ADSORPTION BY POWDERS & POROUS SOLIDS

PRINCIPLES, METHODOLOGY AND APPLICATIONS

F. Rouquerol J. Rouquerol & K. Sing

Academic Press

Adsorption by Powders and Porous Solids

Principles, Methodology and Applications

This Page Intentionally Left Blank

Adsorption by Powders and Porous Solids

Principles, Methodology and Applications

Françoise Rouquerol, Jean Rouquerol and Kenneth Sing

Centre de Thermodynamique et de Microcalorimétrie du CNRS and Université de Provence, 26 rue du 141ème RIA 13003 Marseille France

ACADEMIC PRESS
San Diego London Boston
New York Sydney Tokyo Toronto

This book is printed on acid-free paper.

ISBN 0-12-598920-2

ACADEMIC PRESS
24–28 Oval Road, London NW1 7DX, UK
http://www.hbuk.co.uk/ap/

ACADEMIC PRESS
a division of Harcourt Brace & Company
525 B Street, Suite 1900, San Diego, CA 92101, USA
http://www.apnet.com

Library of Congress Catalogue Card Number: 98-86248
A catalogue record for this book is available from the British Library

Typeset by Mathematical Composition Setters Ltd, Salisbury, Wiltshire
Printed in Great Britain by MPG Books Ltd, Bodmin, Cornwall

99 00 01 02 03 04 MP 9 8 7 6 5 4 3 2 1

Contents

Preface

The growing importance of adsorption (e.g. in separation technology, industrial catalysis and pollution control) has resulted in the appearance of an ever increasing volume of scientific and technical literature on novel adsorbents and catalysts. Also, various new procedures have been introduced over the past few years for the interpretation of adsorption data – particularly for micropore and mesopore size analysis. It is hardly surprising that it is becoming increasingly difficult to obtain a well-balanced view of the significance of the recent developments in such fields as adsorption energetics, network percolation and density functional theory against the background of the more traditional theories of surface coverage and pore filling.

In writing this book, we have endeavoured to give an introductory survey of the principles, methodology and applications of the adsorption of gases and liquids by powders and porous solids. In particular, we hope that this book will meet the needs of all those students and non-specialists who wish to undertake adsorption measurements. In addition, we believe that certain sections of the book will be of interest to those scientists, engineers and other technologists who are already concerned, either directly or indirectly, with the characterization of finely divided or porous solids.

We are conscious of the fact that few people now have the time or inclination to read a scientific volume from cover to cover. Furthermore, we know that some readers are looking for concise information on the general principles or methodology of adsorption, while others are more interested in the adsorptive properties of, say, carbons or oxides. For these reasons we have not adopted the more orthodox arrangement of material, in which the description of each theory is immediately followed by a lengthy discussion of its application. Instead, the format of the present book is as follows. First, a general treatment of the theoretical principles, thermodynamics and methodology of adsorption is given in Chapters 1–5. Secondly, the use of adsorption methods for evaluating the surface area and pore size is discussed (also in general terms) in Chapters 6–8. Thirdly, some typical adsorption isotherms and energies obtained with various adsorbents (carbons, oxides, clays, zeolites) are presented and discussed in Chapters 9–12. Finally, our general conclusions and recommendations are summarized in Chapter 13.

Throughout this book the main emphasis is on the determination and interpretation of adsorption equilibria and energetics. We are not concerned here with the dynamics or chemical engineering aspects of adsorption – both are very important topics which we must leave to other authors! Since we have set out to provide useful

guidance to newcomers to adsorption science, our approach is to some extent didactic. In a book of this nature it would be impossible to achieve a comprehensive review of all aspects of adsorption by powders and porous solids, and the inclusion of material is necessarily selective. By drawing attention to certain publications and overlooking other excellent pieces of research, we risk the displeasure of some members of the international adsorption community. In defence of this approach, we can only plead that the choice of material was dictated by the need to explain and illustrate the general principles which are summarized in Chapter 13.

Many of the ideas expressed in this book have been developed as a result of collaborative research over the past 30–40 years. It would be invidious to name all our co-workers here, but they can be identified in the references listed at the end of each chapter. Our cordial thanks are extended to all those authors and publishers who have readily agreed to the reproduction of published material. For the sake of clarity and consistency of units etc, most figures have been either redrawn or restyled.

We wish to express our grateful thanks to the following people for information supplied privately: D. Avnir, F.S. Baker, F. Bergaya, M. Bienfait, R.H. Bradley, P.J. Branton, P.J.M. Carrott, J.M. Cases, B.H. Davis, M. Donohue, D.H. Everett, G. Findenegg, A. Fuchs, P. Grange, K.E. Gubbins, K. Kaneko, N.K. Kanellopoulos, W.D. Machin, A. Neimark, D. Nicholson, T. Otowa, R. Pellenq, F. Rodriguez-Reinoso, N.A. Seaton, J.D.F. Ramsay, G.W. Scherer, W.A. Steele, F. Stoeckli, J. Suzanne, J. Meurig Thomas, K.K. Unger, and H. Van Damme.

Special thanks are due to our colleagues Y. Grillet, R. Denoyel and P.L. Llewellyn for their forbearance and encouragement, to P. Chevrot for the quality of the art work and to Madame M.F. Fiori for her unfailing dedication in processing the manuscript.

Last, but not least, we should like to pay tribute to the leadership of Dr S. John Gregg, whose many contributions to adsorption and surface science were made over a period of more than 60 years.

List of Main Symbols

As far as possible, the notation used here follows the recommendations of the International Union of Pure and Applied Chemistry.

a	specific surface area
A	surface area
	A(ext) or a(ext) external surface area
b	Langmuir adsorption coefficient
$b(B)$	molality of a solute B
B_m	second virial (molar) coefficient
c	concentration
C	BET constant
d	molecular diameter or particle diameter
E	energy
	E_0 adsorption molar energy at infinitely low coverage
	E_1 adsorption molar energy for the first layer
	E^l liquefaction energy
F	Helmoltz energy defined as $U - TS$
G	Gibbs energy defined as $H - TS$
H	enthalpy defined as $U + pV$
H	distance between the nuclei in the parallel walls of a pore
i	intercept
k_H	Henry's law constant
K	equilibrium constant
K	Kelvin, SI unit
L	Avogadro constant
m	mass
M	molar mass
n	amount of substance
$\boldsymbol{n}$	specific surface excess amount
	n^σ surface excess amount (in the Gibbs representation)
	n^a adsorbed amount (in the layer representation)
	$\boldsymbol{n}_m$ monolayer capacity
	$\boldsymbol{n}_{(sat)}$ Specific surface excess amount corresponding to the saturation of pores
	n_p pore capacity

N number of elementary entities
p pressure
$p°$ standard pressure (usually the saturation pressure)
Q heat
r pore radius
R gas constant
s slope
S entropy
t thickness of multimolecular layer
T thermodynamic temperature
U internal energy

U^σ surface excess (internal) energy

$u^\sigma = \dfrac{U^\sigma}{n^\sigma}$ molar surface excess (internal) energy

$\dot{u}^\sigma = \left(\dfrac{\partial U^\sigma}{\partial n^\sigma}\right)_{T,A.}$ differential surface excess (internal) energy

V volume

$v^\sigma(\mathrm{STP}) = \dfrac{V^\sigma(\mathrm{STP})}{m^s}$ specific gas volume (STP) corresponding to the specific surface excess amount n^σ.

w effective pore width
W work
x mole fraction
y mole fraction
z distance from surface

α polarizability
ε pairwise interaction energy
γ surface tension
Γ surface excess concentration defined as n^σ/A
θ surface coverage, defined as the ratio of two surface excess amounts, one of which is used as a reference
θ Celsius temperature
μ chemical potential
Π spreading pressure
ρ mass density
σ molecular cross sectional area
φ potential energy
ϕ heat flow

CHAPTER 1

Introduction

1.1. Importance of Adsorption

Adsorption occurs whenever a solid surface is exposed to a gas or liquid: it is defined as the enrichment of material or increase in the density of the fluid in the vicinity of an interface. Under certain conditions, there is an appreciable enhancement in the concentration of a particular component and the overall effect is then dependent on the extent of the interfacial area. For this reason, all industrial adsorbents have large specific surface areas (generally well in excess of $100\,m^2\,g^{-1}$) and are therefore highly porous or composed of very fine particles.

Adsorption is of great technological importance. Thus, some adsorbents are used on a large scale as desiccants, catalysts or catalyst supports; others are used for the separation of gases, the purification of liquids, pollution control or for respiratory protection. In addition, adsorption phenomena play a vital role in many solid state reactions and biological mechanisms.

Another reason for the widespread use of adsorption techniques is the importance now attached to the characterization of the surface properties and texture of fine powders such as pigments, fillers and cements. Similarly, adsorption measurements are undertaken in many academic and industrial laboratories on porous materials

such as clays, ceramics and membranes. In particular, gas adsorption has become one of the most widely used procedures for determining the surface area and pore size distribution of a diverse range of powders and porous materials.

The older types of industrial adsorbents (e.g. activated carbons and silica gels) are generally non-crystalline and their surface and pore structures therefore tend to be ill-defined and difficult to characterize. There is, however, a growing number of adsorbents having intracrystalline pore structures (e.g. zeolites and aluminophosphates). Great interest is being shown in the design of other new materials having pores of well-defined size and shape.

1.2. Historical Aspects

Various phenomena which we now associate with adsorption were known in antiquity. The adsorbent properties of such materials as clay, sand and wood charcoal were utilized by the ancient Egyptians, Greeks and Romans (Robens, 1994). These applications were wide-ranging and included the desalination of water, the clarification of fat and oil and the treatment of many diseases.

It has long been known that certain forms of charcoal can take up large volumes of gas. The earliest quantitative studies appear to have been made by Scheele in 1773 and independently by Priestley in 1775 and the Abbé Fontana in 1777 (Deitz, 1944; Forrester and Giles, 1971). The decolorizing properties of charcoal were first investigated by the Russian chemist Lowitz in 1785. The exothermal nature of gas adsorption was noted by de Saussure in 1814 and the first measurements of the heat of adsorption of various gases on charcoal were published by Favre in 1854, who spoke of the wetting of solids by gases. However, it was not until 1881 that the first attempts were made by Chappuis and Kayser to relate the amount of gas adsorbed to the pressure. In that year, Kayser introduced the term *adsorption* and over the next few years the terms *isotherm* and *isothermal curve* were applied to the results of adsorption measurements made at constant temperature (see Forrester and Giles, 1971).

It was observed by Leslie in 1802 that heat was produced when liquid was added to a powder. The heat evolved by the immersion of dry sand in water was described by Pouillet in 1822. This exothermic phenomenon became known in France as the 'Pouillet effect'. Gore (1894) recognized that the amount of heat was related to the surface area of the powder, while Gurvich (1915) suggested that it was also dependent on the polarity of the liquid and the nature of the powder.

The first recorded isotherms of adsorption from solution were probably those reported by van Bemmelen in 1881 (Forrester and Giles, 1972). In his investigations of the 'absorptive' power of soils, van Bemmelen noted the importance of the colloidal structure and drew attention to the relevance of the final state (i.e. equilibrium concentration) of the solution in contact with the soil.

A number of solute–solid isotherms were determined over the next 20 years including those for the uptake of iodine and various dyes by charcoal and other adsorbents, but many of the investigators still believed that the process involved penetration into the solid structure. Freundlich, in 1907, was one of the first to

appreciate the role of the solid surface. He proposed a general mathematical relation for the isotherm, which we now refer to as the Freundlich adsorption equation.

In 1909 McBain reported that the uptake of hydrogen by carbon appeared to occur in two stages: a rapid process of adsorption appeared to be followed by a slow process of absorption into the interior of the solid. McBain coined the term *sorption* to cover both phenomena. In recent years it has been found convenient to use 'sorption' when it is not possible to make a clear distinction between the stages of uptake, and also to use it to denote the penetration of molecules into very narrow pores (Barrer, 1978).

During the early years of the twentieth century, various quantitative investigations of gas adsorption were undertaken. The most important advances in the theoretical interpretation of gas adsorption data were made by Zsigmondy, Polanyi and Langmuir: their ideas set the scene for much of the research undertaken over the past 80 years.

In 1911 Zsigmondy pointed out that the condensation of a vapour can occur in very narrow pores at pressures well below the normal vapour pressure of the bulk liquid. This explanation was given for the large uptake of water vapour by silica gel and was based on an extension of a concept originally put forward by Thomson (Lord Kelvin) in 1871. It is now generally accepted that *capillary condensation* does play an important role in the physisorption by porous solids, but that the original theory of Zsigmondy cannot be applied to pores of molecular dimensions.

The theory proposed by Polanyi in 1914 was developed from an older idea of long-range attractive forces emanating from the solid surface. The adsorbed layer was pictured as a thick compressed film of decreasing density with increase in distance from the surface. The original 'potential theory' did not give an equation for the adsorption isotherm, but instead provided a means of establishing a 'characteristic curve' – relating adsorption potential to amount adsorbed – for a given system. In spite of its initial appeal, it soon became apparent that the principles underlying the potential theory were not consistent with the emerging treatment of intermolecular forces. However, more recently the concept of a characteristic curve has been modified and adopted by Dubinin and his co-workers in their theory of micropore filling.

The year 1916 brought a radical change in the approach to surface science. In that year the first of Langmuir's monumental papers appeared (1916, 1917, 1918). Lord Rayleigh's earlier conclusion that certain films of polar oils on water were one molecule thick had not received the attention it deserved and Langmuir's great contribution was to bring together all the available evidence to support the unifying concept of the monomolecular layer (the *monolayer*). He proposed that adsorption on both liquid and solid surfaces normally involved the formation of a monomolecular layer. In retrospect it is not surprising that the advent of the Langmuir theory produced a renaissance in surface science.

Langmuir's work on gas adsorption and insoluble monolayers prepared the way for more progress to be made in the interpretation of adsorption from solution data. In the light of the Langmuir theory, it seemed logical to suppose that the plateau of a solute isotherm represented monolayer completion and that the monolayer capacity could be derived by application of the Langmuir equation.

Another important stage in the history of gas adsorption was the work of Brunauer and Emmett, which preceded the publication of the Brunauer–Emmett–Teller (BET) theory in 1938. In 1934 Emmett and Brunauer made their first attempt to use low-temperature adsorption of nitrogen to determine the surface area of an iron synthetic ammonia catalyst. They noted that the adsorption isotherms of a number of gases, measured at temperatures at, or near, their respective boiling points, were all S-shaped with certain distinctive features. Others, including Langmuir, had recognized that this type of adsorption was not always restricted to monolayer coverage and an empirical approach was adopted by Emmett and Brunauer (1937) to ascertain the stage at which the multilayer adsorption began. They eventually decided that completion of the monolayer was characterized by the beginning of the middle nearly linear section of the adsorption isotherm (designated Point B – see Figure 1.7). The surface area was then evaluated from the amount adsorbed at Point B by making the further assumption that the completed monolayer was in a close-packed state. In 1938 the publication of the BET theory appeared to provide a sound basis for the identification of Point B as the stage of monolayer completion and the onset of multilayer adsorption.

It would be difficult to overestimate the historical importance of the BET theory since for over 50 years it has attracted an enormous amount of attention (Davis, 1991). Indeed, the BET method is now accepted as a standard procedure for the determination of the surface area of a wide range of fine powders and porous materials. On the other hand, it is generally recognized that the theory is based on an oversimplified model of multilayer adsorption and that the reliability of the BET method is questionable unless certain conditions are fulfilled.

There was a growing awareness in the early 1930s that a distinction could be made between physical adsorption (i.e. *physisorption*) in which the van der Waals interactions are involved and chemical adsorption (i.e. *chemisorption*) in which the adsorbed molecules are attached by chemical bonding. Taylor (1932) introduced the concept of 'activated adsorption' which, by analogy with the familiar idea of an energy of activation in chemical kinetics, attempted to explain the marked increase in rate of adsorption with rise in temperature in terms of surface bond formation. The activated adsorption theory aroused a good deal of early criticism and with the subsequent improvement of high vacuum techniques it was established that chemisorption of certain gases can take place very rapidly on clean metal surfaces. However, there are other chemisorption systems which do appear to exhibit some features of activated adsorption.

In his 1916 paper, Langmuir had stated that with highly porous adsorbents such as charcoal 'it is impossible to know definitely the area on which the adsorption takes place' and that 'there are some spaces in which a molecule would be closely surrounded by carbon atoms on nearly all sides'. He concluded that equations derived for plane surfaces were not applicable to adsorption by charcoal. Unfortunately, these observations have been overlooked by many investigators, who have applied the simple Langmuir monolayer equation to adsorption data obtained with zeolites and activated carbons.

The significance of Langmuir's comments was appreciated, however, by Dubinin

and his co-workers in Moscow, who put forward additional evidence to show that the mechanism of physisorption in very narrow pores is not the same as that in wider pores: or on the open surface. Dubinin argued that the 'micropores' are filled at low relative pressure by a volume-filling process. By studying a wide range of activated carbons, he identified three groups of pores of different width: *micropores*, transitional pores (now termed *mesopores*) and *macropores*. This classification has been refined (see Table 1.3), but the principles remain the same as those adopted by Dubinin (1960).

Another Russian scientist who played a leading role in the advancement of the understanding of adsorption mechanisms was A.V. Kiselev. With the help of a large team of co-workers and by making a systematic investigation of various well-defined adsorbents (notably oxides, carbons and zeolites), Kiselev was able to demonstrate that certain specific interactions were involved in the adsorption of polar molecules on polar or ionic surfaces. At the same time, in the UK the specificity of physisorption was under investigation by Barrer – especially in the context of his pioneering work on the properties of the molecular sieve zeolites.

In an early discussion of the adsorption of gases by solids, Rideal (1932) had stressed the fundamental importance of the nature and extent of the solid surface and had pointed out that it was necessary to evaluate the *accessible* area rather than the 'true' specific area. Many attempts have been made to check the accuracy of the values of surface area derived from adsorption data (in particular from the BET theory), but the concept of surface area still remains problematical. In attempting to assess the magnitude of the surface area of a fine powder or porous solid, one is faced with a similar problem to that of a cartographer required to evaluate a coastal perimeter. Obviously, the answer must depend on the scale of the map and the manner in which the measurement is made.

In recent years much attention has been given to the application of fractal analysis to surface science. The early work of Mandelbrot (1975) explored the replication of structure on an increasingly finer scale, i.e. the quality of self-similarity. As applied to physisorption, fractal analysis appears to provide a generalized link between the monolayer capacity and the molecular area without the requirement of an absolute surface area. In principle, this approach is attractive, although in practice it is dependent on the validity of the derived value of monolayer capacity and the tacit assumption that the physisorption mechanism remains the same over the molecular range studied. In the context of physisorption, the future success of fractal analysis will depend on its application to well-defined non-porous adsorbents and to porous solids with pores of uniform size and shape.

Many new adsorbents have been developed over the past 20 years including carbon molecular sieves, new zeolites and aluminophosphates, pillared clays and model mesoporous solids. In addition, various spectroscopic, microscopic and scattering techniques can now be employed for studying the state of the adsorbate and microstructure of the adsorbent. Major advances have been made in the experimental measurement of isotherms and heats of adsorption and in the computer simulation of physisorption.

It has become apparent that the interpretation of adsorption from solution data is

often difficult. Although many isotherms have a similar shape to the classical Langmuir isotherm, they rarely obey the Langmuir equation over an appreciable range of concentration. It is evident that consideration must be given to the competition between solute and solvent, the solvation of solute and, in many cases, lack of thermodynamic equilibration.

1.3. General Definitions and Terminology

Some of the principal terms and properties associated with adsorption, powders and porous solids are defined in Tables 1.1, 1.2 and 1.3. These definitions are consistent with those proposed by the International Union of Pure and Applied Chemistry (IUPAC) (see Sing *et al.* 1985; Haber, 1991; Rouquerol *et al.*, 1994) and by the British Standards Institution (1958, 1992) and other official organizations (see Robens and Krebs, 1991).

As noted earlier, the term *adsorption* is universally understood to mean the enrichment of one or more of the components in the region between between two bulk phases (i.e. the interfacial layer). In the present context, one of these phases is necessarily a solid and the other a fluid (i.e. gas or liquid). With certain systems (e.g. some metals exposed to hydrogen, oxygen or water), the adsorption process is accompanied by *absorption*, i.e. the penetration of the fluid into the solid phase. As already indicated, one may then use the term *sorption* (and the related terms *sorbent*, *sorptive* and *sorbate*). This is the convention that we shall adopt in the present book. The term sorption is used by some authors to denote the uptake of gas or liquid by a molecular sieve, but we do not favour this practice.

The terms *adsorption* and *desorption* are often used to indicate the direction from which the equilibrium states have been approached. *Adsorption hysteresis* arises when the amount adsorbed is not brought to the same level by the adsorption and desorption approach to a given 'equilibrium' pressure or bulk concentration. The relation, at constant temperature, between the amount adsorbed and the equilibrium pressure, or concentration, is known as the *adsorption isotherm.*

A powder is easily recognized as a mass of small dry particles, but the precise definition is inevitably somewhat arbitrary. The term *fine powder* is also used in an

Table 1.1. Definitions: adsorption

Term	Definition
Adsorption	Enrichment of one or more components in an interfacial layer
Adsorbate	Substance in the adsorbed state
Adsorptive[a]	Adsorbable substance in the fluid phase
Adsorbent	Solid material on which adsorption occurs
Chemisorption	Adsorption involving chemical bonding
Physisorption	Adsorption without chemical bonding
Monolayer capacity	*either* Chemisorbed amount required to occupy all surface sites *or* Physisorbed amount required to cover surface
Surface coverage	Ratio of amount of adsorbed substance to monolayer capacity

[a] Translated into French as 'adsorbable'.

Table 1.2. Definitions: powders

Term	Definition
Powder	Dry material composed of discrete particles with maximum dimension less than about 1 mm
Fine powder	Powder with particle size below about 1 μm
Aggregate	Loose, unconsolidated assemblage of particles
Agglomerate	Rigid, consolidated assemblage or particles
Compact	Agglomerate formed by compression of powder
Acicular	Needle-shaped
Surface area	Extent of available surface as determined by a given method under stated conditions
Specific surface area	Surface area of unit mass of powder, as determined under stated conditions
External surface	Area of external surface of particles, as taking account of roughness (i.e. all cavities which are wider than they are deep), but not porosity
Roughness factor	Ratio of external surface area to area of smoothed envelope around particles
Divided solid	Solid made up of more or less independent particles which may be in the form of a powder, aggregate or agglomerate

imprecise manner, but it seems reasonable to apply it to a material consisting of particles less than about 1 μm (i.e. particles of colloidal dimensions). The unit mass of a fine powder contains a large number of small particles and hence exhibits an appreciable surface area. For example, in the simplest case of an assemblage of spherical particles, all with the same diameter, d, the specific surface area, a, is given by the relation

$$a = 6/\rho\, d \tag{1.1}$$

where ρ is the particle absolute density. Thus, a powder composed of smooth spherical particles of $d = 1$ μm and $\rho = 3$ g cm^{-3} would have a specific surface of 2 m^2 g^{-1}. The same calculation would apply to cubic particles, but in this case d would equal the edge length of the cube. In fact, an area of about 2 m^{2}g^{-1} turns out to be of the same order of magnitude as the lower limit amenable to investigation by the techniques most often used in routine adsorption measurements.

It is evident that it is more difficult to define particle size if the particle shape is not spherical or cubic. With some other simple geometric forms, a single linear dimension, d_x, may be used to calculate the surface area. In particular, when the particle aspect ratio is sufficiently large, d_x is taken as the *minimum* dimension. Thus, if the particles are thin or long (i.e. plates or rods), it is the thickness which mainly determines the magnitude of the specific surface area (Gregg and Sing, 1982).

Perfect spheres are rare, but spheroidal particles are present in some powders produced at high temperature (e.g. pyrogenic silicas) or by the sol-gel process. The term *sphericity* is useful for some purposes. Sphericity has been defined in various ways, the simplest definition being the ratio of the surface area of a sphere of the same volume as a given particle to the actual surface area of that particle (Allen, 1990).

The individual particles (primary particles) in a fine powder are usually clustered together in the form of *aggregates* or *agglomerates*. Loosely bonded aggregates are unconsolidated and non-rigid, but they may be converted into more rigid,

Table 1.3. Definitions: porous solids

Term	Definition
Porous solid	Solid with cavities or channels which are deeper than they are wide
Open pore	Cavity or channel with access to the surface
Interconnected pore	Pore which communicates with other pores
Blind pore[a] (Dead-end pore)	Pore with a single connection to the surface
Closed pore	Cavity not connected to the surface
Void	Space between particles
Micropore	Pore of internal width less than 2 nm
Mesopore	Pore of internal width between 2 and 50 nm
Macropore	Pore of internal width greater than 50 nm
Pore size	Pore width (diameter of cylindrical pore or distance between opposite walls of slit)
Pore volume	Volume of pores determined by stated method
Porosity	Ratio of total pore volume to apparent volume of particle or powder
Total porosity	Ratio of volume of voids and pores (open and closed) to volume occupied by solid
Open porosity	Ratio of volume of voids and open pores to volume occupied by solid
Surface area	Extent of total surface area as determined by given method under stated conditions
External surface area	Area of surface outside pores
Internal surface area	Area of pore walls
True density	Density of solid, excluding pores and voids
Apparent density	Density of material including closed and inaccessible pores, as determined by stated method

[a] In the sense of the French word '*borgne*'.

consolidated agglomerates as a result of sintering or ageing. The breakdown, or partial breakdown, of the consolidated material can be achieved by grinding. The process of agglomeration involves the bridging or cementation of particles and should not be confused with *Ostwald ripening*, which involves the growth of larger particles at the expense of smaller ones. It is evident that an agglomerate may be regarded as a 'secondary' particle, which always contains within it some internal surface. In many cases the *internal surface area* is much larger than the *external surface area* and the agglomerate then possesses a well-defined pore structure.

The classification of pores according to size has been under discussion for many years, but in the past the terms *micropore* and *macropore* have been applied in different ways by physical chemists and some other scientists. In an attempt to clarify this situation, the limits of size of the different categories of pores included in Table 1.3 have been proposed by the International Union of Pure and Applied Chemistry (Everett, 1972; Sing *et al.*, 1985). As indicated, the *pore size* is generally specified as the *pore width*, i.e. the available distance between the two opposite walls. Obviously, pore size has a precise meaning when the geometrical shape is well defined. Nevertheless, for most purposes the limiting size is that of the smallest dimension and this is generally taken to represent the effective pore size. Micropores and mesopores are especially important in the context of adsorption.

The hypothetical types of pores shown in Figure 1.1 relate to the definitions in

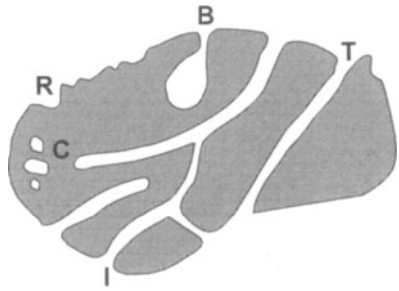

Figure 1.1. Cross-section of a hypothetical porous grain showing various types of pores: closed (C), blind (B), through (T), interconnected (I), together with some roughness (R) (Rouquerol, 1990).

Table 1.3. In addition to *closed pores* and *open pores*, we may distinguish between *blind pores* (or dead-end pores) and *interconnected pores*. Pores which are open at both sides of a membrane or porous plug are termed *through pores*.

Porosity is usually defined as the ratio of the volume of pores and voids to the volume occupied by the solid. However, it should be kept in mind that the recorded value of porosity is not always a simple characteristic property of the material, since it is likely to depend also on the methods used to assess both the pore volume and the volume of the solid. The pore volume is usually regarded as the volume of open pores, but it may include the volume of closed pores. Moreover, the recorded value may depend on the nature of the probe molecule or the experimental conditions.

It is not always easy to distinguish between roughness and porosity or between pores and voids. In principle, a convenient and simple convention is to refer to a solid as porous only if the surface irregularities are deeper than they are wide. Furthermore, the area of a rough surface is regarded as an external surface area, whereas the area of the pore walls is the internal surface area. We prefer to regard the porosity as an intrinsic property of the material and to designate void as the space between particles, which is dependent on the conditions of packing (and the particle coordination number).

It is evident that the description of many real porous materials is complicated by a wide distribution of pore size and shape and the complexity of the pore network. To facilitate the application of certain theoretical principles the shape is often assumed to be cylindrical, but this is rarely an accurate portrayal of the real system. With some materials, it is more realistic to picture the pores as slits or interstices between spheroidal particles. Computer simulation and the application of percolation theory have made it possible to study the effects of *connectivity* and *tortuosity*.

Pore structures can be created in a number of different ways. *Intracrystalline* pores are an inherent part of certain crystalline structures, e.g. of zeolites and certain clays. These pores are generally of molecular dimensions and are arranged as highly regular networks. A second type of porous material is composed of an assemblage of small particles (as mentioned earlier). The pore structure of the consolidated system (e.g. a xerogel) is mainly dependent on the size and packing density of the primary particles: the process is therefore *constitutive*. A third route is *subtractive* since inherent parts of the original structure are removed to create the pores, e.g. the thermal

decomposition of a hydroxide or carbonate or a leaching process to produce porous glass.

1.4. Physisorption and Chemisorption

Adsorption is brought about by the interactions between the solid and the molecules in the fluid phase. Two kinds of forces are involved, which give rise to either physical adsorption (physisorption) or chemisorption. Physisorption forces are the same as those responsible for the condensation of vapours and the deviations from ideal gas behaviour, whereas chemisorption interactions are essentially those responsible for the formation of chemical compounds.

The most important distinguishing features may be summarized as follows:

(a) Physisorption is a general phenomenon with a relatively low degree of specificity, whereas chemisorption is dependent on the reactivity of the adsorbent and adsorptive.
(b) Chemisorbed molecules are linked to reactive parts of the surface and the adsorption is necessarily confined to a monolayer. At high relative pressures, physisorption generally occurs as a multilayer.
(c) A physisorbed molecule keeps its identity and on desorption returns to the fluid phase in its original form. If a chemisorbed molecule undergoes reaction or dissociation, it loses its identity and cannot be recovered by desorption.
(d) The energy of chemisorption is the same order of magnitude as the energy change in a comparable chemical reaction. Physisorption is always exothermic, but the energy involved is generally not much larger than the energy of condensation of the adsorptive. However, it is appreciably enhanced when physisorption takes place in very narrow pores.
(e) An activation energy is often involved in chemisorption and at low temperature the system may not have sufficient thermal energy to attain thermodynamic equilibrium. Physisorption systems generally attain equilibrium fairly rapidly, but equilibration may be slow if the transport process is rate-determining.

1.5. Adsorption Interactions

As a molecule approaches the solid surface, a balance is established between the intermolecular attractive and repulsive forces. If other molecules are already adsorbed, both adsorbent–adsorbate and adsorbate–adsorbate interactions come into play. It is at once evident that assessment of the adsorption energy is likely to become exceedingly complicated in the case of a multicomponent system – especially if the adsorption is taking place from solution at a liquid–solid interface. For this reason, in the numerous attempts made to calculate energies of adsorption, most attention has been given to the adsorption of a single component at the gas–solid interface.

The forces responsible for physisorption always include the dispersion attractive interactions (which derive their name from the close connection between their origin and the cause of optical dispersion) and the short-range repulsion. These interactions

do not depend on the polar nature of the adsorbent or adsorptive and are therefore regarded as *non-specific*.

The dispersion *attractive* interactions were first characterized by London (1930) and arise from the rapid fluctuations in electron density in one atom, which induce an electrical moment in a neighbouring atom. By making use of quantum-mechanical perturbation theory, London arrived at the well-known expression for the potential energy, $\varepsilon_D(r)$, of two isolated atoms separated by a distance r:

$$\varepsilon_D(r) = -C/r^6 \tag{1.2}$$

where C is a constant which can be expressed in terms of the polarizabilities of the adsorptive and the adsorbent.

The short-range *repulsion* is the result of the interpenetration of the electron clouds. This repulsive interaction is often expressed in the form:

$$\varepsilon_R(r) = B/r^m \tag{1.3}$$

where B and m are empirical constants, the latter usually being given the value 12. The *total* potential energy, representing the interaction between the two isolated atoms, therefore becomes:

$$\varepsilon(r) = B/r^{12} - C/r^6 \tag{1.4}$$

which is often designated as the (12-6) Lennard-Jones potential (Lennard-Jones, 1932). Although Equation (1.4) is still used in many theoretical and computer simulation studies – and indeed appears to be remarkably successful for some purposes – it has been refined by the inclusion of additional terms to allow *inter alia* for induced dipole–quadrupole and quadrupole–quadrupole interactions.

For the computation of the adsorbent–adsorbate energies, it has been customary to adopt the principle of additivity of the pairwise interactions. Thus, each atom or ion in the surface layers of the solid is regarded as a force centre and the total interaction experienced by the adsorbate molecule is given by the summation

$$\phi_i(z) = \sum_j \varepsilon_{ij}(r_{ij}) \tag{1.5}$$

Now, $\phi_i(z)$ is the potential energy for the molecule i, expressed as a function of its distance z from the plane of the centres of atoms (or ions) in the surface layer; r_{ij} is the distance between the molecule i and each atom (ion) in the solid. In practice, only a limited number of atoms are taken into account because of the rapid decrease in energy with distance. The balance between attractive and repulsive interactions means that a point exists, at distance z_e from the surface, where the potential energy of the molecule is minimum, as represented in Figure 1.2.

Of course, the value of $\phi_i(z)$ must depend not only on the distance from the surface but also on the location on the surface (i.e. in the xy plane). If this is in the form of one face of a perfect crystal, there will be a regular variation of potential energy across the surface. It is not surprising to find that the most favourable site is at the centre of an array of surface atoms (cf. Figure 1.3). The corresponding depth of the potential energy well (at z_e) will depend on the density and crystal structure of the adsorbent and the polarizability and molecular size of the adsorbate.

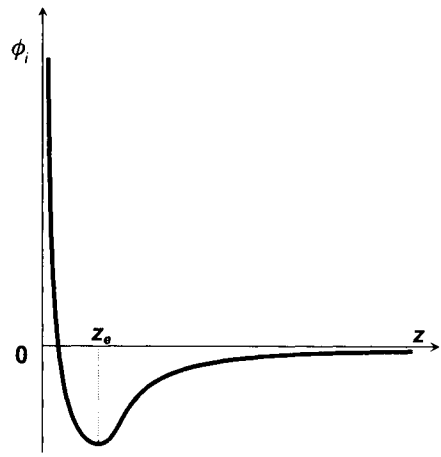

Figure 1.2. Potential energy ϕ_i of a molecule i versus its distance z from the adsorbing surface.

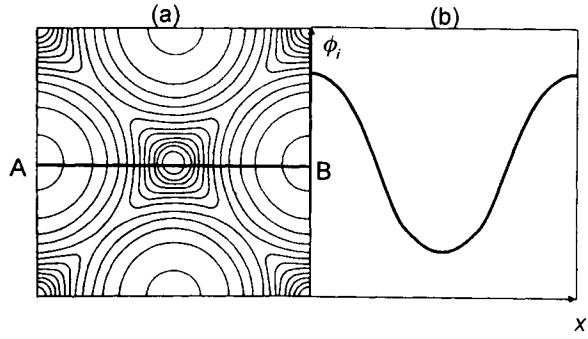

Figure 1.3. (a) Isopotential curves for the adsorption of one He atom on the (1 0 0) face of solid Xe. Intervals between curves are 1.24×10^{-22} J (after Ricca, 1967). (b) Potential energy of an adsorbed He atom moving along line AB.

The easiest path for the movement of the adsorbed molecule across the surface is via a col or 'saddle point' and the energy barrier to translational movement in the xy plane is given by the difference in the corresponding minima potential energies for the two locations (Figure 1.3).

1.6. Mobility of Adsorbed Molecules

The translational movement of adsorbed molecules is governed by the amplitude of the oscillations of $\phi_i(z)$ across the surface and by the available thermal energy. If the variations in $\phi_i(z)$ are much smaller than the mean thermal energy, kT, the energy

barriers between adsorption sites are small enough to be overcome easily at the operational temperature: the adsorbed molecules therefore retain two translational degrees of freedom and can be regarded as *mobile*. On the other hand, if the energy barriers are much larger than kT, the adsorbed molecules are said to be *localized* since they spend most of their time on particular surface sites.

In the hypothetical case of a perfectly homogeneous surface, there is no variation of $\phi_i(z)$ in the xy plane – see Figure 1.4a. It is more realistic to picture a uniform surface, which gives rise to energy wells of the same depth. Now, the potential energy profiles corresponding to mobile and localized adsorption are shown respectively in Figures 1.4b and 1.4c. In the former case, there is a random distribution of

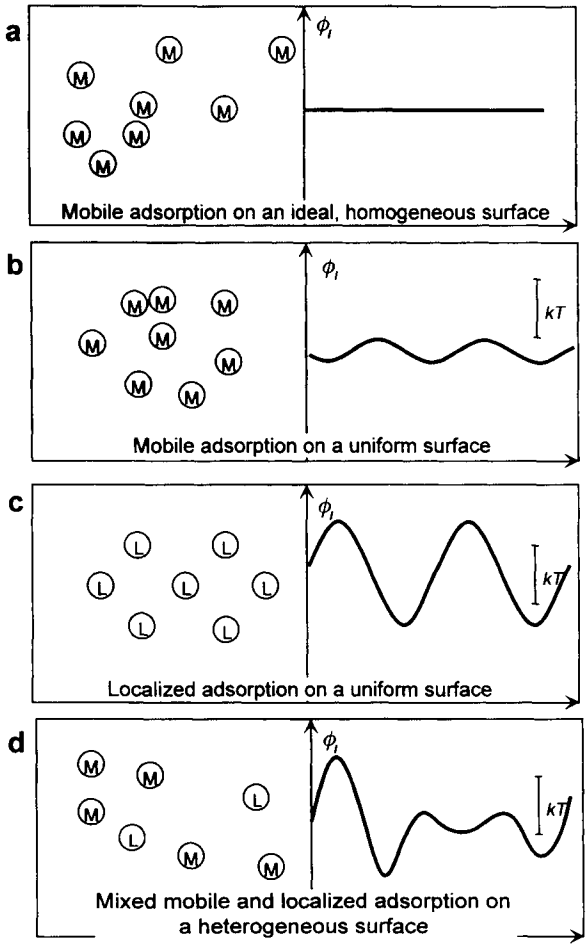

Figure 1.4. Distribution of adsorbed molecules on hypothetical surfaces (left) and corresponding variations of potential energy (right). M, mobile; L, localized. Adsorbate–adsorbate interactions are not taken into account.

adsorbed molecules across the surface; whereas in the latter case, the location of the adsorbed molecules is governed by the surface structure of the adsorbent.

Localization does not prevent the adsorbed molecules from 'hopping' from one site to another (unlike the situation in immobile chemisorption), but it is not compatible with the state of a close-packed completed monolayer.

1.7. Energetics of Physisorption

Provided that the experimental measurements are made under carefully controlled conditions and that the adsorption systems are well characterized, energy of adsorption data can provide valuable information concerning the mechanisms of physisorption.

When a polar molecule is adsorbed on an ionic or polar surface various types of specific interactions may contribute to the *adsorption energy*. A useful general expression for the adsorption energy, E_0, at very low surface coverage was first proposed by Barrer (1966) in the form of the sum

$$E_0 = E_D + E_R + E_P + E_{F\mu} + E_{\dot{F}Q} \tag{1.6}$$

in which E_D and E_R represent the non-specific dispersion and repulsion contributions and the terms E_P, $E_{F\mu}$ and $E_{\dot{F}Q}$ represent, respectively, the three types of specific contributions: the polarization, field-dipole and field gradient-quadrupole energies.

For convenience, we may write Equation (1.6) in the form

$$E_0 = E_{ns} + E_{sp}$$

with E_{ns} now in place of $(E_D + E_R)$ representing the *non-specific* contributions and E_{sp} representing the various *specific* contributions.

If we wish to study the adsorbent–adsorbate interactions we must undertake adsorption calorimetry or analysis of the isotherm data at very low surface coverage. It is only under these conditions that we can eliminate, or at least minimize, the adsorbate–adsorbate interactions. At higher coverage, an additional (self-potential) term, E_{aa}, must be added to E_0 to allow for the latter interactions.

It is evident that the adsorption energy is controlled by the nature of the adsorption *system* (i.e. by both adsorbent and adsorptive). There are a few adsorbents which give rise to essentially non-specific interactions with a wide range of different adsorptives. The most important non-porous adsorbent of this type is graphitized carbon black, which in its most uniform state has a surface structure composed almost entirely of the graphitic basal planes. When a polar molecule is adsorbed on this surface, E_{ns} is much larger than E_{sp}, which is unlikely to contribute more than 10% to the total interaction energy. In the case of graphite, the E_{sp} contribution is largely due to the polarization component arising from the interaction between a polar adsorptive molecule and the induced dipoles in the graphite lattice.

It follows from Equations (1.2) and (1.5) that the magnitude of E_{ns} is dependent on the polarizabilities of the adsorptive and the adsorbent and the density of the principal force centres in the outer part of the adsorbent (i.e. in the surface layer). It is only

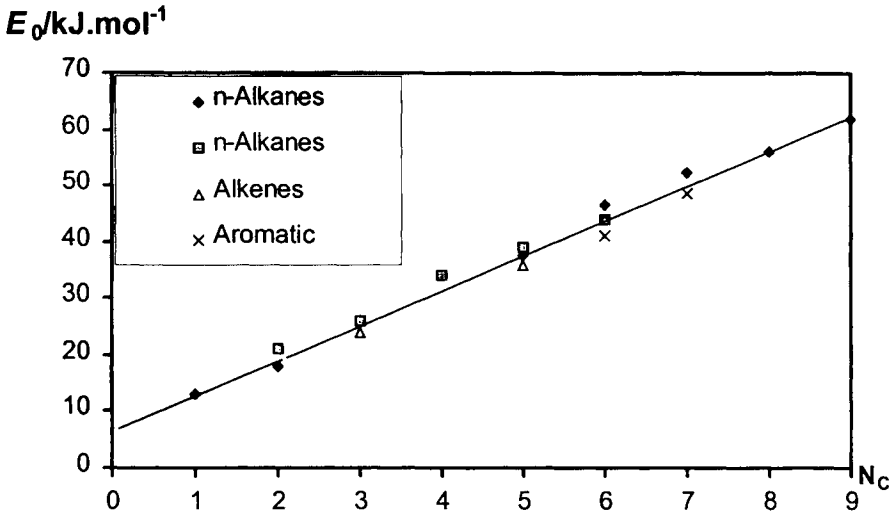

Figure 1.5. 'Zero' coverage energy of adsorption versus carbon number, N_C, on graphitized carbon. *n*-Alkanes, after Avgul and Kiselev (1965) and Carrott and Sing (1987); alkenes, after Carrott *et al.* (1989); aromatic, after Avgul and Kiselev (1965).

when the E_{sp} contribution becomes significant that the polarity of the adsorptive molecule is important.

The results shown in Figure 1.5 illustrate this behaviour. Here E_0 is measured from the enthalpy of adsorption, $[\Delta_{ads}h_0]$ (determined by the chromatographic method at very low surface coverage, as explained in Chapter 3). E_0 is plotted against the number of carbon atoms, N_C, in the various series of hydrocarbons. It is striking that there is an almost common linear relation between E_0 and N_C. Thus, for a given N_C, quite close agreement is obtained between the corresponding values of E_0 for the series of alkanes, alkenes and aromatic hydrocarbons (Cao *et al.*, 1991).

By plotting experimental and theoretical low-coverage enthalpies of adsorption as a function of the molecular polarizability, Avgul and Kiselev (1970) also obtained a linear relation for a wide range of polar and non-polar molecules on graphitized carbon black (including noble gases, dimethyl ketone, ethyl ether and a series of alcohols). We may conclude that there is ample evidence to confirm the essentially non-specific nature of the interactions between the surface of graphitized carbon and all types of gas molecules.

The low-coverage energy data for the adsorption of *n*-hexane and benzene on various non-porous solids in Table 1.4 illustrate the importance of the surface structure of the adsorbent and the nature of the adsorptive. Since *n*-hexane is a non-polar molecule, $E_{ns} \gg E_{sp}$, and therefore the value of E_0 is dependent on the overall dispersion forces and hence on the density of the force centres in the outer part of the adsorbent (i.e. its surface structure). Dehydroxylation of a silica surface involves very little change in surface structure and therefore no significant difference in the value of E_0 for *n*-hexane. However, replacement of the surface hydroxyls by alkylsilyl groups

Table 1.4. Enthalpies in kJ mol^{-1} of adsorption at low coverage for *n*-hexane and benzene on graphitized carbon, silica (hydroxylated, dehydroxylated and modified), and barium sulfate

Adsorbent	n-Hexane	Benzene	Reference
Graphitized carbon black	42	42	Avgul and Kiselev (1965)
Hydroxylated silica	46	55	Kiselev (1965)
Dehydroxylated silica	48	38	Kiselev (1965)
Trimethylsilylated silica	29	34	Kiselev (1967)
Barium sulfate	47	70	Belyakova *et al.* (1970)

has resulted in a much greater effect. In this case the weakening of the adsorbent–adsorbate interactions is mainly due to the fact that the surface modification has resulted in a reduction in the density of the force centres.

The polarizabilities of benzene and hexane are very similar, but because of its electronic structure benzene exhibits significant specificity in its interaction with ionic or polar surfaces (e.g. hydroxylated silica and barium sulphate). Considerable attention has been given to the specificity associated with hydroxylated silica, but some specific adsorbent–adsorbate interactions are enhanced to an even greater extent by the exposure at the surface of ionic sites. This is illustrated by the benzene data on $BaSO_4$ in Table 1.4 and the nitrogen data on rutile in Table 1.5.

One might expect argon and nitrogen to be similar in their physisorption behaviour since their physical properties are not very different (e.g. molecular sizes, boiling points and polarizabilities). However, the energy data in Table 1.5 show that this is true only if the nitrogen interaction is non-specific (e.g. on graphitized carbon). The field gradient-quadrupole term in Equation (1.6) makes an important contribution when nitrogen

Table 1.5. Differential enthalpies of adsorption, $|\Delta_{ads}h|$ (kJ mol^{-1}), of argon and nitrogen at 'zero' and half coverage

Adsorbent	Argon		Nitrogen		Reference
	$\theta \to 0$	$\theta = 0.5$	$\theta \to 0$	$\theta = 0.5$	
Graphitized carbon	10	12	10	11	Grillet *et al.* (1979)
Hydroxylated silica (mesoporous)	15	9	> 20	12	Rouquerol *et al.* (1979)
Dehydroxylated silica (mesoporous)	15	9	17	11	
Zinc oxide (450 °C)[a]	12	11	21	20	Grillet *et al.* (1989)
Rutile (150 °C)	13	9	> 20	10	Furlong *et al.* (1980)
(400 °C)	15	11	30	13	
Molecular sieve carbon	20	15[b]	22	17[b]	Atkinson *et al.* (1987)
Microporous carbon	21	15[b]	25	15[b]	Rouquerol *et al.* (1989)
Silicalite I	14	14[b]	15	14[b]	Llewellyn *et al.* (1993a, b)
H-ZSM5 (Si/Al = 16)	14	14[b]	18	15[b]	
$AlPO_4$-5	11	14[b]	13	14[b]	Grillet *et al.* (1993)
Sepiolite	14	15	17	15	Grillet *et al.* (1988)
Attapulgite (130 °C)	15	13	18	17	Cases *et al.* (1991)

[a] Outgassing temperature.
[b] θ = fraction of pore filling.

is adsorbed on such polar or ionic surfaces as hydroxylated silica, rutile and zinc oxide. In the case of rutile, cationic sites are exposed when the adsorbent is outgassed at 400°C and these interact very strongly with nitrogen at low surface coverage.

The results in Table 1.5 also reveal that with some systems the differential enthalpy undergoes a pronounced change with increase in surface coverage, whereas in other cases the change is much smaller (at least up to $\theta = 0.5$).

An *increase* in the enthalpy of adsorption (e.g. with argon on graphitized carbon) is likely to be due to the attractive interactions between adsorbed molecules ('lateral interactions') becoming more important as the population in the monolayer is increased or as micropore filling approaches completion. The more usual progressive *decrease* in the differential enthalpy is generally to be expected if the adsorbent surface is energetically heterogeneous. However, it is necessary to bear in mind that there may be compensatory effects involved. Thus, the computer simulation studies of Steele and Bojan (1989) have indicated that for the adsorption of krypton on a model heterogeneous surface an almost constant overall energy is the result of a significant decrease in the adsorbent–adsorbate interactions being almost exactly balanced by an increase in the lateral adsorbate–adsorbate interactions.

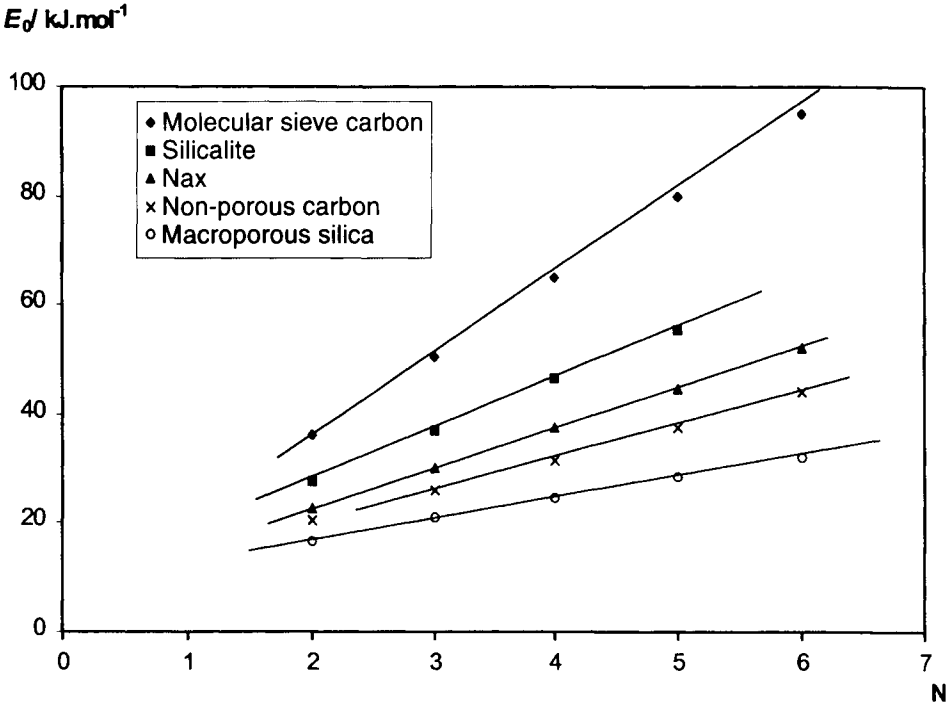

Figure 1.6. 'Zero' coverage energy of adsorption of *n*-alkanes versus carbon number N_C, on three microporous solids (and two others, for comparison). Molecular sieve carbon, after Carrott and Sing (1987); Silicalite after Carrott and Sing (1986); NaX and macroporous silica, after Kiselev (1967); non-porous carbon, after Carrott and Sing (1987) and Avgul and Kiselev (1965).

An important consequence of the additive nature of the molecular interactions is that the entry of adsorbate molecules into pores of molecular dimensions results in an appreciable increase in the adsorption energy over that given by physisorption of the same molecules on the corresponding open surface.

In accordance with the theoretical predictions of Everett and Powl (1976) for physisorption in slit-shaped micropores, the energies of adsorption for certain molecular sieve carbons show an approximately two-fold enhancement over the corresponding values for graphitized carbon (Table 1.5 and Figure 1.6). It will be noted that the molecular sieve zeolites NaX and Silicalite also give appreciably higher energies than macroporous silica, but that the degree of enhancement is not as pronounced as for carbon. To explain these effects one must take into account the differences in solid structure and pore shape. These aspects are discussed in relation to the major adsorbent systems of carbons, oxides and zeolites respectively in Chapters 9, 10 and 11.

1.8. Types of Adsorption Isotherms

The amount of gas adsorbed, n^a, by the mass, m^s, of solid is dependent on the *equilibrium* pressure, p, the temperature, T, and the nature of the gas–solid system. Thus, we may write:

$$n^a/m^s = \mathrm{f}(p, T, \text{system}) \tag{1.7}$$

For a given gas adsorbed on a particular solid at a constant temperature we have

$$n^a/m^s = \mathrm{f}(p)_T \tag{1.8}$$

and if the gas is below its critical temperature, it is possible to write

$$n^a/m^s = \mathrm{f}(p/p^\circ)_T \tag{1.9}$$

where here, the standard pressure p° is equal to the saturation pressure of the adsorptive at T.

Equations (1.8) and (1.9) represent the *adsorption isotherm* which is the relationship between the amount adsorbed by unit mass of solid and the equilibrium pressure (or relative pressure), at a known temperature. The experimental adsorption isotherm is usually presented in graphical form.

1.8.1. Physisorption of gases

Experimental adsorption isotherms recorded in the literature, measured on a wide variety of gas–solid systems, have a wide variety of forms. Nevertheless, the majority of these isotherms which result from *physical adsorption* may conveniently be grouped into six classes in the IUPAC classification (cf. Figure 1.7). The first five types (I to V) of the classification were originally proposed by S. Brunauer, L.S. Deming, W.S. Deming and E. Teller as the BDDT classification (1940), sometimes referred to as the Brunauer classification (1945).

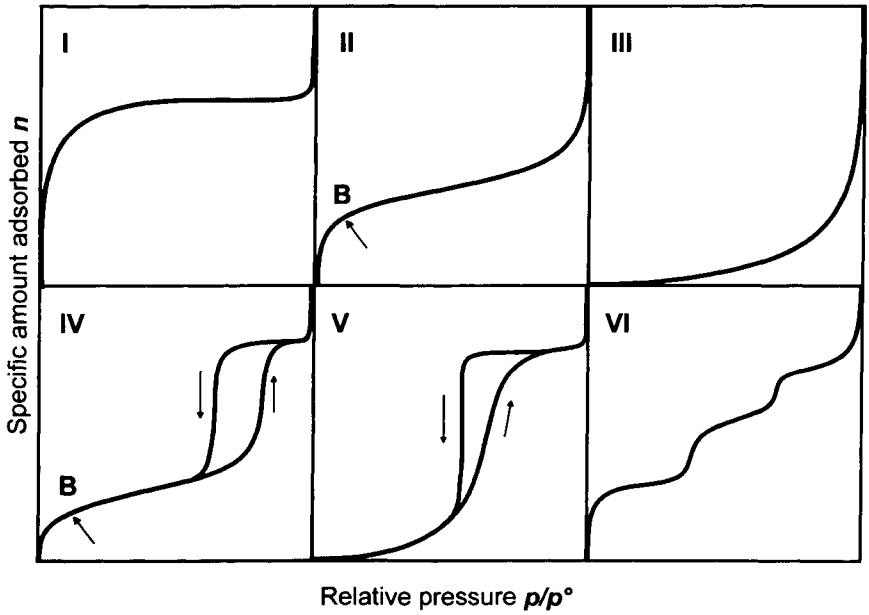

Figure 1.7. The six main types of gas physisorption isotherms, according to the IUPAC classification (after Sing *et al.*, 1985).

The IUPAC 1985 classification of physisorption isotherms, shown in Figure 1.7, included the Type VI which has been more recently observed.

In its most characteristic form, the *Type I* isotherm is concave to the relative pressure ($p/p°$) axis. It rises sharply at low relative pressures and reaches a plateau: the amount adsorbed by the unit mass of solid, n^a/m^s, approaches a limiting value as $p/p° \longrightarrow 1$.

As explained in Section 1.7, enhanced adsorbent–adsorbate interactions occur in micropores of molecular dimensions. A decrease in the micropore width results in both an increase in the adsorption energy and a decrease in the relative pressure at which the micropore filling occurs. The narrow range of relative pressure necessary to attain the plateau is an indication of a limited range of pore size and the appearance of a nearly horizontal plateau indicates a very small external surface area. The limiting adsorption is dependent on the available micropore volume.

The *Type II* isotherm is concave to the $p/p°$ axis, then almost linear and finally convex to the $p/p°$ axis. It indicates the formation of an adsorbed layer whose thickness increases progressively with increasing relative pressure until $p/p° \longrightarrow 1$. When the equilibrium pressure equals the saturation vapour pressure, the adsorbed layer becomes a bulk liquid or solid. If the knee of the isotherm is sharp, the uptake at Point B – the beginning of the middle quasilinear section – is usually considered to represent the completion of the monomolecular layer (monolayer) and the beginning of the formation of the multimolecular layer (*multilayer*). The ordinate of Point B gives an estimation of the amount of adsorbate required to cover the unit mass of solid

surface with a complete monomolecular layer (*monolayer capacity*). Type II isotherms are obtained with non-porous or macroporous adsorbents, which allow unrestricted monolayer–multilayer adsorption to occur at high $p/p°$. If the adsorbent temperature is at, or below, the normal boiling point of the adsorptive, it is not difficult to establish the course of the adsorption–desorption isotherm over the entire range of $p/p°$. Complete reversibility of the desorption–adsorption isotherm (i.e. the absence of adsorption hysteresis) is the first condition to be satisfied for 'normal' monolayer– multilayer adsorption on an open and stable surface.

A *Type III* isotherm is convex to the $p/p°$ axis over the complete range and therefore has no Point B. This feature is indicative of weak adsorbent–adsorbate interactions. True Type III isotherms are not common.

The *Type IV* isotherm, whose initial region is closely related to the Type II isotherm, tends to level off at high relative pressures. It exhibits a hysteresis loop, the lower branch of which represents measurements obtained by progressive addition of gas of the adsorbent, and the upper branch by progressive withdrawal. The hysteresis loop is usually associated with the filling and emptying of the mesopores by capillary condensation. Type IV isotherms are common but the exact shape of the hysteresis loop varies from one system to another.

The *Type V* isotherm is initially convex to the $p/p°$ axis and also levels off at high relative pressures. As in the case of the Type III isotherm, this is indicative of weak adsorbent–adsorbate interactions. A Type V isotherm exhibits a hysteresis loop which is associated with the mechanism of pore filling and emptying. Such isotherms are relatively rare.

The *Type VI* isotherm, or stepped isotherm, is also relatively rare and is associated with layer-by-layer adsorption on a highly uniform surface. The sharpness of the steps is dependent on the system and the temperature.

The above classification is necessarily a simplification since many experimental physisorption isotherms have a composite nature and others are more complex than was formerly thought. Some of the more interesting and unusual isotherms will be discussed in subsequent chapters and the IUPAC classification is refined and extended in Chapter 13. It is, of course, evident that this type of isotherm classification is only applicable to the adsorption of a single-component gas within its condensable range of temperature. Such measurements are extremely useful for the characterization of porous materials. For technological reasons, the study of supercritical gas adsorption is also becoming increasingly important. In a new classification of physisorption isotherms for fluid–solid equilibria, Aranovich and Donohue (1998) have attempted to allow for the more general behaviour of various systems, both below and above the adsorptive critical temperature.

1.8.2. Chemisorption of gases

Chemisorption isotherms generally exhibit a plateau at lower pressures than the micropore filling plateau. This limiting adsorption is due to the completion of a chemically bound monolayer. In our view, these isotherms may be referred to as *Langmuir isotherms*, even if the mechanism involved may not be strictly in

accordance with the Langmuir model. On the other hand we recommend that the term 'Langmuir isotherm' should not be used in the context of physisorption by microporous solids. With some systems, and under certain conditions, the slow rate of chemisorption makes it difficult to obtain equilibrium data. Furthermore, the chemisorption reaction may be undetectable at low temperature or pressure and become significant only when the experimental conditions are changed.

1.8.3. Adsorption from solution

A distinctive feature of adsorption from solution is that it always involves a competition between the solvent and solute which has be taken into account in any complete treatment of the data.

In the case of *adsorption from solution*, the 'apparent adsorption' of a solute at the liquid–solid interface is usually evaluated by measuring the decrease in its concentration when brought into contact with the adsorbent. The adsorption isotherm is then plotted as the apparent adsorption of the solute against the equilibrium concentration.

At low concentrations (i.e. for most practical applications of adsorption) the adsorption from solution isotherms mainly fall into two main types among those listed by Giles and Smith (1974): the *Type L* is concave to the concentration axis (analogous to Type I of the IUPAC classification) and the *Type S* is first convex and then concave to the concentration axis (analogous to Types III or V). A *Type L* isotherm having a long well-defined plateau is generally associated with monolayer adsorption of the solute and minimal competition from the solvent. A *Type S* isotherm is explained by a different balance between the adsorbate–adsorbent and adsorbate–adsorbate interactions: the latter are thought to be responsible for a 'co-operative' adsorption mechanism which produces an upward swing over the first part of the adsorption isotherm.

1.9. Molecular Modelling of Adsorption

With the aid of fast computers it is now possible to predict the adsorption and pore filling of simple molecules by model adsorbents (Cracknell *et al.*, 1995; Nicholson, 1996; Gubbins, 1997; Steele and Bojan, 1997; Nicholson and Pellenq, 1998; Steele and Bojan, 1998; Ravikovitch, Haller and Neimark, 1998). The various computational procedures that have been developed in recent years are based on the statistical mechanics of confined fluids. Before any attempt can be made to solve the equations defining the locations, configurations and movement of individual molecules, it is necessary to specify the exact nature of the adsorption system.

First, a complete description of the adsorbent is required: this must include details of its solid structure, surface chemical structure, pore size and shape. One starts by assuming that the pores in the model adsorbent are all of the same size and shape and that they are unconnected. Secondly, the nature of the fluid–fluid and fluid–solid interactions must be precisely defined since the validity of the calculations is dependent on the accuracy of the intermolecular potential functions.

One way of solving the statistical mechanical equations is by a numerical procedure. This type of approach is called *molecular simulation*. To achieve a satisfactory result, the computer runs must be long enough and the simulated system large enough to overcome statistical uncertainties. In principle, this approach can be applied to fairly complex systems, but a possible disadvantage is that long computing times may be required.

An alternative approach is by the application of an approximate theory. At present, the most useful theoretical treatment for the estimation of the equilibrium properties is generally considered to be the *density functional theory* (DFT). This involves the derivation of the density profile, $\rho(r)$, of the inhomogeneous fluid at a solid surface or within a given set of pores. Once $\rho(r)$ is known, the adsorption isotherm and other thermodynamic properties, such as the energy of adsorption, can be calculated. The advantage of DFT is its speed and relative ease of calculation, but there is a risk of oversimplification through the introduction of approximate forms of the required functionals (Gubbins, 1997).

1.9.1. Intermolecular potential functions

For many purposes, the Lennard-Jones 12-6 potential is considered to be a satisfactory starting point for establishing the pairwise adsorbate–adsorbent and adsorbate–adsorbate interactions. If the adsorbed molecule has a permanent dipole or quadrupole moment, it is necessary to allow for electrostatic interactions and possibly also additional polarization effects. To obtain the required overall fluid–fluid and fluid–solid potential functions, it is customary to assume that the pairwise interactions are additive. With some systems, however, the solid can be regarded as a continuum, and integration is then possible in place of more laborious summation (Steele, 1974).

With methane on graphite, the continuum solid approximation appears to be satisfactory at temperatures as low as 80 K. In this case the diameter of the non-polar methane molecule (0.38 nm) is large in comparison with the C—C spacing (0.14 nm) and therefore the molecule can move parallel to the surface (i.e. at constant z) with little variation in the adsorbent–adsorbate interaction. The continuum solid assumption is more questionable, however, when small molecules are adsorbed at low temperature (e.g. Ar or N_2 at 77 K).

At low temperatures, the simulation of adsorption requires more careful modelling because of the larger contribution of potential energy to the total energy. Furthermore, it has been shown that a permanent quadrupole moment in the adsorbate molecule (of, say, N_2 or CO_2) may have a major influence on the structure of the adsorbed monolayer at low temperature (Steele, 1996). For example, it seems that the remarkable difference between the 2-D phase diagrams for N_2 and O_2 on graphite is in large measure due to the quadrupolar nature of N_2.

It has been pointed out by a number of authors (see Cracknell *et al.*, 1995) that the dispersion, electrostatic and induced (polarization) energy terms can be quantitatively accounted for by quantum-mechanical perturbation theory. However, this is not the case for the short-range repulsion. Some evidence suggests an exponential

decay, rather than the inverse 12th power in Equation (1.4). For this reason, low-coverage isotherm and adsorption energy data are used to refine the evaluation of the adsorbent–adsorbate interaction energy Another source of uncertainty is the magnitude of three-body effects, e.g. involving two adsorbate molecules and a substrate atom, which with some systems are likely to be significant even at very low coverage (Nicholson, 1996).

1.9.2. Molecular simulation

The two simulation methods in general use for solving the statistical mechanical equations are Monte Carlo (MC) and molecular dynamics (MD). The two techniques have several common features, but each has certain advantages and limitations.

Monte Carlo (MC) simulation

In this method a random number generator is used to move and rotate molecules in a random fashion. If the system is held under specified conditions of temperature, volume and number of molecules, the probability of a particular arrangement of molecules is proportional to $\exp(-U/kT)$, where U is the total intermolecular energy of the assembly of molecules and k is the Boltzmann constant. Thus, within the MC scheme the movement of individual molecules is accepted or rejected in accordance with a probability determined by the Boltzmann distribution law. After the generation of a long sequence of moves, the results are averaged to give the equilibrium properties of the model system.

An advantage of MC simulation is that it is not difficult to program. Also, the thermodynamic, canonical, variables may be readily changed. For gas adsorption studies it is generally more useful to specify μ, V, T (the grand canonical variables of chemical potential, volume and temperature) rather than N, V, T (the number of molecules, volume and temperature), so that μ is an independent variable. For this reason grand canonical Monte Carlo (GCMC) molecular simulation has been favoured by most investigators.

Molecular dynamics (MD)

By the application of Newton's equations of motion, the trajectories and velocities of the molecular motion can be obtained. Averaging over time then gives the properties of the system. Since it is possible to simulate a few nanoseconds of real time, transport properties can be evaluated as well as equilibrium states. MD is more difficult to program than MC, but the molecular motions are more realistic and therefore computer graphics can be used to give a more accurate impression of the actual movement of molecules moving through or into pores.

1.9.3. Density functional theory (DFT)

As a means of establishing the density profile, $\rho(r)$, two free energy functionals are introduced: $\Omega[\rho(r)]$ and $F[\rho(r)]$. Ω is a form of thermodynamic potential and is generally known as the grand potential, or grand free energy. In general, for a system

containing a mixture of components, which is characterized by the grand canonical variables T, V, μ_a, ..., μ_i, we may write

$$\Omega = F - \sum \mu_i N_i \tag{1.10}$$

where F is the Helmholtz free energy (see Chapter 2) and N_i is the number of molecules of component i. For a single-component fluid in the presence of a spatially varying external potential $V_{ext}(r)$, the grand potential functional can be expressed in the form

$$\Omega[\rho(r)] = F[\rho(r)] - \int dr\, \rho(r)[\mu - V_{ext}(r)], \tag{1.11}$$

where ρ is the local fluid density at position r and the integration is performed over the pore volume.

The Helmholtz energy F represents the intrinsic free energy in the absence of any external field, whereas Ω is dependent on all the interactions within the pore together with a surface contribution. When Ω is allowed to vary in response to a change in $\rho(r)$, its overall minimum corresponds to the equilibrium density profile of the system. The equilibrium density profile is therefore determined by minimizing the grand potential functional with respect to $\rho(r)$. Since $\rho(r)$ is the local density, the amount adsorbed (usually expressed as the surface excess number of molecules adsorbed) must be obtained by integration over the internal volume of the pore. By repeating this procedure for different values of μ (and hence values of p/p°) it is possible to construct the adsorption isotherm.

The value of DFT is evidently dependent on the accessibility and accuracy of the grand potential functional, Ω [$\rho(r)$]. The usual practice is to treat the molecules as hard spheres and divide the fluid–fluid potential into attractive and repulsive parts. A mean field approximation is used to simplify the former by the elimination of correlation effects. The hard sphere term is further divided into an ideal gas component and an excess component (Lastoskie *et al.*, 1993). The ideal component is considered to be exactly local, since this part of the Helmholtz free energy per molecule depends only on the density at a particular value of r.

The evaluation of the excess free energy is a more difficult problem. This is because in the inhomogeneous fluid the energy distribution is non-local, that is it depends on the correlations within the overall density profile. Various attempts have been made to overcome this difficulty by the introduction of weighting or smoothing functions (Gubbins, 1997). This approach has led to the development of the non-local density functional theory (NLDFT), which *inter alia* has been used for the derivation of the pore size distribution from adsorption isotherm data (see Chapter 7). The use of DFT and MC simulation for the study of micropore filling is also under active investigation (see Chapter 8).

With a number of fairly simple systems, excellent agreement has been obtained between the corresponding DFT-predicted and MC-generated isotherms, 2-D phase transitions and adsorption energies. These are encouraging results, but it must be kept in mind that the computational procedures are not entirely independent. As we have seen, they are dependent on the same model parameters of adsorbent structure and potential functions. At present, there are only a few porous adsorbents which have the

required degree of structural and chemical uniformity to allow rigorous comparisons to be made with experimental adsorption data. The development of a range of chemically pure materials with highly uniform pore structures is a major challenge for the future.

References

Allen T. (1990) Particle Size Measurement, Chapman & Hall, London.

Aranovich G.L. and Donohue, M. (1998) *J. Colloid Interface Sci.*, **200**, 273.

Atkinson D., Carrott P.J.M., Grillet Y., Rouquerol J. and Sing K.S.W. (1987) In: *Proc. Second International Conference on Fundamentals of Adsorption* (A.I. Liapis, ed.), Engineering Foundation and American Institute of Chemical Engineers, New York, p. 89.

Avgul N.N. and Kiselev A.V. (1965) In: *Chemistry and Physics of Carbon* (P.L. Walker, ed.), Marcel Dekker, New York, p. 1.

Avgul N.N. and Kiseler A.V. (1970) In: *Chemistry and Physics of Carbon*, vol. 5 (P.L. Walker, ed.), Marcel Dekker, New York, p. 1.

Barrer R.M. (1966) *J. Colloid Interface Sci.* **21**, 415.

Barrer R.M. (1978) *Zeolites and Clay Minerals as Sorbents and Molecular Sieves*, Academic Press, London.

Belyakova L.D., Kiselev A.V. and Soloyan G.A. (1970), Chromatographia, **3**, 254.

British Standards Institution (1958) British Standard 2955, BSI, London.

British Standards Institution (1992) British Standard 7591, Part 1, BSI, London.

Brunauer S. (1945) *The Adsorption of Gases and Vapours*, Oxford University Press, Oxford.

Brunauer S., Emmett P. H. and Teller E. (1938) *J. Am. Chem. Soc.*, **60**, 309.

Brunauer S., Deming L.S., Deming W.S. and Teller E. (1940) *J. Am. Chem. Soc.* **62**, 1723.

Cao X.L., Colenutt B.A. and Sing K.S.W. (1991) *J. Chromatogr.* **555**, 183.

Carrott P.J.M. and Sing K.S.W. (1986) *Chem. & Ind.* 360.

Carrott P.J.M. and Sing K.S.W. (1987), *J. Chromatogr.* **406**, 139.

Carrott P.J.M., Brotas de Carvalho M. and Sing K.S.W. (1989) *Adsorption Sci. Tech.* **6**, 93.

Cases J.M., Grillet Y., François M., Michot L., Villieras F. and Yvon J. (1991) In: *Characterization of Porous Solids II* (F. Rodriguez-Reinoso, J. Rouquerol, K.S.W. Sing and K.K. Unger, eds), Elsevier, Amsterdam, p. 591.

Cracknell R.F., Gubbins K.E., Maddox M. and Nicholson D. (1995) *Accounts Chem. Res.* **28**, 281.

Davis B.H. (1991) *Chemtech.* 18.

Deitz V. R. (1944) *Bibliography of Solid Adsorbents*, National Bureau of Standards, Washington DC.

de Saussure N.T. (1814) *Gilbert's Ann.* **47**, 113.

Dubinin M. M. (1960) *Chem. Rev.*, **60**, 235

Emmett P. H. and Brunauer S. (1934) *J. Am. Chem. Soc.* **56**, 35.

Emmett P. H. and Brunauer S. (1937) *J. Am. Chem. Soc.* **59**, 1553.

Everett D. H. (1972) *Pure Appl. Chem.*, **31**, 579.

Everett D. H. and Powl J.C. (1976) *J. Chem. Soc., Faraday Trans.* **I, 72**, 619.

Favre P.A. (1854) *C.R. Acad. Sci. Fr.*, **39** (16), 729.

Forrester S. D. and Giles C. H. (1971) *Chem. & Ind.*, 831.

Forrester S. D. and Giles C. H. (1972) *Chem. & Ind.*, 318.

Freundlich H. (1907) *Z. Phys. Chem.*, **57**, 385.

Furlong N.D., Rouquerol F., Rouquerol J. and Sing K.S.W. (1980) *J. Chem. Soc., Faraday Trans.* **I, 76**, 774.

Giles C.H. and Smith D. (1974) *J. Colloid Interface Sci.*, **47**, 3.

Gore G. (1894) *Phil. Mag.*, **37**, 306.

Gregg S.J. and Sing K.S.W. (1982) *Adsorption, Surface Area and Porosity*, Academic Press, London.

Grillet Y., Rouquerol F. and Rouquerol J. (1979) *J. Colloid Interface Sci.*, **70**, 239.

Grillet Y., Cases J.M., François M., Rouquerol J. and Poirier J.E. (1988) *Clays and Clay Minerals*, **36**, 233

Grillet Y., Rouquerol F. and Rouquerol J. (1989) *Thermochim. Acta*, **148**, 191.

Grillet Y., Llewellyn P.L.,Tosi-Pellenq N. and Rouquerol J. (1993) In: *Proc. Fourth International Conference on Fundamentals of Adsorption* (M. Suzuki, ed.), Kodansha, Tokyo, p. 235.
Gubbins K.E. (1997) In: *Physical Adsorption: Experiment, Theory and Applications* (J. Fraissard and W.C. Connor, eds), Kluwer, Dordrecht, p.65.
Gurvich L.G. (1915) *J. Russ. Phys. Chim.*, **47**, 805.
Haber J. (1991) *Pure Appl. Chem.*, **63**, 1227.
Kiselev A.V. (1965) *Disc. Faraday Soc.*, **40**, 205.
Kiselev A.V. (1967) *Adv. Chromatogr.*, **4**, 113.
Langmuir I. (1916) *J. Am. Chem. Soc.*, **38**, 2221.
Langmuir I. (1917) *J. Am. Chem. Soc.*, **39**, 1848.
Langmuir I. (1918) *J. Am. Chem. Soc.*, **40**, 1361.
Lastoskie C., Gubbins K.E. and Quirke N. (1993) *J. Phys. Chem.*, **97**, 4786.
Lennard-Jones J. E. (1932) *Trans. Faraday Soc.*, **28**, 333.
Llewellyn P.L., Coulomb J.P., Grillet Y., Patarin J., Lauter H., Reichert H. and Rouquerol J. (1993a) *Langmuir*, **9**, 1846.
Llewellyn P.L., Coulomb J.P., Grillet Y., Patarin J., André G. and Rouquerol J. (1993b) *Langmuir*, **9**, 1852.
London F. (1930) *Z. Phys.*, **63**, 245.
Mandelbrot B.B. (1975) *Les Objets Fractals: Forme, Hasard et Dimension*, Flammarion, Paris.
McBain J. W. (1909) *Phil. Mag.*, **18**, 916.
Nicholson D. (1996) *J. Chem. Soc., Faraday Trans.* **92**, 1.
Nicholson D. and Pellinq R.J.M. (1998) In: *Advances in Colloid and Interface Science*, vols 76 and 77 (A.V. Neimark, ed.), Elsevier, Amsterdam, pp. 76–77.
Overbeek J. Th. G. (1970) In: *Surface Area Determination* (D.H. Everett and R.H. Ottewill, eds), Butterworths, London, p. 3.
Polanyi M. (1914) *Verb. Deutsch Phys.* Ges., **16**, 1012.
Pouillet M.C.S. (1822) *Ann. Chim. Phys.*, **20**, 141.
Ravikovitch P., Haller G. and Neimark A.V. (1998) In: *Advances in Colloid and Interface Science*, vols 76 and 77 (A.V. Neimark, ed.) Elsevier, Amsterdam, p. 203.
Ricca, F., Pisani, C. and Garrone, E. (1971) In: *Adsorption–Desorption Phenomena*, Academic Press, London, p. 111.
Rideal E.K. (1932) In: *The Adsorption of Gases by Solids*, Disc. Faraday Society, London, p. 139.
Robens E. (1994) In: *Characterization of Porous Solids III* (J. Rouquerol, F. Rodriguez-Reinoso, K.S.W. Sing and K.K. Unger, eds), Elsevier, Amsterdam, p.109.
Robens E. and Krebs K.-F. (1991) In: *Characterization of Porous Solids II* (F. Rodriguez-Reinoso, J. Rouquerol, K. S. W. Sing and K. K. Unger, eds), Elsevier, Amsterdam, p. 133.
Rouquerol J. (1990) *Impact of Science on Society*, UNESCO, Paris, vol. 157, p. 5.
Rouquerol J., Rouquerol F., Pérès C., Grillet Y. and Boudellal M. (1979) In: *Characterization of Porous Solids* (S.J. Gregg, K.S.W. Sing and H.F. Stoeckli, eds.) Society of Chemical Industry, London, p. 107.
Rouquerol J., Rouquerol F. and Grillet Y. (1989) *Pure Appl. Chem.*, **61**, 1933.
Rouquerol J., Avnir D., Fairbridge C.W., Everett D.H., Haynes J.H., Pernicone N., Ramsay J.D.F., Sing K.S.W. and Unger K.K. (1994) *Pure Appl. Chem.*, **66**, 1739.
Sing K. S. W., Everett D.H., Haul R.A.W., Moscou L., Pierotti R.A., Rouquerol J. and Siemieniewska T. (1985) *Pure Appl. Chem.*, **57**, 603.
Steele W.A. (1996) *Langmuir*, **12**, 145.
Steele W.A. (1974) *The Interaction of Gases with Solid Surfaces*, Pergamon, Oxford.
Steele W.A. and Bojan M.J. (1989) *Pure Appl. Chem.*, **61**, 1927.
Steele W.A. and Bojan M.J. (1997) In: *Characterization of Porous Solids IV* (B. McEnaney, T.J. Mays, J. Rouquerol, F. Rodriguez-Reinoso, K.S.W. Sing and K.K. Unger, eds), Royal Society of Chemistry, London, p. 49.
Steele W.A. and Bojan, M.J. (1998) In: *Advances in Colloid and Interface Science*, vols 76 and 77. (A.V., Neimark, ed.) Elsevier, Amsterdam, p. 153.
Taylor H. S. (1932) In: *The Adsorption of Gases by Solids*, Disc. Faraday Society, London, p. 131.
Thomson W.T. (Lord Kelvin) (1871) *Phil. Mag.*, **42** (4), 448.
Zsigmondy A. (1911) *Z. Anorg. Chem.*, **71**, 356.

CHAPTER 2

Thermodynamics of Adsorption at the Gas–Solid Interface

2.1. Introduction

The major advances in the application of classical thermodynamics to gas adsorption were made many years ago. In particular, the work of Guggenheim (1933, 1940), Hill (1947–1952), Defay and Prigogine (1951) and Everett (1950, 1972) led to a greatly improved understanding of the fundamental principles involved in the application of

thermodynamics to various adsorption systems (see also Young and Crowell, 1962; Ross and Olivier, 1964; Letoquart *et al.*, 1973; Myers, 1987; Kadlec, 1989).

The aim of this chapter is simply to introduce a selection of the most appropriate thermodynamic quantities for the processing and interpretation of adsorption isotherm and calorimetric data, which are obtained by the methods described in Chapter 3. We do not consider here the thermodynamic implications of capillary condensation, since these are dealt with in Chapter 7. Special attention is given to the terminology and the definition of certain key thermodynamic quantities, for example, the difference between corresponding molar integral quantities and differential quantities.

In order to facilitate this operational approach, we adopt the following conventions and simplifying assumptions:

(a) We consider only the case of a single gas adsorbed on a solid adsorbent.
(b) The adsorbent is assumed to remain inert and therefore to undergo no change in its surface area, internal energy or entropy at any stage of physisorption.
(c) By making use of the 'Gibbs dividing surface' we define the associated 'surface excess' properties, which are directly assessed from experimental measurements, without making any assumptions concerning the state, location or thickness of the adsorbed layer.
(d) Since the role of the adsorbent is only to provide an adsorption potential, we may picture the adsorption as a transition from a single 3-D gas phase to a 2-D adsorbed film. However, the latter may consist of more than one 2-D phase. At equilibrium, the chemical potential of the adsorptive is the same in all phases and therefore two independent variables are sufficient to characterize each phase.
(e) To process the information provided by the adsorption isotherm data, we shall adopt the Helmholtz energy ($=U - TS$) as the primary thermodynamic potential since this is most suitable for experiments carried out at constant temperature and surface area.
(f) To derive an equation of state for the adsorbate, it is necessary to select an additional intensive variable. For this purpose, it is convenient to define the spreading pressure (i.e. the decrease in surface tension), which may be regarded as a form of '2-D pressure'. The use of the two intensive variables (gas pressure and spreading pressure) also allows us to obtain the integral molar quantities, which are required to compare experimental data with statistical thermodynamic models.
(g) We follow the IUPAC recommendations: see Mills *et al.* (1993) and also Everett (1972) who *inter alia* discourage the use of the imprecise term 'heat of adsorption'.

2.2. Quantitative Expression of Adsorption

Without any independent information concerning the structure of the adsorbed layer, we might suppose that the local concentration, c ($=\mathrm{d}n/\mathrm{d}V$), of the adsorbable component decreases progressively with increased distance, z, from the adsorbent

surface; at distance $z = t$, this concentration reaches the constant value of the gas phase c^g. This form of hypothetical variation of local concentration is shown schematically in Figure 2.1a, where we also identify three zones (I, II and III).

We shall assume that there is no penetration of gas into the solid (i.e. no *absorption*) so that zone I is occupied solely by the adsorbent and therefore $c^s = 0$. In zone III, the adsorbable gas is at sufficient distance from the solid surface to have a uniform concentration, c^g, and here $z > t$. In this region the concentration is dependent only on the equilibrium pressure and temperature. In Figure 2.1a, zone II is the 'adsorbed layer', which is an intermediate region confined within the limits $z = 0$ and $z = t$. Here, the local concentration, c, is higher than the concentration of the gas in zone III and is dependent on z.

It follows from this simple picture that the volume, V^a, of the adsorbed layer can be expressed as the product of the interfacial area, A, and the thickness, t. Thus

$$V^a = At \tag{2.1}$$

We may define the amount adsorbed, n^a, of the substance in the adsorbed layer as

$$n^a = \int_0^{V^a} c \, dV$$

$$= A \int_0^t c \, dz \tag{2.2}$$

In Figure 2.1a, n^a is equivalent to the hatched area (d + e).

The total amount, n, of the adsorbable substance in the whole system can be divided into two parts, the amount adsorbed and the amount remaining in the gas phase:

$$n = A \int_0^t c \, dz + c^g V^g$$

where the volume occupied by the gas at the concentration c^g is V^g, therefore:

$$n^a = n - c^g V^g \tag{2.3}$$

It is evident that the exact evaluation of n^a requires a knowledge of either the exact value of V^g or of the variation of the local concentration, c, with respect to z. In practice, it is not easy to attain either of these requirements.

To overcome this problem, Gibbs (1877) proposed an alternative approach. This makes use of the concept of 'surface excess' to quantify the amount adsorbed. Comparison is made with a reference system, which is divided into two zones (A, of volume $V^{s,\circ}$ and B, of volume $V^{g,\circ}$) by an imaginary surface – the *Gibbs dividing surface* (or GDS) – which is placed parallel to the adsorbent surface. The reference system occupies the same volume V as the real system, so that:

$$V = V^{s,\circ} + V^{g,\circ} = V^s + V^a + V^g \tag{2.4}$$

In the reference system the concentration of the gaseous adsorptive remains constant

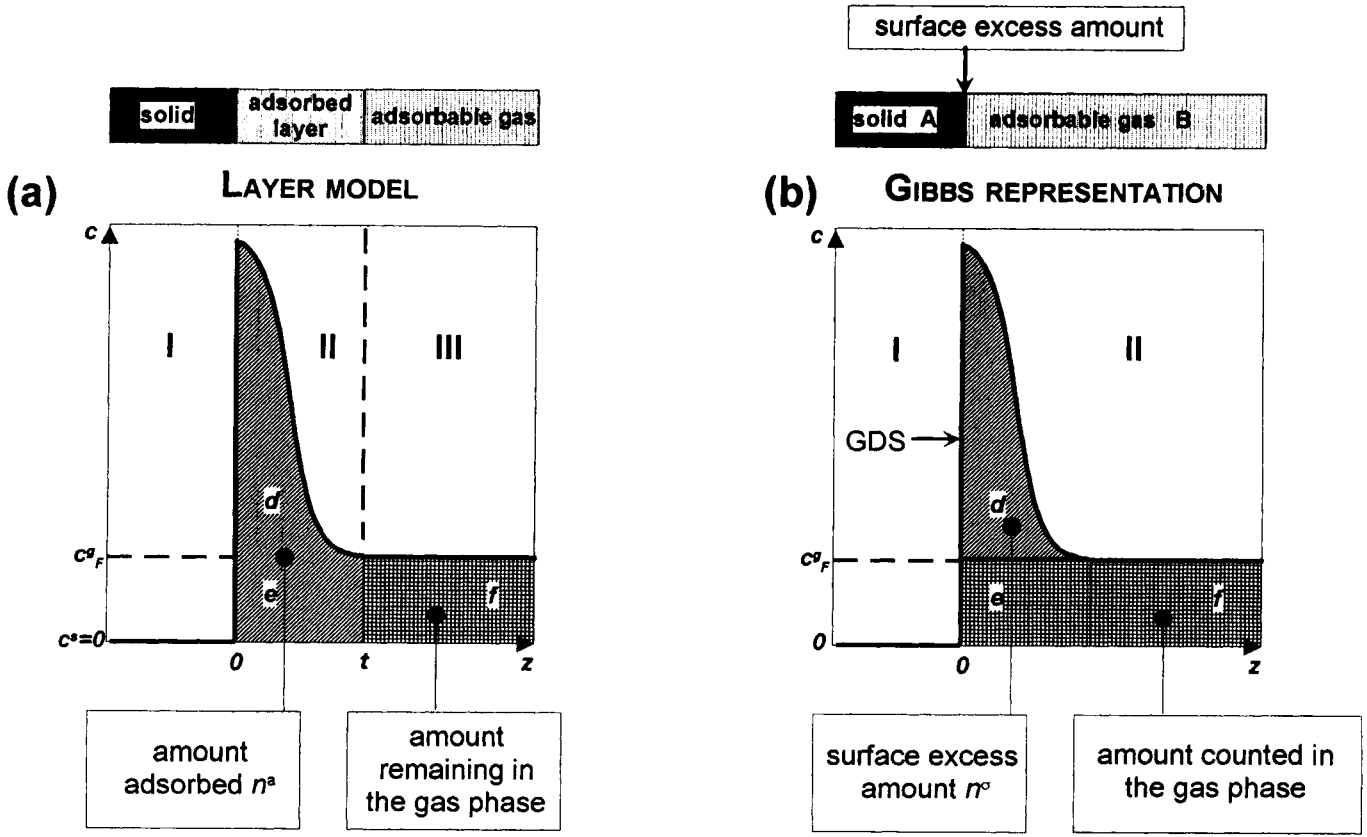

Figure 2.1. The Gibbs representation of the surface excess amount. c, local concentration dn/dV of adsorbable gas; z, distance from the surface.

in the volume $V^{g,\circ}$, i.e. up to the GDS. This is shown in pictorial form in Figure 2.1b. In this model, the *surface excess amount*, n^σ, represented by hatched area d, is defined as the difference between the total amount, n, of the adsorptive (hatched and crossed areas) and the amount which would be present in the volume $V^{g,\circ}$ of the reference system if the final equilibrium concentration c^g were constant up to the GDS (crossed area e + f). Thus:

$$n^\sigma = n - c^g V^{g,\circ}$$

It is convenient (although, in principle, not compulsory), for the sake of the physical interpretation of the data, to locate the GDS exactly on the surface which is accessible to the adsorptive used, so that $V^{g,\circ} = V^a + V^g$. This is what was actually done in Figure 2.1b. The experimental determination of $V^{g,\circ}$ in order to meet the above requirement is examined in Section 3.4.1.

Under these conditions:

$$n^\sigma = n - c^g V^g - c^g V^a \tag{2.5}$$

Combining with Equation (2.3), one gets:

$$n^a = n^\sigma + c^g V^a \tag{2.6}$$

In Figure 2.1b, the surface excess amount n^σ is represented by hatched area d; whereas the amount adsorbed n^a, which also includes term $c^g V^a$, is represented in Figure 2.1a by area (d + e).

Generally, the experimental conditions are such that the final concentration c^g of the gas is small and the volume V^a of the adsorbed layer is negligible in comparison with the gas volume V^g. Under these conditions

$$n^a \approx n^\sigma \tag{2.7}$$

However, at high temperature or pressure it may become necessary to make some allowance for the difference between these two quantities.

The amounts n^a and n^σ are extensive quantities, which depend on the extent of the interface. The related 'surface excess concentration', Γ, is an intensive quantity, which is defined as

$$\Gamma = n^\sigma / A \tag{2.8}$$

where the surface area, A, is associated with the mass m^s of the adsorbent. The specific surface area is therefore:

$$a = A/m^s \tag{2.9}$$

What is usually measured and recorded is the specific surface excess amount n^σ/m^s, where

$$n^\sigma/m^s = \Gamma a$$

As we have seen already, n^σ/m^s is dependent on the equilibrium pressure, p, and the adsorbent temperature, T. The usual practice is to maintain constant temperature

and then the relation

$$n^{\sigma}/m^{s} = f(p)_T \tag{2.10}$$

is the adsorption isotherm.

For the sake of simplicity in some later sections of this book, we adopt the *symbol* n to denote the *specific surface excess amount* n^{σ}/m^{s}. Also, for convenience, this quantity will be often referred to as *amount adsorbed.*

The Gibbs representation provides a simple, clear-cut mode of accounting for the transfer of adsorptive associated with the adsorption phenomenon. The same representation is used to define surface excess quantities assumed to be associated with the GDS for any other thermodynamic quantity related with adsorption. In this way, surface excess energy (U^{σ}), entropy (S^{σ}) and Helmholtz energy* (F^{σ}) are easily defined (Everett, 1972) as:

$$U^{\sigma} = U - U^{g} - U^{s} \tag{2.11}$$

$$H^{\sigma} = H - H^{g} - H^{s} \tag{2.12}$$

$$S^{\sigma} = S - S^{g} - S^{s} \tag{2.13}$$

$$F^{\sigma} = F - F^{g} - F^{s} \tag{2.14}$$

where U, H, S and F refer to the whole adsorption system at equilibrium (of total volume V and of total solid–gas interface area A), U^{s}, H^{s}, S^{s} and F^{s} refer to the solid adsorbent (zone I in Figure 2.1b), U^{g}, H^{g}, S^{g} and F^{g} refer to the gaseous adsorptive. Since the Gibbs representation is used in all the following sections of this chapter the superscripts g,o and s,o are replaced by g and s, thus V^{g} replaces $V^{g,o}$.

For the sake of completeness, U^{σ} and H^{σ} are separately defined above. Actually, when the enthalpy is defined in the standard way ($H = U + pV$), the Gibbs representation results in a useful simplification since the surface excess volume $V^{\sigma} = 0$ and we can write $H^{\sigma} = U^{\sigma}$ (as in Sections 2.4.2 and 2.5.1).

2.3. Thermodynamic Potentials of Adsorption

The simplest gas–solid adsorption system consists of a mass m^{s} of solid adsorbent, of surface area A, and an amount n of a single adsorbable gas contained in volume V at temperature T.

When the adsorptive gas is brought into contact with the clean adsorbent, part of it leaves the gas phase and becomes adsorbed (i.e. $dn^{\sigma} > 0$). If the adsorption takes place at constant T, V, A and n, the Helmholtz energy $F_{T,V,A,n}$ is the thermodynamic potential of the adsorption system since this potential attains the minimum value at equilibrium:

$$\left(\frac{\partial F}{\partial n^{\sigma}}\right)_{T,V,A,n} = 0 \tag{2.15}$$

* Traditionally called *énergie libre* in French. Note that by adopting the symbol F we avoid confusion with the area A.

At equilibrium the surface excess amount is $n^\sigma = n - n^g$, where n^g is the amount of adsorptive in the gas phase, up to the GDS.

From Equations (2.14) and (2.15), we arrive at the general condition of equilibrium:

$$\left(\frac{\partial F}{\partial n^\sigma}\right)_{T,V,A,n} = \left(\frac{\partial F^\sigma}{\partial n^\sigma}\right)_{T,A} + \left(\frac{\partial F^g}{\partial n^\sigma}\right)_{T,V} + \left(\frac{\partial F^s}{\partial n^\sigma}\right)_{T,A} = 0 \tag{2.16}$$

which applies to a system in which the adsorptive is distributed between the adsorbed phase, at the surface excess concentration $\Gamma = n^\sigma/A$, and the gas phase, at the concentration $c^g = n^g/V^g$.

It is usually assumed that the properties of the bulk of the adsorbent are not affected by physisorption and therefore that its internal energy and its entropy do not change on adsorption, so that:

$$\left(\frac{\partial F^s}{\partial n^\sigma}\right)_{T,A} = 0 \tag{2.17}$$

However, this is not always true. Complications arise, for example, if the adsorbent undergoes some form of elastic deformation or if the pore structure is modified as a result of the adsorption process. We adopt this convention in order to simplify the thermodynamic treatment. Similarly, we assume that the area of the Gibbs dividing surface is equal to the constant surface area of the adsorbent. We must not forget that we have made these simplifying assumptions when we come to interpret experimental data – especially if there is any indication of low pressure hysteresis.

With the assumption of an inert adsorbent, we may consider the physisorption process as a simple phase change of the adsorptive from the gaseous state to an adsorbed state on the surface A of the adsorbent. Since for a closed adsorption system at equilibrium $dn = dn^\sigma + dn^g = 0$, we may express the condition of equilibrium in the form

$$\left(\frac{\partial F^\sigma}{\partial n^\sigma}\right)_{T,A} = -\left(\frac{\partial F^g}{\partial n^\sigma}\right)_{T,V} = +\left(\frac{\partial F^g}{\partial n^g}\right)_{T,V} \tag{2.18}$$

The term $(\partial F^g/\partial n^g)_{T,V}$ is the chemical potential of the gas, μ^g. Similarly, for the equilibrium state of the adsorbed phase, which is characterized by the variables A and T, we may define a surface excess chemical potential by the relation

$$\mu^\sigma = \left(\frac{\partial F^\sigma}{\partial n^\sigma}\right)_{T,A} \tag{2.19}$$

Then using Equations (2.18) and (2.19) we can write:

$$\mu^\sigma = \mu^g \tag{2.20}$$

Thus, for each equilibrium state, the chemical potential of the adsorbate is equal to that of the adsorptive in the gas phase. In the case of a single adsorptive, the adsorbed state may be regarded as a one-component phase, which has lost one degree of freedom. Equation (2.18) indicates that it is sufficient to specify two of the variables

which characterize the gaseous adsorptive in order to define the adsorbed state for a particular adsorption system.

In the measurement of the adsorption isotherm, $\Gamma = f(p)_{T,A}$, the variables T and A are held constant. If we wish to obtain the analytical relation between Γ and p from Equation (2.20), then it is necessary to find another adsorption potential. For this purpose we must characterize the adsorbed phase by another intensive variable.

It is well known that the effect of surface tension is to minimize the area of a liquid surface. From a thermodynamic standpoint, the notion of surface tension can also be applied to a solid surface, although its physical significance is more difficult to explain. For our present purpose, we may adopt an analogous definition of the surface tension of a clean solid adsorbent to that for a clean liquid surface. Thus,

$$\left(\frac{\partial F^{s}}{\partial A}\right)_{T,V^{s}} = \gamma_T^{s} \tag{2.21}$$

which relates the Helmholtz energy F^s of the solid adsorbent to its surface area A, γ_T^s being the surface tension of the clean solid at the temperature T.

Furthermore, as with a liquid, the surface tension of the adsorbent is reduced as a result of physisorption (Hill, 1968). This lowering of the surface tension is called the *spreading pressure* and denoted by Π so that:

$$\Pi = \gamma^{s} - \gamma \tag{2.22}$$

The spreading pressure Π is an intensive variable which characterizes the adsorbed phase at the given surface excess concentration $\Gamma\,(=n^{\sigma}/A)$.

Introduction of the surface tension γ and surface area A in the expressions for H, F and G simply leads to a set of Legendre transforms (Moore, 1972; Alberty and Silbey, 1992) (also known as generalized functions) $\hat{H}$, $\hat{F}$ and $\hat{G}$. Thus,

$$\hat{H} = H - \gamma A, \qquad \hat{F} = F - \gamma A, \qquad \hat{G} = G - \gamma A \tag{2.23}$$

We can now characterize the state of equilibrium of the complete adsorption system by its transformed Gibbs energy*, $\hat{G}$, defined as

$$\hat{G} = F + pV - \gamma A \tag{2.24}$$

For an adsorption process which would be carried out at constant T, p, γ and n, the transformed Gibbs energy $\hat{G}_{T,p,\gamma,n}$ would be the thermodynamic potential of adsorption which would attain the minimum value at equilibrium:

$$\left(\frac{\partial \hat{G}}{\partial n^{\sigma}}\right)_{T,p,\gamma,n} = 0 \tag{2.25}$$

We may define the *transformed surface excess Gibbs energy* by the relation

$$\hat{G}^{\sigma} = \hat{G} - G^{g} - \hat{G}^{s} \tag{2.26}$$

where $G^g(=n^g\mu^g)$ is the Gibbs energy of the adsorptive remaining in the gaseous state

* Gibbs energy is traditionally called *enthalpie libre* in French.

(characterized by T and p), and $\hat{G}^s$ is the transformed Gibbs energy of the solid adsorbent (characterized by T and γ^s), defined as:

$$\hat{G}^s = F^s + pV^s - \gamma^s A \tag{2.27}$$

In the case of an inert solid, V^s remains constant and therefore the only variation in volume is that of the gaseous phase, V^g.

From Equations (2.23)–(2.27) and taking into account that in the simplified Gibbs approach the excess volume equals zero, we obtain the relation between $\hat{G}^\sigma$ and F^σ:

$$\hat{G}^\sigma = F^\sigma + \Pi A = n^\sigma \mu^\sigma \tag{2.28}$$

which becomes $\hat{G}^\sigma = \hat{H}^\sigma - TS^\sigma$ if we define a transformed surface excess enthalpy $\hat{H}^\sigma$ as:

$$\hat{H}^\sigma = U^\sigma + \Pi A \tag{2.29}$$

We have seen that, for each equilibrium state, the adsorptive has the same chemical potential in the gas phase and in the adsorbed phase, and that, for a given system, only two variables are required to provide a thermodynamic description of each of these phases. Consequently, there is a relation between the two intensive variables Π and p.

Let us suppose that under conditions of equilibrium a reversible change is made in the gas pressure and surface excess concentration of $\mathrm{d}p$ and $\mathrm{d}\Gamma$, respectively, and that the corresponding change in the spreading pressure is $\mathrm{d}\Pi$. Since the chemical potential must change by the same amount throughout the system, we may write:

$$\left(\frac{\partial \mu^\sigma}{\partial \Pi}\right)_{T,A} \mathrm{d}\Pi = \left(\frac{\partial \mu^g}{\partial p}\right)_{T,V} \mathrm{d}p \tag{2.30}$$

Furthermore, we may express the change in the chemical potential with the spreading pressure in the form of a generalized Gibbs–Duhem type equation:

$$\mathrm{d}\mu^\sigma = -\frac{S^\sigma}{n^\sigma}\mathrm{d}T + \frac{A}{n^\sigma}\mathrm{d}\Pi \tag{2.31}$$

Equation (2.31) is analogous to that obtained for a pure gas:

$$\mathrm{d}\mu^g = -\frac{S^g}{n^g}\mathrm{d}T + \frac{V^g}{n^g}\mathrm{d}p \tag{2.32}$$

By combining Equations (2.30), (2.31) and (2.32) we derive, at constant temperature T, the following relation between p and Π :

$$\frac{1}{\Gamma}\mathrm{d}\Pi = v^g \mathrm{d}p \tag{2.33}$$

where $1/\Gamma$ is the reciprocal of the surface excess concentration and v^g is the gaseous molar volume.

The value of the spreading pressure Π, at any value of Γ, may be calculated by integration of Equation (2.33) between $p = 0$ and p, and correspondingly $\Pi = 0$ and Π, after replacing v^g by RT/p (assuming the gas to be ideal), so that:

$$\Pi = RT \int_0^p \frac{\Gamma}{p} \mathrm{d}p \tag{2.34}$$

Equation (2.34) is often referred to as the *Gibbs adsorption equation* where the interdependence of Γ and p is given by the adsorption isotherm. The Gibbs adsorption equation is a surface equation of state which indicates that, for any equilibrium pressure and temperature, the spreading pressure Π is dependent on the surface excess concentration Γ. The value of spreading pressure, for any surface excess concentration, may be calculated from the adsorption isotherm drawn with the coordinates $\boldsymbol{n}/p$ and p, by integration between the initial state ($\boldsymbol{n} = 0$, $p = 0$) and an equilibrium state represented by one point on the isotherm.

A mathematical difficulty arises in the evaluation of the integral in the region below the first experimental point ($p = p_1$). First, the exact form of the adsorption isotherm is unknown in this range and secondly the ratio $\boldsymbol{n}/p$ is indeterminate as p tends to zero. A possible solution is to assume a linear variation of $\boldsymbol{n}$ versus p (i.e. Henry's law, as explained in Chapter 4) and then

$$\int_0^{p_1} \frac{\boldsymbol{n}}{p} \mathrm{d}p = kp_1 = (\boldsymbol{n})_{p_1}$$

The assumption of linearity can be verified most easily by plotting the isotherm in a semi-logarithmic form, i.e. $\boldsymbol{n}$ versus $\ln p$. An excessive curvature would indicate the need for another form of approximation.

For equilibrium pressures higher than p_1, for which surface excess concentration can be measured, the value of the integral term of Equation (2.34) is obtained by evaluation of the area under the curve $\boldsymbol{n}/p = \mathrm{f}(p)$, between pressures p_1 and p.

2.4. Thermodynamic Quantities Related to the Adsorbed States in the Gibbs Representation

By adopting the usual conventions of chemical thermodynamics, we are able to derive from the surface excess chemical potential μ^σ a number of useful surface excess quantities. Our purpose here is to draw attention to the difference between the molar and the differential surface excess quantities.

2.4.1. Definitions of the molar surface excess quantities

The surface excess chemical potential can be obtained by partial differentiation of $\hat{G}^\sigma$ (defined in Equation 2.28) with respect of the surface excess amount n^σ, with the

intensive variables T and Π remaining constant, so that:

$$\mu^{\sigma} = \left(\frac{\partial \hat{G}^{\sigma}}{\partial n^{\sigma}}\right)_{T,\Pi} \tag{2.35}$$

Alternatively, the chemical potential of the adsorbed phase is equal to the transformed Gibbs energy *divided* by the surface excess amount, i.e. the transformed *molar* surface excess Gibbs energy:

$$\mu^{\sigma} = \left(\frac{\partial \hat{G}^{\sigma}}{\partial n^{\sigma}}\right)_{T,\Pi} = \frac{\hat{G}^{\sigma}_{T,\Gamma}}{n^{\sigma}} \tag{2.36}$$

Similarly, for other surface excess thermodynamic quantities, the corresponding molar quantities are as follows:

- the molar surface excess internal energy, $u^{\sigma}_{T,\Gamma} = \dfrac{U^{\sigma}_{T,\Gamma}}{n^{\sigma}}$ (2.37)
- the molar surface excess entropy, $s^{\sigma}_{T,\Gamma} = \dfrac{S^{\sigma}_{T,\Gamma}}{n^{\sigma}}$ (2.38)
- the molar surface excess Helmholtz energy, $f^{\sigma}_{T,\Gamma} = \dfrac{F^{\sigma}_{T,\Gamma}}{n^{\sigma}}$ (2.39)
- the transformed molar surface excess enthalpy, $\hat{h}^{\sigma}_{T,\Gamma} = u^{\sigma}_{T,\Gamma} + \dfrac{\Pi}{\Gamma}$ (2.40)

By combining Equations (2.36)–(2.40) we obtain:

$$\mu^{\sigma}_{T,\Gamma} = u^{\sigma}_{T,\Gamma} + \frac{\Pi}{\Gamma} - T s^{\sigma}_{T,\Gamma} \tag{2.41}$$

2.4.2. Definitions of the differential surface excess quantities

We now return to the definition of the surface excess chemical potential μ^{σ} given by Equation (2.19) where the partial differentiation of the surface excess Helmholtz energy, F^{σ}, with respect to the surface excess amount, n^{σ}, is carried out so that the variables T and A remain constant. This partial derivative is generally referred to as a *differential quantity* (Hill, 1949; Everett, 1950). Also, for any surface excess thermodynamic quantity X^{σ}, there is a corresponding differential surface excess quantity $\dot{x}^{\sigma}$. (According to the mathematical convention, the upper point is used to indicate that we are taking the derivative.) So we may write:

- the differential surface excess internal energy, $\dot{u}^{\sigma}_{T,\Gamma} = \left(\dfrac{\partial U^{\sigma}}{\partial n^{\sigma}}\right)_{T,A}$ (2.42)
- the differential surface excess entropy, $\dot{s}^{\sigma}_{T,\Gamma} = \left(\dfrac{\partial S^{\sigma}}{\partial n^{\sigma}}\right)_{T,A}$ (2.43)

By combining Equations (2.19) and (2.42)–(2.43) we obtain:

$$\mu^{\sigma}_{T,\Gamma} = \dot{u}^{\sigma}_{T,\Gamma} - T\dot{s}^{\sigma}_{T,\Gamma} \tag{2.44}$$

and the transformed differential surface excess enthalpy may be written:

$$\hat{h}^{\sigma}_{T,\Gamma} = \dot{u}^{\sigma}_{T,\Gamma} + A\left(\frac{\partial \Pi}{\partial n^{\sigma}}\right)_{T,A} \tag{2.45}$$

Note that since the surface excess enthalpy, H^{σ}, is defined as $U^{\sigma} + pV^{\sigma}$, $H^{\sigma} = U^{\sigma}$. Similarly, the differential surface excess enthalpy, $\dot{h}^{\sigma}$, equals the differential surface excess internal energy, $\dot{u}^{\sigma}$.

It is of importance to both experimentalists and theoreticians that the differential and the integral molar excess quantities should not be confused.

2.5. Thermodynamic Quantities Related to the Adsorption Process

If the adsorption isotherm is entirely reversible (i.e. the adsorption and desorption paths coincide), we can assume that thermodynamic equilibrium has been established and maintained over the complete range of p/p°. It is then possible to obtain useful thermodynamic quantities from the adsorption isotherm, by applying Equation (2.20), since each point on the isotherm represents a particular adsorbed state defined by one value of Γ (or $\boldsymbol{n}$) and one value of the equilibrium pressure p (at temperature T).

Since adsorption is carried out experimentally when the variables T, V and A are held constant, it is logical to use the differential quantities introduced in Equations (2.19), (2.42) and (2.43). So, taking the differential surface excess Helmholtz energy as the surface excess chemical potential, and assuming the gas to be ideal, Equation (2.20) may now be written as:

$$\dot{u}^{\sigma}_{T,\Gamma} - T\dot{s}^{\sigma}_{T,\Gamma} = u^{g}_{T} + RT - Ts^{g}_{T,p} \tag{2.46}$$

where u^{g}_{T} is the molar internal energy of the ideal gaseous adsorptive, which depends only on the temperature T, and $s^{g}_{T,p}$ is the molar entropy of the ideal gaseous adsorptive, which depends on T and p. Thus

$$s^{g}_{T,p} = s^{g,\circ}_{T} - R\ln\left(\frac{p}{p^{\circ}}\right) \tag{2.47}$$

where $s^{g,\circ}_{T}$ is the molar standard entropy of the ideal gaseous adsorptive at temperature T and at the standard pressure $p^{\circ} = 10^{5}$ Pa.

By combining Equations (2.46) and (2.47) we obtain:

$$\ln\left(\frac{p}{p^{\circ}}\right) = \frac{\dot{u}^{\sigma}_{T,\Gamma} - u^{g}_{T} - RT}{RT} - \frac{\dot{s}^{\sigma}_{T,\Gamma} - s^{g,\circ}_{T}}{R} \tag{2.48}$$

2.5.1. Definitions of the differential quantities of adsorption

The 'differential quantities of adsorption', are the differences between the differential surface excess quantities and the same molar quantity, as in Equation (2.46) or (2.48).

The *differential energy of adsorption*, $\Delta_{\text{ads}}\dot{u}_{T,\Gamma}$, is thus

$$\Delta_{\text{ads}}\dot{u}_{T,\Gamma} = \dot{u}^{\sigma}_{T,\Gamma} - u^{\text{g}}_{T} \tag{2.49}$$

The differential energy of adsorption can also be regarded as the change of internal energy of the complete adsorption system, produced by the adsorption of an infinitesimal surface excess amount $\mathrm{d}n^{\sigma}$, when temperature, volume and surface area are held constant (and assuming the adsorbent to be inert and that its internal energy is not changed). Thus,

$$\Delta_{\text{ads}}\dot{u}_{T,\Gamma} = \left(\frac{\partial U}{\partial n^{\sigma}}\right)_{T,V,A} \tag{2.50}$$

In fact, the differential energy of adsorption may be obtained *directly* by the calorimetric measurement of the heat evolved by adsorption (see Sections 2.7 and 2.8).

We can define the *differential enthalpy of adsorption*, $\Delta_{\text{ads}}\dot{h}_{\text{T},\Gamma}$, as:

$$\Delta_{\text{ads}}\dot{h}_{T,\Gamma} = \dot{u}^{\sigma}_{T,\Gamma} - u^{\text{g}}_{T} - RT \tag{2.51}$$

The differential enthalpy of adsorption may be obtained *indirectly* by the isosteric method (cf. Section 2.6.1). In the past, it was often referred to as the 'isosteric heat' and denoted by $-q_{\text{st}}$. This term is now discouraged, and should be replaced by the *isosteric enthalpy of adsorption*. The differential energy and differential enthalpy of adsorption are related by the expression:

$$\Delta_{\text{ads}}\dot{h}_{T,\Gamma} = \Delta_{\text{ads}}\dot{u}_{T,\Gamma} - RT \tag{2.52}$$

To compare energies of adsorption for different adsorptives, it is convenient to evaluate the difference between the differential surface excess internal energy and the molar internal energy of the bulk adsorptive (liquid or solid) at the same temperature: that is the difference between the differential energy of adsorption and the molar energy of condensation of the liquid ($\Delta_{\text{liq}}u_T$) or of the solid, ($\Delta_{\text{sol}}u_T$). Lamb and Coolidge (1920) introduced the term 'net heat of adsorption', which was adopted by Brunauer, Emmett and Teller (1938) (see also Brunauer, 1945), and has been used by many other authors. However, since the original term is somewhat ambiguous, we recommend that it should be replaced by the 'net molar energy of adsorption'.

We have already seen that the differential surface excess energy is equal to the differential surface excess enthalpy; consequently, we can write:

$$\dot{u}^{\sigma}_{T,\Gamma} - u^{\text{l}}_{T} = \Delta_{\text{ads}}\dot{h}_{T} - \Delta_{\text{liq}}h_{T} \tag{2.53}$$

This difference is the 'net differential enthalpy of adsorption' and could also be called the 'net isosteric enthalpy of adsorption'.

The *differential entropy of adsorption*, $\Delta_{\text{ads}}\dot{s}_{T,\Gamma}$, is:

$$\Delta_{\text{ads}}\dot{s}_{T,\Gamma} = \dot{s}^{\sigma}_{T,\Gamma} - s^{\text{g}}_{T,p} \tag{2.54}$$

The *differential standard entropy of adsorption*, $\Delta_{ads}\dot{s}^{\circ}_{T,\Gamma}$, is:

$$\Delta_{ads}\dot{s}^{\circ}_{T,\Gamma} = \dot{s}^{\sigma}_{T,\Gamma} - s^{g,\circ}_{T} \tag{2.55}$$

The differential entropy of adsorption can be readily calculated from the differential enthalpy of adsorption since from Equations (2.46), (2.51) and (2.54) we obtain:

$$\Delta_{ads}\dot{s}_{T,\Gamma} = \frac{\Delta_{ads}\dot{h}_{T,\Gamma}}{T} \tag{2.56}$$

It is important not to confuse the differential (or isosteric) enthalpy of adsorption with the *transformed differential enthalpy of adsorption* $\Delta_{ads}\hat{h}_{T,\Gamma}$, which is derived from Equation (2.45):

$$\Delta_{ads}\hat{h}_{T,\Gamma} = \dot{u}^{\sigma}_{T,\Gamma} + A\left(\frac{\partial \Pi}{\partial n^{\sigma}}\right)_{T,A} - u^{g} - RT \tag{2.57}$$

so that:

$$\Delta_{ads}\hat{h}_{T,\Gamma} = \Delta_{ads}\dot{h}_{T,\Gamma} + A\left(\frac{\partial \Pi}{\partial n^{\sigma}}\right)_{T,A} \tag{2.58}$$

2.5.2. Definitions of the integral molar quantities of adsorption

The difference between a molar surface excess thermodynamic quantity $x^{\sigma}_{T,\Gamma}$ and the corresponding molar quantity $x^{g}_{T,p}$ for the gaseous adsorptive at the same equilibrium T and p is usually called the *integral molar quantity of adsorption*, and is denoted $\Delta_{ads}x_{T,\Gamma}$:

$$\Delta_{ads}x_{T,\Gamma} = x^{\sigma}_{T,\Gamma} - x^{g}_{T,p}$$

We can thus define the *integral molar energy of adsorption*:

$$\Delta_{ads}u_{T,\Gamma} = u^{\sigma}_{T,\Gamma} - u^{g}_{T} \tag{2.59}$$

and the *integral molar entropy of adsorption*:

$$\Delta_{ads}s_{T,\Gamma} = s^{\sigma}_{T,\Gamma} - s^{g}_{T,p} \tag{2.60}$$

We may derive the relation between these integral molar quantities of adsorption from Equations (2.20) using the expression of surface excess chemical potential μ^{σ} given by Equation (2.41) and assuming the gas to be ideal:

$$u^{\sigma}_{T,\Gamma} + \frac{\Pi}{\Gamma} - Ts^{\sigma}_{T,\Gamma} = u^{g}_{T} + RT - Ts^{g}_{T,p} \tag{2.61}$$

Then, from Equation (2.40), the *transformed integral molar enthalpy of adsorption* is obtained:

$$\Delta_{ads}\hat{h}_{T,\Gamma} = u^{\sigma}_{T,\Gamma} + \frac{\Pi}{\Gamma} - u^{g}_{T} - RT \tag{2.62}$$

and therefore:

$$\Delta_{\text{ads}} s_{T,\Gamma} = \frac{\Delta_{\text{ads}} \hat{h}_{T,\Gamma}}{T} \tag{2.63}$$

The quantity $\Delta_{\text{ads}}\hat{h}$ was called the 'equilibrium heat of adsorption' by Hill (1949) and Everett (1950), but this is no longer appropriate.

Equation (2.63), which relates two integral molar quantities of adsorption, must not be confused with Equation (2.56), which relates two differential quantities of adsorption. Note that the differential enthalpy of adsorption is defined without reference to the spreading pressure, whereas this is necessary for the integral molar transformed enthalpy of adsorption in Equation (2.62). It is only in the exceptional case when the differential energy of adsorption does not vary with Γ (e.g. at low coverage on highly homogeneous surfaces) that the differential energy of adsorption equals the integral molar energy of adsorption.

2.5.3. Advantages and limitations of differential and integral molar quantities of adsorption

In any investigation of the energetics of adsorption, a choice has to be made of whether to determine the differential or the corresponding integral molar quantities of adsorption. The decision will affect all aspects of the work including the experimental procedure and the processing and interpretation of the data.

When the main purpose of the gas adsorption measurements is to characterize the adsorbent surface or its pore structure, the preferred approach must be to follow the change in the thermodynamic quantity (e.g. the adsorption energy) with the highest available resolution. This immediately leads to a preference for the differential option, simply because the integral molar quantity is equivalent to the *mean* value of the corresponding differential quantity taken up to a recorded amount adsorbed. Their relationship is indicated by the mathematical form of Equation (2.64), which is explained in the following section.

Numerous examples are given in later chapters of the application of microcalorimetric measurements. In this chapter it is sufficient to refer briefly in general terms to the advantages of studying the changes in differential energies or enthalpies of adsorption. Thus, high initial values of $\Delta_{\text{ads}}\dot{u}$ or $\Delta_{\text{ads}}\dot{h}$ are associated with the interaction of adsorptive molecules with highly active surface sites and/or their entry into narrow pores (i.e. ultramicropores). A fairly sharp decline in the differential quantity is indicative of pronounced energetic heterogeneity; whereas an increase is generally the result of adsorbate – adsorbate interaction, which in some cases can be related to 2-D phase changes. To satisfy the condition for adsorption on a uniform surface, such as the basal plane of pure graphite, one would normally expect that over an appreciable range of monolayer coverage the differential energy would either remain constant or gradually increase.

The integral molar quantities are of importance for modelling adsorption systems or in the statistical mechanical treatment of physisorption. For example, they are required for comparing the properties of the adsorbed phase with those of the bulk

gas or liquid. As originally pointed out by Hill (1951), the differential quantities are not sufficient to give a complete thermodynamic description of an adsorption system. To compare the experimental data with theoretical (e.g. statistical mechanical) values, it is necessary to evaluate integral molar adsorption energies and entropies.

Some experimental techniques are to be preferred for the accurate determination of integral quantities (e.g. from energy of immersion data or a calorimetric experiment in which the adsorptive is introduced in one step to give the required coverage), while others are more suitable for providing high-resolution differential quantities (e.g. a continuous manometric procedure). It is always preferable experimentally to determine the differential quantity directly, since its derivation from the integral molar quantity often results in the loss of information.

2.5.4. Evaluation of integral molar quantities of adsorption

The evaluation of an integral quantity of adsorption, $\Delta_{ads}X$, requires the integration of the corresponding differential quantity between $\Gamma = 0$ and the given surface excess concentration when the variables T, V and A are held constant. The thermodynamic quantity X characterizes the complete adsorption system and therefore the integral quantity of adsorption is strictly made up of the three contributions resulting from the changes in the properties of the adsorbed phase, the gaseous adsorptive and the adsorbent. As before, we shall assume the gas to be ideal and the adsorbent to be inert. In carrying out the required integration, we must be careful to specify which variables are held constant and must also define the limiting equilibrium states. In addition, we must keep in mind that we are dealing with a closed system $dn = 0 = dn^{\sigma} + dn^{g}$.

Integral molar energy of adsorption

Integration of the differential energy of adsorption is quite straightforward from Equation (2.50). Since the gas is ideal, its molar internal energy does not vary with pressure so that:

$$\Delta_{ads}u_{T,\Gamma} = \frac{1}{n^{\sigma}}\int_0^{n^{\sigma}} \Delta_{ads}\dot{u}_{T,\Gamma}\,dn^{\sigma} \tag{2.64}$$

The integral molar energy of adsorption is therefore obtained by integrating the differential energy of adsorption between the limits 0 and n^{σ}. It equals the mean of the differential energy of adsorption over the range of surface excess concentration from 0 to Γ.

Integral molar entropy of adsorption

The integration of the differential entropy of adsorption between 0 and Γ is conveniently carried out with the variables T, V and A held constant:

$$\int_0^{n^{\sigma}} (\Delta_{ads}\dot{s}_{T,\Gamma})\,dn^{\sigma} = \int_0^{n^{\sigma}} \left(\frac{\partial S^{\sigma}}{\partial n^{\sigma}}\right)_{T,A} dn^{\sigma} - \int_0^{n^{\sigma}} s^{g}_{T,p}\,dn^{\sigma} \tag{2.65}$$

To integrate the second term of the right-hand side of the Equation (2.65), it must be taken into account that the molar entropy of the gaseous adsorptive depends on the pressure which varies from 0 to p when n^σ varies from 0 to n^σ (cf. Equation 2.47). So integration by parts gives:

$$\int_0^{n^\sigma} s^g \, dn^\sigma = n^\sigma s^g - \int_0^{n^\sigma} n^\sigma \, ds^g = n^\sigma s^g + R \int_0^{n^\sigma} n^\sigma \, d \ln [p] \tag{2.66}$$

From Equations (2.56), (2.65) and (2.66) we obtain:

$$\Delta_{ads} s_{T,\Gamma} = \frac{1}{n^\sigma} \int_0^{n^\sigma} \frac{\Delta_{ads} \dot{h}}{T} \, dn^\sigma + \frac{R}{n^\sigma} \int_0^{n^\sigma} n^\sigma \, d \ln [p] \tag{2.67}$$

Comparison of Equations (2.61) and (2.67) shows that the second term of the right-hand side of Equation (2.67) is due to the spreading pressure, which is related to the interactions between adsorbed molecules, often referred to as the 'lateral interactions'. It is only at very low coverages, where the spreading pressure is negligible, that the integral molar entropy of adsorption is simply dependent on the adsorbate–adsorbent interaction.

In the general case, the integral molar entropy of adsorption is not equal to the mean differential entropy of adsorption over the range of surface excess concentration from 0 to Γ, because of the extra term of the right-hand side of Equation (2.67).

2.6. Indirect Derivation of the Quantities of Adsorption from a Series of Experimental Physisorption Isotherms: The Isosteric Method

2.6.1. Differential quantities of adsorption

To obtain differential enthalpies of adsorption from physisorption isothermal data, it is advisable to measure a series of adsorption isotherms at different temperatures (see Section 2.8.3).

If we differentiate Equation (2.48) with respect to the adsorption temperature, so that the surface excess concentration Γ (or $\boldsymbol{n}$) remains constant, and assume that $\Delta_{ads}\dot{h}_{T,\Gamma}$ and $\Delta_{ads}\dot{s}_{T,\Gamma}$ do not vary, we obtain:

$$\left(\frac{\partial}{\partial T} \ln [p] \right)_\Gamma = - \frac{\Delta_{ads} \dot{h}_{T,\Gamma}}{RT^2} \tag{2.68}$$

and therefore:

$$\Delta_{ads} \dot{h}_{T,\Gamma} = R \left(\frac{\partial \ln [p]}{\partial (1/T)} \right)_\Gamma$$

where $[p]$ is the numerical value of the equilibrium pressure corresponding to the surface excess concentration Γ (or $\boldsymbol{n}$).

It is evident that Equation (2.68) is analogous to the well-known Clausius–Clapeyron equation for a one component gas–liquid system. Integration of Equation (2.68) between the limits of equilibrium pressures and temperatures of p_1, p_2 and T_1, T_2 gives:

$$\Delta_{ads}\dot{h} = -\frac{RT_1T_2}{T_2 - T_1}\ln\frac{p_2}{p_1} \tag{2.69}$$

The usual method of calculating $\Delta_{ads}\dot{h}$ from a series of adsorption isotherms obtained at different temperatures is to plot $\ln [p]_\Gamma$ for a given Γ (or $\boldsymbol{n}$) as a function of $1/T$. This method of calculation of the differential enthalpy based on the use of Equations (2.68) and (2.69) is called the *isosteric method*. By applying Equation (2.68) at different values of Γ (or $\boldsymbol{n}$), we can determine the variation of $\Delta_{ads}\dot{h}$ with Γ.

We can verify with Equation (2.68) that $\Delta_{ads}\dot{h} < 0$ since, for physical adsorption, the equilibrium pressure necessary to obtain the surface excess concentration Γ (or $\boldsymbol{n}$) increases with the adsorption temperature. It follows that $\Delta_{ads}\dot{s}$ is necessarily negative. However, since the differential entropy of adsorption, at constant T, given by Equation (2.56) is directly proportional to the differential enthalpy of adsorption, its calculation is not of great value.

The differential standard entropy of adsorption $\Delta_{ads}\dot{s}^\circ_{T,\Gamma}$ may also be deduced from Equations (2.47), (2.55) and (2.56):

$$\Delta_{ads}\dot{s}^\circ_{T,\Gamma} = \Delta_{ads}\dot{h}_{T,\Gamma} - R\ln\frac{p}{p^\circ} \tag{2.70}$$

It will be seen in Section 2.8.3 that the isosteric procedure is not always reliable and should not be used at very low pressure unless the equilibrium pressures are measured with very high accuracy.

2.6.2. Integral molar quantities of adsorption

By making use of Equations (2.47) and (2.63) we can arrive at:

$$\ln\left(\frac{p}{p^\circ}\right) = \frac{\Delta_{ads}\hat{h}_{T,\Gamma}}{RT} - \frac{\Delta_{ads}s^\circ}{R} \tag{2.71}$$

If we differentiate Equation (2.71) with respect to the reciprocal of temperature $1/T$, so that the spreading pressure Π remains constant, we obtain:

$$\Delta_{ads}\hat{h}_{T,\Gamma} = R\left(\frac{\partial \ln(p)}{\partial(1/T)}\right)_\Pi \tag{2.72}$$

This equation, which gives the transformed integral molar enthalpy of adsorption for the adsorption equilibrium characterized by the variables T and Γ (or $\boldsymbol{n}$), must not be confused with Equation (2.68), which gives the differential enthalpy of adsorption. Indeed, by combining Equations (2.31), (2.44), (2.56) and (2.63) we obtain the

relation between these two enthalpies of adsorption:

$$\Delta_{ads}\hat{h} = \Delta_{ads}\dot{h} + \frac{T}{\Gamma}\left(\frac{\partial \Pi}{\partial T}\right)_{\Gamma} \tag{2.73}$$

Equation (2.72) is not easy to use in the general case in which the spreading pressure is unknown. But in the particular case of stepwise isotherms where there are two adsorbed phases in equilibrium with the gaseous adsorptive (i.e. in the case of a univariant adsorption system), Larher (1968, 1970) showed that the isosteric method may be used with the transition pressure p^n to give integral molar energies u^n and entropies s^n of the 'quasi-layer':

$$\ln\left(\frac{p^n}{p^\infty}\right) = \frac{u^n - u^\infty}{RT} - \frac{1}{R}(s^n - s^\infty) \tag{2.74}$$

Here the standard state is the bulk adsorptive (liquid or solid) characterized by its molar energy (u^∞) and entropy (s^∞) and the saturation pressure p^∞.

2.7. Derivation of the Adsorption Quantities from Calorimetric Data

Microcalorimeters are well suited for the determination of differential enthalpies of adsorption, as will be commented on in Sections 3.2.2 and 3.3.3. Nevertheless, one should appreciate that there is a big step between the measurement of a 'heat' of adsorption and the determination of a meaningful energy or enthalpy of adsorption. The measured heat depends on the experimental conditions (e.g. on the extent of reversibility of the process, the dead volume of the calorimetric cell and the isothermal or adiabatic operation of the calorimeter). It is therefore essential to devise the calorimetric experiment in such a way that it is the change of state which is assessed and not the mode of operation of the calorimeter.

We shall examine here the two major procedures for gas adsorption calorimetry (cf. Section 3.3.3). Both procedures make use of a diathermal, heat-flowmeter, Tian–Calvet microcalorimeter (cf. Section 3.2.2).

2.7.1. Discontinuous procedure

The most common calorimetric technique is the *discontinuous procedure* where the adsorptive is introduced in successive steps. The calorimetric cell with its contents (adsorbent and adsorptive) must be considered as an *open* system (cf. Figure 3.15). It is only when the adsorptive is introduced *reversibly* and when the *step is small enough* (so that the amount introduced can be written dn and the pressure increase dp) that the derivation of a differential energy of adsorption (as defined by Equations (2.49) and (2.50)) is possible. Under these conditions, and taking into account the internal energy contributed by the gaseous adsorptive, we can write:

$$dU = dQ_{rev} + dW_{rev} + u_T^g\, dn \tag{2.75}$$

where dQ_{rev} is the heat reversibly exchanged with the surroundings at temperature T, dW_{rev} is the reversible work of the gas against the external pressure, u_T^g is the molar internal energy of the adsorbable gas at temperature T, and dn is the amount of adsorbable gas introduced during a given step.

Rouquerol and Everett (Rouquerol *et al.*, 1980) have shown that the calculation of dW_{rev} is easily accomplished if one notionally splits the volume of the whole adsorption system into two parts, V_A (external to the calorimetric cell, but in contact with the thermostat) and V_C (located within the calorimetric cell, see Figure 3.15). If we assume a reversible compression of an ideal gas by reduction of volume V_A, the whole system exchanges work with the surroundings:

$$dW_{rev}(A + C) = RT\, dn^\sigma + (V_A + V_C)\, dp \tag{2.76}$$

where dn^σ is the amount adsorbed during the compression.

The work received by the calorimetric cell is only:

$$dW_{rev}(C) = RT\, dn^\sigma + V_C\, dp \tag{2.77}$$

By combining the above equations, we obtain:

$$d(n^g u^g + n^\sigma u^\sigma)_{T,V,A} = dQ_{rev} + RT\, dn^\sigma + V_C\, dp + u^g(dn^g + dn^\sigma) \tag{2.78}$$

or

$$\left(\frac{dQ_{rev}}{dn^\sigma}\right)_{T,A} + V_C\left(\frac{dp}{dn^\sigma}\right)_{T,A} = \left[\left(\frac{dU^\sigma}{dn^\sigma}\right)_{T,A} - u^g - RT\right] = \Delta_{ads}\dot{h}_{T,\Gamma} \tag{2.79}$$

which provides a means for the experimental assessment of the differential enthalpy adsorption, $\Delta_{ads}\dot{h}_{T,\Gamma}$.

One sees that the use of Equation (2.79) requires a knowledge of the following experimental quantities: dQ_{rev} (heat measured by the calorimeter), dn^σ (amount adsorbed), dp (increase in equilibrium pressure) and V_C (dead volume of the part of the cell immersed in the heat-flowmeter of the microcalorimeter; cf. Figure 3.15.). If the conditions of small and reversible introduction of adsorptive are not fulfilled, the quantity assessed by Equation (2.79) can be described as a 'pseudo-differential' enthalpy of adsorption (see Figure 3.16a).

2.7.2. Continuous procedure

In principle, the *continuous procedure*, where the adsorption takes place continuously and slowly, under quasi-equilibrium conditions, meets the above requirement of reversibility (Rouquerol *et al.* 1972). In this experiment, the basic experimental quantities from which one wishes to derive the differential enthalpy of adsorption are the rate of adsorption, f^σ, and the corresponding heat flow, ϕ.

When the rate of introduction of the adsorptive, $f = dn/dt$, is constant (cf. Section 3.3.2), the rate of adsorption, f^σ, is slightly different. Thus:

$$f^\sigma = \frac{dn^\sigma}{dt} = f - \frac{V_e}{RT_e}\frac{dp}{dt} - \frac{V_C}{RT_C}\frac{dp}{dt} \tag{2.80}$$

where V_e and T_e are the volume and temperature of the external manometric device.

The corresponding heat flow is:

$$\phi = \frac{dQ_{rev}}{dt} = \frac{dQ_{rev}}{dn^\sigma} \times \frac{dn^\sigma}{dt} = f^\sigma \times \left(\frac{dQ_{rev}}{dn^\sigma}\right)_{T,A} \tag{2.81}$$

By introducing Equation (2.81) into Equation (2.79), we obtain:

$$\Delta_{ads}\dot{h} = \left(\frac{dQ_{rev}}{dn^\sigma}\right)_{T,A} + V_C\left(\frac{dp}{dn^\sigma}\right)_{T,A} = \frac{\phi}{f^\sigma} + V_C \frac{dp}{dt}\frac{dt}{dn^\sigma}$$

$$\Delta_{ads}\dot{h} = \frac{1}{f^\sigma}\left(\phi + V_C \frac{dp}{dt}\right) \tag{2.82}$$

It is evident that a knowledge of f^σ (rate of adsorption) and ϕ (heat flow) is not enough to derive a continuous curve of differential enthalpy of adsorption. One must also know the dead volume V_C of the calorimetric cell proper and the derivative of the quasi-equilibrium pressure with time. Note that when this derivative is very small (i.e. in the nearly vertical parts of an adsorption isotherm), Equation 2.82 becomes simply:

$$\Delta_{ads}\dot{h} \approx \frac{\phi}{f} \tag{2.83}$$

and under these conditions $f^\sigma \approx f$. This means that if f is constant, the recording of heat flow ϕ versus time gives a direct measure of $\Delta_{ads}\dot{h}$ versus amount adsorbed.

2.8. Methods for the Determination of Differential Enthalpies of Adsorption

Our aim in this section is to outline the advantages and limitations of the main experimental procedures now available for the determination of the differential enthalpies of adsorption. Both thermodynamic and practical aspects are summarized here, but the latter are discussed in more detail in Chapters 3 and 5.

2.8.1. Gas adsorption calorimetry

The essential requirements for the application of this direct method are a sensitive microcalorimeter (preferably of the heat-flow type, as described in Section 3.2.2) combined with equipment for the determination of the amount adsorbed. Although the assemblage of the apparatus is somewhat demanding, once the effort has been made the advantages of calorimetry are as follows:

1. In contrast to the isosteric and chromatographic methods, the derivation of differential enthalpies does not involve any assumptions provided that the experiments are carried out sufficiently slowly to ensure equilibration in the adsorption and gas compression.

2. Accurate thermal data can be obtained, even at low pressures. This method is therefore recommended for studying the energetics of micropore filling or adsorption on high energy sites.
3. When used along with a continuous measurement of the isotherm, a continuous, high-resolution curve of $\Delta_{ads}\dot{h}$ versus n is obtained. This allows one to detect and characterize substeps associated with 2-D phase changes (Grillet *et al.*, 1979).

2.8.2. Immersion calorimetry

As described in Section 5.2.1, immersion calorimetry provides an indirect method for determining adsorption energies. The net molar integral energy of adsorption can be obtained from the energy of immersion of the dry solid, but the evaluation of differential energies is more difficult. In this case, a number of independent heat measurements must be made after the progressive pre-coverage of the adsorbent surface. This approach is therefore sample-consuming (since a fresh sample is required for each pre-coverage point) and time-consuming (the weighing, outgassing etc. may take a day for each point). Moreover, the method is limited to easily condensable adsorptives (mainly water and organic vapours). On the other hand, there are some practical advantages:

1. Provided that sufficient care is taken in the experimentation, the results are more accurate than can be obtained by the isosteric method, especially at low surface coverage (Harkins, 1952; Zettlemoyer and Narayan, 1967).
2. In some respects the technique is less demanding than gas adsorption calorimetry. For example, the calorimeter and pre-adsorption rig are separate and therefore easy to handle.
3. Condensable vapours pose problems with the other methods. Some of these difficulties (e.g. temperature gradients and spurious condensation) can be avoided by the measurement of energies of immersion.

2.8.3. The isosteric method

As explained in Section 2.6.1, the application of the isosteric method relies on the principles embodied in Equation (2.68). In practice, the isosteric procedure is applied to at least two isotherms at different temperatures, which must not be too far apart. A temperature range of, say, 10 K is often considered to be a good compromise. Whenever possible, more than two isotherms should be measured and the plot of $\ln [p]$ versus $1/T$ checked for linearity. As noted earlier, the isosteric method is very sensitive to any error in the measurement of the equilibrium pressure. Systematic comparisons between the values of differential enthalpy determined by the calorimetric and isosteric methods have revealed serious inaccuracies in the isosteric values at low pressures or low surface coverage (Rouquerol *et al.* 1972; Grillet *et al.*, 1976). It turns out that one must be particularly careful when applying the isosteric method at surface coverage <0.5. A further constraint is that for each constant n^{σ}, there should be no 2-D phase change over the temperature studied.

In spite of these limitations, two valuable features of the isosteric method should be recognized:

1. It is a simple and generally applicable procedure for the evaluation of differential enthalpies of adsorption.
2. The accuracy of the method improves as the pressure is increased; this is unlike calorimetry, which tends to become less accurate at higher pressures.

2.8.4. The chromatographic method

The gas chromatographic method is based on the relation between the differential enthalpy of adsorption at 'zero' coverage and the temperature dependence of the Henry's law constant, k_H, as expressed in the form of Equation (4.3). In the low-pressure region, where Henry's law applies, the specific retention volume, V_s, is a linear function of k_H (Purnell, 1962; Littlewood, 1970). This relationship makes it possible to make use of elution chromatography since

$$\Delta_{ads}\dot{h} = RT^2 \left[\partial(\ln V_s)/\partial T\right]_n \tag{2.84}$$

The successful application of the method is dependent on a number of requirements (Gravelle, 1978). The chromatographic column must be operating under almost ideal conditions to give sharp, symmetrical peaks and the carrier gas must not be adsorbed. Ideal gas behaviour is generally a good approximation, but if not then the non-ideality of the adsorptive vapour must be taken into account (Blu *et al.*, 1971).

The advantages of the method are as follows:

1. In principle, the differential enthalpy is determined at very low surface coverage.
2. Measurements are rapid and with standard commercial equipment the retention time measurements can be made over a wide range of temperature.
3. Adsorptives with low vapour pressures can be studied.

References

Alberty R.A. and Silbey R.J. (1992) In: *Physical Chemistry*, John Wiley, New York, p. 108.
Blu G., Jacob L. and Guiochon G. (1971) *J. Chromatogr.* **61**, 207.
Brunauer S. (1945) *The Adsorption of Gases and Vapors: Physical Adsorption*, Vol. I, Princeton University Press, Princeton.
Brunauer S., Emmett P.H. and Teller E. (1938) *J. Am. Chem. Soc.* **60**, 309.
Defay R. and Prigogine I. (1951) *Tension Superficielle et Adsorption*, Dunod, Paris.
Everett D.H. (1950) *Trans. Faraday. Soc.* **46**, 453, 942, 957.
Everett D.H. (1972) *Pure Appl. Chem.* **31**(4) 579.
Gibbs J.W. (1877), *Collected Works*, Longmans Green and Co., New York.
Gravelle P.C. (1978) *J. Thermal Anal.* **14**, 53.
Grillet Y., Rouquerol F. and Rouquerol J. (1976) *Revue Générale de Thermique* **171**, 237.
Grillet Y., Rouquerol F. and Rouquerol J. (1979) *J. Colloid Interface Sci.* **70**, 239.
Guggenheim E.A. (1933) *Modern Thermodynamics by the Methods of J.W. Gibbs*, Methuen, London.
Guggenheim E.A. (1940) *Trans. Faraday Soc.* **36**, 397.
Harkins W.D. (1952) *The Physical Chemistry of Surface Films*, Reinhold, New York, p. 268.
Hill T.L. (1947) *J. Chem. Phys.* **15**, 767.

Hill T.L. (1949) *J. Chem. Phys.* **17**, 507, 520.
Hill T.L. (1950) *J. Chem. Phys.* **18**, 246.
Hill T.L. (1951) *Trans. Faraday Soc.* **47**, 376.
Hill T.L. (1952) *Adv. Catalysis* **4**, 212.
Hill T.L. (1968) *Thermodynamics for Chemists and Biologists*, Addison-Wesley, Reading, MA.
Hill T.L., Emmett P.H. and Joyner L.J. (1951) *J. Am. Chem. Soc.* **73**, 5102.
Kadlec O. (1989) *Pure Appl. Chem.* **61**, 1867.
Lamb A.B. Coolidge A.S. (1920) *J. Am. Chem. Soc.* **42**, 1146.
Larher Y. (1968) *J. Chim. Phys. Fr.* 974.
Larher Y. (1970) PhD thesis, Paris.
Letoquart C., Rouquerol F. and Rouquerol J. (1973) *J. Chim. Phys. Fr.* **70**, (3), 559.
Littlewood A.B. (1970) *Gas Chromatography*, Academic Press, New York.
Mills I., Cvitas T., Homann K., Kallay N. and Kuchitsu K. (1993) *Quantities, Units and Symbols in Physical Chemistry*, 2nd edn, Blackwell Scientific, London.
Moore W.J. (1972) In: *Physical Chemistry*, 5th edn, Longman, London, p.96.
Myers A.L. (1987) In: *Fundamentals of Adsorption II* (A.I. Liapis, ed.) Engineering Foundation, New York, p. 3.
Purnell H. (1962) *Gas Chromatography*, Wiley, New York.
Ross S. and Olivier J.P. (1964) *On Physical Adsorption*, Interscience, New York.
Rouquerol F., Partyka S. and Rouquerol J. (1972) In: *Thermochimie*, Colloques Internationaux du CNRS, no. 201, Editions du CNRS, Paris, p. 547.
Rouquerol F., Rouquerol J. and Everett D.H. (1980) *Thermochim. Acta*, **41**, 311.
Young D.M. and Crowell A.D. (1962) *Physical Adsorption of Gases*, Butterworths, London.
Zettlemoyer, A.C. and Narayan K.S. (1967) In: *The Solid–Gas Interface* (E.A. Flood, ed.), Marcel Dekker, New York, p. 152.

CHAPTER 3

Methodology of Adsorption at the Gas–Solid Interface

3.1. Introduction

The aim of this chapter is to introduce the major experimental procedures for the determination of adsorption isotherms and energies of adsorption. These measurements provide the essential physisorption data, which are discussed in other chapters. Indeed, even if a research project is directed towards, say, a spectroscopy study of adsorption, one cannot avoid having recourse to adsorption isotherm data.

It is perhaps worth noting that when a quantity, other than the amount adsorbed, is plotted against the equilibrium pressure (or p/p°) this quantity should always be clearly defined (e.g. the differential or integral energy or a crystalline parameter of the adsorbent). In our opinion, it is important to reserve the expression 'adsorption isotherm' for the relation between the amount adsorbed and the equilibrium pressure, thereby emphasizing its basic character. Gas adsorption measurements are not difficult to accomplish, provided that care is taken in the choice of equipment and the design of the operational procedure. Before any measurements are undertaken, it is useful to pose the following questions:

(a) What is the purpose of the work?
(b) Which technique is most suitable for the particular gas–solid system and the required conditions (i.e. the temperature and range of pressure)?
(c) What operational procedure should be followed to obtain data with the desired accuracy and thermodynamic consistency?

Obviously, the choice of technique and experimental conditions will depend on whether the measurements are to be used for, say, the routine determination of surface area and pore size, or for fundamental research, or for the acquisition of chemical engineering data. However, if the results are to have any real scientific value it is essential that they are obtained under carefully controlled and well-defined conditions.

The three different physical properties which can be utilized for determining an adsorption isotherm are pressure, mass and gas flow. To evaluate the adsorption energy, it is also necessary to determine either a heat flow or a temperature change. These five basic parameters of adsorption methodology are discussed in Section 3.2.

Whichever property (i.e. pressure, mass or gas flow) is selected for the determination of the amount adsorbed, one must choose between the two experimental procedures

generally referred to as discontinuous or continuous techniques. The advantages and limitations of these alternative procedures are discussed in Section 3.3.

Finally, the many experimental details which are essential for the determination of a meaningful adsorption experiment are dealt with in Section 3.4.

3.2. Basic Aspects of Methodology

3.2.1. Determination of the amount adsorbed

Gas adsorption manometry

This method is based on the measurement of the gas pressure in a calibrated, constant volume, at a known temperature.

The expression 'volumetric determination', which is still employed by some investigators, dates from the time when adsorption measurements were made with a mercury burette and manometer (as in Figure 3.1). The technique for determining an

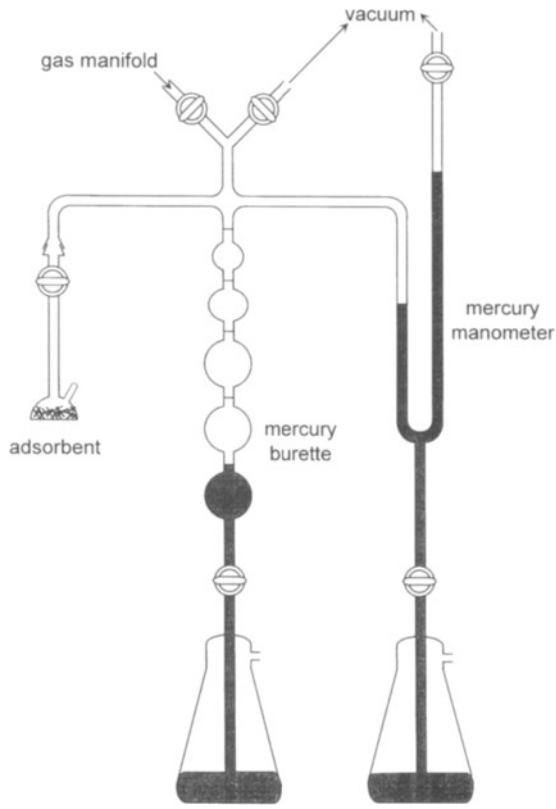

Figure 3.1. Original 'BET' apparatus (gas adsorption volumetry) (after Emmett, 1942).

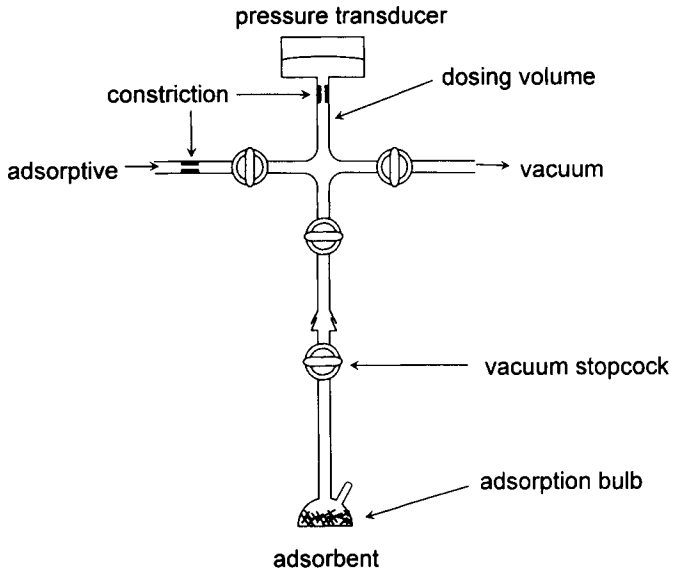

Figure 3.2. Simple gas adsorption manometry.

adsorption isotherm is often referred to as the 'BET volumetric method' since it was the type of measurement made originally by Emmett and Brunauer (1937) and described by Emmett (1942). Many physisorption isotherms are still presented as the volume of gas (STP) adsorbed versus the relative pressure. However, mercury burettes are no longer generally used and it is therefore becoming inappropriate to refer to a volumetric procedure when the amount adsorbed is evaluated by the change of gas pressure rather than volume.

Simple gas adsorption manometry. A simple modern set-up with three valves and a capacitance pressure transducer is shown in Figure 3.2. The 'dosing volume' is within the central cross, i.e. in the connecting tubes between the valves and the pressure transducer.

The technique of gas adsorption manometry is now probably the most widely used: it is simple and effective since the pressure transducer provides all the information required to determine the adsorption isotherm. Thus, the pressure and temperature of each dose of gas are measured and the gas is allowed to enter the adsorption bulb. After adsorption equilibrium has been established, the amount adsorbed is calculated from the change in pressure. The most critical features of adsorption manometry are summarized in the following checklist, with more detailed comments given in Section 3.4.

(a) The effective volume occupied by the adsorbent must be assessed so that the remaining 'dead space' volume can be determined. The procedure to be adopted is dependent on the exact location of the Gibbs dividing surface.
(b) Allowance must be made for differences in temperature of gas in the various parts

of the apparatus. In the common case of adsorption at liquid nitrogen temperature, gradients of more than 100 K cm^{-1} are common in the neck of the adsorbent bulb.

(c) The accuracy of the adsorption isotherm is governed by the accuracy of the pressure measurement.

(d) Determination of a full adsorption isotherm up to $p/p° \approx 1$ is possible provided that condensation of the vapour does not take place on another part of the assembly before it occurs on the adsorbent itself. Special care is therefore required to ensure that the sample is really the coolest point of the assembly.

(e) Deviations from ideal gas behaviour must be allowed for (cf. Sections 3.4.8).

(f) Attainment of adsorption equilibrium may take hours.

Gas adsorption manometry with reservoir and double pressure measurement. The corresponding set-up is shown in Figure 3.3. One pressure transducer is used to determine the amount of adsorptive remaining in the reservoir, while the second is used to determine the adsorption equilibrium pressure and also the amount of unadsorbed gas in the central cross and adsorption bulb. This arrangement gives an integral measure-

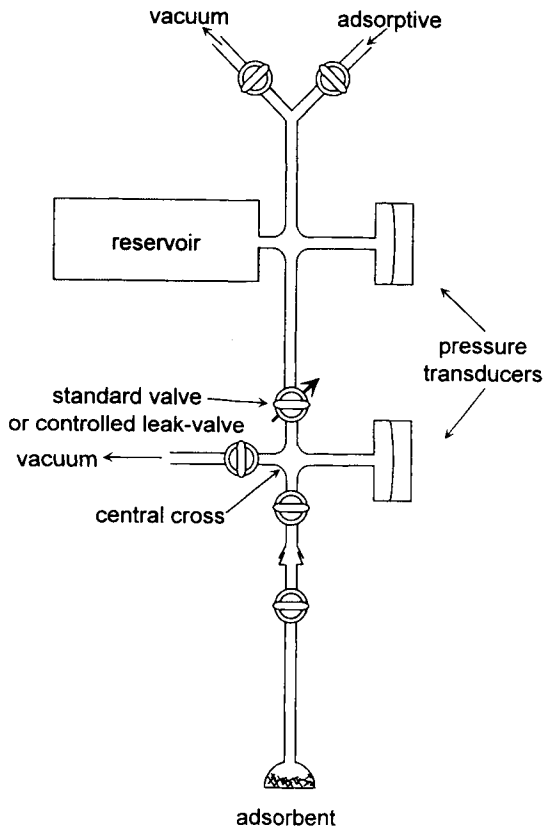

Figure 3.3. Gas adsorption manometry with reservoir and double pressure measurement.

ment of the amount adsorbed and avoids the addition of successive errors resulting from a dosing device (Rouquerol and Davy, 1991). It lends itself, as we shall see later, to both discontinuous and continuous procedures.

Differential gas adsorption manometry. In the earliest form of this technique (Schlosser, 1959), represented in Figure 3.4, two carefully matched capillaries feed two bulbs (adsorption and reference) from a common reservoir of adsorptive. The pressure difference between the two sides provides a direct measurement of the amount adsorbed on the sample side, provided the gas flow rate through the two capillaries is the same: this is no longer true when the difference between the two downstream pressures (on sample side and reference side) is too great. For this reason, this technique is limited to downstream pressures lower than, say, 50 mbar. This allows one to determine surface areas by adsorbing Ar at 77 K, but not N_2.

A simplified form of differential gas adsorption manometry (Haul and Dümbgen, 1960, 1963) is represented in Figure 3.5. Nitrogen under atmospheric pressure is introduced into both sides at room temperature. The intermediate valve is closed and the two bulbs are immersed in liquid nitrogen. When equilibrium is reached, the pressure difference gives the amount adsorbed. No vacuum is needed (only flushing with

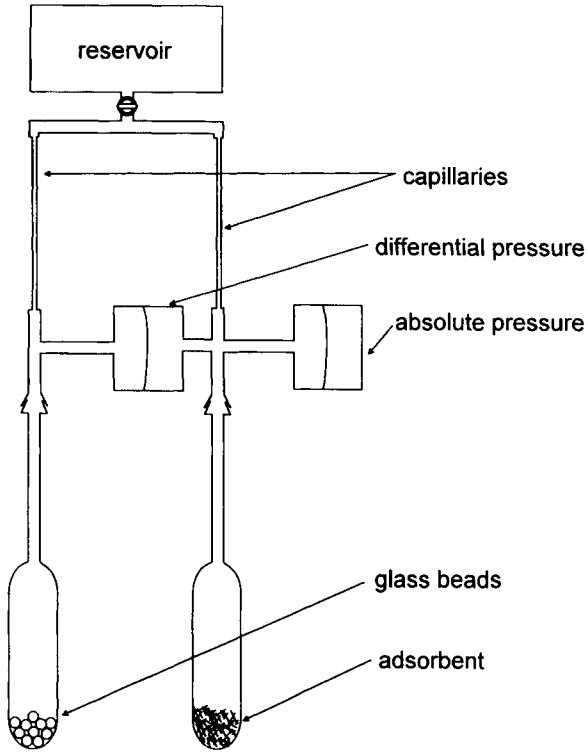

Figure 3.4. Differential gas adsorption manometry with capillaries (valves for initial evacuation of equipment or filling of reservoir not represented) (after Schlosser, 1959).

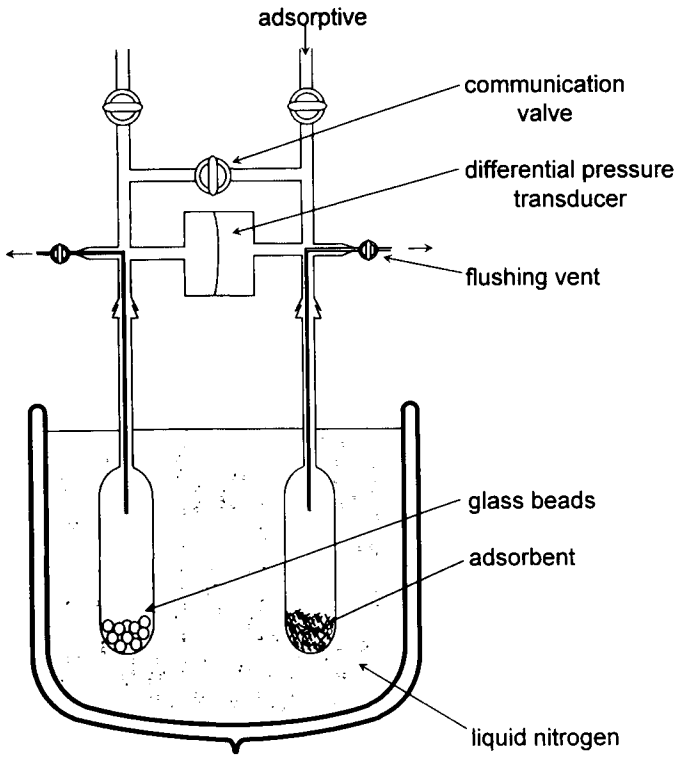

Figure 3.5. Differential gas adsorption manometry from atmospheric pressure (after Haul and Dümbgen, 1960).

nitrogen – hence the two flushing vents and valves) but the single experimental point may not fall in the BET region. This technique was proposed for routine work and needs to be calibrated, for any new type of sample.

At the other extreme, a sophisticated form of differential gas adsorption manometry (Camp and Stanley, 1991; Webb, 1992) is shown in Figure 3.6. It can be considered as combining the best features of the equipment in Figures 3.3 and 3.5. The differential assembly allows one to eliminate the dead volume correction, provided that the dead volume of the reference side is properly adjusted by means of the glass beads. In addition, an integral measurement is possible by the use of the two reservoirs and an extra differential manometer.

Gas flow techniques

In this approach a gas flowmeter is used to determine the amount adsorbed. It can be of a differential type, as in Figure 3.7 (e.g. with a differential catharometer or a differential pressure drop flowmeter) or a simple form with either a sonic nozzle (Figure 3.8) or a thermal detector (Figure 3.9). The last provides a signal which depends on the heat capacity, thermal conductivity and mass flow of the gas: it is usually referred to as a 'mass' flowmeter although there is no direct measurement of mass.

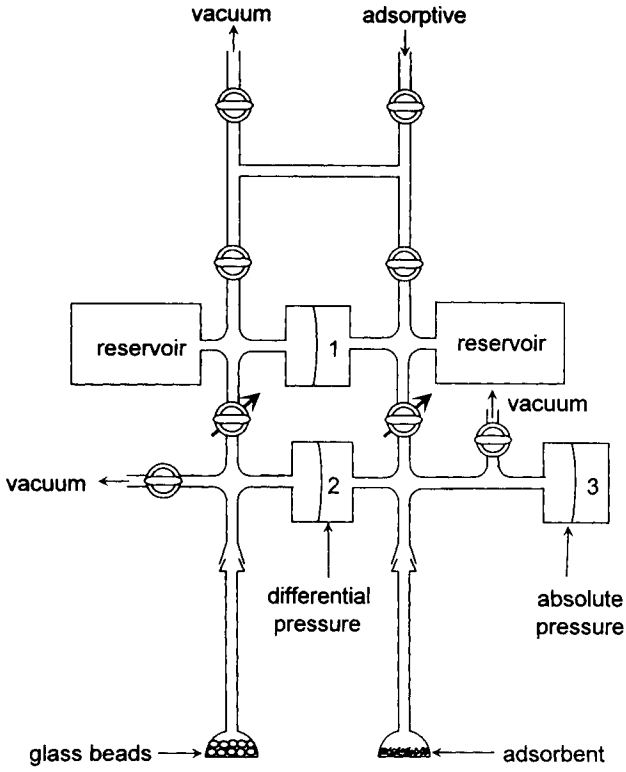

Figure 3.6. Differential gas adsorption manometry with double reservoir and triple pressure measurement (after Camp and Stanley, 1991).

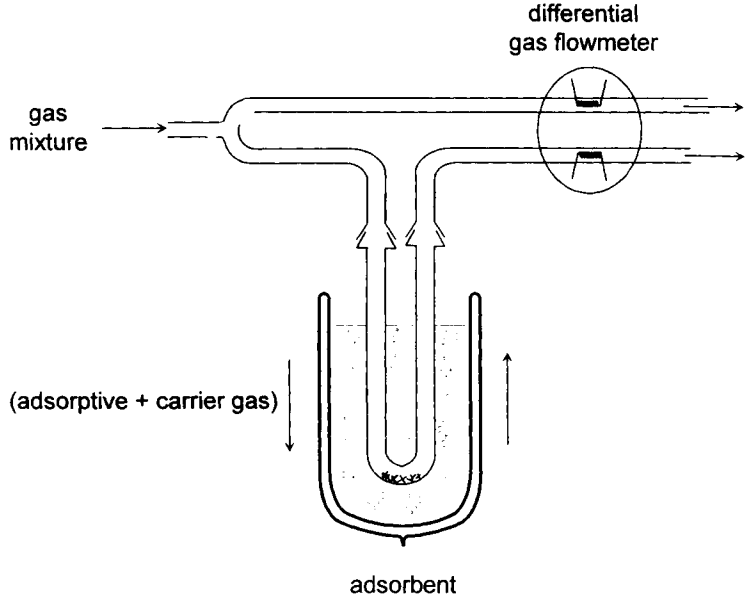

Figure 3.7. Differential flow technique for gas adsorption (after Nelsen and Eggertsen, 1958).

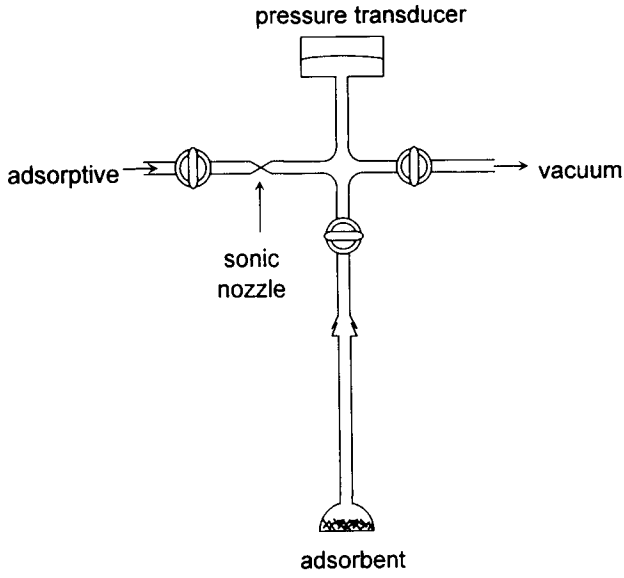

Figure 3.8. Single flow technique for gas adsorption, with sonic nozzle (after Rouquerol, 1972, and Grillet *et al.*, 1977a).

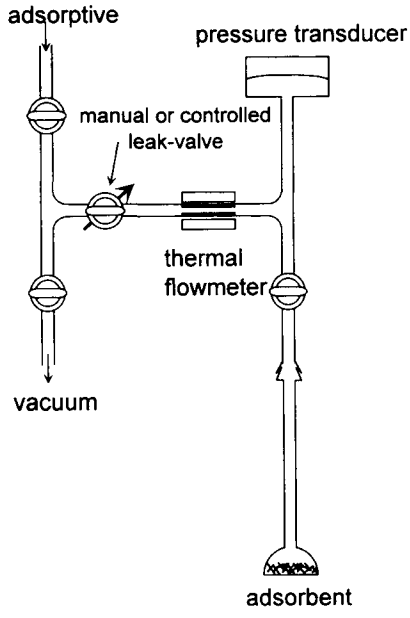

Figure 3.9. Simple gas adsorption flow technique using a thermal gas flowmeter (after Pieters and Gates, 1984).

An advantage of gas flow techniques is that they can be used for two very different types of procedures, i.e. either the discontinuous point-by-point procedure with a non-adsorbable carrier gas (cf. Section 3.3.1) or a continuous adsorption procedure (Section 3.3.2). The limitation is that the amount adsorbed is evaluated by integration of the gas flow over a period which may range from five minutes to several hours. Therefore, great stability and accuracy of the flowmeter are essential. The checklist given above for gas adsorption manometry is equally applicable to gas flow techniques.

Gas adsorption gravimetry

A spring balance for the determination of the amount adsorbed (measurement of mass) was first used by McBain and Bakr (1926). In its simplest form the apparatus consists of an adsorbent bucket attached to the lower end of a fused silica spring, which is suspended within a vertical glass tube as in Figure 3.10.

Spring balances are still used in certain research investigations when adsorption equilibration is very slow, e.g. for the study of hysteresis phenomena. For this purpose, it is advisable to replace the mercury manometer by a modern pressure gauge. However, in recent years spring balances have been largely superseded by electronic microbalances. The essential features of an electronic, null adsorption microbalance are indicated in Figure 3.11.

It is evident that two independent sets of measurements are required in the

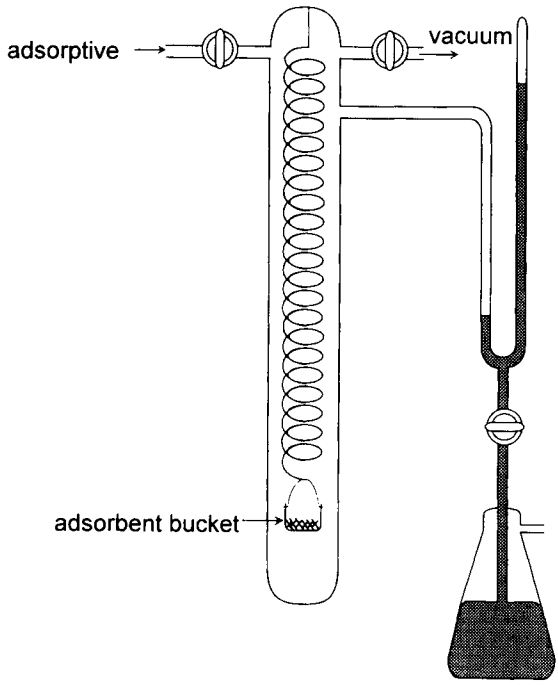

Figure 3.10. The McBain spring adsorption balance (after McBain and Bakr, 1926).

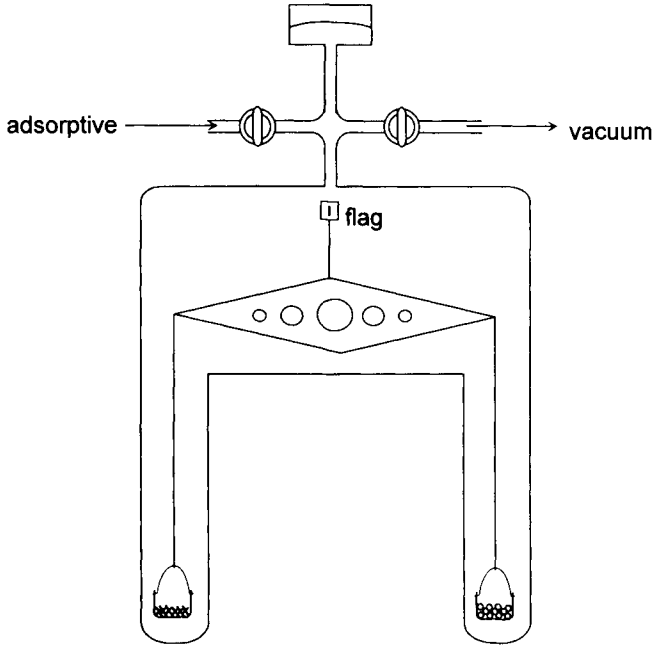

Figure 3.11. Electronic, null, adsorption microbalance.

application of adsorption gravimetry: that of the amount adsorbed (from the increase in mass) and that of the equilibrium pressure. The gravimetric technique is particularly useful for studying the adsorption of a condensable vapour since any uncontrolled condensation on the wall of the balance does not affect the measurement of amount adsorbed, but obviously condensation on the moving parts of the balance must be avoided. In the context of surface area determination, the sensitivity of a gravimetric procedure can be illustrated in the following manner. A monolayer which covers 10 m^2 of surface would be equivalent to: ca. 1 mg of He, 3 mg of N_2, H_2O or C_4H_{10}, 5 mg of Ar and 9 mg of Kr.

There are a number of potential sources of error in gravimetric measurements and particular attention is drawn to the following:

(a) The direct measurement of mass does not eliminate the problem of the evaluation of the dead space. The adsorbent volume correction is now transformed into a buoyancy correction.
(b) There is always poor thermal transport between the adsorbent and the surrounding thermostat. Thus, at low temperature (e.g. 77 K) and low pressure, the adsorbent temperature is likely to be appreciably above that of the cryostat bath.
(c) After the outgassing stage, the sample bucket is often electrostatically charged and tends to stick to the walls of the hang-down tube. Various methods are available for overcoming this problem.

A different type of extremely sensitive gravimetric technique is based on the effect of change of mass on the resonance frequency of a vibrating quartz crystal (see Figure 3.12). In this case, the adsorbent must be firmly attached to the crystal. Its area can be as small as a few square centimetres and mass changes as low as 10^{-2} μg can be detected from the frequency shift (Krim and Watts, 1991).

3.2.2. Gas adsorption calorimetry

Since over a hundred different types of calorimeter have been described in the literature, it is perhaps helpful to distinguish between the four main categories – all of which have been used at various times to study physisorption systems. This is easily done by reference to Figure 3.13 and considering the temperature of the sample cell, the temperature of the surroundings and the way they are connected to each other.

- *Adiabatic calorimeters*: sample temperature is followed by surroundings temperature. This is done in order to prevent any exchange of thermal energy between sample and surroundings.
- *Diathermal-conduction calorimeters*: sample temperature follows surroundings temperature by simple conduction. Either a *heat flowmeter* or a *phase change* detection system is used.

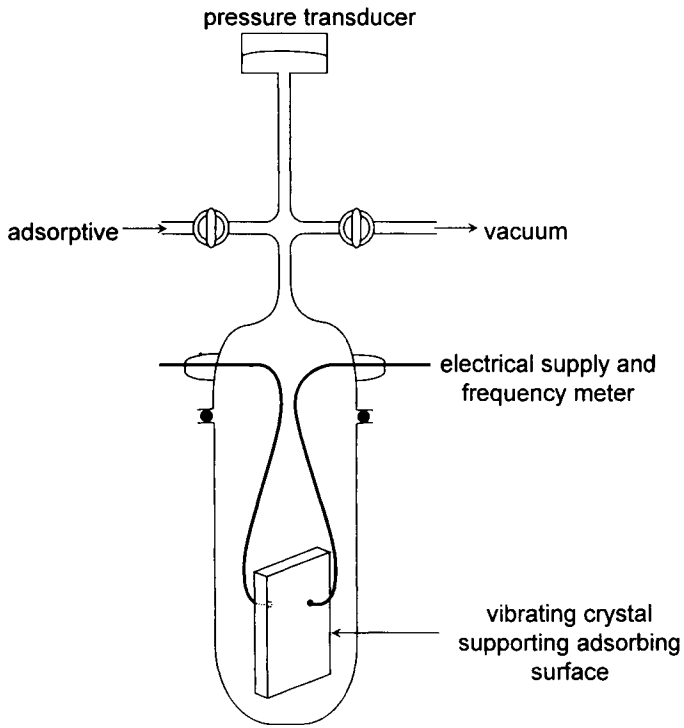

Figure 3.12. Vibrating crystal adsorption balance.

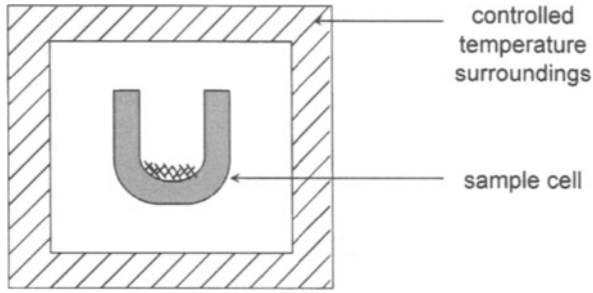

Figure 3.13. Schematic representation of a calorimeter.

- *Diathermal-compensation calorimeters*: here again, sample temperature follows surroundings temperature (usually constant in adsorption experiments), but now by means of a power compensation within the sample cell (i.e. Joule or Peltier effect). This reduces the response time.
- *Isoperibol calorimeters*: no special connection between sample temperature and surroundings temperature and, generally, the latter is kept constant. This is the conventional 'temperature rise', 'Thomsen', or 'Berthelot' calorimeter. The word 'isoperibol' was coined by Kubachewski and Hultgren (1962), from the Greek, to mean 'with isothermal surroundings'.

Adiabatic adsorption calorimetry

Here, the heat evolved on adsorption increases the temperature of the sample and its container (usually a copper cylinder). The heat is prevented from flowing to the peripheral shield (the 'surroundings') by an appropriate control of the shield temperature. Thus, the shield is usually maintained at the same temperature as the sample container by the use of a differential thermocouple and a heat coil – as indicated in Figure 3.14. The temperature rise is measured by means of a resistance thermometer attached to the sample container.

Adiabatic calorimetry is particularly useful for the study of closed adsorption systems at low temperatures (where radiation losses are small) and for temperature scanning experiments. It is the preferred type of measurement for the determination of the heat capacity of adsorption systems, especially in the temperature range 4–300 K (Morrison *et al.*, 1952; Dash, 1975). The temperature scan is obtained by means of the Joule effect applied to the sample container: the sample heating coil shown in Figure 3.14 is used for this purpose.

In some respects, adiabatic calorimetry provides information which is complementary to that provided by heat-flow calorimetry. The latter allows a study to be made of the full composition range at constant temperature, whereas the adiabatic calorimetry study is carried out over the prescribed range of temperature with a constant amount of adsorptive in the adsorption cell (of course, this does not mean that a constant amount is adsorbed). Adiabatic calorimetry allows direct measurements of the heat capacities of adsorbed films, although they are difficult to make accurately

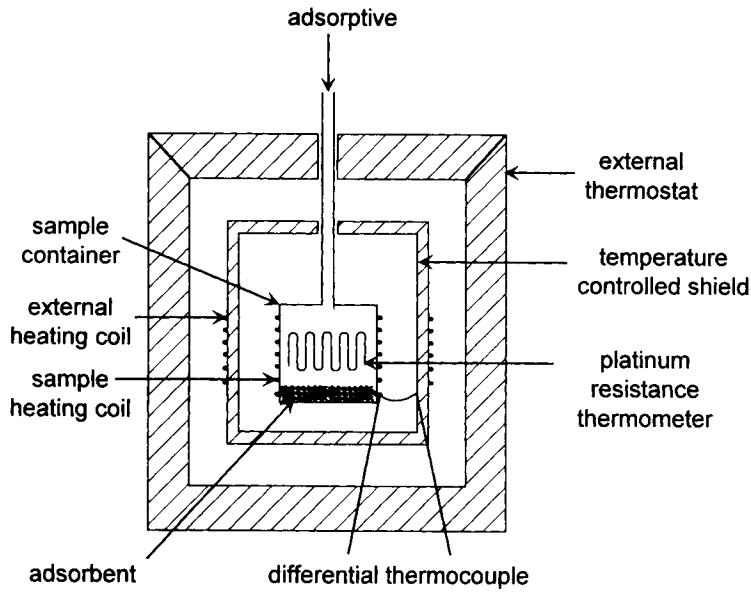

Figure 3.14. Gas adsorption cell (or sample container) in an adiabatic calorimeter.

because the mass of the film is usually a small fraction of the total mass of the calorimetric cell and sample. Fortunately, phase changes of the adsorbed film give rise to large changes in heat capacity which are easily detected by adiabatic calorimetry: this technique can be used in the same way as thermal analysis (for 3-D systems) to determine phase diagrams of 2-D systems (Morrison, 1987). Because of the desorption that takes place on heating it is necessary to allow for the enthalpy of desorption (e.g. by application of the isosteric method).

Diathermal-conduction adsorption calorimetry

This is now the most useful category for adsorption studies, especially for isothermal measurements. There are two main types.

Phase-change adsorption calorimetry. This was the earliest type of diathermal-conduction calorimetry and was originally developed in the form of 'ice calorimetry' by Lavoisier and Laplace (1783), who weighed the liquid water, and by Bunsen (1870), who measured the change of volume. Dewar (1904) devised an elegant adsorption calorimeter at liquid air temperature: the heat was evaluated from the volume of air vaporized. Of course, the temperature of the calorimeter is imposed by the temperature of the phase change. Because these calorimeters lack adaptability and cannot be readily automated, they are mainly of historical interest.

Heat-flow adsorption microcalorimetry. The most important type of isothermal calorimeter in current use is that based on the principle of the heat flowmeter, which was first applied by Tian (1923) and improved by Calvet (Calvet and Prat, 1958,

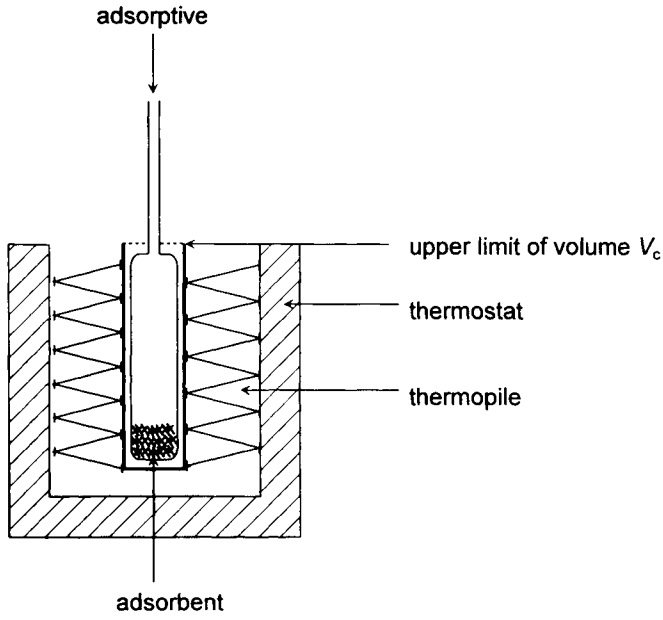

Figure 3.15. Gas adsorption cell in a Tian–Calvet thermopile.

1963), who also introduced a differential assembly. The Tian–Calvet thermopile (with up to 1000 thermocouples) is used to control and measure the heat flux between the sample and the thermostat (cf. Figure 3.15). Measurement of the heat flux is possible even for ΔT as small as 10^{-6} K.

This type of isothermal calorimeter is especially suitable for the study of open systems (i.e. with the introduction and withdrawal of gas) and is therefore highly recommended for the determination of energies of adsorption.

A simplified version of the heat-flow gas adsorption microcalorimeter has only one thermal sensor in close contact with the sample (instead of a multiple integrating heat flowmeter surrounding the sample). It may be complemented by a second sensor acting as a reference. The thermal sensor can be embedded within the sample, while a continuous flow of carrier gas brings the adsorptive at the desired partial pressure through the bed of adsorbent (Groszek, 1966). This set-up is suitable for some preliminary or routine work. In another version, the 'calorimetric bead system', the temperature sensor is embedded in a bead of solid adsorbent, directly cooled by the surrounding gas medium (Jones *et al.*, 1975). These arrangements are simple and sensitive but are not reliable for quantitative measurement.

In a standard set-up for heat-flow gas adsorption microcalorimetry, the adsorbent bulb, (which is located in the thermopile (Figure 3.15)), is connected to a device to allow the simultaneous determination of the adsorption isotherm by one of the techniques listed in the previous sections. The simultaneous determination of the amount adsorbed and corresponding heat evolution allows one to assess the energy of adsorption (for the exact procedure, see Section 3.3.3) provided the following points are

taken into account:

- The adsorptive must be carefully brought to the temperature of the microcalorimeter before entering the adsorption bulb.
- It must also be introduced very slowly, so that the heat effect corresponding to the gas compression in the calorimeter may be calculated accurately, as explained by Rouquerol and Everett (Rouquerol *et al.*, 1980). This also helps to meet the previous requirement of efficient adsorptive pre-cooling or pre-heating.
- The outgassing must be carried out carefully, bearing in mind that the adsorption bulbs used in a microcalorimeter usually have much longer necks than standard adsorption bulbs. Also, this arrangement may drastically change the actual residual pressure in the immediate vicinity of the sample during outgassing.

Diathermal-compensation adsorption calorimetry

At a time when the means for recording and integrating the signal from a heat flowmeter were of limited accuracy, Tian (1923) proposed a way of compensating the major part of the heat liberation by a steady Peltier or Joule effect taking place just against the sample. This idea was refined and adapted to adsorption experiments by Kiselev and his co-workers (Dzhigit *et al.*, 1962). By means of a continuous Joule effect in the vicinity of the adsorbent, they maintained a constant temperature difference ΔT through the heat flowmeter. As soon as adsorption produced an evolution of heat, the Joule effect was interrupted discontinuously, just enough to keep ΔT unchanged. The heat evolved on adsorption was simply derived from the sum of all non-heating periods. This approach was no longer used when the quality of the recordings allowed an accurate integration. Nevertheless, it would be worthwhile updating it (with proportional, integral and differential – PID – control and with integration of the variable Joule power) with the objective of speeding up the experiments, since this *in situ* power compensation shortens the time needed to reach the desired thermal equilibrium. The same can be done using a Peltier effect (keeping $\Delta T = 0$).

Isoperibol adsorption calorimetry

The first experiments of gas adsorption calorimetry by Favre (1854) were made with an isoperibol calorimeter. More recently, refinements were introduced by Beebe and his co-workers (1936) and by Kington and Smith (1964). Because of the uncontrolled difference between the temperature of the sample and that of the surroundings, Newton's law of cooling must be applied to correct the observed temperature rise of the sample. In consequence, any slow release of heat (over more than, say, 30 minutes), which would produce a large uncertainty in the corrective term, cannot be registered. For this reason, isoperibol calorimetry cannot be used to follow slow adsorption equilibria. However, its main drawback is that the experiment is never isothermal: during each adsorption step, a temperature rise of a few kelvins is common. The corresponding desorption (or lack of adsorption) must then be taken into account and, after each step, the sample must be 'thermally earthed' so as to start each step at the same temperature. In view of these drawbacks,

isoperibol calorimeters cannot be recommended for studying the energetics of gas adsorption.

3.3. Operational Procedures

Whatever quantity is used to determine the amount adsorbed (pressure, mass or gas flow), one has to choose between the two basic procedures, discontinuous and continuous. In the past there has been some misunderstanding about the significance of these terms. We prefer to focus attention on the adsorption phenomenon itself, as will be made clear in the following sections.

3.3.1. Discontinuous procedures for determining the adsorption isotherms

The discontinuous procedure is the conventional technique. It is also referred to as the point-by-point procedure. The adsorptive is introduced in successive amounts and at each stage the measurement is made only when adsorption equilibrium is attained. In this way each point on the adsorption isotherm is determined. The original BET technique (Figure 3.1) and all conventional manometric measurements (Figure 3.2) are based on the discontinuous procedure. This is still the procedure most often used with adsorption balances (Figures 3.10–3.12). In principle, it takes account of the requirement that each experimental point of the adsorption isotherm should correspond to thermodynamic equilibrium.

The discontinuous manometric procedure (see Figure 3.2)
The successive steps in the determination of an adsorption–desorption isotherm are normally as follows (more detailed information on particular steps is given in Section 3.4):

1. Adsorbent sample introduced into adsorbent bulb and initial mass recorded (see Section 3.4.2).
2. Adsorbent evacuated under controlled conditions (see Section 3.4.3) and dosing volume also evacuated.
3. Dose of gas (e.g. He, N_2 or Ar) introduced into pre-calibrated dosing volume and p and T measured.
4. Gas expanded into adsorbent bulb at room temperature and new p and T measured.

   Steps 3 and 4 are not required if the 'dead space' volume is determined in another way.
5. Adsorbent and dosing volume evacuated and adsorbent brought to adsorption temperature (e.g. 77 K).
6. Dose of adsorptive (e.g. N_2 or Ar) introduced into dosing volume and p and T measured.
7. Gas allowed to enter adsorbent bulb and time allowed for equilibration.
8. Equilibrium p (and T) of unadsorbed gas recorded.

9. Adsorbent bulb valve (stopcock) closed.
10. Steps 6–9 repeated a number of times to construct adsorption isotherm.
11. First stage of desorption by removal of a measured dose of adsorptive from dosing volume.
12. Gas released from adsorbent bulb into dosing volume and time allowed for equilibration.
13. Equilibrium p and T of gas in bulb and dosing volume recorded.
14. Steps 11–13 repeated to obtain series of desorption points.
15. Adsorbent bulb evacuated.
16. Adsorbent mass determined under dry ambient pressure (alternatively, this mass determined at Step 2, after outgassing, taking into account initial mass of air).

Note that in this procedure the main decision required by the experimenter is the size of the dose. Of course, this will depend on the adsorption capacity of the sample and the number of experimental points desired. For a new, unknown sample, a first exploratory experiment with large doses is useful. Also, the fact that the final accuracy is an inverse function of the number of experimental points (because of the additivity of the errors made at each introduction of adsorptive) must be kept in mind. The introduction of the desired dose is made easier if the gas flow is restricted by a constriction or a needle valve.

The discontinuous gravimetric procedure

Although the problems associated with the selection of the dose size are avoided, other decisions must be made which affect the accuracy of gravimetric measurements. These are considered in more detail in Sections 3.4.4 and 3.4.6.

The steps normally involved in this procedure are as follows:

1. Adsorbent sample weighed in adsorbent bucket/pan.
2. Adsorbent evacuated *in situ* under controlled conditions and mass loss recorded.
3. Non-adsorbable gas introduced at room temperature up to *c.* atmospheric pressure and apparent mass change recorded (to obtain buoyancy correction).
4. Balance case evacuated and adsorbent brought to required temperature.
5. Adsorptive introduced up to desired p and time allowed for equilibration.
6. Equilibrium p, adsorbent T and mass change recorded.
7. Steps 5 and 6 repeated a number of times to construct isotherm.
8. For desorption, removal of adsorptive to pre-determined p and time allowed for equilibration.
9. First desorption point determined – as in Step 6.
10. Steps 8 and 9 repeated to obtain desorption isotherm.
11. Adsorbent evacuated and T restored to ambient.
12. Dry gas (e.g. N_2 or air) admitted and final sample mass recorded at $p = 1$ atm.

Note that the gravimetric procedure involves an integral measurement: at any time, the total amount adsorbed is known from the total mass uptake, with an accuracy which does not depend on the number of previous equilibrium points. Another interesting feature stems from the relatively large volume of adsorption balances

(typically 0.5–2 litres) and from the small samples used (typically 20–100 mg). It follows that adsorption does not greatly disturb the pressure in the balance. The pressure of each experimental point can therefore be approximately pre-set, even with an unknown sample. This makes it easy to get experimental points evenly distributed over the pressure scale. In the case of a steep initial rise of the adsorption isotherm (e.g. in the case of primary micropore filling), the introduction of adsorptive requires careful control. In this case, a previous knowledge of the adsorption capacity of the sample is required, just as for the discontinuous manometric procedure.

The discontinuous carrier gas flow procedure (see Figure 3.7)

The steps of this procedure, devised by Nelsen and Eggertsen (1958) and modified by Atkins (1964) and Karp *et al.* (1972), are usually as follows:

1. Adsorbent sample is weighed in the flow-through adsorbent bulb or U-tube.
2. Adsorbent outgassed by passage of carrier gas (e.g. He) or gas mixture (if not adsorbed at outgassing T).
3. Adsorbent brought to operational T (usually 77 K), while gas mixture of known composition passes through sample (at rate of 10–50 $cm^3\ min^{-1}$).
4. Time allowed for adsorption equilibration as indicated by flowmeter signal.
5. Adsorbent heated to achieve rapid desorption and change in flowmeter signal recorded until all adsorbate removed.
6. Integration of recorded desorption peak.
7. If additional points are required, gas composition changed and Steps 3–6 repeated.
8. Sample removed at ambient T and p and weighed.

Advantages of this procedure are: (a) rapidity (heat exchanges are favoured by the gas mixture flowing at atmospheric pressure); (b) sensitivity (surface areas as low as 0.5 m^2 can be measured); and (c) simplicity (it does not require vacuum or dead volume calibration). The main interest of this procedure is to provide one experimental point for the application of the single point BET determination (cf. Chapter 6). Thus, one adsorptive–carrier gas mixture (for example 10% N_2, 90% He) can be stored and used as required. Measurement of equilibrium pressure is not required, but the atmospheric pressure, p, should be known. In the above example, the equilibrium pressure is: $p/9$. If possible, the mixture is chosen so that the determination is made within the expected linear range of the BET plot.

The limitations are: (a) the carrier gas (usually helium) may be adsorbed in micropores at 77 K; (b) the determination of successive experimental points involves successive cycles of cooling, flushing with new mixture and heating; and (c) adsorption equilibration is not always easy to establish (tailing of the signal).

There is sometimes a tendency to call the above procedure 'dynamic', 'continuous flow' or 'chromatographic' (although no chromatographic effect is studied here). To avoid confusion with the case where a continuous adsorption takes place (which is dealt with in the next section), we prefer to refer to it as a 'discontinuous carrier-gas flow procedure'.

3.3.2. Continuous procedures for determining the adsorption isotherms

The continuous approach is more recent and is not yet widely used. In contrast to a discontinuous procedure, the adsorptive is now continuously 'feeding' the adsorbent, so that the 'point' on the adsorption isotherm is continuously moving along the path of the isotherm. By using the term 'adsorption isotherm' we imply that the adsorption system is always at thermodynamic equilibrium. Since the system is now continuously changing we should strictly speak of 'quasi-equilibrium' (Rouquerol *et al.*, 1988). The fact that this condition was not fulfilled in the first experiments of this type (Innes, 1951; Lange, 1963) unfortunately delayed the development of this procedure.

A slow introduction of the adsorptive is required, and we must ensure that it is slow enough to give – within the limits of the accuracy and sensitivity of the equipment used – the true thermodynamic adsorption isotherm. With most systems, the check is simple and does not even need any comparison with point-by-point measurements. It is sufficient to compare the recorded adsorption isotherms for two different rates of introduction of the adsorptive (say, in ratio of 1 to 2). If the isotherms are identical, they can be regarded as equilibrium adsorption isotherms. Experience shows that the flowrates needed are as low as 50–500 μmol h^{-1} (i.e. around 1–10 cm^3 (STP) h^{-1}). The main advantage of this procedure is that it provides – if used under true quasi-equilibrium conditions – an infinite number of experimental points and, therefore, unsurpassed resolution. Various experimental techniques can be used to apply this approach.

The continuous gravimetric procedure

This simply needs a leak-valve to provide a slow, but not necessarily constant, flow rate of the adsorptive into the balance. This was the first procedure to provide a means of direct on-line recording of the adsorption isotherm. In its original form (Rouquerol and Davy, 1978) the procedure is as follows:

Steps 1–4 (Adsorbent weighed and evacuated, buoyancy correction determined and temperature adjusted) are the same as for the discontinuous procedure.

5. Leak-valve opened to obtain pre-determined rate of p increase (typically 20–100 mbar h^{-1}). Manifold p must be at least 20% above maximum quasi-equilibrium p.
6. Mass change versus quasi-equilibrium p simultaneously recorded. Sample T recorded.
7. If necessary, readjustment of leak-valve to reduce time required to determine complete isotherm.
8. If desorption measurements are required, evacuation of gas manifold to reverse direction of gas flow.
9. Dry gas admitted to atmospheric p and final sample mass recorded.

The automation of the leak-valve can provide either an approximately constant rate of adsorption (i.e. a constant derivative of the mass signal versus time) or a constant rate of pressure increase.

The continuous sonic nozzle procedure (see Figure 3.8)
The approach developed by Rouquerol (1972) and Grillet *et al.* (1977a) involves the following steps:

Steps 1 and 2 (Adsorbent weighed and evacuated) are the same as in the discontinuous manometric procedure.

3. Calibration of gas flow rate: adsorptive allowed to flow through sonic nozzle into the calibrated volume. Flow rate obtained from slope of p versus t curve.
4. Determination of 'dead space' volume by gas expansion into adsorption bulb and measurement of new pressure; another method is to determine the modified slope of the p versus t curve.
5. Adsorbent and calibrated volume evacuated.
6. Adsorbent isolated and brought to required temperature.
7. Adsorptive introduced through sonic nozzle, while evacuation continues.
8. Closure of evacuation valve (starting time of experiment) and opening valve to adsorbent.
9. Quasi-equilibrium p versus t recorded.
10. Adsorbent evacuated after final p attained.
11. Adsorbent mass recorded (alternatively, this mass determined at Step 2, after outgassing).

The sonic nozzle is capable of providing a constant gas flow irrespective of the change of downstream pressure. Its successful application is dependent on the maintenance of a high upstream pressure. In theory, the pressure ratio should be at least 2, but in practice it is advisable to keep the pressure ratio above 6. At present, the sonic nozzle technique is the only reliable method for controlling low gas flow (e.g. ~0.01 $cm^3 h^{-1}$, which is required for krypton adsorption measurements on powders of low surface area).

Note that the pressure versus time curve gives a direct measure of pressure versus the amount of adsorptive introduced through the sonic nozzle. This curve must be corrected for the unadsorbed amount (i.e. the dead space correction) to provide the real adsorption isotherm.

More flexibility (including the possibility of determining the desorption branch) is obtained, at the expense of stability, by the continuous gas-flow controlled procedure (Venero and Chiou, 1988), presented in Figure 3.9. Here, the flow of adsorptive is set at a pre-determined value and then controlled by a loop including the flowmeter and the leak-valve. With a thermal 'mass' flowmeter of good quality, flow rates can be correctly controlled down to *c.* 5 $cm^3 h^{-1}$. With microporous adsorbents, and also when a low specific surface area necessitates the use of large amounts of sample, the flow rate may prove to be a limitation (i.e. not low enough to ensure the required quasi-equilibrium conditions).

The continuous manometric procedure (see Figure 3.3)
In this case the pressure of the gas reservoir is continuously monitored as it slowly supplies the adsorptive to the sample, with the help of a controlled leak-valve. The

procedure is similar to that with the sonic nozzle, except that Step 3 (calibration of gas flow rate) is not required: this rate is derived from the pressure versus time relation for the reservoir. There is either a fine control of the leak-valve (Ajot *et al.*, 1991), so that the rate remains constant and is used to determine the amount adsorbed, or a more flexible control (Rouquerol and Davy, 1991), since the amount adsorbed can be derived from the residual pressure in the reservoir.

The continuous differential manometric procedure (see Figures 3.4–3.6)
The steps involved in the operation of the differential manometric equipment in Figure 3.6. (Camp and Stanley, 1991) are as follows:

1. Adsorbent weighed and introduced into adsorbent bulb and equivalent volume of glass beads put into the reference cell.
2. Adsorbent outgassed.
3. The two reservoirs filled with adsorptive at the same p (high enough to complete experiment).
4. Both sides of differential transducer 2 evacuated and both bulbs brought to desired adsorption temperature.
5. Leak-valve on reference side opened to provide desired rate of pressure increase.
6. Leak-valve above sample automatically adjusted to cancel unbalance of transducer 2. Simultaneously, p from transducers 1 (amount adsorbed) and 3 (equilibrium pressure) recorded.
7. When desorption branch desired, reservoirs evacuated and then filled slowly through leak-valves, with same control loop and recordings as above.
8. At the end, bulbs evacuated.

3.3.3. Calorimetric procedures

Calorimetry must be associated with a means for determining the amount adsorbed. In principle, any technique could be used to determine the adsorption isotherm, but in practice the most frequently used methods for the study of physisorption are: (1) the discontinuous, point-by-point, manometric procedure; (2) the continuous sonic nozzle procedure; and (3) adsorption gravimetry. The first has the advantage of using a conventional assembly (Holmes and Beebe, 1961; Morrison *et al.*, 1952; Isirikyan and Kiselev, 1962; Gravelle, 1972; Della Gatta *et al.*, 1972), whereas the second can provide a continuous measurement of the differential energy of adsorption, with high resolution (Rouquerol, 1972; Grillet *et al.*, 1977b). A fourth procedure can also be used in the case of low-pressure chemisorption, namely the pulse procedure with carrier gas (Gruia *et al.*, 1976).

Discontinuous manometry
As indicated in Section 2.7.1, a discontinuous calorimetric–manometric experiment can be designed to provide the essential experimental data for insertion in the

following equation:

$$\Delta_{\text{ads}}\dot{h}_{T,\Gamma} = \left(\frac{\mathrm{d}Q_{\text{rev}}}{\mathrm{d}n^{\sigma}}\right)_{T,A} + V_{\text{C}}\left(\frac{\mathrm{d}p}{\mathrm{d}n^{\sigma}}\right)_{T,A} \tag{3.1}$$

which is in principle applicable to very small steps.

Thus in addition to the data required to determine the surface excess amount (cf. Section 3.3.1), one needs to know $\mathrm{d}Q_{\text{rev}}$ (the heat exchanged reversibly during each adsorption step) and V_{C} (the volume – dead space – of that part of the adsorption bulb which is located within the calorimetric detector (cf. Figure 3.15). V_{C} is evaluated by liquid weighing or by geometrical considerations and corrected for the sample volume.

The main steps of a typical experiment are as follows:

1. Adsorbent sample introduced and weighed in adsorption bulb.
2. Adsorbent outgassed (see Section 3.4.3) and new mass measured.
3. Adsorption bulb introduced into calorimeter and attached to manometric equipment.
4. When thermal equilibrium reached (i.e. after *c.* 3–5 hours), the dead space volume is determined as in Steps 3 and 4 of the discontinuous manometric procedure in Section 3.3.1. In the case of low-temperature calorimetry this must be done between Steps 2 and 3, by simply connecting the adsorption bulb to the manometric equipment.
5. Adsorption bulb and dosing volume evacuated and sample bulb isolated.
6. First dose of adsorptive introduced and measured (T, p) in dosing volume.
7. Stopcock of sample bulb gently opened for slow introduction of adsorptive (to allow efficient heat exchange between thermostat and adsorptive before it reaches the adsorption bulb and to establish thermodynamic equilibrium).
8. Calorimetric signal continuously recorded during the complete step.
9. Equilibrium p and T measured when calorimetric signal returns to baseline.
10. Adsorption bulb isolated.
11. Steps 6–10 repeated until required range of p/p° is covered.

Because small steps are time-consuming and demanding (in terms of the sensitivity and quality of the baseline), the above procedure is normally used to provide a limited number of adsorption steps. The data are then presented in the form of pseudo-differential energies of adsorption, as in Figure 3.16a. A more elaborate way of processing of the data involves plotting the integral molar enthalpy of adsorption versus n^{σ} (see Section 2.7.1) followed by the derivation of the differential enthalpies. Myers and his co-workers have devised and used an elegant discontinuous calorimetric-manometric procedure with a quadrupole gas analyser to study the co-adsorption of two gases by zeolites at near-ambient temperatures (Dunne *et al.*, 1996, 1997).

Continuous sonic nozzle procedure

The continuous calorimetric sonic nozzle experiment, as described in Section 2.7.2,

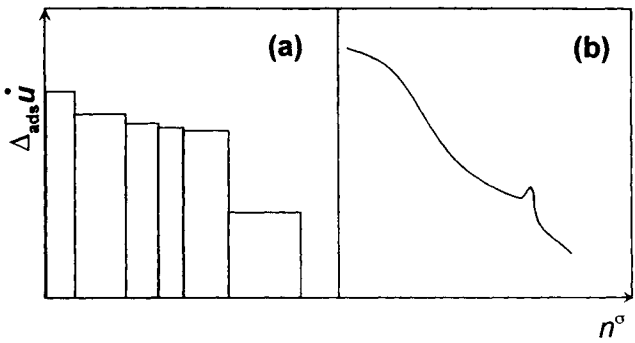

Figure 3.16. Pseudo-differential (left) and differential (right) energies of adsorption, as obtained with a discontinuous or continuous procedure, respectively.

involves the use of the following equation:

$$\Delta_{ads}\dot{h} = \frac{1}{f^{\sigma}}\left(\phi + V_C \frac{dp}{dt}\right) \tag{3.2}$$

The 'rate of adsorption' f^{σ} is determined with the help of Equation (2.80) from the experimental rate of introduction, f, of the adsorptive, the dead volumes V_C and V_E and their temperatures T_C and T_E, and the slope dp/dt. The only extra information needed is a continuous recording of the heat-flow ϕ from the beginning to the end of the experiment. To obtain these data, a convenient procedure is described in the following steps.

Steps 1–5 as for the discontinuous experiment. Dead space volume determination (Step 4) also possible by the discontinuous sonic nozzle procedure (Section 3.3.2).

6. Adsorbent bulb and calibrated volumes evacuated. Adsorbent bulb isolated.
7. Gas flow rate calibrated (cf. Step 3 of continuous sonic nozzle procedure).
8. Calibrated volume evacuated, while adsorptive still introduced at constant rate.
9. Evacuation valve closed (starting time of experiment).
10. Adsorption bulb opened and heat-flow $\phi = (dQ/dt)_T$ and quasi-equilibrium pressure p recorded.
11. Adsorbent bulb evacuated when final pressure reached.

The results can be presented in the form of a continuous curve of differential enthalpies of adsorption $\Delta_{ads}\dot{h}$ versus n^{σ}, as shown in Figure 3.16b, with a resolution which is much higher than that obtained by the discontinuous procedure (Figure 3.16a). If the adsorption calorimeter cannot be easily connected to a well-calibrated and well-temperature-controlled adsorption sonic nozzle set-up, or when the adsorption isotherm is difficult to determine (e.g. if very small amounts are adsorbed), there remains the possibility of determining, separately, the adsorption isotherm by any of the discontinuous or continuous procedures described in Sections 3.3.1 or 3.3.2. A simple procedure can be applied which does not require the gas flow rate calibration:

the simple recordings of quasi-equilibrium pressure and heat-flow versus time is all that is required for the determination of the isotherm and the adsorption energy. If V_C can be calculated (from the dead volume of the empty adsorption bulb and the density of the adsorbent), then one can omit all calibration steps (included in Steps 4 to 8 in the above procedure).

Gravimetry

Gravimetry can be associated with adsorption calorimetry, either by using two samples (one in the microcalorimeter, the other in the microbalance) in contact with the same atmosphere of adsorptive (Gravelle, 1972) or using a single sample, located in the cylindrical pan of a microbalance and surrounded by a Tian–Calvet thermopile (Le Parlouer, 1985).

3.3.4. Simultaneous gravimetry and manometry

Gravimetry can also be associated with adsorption manometry, which is a simple and safe way to study co-adsorption of two gases, provided their molar masses are sufficiently different (Keller *et al.*, 1992). The manometric experiment provides a total amount adsorbed $n^{\sigma}_{tot} = n^{\sigma}_1 + n^{\sigma}_2$, whereas the gravimetric experiment provides the total mass adsorbed $m^{\sigma}_{tot} = m^{\sigma}_1 + m^{\sigma}_2$. Since $n^{\sigma}_1 M_1 = m^{\sigma}_1$ and $n^{\sigma}_2 M_2 = m^{\sigma}_2$ we have two unknowns, n^{σ}_1 and n^{σ}_2, and two equations. From these we can obtain, for instance:

$$n^{\sigma}_1 = (m^{\sigma}_{tot} - n^{\sigma}_{tot} M_2)/(M_1 - M_2) \tag{3.3}$$

On practical grounds, some difficulties stem from the large volume of adsorption balances: to measure pressure changes due to adsorption accurately, one must usually place a considerable amount of the adsorbent outside the balance pan (because of the limited loading capacity of the balance) yet close enough to be at the same temperature.

Other techniques that have been introduced recently in association with adsorption manometry include the use of a magnetic suspension balance (Dreisbach *et al.*, 1996) and a rotational pendulum (Keller, 1995).

3.4. Details of the Operational Stages

3.4.1. Calibration of volumes

Dosing volumes

Most experiments described in Section 3.2.1 (with the exception of adsorption gravimetry) rely on the use of a calibrated volume. The basic calibration can be carried out in two ways: directly or indirectly. Direct calibration implies that this part of the equipment can be isolated, removed and weighed (either evacuated or filled with dry air), filled with an outgassed liquid of known density and then weighed again.

A practical limitation comes from the loading capacity of modern analytical balances. It is difficult to find a balance with a sensitivity of 0.1 mg and a loading capacity of more than *c.* 300 g. This means that the stainless steel gas storage vessels

used in most modern equipment are generally too heavy to be weighed accurately. Indirect calibration implies the use of an external calibrated volume in place of the adsorption bulb. The experiment is similar to that for determining the dead space volume of the adsorption bulb. Maximum accuracy will be obtained if the initial dose of gas admitted to the volume to be calibrated makes use of the full working range of the pressure transducer and if the external calibrated volume is roughly equal to the total volume to be calibrated (i.e. including the pressure transducer and connecting tubing). If there is a difference in temperature, it will be necessary to make a correction for thermal expansion.

In indirect calibration there is inevitably some loss of accuracy in using a separate bulb, but there is also the opportunity to use a glass bulb which can be properly cleaned. Any gas bubbles can be seen and withdrawn, and also there are no inaccessible regions in the vicinity of metal fittings and valves.

Dead space volumes

As we have already seen, for the application of most manometric techniques for the determination of the amount adsorbed it is necessary to have an accurate knowledge of the volumes of two parts of the overall dead space. The first is the connecting volume located between the stopcock above the adsorbent bulb and the lowest valve of the dosing volume (see Figure 3.2). The second, and more important, volume is that of the dead space within the adsorbent bulb. Although the connecting volume does not need to be determined for each experiment, its value can be checked in the first stage of the gas expansion calibration procedure.

The determination of the dead space volume of the adsorbent bulb is not quite as straightforward as one might think. It is necessary to consider the following three questions: (1) How do we define the remaining gas volume in relation to the volume occupied by the adsorbent? (2) What is the most suitable procedure? (3) If gas expansion is to be used, then which gas (e.g. He or N_2) should be adopted, and at what temperature?

It follows from the discussion of the quantitative expression of adsorption in Chapter 2 that the most appropriate demarcation between the gas and the adsorbed phase is the Gibbs dividing surface (GDS). This enables us to express the adsorption data in terms of the surface excess and avoids having to determine (or assume) the absolute thickness of the adsorbed layer.

The next question is: where should we locate the Gibbs dividing surface? For several reasons it is most convenient to locate the GDS as closely as possible to the solid surface. By doing so we can minimize the effect of operational temperature and facilitate the comparison of adsorption data.

Two main routes are available for evaluating the volume up to that surface: the direct one of measuring the volume accessible to a gas, which is not adsorbed at the temperature and pressure of the dead volume determination, and the indirect one, of simply subtracting from the volume of the empty bulb the estimated volume of the sample.

The direct route has in the past been preferred and considered to be safer, although, as will become evident, opinions are now less clear-cut. The direct route involves

expanding a gas into the adsorption bulb already containing the adsorbent sample. The exact location of the Gibbs dividing surface is dependent on the gas and temperature (especially if the sample is microporous). In the simplest situation, the whole adsorption bulb (up to the top of its stopcock) is maintained at the sample temperature during the subsequent adsorption experiment, whereas all other volumes of the set-up can be considered to be entirely at the controlled ambient temperature. In this case, only one determination must be made, namely that of the volume V_f of the bulb containing the sample. This is acceptable for adsorption experiments at around room temperature, but not for experiments carried out at 77 K. As illustrated in Figure 3.17, there is a considerable temperature change in the CD portion of the bulb neck. In principle, it should be possible to determine carefully the volumes between levels A and B (the bulb proper), C and D (where the gradients lie) and D and F (including the stopcock), and then make a simplifying assumption about the temperature gradients between C and D in order to calculate the amount of gas enclosed.

However, there is another experimental procedure that can take into account these gradients much more accurately – provided they are reproducible. This procedure is as follows:

1. Determination of the volume V_e of the empty bulb at ambient temperature (i.e. in the air thermostat) by expansion of gas from the dosing volume.
2. Determination of the apparent volume V_a which, at ambient temperature, would enclose the same amount of gas as the empty bulb immersed in liquid nitrogen at controlled and reproducible depth, under the same pressure.
3. Determination of volume V_f of bulb filled with adsorbent at ambient temperature.

From V_a and V_e, we can obtain two imaginary volumes, V_{up} and V_{lo}, making up V_e. We can picture V_{up} as a volume totally at room temperature (upper part of the bulb) and V_{lo} as a volume totally immersed in liquid nitrogen. In this representation there is no transition volume with temperature gradients, but V_{up} (at room temperature) and V_{lo} (at 77 K) are such as to accommodate exactly the same amount of gas as the empty

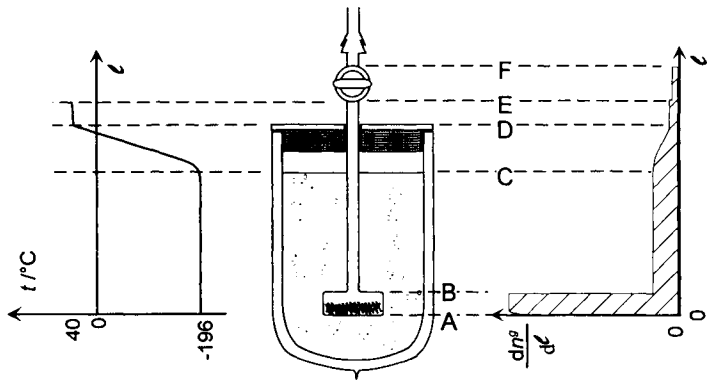

Figure 3.17. Temperature (left) and amount of adsorptive in the gas phase (hatched area, right) as one moves from bottom to top of an adsorption bulb immersed in liquid nitrogen.

bulb when immersed in liquid nitrogen during Step 2 (with reproducible but unknown temperature gradients). V_{up} does not depend on the presence or absence of the sample. From V_f and V_{up} we therefore obtain the modified V_{lo}, which takes account of the presence of the adsorbent. Since V_{up} remains constant, only Step 3 is required for a new sample.

The gas to be used in the dead space determination must be carefully selected. In the procedure described, Step 1 can be carried out with any permanent gas (e.g. helium or nitrogen), whereas for Step 2 it is advisable to use a gas with the same virial coefficient B_m as the adsorptive, since B_m and the subsequent correction can vary considerably from one gas to another (see Section 3.4.8). Since the measured value of V_a depends on the virial coefficient B_m of the gas used, the simplest procedure is to use the adsorptive itself. Step 3 is also preferably carried out with a gas whose accessibility to the sample is comparable to that of the adsorptive: here again the adsorptive itself, at a temperature at which it is known not to adsorb, is the best.

As can be seen, helium, in contrast to what was once assumed, is not necessarily the best gas to select for the determination of dead space. It is sometimes thought that helium allows dead space to be determined directly at 77 K in the presence of the sample, since it will not adsorb. However, since its virial coefficient is much smaller than that of most adsorptives (see Table 3.2), and because of the possibility of adsorption in micropores (see Chapter 9), its use cannot be recommended. This problem has been discussed recently by Neimark and Ravikovitch (1997).

The indirect route for determining the dead space volume makes use of an estimated volume of the adsorbent sample. This volume can be obtained in two ways:

(a) From the theoretical density. This leads to a dead space which, by definition, contains all pores of any size (including closed pores and also any micropores inaccessible to the adsorptive).
(b) From pycnometric measurements (in a liquid or in a gas) carried out separately. In this case the nature and temperature of the fluid must always be stated.

Both have the advantage of giving a sample volume (and therefore a location of the dividing surface) which is, by definition, perfectly reproducible from one adsorption bulb to another and from one laboratory to another. Even if not always realistic, it is a sound convention, if the aim is to obtain reproducible measurements and calculations and is consistent with the spirit of the Gibbs representation. It is, for these reasons, certainly well suited for the study of reference materials. Of course, this approach would replace Step 3 in the procedure described above, whereas Steps 1 and 2 would remain necessary.

In the case of differential or twin arrangements of adsorption manometry (cf. Figures 3.4–3.6), the dead volume determination is not required, but the volume equalization and the symmetry of the set-up are essential. The volume equalization is usually obtained with glass beads on the reference side and sometimes also with adjustable bellows or a piston. The check or adjustment is normally carried out at ambient temperature: the introduction of an identical amount of gas on both sides must result in a zero pressure difference between them.

3.4.2. Sample mass

The first problem to be faced is what amount of adsorbent should be used for the adsorption experiment. This of course depends *inter alia* on the sensitivity of the measuring equipment and the texture and surface properties of the adsorbent.

With most modern equipment, the most reliable measurements are generally obtained with total areas ranging from 20 to 50 m^2 in the adsorption bulb. For materials with specific surface areas under 1 $m^2 g^{-1}$ a mass of 10 g or more may be found necessary, but the improvement in sensitivity is counterbalanced by the unavoidable pressure and temperature gradients within the sample.

At the other extreme, with materials of specific surface area above 500 $m^2 g^{-1}$ one must be careful not to reduce the mass of sample by too much: it must remain representative of the batch of adsorbent and it must be weighed with an accuracy consistent with the accuracy provided by the adsorption measurement. For these two reasons, it is usually unwise to use a sample mass under, say, 50 mg. If the full adsorption–desorption isotherm is to be determined, one can be limited by the capacity of adsorptive reservoir or dosing volume or by the automatic control range of the electronic microbalance (typically, between 50 and 100 mg with sensitivity $\geqslant 1$ μg). It therefore often happens that the measurement of one isotherm cannot provide the best determination of the specific surface area and at the same time the best determination of the full adsorption–desorption isotherm.

The second problem is to obtain a meaningful mass measurement in the case of a reactive adsorbent (e.g. one that may absorb or chemisorb H_2O, CO_2, etc.). This requires a careful measurement of the mass of adsorbent in its initial state and of the mass change undergone on outgassing – since the reference mass will be that of the outgassed sample. This mass change includes the mass of air initially present in the adsorption bulb. This can be calculated from the dead volume of the adsorption bulb and from the density of the air (at a given ambient temperature, pressure and humidity). The adsorbent bulb can also be evacuated at room temperature prior to being weighed, but care must then be taken not to change the sample mass by some desorption. Therefore, this evacuation must be short and not severe: the pressure in the bulb must not be lower than a few mbar to limit water desorption. This should result in an error of less than 1% in the calculated mass of air.

3.4.3. Outgassing the adsorbent sample

Aim of the outgassing

Of particular importance are investigations of the adsorptive properties of powders and porous solids in relation to particular applications. This means that a reproducible initial state of the adsorbent surface should be consistent with the proposed application of the adsorbent. This is why we do not always require a 'perfectly clean' surface, which would usually involve ultra high vacuum (say, a residual pressure less than 10^{-6} mbar) and high temperatures (say, above 1000°C). Instead, our aim is: (a) to eliminate most of the species physisorbed during storage of the sample (e.g. H_2O, CO_2); (b) to avoid any drastic change as a result of ageing, sintering or modification

of surface functional groups; and (c) to reach a well-defined, reproducible, intermediate state that would be suitable for the proposed experiments (e.g. adsorption isotherm measurements or adsorption calorimetry). This state can be attained by an appropriate form of vacuum outgassing or by a gas displacement process.

Conventional vacuum outgassing

This type of outgassing is attractive because: (a) it is *clean* by definition; (b) it allows the operator to use a lower outgassing temperature than would be necessary under atmospheric pressure and static conditions; and (c) it leaves the surface exposed to a vacuum which is precisely what is required to start most adsorption experiments. It might seem that this type of outgassing simply needs a sample container, a furnace or oven (with temperature control and, if possible, heating rate or 'ramp' control) and a vacuum (cf. Figure 3.18). In practice, two main problems may have to be faced, namely the spurting of fine powders from the sample container and changes which may occur during the reduction of pressure and increase of temperature.

The problem of the spurting of fine powders can be solved in several ways. First, spurting can be prevented by using a glass-wool pad (or a glass frit) in the tube above the sample. This practice is simple but adds an uncontrolled barrier between the vacuum line and the region around the sample; it therefore leads to a lack of control in the outgassing. Second, spurting can be prevented by controlling manually the opening of the valve connecting the sample to the vacuum line. However, this may be quite time-consuming. For example, samples prepared by the sol-gel method may need several hours of slow pumping at room temperature before the stopcock can be completely open. One can then operate in two ways: either by directly observing the sample as the vacuum valve is opened, little by little, or by keeping the gas flow from the sample lower than a pre-selected value which is known, from prior experience, to be safe for the particular sample. Monitoring the gas flow can be achieved by using a

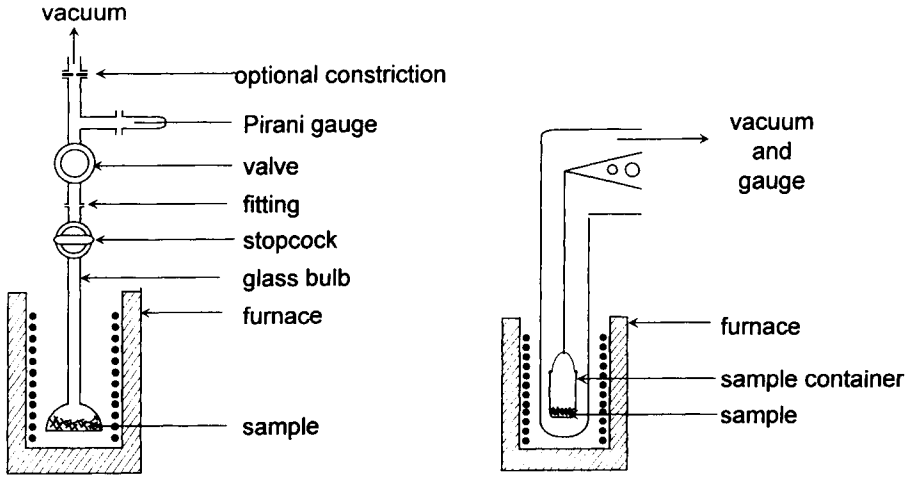

Figure 3.18 : Vacuum outgassing from a bulb for adsorption manometry (left) or from the sample container of an adsorption microbalance (right).

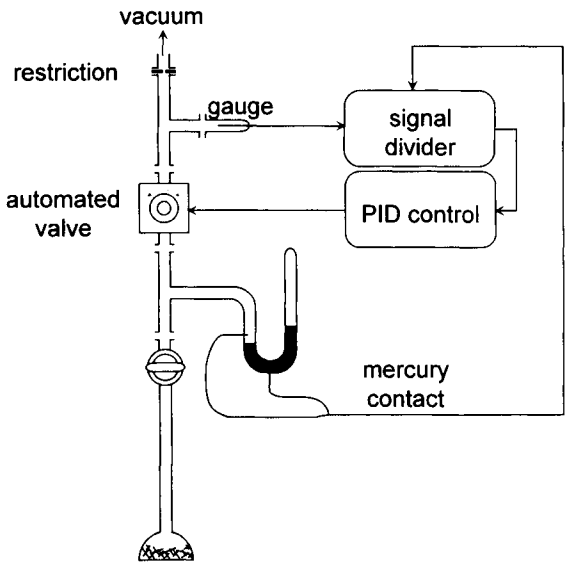

Figure 3.19. Antispurting automatic set-up for sample evacuation.

Pirani gauge upstream, and possibly a constriction (convenient size: 1 to 3 mm bore and 10 mm length) as shown in Figure 3.18. When the valve is completely open, some manual control of the heating may still be needed.

A more complete way of preventing spurting is to introduce two automatic controls, one for opening the vacuum valve and the other for controlling the sample temperature (see the next section). The automatic control of the vacuum valve is similar to that used in the manual procedure and is illustrated in Figure 3.19. The signal from a Pirani gauge feeds a PID controller acting upon an automated valve (e.g. a standard diaphragm vacuum valve of 10 or 20 mm bore). Experience shows that, on outgassing an adsorbent, two successive stages can be identified: (1) the pumping of air down to a pressure of, say, 25 mbar, and (2) the desorption proper, which usually involves the removal of water. Since only a small part of the air pumped comes from the sample itself, the first step can be carried out much more rapidly than the second. A mercury contact control unit can be used to switch the controller from stage (1) to stage (2).

Convenient pumping rates are, for instance, 0.5 dm^3 (STP) h^{-1} during stage (1) (so that it will require around 15 minutes) and 50 cm^3 (STP) h^{-1} during stage (2). It takes *c.* 5 minutes to pump 5% physisorbed water from a 100 mg sample, but 1.5 hour to pump 10% physisorbed water from a 1 g sample.

Controlled vacuum outgassing by means of CRTA

We have just seen how to avoid (either manually or automatically) spurting of the sample on evacuation, at room temperature. However, when the sample temperature is raised there is a further risk of spurting and of uncontrolled changes of the sample itself. The technique for overcoming these problems follows the general principle of controlled rate thermal analysis (CRTA) (Rouquerol, 1970, 1989), where the heating

is directly controlled by the behaviour of the sample itself (i.e. by feedback from the sample). A simple form of CRTA, which is well adapted for outgassing purposes, is presented in Figure 3.20.

The adsorbent bulb is continuously evacuated through a calibrated diaphragm D (convenient size: 1 mm bore, 1 cm long). The pressure drop through the diaphragm is monitored by a simple Pirani gauge. This signal is fed to PID heating control which heats the sample in such a way as to maintain a constant pressure drop. Thus, both the residual vacuum around the sample (typical values: 5–100 μbar) and the rate of outgassing (typical rates: 1–10 mg lost per hour) are controlled at the same time. Controlling the rate of outgassing means that we also control the pressure and temperature gradients through the sample. These can be lowered at will, simply by reducing the rate of outgassing. The recorded temperature curve is representative of the thermal path followed by the sample and has the advantage of being obtained directly with the sample located in its adsorption bulb. The reproducibility of the heat treatment is easily checked by comparing the temperature curves. Finally, this type of thermal treatment provides a way of studying the effect of outgassing and heating on the properties of the adsorbent and providing a characteristic temperature curve.

In conventional heating the sample is brought linearly to a given temperature and, since the sample is far from equilibrium, it is kept at that temperature for a certain time (commonly between 2 and 10 hours). This results in a mass–temperature curve which is often far removed from the characteristic curve for the adsorbent (cf. points 1 and 2 in Figure 3.21). In some cases, this can invalidate any discussion of the significance of the results. However, since quasi-equilibrium can be reached at any time during a CRTA experiment, it is possible to stop the heat treatment (and even to quench the sample) at any point of the curve common to all samples (cf. points 3, 4

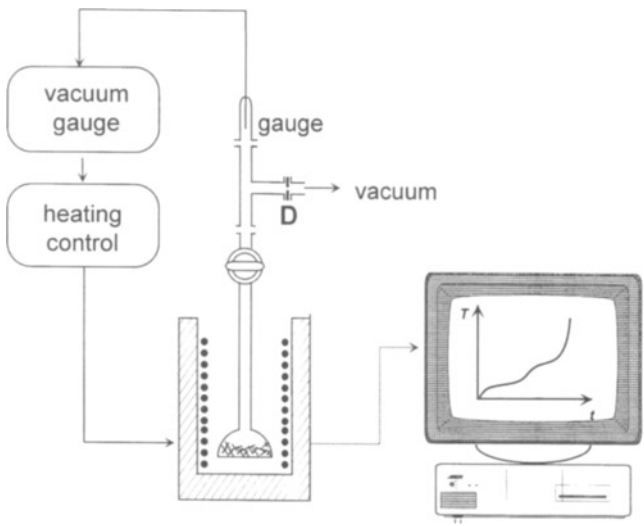

Figure 3.20. Simple set-up for CRTA outgassing.

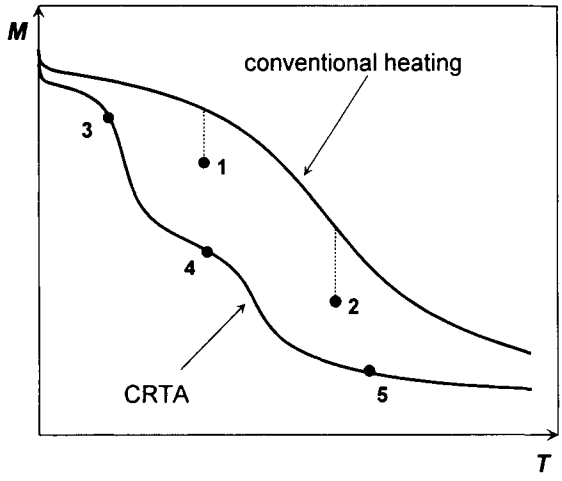

Figure 3.21. Representative points of samples outgassed by conventional heating (1 and 2) or by CRTA (3, 4 and 5).

and 5 in Figure 3.21). The CRTA approach can be used for the outgassing of a sample located either in a standard adsorption bulb or in the pan of a microbalance (Rouquerol and Davy, 1978).

Outgassing with a carrier gas

The carrier gas can be any non-reacting gas (e.g. nitrogen, argon or helium) with no more than, say, 100 ppm humidity. To achieve good reproducibility, only metal or viton tubes must be used between the gas bottle and the sample container. The latter can be in the shape of a U-tube, with the sample in the bottom, or in the shape of a standard adsorption bulb into which a long, hollow, needle is introduced and used as the gas inlet.

Heating of the sample is carried out in the same way as in vacuum. In principle, one could again choose between a conventional form of linear heating (followed by a temperature plateau) and a CRTA treatment, the rate of outgassing now being controlled with the help of a highly sensitive, differential gas flowmeter (J. Rouquerol and J.M. Fulconis, personal communication). In fact, the main advantage of outgassing with a carrier gas is the simplicity of the technique (no vacuum, no spurting of the sample and good thermal exchange – particularly if the carrier gas is helium). An interesting compromise is simply to monitor the outgassing of the sample by the use of a catharometer (with helium as the carrier gas, it is possible to detect the release of water vapour).

3.4.4. Buoyancy correction

The buoyancy correction needed in adsorption gravimetry has the same origin as the dead space correction in adsorption manometry: it is due to the volume of the sample

or, more precisely, to the 'envelope' of the dividing surface and the resulting change in the apparent amount adsorbed (Rouquerol *et al.*, 1986). This means that any errors – or deliberate changes – in the location of the dividing surface must have the same effect in gravimetry as in manometry. Here again, we can choose between a direct or an indirect approach, and we can cancel out part or the whole of this correction by using a symmetrical set-up.

Direct approach

The direct determination of the buoyancy is carried out with a gas which does not adsorb at the temperature of the determination: it must be chosen in the same way as the gas for Step 3 in the previous section. Helium should be avoided – this light gas does not lend itself to the precise determination required since the buoyancy correction is directly proportional to the molar mass of the gas used.

Indirect approach

The indirect determination of the buoyancy is obtained by the assessment of the sample volume from its density or by pycnometry – as in the previous section and with the same implications for the location of the Gibbs dividing surface.

Symmetrical balance

A symmetrical balance provides a means of minimizing these corrections. To obtain the best compensation, one can adjust the mass and volume on the reference side, for instance by the use of glass beads and gold wires (Mikhail and Robens, 1983). This compensation is no more accurate than the determination of the buoyancy effect as

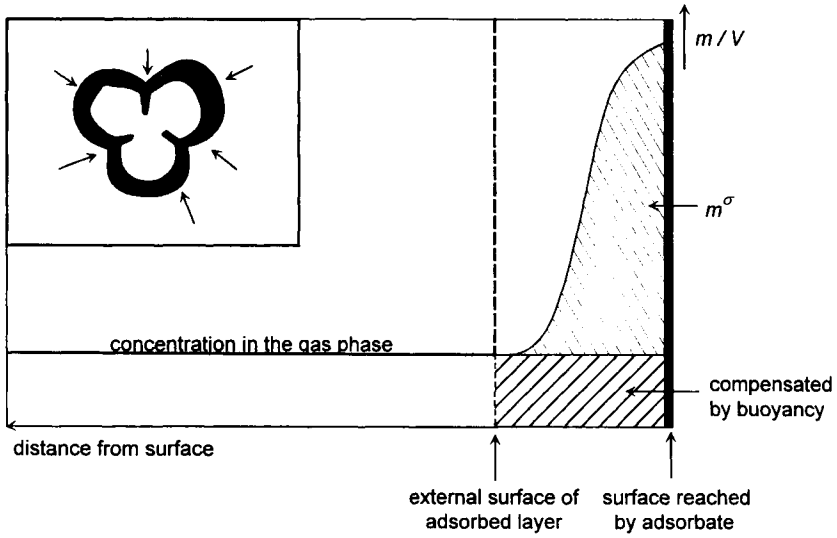

Figure 3.22. Buoyancy in relation to the Gibbs representation: the surface excess mass m^σ and the corresponding buoyancy effect is indicated (top left).

described just above, but it may allow the balance to be used over a smaller range, where a higher sensitivity is available.

A pertinent question is: as the volume of the adsorbed phase increases, do we have to take into account the corresponding increase of buoyancy? (e.g. the buoyancy doubles after saturation of an adsorbent with 50% porosity). The answer is no, provided we want to assess the surface excess mass m^{σ}. As illustrated in Figure 3.22, because of the buoyancy effect, we do not measure the total mass of the adsorbed layer (shaded + hatched areas) but simply a surface excess mass (hatched area only). Thus, adsorption gravimetry and the Gibbs representation are highly compatible (Findenegg, 1997).

Finally, it may be worth considering the effect of buoyancy correction on the magnitude of the error in the determination of the BET(N_2) surface area. This is indicated in Figure 3.23 for surface areas ranging from 1 to 1000 $m^2 g^{-1}$ and adsorbent densities in the range 1 to 8. The buoyancy is calculated by taking into account the density of nitrogen vapour at a temperature of 77 K and a pressure of 100 mbar, which is assumed enough to complete the monolayer. For a sample of 1 $m^2 g^{-1}$, with a density of 2 (for instance, a finely ground quartz), the error amounts to 80%! At the other extreme, for a sample of 1000 $m^2 g^{-1}$, with a density of 1.5 (for instance, an active carbon), the error will be as small as 0.1%.

3.4.5. Adsorption equilibrium

By convention, 'adsorption isotherms' are generally assumed to correspond to a thermodynamic equilibrium: if this is not true, use of the term 'adsorption isotherm' is questionable. The confirmation of adsorption equilibrium is therefore of crucial significance.

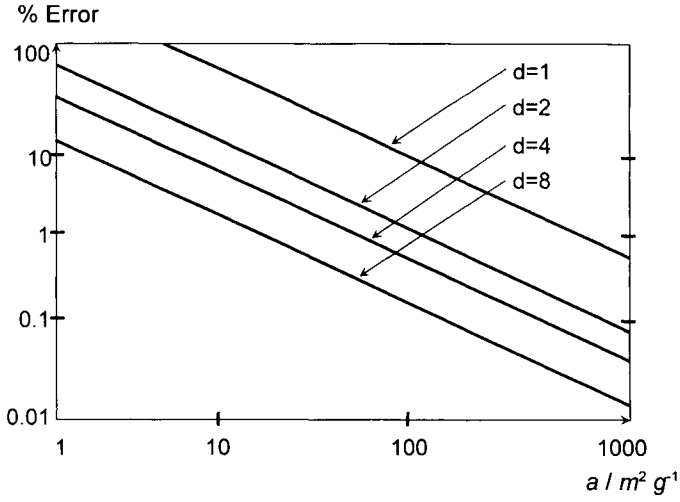

Figure 3.23. Gas adsorption gravimetry: percentage error in surface area as a result of neglecting totally the buoyancy effect on the adsorbent (assumptions: nitrogen BET, monolayer at 100 mbar, bulk density of adsorbent from 1 to 8).

Let us first consider the case of a discontinuous, point-by-point procedure. An 'absolute' or 'perfect' equilibrium can of course never be attained, since it is limited by the fluctuations of (a) the adsorbent temperature, (b) the residual gas temperature, and (c) the baseline of the pressure transducer. As a consequence, after a certain time, the system is as close as it will ever get to true equilibrium. Nevertheless, this time may be relatively long (e.g. it may take hours to determine each point). The experimenter may then decide to be less demanding in order to save time. A convenient way to operate, which lends itself to automation, is the following:

1. Determine the height of the minimum pressure step which can be safely detected (say, 3 or 5 times the fluctuation amplitude observed for the pressure signal).
2. Select an 'observation period': equilibrium will be considered to be reached if, over that period, the pressure changes by less than the 'minimum pressure step' determined above.
3. Only then, read and store the data (equilibrium pressure and temperatures). The longer the preselected 'observation period' (usual range: 0.5 to 5 min), the more demanding the equilibrium requirement.

We have already pointed out (cf. Section 3.3.1) that the point-by-point procedure does not always ensure the establishment of a meaningful equilibrium: the adsorptive must be introduced slowly enough to avoid some undesirable scanning within the hysteresis loop. Indeed, when an adsorption system reaches a state corresponding to the adsorption branch of a hysteresis loop, the sudden introduction of a new dose of adsorptive may well favour the initial adsorption on the upper layers of the adsorbent; subsequently, these layers will undergo the desorption of part of their adsorbate which will be transferred to lower layers. The resulting experimental point will therefore be located somewhere within the hysteresis loop, instead of on the true adsorption branch. It follows that, in the pressure range of the hysteresis loop, a slow introduction and removal of adsorptive is highly recommended.

Let us now consider the *continuous, quasi-equilibrium procedures*. Since the safest and simplest check is to look for the superimposition of two successive adsorption isotherms, this requires one to be able to operate at two different flow rates and, if necessary, to reduce the rate until the test is satisfied. For this reason, it is inadvisable to employ any technique which would not allow the possibility of reducing the flow rate beyond the value finally selected. Also, equipment designed to maintain the pressure over the adsorbent at a predetermined level does not necessarily guarantee equilibrium conditions: again, this should be checked by two successive experiments using different flow rates.

3.4.6. Temperature

The *adsorption temperature* is the first, basic datum of an adsorption isotherm. It must be stable over the whole experiment (usually to within 0.1 K): in the case of nitrogen adsorption at 77 K, such a temperature fluctuation would produce a *c.* 10 mbar variation in the saturation pressure. In adsorption manometry, the adsorption

bulbs are usually immersed in a thermostat or cryostat with which they are in good thermal contact. In adsorption gravimetry, the situation is more complex, because of the poor thermal contact between the sample pan and the surroundings. This is especially critical when the adsorbent is at cryogenic temperatures. A systematic investigation (Partyka and Rouquerol, 1975) has shown that the thermal exchange in a balance can be significantly improved by using a relatively tall (e.g. 80 mm × 10 mm) blackened bucket and by placing black thermal shields above the bucket. Nevertheless, even with these precautions, if the pressure is below 10^{-2} mbar, it is virtually impossible to achieve good thermal equilibrium between the sample and a 77 K cryostat (cf. Figure 3.24). It follows that it is pointless to wait for equilibrium to be established until the pressure is at least 10^{-2} mbar. This limitation must be kept in mind when adsorption gravimetry is used to study the adsorption of nitrogen by ultramicroporous solids. Above 10^{-2} mbar, the sample is no more than 0.2 K warmer than the surrounding cryostat, but even this is enough to cut off a part of the adsorption isotherm close to saturation.

The *cabinet temperature* must also be kept constant, especially when the adsorptive reservoir is included in the calibrated part of the apparatus (as in Figures 3.3 and 3.4). The pressure transducers are very sensitive to temperature variation and it is preferable to have the transducer at the same temperature as the rest of the set-up rather than to use individually controlled heaters.

3.4.7. Pressure

Nowadays, *membrane capacitance pressure transducers* are the most widely used manometers for adsorption studies. A single pressure transducer can be chosen to cover a wide pressure range, but since they lose part of their performances over the lowest few percent of the range, it is usually advisable to have two (e.g. 0–10 and

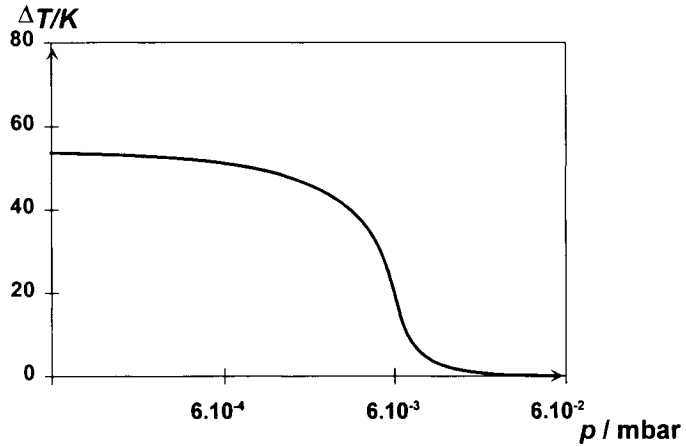

Figure 3.24. Gas adsorption gravimetry: temperature difference between sample and cryostat (at 77 K) as the vacuum around the sample is progressively reduced (after Rouquerol and Davy, 1978).

0–1000 mbar, for N_2 adsorption). It should also be noted that these transducers are fragile and that special care must be taken to avoid sudden pressure changes (this is the reason for the constrictions shown in Figure 3.2) or deposition of powder or condensation of liquid on the membrane.

For the measurement of low pressures (as required to investigate micropore filling or for krypton or xenon adsorption at 77 K), it may be necessary to take into account the phenomenon of 'thermomolecular flow' or 'thermal transpiration'. This happens when two parts of the equipment are maintained at different temperatures and they are connected by tubing in which the free mean path of the gas molecules is of the order of magnitude of (or above) the tube diameter. The phenomenon results in a steady pressure difference between the ends of the tubing. According to Knudsen (1910), when the mean free path is several times the tube diameter, the pressure ratio is given by the simple relationship:

$$\frac{p_B}{p_G} = \sqrt{\frac{T_B}{T_G}} \tag{3.4}$$

where subscripts B and G stand for 'sample bulb' and 'pressure gauge', respectively. Thus with a sample bulb at 77 K and a pressure gauge at 300 K, the pressure measured by the gauge is nearly twice the true pressure above the sample! In intermediate situations, this effect is smaller and directly depends on the relative size of the mean free path and tube diameter. In these conditions, empirical equations have to be used to estimate the pressure ratio. The most popular equation (Takaishi and Sensui, 1963) employed at present can be written as follows:

$$\frac{p_B}{p_G} = 1 + \frac{\sqrt{T_B/T_G} - 1}{10^5 AX^2 + 10^2 BX + C\sqrt{X} + 1} \tag{3.5}$$

where A, B and C are constants that depend on the gas (see Table 3.1), and

$$X = \frac{1.5 p_G D}{T_B + T_G} \tag{3.6}$$

where D is the diameter (in mm) of the tube (usually the 'neck' of the sample bulb), p_G is expressed in mbar, and T_B and T_G are in kelvins.

The results given in the lower part of Table 3.1 (methane and onwards) are considered to be less reliable, especially if they are to be used out of the T_B range over which the measurements were carried out (T_G is room temperature).

The direct determination of the saturation pressure of the adsorptive has the advantage of providing the real $p°$ and, with nitrogen, of allowing one to calculate the adsorption temperature to the nearest 0.01 K. Since the surface layer of a cryogenic liquid tends to become colder (because of evaporation) than the lower part of the liquid (Nicolaon and Teichner, 1968), it is necessary to condense the adsorptive in the bottom of a double-walled ampoule, so that the location of the condensation is very close to the adsorbent sample. Measurement of the sample temperature by means of a resistance thermometer is more straightforward, but requires calibration against the saturation vapour pressure thermometer.

Table 3.1. Thermal transpiration: coefficients of the Takaishi and Sensui equation, for various gases.

Gas	*A*	*B*	*C*	Temperature range (K)
Hydrogen	1.24	8.00	10.6	14–673
Neon	2.65	1.88	30.0	20.4–673
Argon	10.8	8.08	15.6	77–673
Krypton	14.5	15.0	13.7	77–673
Methane	14.5	15.0	13	473–673
Xenon	35	41.4	10	77–90
Helium	1.5	1.15	19	4.2–90
Nitrogen	12	10	14	77–195
Oxygen	8	17.5	–	90

3.4.8. Correction for non-ideality

At the temperatures normally used for physical adsorption, the correction for the non-ideality of real gases generally amounts to several percent. It can be reasonably taken into account by using the first two terms of the virial equation:

$$v^{\circ}_{\text{real}} = \frac{V}{n} = v^{\circ}_{\text{id}} + B_{\text{m}} \tag{3.7}$$

where v°_{real} and v°_{id} are the real and ideal molar volumes of the gas at a given temperature T and reference pressure (normally 1 bar), respectively, V is the total volume occupied by the given amount of gas, and B_{m} is the second molar virial coefficient, which is usually negative under the conditions of physisorption experiments. Its value for a large number of gases can be found in a critical compilation by Dymond and Smith (1969) and in the thermodynamic tables published by Marsh (1985).

To determine the real amount of gas present in a given volume V, at temperature T and pressure p, it is convenient to use the relation:

$$n = \frac{V}{T} \times \frac{273.15}{22711}\left(1 + \frac{\alpha p}{100}\right) \tag{3.8}$$

where V is expressed in cm^3 and p in bar and where $\alpha = -100B_{\text{m}}/v^{\circ}_{\text{id}} = -(10B_{\text{m}}/RT) \times p^{\circ}$.

Values of α for a number of gases and temperatures used in adsorption studies are given in Table 3.2. They were calculated with help of the data provided by Dymond and Smith (1969). A detailed study of the incidence of these corrections on the adsorption isotherms and the BET surface areas was made by Jelinek *et al.* (1990).

An elegant way to avoid this non-ideality correction, especially when operating at high pressures (up to 16.5 MPa), where it can become predominant, was proposed by Bose *et al.* (1987). In their method, for each equilibrium point the density of the adsorptive is determined experimentally from its dielectric constant, which is measured in a gas capacitance cell at the same temperature and pressure as the adsorption system studied. The rest of their adsorption procedure is comparable to the

Table 3.2. Correction for non-ideality for a few gases commonly used in adsorption experiments.

Gas	Formula	T (K)	α = % correction
Nitrogen	N_2	77.3	4.0
		90.0	3.1
Argon	Ar	77.3	4.8
		90.0	3.6
Oxygen	O_2	77.3	5.1
		90.0	3.8
Helium	He	77.3	0.2
Carbon monoxide	CO	77.3	1.3
Ammonia	NH_3	273.15	1.5
		298.15	1.2
Neopentane	$(CH_3)_4C$	273.15	4.4
		298.15	3.9
n-Butane	C_4H_{10}	273.15	4.1
		298.15	3.2

discontinuous manometric procedure (see Section 3.3.1), the dosing volume being made up of the gas capacitance cell at the temperature of the adsorbent.

3.4.9. Presentation and use of the experimental data

The raw experimental data (temperatures, pressures, flow-rates, equilibration times, sample treatment) should be stored, together with all calibration data of the set-up. It is highly desirable to plot the adsorption isotherm as soon as possible and preferably during the experiment itself.

The commercial software generally includes a smoothing procedure in the first processing stage of the experimental data. This certainly improves the appearance of the data and may be useful for routine measurements, but the smoothing tends to hide systematically small events (including small phase changes) which may be highly informative about the mechanism of adsorption. It is therefore preferable to store the data in their raw form, before any smoothing has been applied, so that the experimental results are available for subsequent analysis.

References

Ajot H., Joly J.F., Raatz F. and Russmann C. (1991) In: *Studies in Surface Science and Catalysis*, vol. 62, Elsevier, Amsterdam, p. 161.
Atkins J.H. (1964) *Anal. Chem.* **36**, 579.
Beebe R.A., Low G.W. and Goldwasser S. (1936) *J. Am. Chem. Soc.* **58**, 2196.
Bose T.K., Chahine R., Marchildon L. and St Arnaud J.M. (1988) *Rev. Sci. Instrum.* **58**(12), 2279.
Bunsen R.W. (1870) *Ann. Phys.* **141**, 1.
Calvet E. and Prat H. (1958) *Récents Progrès en Microcalorimétrie*, Dunod, Paris.
Calvet E. and Prat H. (1963) *Recent Progress in Microcalorimetry*, Pergamon Press, Oxford.
Camp R.W. and Stanley H.D. (1991) *American Laboratory* September, p. 34.
Dash J.G. (1975) *Films on Solid Surfaces*, Academic Press, New York.

Della Gatta G., Fubini B. and Venturello G. (1977) In: *Thermochimie*, Colloques Internationaux du CNRS, no. 201, Editions du CNRS, Paris, p. 565.
Dewar J. (1904) *Proc. Roy. Soc. A* **74**, 122.
Dreisbach F., Staudt R., Tomalla M. and Keller, J.U. (1996) In: *Fundamentals of Adsorption V* (M.D. Le Van, ed.), Kluwer, Dordrecht, p. 259.
Dunne J.A., Mariwala R., Rao M., Sircar S., Gorte R.J. and Myers A.L. (1996) *Langmuir* **12**, 5888.
Dunne J.A., Rao, M., Sircar S., Gorte R.J. and Myers A.L. (1997) *Langmuir* **13**, 4333.
Dymond J.H. and Smith E.B. (1969) *The Virial Coefficient of Gases: A Critical Compilation*, Clarendon Press, Oxford.
Dzhigit O.M., Kiselev A.V. and Muttik G.G. (1962) *J. Phys. Chem.* **66**, 2127.
Emmett P.H. and Brunauer S. (1937) *J. Am. Chem. Soc.* **56**, 35.
Emmett P.H. (1942) *Adv. Colloid Sci.* **1**, 3.
Favre P.A. (1854) *C.R. Acad. Sci.* Paris **39**, 729.
Findenegg G. (1997) In: *Proceedings of NATO-ASI on Physical Adsorption: Experiments, Theory and Applications* (J. Fraissard, ed.), Kluwer Academic Publishers, Dordrecht, p. 151.
Gravelle P.C. (1972) *Adv. Catalysis* **22**, 191.
Grillet Y., Rouquerol J. and Rouquerol F. (1977a) *J. Chim. Phys.* **74**(2), 179.
Grillet Y., Rouquerol J. and Rouquerol F. (1977b) *J. Chim. Phys.* **74**(7–8), 778.
Groszek A.J. (1966) *Lubrication Sci. Technol.* **9**, 67.
Gruia M., Jarjoui M. and Gravelle P.C. (1976) *J. Chim. Phys.* **73**(6), 634.
Haul R. and Dümbgen G. (1960) *Chem. Ing. Tech.* **32**, 349.
Haul R. and Dümbgen G. (1963) *Chem. Ing. Tech.* **35**, 586.
Holmes J.M. and Beebe R.A. (1961) *Adv. Chem. Ser.* **33**, 291.
Innes W.B. (1951) *Anal. Chem.* **23**(5), 759.
Isirikyan A.A. and Kiselev A.V. (1962) *J. Phys. Chem.* **66**, 210.
Jelinek L., Dong P. and Kovats E. (1990) *Adsorption Sci. Tech.* **7**(3), 140.
Jones A., Firth J.G. and Jones T.A. (1975) *J. Phys. E.* **8**, 37.
Karp S., Lowell S. and Mustacciulo A. (1972) *Anal. Chem.* **44**, 2395.
Keller J.U. (1995) *Adsorption* **1**, 283.
Keller J.U., Staudt R. and Tomalla M. (1992) *Ber. Bunsenges. Phys. Chem.* **96**(1), 28.
Kington G.L. and Smith P.S. (1964) *J. Sci. Instrum.* **41**, 145.
Knudsen M. (1910) *Ann. Physik* **31**, 210, 633.
Krim J. and Watts E.T. (1991) In: *Third International Conference on Fundamentals of Adsorption* (A.B. Mersmann and S.E. Scholl, eds), Engineering Foundation, New York, p. 445.
Kubaschewski O. and Hultgren R. (1962) In: *Experimental Thermochemistry*, vol. II (H.A. Skinner, ed.), Interscience Publishers, London, p. 351.
Lange K.R. (1963) *J. Colloid Sci.* **18**, 65.
Lavoisier A.L. and de Laplace P.S. (1783) In: *Mémoire sur la chaleur*, C. R. Académie Royale des Sciences, 28 June.
Le Parlouer (1985) *Thermochimica Acta* **92**, 371.
McBain J.W. and Bakr A.M. (1926) *J. Am. Chem. Soc.* **48**, 690.
Marsh K.N. (1985) *TRC – Thermodynamics Tables*, Texas Engineering Experimental Station, College Station, TX.
Mikhail R.S. and Robens E. (1983) In: *Microstructure and Thermal Analysis of Solid Surfaces*, John Wiley & Sons, Chichester, p. 388.
Morrison J.A., Drain L.E. and Dugdale J.S. (1952) *Can. J. Chem.* **30**, 890.
Morrison J.A. (1987) *Pure Appl. Chem.* **59**(1), 7.
Neimark A.V. and Ravikovitch P.I. (1997) *Langmuir* **13**, 5148.
Nelsen F.M. and Eggertsen F.T. (1958) *Anal. Chem.* **30**, 1387.
Nicolaon G.A. and Teichner S.J. (1968) *J. Chim. Phys.* **64**, 870.
Partyka S. and Rouquerol J. (1975) In: *Progress in Vacuum Microbalance Techniques*, vol. 3 (C. Eyraud and M. Escoubès, eds), Heyden, London, p. 83.
Pieters, W.J.M. and Gates W.E. (1984) US Patent 4 **489**, 593.
Rouquerol J. (1970) *J. Therm. Anal.* **2**, 123.

Rouquerol J. (1972) In: *Thermochimie*, Colloques Internationaux du CNRS, no. 201, Editions du CNS, Paris, p. 537.
Rouquerol J. and Davy L. (1978) *Thermochim. Acta* **24**, 391.
Rouquerol F., Rouquerol J. and Everett D. (1980) *Thermochim. Acta* **41**, 311.
Rouquerol J., Rouquerol F., Grillet Y. and Triaca M. (1986) *Thermochim. Acta* **103**, 89.
Rouquerol J., Rouquerol F., Grillet Y. and Ward R.J. (1988) In: *Characterization of Porous Solids* (K.K. Unger *et al.*, eds), Elsevier Science Publishers, Amsterdam, p. 317.
Rouquerol J. (1989) *Thermochim. Acta* **144**, 209.
Rouquerol J. and Davy L. (1991) French Patent on device for integral and continuous measurement of gas adsorption and desorption, filed 25/10/1991.
Schlosser E.G. (1959) *Chem. Ing. Tech.* **31**, 799.
Takaishi T. and Sensui Y. (1963) *Trans. Faraday Soc.* **59**, 2503.
Tian A. (1923) *Bull. Soc. Chim. Fr.* **33**(4), 427.
Venero A.F. and Chiou J.N. (1988) *Proc. Materials Research Society: microstructure properties and catalysis* **111**, 235.
Webb P.A. (1992) *Powder Handling and Processing* **4**(4), 439.

CHAPTER 4

Interpretation of Physisorption Isotherms at the Gas–Solid Interface

4.1. Introduction

As explained in Chapter 1, the shape of an adsorption isotherm provides useful preliminary information concerning the mechanisms of physisorption, and hence the nature of the adsorbent. For example, a reversible Type II adsorption–desorption isotherm is generally associated with the formation of an adsorbed layer which progressively thickens as the equilibrium pressure is increased up to the saturation pressure: this form of monolayer–multilayer physisorption is observed on an open and stable surface of a non-porous adsorbent.

The physisorption isotherm on a mesoporous or macroporous adsorbent follows the same monolayer–multilayer path as on the corresponding non-porous surface until the secondary process of capillary condensation occurs. In the case of a macroporous solid, the deviation from the standard monolayer–multilayer isotherm does not take place until very high relative pressures are attained (with nitrogen adsorption at 77 K, this would be at $p/p^\circ > 0.99$).

It was shown in Chapter 1 that enhanced adsorbent–adsorbate interactions occur in

pores of molecular dimensions and that the increased adsorption energy is largely responsible for the observed distortion of the initial part of the adsorption isotherm. Thus, the filling of narrow micropores takes place at very low $p/p°$. In the simplest case, physisorption by a microporous solid gives a Type I isotherm in the IUPAC classification. The nearly horizontal plateau is generally a clear indication of a very small external surface area.

The main purpose of the present chapter is to introduce the underlying principles which will serve as a basis for the discussion of physisorption isotherms presented in later chapters. It is not our intention to give a general survey of the theories of physisorption at the gas–solid interface; instead, our aim is to provide sufficient information to enable the newcomer to surface science to appreciate the advantages and limitations of the most widely used procedures for the analysis of experimental adsorption isotherms. Our selection of theoretical material is necessarily somewhat arbitrary in view of the vast literature on physisorption. The decision to include a particular concept or equation is based on either its historical importance or its current usage. Thus, a few equations were considered worthy of inclusion in this chapter, although for our purpose they do not merit further discussion or application in subsequent chapters.

Capillary condensation *per se* is not discussed in this chapter since it involves the formation of a liquid-like meniscus. This aspect of physisorption by the filling of mesopores is dealt with in Chapter 7 in relation to the assessment of the mesopore size distribution.

4.2. Physisorption isotherms on non-microporous solids

4.2.1. Henry's law and virial equations

The simplest interpretation of the behaviour of the adsorbed phase is to suppose that, at very low surface excess concentration, the adsorbate molecules are independent of each other. By assuming that the dilute adsorbed phase behaves as a two-dimensional ideal gas, regardless of the nature of the adsorption, we may write the limiting equation of state in the form

$$\Pi A = nRT \tag{4.1}$$

where Π is the spreading pressure, as defined by Equation (2.22).

From Equations (4.1) and (2.33), we obtain

$$n = k_H p \tag{4.2}$$

where n is used to represent the specific surface excess amount (cf. Chapter 2) and k_H is generally known as the Henry's law constant. Thus, at sufficiently high temperatures and sufficiently low pressures, n, or the surface excess concentration, Γ, should vary linearly with the equilibrium gas pressure.

It is possible to obtain the differential enthalpy of adsorption at 'zero' coverage, $\Delta_{ads}\dot{h}_o$, from the variation of the Henry's law constant with temperature, since from

Equation (2.68)

$$\Delta_{ads}\dot{h}_o = RT^2(\partial(\ln k_H)/\partial T)_n \tag{4.3}$$

The evaluation of $\Delta_{ads}\dot{h}_o$ is achieved by plotting ln $[k_H]$ against $1/T$, provided that $\Delta_{ads}\dot{h}_o$ remains constant over the temperature range studied.

Although the initial Henry's law region is well documented with some physisorption isotherms, there are others which deviate from linearity at the lowest pressures so far recorded. Convex curvature with respect to the adsorption axis in this region is likely to be due to the effect of either surface heterogeneity or microporosity. In particular, specific adsorbent–adsorbate interactions are often associated with energetic heterogeneity and it is not surprising to find that the corresponding isotherms tend to be non-linear at low surface coverage. In some cases, a small knee is evident at very low $p/p°$ and then the isotherm becomes linear over an appreciable range of higher $p/p°$. If adsorption energy data are also available, it can be established whether the knee is associated with adsorption on a small high-energy fraction of the surface or whether adsorbate–adsorbate interactions are detectable over the linear range.

A number of different empirical equations have been proposed to allow for the deviations of physisorption isotherms from Henry's law. An approach which is analogous to that used in the treatment of imperfect gases and non-ideal solutions is to adopt a virial treatment. Kiselev and his co-workers (Avgul *et al.* 1973) favoured the form

$$p = \boldsymbol{n} \exp (C_1 + C_2\boldsymbol{n} + C_3\boldsymbol{n}^2 + \cdots) \tag{4.4}$$

where the coefficients (C_1, C_2, C_3) are characteristic constants for a given gas–solid system and temperature. An alternative, and in some respects more useful, linear form (Cole *et al.*, 1974) is:

$$\ln (\boldsymbol{n}/p) = K_1 + K_2\boldsymbol{n} + K_3\boldsymbol{n}^2 + \cdots \tag{4.5}$$

Thus, by extrapolation of the virial plot of ln $(\boldsymbol{n}/p)$ versus $\boldsymbol{n}$, it is possible to obtain k_H, since

$$k_H = \lim_{p \to 0} (\boldsymbol{n}/p) \tag{4.6}$$

The advantage of using Equation (4.5) is that the linearity of the semi-logarithmic plot generally extends well above the Henry's law limit and therefore the evaluation of k_H by extrapolation is more reliable.

Virial treatment provides a general method of analysing the low-coverage region of an adsorption isotherm and its application is not restricted to particular mechanisms or systems. If the structure of the adsorbent surface is well defined, virial treatment also provides a sound basis for the statistical mechanical interpretation of the adsorption data (Pierotti and Thomas, 1971; Steele, 1974). As indicated above, K_1 in Equation (4.5) is directly related to k_H and therefore, under favourable conditions, to the gas–solid interaction.

In the simplest case of the adsorption of a spherical non-polar molecule on a

smooth, energetically uniform surface, k_H is given by the configurational integral

$$k_H = \frac{1}{kT}\int_V [\exp(-\phi(z)/kT) - 1]\,dz \tag{4.7}$$

where $\phi(z)$ is the potential energy of adsorption expressed as a function of the distance z of the adsorbed molecule from the surface plane. In this case it is assumed that ϕ is independent of the location in the xy plane (i.e. the plane parallel to the surface), but a position vector must be introduced in the more general treatment.

The higher coefficients in Equations (4.4) and (4.5) are more complex and depend on 'mixed' interactions between the adsorbed molecules and with the adsorbent. Although a good deal of attention has been given to the difficult problems associated with surface heterogeneity (Rudzinski and Everett, 1992), the theoretical interpretation of the derived virial coefficients remains speculative.

4.2.2. The Hill–de Boer equation

If one pictures the adsorbed monolayer as a two-dimensional imperfect gas, it seems reasonable to assume the applicability of a two-dimensional form of the van der Waals equation in which the gas pressure is replaced by the spreading pressure and the volume by the surface area. By combining this with the Gibbs adsorption equation – Equation (2.34) – de Boer (1968) obtained the equation

$$p = \frac{\theta}{k_H(1-\theta)}\exp\left(\frac{\theta}{1-\theta} - k_2\theta\right) \tag{4.8}$$

where θ is the surface coverage, k_H is the Henry's law constant, and k_2 is a second empirical constant. A similar form of equation was proposed independently by Hill and therefore Equation (4.8) is generally known as the Hill–de Boer equation.

Equation (4.8) may be rearranged to give the linear form

$$\begin{aligned} k_2\theta + \ln k_H &= \frac{\theta}{1-\theta} + \ln\left(\frac{\theta}{1-\theta}\right) - \ln[p] \\ &= W(p,\theta) \end{aligned} \tag{4.9}$$

Accordingly, the plot of W against θ should provide a means of obtaining k_H and k_2. However, this obviously requires prior knowledge of the monolayer capacity, n_m, since $\theta = n/n_m$.

We have seen already that the surface of graphitized carbon black is energetically remarkably homogeneous and therefore we would expect it to be a suitable substrate for testing the validity of the Hill–de Boer equation. A number of investigators have reported an appreciable range of fit of Equation (4.8), although generally this is not found above $\theta = 0.5$ (Sing, 1973).

Broekhoff and van Dongen (1970) suggested that it is not appropriate to use the BET monolayer capacity to calculate θ. Instead, they proposed that appropriate values of the three adjustable parameters (θ, k_H and k_2) should be selected to obtain the best fit. When applied in this manner, Equation (4.8) was claimed to be a useful

empirical relation and applicable to a wide range of isotherms on graphitized carbon.

Several attempts have been made to extend the application of the Hill–de Boer equation to heterogeneous surfaces, following the approach originally adopted by Ross and Olivier (1964). The surface is pictured as an assembly of small uniform patches. The Hill–de Boer equation is used to describe the form of the isotherm on each 'homotattic' patch and the weighted sum is then employed to give the composite isotherm for the heterogeneous surface. This approach has led to extensive interest in the effects of surface heterogeneity on the physisorption of gases (Rudzinski and Everett, 1992).

4.2.3. The Langmuir theory

Although the simple Langmuir equation is more applicable to some forms of chemisorption, the underlying theory is of great historical importance and has provided a starting point for the development of the BET treatment and of other more refined physisorption isotherm equations. It is therefore appropriate to consider briefly the mechanism of gas adsorption originally proposed by Langmuir (1916, 1918).

The original derivation of the Langmuir equation (Langmuir, 1916) is a kinetic one. The adsorbent surface is pictured as an array of N^s equivalent and independent sites for localized adsorption (one molecule per site). The fraction of sites occupied by N^a molecules is $\theta = N^a/N^s$.

From the kinetic theory of gases, the rate of adsorption is dependent on the pressure and the fraction of bare sites $(1 - \theta)$. The rate of desorption is dependent on θ and on the energy of activation, E (i.e. equivalent to an energy of adsorption expressed as a positive quantity). Equilibrium is obtained for the values of θ and p for which the rates of adsorption and desorption are equal. Thus, the net rate of adsorption is zero:

$$\frac{dN^a}{dt} = \alpha p(1 - \theta) - \beta\theta \exp\left(-\frac{E}{RT}\right) = 0 \tag{4.10}$$

where α and β are characteristic constants for the given gas–solid system.

If, in an ideal case, the probability of desorption of an adsorbed molecule from the surface is independent of the surface coverage (i.e. there are no lateral interactions between the adsorbed molecules), then the value of E is constant for a particular adsorption system. Equation (4.10) is then applicable over the complete range of monolayer coverage. By rearrangement and simplification of Equation (4.10), we arrive at the familiar Langmuir isotherm equation,

$$\theta = bp/(1 + bp) \tag{4.11}$$

where b, the 'adsorption coefficient', is exponentially related to the positive value of the energy of adsorption, E, as

$$b = K \exp(E/RT) \tag{4.12}$$

Here the pre-exponential factor, K, is equal to the ratio of the adsorption and desorption coefficients, α/β. Alternatively, b may be regarded as a function of the enthalpy and entropy of adsorption (Everett, 1950; Barrer, 1978, p. 117).

In his early treatment, Langmuir assumed that the energy of adsorption for the first layer is generally considerably larger than for the second and higher layers, and therefore multilayer formation is possible only at much greater pressures than the pressure required for monolayer completion. Thus, the formation of second or higher layers would be indicated by the appearance of a discontinuous isotherm. In fact, this situation does arise in the case of a stepwise, Type VI, isotherm. However, the lateral adsorbate–adsorbate interactions, which are associated with all known stepwise isotherms, are not compatible with the Langmuir model.

It is evident that Equation (4.11) is of a very general mathematical form (i.e. a hyperbolic function). At low θ it reduces to Henry's law; at high surface coverage, a plateau is reached as $\theta \longrightarrow 1$. Other equations of the same mathematical form as Equation (4.11) have been derived from a classical thermodynamic standpoint (Brunauer, 1945) and by application of the principles of statistical mechanics (Fowler, 1935).

Equation (4.11) is usually applied in the linear form

$$p/\boldsymbol{n} = 1/\boldsymbol{n}_{\mathrm{m}}b + p/\boldsymbol{n}_{\mathrm{m}} \tag{4.13}$$

where $\boldsymbol{n}$ is the specific amount of gas adsorbed at the equilibrium pressure p and $\boldsymbol{n}_{\mathrm{m}}$ is the monolayer capacity (as before, $\theta = \boldsymbol{n}/\boldsymbol{n}_{\mathrm{m}}$).

Many systems give linear plots of $p/\boldsymbol{n}$ against p over a limited ranges of pressure, but such linearity does not by itself imply conformity with the Langmuir model. As already indicated, a second condition is that the energy of adsorption should be independent of surface coverage. Thirdly, the differential entropy of adsorption should vary in accordance with the ideal localized model (Everett, 1950). That no real system has been found to satisfy all these requirements is not surprising in view of the complexities noted here and in subsequent chapters.

Various attempts have been made to modify the Langmuir model. One of the best known is that of Fowler and Guggenheim (1939), which allowed for adsorbate–adsorbate interactions in a localized monolayer on a uniform surface. However, on an empirical basis the Fowler–Guggenheim equation turns out to be no more successful than the original Langmuir isotherm. The highly complex problem of localized adsorption on heterogeneous surfaces has been discussed by Rudzinski and Everett (1992).

4.2.4. The Brunauer–Emmett–Teller (BET) theory

By introducing a number of simplifying assumptions, Brunauer, Emmett and Teller (1938) were able to extend the Langmuir mechanism to multilayer adsorption and obtain an isotherm equation (the BET equation), which has Type II character. The original BET treatment involved an extension of the Langmuir kinetic theory of monomolecular adsorption to the formation of an infinite number of adsorbed layers.

According to the BET model, the adsorbed molecules in one layer can act as

adsorption sites for molecules in the next layer and, at any pressure below the saturation vapour pressure p° fractions of the surface (θ_0, θ_1, θ_2, ..., θ_i, ...) are covered by 0, 1, 2, ..., i, ... layers of adsorbed molecules (θ_0 of course, represents the fraction of bare surface). It follows that the adsorbed layer is envisaged not to be of uniform thickness, but instead to be made up of random stacks of molecules.

If it is assumed that at equilibrium, characterized by the pressure p, the fractions of bare and covered surface, θ_0 and θ_1, remain constant, we can equate the rate of condensation on the bare surface to the rate of evaporation from the first layer:

$$a_1 p\theta_0 = b_1\theta_1 \exp\left(-\frac{E_1}{RT}\right) \tag{4.14}$$

where a_1 and b_1 are adsorption and desorption constants for the first layer and E_1 is the positive value of the so-called 'energy of adsorption in the first layer'. It is assumed that a_1, b_1 and E_1 are independent of the quantity of adsorbed molecules already present in the first layer, i.e. as in the Langmuir mechanism, no allowance being made for lateral adsorbate–adsorbate interactions.

In the same way, at the equilibrium pressure p, the fractions of the surface $\theta_2, \theta_3, \ldots, \theta_i, \ldots$ must also remain constant and we may therefore write:

$$a_2 p\theta_1 = b_2\theta_2 \exp\left(-\frac{E_2}{RT}\right) \tag{4.15}$$

$$a_3 p\theta_2 = b_3\theta_3 \exp\left(-\frac{E_3}{RT}\right) \tag{4.16}$$

$$\vdots \qquad \vdots$$

$$a_i p\theta_{i-1} = b_i\theta_i \exp\left(-\frac{E_i}{RT}\right) \tag{4.17}$$

where θ_{i-1} and θ_i represent respectively the fractions of surface covered by $i-1$ and i layers; a_i and b_i are adsorption and desorption constants; and E_i is the energy of adsorption in the ith layer.

The sum of the fractions of surface equals unity:

$$\theta_0 + \theta_1 + \cdots + \theta_i + \cdots = 1 \tag{4.18}$$

Moreover, the total adsorbed amount can be expressed as:

$$n = n_m[1\theta_1 + 2\theta_2 + \cdots + i\theta_i + \cdots] \tag{4.19}$$

In principle, each adsorbed layer has a different set of values of a_i, b_i and E_i, but the derivation of the BET isotherm equation is dependent on two main assumptions:

(a) In the second and all higher layers, the energy of adsorption E_i has the same value as the liquefaction energy, E_L, of the adsorptive (i.e. $E_2 = E_i = E_L$).
(b) The multilayer has infinite thickness at $p/p^\circ = 1$ ($i = \infty$).

Let

$$\frac{b_2}{a_2} = \frac{b_3}{a_3} = \cdots = \frac{b_i}{a_i} = g \tag{4.20}$$

where g is a constant, since all the layers (except the first) have the same properties. We can now express $\theta_1, \theta_2 \ldots \theta_i, \ldots$ in terms of θ_0:

$$\theta_1 = y\theta_0 \qquad \text{where } y = \frac{a_1}{b_1} p \exp\left(\frac{E_1}{RT}\right) \tag{4.21}$$

$$\theta_2 = x\theta, \qquad \text{where } x = \frac{p}{g} \exp\left(\frac{E_L}{RT}\right) \tag{4.22}$$

$$\theta_3 = x\theta_2 = x^2\theta \tag{4.23}$$

$$\vdots \quad \vdots \quad \vdots$$

$$\theta_i = x^{i-1}\theta_1 = yx^{i-1}\theta_0 \tag{4.24}$$

We may define a constant C so that:

$$C = \frac{y}{x} = \frac{a_1}{b_1} g \exp\left(\frac{E_1 - E_L}{RT}\right) \tag{4.25}$$

then:

$$\theta_i = Cx^i\theta_0 \tag{4.26}$$

So we can write:

$$\frac{n}{n_m} = \sum_{i=1}^{\infty} i\theta^i = C \sum_{i=1}^{\infty} ix^i \times \theta_0 \tag{4.27}$$

Taking account of the value of the sum of an infinite geometric progression:

$$\sum_{i=1}^{\infty} x^i = \frac{x}{1-x} \tag{4.28}$$

and of the value of the term $\sum_{i=1}^{\infty} ix^i$:

$$\sum_{i=1}^{\infty} ix^i = \frac{x}{(1-x)^2} \tag{4.29}$$

and since $\theta_0 = 1 - \sum_1^{\infty} \theta_i$, we obtain from Equations (4.26) and (4.27):

$$\frac{n}{n_m} = \frac{Cx}{(1-x)(1-x+Cx)} \tag{4.30}$$

Since at the saturation vapour pressure $p°$, the total adsorbed amount is supposed

infinite, it follows that $x = 1$ and (from Equation 4.22) that:

$$x = \frac{p}{p^\circ} \tag{4.31}$$

Equation (4.30) can now be written in the usual form:

$$\frac{p}{n(p^\circ - p)} = \frac{1}{n_m C} + \frac{C-1}{n_m C} \times \frac{p}{p^\circ} \tag{4.32}$$

This 'linear transformed BET equation', provides the basis for the BET plot of experimental isotherm data (cf. Chapter 6).

The constant C, which is strictly given by Equation (4.25), is often assumed to be exponentially related to E_1 by the simplified equation:

$$C \approx \exp\left(\frac{E_1 - E_L}{RT}\right) \tag{4.33}$$

Here, E_1 is defined as a positive quantity and interpreted by Brunauer (Brunauer, 1945, p.158) as the 'average heat of adsorption on the *less active* part of the adsorbing surface'.

Originally $E_1 - E_L$ was known as the 'net heat of adsorption' (Lamb and Coolidge, 1920). It is now recommended that the more general term 'net molar energy of adsorption' should be adopted (cf. Chapter 2).

An alternative and elegant derivation of the BET equation is by a statistical mechanical treatment (Hill, 1946; Steele, 1974). The adsorbed phase is pictured as a lattice gas: that is molecules are located at specific sites in all layers. The first layer is localized and these molecules act as sites for molecules in the second layer, which in turn act as sites for molecules in the third layer, and so on for the higher layers. As the surface is assumed to be planar and uniform, it follows that all surface sites are identical. It is also assumed that the occupation probability of a site is independent of the occupancy of neighbouring sites. This is equivalent to the assumption that there are no lateral interactions between adsorbed molecules. In accordance with the BET model, the probability for site occupation is zero unless all its underlying sites are occupied. Furthermore, it is assumed that it is only the molecular partition function for the first layer which differs from that for molecules in the liquid state.

The statistical thermodynamic treatment of the BET theory has the advantage that it provides a satisfactory basis for further refinement of the theory by, say, allowing for adsorbate–adsorbate interactions or the effects of surface heterogeneity. By making the assumptions outlined above, Steele (1974) has shown that the problems of evaluating the grand partition function for the adsorbed phase could be readily solved. In this manner, he arrived at an isotherm equation, which has the same mathematical form as Equation (4.32). The parameter C is now defined as the ratio of the molecular partition functions for molecules in the first layer and the liquid state.

As mentioned above, the mathematical form of Equation (4.32) gives a curve having the general shape of a Type II isotherm, which has also been called an S-shaped, or sigmoid, isotherm (Brunauer, 1945). However, if $C < 2$, the shape is

changed and the point of inflection is lost. The BET equation then gives a Type III isotherm. In practice, the range of validity of Equation (4.32) is always confined to a limited part of the isotherm.

If the adsorption at saturation is restricted to a finite number of layers, N, the BET treatment leads to a modified equation which includes this additional parameter (cf. Chapter 6). Naturally, in the special case when $N = 1$, the extended BET equation corresponds to the Langmuir equation.

The BET model appears to be unrealistic in a number of respects. For example, in addition to the Langmuir concept of an ideal localized monolayer adsorption, it is assumed that all the adsorption sites for multilayer adsorption are energetically identical and that all layers after the first have liquid-like properties. It is now generally recognized that the significance of the parameter C is oversimplified and that Equation (4.33) cannot provide a reliable evaluation of E_1.

A recent molecular simulation study (Seri-Levy and Avnir, 1993) has also revealed the artificial nature of the BET model and has illustrated the effect of taking adsorbate–adsorbate interactions into account. Thus, the addition of lateral interactions appears to flatten the BET stacks into more realistically shaped islands.

In spite of the inadequacy of the underlying theory, the BET equation remains the most used of all adsorption isotherm equations. The reasons for this situation and the advantages and limitations of the BET method are discussed in Chapter 6.

4.2.5. Multilayer equations

An extension to the BET model was put forward by Brunauer, Deming, Deming and Teller (BDDT) in 1940. The BDDT equation contains four adjustable parameters and was designed to fit the isotherm Types I–V. From a theoretical standpoint, the BDDT treatment appears to offer very little more than the original BET theory and the cumbersome equation has very rarely been applied to experimental data.

Several other attempts have been made to modify the BET equation in order to improve the agreement with isotherm data in the multilayer region. Brunauer *et al.* (1969) pointed out that the BET assumption of an infinite number of molecular layers at saturation pressure is not always justified. By replacing p by kp, where k is an additional parameter with a value less than unity, they arrived at the following equation, which has the same form as that originally proposed by Anderson (1946):

$$\frac{kp}{n(p^\circ - kp)} = \frac{1}{n_m C} + \frac{(C-1)}{n_m C} \times \frac{kp}{p^\circ} \tag{4.34}$$

On an empirical basis, this Anderson–Brunauer equation can be applied to some isotherms (e.g. nitrogen and argon at 77 K on various non-porous oxides) over a much wider range of p/p° than the original BET equation.

When the adsorbate reaches a thickness of several molecular layers, the effects of surface heterogeneity are considerably reduced. If the temperature is not too low, some – but not all – multilayers appear to undergo a continuous increase in thickness as the pressure approaches saturation and bulk behaviour is gradually developed (Venables *et al.*, 1984). With such systems, it seems reasonable to assume that the

molar entropy of the thick multilayer is the same as that of the bulk liquid. In that case, the course of the isotherm would be determined solely by the energy of adsorption.

By assuming that the dispersion interactions are dependent on z^{-3} (i.e. by integration of the additive r^{-6} terms), Hill (1952) arrived at the multilayer isotherm equation

$$\ln (p^\circ/p) = k/\theta^3 \tag{4.35}$$

where k is a constant for a given gas–solid system.

Because of the experimental difficulty of making accurate measurements at very high p/p°, it is not easy to verify this expression. However, a more general equation,

$$\ln (p^\circ/p) = k/\theta^s \tag{4.36}$$

in which the parameter s is a non-integer, has been found to be more readily applicable (Steele, 1974). Although it was first proposed by Halsey (1948), Equation (4.36) is now known as the Frenkel–Halsey–Hill (FHH) equation and the widely used plot of log [log (p°/p)] against log (n) is generally referred to as the FHH plot.

Nitrogen isotherms (at 77 K) on non-porous oxides and carbons have been found to give linear FHH plots over a wide range of p/p°, corresponding to *c.* 1.5–3 molecular layers (Carrott and Sing, 1989). With these systems, the individual values of s are remarkably constant. Other adsorptives, such as hydrocarbons and water vapour, give values of s which appear to depend on the surface structure of the adsorbent.

Rudzinski and Everett (1992, p. 368) have drawn attention to a possible relation between the value of s and the degree of surface heterogeneity. The interesting suggestion is made that an increase in heterogeneity is likely to extend the range of influence of the surface on the multilayer structure, consequently causing a reduction in the value of s. However, more evidence is required to test this hypothesis.

In spite of its semi-empirical origin, the FHH equation does provide a means of identifying the different effects of micropore and mesopore filling (Carrott *et al.*, 1982). Capillary condensation in mesopores necessarily restricts the range of linearity of the FHH plot and tends to reduce the value of s. Although micropore filling may not significantly affect the linearity of the FHH plot, it does lead to an increase in s. These aspects are discussed in relation to fractal analysis in a recent paper by Sahouli *et al.* (1997).

4.3. Phase Changes in Physisorbed Layer

Since physisorbed molecules interact with each other, we would expect to find 2-D states and phase changes which are analogous to those found in 3-D condensed matter (Gregg, 1961, p. 62). However, we must keep in mind that the structure of a physisorbed layer is dependent, not only on the adsorbate–adsorbate interactions, but also on the magnitude and disposition of the adsorbent–adsorbate interactions.

It can be seen that 2-D phase changes are unlikely to be easily detectable unless the adsorbent surface is chemically and physically uniform. The early literature contains a number of claims for the existence of isotherm discontinuities, which appeared to

be associated with 2-D phase changes. Many of these discontinuities were subsequently thought to be spurious and were probably due to faulty technique (see Young and Crowell, 1962). However, the adsorption of CH_4 on MoS_2 was first shown by Bonnetain *et al.* (1952) to give a genuine stepwise isotherm. The existence of first-order 2-D phase changes was also firmly established by the work of Ross and Clark (1954), in which isotherms of C_2H_6 on cubic crystals of NaCl were measured at different temperatures.

Most of the well-documented investigations of 2-D phase changes have featured the adsorption of Ar, Kr and Xe on the basal, (0 0 0 1), face of graphite (see Dash, 1975; Suzanne and Gay, 1996), but detailed work has also been undertaken on a number of other systems such as Ar, Kr and CH_4 on layered halides (Larher, 1992) and cubic crystals of MgO (Coulomb *et al.*, 1984). In addition, phase diagrams have been constructed for the adsorption of certain polar molecules on graphite (Terlain and Larher, 1983).

In the systematic investigations undertaken by Thomy and Duval (1970; Thomy *et al.*, 1972) of krypton adsorption on exfoliated graphite, a series of isotherms was determined over the temperature range 77 to 100 K. Stepwise multilayer character

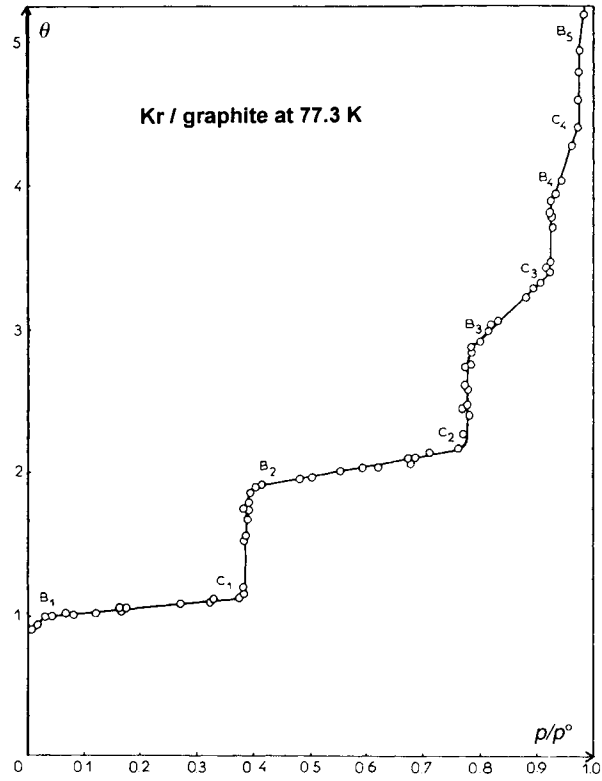

Figure 4.1. Complete adsorption isotherm of krypton on exfoliated graphite at 77.3 K (courtesy Thomy *et al.*, 1972).

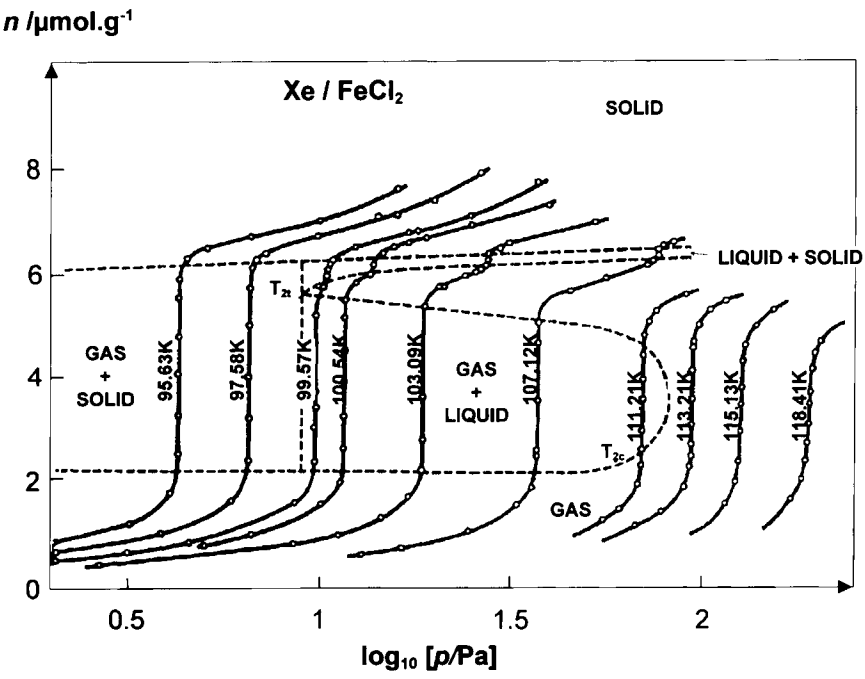

Figure 4.2. Adsorption isotherms of xenon on $FeCl_2$ (courtesy of Larher, 1992).

was displayed up to four molecular layers, as can be seen in Figure 4.1. Each vertical 'riser' (at constant $p/p°$) can be regarded as a phase transition between one adsorbed layer and the next higher layer.

In the sub-monolayer range, three distinctive regions were identified and attributed by Thomy and Duval to 2-D 'gas', 'liquid' and 'solid' phases. These measurements provided the first unambiguous evidence for the existence of sub-steps in the monolayer region of a stepwise, Type VI, isotherm.

To illustrate the interpretation of such sub-steps, the monolayer isotherms for the adsorption of Xe on $FeCl_2$ (Larher, 1992) are shown in Figure 4.2. At temperatures below 99.57 K, there is a single vertical step, which corresponds to the transformation of 2-D gas to the solid phase. Very little further compression of the monolayer is possible before its completion at Point B. A smaller sub-step becomes apparent at temperatures above 99.57 K. As a result of the careful studies of Thomy and Duval and Larher, the consensus interpretation is that this small sub-step represents a first-order transition between the 2-D liquid and solid phases. It is evident that, in the case of the $Xe/FeCl_2$ system, 99.57 K is the two-dimensional triple point.

Two-dimensional phase diagrams are often displayed in the form of ln $[p]$ against $1/T$ (at a constant specific amount adsorbed), which provides a convenient way of indicating the conditions for the coexistence of two phases (see Figure 4.3). Indeed, the application of the Phase Rule indicates that when two adsorbed phases coexist in equilibrium, the system has one degree of freedom: therefore, at constant

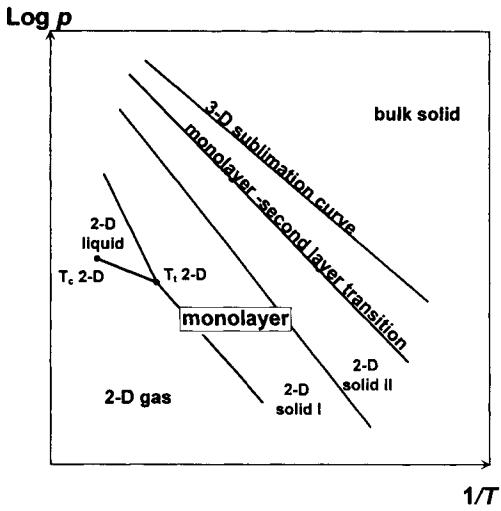

Figure 4.3. Phase diagram for physisorbed rare gas atoms or molecules on uniform solid surfaces such as the basal plane of graphite (after Suzanne and Gay, 1996).

temperature, the pressure must also remain constant. The co-existence of three adsorbed phases requires the loss of the one degree of freedom and the system then becomes invariant at the 2-D triple point.

The limiting temperature for 2-D condensation is the 2-D critical temperature, T_{2c}, which marks the upper limit for the first-order transition associated with the formation of a 'liquid' monolayer. According to Larher (1992), for the Xe/$FeCl_2$ system in Figure 4.3, $T_{2c} = 112$ K.

Larher (1992) has discussed certain aspects of the 2-D phase behaviour of different systems. If the adsorbate–adsorbate interaction is not perturbed to any significant extent by the adsorbent, the law of corresponding states should apply to 2-D systems. In that case, we would expect the ratio of the 2-D and 3-D critical temperatures, T_{2c}/T_{3c}, to be constant. It turns out that values close to $T_{2c}/T_{3c} = 0.39$ are obtained for Ar, Kr and Xe on certain layered chlorides (e.g. $NiCl_2$) and also for Ar, and Xe on the basal face of graphite. Larher concludes that the corresponding value of T_{2c} (i.e. $0.39T_{3c}$) can be regarded as an 'ideal' critical temperature for 2-D condensation on a smooth planar surface.

Higher values of T_{2c}/T_{3c} in the range 0.50–0.55 were reported for the adsorption of Ar on some other dihalides such as $CdBr_2$ and FeI_2 (Larher, 1992). In these cases there appeared to be a somewhat larger degree of incompatibility between the lattice parameters of the crystalline surface and the densest plane – the (1 1 1) plane – of the rare gas crystal. Larher suggests that within a certain range of size incompatibility the most useful quantitative description of monolayer condensation is by a lattice gas model.

Various particle scattering, electron and neutron diffraction and electron spectroscopic techniques have been used to study the structure of physisorbed monolayers

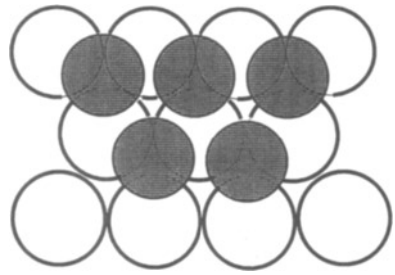

Figure 4.4. Representation of an epitaxial monolayer, i.e. in registry with the adsorbent structure.

(Block *et al.*, 1990). Heat capacity measurements have also provided strong evidence for the development of different 2-D solid structures. Epitaxial monolayers have been reported for some systems (see Dash, 1975) in which the adsorbed atoms are arranged in regular patterns in registry with adsorbent structure, as in Figure 4.4.

In recent years, a number of different 'commensurate' and 'incommensurate' monolayer structures have been identified (Suzanne and Gay, 1996). In the important case of the graphite (0 0 0 1) face, the commensurate hexagonal structure can be compared with 3-D (1 1 1) plane of the face-centred cubic (f.c.c.) structure of the rare gases. The lattice mismatch is small for Xe and Kr and much larger for Ar and Ne. The compression of the monolayer from a localized epitaxial state to the close-packed state was suggested as the origin of sub-steps given by Xe and Kr on graphite (Price and Venables, 1976). The argon sub-step at 77 K is more likely to be due to a transformation from the 2-D liquid to the solid (as in Figure 4.3). The latter system is discussed in more detail in Chapter 9.

Knowledge of the effective molecular area is of particular importance when gas adsorption is used for the determination of surface area (see Chapter 6). It is often assumed that the completed monolayer is in a 'liquid' close-packed state, but it is now apparent that we must question the soundness of this assumption. The recent studies of phase transitions and monolayer structures lead us to the conclusion that the degree of molecular packing is dependent on the adsorption system (both adsorbent and adsorptive) and the operational conditions of pressure and temperature (Steele, 1996).

4.4. Physisorption by Microporous Solids

4.4.1. Introduction

According to the IUPAC classification (Everett, 1972; Sing *et al.*, 1985), the upper limit of the internal micropore width is about 2 nm. A characteristic property of microporous adsorbents is that they give Type I physisorption isotherms (see Figure 1.7). As noted previously, the most distinctive feature of a Type I isotherm is the long, almost horizontal plateau, which extends across most, if not all, of the

multilayer range up to $p/p^\circ \longrightarrow 1$. This distinctive shape is generally considered to be a clear indication of a very small external surface area and of the absence of any significant mesoporosity.

That micropores are filled reversibly in the p/p° range below the normal onset of capillary condensation is now indisputable, but the mechanisms involved in micropore filling are still under discussion – as they have been for over 40 years. However, it is now apparent that the micropore filling process is dependent on both the ratio of the pore width to the molecular diameter (w/d) and the pore shape.

The close proximity of the pore walls in the narrowest micropores produces an increased adsorbent–adsorbate interaction energy and this in turn results in the distortion of the initial part of the isotherm. If the pore width w is no more than a few molecular diameters d, the enhanced interactions lead to complete pore filling at very low p/p°. In slit-shaped pores, the increased adsorption energy is unlikely to be significant beyond a pore width of about $2d$, whereas in cylindrical pores the enhancement may extend up to a pore diameter of $3–4d$ (see Figure 4.5; Everett and Powl, 1976).

The filling of these molecular-sized pores, which is associated with the isotherm distortion at very low p/p°, has been called 'primary micropore filling'. Wider micropores are filled by a 'secondary', or co-operative, process over a range of higher p/p° (Sing, 1979). These processes are discussed in some detail in subsequent chapters.

4.4.2. Henry's law and virial analysis

In the special case of the physisorption of a simple non-polar gas by a 'homogeneous' microporous solid, as Everett (1970) has pointed out, we may relate the Henry's law constant, k_H, to the potential energy of adsorption, ϕ, by an expression analogous to

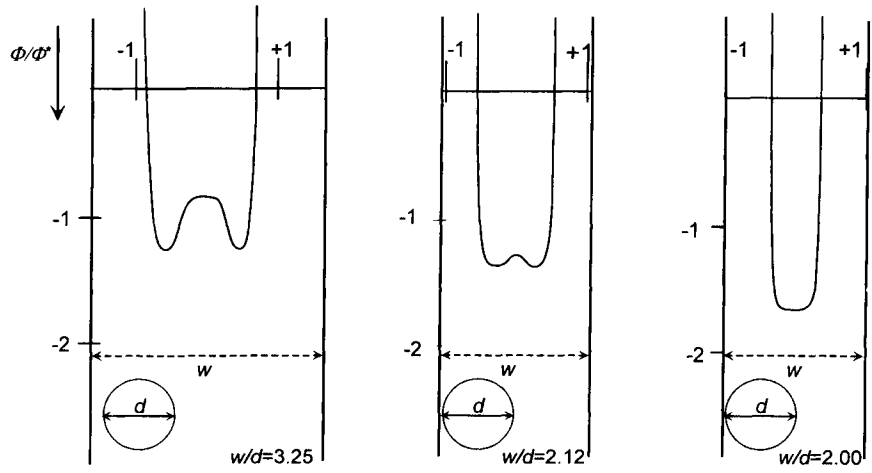

Figure 4.5. Enhancement of energy of adsorption Φ/Φ^* in slit-shaped pores of various widths (after Everett and Powl, 1976).

Equation (4.7). Assuming that ϕ is essentially constant within each pore, we have

$$k_H = \frac{v_p}{RT}\left[\exp\left(-\frac{\phi}{kT}\right) - 1\right] \tag{4.37}$$

where v_p is the accessible specific pore volume.

Since primary micropore filling is associated with high adsorption affinity, adsorption isotherm measurements at very low fractional pore filling are best made at elevated temperature. Unfortunately, the energetic heterogeneity exhibited by many microporous adsorbents results in isotherm curvature, even at the lowest recorded pressures. However, there are a few crystalline molecular sieves which have remarkably regular tubular pores and which have been found to give linear nitrogen isotherms over wide ranges of pressure at temperatures of around 300 K (Reichert *et al.*, 1991). In these cases, the Henry's law behaviour is consistent with a nearly constant adsorption energy over an appreciable range of fractional pore filling.

If the isotherm curvature is not too great, the simple virial plot of ln (n/p) versus n provides a useful means of obtaining k_H. Although the linear range of these plots is generally confined to very low values of n, the evaluation of k_H is achieved by extrapolation and the application of Equation (4.6) (Cole *et al.*, 1974; Carrott and Sing, 1989).

Avgul and Kiselev (1970), Barrer (1978) and others (Ruthven, 1984) have used equations of the virial form to analyse physisorption data obtained with molecular sieve zeolites. In their investigations of the adsorption of the noble gases and lower hydrocarbons, Avgul *et al.* (1973) were able to demonstrate that, at low pore filling/surface coverage, Equation (4.4) can be applied to the isotherms on both X-type zeolites and graphitized carbons. From an empirical standpoint this confirms the utility of the virial analysis of adsorption data, but it does not resolve the problems involved in the interpretation of the higher coefficients (Rudzinski and Everett, 1992).

4.4.3. The Langmuir–Brunauer theory

The fact that many Type I isotherms appear to obey a simple form of Langmuir equation – Equation (4.13) – over a wide range of pressure was for many years accepted as confirmatory evidence for the Langmuir model. According to this view (Brunauer, 1945), the limiting plateau would be the result of monolayer adsorption on the pore walls.

In practice, a long range of linearity of the plot of p/n against p may be somewhat misleading since the change in n may be quite small. A more rigorous test of the conformity of an experimental isotherm to Equation (4.11) is to plot the quotient $\theta/p(1-\theta)$ against θ. Such plots of the 'Langmuir quotient' have been constructed by Barrer (1978) for the adsorption of various gases by zeolites. In some cases the quotient remains almost constant over a wide range of θ, but a significant variation is generally observed – especially at lower temperatures. However, as pointed out earlier, even this test is insufficient to support the validity of the model because the

Langmuir equation contains the two disposable constants, n_m and b, which cannot be evaluated by any independent method.

It is now generally accepted that there is no sound reason why isotherms on microporous solids should conform any more closely to the classical Langmuir mechanism than isotherms on non-porous or mesoporous adsorbents. Indeed, a considerable amount of the evidence now available gives strong support to the view that the limiting uptake is controlled rather by the accessible micropore volume than by the internal surface area (Gregg and Sing, 1982).

In the context of gas separation (see Yang, 1987) or for some other purposes, it may be expedient to apply an equation of the Langmuir form; but we consider it advisable to treat this as empirical relation. Thus, we may write

$$\frac{n}{n_L} = \frac{bp}{1+bp} \tag{4.38}$$

where the parameters n_L and b are to be regarded as empirical constants within stated ranges of p and T.

We have concluded that the limiting uptake at the plateau of a Type I isotherm is not directly related to the surface area. However, it is now appropriate to return briefly to the initial stage of physisorption by microporous solids and consider the question: does monolayer adsorption ever precede micropore filling ?

Some time ago Brunauer (1970) argued that monolayer adsorption of nitrogen and other small molecules does occur on the walls of micropores wider than about 0.7 nm. Although as we have seen, Brunauer's original theory is now questionable, some recent evidence does support his view that monolayer adsorption can take place on the walls of the wider micropores before secondary micropore filling occurs. These aspects are discussed in later chapters.

4.4.4. The Dubinin–Stoeckli theory

Dubinin was the pioneer of the concept of micropore filling. His approach was based on the early potential theory of Polanyi, in which the physisorption isotherm data were expressed in the form of a temperature-invariant 'characteristic curve'.

In 1947 Dubinin and Radushkevich put forward an equation for the characteristic curve in terms of the fractional filling, W/W_0, of the micropore volume, W_0. This relation is usually expressed in the form

$$W/W_0 = \exp\,[-(A/E)^2] \tag{4.39}$$

where A, the Polanyi 'adsorption potential', is an adsorption affinity,

$$A = -RT \ln (p/p^\circ) \tag{4.40}$$

and E is a characteristic energy for the given system.

The isotherm equation is obtained by combining Equations (4.39) and (4.40). With the introduction of a scaling factor, β, it becomes

$$W/W_0 = \exp\{-[RT \ln (p^\circ/p)]^2/(\beta E_0)^2\} \tag{4.41}$$

where E_0 is a 'characteristic energy'.

Another parameter, the 'structural constant', B, is defined as

$$B = 5.304(R/E_0)^2 \tag{4.42}$$

Rearrangement of Equation (4.41) gives the Dubinin–Radushkevich, DR, equation in its usual form

$$\log_{10}\left[\frac{W}{W_0}\right] = -D\log_{10}^2\left(\frac{p^\circ}{p}\right) \tag{4.43}$$

where D is given by the equation:

$$D = 0.434B(T/\beta)^2 \tag{4.44}$$

According to Equation (4.43), a linear relationship should be obtained between $\log_{10}(n)$ and $\log_{10}^2(p^\circ/p)$. In fact, a number of microporous carbons have been found to give linear DR plots over a wide range of p/p° (Dubinin, 1966); but in many other cases, as in Figure 9.11c, the linear region is restricted to a very limited range of low p/p° (Gregg and Sing, 1982; Carrott *et al.*, 1987). DR plots obtained with zeolites are generally non-linear over virtually the complete isotherm (Dubinin, 1975).

To allow for the deficiencies of the DR equation, Dubinin and Astakhov (1970) put forward a more general form of characteristic curve,

$$W/W_0 = \exp\left[-(A/E)^N\right] \tag{4.45}$$

where N is another empirical constant.

Dubinin (1975) reported values of N between 2 and 6. Some molecular sieve carbons and zeolites gave $N = 3$. However, in view of the empirical nature of N, it is not surprising to find that usually the 'best' values are not integers. The particular value of N may also depend on the range of the isotherm and the operational temperature.

To overcome these difficulties, Stoeckli (Stoeckli, 1977; Stoeckli *et al.*, 1979) suggested that the original DR equation only holds for those carbons with a narrow micropore size distribution. According to this view, the overall isotherm on a heterogeneous microporous solid is made up of the sum of the contributions from the different groups of pores. Thus,

$$W = \sum_j W_{0,j}\exp[-B_j(T/\beta)^2\log_{10}^2(p^\circ/p)] \tag{4.46}$$

where $W_{0,j}$ represents the pore volume of the jth group.

For a continuous distribution, the summation is replaced by integration and then

$$W(y) = \int_0^\infty \mathrm{f}(B)\exp[-By]\,\mathrm{d}B \tag{4.47}$$

where f(B) is a micropore size distribution function and

$$y = (T/\beta)^2\log_{10}^2(p^\circ/p) \tag{4.48}$$

By assuming a Gaussian pore size distribution, Stoeckli was able to simplify

Equation (4.47) and obtain an isotherm equation in which the distribution function, f(B) was expressed in an analytical form (Huber *et al.*, 1978; Bansal *et al.*, 1988). In principle, f(B) provides an elegant basis for relating the micropore size distribution to the adsorption data. However, it must be kept in mind that the validity of the approach rests on the assumption that the DR equation is applicable to each pore group and that there are no other complicating factors such as differences in *surface* heterogeneity.

4.4.5. Empirical isotherm equations

Many different equations have been applied to physisorption isotherms on microporous adsorbents. The first and best known empirical equation was proposed by Freundlich (1926) in the form

$$n = kp^{1/m} \tag{4.49}$$

where k and m are constants ($m > 1$).

According to Equation (4.49), the plot of ln [n] against ln [p] should be linear. In general, activated carbons give isotherms which obey the Freundlich equation in the middle range of pressure (Brunauer, 1945), but the agreement is usually poor at high pressures and low temperatures. These limitations are partly due to the fact that the Freundlich isotherm does not give a limiting value of n as $p \longrightarrow \infty$.

It is possible to achieve an improved fit at higher pressures by a combination of the Freundlich and Langmuir equations (Sips, 1948),

$$n/n_L = (kp)^{1/m}/[1 + (kp)^{1/m}] \tag{4.50}$$

where n_L is the limiting adsorption capacity. Equation (4.50) has been applied as a 'generalized Freundlich' isotherm to multisite occupancy by long-chain hydrocarbons (Rudzinski and Everett, 1992, p. 491). However, as in the case of the Freundlich isotherm itself, the Sips equation does not reduce to Henry's law as $p \longrightarrow 0$.

Another empirical variant is Toth equation,

$$n/n_L = p/(b + p^m)^{1/m} \tag{4.51}$$

which also contains three adjustable parameters (n_L, b and m), but has the advantage that it appears to give the correct limits for both $p \longrightarrow 0$ and $p \longrightarrow \infty$. Thus, although it was originally proposed for monolayer adsorption (Toth, 1962), the Toth equation actually gives a more extensive range of fit when applied to Type I isotherms (Rudzinski and Everett, 1992).

In spite of the availability of modern computer-aided techniques for curve fitting, these and other relatively simple, empirical equations are still found to be useful for the analysis of chemical engineering data (e.g. in the context of pressure swing adsorption or other separation processes).

There is a growing interest in the presentation of physisorption isotherms in a generalized integral form. This approach was first applied to physisorption in the submonolayer region (Adamson *et al.*, 1961), but much of the current interest is centred on the analysis of micropore filling isotherms. An apparent advantage is that it provides a means of constructing a series of model isotherms by systematically

combining various hypothetical 'local' isotherms with either hypothetical or computed energy distribution functions.

The starting point is an expression for the overall adsorption, $n(p, T)$, in the form:

$$n(p,T) = n_0 \int \theta(p,T,E)\mathrm{f}(E)\,\mathrm{d}E \tag{4.52}$$

where n_0 represents either the monolayer capacity or the micropore capacity, $\theta(p, T, E)$ is the local isotherm corresponding to the adsorption energy E, and $\mathrm{f}(E)$ is the distribution function for the adsorption energy over a specified range of energy.

Stoeckli (1993) has pointed out that the Dubinin–Astakhov equation (Equation (4.45)) can be derived from Equation (4.52), but McEnaney (1988) and others (e.g. Jaroniec *et al.* 1997) have drawn attention to the difficulty in arriving at an unambiguous interpretation of the energy distribution function. Indeed, Stoeckli *et al.* (1998) have now pointed out that Equation (4.45) can be usefully applied to a number of adsorption isotherms on non-porous solids. A comprehensive review of the significance and application of Equation (4.52) is given by Rudzinski and Everett (1992).

4.5. Conclusions

In view of the complexity of physisorption mechanisms and the heterogeneity of most solid surfaces and pore structures, it is not surprising to find that all the theoretical models summarized in this chapter have practical limitations of one kind or another. Furthermore it must be re-emphasized that the range of fit of a particular equation is not enough by itself to establish the validity of the underlying theory.

In the range of very *low pressure*, adsorption takes place on the most active sites on the surface or within very narrow pores. At somewhat higher pressures, the less active sites are occupied or alternatively the wider micropores are filled. The molecular interactions are dependent on the particular surface composition and/or the pore structure. For this reason no relatively simple theoretical treatment can be expected to fit the entire adsorption isotherm or to be applicable equally well to both Type I and Type II isotherms.

The determination of the energy of adsorption is the most direct way of studying surface heterogeneity, but as adsorption calorimetry is experimentally more demanding than the measurement of the isotherm, this approach has inevitably attracted less attention. However, as will become evident in subsequent chapters, there is much to be gained by employing the two experimental techniques in combination.

From a practical standpoint, the BET equation must be regarded as the most important of the physisorption equations considered in this chapter. It is a curious paradox that the success of the BET method for surface area determination does not depend on the validity of the BET *theory*. However, although the method has come to be accepted as an internationally approved procedure, certain conditions must be satisfied before the reliability of the derived BET areas can be established. For this

purpose, empirical methods of isotherm analysis are extremely useful. These procedures are introduced in Chapters 6, 7 and 8.

The pragmatic approach adopted in the following chapters involves the identification and characterization of the various mechanisms of adsorption and pore filling. By making use of standard data on well-defined adsorbents and proceeding step-by-step, we endeavour to extract the maximum amount of useful information without having to rely completely on any of the oversimplified models discussed in this chapter.

References

Adamson A.W., Ling I. and Datta S.K. (1961) *Adv. Chem. Series* **33**, 62.

Anderson R.B. (1946) *J. Am. Chem. Soc.* **68**, 686.

Avgul N.N. and Kiselev A.V. (1970) In: *Chemistry and Physics of Carbon*, vol. 6 (P.L. Walker, ed.), Marcel Dekker, New York, p.1

Avgul N.N., Bezus A.G., Dobrova E.S. and Kiselev A.V. (1973) *J. Colloid Interface. Sci.* **42**, 486.

Bansal R.C., Donnet J.B. and Stoeckli H.F. (1988) *Active Carbon*, Marcel Dekker, New York.

Barrer (1978) *Zeolites and Clay Minerals as Sorbents and Molecular Sieves*, Academic Press, London, p. 117.

Block J.H., Bradshaw A.M., Gravelle P.C., Haber J., Hansen R.S., Roberts M.W., Sheppard N. and Tamaru K. (1990) *Pure Appl. Chem.* **62**, 2297.

Bonnetain L., Duval X. and Letort M. (1952) *C.R. Acad. Sci. Fr.* **234**, 1363.

Broekhoff J.C.P. and van Dongen R.H. (1970) In: *Physical and Chemical Aspects of Adsorbents and Catalysts* (ed. B.G. Linsen), Academic Press; London, p. 63.

Brunauer S. (1945) *The Adsorption of Gases and Vapours*, Princeton University Press, Princeton.

Brunauer S. (1970) In: *Surface Area Determination* (D.H. Everett and R.H. Ottewill, eds.) Butterworths, London, p. 63.

Brunauer S., Emmett P.H. and Teller E. (1938) *J. Am. Chem. Soc.* **60**, 309.

Brunauer S., Deming L.S., Deming W.L. and Teller E. (1940) *J. Am. Chem. Soc.* **62**, 1723.

Brunauer S., Skalny J. and Bodor E.E. (1969) *J. Colloid Interface Sci.* **30**, 546.

Carrott P.J.M. and Sing K.S.W. (1989) *Pure Appl. Chem.* **61**(11) 1835.

Carrott P.J.M., McLeod A.J. and Sing K.S.W. (1982) In: *Adsorption at the Gas–Solid and Liquid–Solid Interface* (J. Rouquerol and K.S.W. Sing, eds.) Amsterdam, p. 403.

Carrott P.J.M., Roberts R.A. and Sing K.S.W. (1987) *Carbon* **25**(6), 769.

Cole J.H., Everett D.H., Marshall C.T., Paniego A.R., Powl J.C. and Rodriguez-Reinoso F. (1974) *J. Chem. Soc., Faraday Trans. I* **70**, 2154.

Coulomb J.P., Sullivan T.J. and Vilches (1984) *Phys. Rev. B* **30**(8), 4753.

Dash J.G. (1975) *Films on Solid Surfaces*, Academic Press, New York.

de Boer J.H. (1968) *The Dynamical Character of Adsorption*, Oxford University Press, London, p. 179.

Dubinin M.M. (1966) In: *Chemistry and Physics of Carbon* (P.L. Walker, ed.), Marcel Dekker, New York, p. 51.

Dubinin M.M. (1975) In: *Progress in Surface and Membrane Science*, vol. 9 (D.A. Cadenhead ed.), Academic Press, New York, p. 1.

Dubinin M.M. and Astakhov V.A. (1970) *Adv. Chem. Series* **102**, 69.

Dubinin M.M. and Radushkevich L.V. (1947) *Proc. Acad. Sci.* USSR, **55**, 331.

Everett D.H. (1950) *Trans. Faraday Soc.* **46**, 453, 942, 957.

Everett D.H. (1970) In: *Surface Area Determination* (D.H. Everett and R.H. Ottewill, eds.), Butterworth, London, p. 181.

Everett D.H. (1972) *Pure Appl. Chem.* **31**, 579.

Everett D.H. and Powl J.C. (1976) *J. Chem. Soc., Faraday Trans. I* **72**(3), 619.

Fowler R.H. (1935) *Proc. Cambridge Phil. Soc.* **31**, 260.

Fowler R.H. and Guggenheim E.A. (1939) *Statistical Thermodynamics,* Cambridge University Press, London, p. 429.
Freundlich H. (1926) *Colloid and Capillary Chemistry*, Methuen, London, p. 120.
Gregg S.J. (1961) *The Surface Chemistry of Solids*, Chapman & Hall, London.
Gregg S.J. and Sing K.S.W. (1982) *Adsorption, Surface Area and Porosity*, Academic Press, London.
Halsey G.D. (1948) *J. Chem. Phys.* **16**, 93.
Hill T.L. (1946) *J. Am. Chem. Soc.* **68**, 535.
Hill T.L. (1952) *Adv. Catalysis* **4**, 211.
Huber U., Stoeckli H.F. and Houriet J.P. (1978) *J. Colloid Interface Sci.* **67**(2), 195.
Jaroniec M., Kruk M. and Choma J. (1997) In: *Characterization of Porous Solids IV* (B. McEnaney, T.J. Mays, J. Rouquerol, F. Rodriguez-Reinoso, K.S.W. Sing and K.K. Unger, eds.) Royal Society of Chemistry, London, p. 163.
Lamb A.B. and Coolidge A.S. (1920) *J. Am. Chem. Soc.* **42**, 1146.
Langmuir I. (1916) *J. Am. Chem. Soc.* **38**, 2221.
Langmuir I. (1918) *J. Am. Chem. Soc.* **40**, 1361.
Larher Y. (1992) *Surface properties of layered structures* (G. Benedek, ed.), Kluwer, Dordrecht, p. 261.
McEnaney B. (1988) *Carbon* **26**, 267.
Pierotti R.A. and Thomas H.E. (1971) In *Surface and Colloid Science* (E. Matijevic, ed.) Wiley-Interscience, New York, p. 93.
Price G.L. and Venables J.A. (1976) *Surface Sci.* **59**(2), 509.
Reichert H., Muller U., Unger K.K., Grillet Y., Rouquerol F., Rouquerol J. and Coulomb J.P. (1991) In: *Characterization of Porous Solids II* (F. Rodriguez-Reinoso, J. Rouquerol, K.S.W. Sing and K.K. Unger, eds.), Elsevier, Amsterdam, p. 535.
Ross S. and Clark H. (1954) *J. Am. Chem. Soc.* **76**, 4291.
Ross S. and Olivier J.P. (1964) *On physical adsorption*, Wiley-Interscience, New York.
Rudzinski W. and Everett D.H. (1992) *Adsorption of Gases on Heterogeneous Surfaces*, Academic Press, London.
Ruthven D.M. (1984) *Principles of Adsorption and Adsorption Processes*, Wiley-Interscience, New York.
Sahouli, B., Blacher, S. and Brouers, F. (1997) *Langmuir* **13**, 4391.
Seri-Levy, A. and Avnir, D. (1993) *Langmuir* **9**, 2523.
Sing K.S.W. (1973) In: *Colloid Science I*, The Chemical Society, London, p. 30.
Sing K.S.W. (1979) In: *Characterization of Porous Solids* (S.J. Gregg, K.S.W. Sing and H.F. Stoeckli, eds.), Society of Chemical Industry, London, p. 98.
Sing K.S.W., Everett D.H., Haul R.A.W., Moscou L., Pierotti R.A., Rouquerol J. and Siemieniewska T. (1985) *Pure Appl. Chem.* **57**, 603.
Sips R. (1948) *J. Chem. Phys.* **16**, 490.
Steele W.A. (1974) *The Interaction of Gases with Solid Surfaces*, Pergamon, New York, p. 131.
Steele W.A. (1996) *Langmuir* **12**, 145.
Stoeckli H.F. (1977), *J. Colloid Interface Sci.* **59**, 184.
Stoeckli H.F. (1993) *Adsorption Sci. Tech.* **10**, 3.
Stoeckli H.F., Houriet J.P., Perret A. and Huber U. (1979) In: *Characterization of Porous Solids* (S.J. Gregg, K.S.W. Sing and H.F. Stoeckli, eds.), Society of Chemical Industry, London, p. 31.
Stoeckli, F., Hugi-Cleary, D. and Centeno, T.A. (1998), *J. Eur. Ceramic. Soc.* in press.
Suzanne J. and Gay J.M. (1996) In: *Handbook of Surface Science*, vol. 1, Physical Structure (W.N. Unertl, vol. ed., N.V. Richardson and S. Holloway, series eds), North-Holland Elsevier, Amsterdam, p. 503.
Terlain A. and Larher Y. (1983) *Surface Sci.* **125**, 304.
Thomy A. and Duval X. (1970) *J. Chim. Phys. Fr.* **67**, 1101.
Thomy A., Regnier J. and Duval X. (1972) In: *Thermochimie*, Colloques Internationaux du CNRS no. 201, Editions du CNRS, Paris, p. 511.
Toth J. (1962) *Acta Chim. Acad. Sci. Hung.* **35**, 416.
Venables J.A., Seguin J.L., Suzanne I. and Bienfait M. (1984) *Surface Sci.* **145**, 345.
Yang R.T. (1987) *Gas Separation by Adsorption Processes*, Butterworths, London.
Young D.M. and Crowell A.D. (1962) *Physical Adsorption of Gases*, Butterworths, London, p. 124.

This Page Intentionally Left Blank

CHAPTER 5

Adsorption at the Liquid–Solid Interface: Thermodynamics and Methodology

5.1. Introduction

Adsorption at the liquid–solid interface is of great importance in industry and everyday life (e.g. in detergency, adhesion, lubrication, flotation of minerals, water treatment, oil recovery, and in pigment and particle technology). Adsorption from solution measurements have been used for many years for the determination of the surface area of certain industrial materials. Immersion microcalorimetry has also been applied for the characterization of such materials as clays and activated carbons. The application of the energetics of immersion is based on the observation by Pouillet in 1822 that the immersion of an insoluble solid in a liquid is a measurable exothermic phenomenon. To gain an understanding of liquid–solid adsorption phenomena, it is not enough to know the surface area and porosity of the adsorbent. In addition, it is necessary to know how the solid behaves in the liquid medium.

The comparison with adsorption at the gas–solid interface is further complicated by the fact that some adsorbents cannot be outgassed without an irreversible change in their texture. Also, changes in texture may occur when the adsorbent is immersed in a pure liquid or a solution. For these reasons, it is necessary to utilize special methods which provide direct information on the particular liquid–solid interactions.

In this chapter, our aim is to give an introductory account of the methodology and underlying thermodynamic principles of adsorption at the liquid–solid interface. We are mainly, but not exclusively, concerned with the characterization of the liquid–solid interface. In this context, there are two relevant topics:

(a) the energetics of immersion of solids in liquids;
(b) isothermal adsorption from solutions.

Many attempts have been made to employ immersion calorimetry and solution adsorption measurements for the determination of the surface area of porous and non-porous materials (see Gregg and Sing, 1967), but in our view insufficient attention has

been given to either the basic principles involved or the limitations of the experimental procedures used by most investigators.

Our approach to the thermodynamics of adsorption and immersion remains simple, although rigorous, and close to the experiment. This is why the thermodynamic treatment of the energetics of immersion in Section 5.2 is confined to the simple system of a solid immersed in a pure liquid. Similarly, in Section 5.3 consideration is given only to the adsorption from binary solutions. The thermodynamic nomenclature and definitions proposed here are consistent with the recommendations of IUPAC (Everett, 1972, 1986).

5.2. Energetics of Immersion of Solid in Pure Liquid

5.2.1. Thermodynamic background

In Chapter 2 we have introduced a number of thermodynamic surface excess quantities (Equations (2.11)–(2.14)) in the case of a simple gas adsorption system involving a single adsorptive. These quantities were expressed as a function of the surface excess amount, n^σ. In the case of the process of immersion of a solid in a pure liquid, the same surface excess quantities can still be defined and it is useful to express them as a function of the surface area. Thus:

$$U^\sigma = Au^i \tag{5.1}$$

$$H^\sigma = Ah^i \tag{5.2}$$

$$S^\sigma = As^i \tag{5.3}$$

$$F^\sigma = Af^i \tag{5.4}$$

where A is the area of the solid–fluid interface and u^i, h^i, s^i and f^i (with superscript 'i') denote the *areal* surface excess energy, enthalpy, entropy and Helmholtz energy, respectively (here again, since we have adopted the Gibbs representation, there is no difference between U^σ and H^σ, because $V^\sigma = 0$). The areal surface excess quantities are characteristic of the nature of the interface, which must be stated.

Definition of immersion quantities

The energy (or enthalpy) of immersion $\Delta_{imm}U$ (or $\Delta_{imm}H$) is defined (Everett, 1972) as the energy (or enthalpy) change, at constant temperature, when a solid surface is completely immersed in a wetting liquid in which the solid is insoluble and unreactive. The initial state of the solid surface must of course be specified: the extent of any preliminary outgassing and the nature of the surrounding medium (vacuum or vapour of the liquid at a given partial pressure). Each initial state leads indeed to a different surface excess energy U^σ since:

$$U^\sigma = U - U^s - U^l - U^g \tag{5.5}$$

where U is the internal energy of the whole system in equilibrium and U^s, U^l and U^g are the internal energies of the bulk solid, liquid and vapour phases, respectively.

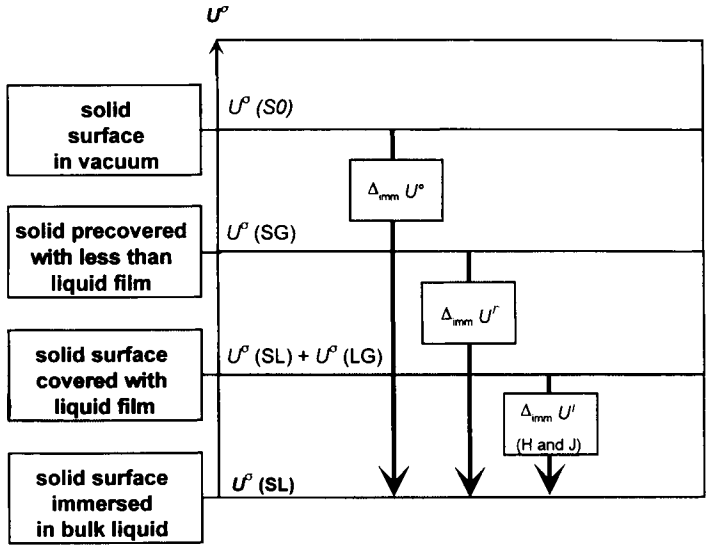

Figure 5.1. Dependence of the energy of immersion on the initial coverage of the solid surface ('H and J' stands for 'Harkins and Jura procedure').

The dependence of U^σ on a few typical states of the system is represented in Figure 5.1. The upper level corresponds to the clean solid (i.e. in vacuum) whose surface excess energy is denoted U^σ (S0) and, as stated earlier, is proportional to its surface area:

$$U^\sigma(\mathrm{S0}) = Au^{\mathrm{i}}(\mathrm{S0}) \tag{5.6}$$

The lowest level corresponds to the immersed solid, with a solid–liquid interface whose surface excess energy is now denoted U^σ(SL), with

$$U^\sigma(\mathrm{SL}) = Au^{\mathrm{i}}(\mathrm{SL}) \tag{5.7}$$

Two intermediate levels deserve consideration, depending on the pre-coverage of the solid surface. If the solid surface has adsorbed less than a liquid film, then the surface excess energy is located at the solid–vapour interface, U^σ (SG), and it can be written (always assuming the adsorbent to be inert):

$$U^\sigma(\mathrm{SG}) = U^\sigma(\mathrm{S0}) + n^\sigma(u^\sigma - \mathrm{u}^{\mathrm{l}}) \tag{5.8}$$

where n^σ is the surface excess amount and u^σ the molar surface excess energy. In accordance with Equation (5.1) we can write

$$U^\sigma(\mathrm{SG}) = Au^{\mathrm{i}}(\mathrm{SG}) \tag{5.9}$$

In Figure 5.1 we see that for a solid surface covered with a liquid film we obtain U^σ(SL) + U^σ(LG). It is useful to separate these two terms as follows:

$$U^\sigma(\mathrm{SL}) = Au^{\mathrm{i}}(\mathrm{SL}) \tag{5.10}$$

at the solid–liquid film interface and

$$U^{\sigma}(\mathrm{LG}) = Au^{\mathrm{i}}(\mathrm{LG}) \tag{5.11}$$

at the liquid film–vapour interface.

The maximum energy of immersion, which we designate $\Delta_{\mathrm{imm}}U^{\circ}$, is liberated when the vacuum–solid interface is replaced by the liquid–solid interface. Thus, for the immersion of an outgassed adsorbent of surface area A, we obtain:

$$\Delta_{\mathrm{imm}}U^{\circ} = A[u^{\mathrm{i}}(\mathrm{SL}) - u^{\mathrm{i}}(\mathrm{S0})] \tag{5.12}$$

where $u^{\mathrm{i}}(\mathrm{SL})$ and $u^{\mathrm{i}}(\mathrm{S0})$ are the areal surface excess energies corresponding to $U^{\sigma}(\mathrm{SL})$ and $U^{\sigma}(\mathrm{S0})$ in Figure 5.1. (Note that since the process is exothermic, the $\Delta_{\mathrm{imm}}U$ values are all negative.)

When area A is already covered with a physisorbed layer at surface excess concentration Γ (i.e. n^{σ}/A), the energy of immersion becomes

$$\Delta_{\mathrm{imm}}U^{\Gamma} = \mathrm{A}[u^{\mathrm{i}}(\mathrm{SL}) - u^{\mathrm{i}}(\mathrm{SG})] \tag{5.13}$$

Finally, when the adsorbed layer is thick enough to behave as a liquid film, the energy of immersion, $\Delta_{\mathrm{imm}}U^{\mathrm{l}}$, which corresponds to the disappearance of the liquid–gas interface, is simply:

$$\Delta_{\mathrm{imm}}U^{\mathrm{l}} = -Au^{\mathrm{i}}(\mathrm{LG}) \tag{5.14}$$

The above equations are all based on the internal energy. Similar equations can be written with the enthalpy since the surface excess enthalpy and energy are identical in the Gibbs representation when $V^{\sigma} = 0$ (Harkins and Boyd, 1942). Therefore the various energies of immersion defined by Equations (5.6)–(5.8) are all virtually equal to the corresponding enthalpies of immersion, i.e. ($\Delta_{\mathrm{imm}}H^{\circ}$, $\Delta_{\mathrm{imm}}H^{\Gamma}$ and $\Delta_{\mathrm{imm}}H^{\mathrm{l}}$), thus:

$$\Delta_{\mathrm{imm}}H^{\circ} = \Delta_{\mathrm{imm}}U^{\circ} \tag{5.15}$$

The latter definition of the enthalpy of immersion is that given by Everett (1972, 1986).

Nevertheless, in this chapter we shall refer to the energy of immersion which is unambiguous and consistent with our thermodynamic treatment.

In fact, 'energy of immersion' was the term originally used by Harkins in his early papers (Harkins and Dahlstrom, 1930), before resorting to the usual laboratory term of 'heat of immersion'. Although the latter term is still used by a few authors, it is to be discouraged since 'heat' is not a precise term and is not directly related to any thermodynamic state of the system: as will be stressed in Section 5.2.2 describing experimental techniques, in practice, the microcalorimetric measurement of the heat exchanged is never equal to the required energy of immersion.

Relation between the energies of immersion and gas adsorption

The process of the immersion of a clean solid surface (which gives rise to $\Delta_{\mathrm{imm}}U^{\circ}$)

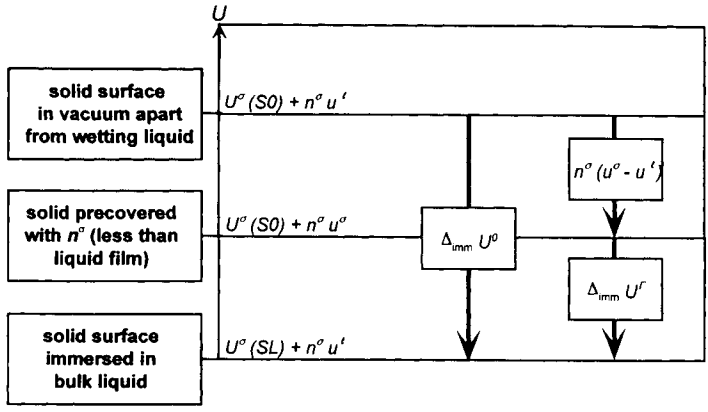

Figure 5.2. Relation between energy of immersion and net molar integral energy of adsorption $n^{\sigma}(u^{\sigma} - u^{l})$.

can be notionally separated into two successive steps (see Figure 5.2):

1. An adsorption step, during which an amount of liquid n^{σ} is vaporized from the liquid phase (with a molar energy of vaporization $\Delta_{vap}u$) and adsorbed on the solid surface (with an integral molar adsorption energy $\Delta_{ads}u$, precisely defined for an adsorption process at constant volume (cf. Equation (2.59)), at temperature T and for the surface excess concentration $\Gamma = n^{\sigma}/A$.
2. An immersion step proper, during which the solid with its pre-adsorbed layer is immersed in the liquid.

Let us now consider the case where the first step takes place out of the calorimeter. The corresponding energy change is:

$$\Delta_{ads}U + \Delta_{vap}U = n^{\sigma}(\Delta_{ads}u + \Delta_{vap}u) = n^{\sigma}(u^{\sigma} - u^{l}) \tag{5.16}$$

The second step, which takes place in the calorimeter, gives rise to an energy of immersion $\Delta_{imm}U^{\Gamma}$ which is of course smaller than $\Delta_{imm}U^{\circ}$ and directly depends on Γ, i.e. on the pre-coverage.

If we now add the energy changes for the two steps, we get:

$$\Delta_{imm}U^{\circ} = n^{\sigma}(u^{\sigma} - u^{l}) + \Delta_{imm}U^{\Gamma} \tag{5.17}$$

It thus becomes possible to assess the net molar integral energy of adsorption $(u^{\sigma} - u^{l})$ from the difference between the energy of immersion of the outgassed adsorbent and that of the adsorbent with a pre-adsorbed surface excess concentration, as was originally pointed out by Hill (1949).

Differentiation of Equation (5.17) with respect to n^{σ} provides the differential energy of adsorption:

$$\Delta_{ads}u = \frac{\partial}{\partial n^{\sigma}}(\Delta_{imm}U^{\circ} - \Delta_{imm}U^{\Gamma}) - \Delta_{vap}u \tag{5.18}$$

Similarly, we can derive the differential (or isosteric) enthalpy of adsorption (defined by Equation (2.51)):

$$\Delta_{\text{ads}}\dot{h} = \frac{\partial}{\partial n^{\sigma}}(\Delta_{\text{imm}}U^{\circ} - \Delta_{\text{imm}}U^{\Gamma}) - \Delta_{\text{vap}}h \tag{5.19}$$

It is with this type of equation that, for instance, Micale *et al.* (1976) was able to check the consistency of the isosteric approach (from gas adsorption isotherms) with immersion calorimetry, for the water–microcrystalline $Ni(OH)_2$ system.

Finally, when integral molar energies of adsorption are directly measured by gas adsorption calorimetry, it is possible to obtain the corresponding integral molar entropies of adsorption from Equations (2.65) and (2.66).

If the integral molar entropy of the adsorbed phase is to be compared with the molar entropy of the immersion liquid, it is necessary to express the molar entropy of the gas as a function of the relative pressure and the enthalpy of vaporization. Thus,

$$s^{g} = s^{l} - R\ln\frac{p}{p^{\circ}} + \frac{\Delta_{\text{vap}}h}{T} \tag{5.20}$$

The integral molar entropy of adsorption then becomes (as indicated by Jura and Hill, 1952):

$$(s^{\sigma} - s^{l}) = \frac{1}{T}\left[\frac{1}{n^{\sigma}}(\Delta_{\text{imm}}U^{\circ} - \Delta_{\text{imm}}U^{\Gamma}) + \frac{\Pi}{\Gamma}\right] - R\ln\frac{p}{p^{\circ}} \tag{5.21}$$

where Π is the spreading pressure of the adsorbed film characterized by the surface excess concentration Γ, which can be calculated from the adsorption isotherm (cf. Chapter 2).

Relation between the energies of immersion and adhesion

The concept of the energy of adhesion between a liquid and a solid was originally proposed and defined by Harkins (1952) as a means of characterizing the 'de-wetting' of a solid to produce a solid surface (in vacuum) and an equal area of liquid surface (in the presence of saturated vapour). The corresponding internal energy change, which we prefer to refer to as the energy of separation, $\Delta_{\text{sep}}U$, is given by

$$\Delta_{\text{sep}}U = A[u^{l}(\text{S0}) + u^{l}(\text{LG}) - u^{l}(\text{SL})] \tag{5.22}$$

It follows from Equations (5.12) and (5.14) and Figure 5.3 that:

$$\Delta_{\text{sep}}U = -[\Delta_{\text{imm}}U^{\circ} + \Delta_{\text{imm}}U^{l}] \tag{5.23}$$

It is somewhat misleading that Harkins used the term 'energy of *adhesion*' to denote an 'energy of *separation* of a liquid from the surface of a solid' (Harkins, 1952). It seems more consistent to define the energy of adhesion $\Delta_{\text{adh}}U$, with the same sign as the immersion quantities, so that:

$$\Delta_{\text{adh}}U = -\Delta_{\text{sep}}U \tag{5.24}$$

The above relationships are represented in Figure 5.3, where the upper level of

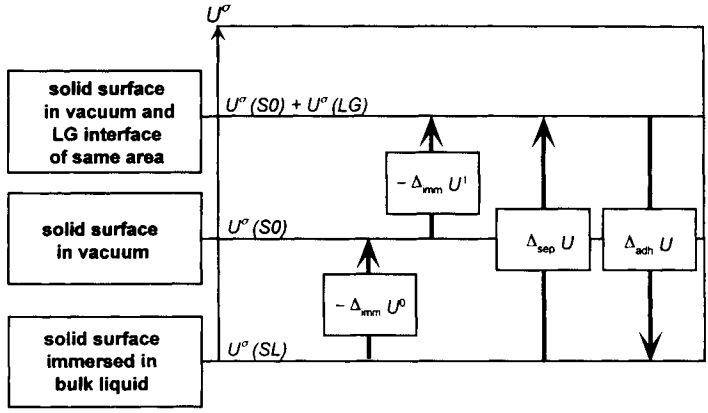

Figure 5.3. Relation between energies of immersion, separation and adhesion.

surface excess energy corresponds to the equal area of solid–vacuum and liquid–vapour interfaces.

Relation between the areal surface excess energy and the surface tension

As indicated in Chapter 2, the adsorbent surface is characterized by a surface tension γ whose magnitude depends on the nature of the surrounding medium (liquid, gas or vacuum) with which the adsorbent is in equilibrium. The isothermal extension of the surface area A, with no other change in the thermodynamic state of the system of adsorption, results in an increase dF of the Helmholtz energy of the system. Thus, the surface tension, γ, is defined as:

$$\gamma = \left(\frac{\partial F}{\partial A}\right)_{T,V,n^\sigma} \tag{5.25}$$

It is convenient to separate the contributions of internal energy U and entropy, S, of the system so that

$$\left(\frac{\partial F}{\partial A}\right)_{T,V,n^\sigma} = \left(\frac{\partial U}{\partial A}\right)_{T,V,n^\sigma} - T\left(\frac{\partial S}{\partial A}\right)_{T,V,n^\sigma} \tag{5.26}$$

and by taking account Equations (5.1), (5.3) and (5.25) we obtain

$$\gamma = u^i - Ts^i \tag{5.27}$$

Since

$$S = -\left(\frac{\partial F}{\partial T}\right)_{A,V,n^\sigma} \tag{5.28}$$

and by making use of Equations (5.25), (5.26) and (5.28), we arrive at:

$$\left(\frac{\partial U}{\partial A}\right)_{T,V} = \gamma - T\left(\frac{\partial \gamma}{\partial T}\right)_A \tag{5.29}$$

It is noteworthy that Equation (5.29) is analogous to the well-known equation for the isothermal expansion of bulk gas:

$$-\left(\frac{\mathrm{d}U}{\mathrm{d}V}\right)_T = p - T\left(\frac{\partial p}{\partial T}\right)_V \tag{5.30}$$

where p is the pressure and V the volume. Of course, $(\partial U/\partial V)_p$ is zero in the case of an ideal gas.

The term $(\mathrm{d}U/\mathrm{d}A)_{T,V,n^\sigma}$ was referred to as the 'total extension energy of the surface per unit increase of area' by Einstein (1901). It is indeed the sum of the work, γ, which must be supplied to extend the surface by one unit of area and the heat which must be supplied to carry out this extension reversibly and isothermally.

We can also obtain the areal surface excess entropy from Equations (5.25) and (5.29):

$$s^{\mathrm{i}} = -\left(\frac{\partial \gamma}{\partial T}\right)_A \tag{5.31}$$

Various types of wetting

In the preceding sections, we have been mainly concerned with one form of wetting, namely 'immersion'. It is, however, useful to distinguish between the various types of wetting that are illustrated in Figure 5.4.

The four major types of wetting are as follows (the first three following Everett's definitions, 1972):

1. *Immersional wetting* (which we simply call *immersion* and denote by subscript 'imm') is a process in which the surface of a solid, initially in contact with vacuum or a gas phase, is brought in contact with a liquid without changing the area of the interface. Here, a solid–gas (or solid–vacuum) interface is replaced by a solid–liquid one of the same area.
2. *Adhesional wetting* (which we shall call *adhesion* and denote by subscript 'adh') is a process by which an adhesional union is formed between two pre-existing surfaces (one of them being solid and the other liquid). Here, two initial interfaces (solid–gas and liquid–gas) are replaced by one (solid–liquid).
3. *Spreading wetting* is a process in which a drop of liquid spreads over a solid substrate (the liquid and solid being previously in equilibrium with the vapour). Here, the solid–vapour interface is replaced by two new interfaces (solid–liquid and liquid–vapour) of same area.
4. *Condensational wetting* is a process in which a clean solid surface (initially in vacuum) adsorbs a vapour up to the formation of a continuous liquid film. Here, the solid–vacuum interface is replaced by two new interfaces (solid–liquid and solid–vapour) of the same area, as in spreading wetting. The difference between condensational and spreading wetting is in the initial state, the liquid film being formed from a vapour in one case and from a drop in the other case.

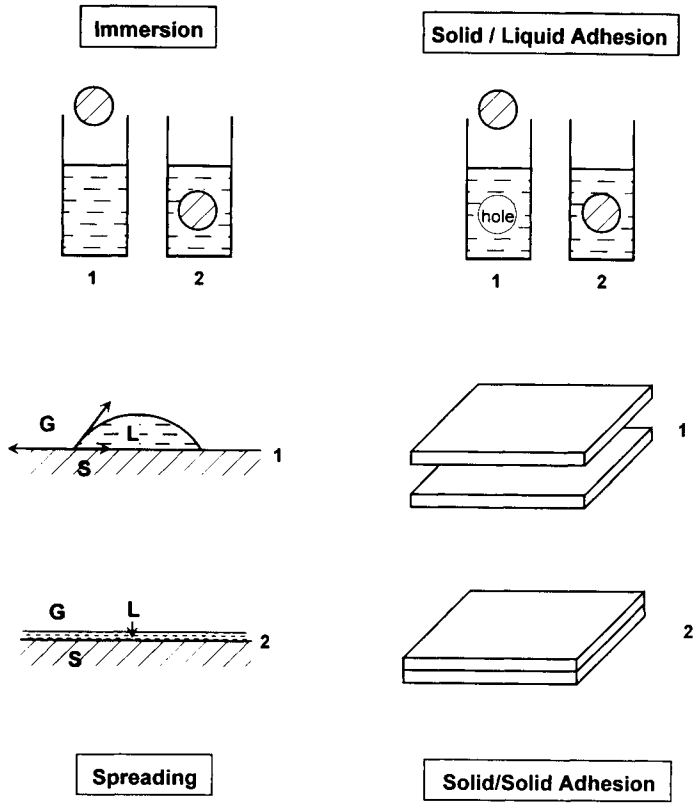

Figure 5.4. Interfaces lost or formed during immersional, adhesional and spreading wetting and during solid–solid adhesion.

At this stage, it may be noted (Jaycock and Parfitt, 1981) that the above types of wetting do not all have the same contact angle requirement ($\theta < 90°$) for spontaneous occurrence. Thus:

(a) adhesional wetting requires $\theta < 180°$, which is of course the most general case;
(b) immersional wetting requires $\theta < 90°$ (otherwise external work must be applied);
(c) spreading and condensational wetting require $\theta = 0$.

Wettability of a solid surface: definition and assessment

The concept of wettability of a solid by a liquid is directly related to the wetting processes. This concept is specially useful in the fields of detergency, lubrication or enhanced oil recovery. In the context of the oil industry, proposals were made by Briant and Cuiec (1972) for the experimental assessment of wettability, which was defined in terms of the thermodynamic affinity of a solid surface for a liquid.

According to this approach wettability is equated to the work exchanged by the immersion system with its surroundings when the process of immersional wetting of

a given area of the clean solid surface is carried out reversibly. Thus:

$$\int_{\text{imm}} -\left(\frac{\partial F}{\partial A}\right)_{T,V} \mathrm{d}A = [\gamma\lfloor(S0) - \gamma(SL)\rfloor A \tag{5.32}$$

where γ(S0) and γ(SL) are the surface tensions of the solid surface in the presence of vacuum and a liquid film.

The wettability, which we propose to denote $\Delta_{\text{imm}}\gamma$, is directly measured by the difference between two surface tensions. This difference was called the 'adhesion tension' by Adamson (1967) and the 'work of immersional wetting per unit area' by Everett (1972). It has also been referred to as the 'wetting tension'.

In Equation (5.32) the difference in γ is positive in the case of spontaneous wetting of the solid by the liquid.

It may be useful to distinguish between the initial conditions when the solid is either in vacuum (the wettability will then be denoted $\Delta_{\text{imm}}\gamma^{\circ}$) or when it is in equilibrium with a gas phase, with a surface excess concentration Γ (the wettability being then denoted $\Delta_{\text{imm}}\gamma^{\Gamma}$):

$$\Delta_{\text{imm}}\gamma^{\circ} = \gamma(\text{S0}) - \gamma(\text{SL}) \tag{5.33}$$

$$\Delta_{\text{imm}}\gamma^{\Gamma} = \gamma(\text{SG}) - \gamma(\text{SL}) \tag{5.34}$$

The following three main routes are available to assess the wettability. The first method is dependent on the measurement of contact angles, while the second and third make use of energy of immersion and adsorption isotherm data.

Assessment of wettability from the contact angle. A favourable case is when a contact angle θ can be measured between the liquid and solid in equilibrium with the vapour, so that the Young–Dupré equation can be applied. As early as 1805, Young considered the possibility of such an equilibrium between surface tensions, but it was only in 1869 that Dupré put it in the well-known form of equation:

$$\gamma(\text{SG}) = \gamma(\text{SL}) + \gamma(\text{LG}) \cos\theta \tag{5.35}$$

and hence:

$$\Delta_{\text{imm}}\gamma = \gamma(\text{LG}) \cos\theta \tag{5.36}$$

This allows us to derive the wettability simply from θ and the surface tension of the liquid. This method was used for instance by Whalen and Lai (1977) in their systematic study of the wetting of modified surfaces of glass.

Assessment of wettability from the energy of immersion. Since it is equal in magnitude to the Helmholtz free energy of immersion per unit area (cf. Equation (5.32)), the wettability can be written as:

$$\Delta_{\text{imm}}\gamma = -\frac{\Delta_{\text{imm}}F}{A} \tag{5.37}$$

The problem is now to evaluate $\Delta_{\text{imm}}F$. This can be done with help of a useful

observation by Briant and Cuiec (1972): these investigators confirmed that, for a number of solid–liquid systems, the following approximate relationship holds:

$$k = \frac{\Delta_{imm}F}{\Delta_{imm}U} = \frac{\gamma(LG)}{u^{i}(LG)} = \frac{\gamma(LG)}{\gamma(LG) - T(\partial\gamma(LG)/\partial T)} \tag{5.38}$$

This means that the ratio $\Delta_{imm}F/\Delta_{imm}U$ can be assessed from the liquid-phase ratio $\gamma(LG)/u^{i}(LG)$.

Combining Equations (5.37) and (5.38) we obtain:

$$\Delta_{imm}\gamma = -k \times \Delta_{imm}U \tag{5.39}$$

which allows us to make use of the energy of immersion, provided k is known. Values of k, calculated by Briant and Cuiec (1972) for liquids commonly used in immersion, are given in Table 5.1.

In fact, the validity of Equation (5.38) is supported by the observation by Robert (1967) that the energies of immersion of carbon blacks in a number of hydrocarbons of the same family (e.g. *n*-alkanes from 7 to 16 carbon atoms) could be ranked exactly in the same order as the 'adsorbability' of these hydrocarbons.

Assessment of wettability from the gas adsorption isotherm. If the solid is covered with a liquid film in equilibrium with saturated vapour $p°$, the spreading pressure of the film can be derived from Equation (2.22). Thus:

$$\Pi(p°) = \gamma(S0) - (\gamma(SL) + \gamma(LG)) \tag{5.40}$$

This expression can be combined with Equation (5.33) to provide the following expression for the wettability of a clean surface:

$$\Delta_{imm}\gamma° = \Pi(p°) + \gamma(LG) \tag{5.41}$$

The spreading pressure $\Pi(p°)$ can be calculated from the Gibbs equation (2.34) by integration from $p/p° = 0$ up to 1. However, this is dependent on the availability of highly accurate data at low $p/p°$. Briant and Cuiec (1972) evaluated the resulting uncertainty of the wettability to be *c.* 10%.

Table 5.1. Calculation of k from Equation (5.38) for a number of liquids (Briant and Cuiec, 1972)

Liquid	t (°C)	γ(LG) (mJ m^{-2})	$-T(\partial\gamma$ (LG)$/\partial T)$ (mJ m^{-2})	γ(LG) $- T(\partial\gamma$ (LG)$/\partial T)$ (mJ m^{-2})	k
Water	37	70	50.5	120.5	0.58
	47	68.4	52.1	120.5	0.57
Heptane	55	16	30.5	46.5	0.34
Cyclohexane	43	21.6	36	57.6	0.37
Benzene	35	26.9	40.1	67	0.40
Paraxylene	38	26.5	32.6	59.1	0.45

5.2.2. Experimental techniques of immersion microcalorimetry in pure liquid

Of the four types of wetting phenomena examined in the previous section, only immersional wetting lends itself to direct microcalorimetric measurement: spreading and adhesion experiments would involve too small interfacial areas (say, no more than *c.* 100 cm^2), whereas condensational wetting would require measurements up to $p/p^\circ = 1$. As we saw in Chapter 3, these are the conditions where accurate measurements of the amounts of gas adsorbed are difficult to achieve. For this reason we confine the following recommendations to immersion microcalorimetry.

In principle, to carry out immersion microcalorimetry, one simply needs a powder, a liquid and a microcalorimeter. Nevertheless, it was early realized that the heat effects involved are small and the sources of errors and uncertainties numerous. Many attempts have been made to improve immersion microcalorimetric techniques. Before commenting on this type of experiment, we describe the equipment and procedure which has been found by Rouquerol and co-workers to be of particular value for energy of immersion measurements (Partyka *et al.*, 1979).

Recommended immersion microcalorimetric equipment and experimental procedure

Figure 5.5 shows the set-up, at a stage which is just prior to the immersion of the solid. Here, the sample (1) is located in a glass bulb (2) with a fragile tip (3). The sample has already been outgassed, out of the microcalorimeter, and has been left either under vacuum or under a given vapour pressure of the immersion liquid. The bulb has been sealed off and attached, through fitting (4), to a thin glass rod. This assembly has been introduced into the microcalorimeter cell and tightly closed. The glass rod is able to slide down through O-ring (5) (located outside the calorimeter to avoid detecting friction effects). The heat flowmeter (6) (a Tian–Calvet thermopile) surrounds the microcalorimetric cell containing the immersion liquid (7) and the glass bulb.

With the above set-up, the *essential steps* for a safe and convenient experiment are as follows:

1. Introduction and weighing of adsorbent in immersion bulb.
2. Outgassing of adsorbent with one of the procedures described in Section 3.4.3.
3. If pre-adsorption is required, equilibration of sample with desired relative vapour pressure of immersion liquid.
4. Sealing of ampoule neck at *c.* 2 cm above the bulb if necessary immersed in cooling bath to protect the sample.
5. Determination of weight of sealed bulb.
6. Connection of top of sample bulb to glass rod (3 mm diameter) by means of Teflon plug.
7. Introduction of sample bulb (2) into stainless steel calorimetric cell already filled with immersion liquid (7).
8. Tight closure of this set-up, with some lubricant on O-ring (5) and with end of capillary tip of sample bulb *c.* 5 mm above bottom of microcalorimetric cell.

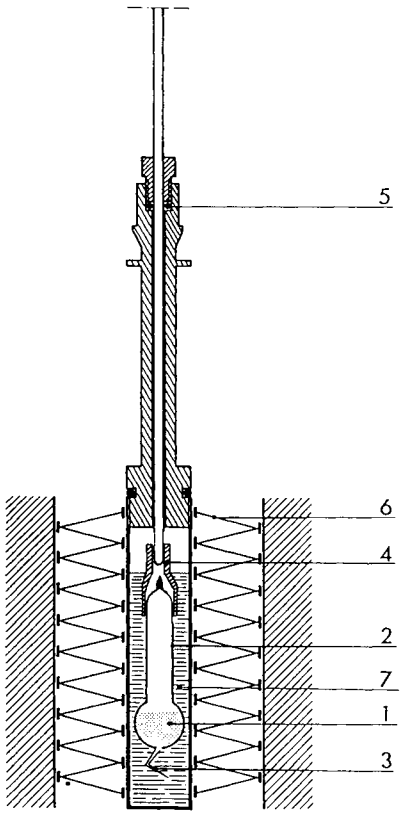

Figure 5.5. Set-up for immersion microcalorimetry (see text for details).

9. Allowance of time for temperature equilibration in the microcalorimeter (this may require 3 hours for high sensitivity).
10. Breaking of capillary tip by slowly and gently depressing glass rod until microcalorimetric signal starts to respond.
11. Recording of microcalorimetric signal until it returns to baseline (this usually requires *c.* 30 min).
12. Careful removal of sample bulb and broken tip from microcalorimetric cell.
13. Determination of weight of sample bulb filled with immersion liquid (only wiped outside), together with broken tip.
14. Determination of dead volume V of sample bulb from the information gained in Steps 5 and 13, knowing mass and density of immersion liquid.
15. Determination of total experimental heat of immersion by integration of the whole microcalorimetric signal (including the small endothermal peak due to vaporization of the first droplet of immersion liquid into dead volume, just before immersion proper (Partyka *et al.*, 1979).
16. Calculation of correction terms and, finally, of the energy of immersion.

Evaluation of the correction terms

The two correction terms involved in the above experiment are:

(a) The *energy of bulb breaking*, W_b, which is the exothermal sum of the work provided by the operator, plus the energy released by pre-existing stresses in the glass bulb, minus the energy absorbed by the formation of new glass–liquid interfaces. Typical values of W_b for a fine tip of the shape represented in Figure 5.5 are around 5 mJ. The W_b value must be determined by blank experiments with similar bulbs.

(b) The *energy of vaporization*, $\Delta_{vap}U$, of the immersion liquid into the dead volume V of the glass bulb, which is endothermal:

$$\Delta_{vap}U = \Delta_{vap}u\,\frac{(p^\circ - p)V}{RT} \tag{5.42}$$

where $\Delta_{vap}u$ is the molar energy of vaporization, p is the pressure in the bulb (vacuum, or equilibrium pressure) and p° the saturation vapour pressure of the immersion liquid.

To obtain an impression of the order of magnitude of the correction terms, let us suppose that, in a typical experiment corresponding to the immersion of *c.* 2 m^2 of ground sand in water (Partyka *et al.*, 1979) the total heat measured is 1042 mJ. In this case the above correction terms are *c.* −6 mJ and +76 mJ, respectively, and therefore:

$$\Delta_{imm}U = 1042\text{ mJ} - 6\text{ mJ} + 76\text{ mJ} = 1112\text{ mJ} \tag{5.43}$$

If other types of equipment and experimental procedures are used, one may also have to take into account:

- The energy absorbed by the continuing evaporation of the immersion liquid – if the set-up is not air-tight.
- The work due to atmospheric pressure when the free level of the liquid is depressed, as it enters the bulb; this term, equal to $V(p_{atm} - p^\circ)$, is quite small and in the experiment quoted above would probably amount to no more than −2 mJ.
- The energy dissipated by stirring, which is often used to ensure a satisfactory dispersion and wetting of the powder.

Critical aspects of immersion microcalorimetric techniques

The microcalorimeter. In the past, most immersion microcalorimetry was carried out with two of the four main categories listed at the beginning of Section 3.2.2, namely, isoperibol microcalorimeters, i.e. conventional 'temperature rise' type, and diathermal-conduction microcalorimeters using a form of heat flowmeter. The isoperibol microcalorimeters were the only type used until the 1960s: they are easily constructed and are well suited for room temperature operation. Improvements were made in the temperature stability of the surrounding isothermal shield and the sensitivity of the temperature detector. Initially the temperature detector was a single thermocouple, then a multicouple with up to 104 junctions (Laporte, 1950), and

finally a thermistor (Zettlemoyer *et al.*, 1953). Differential or twin mountings were adopted in order to cancel external sources of disturbances (Bartell and Suggitt, 1954; Mackrides and Hackerman, 1959; Whalen, 1961). Nevertheless, the limitations of this type of microcalorimetry are: (1) the need for rapid experiments (heat effects must last less than a few minutes, in order to minimize the cooling corrections); (2) the need for complete breaking of the sample bulb and efficient stirring of the powder; and consequently (3) questionable reproducibility and accuracy owing to these extra heat effects. The availability, in the 1960s, of heat flowmeter microcalorimeters increased the possibilities of the immersion method. The improvements included: (a) much higher sensitivity (at least, two orders of magnitude higher); (b) long-term stability which allows wetting phenomena to be studied over hours (even over days if needed); (c) more time available for the wetting process and hence to let the liquid enter the sample bulb through a thin capillary, whose energy of breaking is at least one order of magnitude smaller than that of the complete bulb; and also (d) the possibility of avoiding stirring.

The sample container. This is the most critical part of the experiment. The choice must be made between a sealed glass bulb or another type of container. The latter usually look simpler to operate: some are simply closed by a plug or by a cover with a mercury seal and are located above the liquid. The experiment is then started by simply pulling the plug and turning the bucket upside down (Gonzalez-Garcia and Dios-Cancela, 1965) or when possible by inverting the whole calorimeter (Vanderdeelen *et al.*, 1972; Nowell and Powell, 1991). Another possibility is to insert a pellet of powder, protected on top and bottom by a patch of polymer film, into a tube standing above the liquid. A rod can be used to start the experiment by pushing the pellet out of the tube (Magnan, 1970). Another procedure (Jehlar *et al.*, 1979) is to outgas the powder in a stainless steel cage fitted into the cylindrical cell of a calorimeter. After outgassing, the cage is covered and sealed with mercury. The immersion liquid is poured over the mercury, the cell is closed and made tight by means of a mercury seal and then introduced into the microcalorimeter. When thermal equilibrium is reached, the experiment is started by pulling the cage into the immersion liquid. It is also possible to use a thin metal foil to isolate either the sample (Everett and Findenegg, 1969) or the liquid (Partyka *et al.*, 1975), or simply to use a valve to allow the immersion liquid to flood the sample maintained under vacuum.

The limitation of all these systems lies in the difficulties encountered either in the outgassing or in the air-tight storage of the sample during the thermal equilibration of the microcalorimeter (large variations of the recorded energy of immersion can result from a very small pre-adsorption of the vapour). These difficulties are avoided by the use of *sealed glass bulbs*, which provide the safest operation. Here again, a choice must be made: either the bulbs are to be completely broken or they are designed with a brittle end which is the only part broken. Complete breakage lends itself to excellent wetting (provided it is assisted by thorough stirring) and also to the special case of immersion in a solution. However, the energy of breakage has been reported to range from 57 mJ (Zimmermann *et al.*, 1987) to 3050 mJ (Bartell and Suggit, 1954), although it is most often in the 200–400 mJ range (Zettlemoyer *et al.*, 1953). The unavoidable uncertainty

in these values for the energy of breakage, added to the extra energy introduced by stirring, mean that this approach is only fully justified for immersion in solution. For immersion in pure liquids, the *brittle end* approach is preferable. With special care, one can use thin capillary tips 'barely able to sustain the weight of the ampoule' (Everett *et al.*, 1984), giving a heat of breaking as small as *c.* 0.2 mJ.

The immersion liquid. To study surface phenomena, the liquid must not dissolve the solid and any chemical interaction must not occur in depth. Depending on the purpose, features that are worth considering when selecting an immersion liquid are: (a) its wetting properties for the solid under study; (b) the polarity and molecular size and shape; (c) its saturation vapour pressure at the immersion temperature; and (d) its corresponding enthalpy of vaporization. One would like the product of these two latter quantities to remain small, so that the vaporization into the dead volume of the bulb does not influence too much the quality of the results. The purity of the immersion liquid is essential: if the latter is non-polar (an alkane for instance), the least amount of any polar impurity (alcohol, water) can drastically change the immersion microcalorimetry results. This was early realized by Harkins and Dahlstrom (1930), who spent more than two weeks drying their benzene for immersion and the necessary glassware by making use of 'considerable quantities of sodium wire', of sulfuric acid and of phosphorus pentoxide. The data in Figure 5.6, redrawn from a later

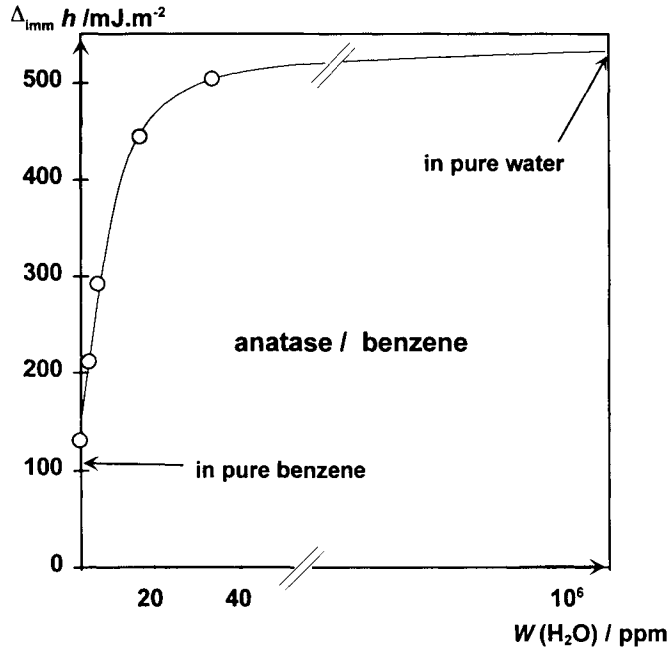

Figure 5.6. Immersion of 1 g TiO_2 (anatase) of 9.24 $m^2\ g^{-1}$ into 8.74 g of benzene: influence of residual water concentration W on $\Delta_{imm}h$ (after Harkins and Boyd, 1942).

paper from the same laboratory (Harkins and Boyd, 1942), show the drastic influence of the residual water concentration in benzene on the enthalpy of immersion of an anatase sample: 20 ppm of water are enough to triple the enthalpy measured! Nowadays, previously degassed 4A zeolite is successfully used as a getter to eliminate any residual water.

Wetting of the powder. Evacuating the immersion bulb prior to sealing it is probably the most efficient means of achieving the desired wetting after breaking the bulb. Nevertheless, it may happen that a powder is not easily wettable and tends to produce aggregates which also are not easily wetted. This situation results in a lack of good reproducibility. It is often thought that this problem can be overcome by efficient stirring, after complete breakage of the bulb, and that therefore one must be prepared to accept the limitations associated with stirring, bulb breakage, etc. However, this is not entirely true: a solution is to use a microcalorimeter able to detect and measure precisely the heat evolution over periods of up to 30 minutes, and in addition to use a bulb with a central constriction. The liquid entering through the broken tip pushes the powder up to the restricted part and percolates through the powder, eventually filling the upper chamber (Laffitte and Rouquerol, 1970).

The dead volume in the bulb. This dead volume allows some evaporation of liquid and a corresponding heat absorption. For example, 1 cm^3 of dead volume, when filled with water vapour at 25°C, absorbs *c.* 80 mJ. Depending on the design and filling of the bulb, this dead volume ranges between 0.2 (Everett *et al.*, 1984) and more than 10 cm^3. Two reasons for this dead volume are (1) the fact that, except for highly wettable powders, it is usually preferable to leave the powder loose rather than compact it; and (2) that some distance – and therefore some volume – must be left between the sample and the glass seal to avoid damaging the sample. This distance is typically around 2 cm. For fragile samples one may use a longer distance or keep the bulb immersed in water or liquid nitrogen during the sealing. In order to restrict the corresponding volume, one can, at will, either introduce a glass rod or limit the diameter of the neck, provided the conditions for a satisfactory outgassing are still ensured.

Finally, it is worth mentioning the interesting experiments by Chessick *et al.* (1954) of determining the enthalpies of immersion of various solids in liquid nitrogen. This was undertaken by simply measuring the amount of gaseous nitrogen vaporized during the experiment, and therefore exactly following the principle of the diathermal, phase change, liquid air calorimeter devised by J. Dewar in 1904. The aim was to determine the surface area of a solid by means of a liquid which was not expected to interact with any functional groups on the surface. The results obtained with samples of carbon black, calcium silicate, alumina and magnesia seem to support this view. Nevertheless, this type of calorimeter is not easy to operate because of the difficulty in obtaining a stable rate of boiling and the strong response of the calorimeter to the least change in atmospheric pressure. For example, if say 250 cm^3 of liquid nitrogen were consumed, a pressure variation of 1 mbar would

produce a heat release of 8 J. The idea, though, certainly deserves to be reconsidered with the aid of modern technological components.

5.2.3. Applications of immersion microcalorimetry in pure liquid

If properly used, immersion calorimetry is a versatile, sensitive and accurate technique which has many advantages for the characterization of porous solids and powders. An indication of these possibilities is given in Figure 5.7. The major areas of application are outlined in this section and reference made to specific examples which are discussed in more detail in other chapters.

It should be kept in mind that any change in surface area, surface chemistry, or microporosity will result in a change in the energy of immersion. Because immersion calorimetry is quantitative and sensitive, and because the technique is not too difficult to apply in its simplest form, it can be used for quality testing. The preliminary outgassing requires the same care as for a BET measurement, but, from an operational standpoint, energy of immersion measurements are probably less demanding than gas adsorption measurements.

Evaluation of the wettability

This involves application of Equation (5.35), following Briant and Cuiec's method (1972), and is straightforward with immersion liquids for which parameter k is already known: water, heptane, cyclohexane, benzene and paraxylene (cf. Table 5.1). Otherwise, it needs to be calculated from γ(LG) and its variation with temperature (cf. Equation (5.34)). This approach was successfully used by Schultz *et al.* (1977) and, more recently, by Douillard *et al.* (1995).

Determination of the polarity of solid surfaces

The polarity of a solid surface can be regarded as the strength of its average electrostatic field F. This field interacts with permanent or induced dipoles of adsorbed molecules, whereas its gradient interacts with permanent or induced quadrupoles. These interactions give rise to components of the adsorption energy such as $E_{F\mu}$ (with permanent dipoles), E_p (polarization contribution) or E_{FQ} (with permanent quadrupoles). Therefore, the selection of the appropriate immersion systems, differing mainly in the molecular dipole moment μ of the immersion liquid, can be expected to provide information on the value of $E_{F\mu}$ since:

$$E_{F\mu} = -F\mu \tag{5.44}$$

This was the basis of the approach by Chessick *et al.* (1954, 1955) and Zettlemoyer *et al.* (1958), which involved the use of a series of immersion liquids such as butyl derivatives differing only in their polar groups: 1-butanol, 2-butanol, butanal, 1-aminobutane, 1-chlorobutane, butanoic acid. With the polar surfaces studied (rutile, CaF_2, Aerosil, alumina), an approximately linear relation was found between the energy of immersion and the dipole moment. The slope gave directly the average field strength (for instance, 820 $V/\mu m^{-1}$ on a rutile titanium (IV) oxide) and the

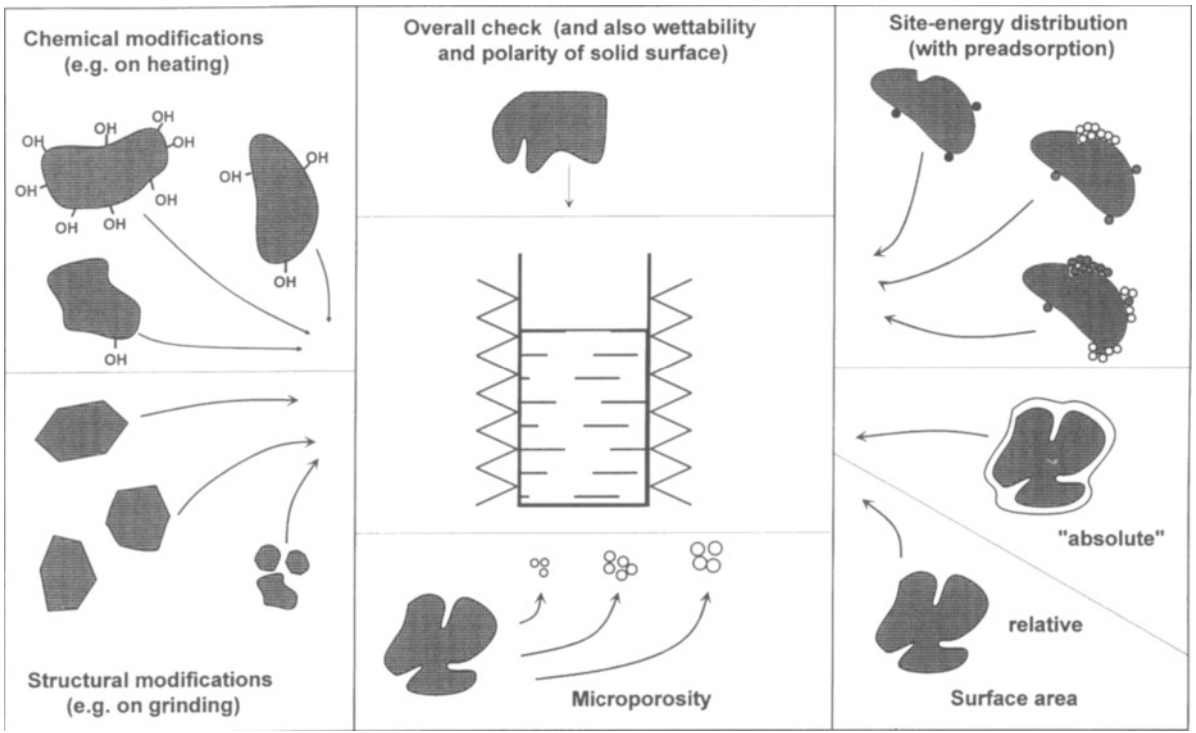

Figure 5.7. Applications of immersion microcalorimetry.

intercept gave the average value for the dispersion contribution E_d to the adsorption energy.

The polarization contribution E_p itself could be calculated from F and the polarizability α of the adsorbate, using:

$$E_p = -\frac{F^2\alpha}{2} \tag{5.45}$$

(For a warning about pitfalls to be avoided in this type of approach, see Chessick, 1962.)

A similar linear variation of the energy of immersion with the dipole moment was observed by Gonzalez-Garcia and Dios-Cancela (1965) when immersing montmorillonites in water, ethylene glycol, acetonitrile and dimethyl sulfoxide, although the relationship was more complicated – as is usual with clays – because of the hydration of the exchangeable cations.

Schröder (1979) was able to improve this approach by using a refined expression of the Gibbs free energy of adhesion as a function of the various intermolecular attraction energies between the liquid and the solid. In this way, by using up to 10 different immersion liquids with known parameters, he has calculated the apparent dipole moment and polarizability characterizing the immersion behaviour of various pigment surfaces (e.g. rutile, iron oxide and several phtalocyanines).

As stressed by Jaycock and Parfitt (1981), immersion calorimetry is thus a potential source of fundamental data and is certainly worth further use for this purpose.

Study of surface modification

One type of chemical modification which has been successfully studied by immersion microcalorimetry in water is the dehydration and dehydroxylation of oxides (see Chapter 10). The oxides studied were mainly silica (Young and Bursh, 1960; Brunauer *et al.*, 1956; Whalen 1961a,b), titania (Wade *et al.*, 1961; Zettlemoyer and Chessick, 1964), alumina (Wade and Hackerman, 1964) and iron oxides (Furuichi *et al.*, 1982; Watanabe and Seto, 1988). The outgassing temperature above which the dehydration was no longer reversible was easily shown from the maximum in the curve of energy of immersion versus outgassing temperature. Also, the influence of dehydroxylation of silicas on their energy of immersion in benzene (which interacts with hydroxyls through its π-electron cloud), but not in cyclohexane (which does not undergo specific interactions), was clearly shown by Whalen (1962), who evaluated the benzene–hydroxyl energy of interaction (from 0.04 to 0.26 μJ per site for his three silicas).

Another modification easily assessed by immersion microcalorimetry is the change in hydrophobicity of a surface, e.g. by oxidizing a graphitized carbon surface. The energy of immersion in water was shown to increase almost linearly with decrease in hydrophobicity (Young *et al.*, 1954) and the energies of immersion of hydrophobic and hydrophilic patches were estimated to be 31 and 730 J m^{-2}, respectively (Healy *et al.*, 1955).

Lyklema (1995) pointed out that, in the absence of immersion calorimetry, the notion of surface hydrophilicity–hydrophobicity remains vague. Once the molar enthalpy of immersion in water is assessed it can readily be compared with the value 44 kJ mol^{-1}, which corresponds to the enthalpy of condensation of water at room temperature. If it is higher, the surface is considered to be hydrophilic; if lower, the surface is defined as hydrophobic.

The change in nature of the oxidized surface can be followed with immersion liquids other than water. By increasing the oxygen content of a carbon black (i.e. Spheron 6) up to 12%, Robert and Brusset (1965) obtained an increase of the energy of immersion in methanol from 140 to as much as 390 mJ m^{-2} (practically the same ratio as that observed with water), whereas the energy of immersion in *n*-hexadecane remained nearly constant, around 100 mJ m^{-2}.

Assessment of the site-energy distribution

This requires a more sophisticated and time-consuming procedure, i.e. by following the energy of immersion versus pre-coverage of the sample by the vapour of the immersion liquid. The vapour will first cover the highest available energy sites, and hence give a pronounced decrease in the energy of immersion. Such a curve is shown in Figure 5.8b.

Figure 5.8 gives the main types of curve listed by Zettlemoyer and Narayan (1967) for this type of immersion calorimetry experiment with pre-coverage of the sample. Curve (a) is obtained with homogeneous surfaces with respect to the immersion liquid (e.g. chrysotile asbestos in water, Zettlemoyer *et al.*, 1953). Curve (b) is given by

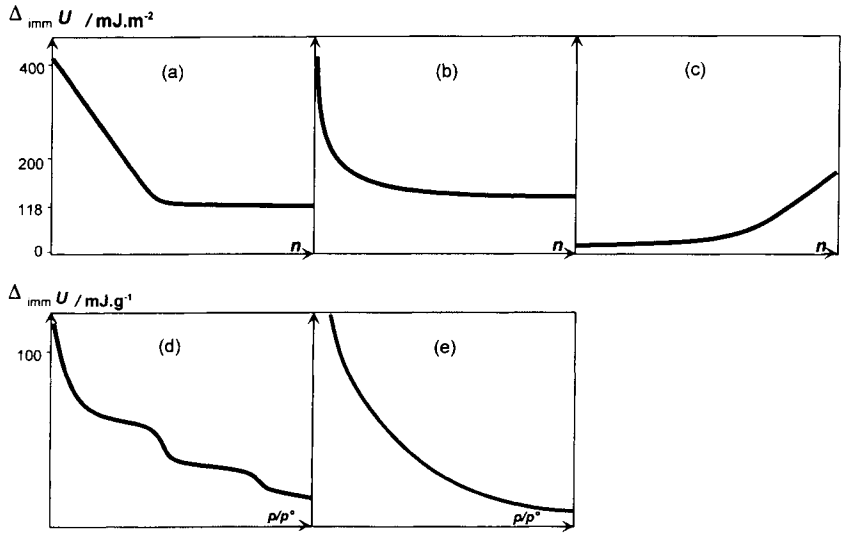

Figure 5.8. Various types of energy of immersion isotherms (after Zettlemoyer, 1965).
(a) Homogeneous surface; (b) heterogeneous surface; (c) hydrophobic surface; (d) swelling of stratified adsorbent; (e) filling of porous adsorbent.

heterogeneous surfaces (e.g. most oxides in water) and curve (c) by the immersion in water of hydrophobic surfaces, with only a few hydrophilic sites (e.g. Graphon). Curves (d) and (e) are only in part related to the site-energy distribution: curve (d) is typical of the swelling of a clay (like Wyoming bentonite in water) where the molecules penetrate through platelets of the mineral at certain relative pressures, whereas curve (e) is typical of the progressive filling of micropores and then possibly mesopores. Because of the difficulty of evaluating the true surface area, the quantities plotted for these last two systems are different from those used in Figures 5.8a to 5.8c.

Since the data provided by the above type of immersion calorimetry experiment can be directly related to the results obtained by gas adsorption calorimetry the question arises: which type of experiment is to be preferred? In fact, immersion calorimetry, although time-consuming, has certain advantages because of the difficulty in handling easily condensable vapours in adsorption manometry.

Assessment of structural modifications of the adsorbent

The surface electrostatic field of a solid strongly depends on the crystallinity of the solid, as can be seen for instance by comparing the areal energies of immersion in water of quartz (510 mJ m^{-2}), precipitated silica (300 mJ m^{-2}) and pyrogenic silica (155 mJ m^{-2}) after a similar outgassing at 140°C (Denoyel *et al.*, 1987). It therefore seems reasonable to consider that there is a direct relationship between the energy of immersion in water and the degree of crystallinity of an oxide such as silica. Furthermore, using immersion microcalorimetry it is possible to follow the changes resulting from intensive grinding of powders such as quartz (Wade *et al.*, 1961), titania and alumina (Wade *et al.*, 1964) or calcite (Cases, 1979).

Assessment of microporosity

Immersion microcalorimetry is able to characterize microporosity in at least three different ways:

1. When progressive pre-coverage is used, a curve of the type shown in Figure 5.8e is given, revealing the filling of micropores, even at very low relative pressures of pre-coverage.
2. When the molecular size of the immersion liquid is close to that of the micropores a delayed diffusion of the liquid can be immediately detected from the slower response of the microcalorimeter, as was clearly shown by Widyani and Wightman (1982) when immersing a microporous activated carbon in propanol.
3. When a set of immersion liquids is used, with an appropriate range of molecular sizes and shapes (i.e. flat, like aromatic molecules, or bulky), the energy of immersion is directly dependent on the extent of the molecular penetration into the porous network. This was shown for example by Atkinson *et al.* (1982) on microporosity and by Denoyel *et al.* (1993).

Assessment of surface area

Immersion calorimetry has an important and unique role in surface area determination. It can provide relative values, which are particularly useful in the study of

microporous adsorbents, and it can also be used (independently of the BET method) to give 'absolute' areas. These aspects are described in Chapter 6.

Further comments on the application of immersion calorimetry

As we have already seen, it is not difficult to undertake accurate energy of immersion measurements provided that the microcalorimetric technique is carefully selected and that certain precautions are taken. It was pointed out by Chessick (1962) that it is deceptively easy to obtain 'heat of wetting' data, but the results will be of very little scientific value unless steps are taken to ensure that the adsorbent and the liquid have been properly prepared and that the conditions of the experiment meet well-defined thermodynamic requirements.

5.3. Adsorption from Liquid Solution

Adsorption from liquid solution is almost a new world in comparison with adsorption from the gas phase: the fundamental principles and methodology are different in almost all respects (Gregg, 1961).

The simplest system now involves a binary solution and the composition of the adsorbed layer is usually unknown. Furthermore, although there is no large density difference (*c.* three orders of magnitude) as in the case of gas adsorption, the sizes, shapes and possible configurations of solute molecules cover a much broader range than in gas adsorption. Indeed, from a statistical mechanical standpoint, it may appear that adsorption at the liquid–solid interface is closer to adsorption at the gas–liquid interface than to adsorption at the gas–solid interface (Everett, 1973). A great effort has been made to improve our understanding of these systems, which are of major importance in many fields of science and technology.

Major advances in the thermodynamic treatment have been made by Defay and Prigogine (1951), Schay (1970), Schay and Nagy (1961, 1972), Schay *et al.* (1972), Nagy and Schay (1963), Kipling, (1965) and Everett (1972, 1973, 1986). These and other authors have given considerable thought to the presentation and utilization of an experimental data adsorption from solution.

Until relatively recently, the fact that an experimental isotherm necessarily contained composite information concerning the adsorption of the two components of a binary solution was considered to be a major problem. For a rigorous interpretation it was felt necessary to process the data to obtain the so-called 'individual adsorption isotherm' or 'separate adsorption isotherm' of each component. However, this is not at all straightforward and requires the introduction of a number of assumptions relating to the structure of the adsorbed layer. The main problem is of course to know the composition of the adsorbed layer. One assumption often used in the case of volatile components is that introduced by Williams (1913): the solid will adsorb the same amount of each component from the vapour in equilibrium with the solution as from the solution itself. This of course implies that the adsorbed layer has the same composition at the liquid–solid and gas–solid interfaces and it requires numerous gravimetric measurements from the vapour

phase. To limit these measurements to two, a further assumption (Elton, 1951) is that the adsorption at both interfaces is confined to a monolayer and that the cross-sectional area of each molecule is independent of coverage, so that it can be derived from the gas adsorption isotherm for each component. This approach was tested by Kipling and Tester (1952) for the adsorption on charcoal from ethanol–benzene mixtures at 20°C. Their results (see Figure 5.9) illustrate the striking difference between the individual isotherms and the original composite isotherm based on the change of concentration. It is important to recognize that the derivation of the individual isotherms requires an oversimplification in the interpretation of the adsorption process. This is why, by following the IUPAC recommendations (Everett, 1986), we stress the need for a few strict rules on the presentation and interpretation of experimental data. In the next section it will be shown how the early assumptions may be avoided by the presentation of 'reduced surface excess amounts' versus concentration, which provides a basis for any further theoretical interpretation of the data.

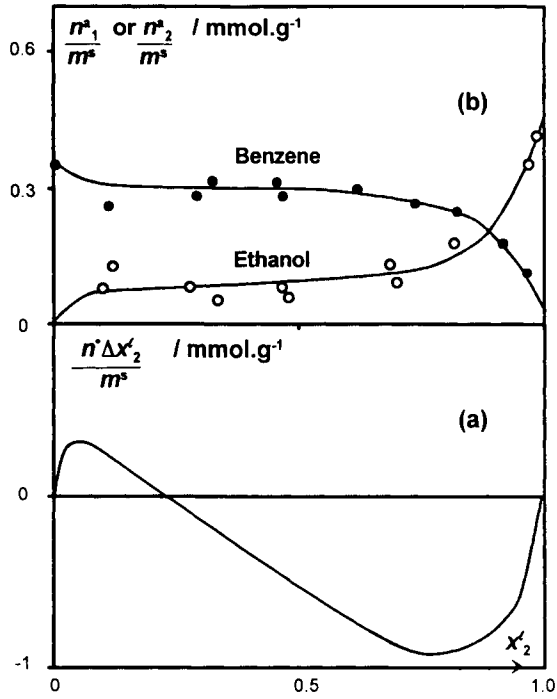

Figure 5.9. Adsorption from ethanol–benzene mixtures onto charcoal at 20°C (after Kipling and Tester, 1952).
(a) Isotherm of 'concentration change' (i.e. of reduced surface excess of ethanol) versus molar fraction of ethanol.
(b) Corresponding separate isotherms.

5.3.1. Quantitative expression of the amounts adsorbed from a binary solution

Scope and limitations of the normal surface excess amounts

As for adsorption from the gas phase, one must be able to express unambiguously and quantitatively the observed adsorption phenomenon without reference to any prior knowledge concerning the structure of the adsorbed layer. For this reason, the concept of the Gibbs dividing surface (GDS) and the associated surface excess amounts are just as useful as for gas adsorption. Figure 5.10 represents the concentration of species 1 and 2 and also the total concentration c (expressed as the amount per unit volume of solution) as one moves away from the adsorbing surface. Figure 5.10a represents a hypothetical adsorption system where the molar volumes of species 1 and 2 are equal, so that any enrichment of the adsorption layer in component 2 (i.e. positive adsorption) is necessarily accompanied by an equal loss of component 1 (i.e. negative adsorption).

Figure 5.10b represents another adsorption system, in which the molar volumes of species 1 and 2 are different, so that adsorption also affects the total concentration c in the solution. Although these are representative of real systems, it must be stressed that in most cases these concentration profiles are unknown.

Finally, Figure 5.10c gives a Gibbs representation of the simple case where the GDS coincides with the real adsorbing surface. By convention, the concentrations in the solution are taken as constant up to the GDS. The hatched areas represent the amounts apparently lost (for component 2) or gained (for component 1) by the solution when the adsorption changes the concentrations from c_1° and c_2° to c_1 and c_2. These are the amounts counted as the 'surface excess amounts' on the GDS, one being positive (for component 2) and the other negative (for component 1). Now, one advantage of the GDS is that it can be located arbitrarily, allowing a change at will of the volume $V^{l,\circ}$ of the liquid. Thus the calculation of the surface excess amount n_i^σ

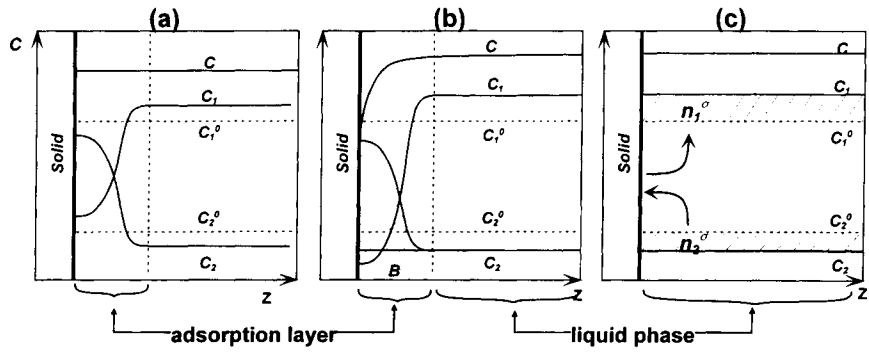

Figure 5.10. Concentrations in a liquid–solid adsorption system (competitive adsorption from binary mixture or solution).
(a) Real state after preferential adsorption of 2 (molecular volumes and cross-sectional areas of 1 and 2 supposed equal).
(b) Same as (a), but with different molecular volumes and/or cross-sectional areas for 1 and 2.
(c) Gibbs representation of system (b) for the case where GDS coincides with real adsorbing surface.

directly follows from its defining equation:

$$n_i^\sigma = n_i - V^{l,\circ} c_i^l \tag{5.46}$$

where n_i is the total amount of component i in the system and c_i^l is its concentration in the liquid after adsorption. It is evident that the value of n_i^σ is linearly dependent on the value taken for $V^{l,\circ}$. This variation of n_i^σ with the position of the GDS is indicated in Figure 5.11. Here, the GDS is taken as parallel to the real solid–liquid interface, of area A. Any displacement, Δz, of the GDS normal to the surface (e.g. from position S to position E), produces a change $A\Delta z$ in the volume $V^{l,\circ}$ in Equation (5.46). The corresponding change in n_i^σ is represented in Figure 5.11 by a straight line, its slope being simply $c_i^l A$. The strong dependence of n_i^σ on the position of the selected GDS must be recognized in any attempt to provide a standard procedure for reporting the experimental data. For this reason, some investigators have preferred to adopt an alternative approach.

The use of relative surface excess amounts

The aim now is to replace n_i^σ by another quantity, which would also rely on the existence of a GDS but which would be invariant with respect to the position of the GDS (Guggenheim and Adam, 1933; Defay, 1941). This can be done by simply writing Equation (5.46) for each component, and then eliminating $V^{l,\circ}$ from these two equations. In this manner we can obtain an equation of the form

$$n_2^\sigma - n_1^\sigma \frac{c_2^l}{c_1^l} = n_2 - n_1 \frac{c_2^l}{c_1^l} \tag{5.47}$$

The variables on the right-hand side are experimental quantities which are independent of the position of the GDS. The left-hand side of the equation must also be

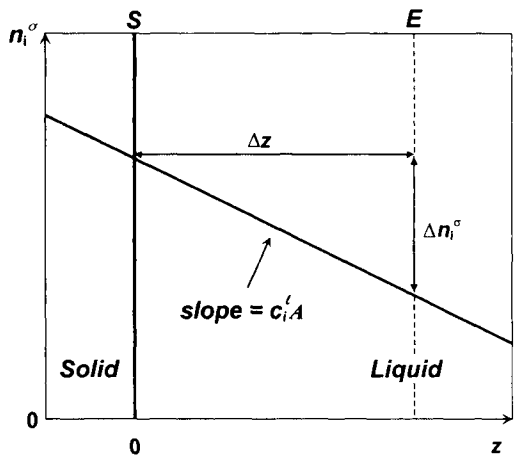

Figure 5.11. Dependence of surface excess amount of component i on location of GDS.
S, GDS of actual adsorbing surface;
E, GDS at distance Δz from adsorbing surface.

independent of the position of the GDS. This function is named '*relative* surface excess of 2 with respect to 1' and is denoted $n_2^{\sigma(1)}$. It is defined as:

$$n_2^{\sigma(1)} = n_2^{\sigma} - n_1^{\sigma} \frac{c_2^{\mathrm{I}}}{c_1^{\mathrm{I}}} \tag{5.48}$$

and operationally:

$$n_2^{\sigma(1)} = n_2 - n_1 \frac{c_2^{\mathrm{I}}}{c_1^{\mathrm{I}}} \tag{5.49}$$

Corresponding equations hold for the relative surface excess of 1 with respect to 2. Thus:

$$n_1^{\sigma(2)} = n_1^{\sigma} - n_2^{\sigma} \frac{c_1^{\mathrm{I}}}{c_2^{\mathrm{I}}} = n_1 - n_2 \frac{c_1^{\mathrm{I}}}{c_2^{\mathrm{I}}} \tag{5.50}$$

In these equations, where the concentrations are expressed as amounts per unit volume, the ratio of concentrations (i.e. $c_2^{\mathrm{I}}/c_1^{\mathrm{I}}$) can be replaced by the ratio of molar fractions (i.e. $x_2^{\mathrm{I}}/x_1^{\mathrm{I}}$). Taking into account that $x_1^{\mathrm{I}} = 1 - x_2^{\mathrm{I}}$, one can then transform Equations (5.48) and (5.47) into:

$$n_2^{\sigma(1)} = n_2 - n_1 \frac{x_2^{\mathrm{I}}}{x_1^{\mathrm{I}}} = n^{\circ} \frac{\Delta x_2^{\mathrm{I}}}{x_1^{\mathrm{I}}} \tag{5.51}$$

where $n^{\circ} = n_1 + n_2$, $n_2 = n^{\circ} x_2^{\mathrm{I},\circ}$ and Δx_2^{I} is the change $x_2^{\mathrm{I},\circ} - x_2^{\mathrm{I}}$ due to adsorption. $n_2^{\sigma(1)}$ is usually divided by m^{s} (the mass of solid adsorbent) to give the '*specific relative* surface excess of 2 with respect to 1'. Alternatively, it can be divided by A to give $\Gamma_2^{(1)}$, the '*areal relative* surface excess of 2 with respect to 1'.

The use of reduced surface excess amounts

Another function invariant with respect to the position of the GDS and named the '*reduced* surface excess amount' was derived at by Defay (1941) in a similar way. Starting again from Equation (5.46), we can write the following two equations:

$$n_2^{\sigma} = n_2 - V^{\mathrm{I},\circ} c_2^{\mathrm{I}} \tag{5.52}$$

$$n^{\sigma} = n^{\circ} - V^{\mathrm{I},\circ} c^{\mathrm{I}} \tag{5.53}$$

where $n^{\sigma} = n_1^{\sigma} + n_2^{\sigma}$, $n^{\circ} = n_1 + n_2$ and $c^{\mathrm{I}} = c_1^{\mathrm{I}} + c_2^{\mathrm{I}}$.

Taking into account that $c_2^{\mathrm{I}}/c^{\mathrm{I}}$ can be replaced by x_2^{I}, we finally obtain:

$$n_2^{\sigma} - n^{\sigma} x_2^{\mathrm{I}} = n_2 - n^{\circ} x_2^{\mathrm{I}} = n^{\circ} \Delta x_2^{\mathrm{I}} \tag{5.54}$$

Here again the right-hand side does not depend on anything other than experimentally measurable quantities, and therefore we conclude that the right-hand side does not depend on the position of the GDS. This function is defined as the '*reduced* surface excess amount of 2':

$$n_2^{\sigma(n)} = n_2^{\sigma} - n^{\sigma} x_2^{\mathrm{I}} \tag{5.55}$$

Usually, this quantity is either made 'specific' after division by m^s or 'areal' after division by A. In the latter case it is denoted by $\Gamma_2^{(n)} = n_2^{\sigma(n)}/A$.

In some instances (especially if the exact molar mass of one component is not known, which often happens with long chain molecules, like those of surfactants) it is more convenient to think in terms of mass. We then use mass fractions w_1^1 or w_2^1 (instead of molar concentrations or molar fractions) and arrive at surface excess *masses*, either relative:

$$m_2^{\sigma(1)} = m_2^\sigma - m_1^\sigma \frac{w_2^1}{w_1^1} = m_2 - m_1 \frac{w_2^1}{w_1^1} \tag{5.56}$$

or reduced:

$$m_2^{\sigma(m)} = m_2^\sigma - m^\sigma w_2^1 = m_2 - m^\circ w_2^1 \tag{5.57}$$

The meaning of relative and reduced surface excess amounts

Although the relative and the reduced surface excess amounts (or masses) do not depend on the position of the GDS, there is a special position of the GDS which cancels the last term of the defining equations ((5.48) and (5.55)) and gives a useful idea of the meaning of these two quantities. For Equation (5.48), this special position of the GDS is the one for which the surface excess amount n_1^σ of component 1 is zero. We then get:

$$n_2^{\sigma(1)} = n_2^\sigma \tag{5.58}$$

so that the relative surface excess amount of 2 with respect to 1 is equal to the surface excess of 2 for the GDS which cancels the surface excess of 1. This is represented in Figure 5.12, which, along the same lines as Figure 5.11, now shows the effect of the

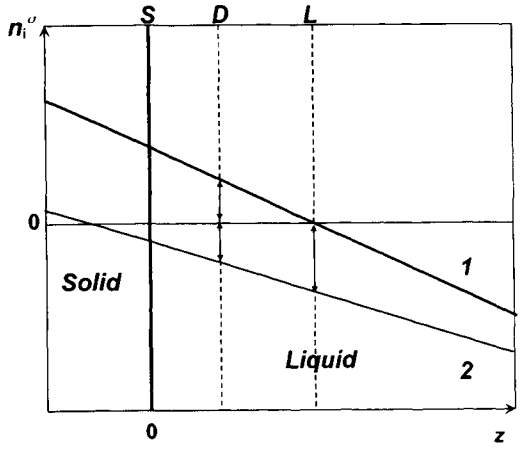

Figure 5.12. Dependence of surface excess amounts of components 1 and 2 on location of GDS. S, GDS of actual adsorbing surface; D, GDS for which $n_1^\sigma + n_2^\sigma = 0$; L, GDS for which $n_1^\sigma = 0$.

location of the GDS on the surface excess amounts of components 1 and 2. Here GDS 'L' provides the special condition for $n_1^\sigma = 0$.

Turning to Equation (5.55), we now require a GDS where n^σ (the whole surface excess amount $n_1^\sigma + n_2^\sigma$) equals zero. In Figure 5.12, this is the case for GDS 'D', where $n_2^\sigma = -n_1^\sigma$.

From Equation (5.55) we now obtain:

$$n_2^{\sigma(n)} = n_2^\sigma = -n_1^\sigma = -n_1^{\sigma(n)} \tag{5.59}$$

which shows that the reduced surface excess amounts of 1 and 2 are equal and opposite in sign. It turns out that this remains true whatever the position of the GDS. As underlined by Defay and Prigogine (1951, p. 26), this representation in terms of the reduced surface excess 'treats the components on an equal footing'. A practical consequence is that the same curve (either U or S as illustrated in Figure 5.13) provides the adsorption isotherm for both components. We also note that it is only when the partial molar volumes of 1 and 2, together with their molecular cross-sectional areas, are equal, that for $n_1^\sigma + n_2^\sigma = 0$ the GDS coincides with the real adsorbing surface.

By combining Equations (5.51), (5.54) and (5.55), we obtain the relationship between the relative and reduced surface excess quantities:

$$n_2^{\sigma(1)} = n_2^{\sigma(n)}/x_1^1 \tag{5.60}$$

and:

$$\Gamma_2^{(1)} = \Gamma_2^{(n)}/x_1^1 \tag{5.61}$$

and also:

$$m_2^{\sigma(1)} = m_2^{\sigma(m)}/w_1^1 \tag{5.62}$$

Adsorption isotherms expressed in reduced surface excess amounts

The reduced surface excess amounts, whose use is recommended by the IUPAC (Everett, 1986), offer much more than a form of precise mathematical accounting of the adsorption experiment: they also offer the most convenient way of reporting the experimental results. For decades this presentation was intuitively chosen as a way of plotting adsorption data, without any reference to the Gibbs formalism. The quantity plotted to represent adsorption of component 2 was often in the form of either $n^\circ\,\Delta x_2^1$, which is consistent with Equation (5.54), or $[m_2 - m^\circ w_2^1]$, which is consistent with Equation (5.57). The isotherm obtained is generally termed a 'composite isotherm' or an 'isotherm of apparent adsorption', or less often an 'isotherm of concentration change'. The term 'composite' refers to the fact that this single isotherm contains information about the adsorption of both components 1 and 2. This is shown in Figure 5.13, which gives the two most important shapes of reduced surface excess (or 'composite') isotherms (S-shape and inverted U-shape) for completely miscible liquids. Depending on the axis chosen, one obtains the isotherm for component 2. These shapes were the basis for a more detailed classification given by Schay and Nagy (1961).

When the adsorption is studied from *dilute solutions* (where by convention, we shall consider that component 1 is the solvent), the experimental isotherms are still plotted, strictly speaking, in terms of reduced surface excess. Nevertheless, since

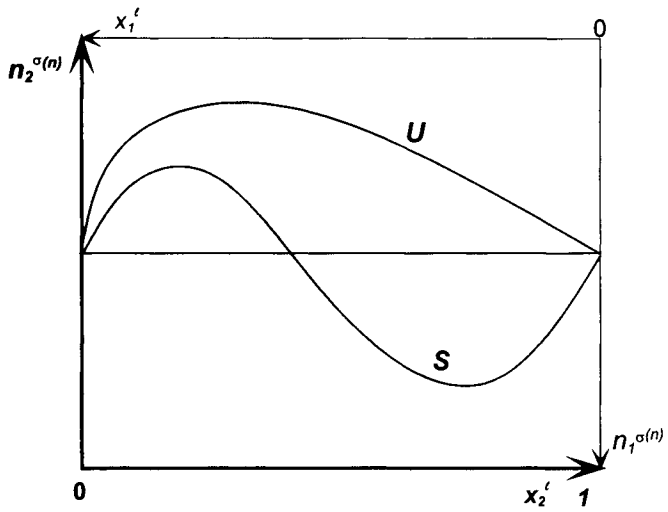

Figure 5.13. The two basic shapes of reduced surface excess (or 'composite') isotherms over the whole concentration range: S-shape (S) or inverted U-shape (U). Thick line axes (zero in bottom left) represent the isotherms for component 2. Thin line axes (zero in top right) represent the isotherms for component 1.

$x_1^l = 1 - x_2^l \approx 1$, one sees, from Equations (5.51), (5.54) and (5.60) that:

$$n_2^{\sigma(1)} \approx n_2^{\sigma(n)} \approx n_2^{\sigma} \tag{5.63}$$

so that any one of these three quantities can be plotted to represent the adsorption data. Although up to 18 different shapes have been distinguished in a detailed classification (Giles *et al.*, 1960), three main shapes are of special interest, as shown in Figure 5.14: a Langmuir or L-shape, stepwise and an S-shape with an inflexion in

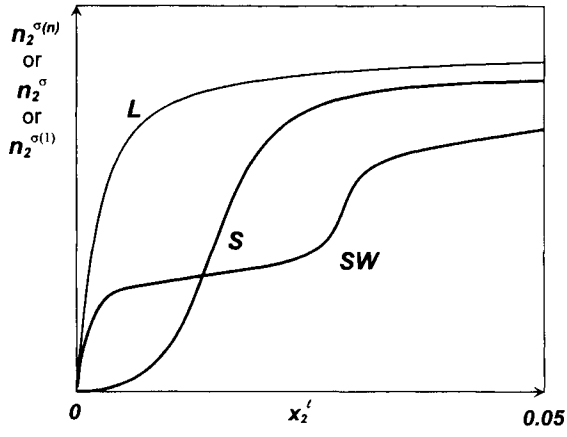

Figure 5.14. Typical shapes of surface excess isotherms from dilute solutions (Langmuir or L-shape, S-shape, stepwise (SW)).

the low-concentration region. If higher concentrations can be attained, the reduced surface excess eventually reaches a maximum, before decreasing as indicated in Figure 5.13.

Since the reduced and relative surface excess isotherms convey composite information on the adsorption of the two components, there is a strong incentive to determine the *individual* (or 'separate') *isotherms*, i.e. the adsorbed amount n_2^a (or n_1^a) versus concentration, mole fraction or mass fraction. It will be recalled that this implies some assumptions about the thickness, composition and structure of the adsorbed layer, and therefore is not to be recommended for reporting adsorption from solution data in a standard form. Indeed, this second step is already part of the theoretical interpretation of the adsorption mechanisms.

5.3.2. Quantitative expression of the energies involved in adsorption from solution

Definition of energies and enthalpies of adsorption from solution

Let us consider the case of a solution with solvent (1) and solute (2). Its composition will be preferably given as a *molality*, i.e. the amount n_2 of solute associated with 1 kg of solvent (this quantity is of course invariant with temperature). Following the IUPAC recommendation (Mills *et al.*, 1993), the molality of the solute will be denoted b_2 to avoid any confusion with m_2, the mass of solute. The amount of solute contained in a mass m of solution of molality b_2 is therefore:

$$n_2 = \frac{b_2 \times m}{1000 + M_2 b_2} \tag{5.64}$$

where M_2 is the molar mass of the solute (in g mol^{-1}). In the solution of molality b_2, each component has a partial molar enthalpy:

$$h_i^1 = \left(\frac{\partial H^1}{\partial n_i}\right)_{T,p,A,n_{j\neq i}} \tag{5.65}$$

where H^1 is the total enthalpy of the solution.

We recall that for condensed phases (either liquid or adsorbed) we are generally able to equate the molar enthalpy and the molar internal energy. Here we shall use enthalpies, simply because they are more common in the literature, but in the following definitions h could be replaced by u.

Just as for gas adsorption, we can define a partial differential enthalpy of adsorption of a component, $\Delta_{ads}\dot{h}_i$, which would correspond to the adsorption, from a solution of molality b_i, of an infinitesimal amount of component i, dn_i, on a solid surface already covered with solute at a reduced surface excess concentration $\Gamma_i^{(n)}$:

$$\Delta_{ads}\dot{h}_i = \dot{h}_i^{\sigma(n)} - h_i^1(b_i) \tag{5.66}$$

where $\dot{h}_i^{\sigma(n)}$ is the reduced surface excess enthalpy of the component i:

$$\dot{h}_i^{\sigma(n)} = \left(\frac{\partial H^\sigma}{\partial n_i^{\sigma(n)}}\right)_{T,p,A,n_j \neq n_i} \tag{5.67}$$

H^σ being the total surface excess enthalpy.

Now, in case of adsorption of a finite amount of component i, there is a resulting change in the molality of the solution: it follows that the partial enthalpy of component i changes not only in the solution, but also at the adsorbing surface. Rather than integrating Equation (5.66) with an ever-changing initial state, it turns out to be more convenient to refer to a constant reference state comprising a clean solid surface and a pure liquid for the solvent (molar enthalpy $h_1^*(1)$) or an infinitely diluted state for the solute (molar enthalpy $h_2^\infty(1)$). We can define a standard integral molar enthalpy of adsorption for each component, so that we may write for the solvent:

$$\Delta_{ads} h_1^\circ = h_1^{\sigma(n)} - h_1^*(1) \tag{5.68}$$

and for the solute:

$$\Delta_{ads} h_2^\circ = h_2^{\sigma(n)} - h_2^\infty(1) \tag{5.69}$$

Definition of displacement enthalpies (and energies)

The enthalpies of adsorption as already defined are adequate for an experiment when a clean adsorbent is immersed in the solution, but they are not suited for other experiments, which are usually more accurate where the adsorbent is initially immersed in the pure solvent. When the pure solvent is replaced by a solution of molality b_2, adsorption of the solute can only take place by *displacement of the solvent*. The word 'displacement' is used here to indicate that the adsorption of the amount $n_2^{\sigma(n)}$ of solute produces the desorption of a corresponding (but usually not equal) amount of solvent. Following Kiraly and Dekany (1989), let us call r the amount of solvent displaced (i.e. desorbed) by one mole of solute, therefore producing a change in composition of the solution and giving an enthalpy of mixing, $\Delta_{mix}H$, which is part of the overall heat effect, Q_{exp}, measured during the experiment. It is preferable not to include $\Delta_{mix}H$ (which is not a property of the interface) in the definition of the enthalpy of displacement, which is therefore:

$$\Delta_{dpl} H_{1,2} = Q_{exp} - \Delta_{mix} H \tag{5.70}$$

Definition of the enthalpies (and energies) of mixing

In principle, the overall enthalpy of dilution can be considered to include one term due to the solute and another one due to the solvent. Thus,

$$\Delta_{mix} H = n_2^l[h_{2f}^l - h_{2i}^l] + n_1^l[h_{1f}^l - h_{1i}^l] \tag{5.71}$$

where the subscripts i and f refer to the initial and final states. For a dilute solution, say with a mass fraction $\leqslant 1\%$, the term due to the solvent can be omitted. $\Delta_{mix}H_2$ must be measured in separate experiments, by the addition of a standard solution to the pure solvent.

5.3.3. Basic experimental methods for the study of adsorption from solution

We may divide the experimental techniques available for the study of adsorption from solution into three main categories: (a) for the determination of adsorption isotherms, (b) for the measurement of the energies involved, and (c) for the provision of extra information on the properties of the adsorbed layer.

Methods for determining the amounts adsorbed

A first distinction must be made between the methods which use one sample for each point on the adsorption isotherm (i.e. immersion methods) and those using a single sample through which the solution of increasing concentration is allowed to flow (i.e. flow-through methods). A critical outline of most of these methods is given by Everett (1986).

Immersion methods. These are the oldest and the easiest to apply with conventional bench-type equipment but may suffer, as we shall see, from a lack of accuracy or from a large sample consumption.

In the *standard immersion method*, the dry sample is immersed in the solution (see Figure 5.15a). In a slightly different version (Rouquerol and Partyka, 1981), the sample is initially covered with the pure solvent (protected from any contact with ambient atmosphere) before receiving an appropriate dose of mother solution (see Figure 5.15b).

Equilibration may take between 1 minute and more than a day, in a thermostatted bath with continuous and slow tumbling. The suspension, still kept at the controlled temperature, is allowed to settle, which may take one full day, or, more frequently, the suspension is centrifuged (taking care, in the case of polymers, not to produce a measurable concentration gradient) and the supernatant is then pipetted and analysed. The analysis may involve differential refractometry, UV or IR spectroscopy (the former mainly for aqueous solutions, the latter for organic solutions), organic carbon analysis, colorimetry (for dye adsorption) or surface tension measurements. As mentioned in Section 5.3.1, this method has the advantage that it directly gives the reduced surface excess amounts. Since one experiment only provides one point of the adsorption isotherm, it is usual to undertake a number of simultaneous measurements (each requiring a fresh sample) in order to cover the desired portion of the adsorption isotherm.

A possible way to increase the accuracy of this immersion approach is to use the *slurry method* and to analyse a weighed sample of the slurry in the bottom of the test-tube, instead of analysing the supernatant (Nunn *et al.*, 1981). One then simply makes use of Equation (5.49), the operational expression of the relative surface excess of the solute with respect to the solvent. Here n_1 and n_2 are the total amounts of solute and solvent in the sample of slurry (either adsorbed or in solution) and c_2^l and c_1^l their concentrations in the solution. If one uses a liquid–solid ratio large enough to avoid any measurable change in concentration on adsorption, then c_2^l and c_1^l are simply the concentrations in the starting solution. The measurement is accurate provided the quantitative analysis of the slurry, which involves measuring the total amounts of 2 and 1

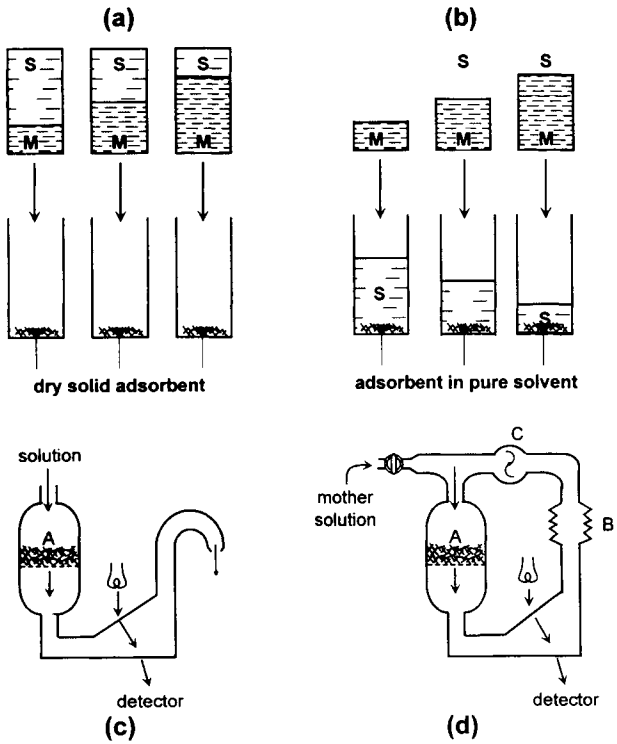

Figure 5.15. Methods to determine amount adsorbed from solution.
(a) Immersion method 1: dry samples covered with solution made of various proportions of pure solvent S and mother solution M. (b) Immersion method 2: samples protected by pure solvent receive various amounts of mother solution. (c) Open-flow method with refractometric detector. (d) Circulation method (A, adsorbent packing; B, expansion bellows or vessel; C, circulating pump).

and also the weight of the dry solid, can itself be carried out accurately. However, this does not solve the problem of sampling: the immersion method relies on the assumption that the various samples used (one for each point of the adsorption isotherm) are all representative of the solid studied.

Flow-through methods. In these methods, only one sample is used and is successively brought into equilibrium with solutions of increasing concentration. Most frequently, the sample is initially equilibrated with the pure solvent. Each increase in concentration produces an adsorption of solute by displacement of solvent from the solid surface. The changes in concentration produced by adsorption are usually monitored by the same techniques as those used in the immersion methods, except that they are now located on-line. A general requirement of these methods is that the sample can form a permeable bed and does not block the filter: this usually requires a grain size over, say, 2 μm and prevents any tendency to gel formation.

In the *open-flow method* (see Figure 5.15c), at each step a fresh solution of

constant concentration continuously flows through the sample and is analysed at the outlet (Schay *et al.*, 1972; Sharma and Fort, 1973). The outlet concentration (c_{out}) is lower than the inlet concentration (c_{in}) as long as adsorption equilibrium is not reached. Integration of the difference in concentration between the inlet and outlet over the mass m ($= m_1 + m_2$) or volume V of the solution flowing through the sample gives the increase in reduced surface excess amount of 2 during this adsorption step. Thus,

$$\Delta n_2^{\sigma(n)} = \int_0^m \Delta w_2 \, \mathrm{d}m \tag{5.72}$$

where $w_2 = m_2/(m_1 + m_2)$, or

$$\Delta n_2^{\sigma(n)} = \int_0^V \Delta c_2 \, \mathrm{d}V \tag{5.73}$$

where $c_2 = n_2/V$.

Because this method makes use of standard HPLC chromatographic equipment (pump, sample cell with filters, on-line detectors), there is a tendency to call it 'chromatographic' or 'frontal chromatographic'. We suggest that this tendency should be resisted: it is misleading since there is no chromatographic effect or phenomenon.

In the *circulation method*, the same solution is continuously passed through the sample, also with continuous monitoring of the concentration, until equilibrium is reached (see Figure 5.15d) (Kurbanbekov *et al.*, 1969; Ash *et al.*, 1973). Although this method requires a less conventional set-up than the immersion or open-flow methods, it presents the following advantages:

1. Conservation of solution, which is important not only to save the solute (e.g. specially synthesized surfactants or proteins), but also the solvent (e.g. high-purity alkanes).
2. Straightforward study of the temperature dependence of adsorption (without any addition of solution).
3. The possible incorporation of a null procedure.

The principle of the null procedure (Nunn and Everett, 1983) is to restore, by injection of an appropriate dose of initial solution, the concentration prior to adsorption. This is done at each adsorption step. A refinement is to arrange that the sample cell is by-passed during the injection of a new dose of solution until the determination of a new amount concentration c_2^j. The flow through is re-started and, as the concentration decreases, it is restored to its initial value c_2^j by addition of a volume ΔV^a of a solution of amount concentration c_2^a. The determination of the increase in reduced surface excess amount of 2 simply requires a knowledge of the void volume V_m of the by-passed section and the concentration c_2^{j-1} of the former adsorption equilibrium. Thus,

$$\Delta n_2^{\sigma(n)} = \Delta V^a (c_2^a - c_2^j) - V_m (c_2^j - c_2^{j-1}) \tag{5.74}$$

One point of interest in this procedure is that it does not require the knowledge of any other volume than V_m. Also, the accuracy of the determination of $n_2^{\sigma(n)}$ does not

depend on the calibration of the detector. A calibration is required for the presentation of the adsorption isotherm, i.e. $n_2^{\sigma(n)}$ versus c_2^j.

Methods for determining adsorption energies

In principle, the following methods are available for the determination of energies, associated with adsorption from solution:

1. The 'isosteric method', based on the temperature dependence of adsorption.
2. The immersion calorimetry method.
3. The batch calorimetry method.
4. The flow-through calorimetry method.

The *isosteric method* can be considered, for adsorption from solution, in a similar manner as for gas adsorption (see Section 2.6.1). For example, by equating the chemical potentials of component 2 (the solute) in its adsorbed state and the liquid phase, by keeping the specific amounts adsorbed constant and by considering a dilute solution, so that the activity can be replaced by a molality ($b_2 = 1000\, n_2/m_1$), we obtain:

$$\Delta_{ads}\dot{h}_2 = -RT^2\left(\frac{\partial(\ln b_2)}{\partial T}\right)_{n_2^{\sigma(n)},\, n_1^{\sigma(n)}} \tag{5.75}$$

In principle, this method of calculating the differential enthalpy of adsorption could be applied to two adsorption isotherms determined at different temperatures, but the following restrictions must be kept in mind:

1. The above equation only holds for dilute solutions.
2. The structures of the adsorbed phase and the solution are assumed to be unchanged over the temperature range considered.
3. Both surface excess amounts must also remain unchanged; this necessarily holds when using *reduced* surface excess amounts by the application of Equation (5.75), since $n_2^{\sigma(n)} = -n_1^{\sigma(n)}$ (see Equation (5.10)) so that it is enough to maintain a constant $n_2^{\sigma(n)}$. This does not hold, however, when *relative* surface excess amounts or simple surface excess amounts are used.

For all these reasons, one should be cautious in the application of the isosteric method (see Lyklema, 1995).

Although the method of *immersion calorimetry in solution* is directly related to immersion calorimetry in pure liquids, its application to solutions is much less rewarding. This is because if one uses the standard sealed glass bulb technique one must now break the bulb completely and stir to obtain a homogeneous solution after adsorption. The resulting heat of breaking and stirring then limits the accuracy of the microcalorimetric measurements, whereas the required sensitivity and reproducibility are usually higher than for a standard immersion microcalorimetry experiment in a pure liquid. These drawbacks mean that, like the isosteric method, this approach to the energetics of adsorption from liquid solutions is not widely used.

In the *batch calorimetry method*, the adsorbent is initially kept in suspension in the pure solvent by means of continuous stirring. The solution is then introduced by

successive doses which eventually fill the sample cell (see Figure 5.16). A particular advantage of this method is that it is suitable for any type of powder, including those of grain size much smaller than 10 μm, which cannot be studied with the flow-through techniques. It is also suitable for kinetic studies, by using the microcalorimeter as a simple detector of the rate of adsorption after the rapid introduction of each new dose.

However, the method has a number of requirements:

1. A sample cell large enough (e.g. 20 to 100 cm^3) to accommodate the stirring device and to receive several successive doses of solution.
2. An efficient heat exchanger so that the doses of added solution are, say, within 10^{-3} K of the temperature of the microcalorimeter.
3. A stirring device able to keep the powder in suspension with a minimum heat evolution.
4. A high calorimetric sensitivity, since the energies of *displacement* to be measured are usually very small.
5. The previous determination of the adsorption isotherm by one of the methods listed in Section 5.3.3.

Two operational arrangements fulfilling the above requirements are represented in Figures 5.16b and 5.16c. For convenience, both are incorporated in a Tian–Calvet microcalorimeter with large cells (i.e. *c.* 100 cm^3). The first device uses a disc stirrer (up and down movement) and cancels any temperature difference between the added solution and the adsorbent by placing both the adsorbent and the solution reservoir in the top part of the microcalorimetric cell (Rouquerol and Partyka, 1981). The second device uses a propeller which is given very fast half-turns (*c.* 10 per minute) by means of a hindered magnetic transmission which serves to damp the vibrations from the motor.

A long heat exchanger (2 m long coil) allows the solution to reach the microcalorimetric cell at the right temperature. In this set-up, the full volume of the cell is available for progressive filling (Nègre *et al.*, 1985; Rouquerol, 1985). Both arrangements can be used from 25 to 200°C (the upper temperatures being useful for studying adsorption from organic solutions) and their thermal stability permits adsorption measurements to be made over several hours. Typically, 0.5 g of adsorbent is kept in suspension in 15 g of pure solvent, whereas the added solution is introduced by steps of 5 g by means of a peristaltic pump operating at a flow-rate of 60 mg min^{-1}. The amount of heat Q_{exp} measured during each step must be corrected for the enthalpy of mixing, $\Delta_{mix}H$, as indicated in Equation (5.70), and referred to the change in surface excess reduced amount, $\Delta n_2^{\sigma(n)}$, in order to obtain the corresponding change in integral enthalpy of displacement of solvent 1 by solute 2, $\Delta_{mix}H_{1\text{-}2}$. At the end of each adsorption step, the molality of the solution is required to derive $\Delta_{mix}H$ and the reduced surface excess amount $n_2^{\sigma(n)}$ to derive $\Delta n_2^{\sigma(n)}$. This is done by reference to a previously determined adsorption isotherm $n_2^{\sigma(n)} = f(b_2)$ and from the knowledge of the initial amount of solvent and of the successive increments of solution introduced. The calculation can be conveniently presented in a graphical from (Nègre, 1984); the principle, in the form proposed by Trompette (1995), is explained in Figure 5.17.

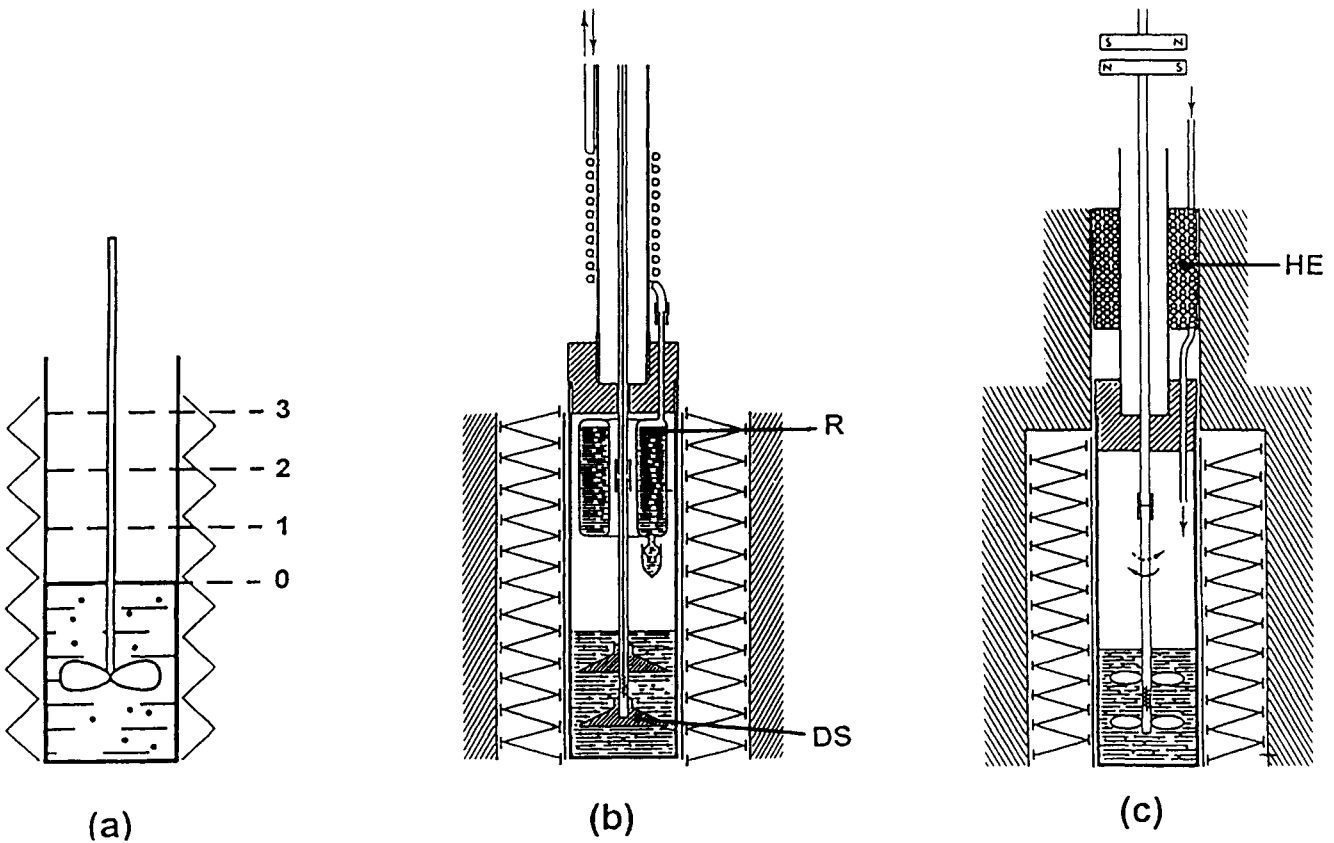

Figure 5.16. Batch calorimetry method.
(a) Principle: aliquots of mother solution successively added to suspension of solid (initially in pure solvent). (b) Set-up with disc stirrer (DS) and internal reservoir (R) of mother solution (after Rouquerol and Partyka, 1981). (c) Set-up with magnetic stirring and heat exchanger (HE) for mother solution (after Nègre *et al.*, 1985).

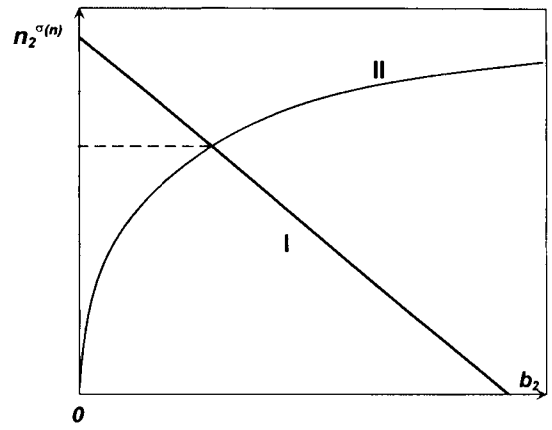

Figure 5.17. Graphical calculation of amount adsorbed in batch calorimetry experiment after introducing amount n_2 of solute (after Trompette, 1995). Curve II is the adsorption isotherm. For straight line I, see text. Crossing represents final adsorption equilibrium.

In Figure 5.17, for a given total amount of solute n_2 introduced into the microcalorimetric cell, the line I gives the dependence of the reduced surface excess amount $n_2^{\sigma(n)}$ on the equilibrium molality b_2. In order to plot line I we first consider the extreme case of $b_2 = 0$, that is all the solute is considered to be adsorbed so that

$$\frac{n_2^{\sigma(n)}}{m^s} = \frac{b_{2,0} \times \Delta m_i}{1000 + b_{2,0} M_2} \times \frac{1}{m^s} \tag{5.76}$$

where $b_{2,0}$ is the molality of the added solution, Δm_i is the mass of the first increment of solution, M_2 is the molar mass of the solute, and m^s is the mass of the adsorbent.

The other extreme of the line is determined by considering that $n_2^{\sigma(n)} = 0$, when all the solute is considered to remain in solution. Then:

$$b_2 = \frac{1000 b_{2,0} \Delta m_i}{(m_0 + \Delta m_i)[1000 + b_{2,0} M_2] - b_{2,0} m_0} \tag{5.77}$$

where m_0 is the initial mass of the pure solvent.

Curve II is simply the adsorption isotherm: the crossing provides the actual values of $n_2^{\sigma(n)}$ and b_2 after the introduction of Δm_i of solution. A blank experiment with the same set-up provides the curve of $\Delta_{mix} H$ versus b_2.

A batch microcalorimetric experiment, very similar to the one just described, is possible with a diathermal heat flowmeter type of microcalorimeter, which is less versatile than the Tian–Calvet microcalorimeter (especially in its temperature range and ultimate sensitivity), but of a simpler design. In the 'Montcal' microcalorimeter (Partyka *et al.*, 1989), the thermopile with up to 1000 thermocouples is replaced by a few thermistors.

Flow-through adsorption microcalorimetry. Flow-through adsorption microcalorimetry is not as versatile as the batch procedure. The grain size must be

over about 20 μm to avoid additional heat effects. Also, the system may require a long time to reach equilibrium (especially in the low-concentration range). Furthermore, the technique may need larger amounts of solution than the batch procedure. On the other hand it has several advantages:

1. The final equilibrium molality, pH or ionic strength for each adsorption point can be selected since these are imposed by the incoming solution.
2. The amount adsorbed can be determined on-line by simply installing the appropriate detector at the outlet of the microcalorimeter (cf. the flow-through method for determining the adsorption isotherm).
3. Both desorption and adsorption can be studied, which is practically impossible with the batch procedure.

Groszek (1966) early developed a simple flow-through adsorption calorimeter, which is somewhat similar to a differential thermal analysis (DTA) system (because of its single-point temperature detector) and is therefore well suited for the detection of thermal effects and for screening experiments. To obtain meaningful results requires more sophisticated equipment, however. A heat flowmeter microcalorimeter is normally used for this purpose. Such a microcalorimeter, especially designed for liquid-flow adsorption and for the complementary determination of $\Delta_{mix}H$, is illustrated in Figure 5.18.

The enthalpy of mixing, $\Delta_{mix}H$ corresponds to the transient decrease in molality which takes place around the adsorbent before the molality of the added solution is eventually restored. If this change in molality is continuously recorded at the outlet of the microcalorimetric cell, then it is not difficult to carry out the integration, provided the enthalpies of mixing alone have been measured separately (Liphard *et al.*, 1980; Denoyel *et al.*, 1982).

5.3.4. Applications of adsorption from solution

The numerous technological applications of adsorption from solution include liquid purification, the stabilization of suspensions, ore flotation, soil science, adhesion, liquid chromatography, detergency, enhanced oil recovery, lubrication, and last but not least, applications in the life sciences (e.g. adsorption by cell membranes, blood vessels, bones, teeth, skin, eyes, and hair).

Assessment of surface area and pore size

The assessment of surface area by adsorption from solution is still a major application, especially when the adsorbent cannot be outgassed or when the analytical techniques available in a laboratory are designed for the study of solutions. Various aspects of this application are examined in Chapter 6.

Assessment of microporosity from adsorption of organic molecules of different shapes and sizes is examined in Chapter 8.

Adsorption (and displacement) mechanisms

If adsorption from solution procedures are to be successfully applied, either in the laboratory or in industry, it is important to have some understanding of the

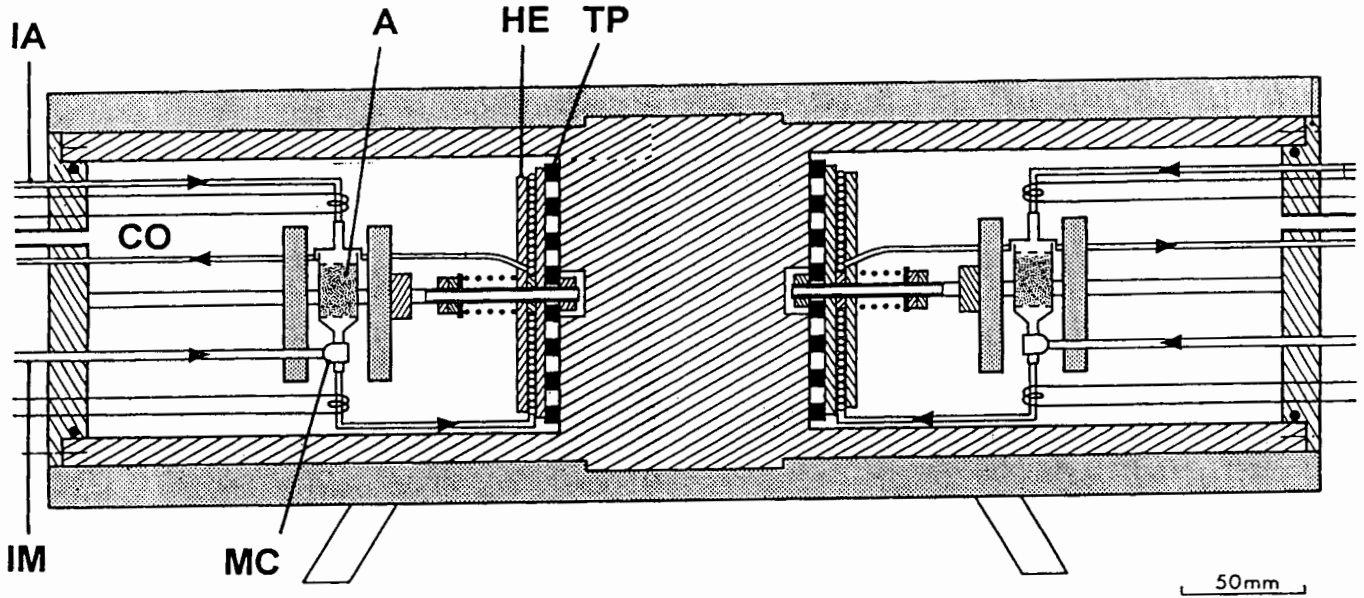

Figure 5.18. Twin liquid-flow adsorption and mixing microcalorimeter.
IA, inlet for adsorption; IM, inlet for mixing; MC, mixing cell; CO, common outlet; A, adsorbent; HE, heat exchanger; TP, thermopile (after Denoyel *et al.*, 1982).

mechanisms involved. The following examples illustrate the various parameters that can influence the adsorption mechanisms. Other aspects of this complex area can be found in the recent review by Lyklema (1995).

The pH of the solution and the resulting surface charge of the adsorbent have a major influence on the adsorption mechanism, even for the adsorption of non-ionic species. This is strikingly seen in the adsorption of the non-ionic polyoxyethylenic surfactants on various surfaces of silica: quartz, macroporous precipitated silica and pyrogenic silica (Denoyel *et al.*, 1990). For instance, at pH = 7, the surface excess density corresponding to the final plateau of the adsorption isotherms increases more than three-fold from quartz to precipitated silica: this was shown to result from the much larger proportion of dissociated silanols in the case of quartz. At pH = 2, which is the zero point of charge, the surface excess density is the same for all silicas and has its maximum value, since all silanols are undissociated. This is an example of the indirect but important effect of surface charge on adsorption.

This work has also revealed that the *crystallinity* of the silica surface affects its adsorbing behaviour through the enhancement of surface charge density and pH (Iler, 1979). Similar phenomena can be used to follow the increase in disorder of solid surfaces on grinding crystalline samples (Cases, 1979).

The presence of *surface OH groups or H_2O molecules* can play a primary role in adsorption. For example, a microcalorimetric study of the adsorption of stearic acid, from heptane solution, on ferric oxide (Husbands *et al.*, 1971) revealed that pre-adsorbed water enhanced adsorption of stearic acid. When adsorption takes place from a dry organic liquid, residual surface water may act as special agent. This was shown for the adsorption of a silane coupling agent (γ-amino-propyl-triethoxysilane) on silica covered with water molecules for $\theta \leqslant 1$ (Trens and Denoyel, 1996). By the simultaneous determination of adsorption isotherms and the enthalpies of displacement (of heptane by various silanes) it was demonstrated that the amine function was able to displace some of the surface water and make it available for the hydrolysis of the silane into trisilanol, whereas the residual water was able to promote the formation of siloxane bonds between the trisilanol molecules and the surface.

With the aid of adsorption flow-microcalorimetry, Groszek (1965, 1970) studied the effect of *chain length* on the behaviour of normal alcohols and the corresponding acids when adsorbed from *n*-heptane on iron oxides. It was found that the behaviour of *n*-butanol and *n*-octadecanol was quite different: the former was strongly adsorbed in a single stage up to an apparent saturation level, whereas the latter was adsorbed in two stages. In the first stage, the molecules of *n*-octadecanol appeared to lie flat on the surface and, in the second stage, to stand vertically away from the surface. The scale of the microcalorimetric signal was enhanced as the length of the solvent molecule approached that of the solute. Groszek concluded that the stability of the adsorbed layer was increased by the formation of a mixed film (solvent + solute) made up of molecules of similar size.

It is in the field of polymer adsorption that the chain length plays a major role. A microcalorimetric procedure has been used to determine the fraction of 'train' segments in contact with the surface (see Figure 5.19). This approach is based on the assumption that the 'loops' and 'tails' are too far away from the surface to contribute

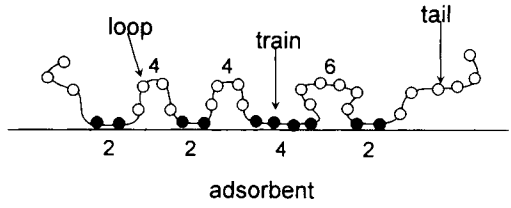

Figure 5.19. Example of a train–loop–tail configuration of an adsorbed chain (after Fleer *et al.*, 1993).

to the measured $\Delta_{dpl}\dot{h}$, and also that the displacement enthalpy of the monomer is an adequate reference (Cohen Stuart *et al.*, 1982; Killmann *et al.*, 1983; Denoyel *et al.*, 1990). This method was found to work well with polyethylene glycol (in the relative molar mass range 400 to 4 000 000) on macroporous silica gel (Trens and Denoyel, 1993). In spite of the very small $\Delta_{dpl}\dot{h}$ per mole of segment (*c.* 3 kJ mol^{-1}; M of segment: 44 g mol^{-1}), it was shown that (a) at low coverage, irrespective of its length, the molecules adsorb in a flat conformation, (b) as coverage increases, the molecules tend to stand up, (c) the molecules must contain more than, say, 5–10 segments to give rise to a complete loop and a second train, and (d) at coverages above 0.5, polymers with more than 500 segments can adsorb only by displacing previously adsorbed molecules.

Finally, one must be aware of possible *modifications of the sample* during the adsorption process itself. This is what was shown to happen when adsorbing a non-ionic surfactant (nonyphenoloxyethylene, with 9–10 ethoxy groups) on kaolin in the presence of 1% NaCl at 40°C. In this case one step only was visible in the normal L-shaped adsorption isotherm whereas two steps were seen in the microcalorimetric recording. The first was attributed to the displacement of water by the surfactant and the second to a partial opening and hydration of the sheet-like structure of kaolin under the action of surfactant and salt (Rouquerol and Partyka, 1981).

A more common situation is the effect of adsorption on the stability of a suspension. This may be favourable (by modifying, for example, the surface charge of the particles, or by increasing the distance between particles) or unfavourable. Such an example of the latter effect was found with non-ionic surfactant Triton TX-100 and silica suspensions. It was found that the adsorption produced micelle-like aggregates which underwent flocculation by a bridging mechanism (Giordano-Palmino *et al.*, 1994). This was strongly supported by the fact that the fastest flocculation occurred at half-coverage, for which the theory predicted an optimum amount of bridging flocculation (La Mer, 1966; Kitchener, 1972).

References

Adamson A.W. (1967) *The Physical Chemistry of Surfaces*, 2nd edn, Interscience, New York.
Ash S.G., Brown R. and Everett D.H. (1973) *J. Chem. Thermodynamics* **5**, 239.
Atkinson D., Mc Leod A.I., Sing K.S.W. and Capon A. (1982) *Carbon* **20**(4), 339.
Bartell F.E. and Suggitt R.M. (1954) *J. Phys. Chem.* **58**, 36.

Briant J. and Cuiec L. (1972) *Comptes-Rendus du 4ème Colloque ARTEP, Rueil-Malmaison*, 7–9 Juin 1971, Technip, Paris.
Brunauer S., Kantro D.L. and Weise C.H. (1956) *Can. J. Chem.* **34**, 1483.
Cases J.M. (1979) *Bull. Minéralogie* **102**, 694.
Chessick J.J. (1962) *J. Phys. Chem.* **66**, 762.
Chessick J.J., Young G.J. and Zettlemoyer A.C. (1954) *Trans. Faraday Soc.* **50**, 587.
Chessick J.J., Zettlemoyer A.C., Healey F.H. and Young G.J. (1955) *Can. J. Chem.* **33**, 251.
Cohen-Stuart M.A., Fleer G.J. and Bijsterbosch B.H. (1982) *J. Colloid Interface Sci.* **90**, 321.
Defay R. (1941) 'Des diverses façons de définir l'adsorption', *Mém. Acad. r. Belg. Cl. Sci.*
Defay R. and Prigogine I. (1951) *Tension Superficielle et Adsorption*, Desoer-Dunod, Liège-Paris.
Denoyel R., Rouquerol F. and Rouquerol J. (1982) In: *Adsorption from Solution* (C. Rochester, ed.), Academic Press, London.
Denoyel R., Rouquerol F. and Rouquerol J. (1987) In: *Fundamentals of Adsorption* (A.I. Liapis, ed.), Eng. Foundation, New York and American Institute of Chemical Engineers, p. 199.
Denoyel R., Durand G., Lafuma F. and Audebert R. (1990) *J. Colloid Interface Sci.* **139**(1), 281.
Denoyel R., Fernandez-Colinas F., Grillet Y. and Rouquerol J. (1993) *Langmuir* **9**, 515.
Dewar J. (1904) *Proc. Roy. Soc.* (London), Ser. A **74**, 122.
Douillard J.M., Zoungrana T. and Partyka S. (1995) *J. Petr. Sci. Eng.* **14**, 51.
Einstein A. (1901) *Ann. Physik* **4**, 513.
Elton G.A.H. (1951) *J. Chem. Soc.* 2958.
Everett D.H. (1972) *Pure Appl. Chem.* **31**(4) 579.
Everett D.H. (1973) In: *Specialist Periodical Reports*, Colloidal Science, vol. 1, The Chemical Society, London, p. 51.
Everett D.H. (1986) *Pure Appl. Chem.* **58**(7), 967.
Everett D.H. and Findenegg G.H. (1969) *J. Chem. Thermodynamics* **1**, 573.
Everett D.H., Langdon A.G. and Maher P. (1984) *J. Chem. Thermodynamics* **16**, 98.
Fleer G.J., Cohen-Stuart M.A., Scheutjens J.M.H.M., Cosgrove T. and Vincent B. (1993) *Polymers at Interfaces*, Chapman & Hall, London, p. 31.
Furuichi R., Ishii T. and Oshima Y. (1982) *Thermochim. Acta* **56**, 31.
Giles C.H., MacEwan T.H., Nakhwa S.N. and Smith D. (1960) *J. Chem. Soc.* 3973.
Giordano-Palmino F., Denoyel R. and Rouquerol J. (1994) *J. Colloid Interface Sci.* **165**, 82.
Gonzalez-Garcia S. and Dios-Cancela G. (1965) *Studia Chemica I*, Salamanca University, Salamanca, p. 37.
Gregg S.J. (1961) *The Surface Chemistry of Solids*, 2nd edn, Chapman & Hall, London.
Gregg S.J. and Sing K.S.W. (1967) *Adsorption, Surface Area and Porosity*, 1st edn, Academic Press, London.
Groszek A.J. (1965) *Chem. & Ind.* 482.
Groszek A.J. (1966) *Lubrication Sci. Technol.* **9**, 67.
Groszek A.J. (1970) *ASLE Trans.* **13**, 278.
Guggenheim E.A. and Adam N.K. (1933) *Proc. Roy. Soc.* **139**, 218.
Harkins W.D. and Boyd G.E. (1942) *J. Am. Chem. Soc.* **64**, 1195.
Harkins W.D. and Dahlstrom R. (1930) *Ind. Eng. Chem.* **22**, 897.
Harkins W.D. (1952) *The Physical Chemistry of Surface Films*, Reinhold, New York, p. 262.
Healey F.H., Yu Y.F. and Chessick J.J. (1955) *J. Phys. Chem.* **59**, 399.
Hill T.L. (1949) *J. Chem. Phys.* **17**, 520.
Husbands D.I., Tallis W., Waldsax J.C.R., Woodings C.R. and Jaycock M.J. (1971) *Powder Technology* **5**, 31.
Iler R.K. (1979) *The Chemistry of Silica*, Wiley, New York.
Jaycock M.J. and Parfitt G.D. (1981) *Chemistry of Interfaces*, John Wiley, Chichester.
Jehlar P., Romanov A. and Biros P. (1979) *Thermochim. Acta* **28**, 188.
Jura G.J. and Hill T.L. (1952) *J. Am. Chem. Soc.* **74**, 1598.
Killman E., Korn M. and Bergmann M. (1983) In: *Adsorption from Solution* (R.H. Ottewill, C.H. Rochester, and A.L.S. Smith, eds), Academic Press, London, p. 259.
Kipling J.J. (1965) *Adsorption from solution of non-electrolytes*, Academic Press, London.

Kipling J.J. and Tester D.A. (1952) *J. Chem. Soc.* 4123.
Kiraly Z. and Dekany I. (1989) *J. Chem. Soc., Faraday Trans.* I **85**, 3373.
Kitchener J.A. (1972) *British Polymer* J. **4**, 27.
Kurbanbekov E., Larionov O.G., Chmutov K.V. and Yudelevich M.D. (1969) *Russ. Phys. Chem.* **43**, 916.
Laffitte M. and Rouquerol J. (1970) *Bull. Soc. Chim. Fr.* 3335.
La Mer V.K. (1966) *Disc. Faraday Soc.* **42**, 248.
Laporte F. (1950) *Ann. Phys.* **5**, 5.
Liphard M., Glanz P., Pilarski G. and Findenegg G.H. (1980) *Progr. Colloid and Polymer Sci.* **67**, 131.
Lyklema J. (1995) *Fundamentals of Interface and Colloid Science. I Fundamentals. II. Solid-liquid Interfaces*, Academic Press, London.
Mackrides A.C. and Hackerman N. (1959) *J. Phys. Chem.* **63**, 594.
Magnan R. (1970) *Am. Ceram. Soc. Bull.* **49**(3), 314.
Micale F.J., Topic M., Cronan C.L., Leidheiser H. Jr and Zettlemoyer A.C. (1976) *J. Colloid Interface Sci.* **55**(3), 540.
Mills I., Cvitas T., Homann K., Kallay N. and Kuchitzu K. (1993) *Quantities, Units and Symbols in Physical Chemistry*, IUPAC, Blackwell Scientific Publication, London, p. 42.
Nagy L.G. and Schay G. (1963) *Acta Chim. Acad. Sci. Hung.* **39**, 365.
Nègre J.Cl. (1984) Thèse Université de Provence, Marseille.
Nègre J.Cl., Denoyel R., Rouquerol F. and Rouquerol J. (1985) *Actes des Journées de Calorimétrie et d'Analyse Thermique (J.C.A.T.)*, Marseille.
Nowell D.V. and Powell M.W. (1991) *J. Therm. Anal.* **37**, 2109.
Nunn C. and Everett D.H. (1983) *J. Chem. Soc. Faraday Trans I.* **79**, 2953.
Nunn C., Schlechter R.S. and Wade W.H. (1981) *J. Colloid Interface Sci.* **80**, 598.
Partyka S., Rouquerol F. and Rouquerol J. (1975) In: *Proc. 4th Int. Conf. on Chemical Thermodynamics of IUPAC*, Montpellier, CRMT Marseille, vol. 7, p. 46.
Partyka S., Rouquerol F. and Rouquerol J. (1979) *J. Colloid Interface Sci.* **68**(1), 21.
Partyka S., Keh E., Lindheimer M. and Groszek A. (1989) *Colloids and Surfaces* **37**, 309.
Pouillet M.C.S. (1822), *Ann. Chim. Phys.* **20**, 141.
Robert L. (1967) *Bull. Soc. Chim. Fr.* **7**, 2309.
Robert L. and Brusset H. (1965) *Fuel* **44**, 309.
Rouquerol J. (1985) *Thermochim. Acta* **95**, 337.
Rouquerol J. and Partyka S. (1981) *J. Chem. Tech. Biotechnol.* **31**, 584.
Schay G. (1970) In: *Surface Area Determination* (D.H. Everett and R.H. Otterwill, eds.), Butterworth, London, p. 273.
Schay G. and Nagy L.G. (1961) *J. Chim. Phys.* 140.
Schay G. and Nagy L.G. (1972) *J. Colloid Interface Sci.* **38**(2), 302.
Schay G., Nagy L.G. and Racz G. (1972) *Acta Chim. Acad. Sci. Hung.* **71**, 23.
Schröder J. (1979) *J. Colloid Interface Sci.* **72**(2), 279.
Schultz J., Tsutsumi K. and Donnet J.B. (1977) *J. Colloid Interface Sci.* **59**(2), 272.
Sharma S.G. and Fort T. (1973) *J. Colloid Interface Sci.* **43**, 36.
Trens P. and Denoyel R. (1993) *Langmuir* **9**, 519.
Trens P. and Denoyel R. (1996) *Langmuir* **12**, 2781.
Trompette J.L. (1995) Thèse, Université des Sciences et Techniques du Languedoc, Montpellier.
Vanderdeelen J., Rouquerol J. and Baert L. (1972) In: *Thermochimie*, Colloques Internationaux du CNRS, no. 201, Editions du CNRS, Paris.
Wade W.H., Hackermann N. (1964) *Adv. Chem. Ser.* **43**, 222.
Wade W.H., Hackermann N., Cole H.D. and Meyer D.E. (1961) *Adv. Chem. Ser.* **33**, 35.
Watanabe H. and Seto J. (1988) *Bull. Chem. Soc. Japan* **61**, 3067.
Whalen J.W. (1961a) *J. Phys. Chem.* **65**, 1676.
Whalen J.W. (1961b) *Adv. Chem. Ser.* **33**, 281.
Whalen J.W. (1962) *J. Phys. Chem.* **66**, 511.
Whalen J.W. and Lai K.Y. (1977) *J. Colloid Interface Sci.* **59**(3), 483.
Widyani E. and Wightman J.P. (1982) *Colloids and Surfaces* **4**, 209.
Williams A.M. (1913) *Medd. k. Veteskapsakad. Nobelinst.* **2**, 27.

Young G.J. and Bursh T.P. (1960) *J. Colloid Interface Sci.* **15**, 361.
Young G.J., Chessick J.J., Healey F.H. and Zettlemoyer A.C. (1954) *J. Phys. Chem.* **58**, 313.
Zettlemoyer A.C. (1965) *Ind. Eng. Chem.* **57**, 27.
Zettlemoyer A.C. and Chessick J.J. (1964) *Adv. Chem. Ser.* **43**, 88.
Zettlemoyer A.C. and Narayan K.S. (1967) In: *The Solid-Gas Interface* vol. I (E.A. Flood, ed.), Marcel Dekker, New York, p. 158.
Zettlemoyer A.C., Young G.J., Chessick J.J. and Healey F.H. (1953) *J. Phys. Chem.* **57**, 649.
Zettlemoyer A.C., Chessick J.J. and Hollabaugh C.M. (1958) *J. Phys. Chem.* **62**, 489.
Zimmermann R., Wolf G. and Schneider H.A. (1987) *Colloids and Surfaces* **22**, 1.

This Page Intentionally Left Blank

CHAPTER 6

Assessment of Surface Area

6.1. Introduction

Many of the most popular methods for determining the surface area of powders and porous materials depend on the measurement of adsorption. The early work of Paneth (1922) involved the use of radioactive indicators and dye adsorption. It had been noted by Marc (1911) that the uptake of dye by an inorganic powder tended to approach a certain saturation level. Paneth set out to show that this level of maximum adsorption corresponded to the formation of a unimolecular layer. In spite of a number of unsolved problems, dye adsorption soon became one of the most widely used techniques for the study of fine powders.

The appearance of Langmuir's comprehensive review of the nature of adsorption (1916, 1918) prompted several investigators to consider the possibility of using gas adsorption for surface area determination. Early attempts were made by Williams (1919) and Benton (1926), but these led to inconclusive findings. The first significant advances were made by Brunauer and Emmett (1935, 1937) and their work prepared the way for the development of the Brunauer–Emmett–Teller (BET) theory in 1938.

Over the past 50 years the BET method has become an extremely popular method for determining the surface area of adsorbents, catalysts and various other finely

divided and porous materials. However, the apparent success of the BET method has tended to overshadow the weakness of the underlying theory.

As was pointed out in Chapter 4, the BET model does not provide a realistic description of any known physisorption system. Indeed, it has been implied by some critics that the BET plot is little more than a mathematical device for locating Point B. This opinion may be too harsh, but it must be acknowledged that if it were removed from the context of surface area determination, the BET theory would be unlikely to continue to attract much interest. This situation reinforces the need to examine the limitations of the BET method and in particular to attempt to define the conditions which govern its application.

Immersion calorimetry was in use over 70 years ago for the characterization of activated charcoals and silica gels. The measurement of 'heat of wetting' appeared to provide a relatively simple way of determining the surface area of a porous adsorbent (Brunauer, 1945).

However, as shown in Chapter 5, it became clear that to be meaningful these measurements should register the change of a thermodynamic function between well-defined states of the system and that the extent of the surface area measured may depend on the experimental procedure.

6.2. The BET Method

6.2.1. Introduction

Two stages are involved in the evaluation of the surface area by the BET method from physisorption isotherm data. First, it is necessary to construct the BET plot and from it to derive the value of the *monolayer capacity*, $\boldsymbol{n}_m$. The second stage is the calculation of the specific surface area, a(BET), from $\boldsymbol{n}_m$, and this requires a knowledge of the average area, σ, occupied by each molecule in the completed monolayer (i.e. *the molecular cross-sectional area*). Questionable assumptions are introduced at each stage and these therefore require careful consideration.

6.2.2. The BET plot

As noted in Chapter 4, the BET equation is conveniently expressed in the linear form:

$$\frac{p/p^\circ}{\boldsymbol{n}(1-p/p^\circ)} = \frac{1}{\boldsymbol{n}_m C} + \frac{C-1}{\boldsymbol{n}_m C}(p/p^\circ) \tag{6.1}$$

Thus, the BET plot of $(p/p^\circ)/[\boldsymbol{n}(1-p/p^\circ)]$ versus p/p° should be a straight line with slope $s = (C-1)/\boldsymbol{n}_m C$ and intercept $i = 1/\boldsymbol{n}_m C$. By solving these two simultaneous equations, we obtain:

$$\boldsymbol{n}_m = 1/(s+i) \tag{6.2}$$

and

$$C = (s/i) + 1 \tag{6.3}$$

In the original work of Brunauer, Emmett and Teller (1938) it was found that Type II nitrogen isotherms on various adsorbents gave linear BET plots over the approximate range $p/p^\circ = 0.05–0.35$. However, subsequent studies have revealed that with most systems the linear range is more restricted (Rouquerol *et al.*, 1964; Gregg and Sing, 1982).

The location and extent of the linear region of a BET plot is dependent on the system and operational temperature; it is therefore inadvisable to fit the 'best' straight line over any predetermined p/p° range (e.g. $p/p^\circ = 0.05–0.30$). Instead, the recommended procedure is to obtain by statistical analysis the best linear fit for that part of the isotherm which includes Point B. Of course, this approach necessarily entails some degree of qualitative judgement and for this reason it is important to record the range of p/p° over which the BET plot is considered to be sufficiently linear.

According to Equation (6.1), the relative pressure corresponding to the monolayer capacity depends on the C value since:

$$\left(\frac{p}{p^\circ}\right)_{n_m} = \frac{1}{\sqrt{C}+1} \tag{6.4}$$

For a given adsorbate–adsorbent system for which the adsorption energy of the first layer is high, and consequently for which the C value is high (>350), the relative pressure corresponding to the monolayer capacity is low (<0.05) and there is a correspondingly sharp Point B. Conversely, when the adsorption energy and C value are low ($C < 20$), the relative pressure corresponding to the monolayer capacity is high (>0.18) and Point B is ill-defined. With the oxides most often used as mesoporous or macroporous adsorbents (e.g. silica and alumina) C values for nitrogen adsorption at 77 K are in the range 80–150, which is consistent with the formation of the monolayer within the relative pressure range of 0.075–0.100. An interesting feature of the BET equation is that it allows for the possibility that when the surface is covered with a 'statistical monolayer', a fraction still apparently remains uncovered. We may note, with Hill (1946), that this fraction $(\theta_0)_{n_m}$ is directly dependent on the value of C:

$$(\theta_0)_{n_m} = \frac{1}{\sqrt{C}+1} \tag{6.5}$$

which means that the higher the C value, the smaller the uncovered fraction of the surface when the statistical monolayer is achieved. One immediately sees that for C values of 1, 9 and 100, the corresponding fractions of uncovered surface are 50%, 25% and *c.* 10%. Returning to the evaluation of $(\theta_0)_{n_m}$, we note that comparison of Equations (6.4) and (6.5) leads to:

$$(\theta_0)_{n_m} = (p/p^\circ)_{n_m} \tag{6.6}$$

which, according to the BET model, provides a simple way of evaluating the fraction of uncovered surface.

The appreciable overlap of the monolayer completion and multilayer development which corresponds to a low C value and to a gradual isotherm curvature results

usually from relatively weak adsorbent–adsorbate interactions together with relatively strong adsorbate–adsorbate interactions. This situation arises in the case of the adsorption of water vapour on carbon (as discussed in Chapter 9). With such systems, the BET monolayer capacity cannot be relied on to give a realistic assessment of the magnitude of total area of the surface. However, it can provide a useful indication of the extent of the 'hydrophilic' area or the extent of the high-energy sites.

For a new, unknown sample, a reliable interpretation of the BET plot requires a certain number of experimental points: 10 is, we consider, a minimum in the range of relative pressures from 0.01 to 0.30. A very simple consistency test is provided by comparing the calculated value of $(p/p^\circ)_{n_m}$ (given by Equation (6.4)) with the value of p/p° corresponding to the BET n_m value obtained by application of Equation (6.1). When these values are very different (say, by more than 10%), it is necessary to change the chosen range of relative pressures. Furthermore, we know that the quantity C must be positive (see Equation (4.33)): any negative intercept on the ordinate of the BET plot is an indication that we are outside the valid range of the BET equation. In applying the BET method it is necessary to reduce any subjectivity in the assessment of the monolayer capacity. To this end, the two above criteria can be complemented by a third (Rouquerol *et al.*, 1964), which limits the application of the BET equation to the pressure range where $n(1 - p/p^\circ)$ continuously increases with p/p°. Justification of this requirement can be seen by applying an alternative form of the BET equation proposed by Keii *et al.*, (1961):

$$\frac{1}{n(1-p/p^\circ)} = \frac{1}{n_m} + \frac{1}{n_m C} \times \frac{1-p/p^\circ}{p/p^\circ} \tag{6.7}$$

This equation was applied by Parra *et al.* (1994) for the processing of experimental data for the adsorption of nitrogen by microporous activated carbons. It is precisely when the term $n(1 - p/p^\circ)$ starts to decrease (as p/p° is increased) that the new plot clearly begins to deviate from linearity. Equation (6.7) is specially suited for the evaluation of a high C value. The intercept on the ordinate gives n_m, and the slope of the plot gives the product $n_m C$. Nevertheless, for general application, we consider that the standard BET plot is still the more appropriate.

As was noted in Chapter 4, the BET treatment leads to a modified equation if the amount adsorbed at the saturation pressure is restricted to a finite number of layers, N. Thus, in place of Equation (6.1), Brunauer, Emmett and Teller (1938) obtained:

$$\frac{n}{n_m} = \frac{C(p/p^\circ)}{1-p/p^\circ} \cdot \frac{1-(N+1)(p/p^\circ)^N + N(p/p^\circ)^{N+1}}{1+(C-1)(p/p^\circ) - C(p/p^\circ)^{N+1}} \tag{6.8}$$

In practice, Equation (6.8) should be regarded as an empirical relation, since a value of N is chosen to give the best fit in the multilayer range. For example, it was found by Brunauer (1945) that, for the adsorption of nitrogen on an iron catalyst at 77 K, by taking $N = 6$ the upper limit of the range of fit could be extended from p/p° of 0.35 to 0.7. In view of the improved range of applicability of Equation (6.8), it might be expected that this equation would be capable of yielding a more reliable evaluation

of n_m. It turns out, however, that the difference in the location of n_m when comparing Equations (6.1) and (6.8) is no more than a few percent provided that $N > 4$. In view of the underlying weakness of the BET theory, we conclude that there is no advantage to be gained by using Equation (6.8) to obtain n_m.

The single point method

For some routine or exploratory work, it is expedient to adopt a simplified experimental procedure, which involves the determination of a single point on the isotherm – preferably within the BET range. The assumption is then made that C is sufficiently large to give an almost zero intercept. If we assume that the intercept is zero, and that $C - 1 \approx C$ we may write:

$$n_m = n(1 - p/p^\circ) \tag{6.9}$$

The validity of this simplifying assumption is evidently dependent on the isotherm shape: the error is likely to be within a few percent provided that $C \approx 100$. Experience confirms that the errors in the estimation of n_m by the single point method become appreciable when $C \leqslant 80$.

6.2.3. Validity of the BET monolayer capacity

As a result of their systematic study of the adsorption of nitrogen and other gases on a number of different adsorbents, Emmett and Brunauer (1937) came to the conclusion that Point B marked the boundary between monolayer and multilayer adsorption. It will be recalled that Point B was defined as the beginning of the middle, nearly linear, region of an adsorption isotherm. On an empirical basis a number of other characteristic features (designated A, C, D, and E) were rejected in favour of Point B. The main reasons for the selection of Point B were: (1) because it gave fairly consistent values of surface area, and (2) because at this point the isosteric heat of adsorption appeared to undergo an appreciable decrease.

The theoretical significance of Point B was clarified with the appearance of the BET theory in 1938. Thus, for nitrogen adsorption on 12 different adsorbents, the values of n_m and the corresponding uptakes at Point B were generally found to be in close agreement (to within *c.* 10%). In fact, the agreement is within a few percent if the C value is sufficiently high to allow a well-defined Point B to be identified (Gregg and Sing, 1982, p. 54). It is therefore clear that any evidence supporting the validity of Point B can be regarded as also supporting the validity of n_m.

Further confirmation for the validity of n_m is provided by energy of adsorption data. For reasons given in Chapter 3 it is preferable to use calorimetry rather than the indirect isosteric method for the evaluation of energies of adsorption. Calorimetric measurements made over the past 50 years have confirmed that some systems exhibit an appreciable decrease in the differential energy of adsorption at or in the region of Point B (Beebe and Young, 1954; Avgul *et al.*, 1962; Holmes, 1967; Berezin *et al.*, 1969; Berezin and Sagatelyan, 1972; Rouquerol *et al.*, 1979). All these results are, of course, consistent with the interpretation that at Point B monolayer adsorption is complete and multilayer adsorption has begun. However, the calorimetric data

discussed in later chapters reveal that monolayer–multilayer physisorption does not occur in strict accordance with the BET model.

Pronounced energetic heterogeneity is shown by many physisorption systems over the complete range of monolayer coverage. However, with highly homogeneous surfaces such as graphite there is a progressive increase of adsorption energy as the monolayer coverage is increased. This is due to adsorbate–adsorbate interactions, which can be detected at quite low surface coverage. As we have seen, neither of these effects is compatible with the BET theory.

Furthermore, the theory is not able to account for the Type VI isotherm, which is the simplest type of layer-by-layer multilayer isotherm. The steps of a Type VI isotherm tend to lose their sharpness as the temperature is raised. However, the results of Prenzlow and Halsey (1957) showed that the mid-point (inflection) of the tread is rather insensitive to change of temperature. This is an indication that in this case it is the step height, and not Point B, which corresponds to the monolayer completion.

The existence of sub-steps poses another problem in the application of the BET method. As will be seen in Chapter 9, the presence of a sub-step is a sign that the monolayer can undergo a phase change, which must result in an increase in the monolayer density. Under these conditions, it is unlikely that the BET method is capable of providing an accurate evaluation of the monolayer capacity.

6.2.4. The BET area

The specific surface area, a(BET), is obtained from the BET monolayer capacity, $\boldsymbol{n}_m$, by the application of the simple relation:

$$a(\mathrm{BET}) = \boldsymbol{n}_m L\sigma \tag{6.10}$$

where L is the Avogrado constant and σ is the average area occupied by each molecule in the completed monolayer. Any successful application of Equation (6.10) is, of course, dependent on whether σ is already known, or at least determinable by some other method. The possibility that σ might vary from one surface to another must also be considered. Emmett and Brunauer (1937) proposed that the molecular cross-sectional area, σ, can be calculated from the density of the liquid adsorptive in the bulk liquid state. Thus,

$$\sigma = f(M/\rho L)^{2/3} \tag{6.11}$$

where f is a packing factor, which for hexagonal close-packing becomes 1.091, ρ is the absolute density of the liquid adsorptive at the operational temperature, and M is the molar mass of the adsorptive.

Values of σ obtained by the application of Equation (6.11) are given in Table 6.1 together with an indication of the range of corresponding values to be found in the literature. It is evident that a very confused picture emerges from the many attempts made to compare the estimated and derived values of σ for a wide range of adsorption systems (see Young and Crowell, 1962; McClellan and Harnsberger, 1967; Gregg and Sing, 1982).

Table 6.1. Molecular areas of some adsorptives

Adsorptive	T (K)	Cross-sectional area σ (nm^2)		
		Literature range[a]	In close-packed liquid monolayer[b]	Customary value
Nitrogen	77	0.13–0.20	0.162	0.162
Argon	77	0.10–0.19	0.138	0.138
Krypton	77	0.14–0.24	0.152	0.202
Xenon	77	0.16–0.25	0.168[c]	0.170
Oxygen	77	0.13–0.20	0.141	0.141
Carbon dioxide	195	0.14–0.22	0.163	0.210
n-Butane	273	0.32–0.53	0.321	0.430
Benzene	293	0.25–0.51	0.307	0.430

[a] Values quoted by McClellan and Harnsberger (1967) and Gregg and Sing (1982).
[b] By application of Equation (6.11).
[c] Taking the density of the solid.

For *the important case* of nitrogen adsorption at 77 K, the value of $\sigma(N_2)$ is *normally* taken as 0.162 nm^2, which was the molecular area originally used by Emmett and Brunauer (1937). If we insert in Equation (6.11) the most recent data available for the liquid density of nitrogen at 77 K we obtain a molecular cross-sectional area of 0.16257 nm^2, but the difference is so small that it is insignificant in comparison with the range of uncertainty of the effective molecular area. Unfortunately, the various attempts made to compare the BET-nitrogen area with independent values have not helped to clarify the situation (see Gregg and Sing, 1982, p. 61).

The most direct approach would be to compare a BET area with the simple geometrical area of a solid mass with no surface roughness, but in practice this is extremely difficult because of the very small uptake of gas. It is not surprising that very few studies of this type have ever been attempted. The few results obtained with electropolished thin metal plates and fine glass fibres seem to confirm that $\sigma(N_2) \approx 0.16$ nm^2 (Rhodin, 1950; Gregg and Sing, 1982, p. 62). Most tests of the validity of the BET area have been carried out with finely divided solids and electron microscopy has generally been used to determine the particle size distribution. There are many sources of error (e.g. the wide size distribution and the shape factors) and we are left with the impression that the agreement between the corresponding values of specific surface area is within about ±20%.

Argon is a possible alternative adsorptive for surface area determination: it is chemically inert and its molecule is symmetrical and monoatomic. Although the polarizabilities of argon and nitrogen are remarkably similar, their electronic structures are quite different. When the molecular area of argon is calculated from extrapolated liquid density at 77 K (Brunauer and Emmett, 1937), the value obtained is $\sigma(Ar) = 0.138$ nm^2, which was the value recommended by McClellan and Harnsberger (1967). Comparison between BET-argon and BET-nitrogen areas have revealed that significant adjustments have to be made in the respective molecular areas, which depend on the adsorbent (see Gregg and Sing, 1982, p. 75). Thus, for graphitized carbon blacks the use of $\sigma(Ar) = 0.138$ nm^2 and $\sigma(N_2) = 0.162$ nm^2

generally gives excellent agreement, but this is not the case for oxides. To obtain agreement, we now find that either the argon molecular area must be increased (to *c.* 0.166 nm^2) or the nitrogen molecular area must be decreased (to *c.* 0.13 nm^2). So far, this problem has not been completely resolved, although recent neutron diffraction and adsorption microcalorimetry studies do indicate that the orientation of the nitrogen quadrupole is dependent on the surface structure. It appears likely that this changes with the progressive dehydroxylation of a silica surface. If the nitrogen molecules are able to interact 'vertically' with surface hydroxyl groups, then $\sigma(N_2)$ could be reduced to *c.* 0.112 nm^2 in the completed monolayer (Rouquerol *et al.*, 1979, 1984).

As will be seen in the later chapters of this book, there is much to be said in favour of using *both* argon and nitrogen for the characterization of solid surfaces. However, there are several reasons why argon adsorption at 77 K could not be adopted in place of nitrogen. First, 77 K is below the triple point of argon (88.8 K) and therefore since its bulk reference state is in doubt, it is not possible to use argon at this temperature for the determination of the mesopore size distribution. Second, the overall character of the argon isotherm at 77 K is much more sensitive than the nitrogen isotherm to any change in the surface structure. Nitrogen does not give any well-defined Type VI isotherms at 77 K and its multilayer development remains remarkably constant from one surface to another.

It is perhaps useful to summarize the merits and limitations of nitrogen as a standard adsorptive. As already noted, the fact that nitrogen has a permanent quadrupole moment is generally considered to be important: this appears to be responsible for the formation of a well-defined monolayer on most surfaces. At the same time, the level of specificity is not high enough to give strong localization on most surfaces at 77 K. An exception to this general rule is the exposure of cationic sites on the surface of some oxides (see Chapter 10).

From an experimental standpoint, the availability of liquid nitrogen and the range of commercial equipment now available make it relatively easy to determine full nitrogen adsorption–desorption isotherms at 77 K. This is an additional reason why nitrogen is now internationally accepted as the standard BET adsorptive (IUPAC: Sing *et al.*, 1985), with the convention that $\sigma(N_2) = 0.162\ nm^2$. Thus, for routine work, it is assumed that the nitrogen monolayer is in a close-packed 'liquid' state at 77 K, irrespective of the actual structure of the BET monolayer.

The IUPAC recommended procedure can be regarded as the first stage in the use of gas adsorption for the characterization of powders and porous solids. It does not rule out a more detailed study of the adsorbate structure or the use of other adsorptives. Indeed, the latter step is extremely important in the characterization of microporous adsorbents. The BET-nitrogen area provides a useful basis for a patent specification or for the comparison of adsorbents studied in different laboratories.

A considerable amount of evidence is now available in support of the view that the effective value of σ is to some extent dependent on: (a) the nature of the adsorbent–adsorbate and adsorbate–adsorbate interactions;(b) the structure of the adsorbent surface; and (c) the operational temperature. The monolayer is likely to be localized if the adsorbent–adsorbate interactions are relatively strong, provided that the

temperature is not too high. The density of the monolayer is controlled by the surface structure, although the adsorbate may not be strictly in registry with the crystal structure of the adsorbent. The mobility of the adsorbed molecules is governed by the height of the energy barrier, ϕ_b, between the adsorption sites in relation to the available thermal energy, kT, as previously illustrated in Figure 1.4. Generally, a high energy barrier is associated with strong adsorbent–adsorbate interactions and this in turn is indicated by a high C value. Thus, we may tentatively conclude that a high C (say, $C > 100$) for low-temperature adsorption (e.g. at 77 K) is a sign of a well-defined localized monolayer.

A low C value is more difficult to interpret. As we have seen, the BET monolayer cannot be determined with high accuracy and the same is true for the corresponding value of σ. This may explain why some reported values of σ appear to be much larger than expected. For example, σ and C values of 0.7 nm^2 and 10, respectively, have been reported for pentane on silica, in comparison with the values of 0.5 nm^2 and 60 for pentane on graphitized carbon (Kiselev and Eltekov, 1957).

When we insert the value $\sigma(N_2) = 0.162$ nm^2 into Equation (6.10) we obtain

$$\frac{a(\mathrm{BET})}{\mathrm{m^2\,g^{-1}}} = 0.097\,\frac{n_m}{\mu\mathrm{mol\,g^{-1}}} \tag{6.12}$$

or when v^σ(STP) is used, we have

$$\frac{a(\mathrm{BET})}{\mathrm{m^2\,g^{-1}}} = 4.35\,\frac{v_m^\sigma(\mathrm{STP})}{\mathrm{cm^3\,g^{-1}}} \tag{6.13}$$

For operational reasons, it becomes more difficult to measure nitrogen adsorption isotherms on low-area adsorbents (if $a < 5$ m^2g^{-1}). To overcome this problem, krypton is widely used. As a consequence of its low $p°$ at 77 K (≈2 mbar), the 'dead space' correction for unadsorbed gas is relatively small and it becomes possible to measure low uptakes of gas with acceptable accuracy.

Unfortunately, as with argon, the interpretation of a krypton isotherm is not always straightforward. At 77 K, krypton is well below its triple point and it would seem necessary to take the solid as the reference state to calculate $p/p°$. Nevertheless, as for argon, there is some evidence, from microcalorimetry and neutron diffraction studies (Grillet *et al.*, 1985), that in the BET region the adsorbate may well be in a liquid-like state. It has therefore become customary, for the construction of the BET plot, to adopt the saturation pressure, $p°$ (liquid), of the supercooled liquid as the effective $p°$ at 77 K. By applying Equation (6.11) and taking the absolute density of the supercooled liquid at 77 K, we obtain a value of 0.152 nm^2 for the molecular area of krypton. Beebe *et al.* (1945) found it necessary to adopt $\sigma(Kr) = 0.195$ nm^2 and this still remains a useful empirical value. However, there is little doubt that, in the context of the BET method, the molecular area does depend to some extent on the surface structure of the adsorbent (see Table 6.1). We conclude that krypton adsorption is particularly useful for routine surface area measurements with low-area powders when a knowledge of the 'absolute' area is not essential. The values used for $p°$ and σ must always be stated.

Over the past 50 years, many others gases have been proposed as suitable adsorptives for surface area determination (see Gregg and Sing, 1982). As indicated in Table 6.1, these have included oxygen and xenon (at low temperature) and organic vapours such as butane and benzene (at near 'ambient' temperatures). An excellent survey of early work on the cross-sectional areas of adsorbed molecules was given by McClellan and Harnsberger (1967). Cascarini de Torre *et al.* (1996) have recently used Monte Carlo computer simulation to study the molecular packing of nitrogen, oxygen and carbon dioxide on the surface of hypothetical amorphous carbons. The derived values of molecular cross-sectional areas are compared with the recommended molecular areas in the literature. Other recent attempts to determine σ values are discussed in Chapters 9 and 10 in the context of the physisorption of gases on carbons and oxides, respectively.

There is no special difficulty in dealing with mesoporous or macroporous materials since the pore filling takes place only in the multilayer region of the isotherm. The situation is quite different if the pores are in the molecular size range, i.e. with molecular sieves or other adsorbents containing narrow micropores. As discussed in Chapters 4 and 8, the value of a(BET) cannot be regarded as a true measure of the internal surface area if an overlap of adsorption forces causes a significant distortion of the isotherm in the sub-monolayer range. Under these circumstances, we recommend that a(BET) should always be designated as the 'BET area' (or as the 'equivalent BET area') and that the range of linearity of the BET plot should be given.

It is evident that Equation (6.1) cannot be applied to isotherms determined at temperatures above the critical temperature of the adsorptive. It follows from Figure 1.4 that the effect of surface heterogeneity is reduced at high temperature. Aranovich and Donohue (1997) have shown that in principle some physisorption isotherms at high pressures and supercritical temperature can be used for surface area determination provided that the adsorption is taken to (but not beyond) high monolayer coverage. By expressing the surface excess amount as a function of the density of the supercritical adsorptive, it becomes possible to evaluate the surface area without recourse to any assumptions concerning the adsorption mechanism or the molecular area.

6.3. Empirical Methods for Isotherm Analysis

6.3.1. Standard adsorption isotherms

As already noted, the detailed course of a physisorption isotherm is dependent on the nature of the gas–solid system and the operational temperature. In view of the wide variation in adsorbent–adsorbate interaction energies discussed in Chapter 1, it is not surprising to find that the shape of the isotherm in the *monolayer* region is especially sensitive to any variation in the surface structure of the adsorbent. However, as already indicated in Chapter 4, the shape of the corresponding *multilayer* isotherm is much less dependent on the adsorbent structure.

This means that the thickness t of an adsorbed multilayer depends essentially on the equilibrium pressure and, in some cases, hardly at all on the nature of the

adsorbent. This thickness can be evaluated after normalizing an adsorption isotherm of Type II, i.e. obtained in the absence of any micropore or mesopore filling. Indeed, it is possible to superpose, over an appreciable multilayer range, a series of normalized nitrogen adsorption isotherms determined at 77 K on non-porous oxides and carbons (de Boer *et al.*, 1966; Carrott and Sing, 1989).

An early normalizing procedure, proposed by Kiselev (1957) to compare adsorption isotherms of hydrocarbons, water vapour, etc. on a series of different adsorbents, was simply to plot the surface excess concentration $\Gamma (=n/A)$, obtained from a knowledge of the BET-nitrogen surface area, A(BET), versus $p/p°$. It is also possible to plot, instead of Γ, the 'reduced adsorption', n/n_m, which still relies on the BET method to determine the monolayer capacity n_m but does not require knowledge of the molecular cross-sectional area σ.

If the multilayer thickness is required, then the next step is to convert the reduced adsorption (i.e. the statistical number of adsorbed layers) into t, by the relation

$$t = \frac{n}{n_m} d' \tag{6.14}$$

where d' is the effective thickness of a monolayer. The assumption is generally made that the absolute density of the adsorbed layer is identical to that of the bulk liquid adsorptive at the operational temperature, so that:

$$d' = \frac{M}{\sigma \times L \times \rho^l} \tag{6.15}$$

where the terms are all as previously defined.

For nitrogen adsorbed at 77 K, from Equations (6.11) and (6.15) and taking $\rho = 0.809$ g cm^{-3}, $\sigma = 0.162$ nm^2 and $M = 28.01$ g mol^{-1}, one finds that $d' = 0.354$ nm. This value, which is an average molecular thickness, compares well with the kinetic diameter of nitrogen (0.364 nm). The notional thickness t of a close-packed nitrogen multilayer then becomes:

$$t = 0.354 n/n_m \tag{6.16}$$

This is the equation used by Lippens and de Boer (1965) to plot a t-curve, i.e. the standard multilayer thickness versus $p/p°$, for nitrogen adsorption at 77 K.

The observation that the t-curves for nitrogen on some apparently non-porous oxides (and carbons) were in fairly good agreement appeared to support the concept of a 'universal multilayer thickness curve' for nitrogen adsorption and appeared to offer the possibility of using this t-curve as a standard isotherm for nitrogen adsorption at 77 K (de Boer *et al.*, 1966). Although this claim is now regarded as an oversimplification, the fact that the multilayer sections of many *nitrogen* adsorption isotherms can be superposed has important implications for both surface area determination and pore size analysis (as will be seen in Chapter 7). The empirical methods described hereafter make use of the concept of the standard isotherm to allow an alternative assessment of the specific surface area and so remove the complete reliance on the BET method.

6.3.2. The t-method

The way in which Lippens and de Boer (1965) made use of the universal t-curve is simple. The experimental isotherm is transformed into a t-plot in the following manner: the amount adsorbed, $\boldsymbol{n}$, is replotted against t, the standard multilayer thickness on the reference non-porous material at the corresponding $p/p°$. Any difference in shape between the experimental isotherm and the standard t-curve is thus revealed as a non-linear region of the t-plot and/or a finite (positive or negative) intercept of the extrapolated t-plot (i.e. at $t = 0$). By this method a specific surface area, denoted $a(t)$, can be calculated from the slope, $s_t = \boldsymbol{n}/t$, of a linear section. From Equations (6.10), (6.11) and (6.15) we then get:

$$a(t) = \frac{M}{\rho} \times \left(\frac{\boldsymbol{n}}{t}\right) \tag{6.17}$$

and, taking $\rho = 0.809$ g cm^{-3} for nitrogen at 77 K:

$$\frac{a(t)}{\text{m}^2\,\text{g}^{-1}} = 0.0346\,\frac{s_t}{\mu\text{mol nm}^{-1}} \tag{6.18}$$

In their original work, Lippens and de Boer (1965) had assumed that monolayer adsorption could occur on the micropore walls in the same manner as on the open surface and on the walls of mesopores. So the t-method did not allow for the special nature of micropore filling. At a somewhat later stage, it was appreciated (Sing, 1967) that, under favourable conditions, a t-plot can provide a means of assessing the micropore volume and the external area. These aspects are more fully discussed in relation to the α_S-method in the next section and in Chapter 8.

The t-method can be improved if the universal nature of the t-curve is no longer assumed. Brunauer *et al.* (1969) suggested that the correct t-curve should be the one having the same C value as the adsorption isotherm under investigation. This approach is no longer considered to be acceptable practice and, it is now generally agreed (IUPAC: Sing *et al.*, 1985) that the appropriate standard isotherm must be determined on a non-porous solid having the same surface structure (i.e. surface chemistry) as that of the test adsorbent. The most serious limitation of the t-method is that it is necessarily dependent on the BET evaluation of the monolayer capacity of the reference material, since t is derived from $\boldsymbol{n}/\boldsymbol{n}_m$: this presents a special problem if the C value is relatively low.

6.3.3. The α_S -method

By a simple modification of the t-method it is possible to avoid the prior evaluation of $\boldsymbol{n}_m$ and thereby extend the analysis to virtually any type of physisorption system (Sing, 1968, 1970).

To convert the standard adsorption data into an alternative dimensionless form, $\boldsymbol{n}_m$ is replaced by $\boldsymbol{n}_S$ the amount adsorbed at a pre-selected relative pressure $(p/p°)_S$. In practice, it is usually convenient to take $(p/p°)_S = 0.4$. The corresponding reduced adsorption is then $\boldsymbol{n}/\boldsymbol{n}_{0.4}$ and is called α_S. The reduced isotherm for the non-porous

reference adsorbent (or 'α_S-curve', i.e. α_S versus $p/p°$) is therefore arrived at empirically without any need to determine the BET monolayer capacity.

The α_S-plot is constructed in an analogous manner to the t-plot, with the α_S data for the particular gas–solid system (at the operational temperature) used in place of the t data. From Equation (6.17), it is easy to verify that:

$$\frac{a_{test}}{a_{ref}} = \frac{n_{test}/(n_{ref})_{0.4}}{n_{ref}/(n_{ref})_{0.4}} \tag{6.19}$$

where $n_{ref}/(n_{ref})_{0.4} = \alpha_S$. So by writing $n_{test}/\alpha_S = s_S$, we obtain:

$$a_{test} = \frac{a_{ref}}{(n_{ref})_{0.4}} \times s_S \tag{6.20}$$

where a_{ref} is the specific surface area of the reference material.

In principle, the α_S-method is not restricted to nitrogen adsorption and can be applied to any gas–solid physisorption system irrespective of the shape of its isotherm: it can be used to check the validity of the BET area and also to identify the individual mechanisms (monolayer–multilayer adsorption, micropore filling or capillary condensation). Numerous examples of different α_S-plots are to be found in subsequent chapters. Here, we are concerned with the general principles of the α_S-method of isotherm analysis with particular reference to the evaluation of surface area. The distinctive features of various hypothetical α_S-plots are revealed in Figure 6.1, where the α_S-plots are classified in relation to isotherms of Types II, IV and I, respectively.

The most straightforward form of α_S-plot is Type II(a) in Figure 6.1, which is for a typical Type II isotherm with a moderate value of C (≈ 100). The extensive range of linearity and the zero intercept are the result of unrestricted monolayer–multilayer adsorption on a non-porous solid of very similar surface structure to that of the reference material. In this case the shapes of the experimental and standard isotherms are virtually identical and therefore the slope of the α_S-plot is directly proportional to the ratio of the surface areas, $a(S)/a_{ref}$. Thus, if the value of a_{ref} is already known, it is a simple matter to calculate a_{test}, which we denote $a(S)$ to indicate it is calculated by the α_S-method.

An α_S-plot of Type II(b) or II(c) (cf. Figure 6.1) is obtained when the multilayer section of the experimental isotherm conforms to that of the standard, but the monolayer section is different. The form of plot II(b) is indicative of relatively strong adsorbent–adsorbate interactions, whereas plot II(c) is associated with significantly weaker interactions. With either II(b) or II(c), $a(S)$ may be calculated from the slope of the linear multilayer region.

Type IV isotherms, which are normally associated with capillary condensation within the mesopore structure, generally give α_S-plots of Type IV as shown in Figure 6.1. In this case, it is the initial part of the isotherm which corresponds to monolayer–multilayer adsorption on the mesopore walls. If the corresponding section of the α_S-plot is linear and back-extrapolates to the origin, the slope provides a measure of $a(S)$ which is now the total surface area. We may also conclude that there are no

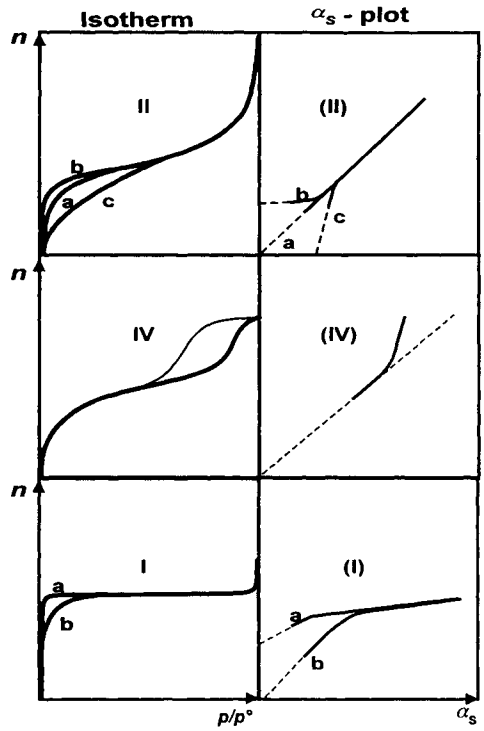

Figure 6.1. Hypothetical α_S-plots (right) and corresponding adsorption isotherms (left). The adsorbent is either non-porous (top), mesoporous (middle), or microporous (bottom).

additional complicating factors such as a micropore filling contribution. The upward deviation is due to the onset of capillary condensation.

The α_S-plots of type I(a) and I(b) are typical of those given by microporous adsorbents. As with the *t*-plot, a long linear multilayer section allows an assessment to be made of the external surface area. Any upward deviation (not represented here) is likely to be due to capillary condensation in a separate mesopore structure. If the intermediate linear region is not too short, its slope can provide a useful indication of the mesopore area. If we are confident that there are no complications associated with different surface chemical structures, we may safely attribute the difference between the shapes of the two α_S-plots I(a) and I(b) to the effects of primary and secondary micropore filling (see Chapters 4 and 8). Thus, the form of plot I(a) is due to distortion of the isotherm in the monolayer region, which is itself associated with the enhanced adsorbent–adsorbate interactions in the pores of molecular dimensions (i.e. primary micropore filling). On the other hand, the initial linear section of I(b), which can be back-extrapolated to the origin, is evidently due to a range of undistorted monolayer adsorption on the walls of wider micropores. It is only in the latter case that we can use the α_S-plot to derive a reliable value of the *internal* surface area.

The α_S-method for surface area determination has been calibrated against certain non-porous reference materials. For example, for N_2 adsorption on a non-porous hydroxylated silica, at 77 K, with $a_{ref} = 154\ m^2\ g^{-1}$ and $(n_{ref})_{0.4} = 2387\ \mu mol\ g^{-1}$, Equation (6.20) may be written as:

$$\frac{a(S-N_2)}{m^2\ g^{-1}} = 0.0645\ \frac{s_S}{\mu mol\ g^{-1}} \tag{6.21}$$

and for the adsorption of argon on the same silica at 77 K, we have:

$$\frac{a(S-Ar)}{m^2\ g^{-1}} = 0.074\ \frac{s_S}{\mu mol\ g^{-1}} \tag{6.22}$$

where $s_S = n/\alpha_S$ is the slope of a linear α_S-plot.

If we wish to use adsorption data where the specific gas volume corresponding to n is expressed in the traditional volume units of cm^3 (STP) g^{-1} (Carruthers *et al.*, 1971), it is necessary to multiply the coefficients of Equations (6.21) and (6.22) by the molar volume of the ideal gas, $0.022414\ cm^3\ \mu mol^{-1}$ (for $\theta = 0°C$ and $p° = 1.01325$ bar). Thus:

$$\frac{a(S-N_2)}{m^2\ g^{-1}} = 2.88\ \frac{v^\sigma/cm^3\ (STP)\ g^{-1}}{\alpha_S} \tag{6.23}$$

and

$$\frac{a(S-Ar)}{m^2\ g^{-1}} = 3.29\ \frac{v^\sigma/cm^3\ (STP)\ g^{-1}}{\alpha_S} \tag{6.24}$$

6.4. Adsorption from Solution

Adsorption from solution measurements have been used for many years for the routine determination of the surface area of certain porous materials such as activated carbons.

For example, adsorptives as diverse as iodine (Puri and Bansal, 1965; Kipling, 1965; Molina-Sabio *et al.*, 1985; Fernandez-Colinas *et al.*, 1989), *p*-nitrophenol (Giles and Nakhwa, 1962; Lopez-Gonzalez *et al.*, (1988), salicylic acid (Fernandez-Colinas *et al.*, 1991a,b) and various surfactants (Somasundaran and Fuerstenau, 1966) have been used for that purpose in dilute aqueous solution. Organic molecules in hydrocarbon solutions have included lauric acid (de Boer *et al.*, 1962).

Solid–solution adsorption systems have been found to give a variety of isotherm types, as classified by Giles *et al.* (1960). Many exhibit the characteristic Type I shape (see Figure 1.7), with the equilibrium concentration, c, replacing $p/p°$. In these cases, over a limited range of c, it is usually possible to apply an empirical equation of Langmuir form

$$n/n_L = bc/(1 + bc) \tag{6.25}$$

where n is the amount of solute adsorbed (per gram of adsorbent) at c, n_L is the amount adsorbed (per gram of adsorbent) at the plateau and b is an empirical constant.

However, this similarity in Type I shape does not mean that the mechanisms involved in solution–solid and gas–solid adsorption are the same. When the adsorbent is microporous, a Type I isotherm may be associated, as for gaseous physisorption, with micropore filling. With some other adsorbents, the plateau of a Type I solute isotherm appears to correspond to monolayer completion in accordance with the classical Langmuir interpretation. But there are a number of reasons why this approach does not always provide a reliable assessment of the overall surface area of an adsorbent. Indeed, solute molecules are generally subject to more specific interactions with the surface than the gas molecules conventionally used (N_2, Ar). An added complication is that adsorbent surfaces are generally heterogeneous. Consequently the apparent molecular area of the solute is likely to depend on the chemical nature of the exposed sites. Furthermore, the structure of the adsorbed phase may depend not only on the interaction between the adsorbed molecules (e.g. hydrogen bonding), but also on the incorporation of solvent. It is evident from the discussion in Chapter 5 that adsorption from solution is a competitive phenomenon between solvent and solute. Therefore, it is considerably more difficult to interpret than the adsorption of a single gas.

The role of the solvent was demonstrated by de Boer and his co-workers (1962). In their study of the adsorption of lauric acid on activated alumina it was found that solvent competition was most pronounced with diethyl ether, rather less so with benzene, and negligible with pentane. In the last case, the plateau of the lauric acid isotherm extended over a very wide range of concentration. This type of isotherm is associated with very high adsorption affinity and is generally due to relatively strong adsorbent–adsorbate interactions. However, the solute monolayer is unlikely to be in a close-packed state, the molecular area being dependent on the surface chemistry. Similarly, it has been found (see Gregg and Sing, 1967) that the apparent molecular area of adsorbed dye molecules is not constant from one type of surface to another. It follows that the problem for the measurement of surface areas by adsorption from solution is to choose a solute which is preferentially adsorbed on a particular type of surface and is able to cover all of that surface at low concentration.

As already mentioned, adsorption from solution is often used to characterize the adsorptive capacity of microporous carbons. As we will see in Chapter 8, recent measurements made with such solutes as iodine (Fernandez-Colinas *et al.*, 1989) or salicylic acid (Fernandez-Colinas *et al.*, 1991a,b) have revealed that it is possible to analyse adsorption from solution data by an extension of the α_S-method and to evaluate both the micropore volume and the external surface area.

6.5. Immersion Microcalorimetry

6.5.1. The modified Harkins and Jura 'absolute method'

For many years immersion microcalorimetry has been found useful for the routine characterization of fine powders and porous materials such as activated carbons and

oxides. In the absence of complicating effects such as micropore filling, it is generally assumed as a first approximation that the magnitude of the energy of immersion of the outgassed solid, $\Delta_{imm}U^{\circ}$ (cf. Chapter 5) is proportional to the extent of the available surface A so that:

$$\Delta_{imm}U^{\circ} = A\Delta_{imm}u^{i,\circ} \tag{6.26}$$

where the areal energy of immersion $\Delta_{imm}u^{i,\circ}$ is characteristic of the nature of a given liquid–solid system.

The technique of immersing a known mass of outgassed solid, with no dissolution, in a given liquid and measuring the heat evolved, would appear to provide a means of determining A by a single measurement, provided that $\Delta_{imm}u^{i,\circ}$ is known for the liquid–solid system. If the surface of the solid sample in the immersion cell is at least 1 m^2, the amount of heat released is not difficult to measure with the microcalorimetric procedure described in Section 5.2.2. Thus, for the routine control of the specific surface areas of a series of well-defined samples, immersion microcalorimetry is a very useful technique.

However, because it is very sensitive to any change in the nature of the surface, the areal energy of immersion in a given liquid is very dependent on the physicochemical properties of the solid, so that the value of $\Delta_{imm}u^{i,\circ}$ cannot be used for the assessment of specific surface area of an unknown solid. An elegant way to solve this problem was proposed by Harkins and Jura (1944) under the name of the 'absolute' calorimetric method for the determination of surface areas (see Figure 6.2). Here, the outgassed powder (state 1) is brought into equilibrium with the saturation vapour pressure of the immersion liquid in order to form an adsorbed film thick enough (5–7 molecular layers) to hide the specific adsorption sites of the powder and to present an external surface identical in nature to that of the bulk liquid (state 2). The pre-coated powder is then immersed in the liquid located in the calorimeter (state 3). The heat released during the loss of the liquid film–vapour interface is related to its area A. Harkins and Jura made use of a basic relationship which is obtained by integrating Equation (5.23) between the two

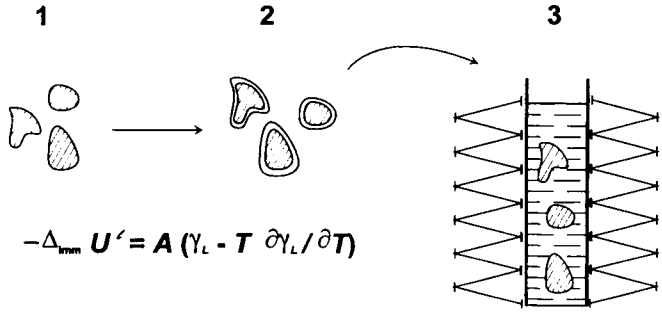

Figure 6.2. Principle of the Harkins and Jura 'absolute' method for determining the surface area.

values of surface area (A, 0):

$$\Delta_{imm}U^{l} = -A\left(\gamma - T\frac{\partial\gamma}{\partial T}\right) \tag{6.27}$$

where γ is the surface tension of the immersion liquid (Harkins and Jura, 1944; Harkins, 1952). Of course the immersion energy $\Delta_{imm}U^{l}$ always has a negative value, and the immersion is an exothermic process. Because A is obtained without any assumption concerning the molecular cross-section of the immersion liquid, Harkins and Jura referred to their method as an 'absolute method'.

The few investigators who have attempted to use the original Harkins–Jura method have encountered a number of inherent difficulties. A major problem is that it is virtually impossible to avoid some interparticle capillary condensation as $p/p^{\circ} \longrightarrow 1$. This inevitably reduces the extent of the available liquid–vapour interface (Wade and Hackerman, 1960). Moreover, the thickness of a pre-adsorbed film as $p/p^{\circ} \longrightarrow 1$ is highly dependent on the shape, size and roughness of the particles.

By taking advantage of the high sensitivity of Tian–Calvet microcalorimetry (see Chapter 3), it was possible to improve the Harkins–Jura procedure (Partyka *et al.*, 1979). It was found that, with a number of non-porous solids, the pre-adsorption of *c* 1.5 molecular layers of water was sufficient to produce a film–vapour interface with the same energy as a bulk liquid–vapour interface. In other words, this statistical thickness of pre-adsorbed water is enough to effectively 'screen' the adsorbent surface, but small enough to prevent any substantial change in surface area (either by capillary condensation or by increase of the apparent radius of the particles). This is obtained by carrying out the pre-adsorption under a relative pressure of 0.5, instead of 1. With the aid of this modified Harkins–Jura technique and the use of a Tian–Calvet microcalorimeter it is possible to obtain surface areas which are in agreement to within 10%, with the nitrogen-BET surface areas (Partyka *et al.*, 1979). Provided that sufficient care is taken, the immersion method is relatively easy to apply and is well suited for the determination of the surface area of insoluble non-porous oxides, ceramics, clays, etc. with specific areas ranging from 1 to 100 $m^2\,g^{-1}$. Of course, water is not a suitable pre-adsorption vapour for the study of hydrophobic surfaces. The limited work carried out so far has indicated that pentanol may be a useful alternative (Partyka *et al.*, 1979).

6.5.2. The surface area of microporous carbons

Immersion calorimetry provides a very useful means of assessing the *total* surface area of a microporous carbon (Denoyel *et al.*, 1993). The basic principle of this method is that there is a direct relation between the energy of immersion and the total area of the microporous material. Indeed, for the two model cases of slit-shaped and cylindrical micropores, the predicted maximum enhancement of the adsorption potential (as compared with that of the flat surface of same nature) is 2.0 and 3.68, respectively (Everett and Powl, 1976). These values are remarkably similar to the increased surface area occupied by a molecule in the narrowest possible slit-shaped and cylindrical pores (i.e. 2.0 in a slit and 3.63 in a cylinder). To apply the method we

must make two assumptions:

1. For a given state of the solid surface the energy of immersion is simply proportional to the surface area available to the immersion liquid for any size and shape of pore.
2. From the viewpoint of the areal energy of immersion, the behaviour of microporous and external solid surfaces is identical.

So far this approach has been applied to activated carbons, taking an ungraphitized carbon black as the reference, and using the set of immersion liquids listed in Table 8.1. The results obtained are consistent with the fact that the ultramicropore surface area accessible to a given immersion liquid is dependent on its molecular size. They open a way for the determination of the surface area of ultramicroporous solids (Denoyel *et al.*, 1993). This method has been successfully applied by Gonzalez *et al.*, (1995) and by Rodriguez-Reinoso *et al.* (1997), who were able to show that the presence of oxygen-containing surface groups does not have much effect on the enthalpy of immersion in methanol or water. The areal enthalpy of immersion of the carbons in non-polar liquids appeared to be independent of the chemical nature of the carbon surface.

6.6. The fractal approach

We have seen that it is often extremely difficult to arrive at exactly the same result when a number of different experimental methods are used for the determination of the specific surface area. Indeed, as Adamson (1990) has pointed out, one should in general *expect* the results to differ!

To illustrate this problem, we note a possible difference between the surface area of a porous solid which is available for adsorption and the area (including that of closed pores) which can scatter low angle X-rays. Even in the former case, the extent of the adsorption is likely to be dependent on the size, shape and electronic nature of the adsorptive molecules in relation to the surface chemistry, roughness and porosity of the adsorbent.

In principle, the fractal approach provides a way of circumventing the intractable problem of evaluating the *absolute* area of a finely divided or porous solid. The aim of fractal analysis is to characterize the *effective* geometry of an adsorbent and hence arrive at a clearer understanding of its behaviour.

The application of fractal geometry may be regarded as a form of resolution analysis: it is a systematic way of studying how the magnitude of a given property (e.g. surface area or pore volume) is altered by a change in the resolution of its measurement (Pfeifer and Obert, 1989; Avnir, 1991, 1997). In general, one makes use of a simple scaling power law of the type

$$(\text{measured property}) = k(\text{resolution})^{D} \tag{6.28}$$

where k and D are constants, which define the degree of resolution.

In the present context, it is useful to express Equation (6.28) in an explicit form,

such as

$$N_m = k\sigma^{-D_a/2} \tag{6.29}$$

where N_m is the number of molecules in the completed monolayer, σ is the adsorptive molecular area and D_a is now the fractal dimension of the accessible surface (Farin and Avnir, 1989).

The magnitude of D_a is determined *inter alia* by the degree of surface roughness or porosity. In principle, a lower limit of $D_a = 2$ is obtained with a perfectly smooth surface on the molecular scale. Most non-porous materials would be expected to exhibit some surface roughness. With such a material, a constant value of D_a between 2 and 3 implies that there is a degree of self-similarity: the shape of the surface irregularities thus remains invariant over a certain range of resolution. The physical structure of a fractal surface will therefore appear similar when viewed at different magnifications.

Fractal plots of log n_m versus log σ for two porous silicas are shown in Figure 6.3 (here, n_m is the BET monolayer capacity). Both plots are linear, giving $D_a = 2.98$ for the silica gel and $D_a = 2.09$ for the controlled pore glass. These values reflect the extremes of the fractal scale, the latter being close to the ideal value for a flat surface.

Some of the many values of D_a compiled by Farin and Avnir (1989) and Avnir *et al.*, (1992) are given in Table 6.2. Most values are within the theoretical fractal range, $D_a = 2$–3 and it is noteworthy that $D_a \approx 2$ for the graphitized carbon blacks and the pillared clays.

The values of D_a of (1.89 ± 0.09) and (1.94 ± 0.10) reported by Van Damme and Fripiat (1985) for pillared clays were derived from the multilayer capacities of nitrogen and various organic adsorptives. The fact that $D_a \approx 2$ appeared to confirm that the basal smectite surface was smooth and that the pillars were regularly distributed. It was argued by Van Damme and Fripiat that a random distribution of the pillars would necessarily lead to some localized molecular sieving and that this in turn would result in $D_a > 2$.

Various other aspects of fractal analysis have been discussed by Van Damme and Fripiat and their co-workers. For example, by extending the BET model to fractal surfaces, Fripiat *et al.* (1986) were able to show that the apparent fractal dimension is reduced by the progressive smoothing of a molecularly rough surface. Alternatively, the effect of a micropore filling contribution is to enhance the fractal dimension.

Other investigators, including Pfeifer and Obert (1989), Pfeifer *et al.* (1990), Krim and Panella (1991), Panella and Krim (1994) and Neimark and Unger (1993), have also studied multilayer adsorption on fractally rough surfaces. In particular, Pfeifer and his co-workers point out that the interpretation of a fractal dimension of a porous surface

Table 6.2. Values of accessible fractal dimension evaluated from adsorption data (taken from Farin and Avnir, 1989)

Adsorbent	Adsorptives	Fractal dimension, D_a
Graphitized carbon blacks	N_2 and alkanes	1.9–2.1
Activated carbons	N_2 and organic molecules	2.3–3.0
Pillared clays	N_2 and organic molecules	1.8–2.0
Silica gels	Alkanes	2.9–3.4
Other oxides	N_2 and alkanes	2.4–2.7

presents problems when it is associated with the BET theory. In contrast, an FHH-fractal treatment appears to be more promising, provided that wetting effects are taken into account. This was exactly the approach adopted by Krim and her co-workers.

In their work on carefully prepared homogeneous silver films, Krim and Panella (1991) and Panella and Krim (1994) applied the FHH equation in the form

$$\ln(p/p^\circ) = -\alpha/(kT\theta^n) \tag{6.30}$$

where the coefficient α is dependent on the nature of the adsorbent–adsorbate and adsorbate–adsorbate interactions and the corresponding fractal dimension is determined by the magnitude of the exponent n (de Gennes, 1985). Nitrogen and oxygen isotherms at 77.4 K gave linear FHH plots over a wide range of multilayer coverage. The values of n for nitrogen on smooth and rough silver substrates were 3.0 and 4.7, respectively, the former giving the expected fractal dimension, $D_a = 2$. However, the value $n \approx 3$ was also obtained for oxygen on the *rough* surface, which was attributed to surface tension effects (since the surface tension of liquid oxygen is much higher than that of liquid nitrogen).

Panella and Krim suggested that the high value $n = 4.7$ was more consistent with the properties of a self-affine surface rather than a self-similar one. Self-affine fractals are associated with asymmetric scaling, that is different scaling relations in different directions (Avnir, 1997).

The FHH-fractal approach was also adopted by Ehrburger-Dolle *et al.* (1994) as part of a systematic study of the properties of silica aerogels. The value $D_a = 2.1$ was evaluated from the linear FHH plot for nitrogen on Aerosil 200, whereas values of 2.64 and 2.95 were obtained from the nitrogen multilayer isotherms on various aerogels. The latter value, which is obviously close to 3, appeared to be consistent with

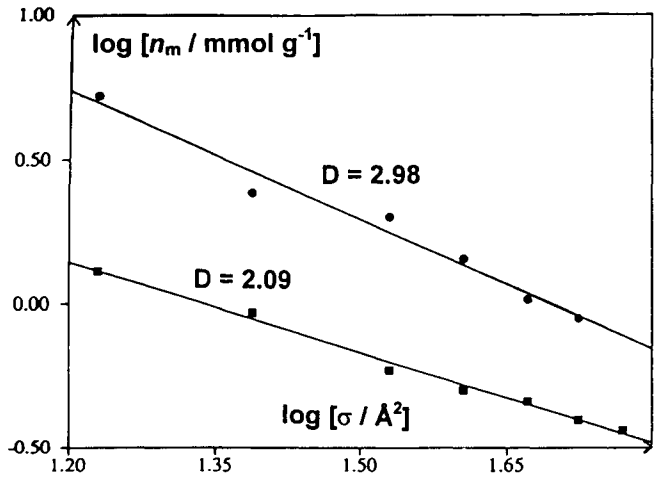

Figure 6.3. Fractal plots for the adsorption of organic vapours on the silica gel and a controlled porous glass (after Farin *et al.*, 1985 and Christensen and Topsoe, 1987): part of Fig. 1, Farin and Avnir, 1989.

volume filling by capillary condensation as the predominant process at high $p/p°$. Evidently, the low fractal dimension given by Aerosil 200 is associated with its molecularly smooth surface.

Another aspect of fractal geometry which has been discussed in some detail by Avnir and his co-workers is the relationship between surface area and particle size. If the particles of a powder are smooth and non-porous, we would expect to find a simple form of inverse relation

$$a = k/d \tag{6.31}$$

where the constant k is dependent on the density and the particle shape.

In practice, Equation (6.31) will not hold if the particles are either rough or porous. If the particles are highly porous, we have the extreme case of a negligible external area in comparison with the internal area.

For the intermediate case between the extremes of smooth and highly porous particles, Farin and Avnir (1988) apply an expression of the form

$$a/a_g = R^{D_r - 2} \tag{6.32}$$

where a is the total apparent specific surface area, a_g is the 'geometric' area, which is based on the average particle radius, R, and D_r is the roughness fractal dimension. Linear fractal plots of log a versus log R have been reported for a number of different porous and non-porous adsorbents (Farin and Avnir, 1989). A selection of the derived values of D_r is given in Table 6.3. Most adsorption measurements were made with nitrogen or krypton at 77 K and it would now be of interest to extend the comparisons to include other adsorptive molecules.

On the whole, the overall pattern of the results in Table 6.3 is as expected. It is not surprising to find that Aerosil and vitreous silica gave low values of D_r which correspond to minimal surface roughness. The high D_r values obtained with the skeletal carbonates and porous silica are also to be expected. Although it is more difficult to understand the significance of some of the intermediate values (e.g. of coke), the linearity of the fractal plots is of practical value.

Table 6.3. Value of the roughness fractal dimension derived from fractal plots of log a versus. log R (Farin and Avnir, 1989)

Adsorbent	Adsorptive	Fractal dimension, D_r
Aerosil	Nitrogen	2.0
Vitreous silica	Nitrogen	2.0
Montmorillonite	Nitrogen	2.0
Quartz	Nitrogen	2.1
Snowit	Nitrogen	2.2
Iceland spar	Krypton	2.2
Coke	Nitrogen	2.5
	Carbon dioxide	2.5
Dolomite	Krypton	2.6–2.9
Biocarbonates	Krypton	2.7–3.0
Porous silica	Nitrogen	3.0
	Ethanol	3.0

On the basis of all these findings, it would seem that a simple fractal approach offers a useful way of detecting and characterizing the effects of surface roughness and porosity. At first sight, fractal analysis appears to be more sophisticated than the traditional and simplifying assumption that the same area is available to all adsorptives. However, it must be kept in mind that, because of experimental constraints, the application of the power law is limited to a fairly short range of molecular size. Furthermore, as Drake *et al.* (1990) have pointed out, the molecular cross-sectional areas are difficult to establish unambiguously. Another limitation of fractal analysis is that the precise nature of the surface roughness or porosity cannot be deduced from a single value of D_a.

In a spirited rebuttal of some of these arguments, Avnir *et al.* (1992) stress the need for caution in accepting molecular areas which are based on a standardized method (usually BET-nitrogen). Indeed, these comments should serve as a useful reminder that we should not expect the effective molecular area of an adsorptive to remain the same on all surfaces. This aspect is discussed in other chapters where we describe the dependence of the monolayer structure on the adsorbent structure (e.g. of graphite and magnesium oxide) and the nature of the adsorbent–adsorbate interactions. In an extreme case of molecular sieving, differences in accessibility are obvious; but with many systems (especially heterogeneous substrates), it is much more difficult to distinguish between the effects of surface roughness and surface structure.

In a critical appraisal of the different methods for determining surface fractal dimensions, Neimark (1990) has stressed the importance of taking account of the different mechanisms of physisorption (e.g. at high p/p° the combination of multilayer adsorption and capillary condensation). Conner and Bennett (1993) have also warned of the risk of an oversimplistic interpretation of a linear log–log fractal plot.

In our view, an oversimplified application of fractal analysis may tend to obscure rather than clarify the interpretation of adsorption data. In practice, there are two complicating factors: (1) the derived values of n_m are not always reliable, and (2) the mechanisms of adsorption and pore filling are dependent on the adsorbent–adsorbate interactions and the ratio of pore width to molecular diameter and may not be the same for all the members of a series of adsorptives on a given adsorbent.

We are drawn to the conclusion that log–log fractal plots are useful for the correlation of adsorption data – especially on well-defined porous or finely divided materials. A derived fractal dimension can also serve as a characteristic empirical parameter, provided that the system and operational conditions are clearly recorded. In some cases, the fractal self-similarity (or self-affine) interpretation appears to be straightforward, but this is not so with many adsorption systems which are probably too complex to be amenable to fractal analysis.

References

Adamson A.W. (1990) *Physical Chemistry of Surfaces*, Wiley, New York, p. 561.
Aranovich G.L. and Donohue M. (1997) *J. Colloid Interface Sci.* **194**, 392.
Avgul N.N., Kiselev A.V., Lygina I.A. and Mikailova E.A. (1962) *Izv. an SSSR, Otd Khim. Nauka* 769.
Avnir D. (1991) *Chem. & Ind.* 912.

Avnir D. (1997) In: *Handbook of Heterogeneous Catalysis*, Vol. 2 (G. Ertl, H. Knozinger and J. Weitkamp, eds), Wiley-VCH, Weinheim, p. 598.
Avnir D., Farin, D. and Pfeifer P. (1992) *New J. Chem.* **16**, 439.
Beebe R.A. and Young D.M. (1954) *J. Phys. Chem.* **58**, 93.
Beebe R.A., Beckwith J.B. and Honig J.M. (1945) *J. Am. Chem. Soc.* **67**, 1554.
Benton A.F. (1926) *J. Am. Chem. Soc.* **48**, 1850.
Berezin G.I., Kiselev A.V., Sagatelyan R.T. and Serdobov M.V. (1969) *Zh. Fiz. Khim.* **43**, 224.
Berezin G.I. and Sagatelyan R.T. (1972) In: *Thermochimie*, Colloques Internationaux du CNRS no. 201, Editions du CNRS, Paris, p. 561
Brunauer S. and Emmett P. H. (1935) *J. Am. Chem. Soc.* **57**, 1754.
Brunauer S. and Emmett P. H. (1937) *J. Am. Chem. Soc.* **59**, 2682.
Brunauer S., Emmett P. H. and Teller E. (1938) *J. Am. Chem. Soc.* **60**, 309.
Brunauer S. (1945) *The Adsorption of Gases and Vapors*, Princeton University Press, Princeton.
Brunauer S., Skalny J. and Bodor E.E. (1969) *J. Colloid Interface Sci.* **30**, 546.
Carrott P.J.M. and Sing K.S.W. (1989) *Pure Appl. Chem.* **61**, 1835.
Carruthers J.D., Payne D.A., Sing K.S.W. and Stryker L. G. (1971) *J. Colloid Interface Sci.* **36**, 205.
Cascarini de Torre L.E., Bottani E.J. and Steele W.A. (1996) *Langmuir* **12**, 5399.
Christensen S.V. and Topsoe H. (1987) Haldor Topsoe Co, Denmark, private communication quoted by Avnir *et al.*, (1992).
Conner W.M. and Bennett C.O. (1993) *J. Chem. Soc., Faraday Trans.* **89**, 4109.
de Boer J.H., Houben G.M.M., Lippens B.C., Meij W.D. and Walgrave W.K.A. (1962) *J. Catalysis* **1**, 1
de Boer J.H., Lippens B.C., Linsen B.G., Broekhoff J.C.P., van den Heuvel A. and Osinga Th.J. (1966) *J. Colloid Interface Sci.* **21**, 405.
Denoyel R., Fernandez-Colinas J., Grillet Y. and Rouquerol J. (1993) *Langmuir* **9**, 515.
Drake J.M., Levitz P. and Klafter J. (1990) *New J. Chem.* **14**, 77.
Ehrburger-Dolle F., Dallamano J., Pajonk G.M. and Elaloui E. (1994) In: *Characterization of Porous Solids III* (J. Rouquerol, F. Rodriguez-Reinoso, K.S.W. Sing and K.K. Unger, eds), Elsevier, Amsterdam p. 715.
Emmett P.H. and Brunauer S. (1937) *J. Am. Chem. Soc.* **59**, 1553.
Everett D.H. and Powl J.C. (1976) *J. Chem. Soc., Faraday Trans. I* **72**, 619.
Farin D., Volpert A. and Avnir D. (1985) *J. Am. Chem. Soc.* **107**, 3368, 5319.
Farin D. and Avnir D. (1988) In: *Characterization of Porous Solids I* (K.K. Unger, J. Rouquerol, K.S.W. Sing, and H. Kral, eds) Elsevier, Amsterdam, p. 421.
Farin D. and Avnir D. (1989) In: *The Fractal Approach to Heterogeneous Chemistry* (D. Avnir, ed.), John Wiley, Chichester, p. 271.
Fernandez-Colinas J., Denoyel R. and Rouquerol J. (1989) *Adsorption Sci. Tech.* **6**, 18.
Fernandez-Colinas J., Denoyel R., Grillet Y., Vandermeersch J., Reymonet J.L., Rouquerol F. and Rouquerol J. (1991a) In: *Fundamentals of Adsorption III* (A.B. Mersmann and S.E. Scholl, eds), Engineering Foundation, New York, p. 261.
Fernandez-Colinas J., Denoyel R. and Rouquerol J. (1991b) In: *Characterization of Porous Solids II* (F. Rodriguez-Reinoso, J. Rouquerol, K.S.W. Sing and K.K. Unger, eds), Elsevier, Amsterdam, p. 399.
Fripiat J.J., Gatineau L. and Van Damme, H. (1986) *Langmuir* **2**, 562.
de Gennes P.G. (1985) In: *Physics of Disordered Materials* (D. Adler, H. Fritzsche and S.R. Ovshinsky, eds), Plenum, New York.
Giles C.H. and Nakhwa S.N. (1962) *J. Appl. Chem.* **12**, 266.
Giles C.H., MacEwan T.H., Nakheva S.N. and Smith D. (1960) *J. Chem. Soc.* 3973.
Gonzalez M.T., Sepulveda-Esoribano A., Molina-Sabio M. and Rodriguez-Reinoso F. (1995) *Langmuir*, **11**, 2151.
Gregg S.J. and Sing K.S.W. (1967) *Adsorption, Surface Area and Porosity*, 1st edn, Academic Press, London, p. 293.
Gregg, S.J. and Sing, K.S.W. (1982) *Adsorption, Surface Area and Porosity*, 2nd edn, Academic Press, London.

Grillet Y., Rouquerol F. and Rouquerol J. (1985) *Surface Sci.* 478.
Harkins W.D. (1952) In: *The Physical Chemistry of Surface Films*, Reinhold Publishing, Division, New York.
Harkins W.D. and Jura, G. (1944) *J. Am. Chem. Soc.* **66**, 1362.
Hill T.L. (1946) *J. Chem. Phys.* **14**, 268.
Holmes J.M. (1967) In: *The Solid-Gas Interface* (E.A. Flood, ed.), Marcel Dekker, New York, p. 127.
Keii T., Takagi T. and Kanataka S. (1961) *Anal. Chem.* **33** (1965).
Kipling J.J. (1965) *Adsorption from Solutions of Non-electrolytes*, Academic Press, London.
Kiselev A.V. (1957) In: *Second International Congress of Surface Activity II* (J.M. Schulman, ed.), Butterworths, London, p. 168.
Kiselev A.V. and Eltekov Y.A. (1957) In: *Second International Congress of Surface Activity II* (J.H. Schulman, ed.), Butterworths, London, p. 228.
Krim J. and Panella V. (1991) In: *Characterization of Porous Solids II* (F. Rodriguez-Reinoso J. Rouquerol, K.S.W. Sing and K.K. Unger, eds), Elsevier, Amsterdam, p. 217.
Langmuir I. (1916) *J. Am. Chem. Soc.* **38**, 2221.
Langmuir I. (1918) *J. Am. Chem. Soc.* **40**, 1361.
Lippens B.C. and de Boer J.H. (1965) *J. Catalysis* **4**, 319.
Lopez-Gonzalez J. de D., Valenzuela-Calahorro C., Navarrete-Guijosa A. and Gomez-Serrano V. (1988) *An. Quim.* **84B**, 47.
McClellan A.L. and Harnsberger H.F. (1967) *J. Colloid Interface Sci.* **23**, 577.
Marc R. (1911) *Z. Phys. Chem.* **75**, 710.
Molina-Sabio M., Salinas-Martinez de Lecea, C., Rodriguez-Reinoso F., Peunte-Ruiz C. and Linares-Solano A. (1985) *Carbon* **23**, 91.
Neimark A.V. (1990) *Adsorption Sci. Tech.* **7**, 210.
Neimark A.V. and Unger, K.K. (1993) *J. Colloid Interface Sci.* **158**, 412.
Panella V. and Krim J. (1994) In: *Characterization of Porous Solids III* (J. Rouquerol, F. Rodriguez-Reinoso, K.S.W. Sing and K.K. Unger, eds), Elsevier, Amsterdam, p. 91.
Paneth F. (1922) *Z. Electrochem* **28**, 113.
Parra J.B., de Sousa J.C., Bansal R.C., Pis J.J. and Pajares J.A. (1994) *Adsorption Sci. Tech.* **11**, 51.
Partyka S., Rouquerol F. and Rouquerol J. (1979) *J. Colloid Interface Sci.* **68** (1), 21.
Pfeifer P. and Obert, M. (1989) In: *The Fractal Approach to Heterogeneous Chemistry* (D. Avnir, ed.), John Wiley, Chichester, p. 11.
Pfeifer P., Obert M. and Cole M.W. (1990) In: *Fractals in the Natural Sciences* (M. Fleischmann, D.J. Tildesly and R.C. Ball, eds), Princeton University Press, Princeton, p.169.
Prenzlow C.F. and Halsey G.D. (1957) *J. Phys. Chem.* **61**, 1158.
Puri B.R. and Bansal R.C. (1965) *Carbon* **3**, 227.
Rhodin T.N. (1950) *J. Am. Chem. Soc.* **72**, 569.
Rodriguez-Reinoso F., Molina-Sabio M. and Gonzalez M.J. (1997) *Langmuir* **13**, 2354.
Rouquerol F., Rouquerol J. and Imelik B. (1964) *Bull. Soc. Chim. Fr.* 635.
Rouquerol J., Rouquerol F., Pérès C., Grillet Y. and Boudellal M. (1979) In: *Characterization of Porous Solids* (S.J. Gregg, K.S.W. Sing and H.F. Stoeckli, eds), London Society of Chemical Industry, p. 107.
Rouquerol J., Rouquerol F., Grillet Y. and Torralvo M.J. (1984) In: *Fundamentals of Adsorption* (A.L. Meyer and G. Belfort, eds), Engineering Foundation, New York, p. 501.
Sing K.S.W. (1967) *Chem. & Ind.* 829.
Sing K.S.W. (1968) *Chem. & Ind.* 1520.
Sing K.S.W. (1970) In: *Surface Area Determination* (D.H. Everett and R.H. Ottewill, eds), Butterworths, London, p. 15.
Sing K.S.W., Everett D.H., Haul R.A.W., Moscou L., Pierotti R.A., Rouquerol J. and Siemieniewska T. (1985) *Pure Appl. Chem.* **57**, 603.
Somasundaran P. and Fuerstenau D.W. (1966) *J. Phys. Chem.* **70**, 90.
Van Damme H. and Fripiat J.J. (1985) *J. Chem. Phys.* **82**, 2785.
Wade W.H. and Hackerman N. (1960) *J. Phys. Chem.* **64**, 1196.
Williams A.M. (1919) *Proc. Roy. Soc.* **A96**, 298.
Young D.M. and Crowell A.D. (1962) *Physical Adsorption of Gases*, Butterworths, London

This Page Intentionally Left Blank

CHAPTER 7

Assessment of Mesoporosity

7.1. Introduction

The aim of this chapter is to discuss in general terms the use of adsorption measurements for the characterization of mesoporous solids (i.e. adsorbents having effective pore widths in the approximate range of 2–50 nm). Our approach here is mainly along 'classical' lines and is based on the concept of capillary condensation and the application of the Kelvin equation. However it is appropriate to include a brief discussion of the relevant aspects of network percolation and density functional theory.

Virtually all the computational procedures used for the analysis of adsorption data start from the assumption that the pores are rigid and of well-defined shape. Many investigators have assumed the mesopores to be either regular cylinders or parallel-sided slits, but in fact there are relatively few real adsorbents which conform exactly to either of these shapes. It is important to keep in mind that most porous adsorbents of technological importance are composed of complex interconnected pores of irregular shape.

Nitrogen adsorption has become generally accepted as the standard method for mesopore size analysis. The recommended experimental and computational procedures involved are described in various official publications (e.g. IUPAC: Sing *et al.*, 1985 and Rouquerol *et al.*, 1994; British Standard 7591, Part 2, 1992). However, the underlying principles of mesopore filling are still not fully understood and in

particular the significance of the lower limit of validity of the Kelvin equation remains unresolved.

A closely related problem is the interpretation of physisorption hysteresis, when it appears in the form of an adsorption–desorption loop in association with capillary condensation–evaporation. Until recently, it was generally assumed that some form of hysteresis loop was a distinctive feature of every Type IV isotherm. With some mesoporous adsorbents, the shape of the loop is known to give a useful indication of the type of pore structure (e.g. the uniformity and shape of the pores).

A few completely reversible Type IV isotherms have been reported within the past few years. One example is that of nitrogen at 77 K on MCM-41. It now seems likely that such behaviour is manifested only if the pores are filled at or below a critical value for the adsorptive at a given temperature.

7.2. Capillary Condensation and the Kelvin Equation

7.2.1. Derivation of the Kelvin equation

It is well known (Defay and Prigogine, 1951) that a spherical interface of radius of curvature r and surface tension γ can maintain mechanical equilibrium between two fluids at different pressures p'' and p'. The phase on the concave side of the interface experiences a pressure p'' which is greater than that on the convex side. The mechanical equilibrium condition is given by the Laplace equation:

$$p'' - p' = \frac{2\gamma}{r} \tag{7.1}$$

Indeed, in the particular case where $r \longrightarrow \infty$, $p'' = p'$, the mechanical equilibrium between two phases separated by a plane interface can only be obtained if their pressures are equal.

If, instead of a spherical surface, one considers any interface having two principal radii of curvature of the surface r_1 and r_2, then the condition of mechanical equilibrium at each point on the interface is:

$$p'' - p' = \gamma\left[\frac{1}{r_1} + \frac{1}{r_2}\right] \tag{7.2}$$

Or introducing the radius r_m of mean curvature defined by:

$$\frac{1}{r_m} = \frac{1}{2}\left[\frac{1}{r_1} + \frac{1}{r_2}\right] \tag{7.3}$$

the equation becomes:

$$p'' - p' = \frac{2\gamma}{r_m} \tag{7.4}$$

which is a generalization of Equation (7.1).

A related phenomenon is the difference in vapour pressure between the flat and curved surfaces of a given liquid. The application of classical thermodynamics (cf. Defay and Prigogine, 1951) allows us to replace the difference in mechanical pressure $\Delta p = p^g - p^l$, by a function of the relative vapour pressure p/p°. The condition for physicochemical equilibrium is:

$$\mu^l = \mu^g \tag{7.5}$$

If we now move from one equilibrium state to another neighbouring equilibrium state at constant temperature, then

$$dp^g - dp^l = d\left(\frac{2\gamma}{r_m}\right) \tag{7.6}$$

and

$$d\mu^l = v^l\, dp^l = d\mu^g = v^g\, dp^g \tag{7.7}$$

which allows Equation (7.6) to be written in the form:

$$d\left(\frac{2\gamma}{r_m}\right) = \frac{v^l - v^g}{v^l}\, dp^g \tag{7.8}$$

If we neglect the molar volume of the liquid v^l in comparison with the molar volume of the vapour v^g, and assume the vapour to be ideal, Equation (7.8) becomes:

$$d\left(\frac{2\gamma}{r_m}\right) = -\frac{RT}{v^l}\frac{dp^g}{p^g} \tag{7.9}$$

If we now integrate this equation from zero curvature ($1/r_m = 0$, $p^g = p^\circ$) to some other state ($1/r_m$, p) and assume that v^l is nearly constant, we have:

$$\ln\frac{p}{p^\circ} = -\frac{2\gamma v^l}{r_K RT} \tag{7.10}$$

which gives the dependence of p/p° on the mean radius of curvature of the meniscus r_m, now replaced by r_K. Equation (7.10) is often referred to as the Kelvin equation since it is closely related to an equation originally proposed by Lord Kelvin (Thomson 1871). Note that in this equation γ and v^l are assumed independent of r_K.

For nitrogen adsorbed at 77.35 K, we can use the following values: $\gamma = 8.85$ m Nm^{-1}; $\rho^l = 0.807$ g cm^{-3}; $M = 28.01$ g mol^{-1}; $V_m^l = 34.71$ cm^3 mol^{-1}. Then:

$$\frac{r_K}{\text{nm}} = -\frac{0.415}{\log_{10}(p/p^\circ)}$$

A more general equation, derived by Everett (1979), is appropriate if the vapour pressure is high or the liquid–vapour adsorptive is close to its critical state.

7.2.2. Application of the Kelvin equation

We are now in a position to consider the significance of Equation (7.10) in relation to physisorption. First, let us consider an assemblage of cylindrical mesopores in which

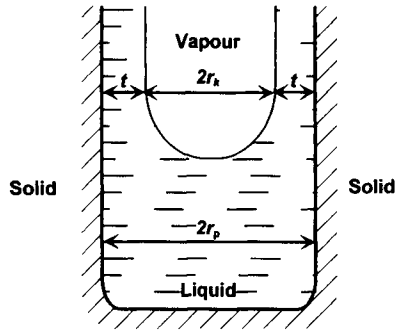

Figure 7.1. Relation between the Kelvin radius r_K and the pore radius r_p in a cylindrical mesopore.

all the pores have exactly the same radius, r_p. In the 'ideal' (and simplified) situation of strict thermodynamic reversibility, we would expect the pore filling to be indicated by a vertical riser in accordance with Equation (7.10).

In this particular case of a cylindrical pore shape, it seems reasonable to assume that the *condensate* has a meniscus of spherical form and radius r_K. However, as some physisorption has already occurred on the mesopore walls, it is evident that r_K and r_p are not equal. If the thickness of the adsorbed multilayer is t, and the contact angle is assumed to be zero, the *radius of the cylindrical pore* is simply

$$r_p = r_K + t \tag{7.11}$$

as in Figure 7.1.

However, if there is a finite contact angle, θ, between the adsorbed film and the capillary condensate, then the relation between r_p and r_K becomes

$$r_p = r_K \cos\theta + t \tag{7.12}$$

In the application of Equation (7.12), it is usually assumed that $\theta = 0$ and therefore $\cos\theta = 1$. The link between r_K and r_p is somewhat more complex when we consider other pore shapes. Two types of particular importance are parallel-sided slits and the interstices between spheroidal particles. At first sight, the former type would appear to be more amenable to analysis.

The form of a meniscus formed in a *slit-shaped pore* cannot be spherical and therefore r_1 and r_2 in Equation (7.2) are no longer equal. In the simplest case its form is hemicylindrical. The curvature is confined to the one axis across the pore, the curvature in the other principal direction being infinite so that $1/r_2 = 0$. We now have $1/r_K = 1/2r_1$ and therefore r_K is directly related to the effective pore width, w_p. It follows that in place of Equation (7.11), we have

$$w_p = r_K + 2t \tag{7.13}$$

We consider next the case of capillary condensation within a *system of packed spheres*: this normally occurs in three stages. The initial adsorption on the overall surface is now accompanied by the first stage of condensation around the points of

contact of the particles. The initial interparticle condensation is reversible, but as the advancing menisci meet the narrow openings between the particles (i.e. the 'windows' or 'throats') are spontaneously filled. The third stage involves the filling of the larger voids (or cavities) within the packed particles.

The initial process of monolayer–multilayer adsorption on the available surface of the packed spherical particles is complicated by two opposing effects. First, there is always a significant reduction in adsorption due to the loss of surface area between adjacent particles (see Figure 7.2a). On the other hand, because of the close proximity of the two surfaces, the adsorption is enhanced in the inner part of the annular space (i.e. similar to small-scale micropore filling).

A saddle-shaped meniscus (or pendular ring) is developed in the first stage of condensation. Application of Equation (7.10) now requires the designation of two radii of curvature of opposite sign, one being concave and the other convex. The Kelvin equation therefore takes the form

$$\ln (p/p^\circ) = -\frac{\gamma v^l}{RT}\left[\frac{1}{r_1} - \frac{1}{r_2}\right] \tag{7.14}$$

where r_1 is the concave radius and r_2 is the convex radius, which is directly related to the particle radius. If we assume that the spherical particles all have the same radius, R, the radius of curvature r_2 as given by Wade (1964, 1965) is $\{[(R+t+r_1)^2 - R^2]^{1/2} - r_1 + R + t\}/2$.

The second and third stages of capillary condensation are evidently dependent on both the particle size and the degree of packing (i.e. the coordination number) of the spherical particles. The windows may be pictured as the space between three or four neighbouring particles as in Figure 7.2. If the particles are in a triangular array, the second stage of condensation is controlled by the radius of the inscribed circle. Although the amount taken up may be relatively small, this stage is important in relation to hysteresis (see Section 7.5).

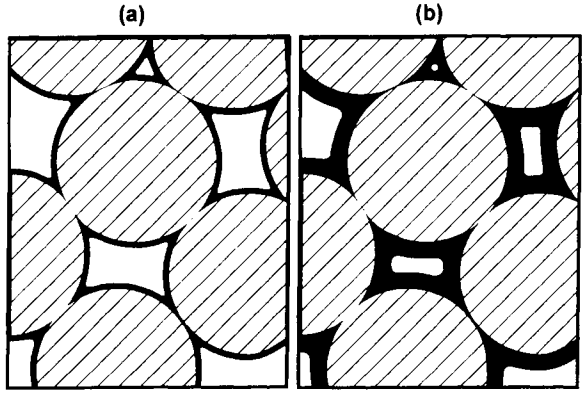

Figure 7.2. Sections of the pore space between solid spheres in irregular packing. First (a) and second (b) stage of condensation.

The overall pore volume of the bed of packed spheres is mainly determined by the size of the inner cavities, which is in turn dependent on the particle radius, R, and the coordination number, N. The effective Kelvin radius corresponding to this major stage of capillary condensation is approximately given by the radius, r_s, of the inscribed sphere within the cavity (Karnaukhov 1971).

A number of theoretical and experimental studies have been made of physisorption by compacted non-porous particles (see Haynes 1975). Pioneering work in this field was carried out by Wade (1964), Broekhoff and Linsen (1970), Karnaukhov (1971) and Kanellopoulos *et al.*, (1983). In his treatment of the random packing of equal spheres, Mason (1971) showed that tetrahedral sub-units could be constructed by taking the edges at random from a distribution function, which was considered to be a characteristic property of the packing. This model was applied by Kanellopoulos *et al.* (1983) to a system of densely packed spheres. A two-dimensional network of irregular tetrahedra was established and cavities within the tetrahedra were assumed to be interconnected through the irregular triangular windows.

A systematic study of the adsorption of nitrogen by packed assemblages of spheroidal particles was undertaken by Adkins and Davis (1986, 1987). After the consideration of various pore filling models, it was concluded that the desorption process can be adequately described by the instability of a Kelvin, hemispherical meniscus in the neck (i.e. the window) of the structure and the adsorption process can be viewed as a delayed Kelvin condensation in the largest dimension of the void structure. This reasoning is consistent with the network-percolation theory of hysteresis, which is discussed in Section 7.5.

In the experimental investigations of Avery and Ramsay (1973), it was found that progressive compaction of very small spheroidal oxide particles led to the sequential change in nitrogen isotherm type from II to IV and finally to I. This was a clear demonstration of a decrease in pore width as a result of increase in particle coordination number.

Table 7.1 gives some of the properties of the pore structures produced by the different degrees of packing of spherical particles. It can be seen that it is only in the case of tetrahedral packing ($N = 4$) that the effective size of the cavities is approximately equal to the particle size.

Simulation studies have been made also on packed beds of other corpuscular systems, such as discs and rods (Karnaukhov 1979). Although this approach is based

Table 7.1. Properties of pore structures obtained by three types of packing of spherical particles of radius R (after Avery and Ramsay, 1973).

Type of packing	N	ε	Radius of spheres inscribed in cavities	Radius of circle inscribed in connecting throats
Hexagonal close-packed	12	0.260	0.225r-octahedral 0.414 r-tetrahedral	0.155r
Primitive hexagonal	8	0.395	0.527r	0.414r 0.155 r
Tetrahedral	4	0.660	1.00r	0.732r

on an oversimplified picture of real powders, it does serve a useful purpose in providing a semi-quantitative analysis of the stages of capillary condensation. These mechanisms have been broadly confirmed by Avery and Ramsay (1973) and by Unger and his co-workers (Bukowiecki *et al.*, 1985).

G.W. Scherer (personal communication) has drawn our attention to a problem which must be faced in the characterization of many aerogels. Even when an aerogel is rigid enough to withstand the capillary pressure which is exercised during the condensation of a vapour, the usual values of Kelvin radius and pore volume may be seriously in error. For example, in the case of a particular silica aerogel it was found that the pore volume registered by nitrogen adsorption amounted to less than 60% of the total pore volume evaluated by other methods. Scherer suggests that the failure of the nitrogen to condense was not due to the pore *size*, but was instead the result of the peculiar curvature of the solid surface. Scherer pictures the gel as a network of intersecting solid cylinders joined at nodes. The adsorption–condensation will begin around the nodes, but will soon be arrested if the distance between the nodes is large in comparison with the radius of the cylinders joining the nodes. Thus, at an early stage the meniscus adopts zero curvature and as a result the overall pore space remains partially empty regardless of the effective pore size, until $p/p^\circ \rightarrow 1$. A quantitative treatment of the condensation process is proposed by Scherer, which involves the evaluation of meniscus shape by minimizing its surface area.

7.3. Mesopore Volume, Porosity and Mean Pore Size

7.3.1. Mesopore volume

It is customary to take the total specific pore volume, v_p, of an adsorbent as the *liquid* volume adsorbed at a predetermined p/p° (e.g. at $p/p^\circ = 0.95$). This procedure is not always satisfactory, however, because the adsorption capacity (i.e. the amount adsorbed as $p/p^\circ \rightarrow 1$) is dependent on the magnitude of the *external* area and also on the upper limit of the pore size distribution.

If a Type IV isotherm has a distinctive plateau, which cuts the p° axis at an angle $\approx 90°$, we may generally arrive at an acceptable assessment of the total mesopore volume v_p. The amount adsorbed, $\boldsymbol{n}(\text{sat})$, at the plateau is a measure of the adsorption capacity and to obtain v_p it is assumed that the adsorbate has the normal molar volume, V_m^l, of the liquid at the operational temperature. This simple method for the determination of the pore volume is based on a general principle, which was put forward 80 years ago by Gurvich (1915) and is still known as the Gurvich rule.

Confirmation of the validity of the Gurvich rule has been obtained with a number of mesoporous adsorbents for a wide range of adsorptives. The results in Table 7.2 are typical of the level of agreement to be expected between the values of $v(\text{sat})$ derived from a number of isotherms determined on a given mesoporous adsorbent. Although the adsorptives differ widely in their chemical and physical properties, the deviation from the mean value of v_p is within *c.* 5 %.

Table 7.2. Uptake at saturation on a silica gel at 25°C, calculated as a volume of liquid and as an amount (from McKee, 1959).

Adsorbate	v(sat) ($cm^3\ g^{-1}$)	n(sat) (mmol g^{-1})
n-Hexane	0.431	3.28
2,3-Dimethylbutane	0.429	3.28
2-Methylpentane	0.431	3.28
n-Heptane	0.431	2.91
2,2,3-Trimethylbutane	0.420	2.88
n-Octane	0.434	2.66
2,2,4-Trimethylpentane	0.439	2.63
2,3,4-Trimethylpentane	0.425	2.66
Cyclohexane	0.421	3.88
Methyl cyclohexane	0.425	3.32
Ethyl cyclohexane	0.426	2.99
Benzene	0.440	4.92
Nitromethane	0.449	8.33
Nitroethane	0.434	6.03
Carbon tetrachloride	0.421	4.30

Some Type IV isotherms do not obey the Gurvich rule. A possible explanation for this failure is that the particular adsorbent has a range of narrow micropores, giving molecular sieving in addition to its mesopore structure. The overall Type IV shape would then be misleading and it would be necessary to undertake a more detailed analysis (e.g. by applying the α_S-method) in order to evaluate the micropore filling contribution with different adsorptives. Another reason for failure of the Gurvich rule may be the lack of rigidity of the mesopore structure.

If the Type IV isotherm has a short plateau, which is followed by an upward swing, the amount adsorbed at the plateau can be regarded as the capacity of the particular range of mesopores. A useful assessment of the upper limit of mesopore size can then be obtained with the aid of the Kelvin equation corrected for multilayer adsorption.

In converting n_p to v_p, we have assumed that the condensate and the adsorbed layer have together an average density close to that of the bulk liquid adsorptive. Strictly, an allowance should be made for differences in density of the various parts of the adsorbate, but these corrections are very difficult to assess and are probably small in comparison with the other uncertainties in the evaluation of v_p.

7.3.2. Porosity

For the present purpose we define the porosity, ε, as the ratio of the total accessible pore volume V_p to the apparent volume of the adsorbent. Thus,

$$\varepsilon = \frac{V_p}{V_p + V^s} \tag{7.15}$$

where V^s is the inaccessible volume of the solid. In general, we should not expect to

find a simple relationship between the porosity and the coordination number of packed spheres. However, Karnaukhov (1971, 1979) has shown that for a wide range of regular packings ($N = 3–12$) an 'ideal' porosity can be specified ($\varepsilon = 0.815–0.260$). In practice, it is not easy to relate the properties of random sphere packings to those of regular packings (Haynes 1975) since the overall pore space may be defined by an infinite variety of local packings.

7.3.3. Hydraulic radius and mean pore size

The ratio of specific pore volume to specific surface area, v_p/a, has been used for many years as a simple means of characterizing the pore size. This volume-to-surface ratio, when applied to a group of pores, is known as the hydraulic radius, r_h, and has an unambiguous physical significance provided that the pore geometry can be specified by a single parameter (Everett 1958).

For example, if the mesopore structure consists of a set of open-ended, non-intersecting cylinders, the mean pore radius, $\bar{r}_p$, is given by

$$\bar{r}_p = 2v_p/a \tag{7.16}$$

which is, of course, based on the assumption that the specific surface area, a, is confined to the cylindrical pore walls. This condition is fulfilled in the case of MCM-41 (see Section 12.3.1).

Other pore structures amenable to this simple treatment are parallel-sided slit-shaped pores or aggregates of parallel plates. The appropriate volume/surface relation is similar to Equation (7.16), but now the mean pore width, $\bar{w}_p$, replaces $\bar{r}_p$. Thus,

$$\bar{w}_p = 2v_p/a \tag{7.17}$$

The mathematical significance of r_h has been established for a number of other pore geometries (Everett, 1958), but with most real systems it is not possible to arrive at an unambiguous evaluation of $\bar{r}_p$ or $\bar{w}_p$ or a useful interpretation of r_K. For example, with an assemblage of packed spheres, as already noted, the porosity is dependent on the packing density as well as the particle size. Similarly, in the case of a network of intersecting pores, the value of r_h is dependent on both the pore radius and the lattice spacing of the intersections.

7.4. Computation of the Mesopore Size Distribution

7.4.1. General principles

Over the period 1945–1970 many different mathematical procedures were proposed for the derivation of the pore size distribution from nitrogen adsorption isotherms. It is appropriate to refer to these computational methods as 'classical' since they were all based on the application of the Kelvin equation for the estimation of pore size. Amongst the methods which remain in current use were those proposed by: Barrett, Joyner and Halenda (1951), apparently still the most popular; Cranston and Inkley

(1957); Dollimore and Heal (1964); and Roberts (1967). In the early work, it was customary to assume the pore shape to be cylindrical, but now the slit-shaped and packed sphere models are considered to be more appropriate for some systems.

There are several reasons why nitrogen (at 77 K) is generally accepted as the most suitable adsorptive for mesopore size analysis. First, the thickness of the N_2 multilayer is largely insensitive to differences in adsorbent particle size or surface structure (Carrott and Sing, 1989). Second, the same isotherm can be used for the evaluation of both the surface area and the mesopore size distribution (Sing *et al.* 1985). However, in spite of these considerations, there is an emerging view that ideally more than one adsorptive should be used for the characterization of mesoporous solids (e.g. see Machin and Murdey 1997; Llewellyn *et al.*, 1997).

In adopting the classical approach, one must necessarily assume that:

1. the Kelvin equation is applicable over the complete mesopore range;
2. the meniscus curvature is controlled by the pore size and shape and $\theta = 0$;
3. the pores are rigid and of well-defined shape;
4. the distribution is confined to the mesopore range;
5. the filling (or emptying) of each pore does not depend on its location within the network;
6. the adsorption on the pore walls proceeds in exactly the same way as on the corresponding open surface.

The relation between pore volume and pore dimensions is presented graphically either in the form of a cumulative plot of pore volume against mean pore size (i.e. v_p versus $\bar{r}_p$) or ideally as a distribution (or frequency curve), dv_p/dr_p versus $\bar{r}_p$ (or $\bar{w}_p$). Since the computation is usually based on the notional removal of the condensate by a step-wise lowering of $p/p°$, in practice the pore size distribution is expressed in the form of $\delta v_p/\delta r_p$ versus $\bar{r}_p$. The computation is somewhat complicated because allowance must be made at each desorption step for the thinning of the adsorbed multilayer in pores from which the capillary condensate has already been removed.

Before any attempt is made to evaluate the pore size distribution, it is necessary to decide which branch of the hysteresis loop of a Type IV isotherm is to be used for the analysis. It will be evident from the discussion of hysteresis in Section 7.5 that this choice is not easy and at this point it may be helpful to summarize the main implications.

A relatively simple pore structure of fairly uniform tubular pores would be expected to give a narrow Type H1 hysteresis loop (see Figure 7.3) and in this case the desorption branch is generally used for the analysis. On the other hand, if there is a broad distribution of interconnected pores it would seem safer to adopt the adsorption branch since the location of the desorption branch is largely controlled by network-percolation effects. If a Type H2 loop is very broad, neither branch can be used with complete confidence because of the possibility of a combination of effects (i.e. both delayed condensation and network-percolation). Furthermore, the condensate becomes unstable and pore emptying occurs when the steep desorption branch is located at a critical $p/p°$ (i.e. at *c.* 0.42 for N_2 adsorption at 77 K).

7.4.2. Computation procedure

The plateau of a Type IV isotherm is normally taken as the starting point for the computation of the mesopore size distribution. If all the pores are full, the first step in the notional desorption process (e.g. from $p/p°$ of 0.95 to 0.90) involves only the removal of capillary condensate. Each subsequent step involves both the removal of condensate from the *cores* of a group of pores and the thinning of the multilayer in the larger pores (i.e. those pores already emptied of condensate). In the following treatment the symbol v_K is used to represent the inner core volume and, as before, v_p is the pore volume. The corresponding radii are r_K and r_p.

Let us suppose that the amount of nitrogen removed in each desorption step 'j' is $\delta n(j)$; for the purpose of the pore size calculations, this amount is expressed as the volume $\delta v^l\ (j)$, of *liquid* nitrogen. In the first desorption step ($j = 1$) the initial removal is the result of capillary evaporation alone and therefore the volume of core space released is equal to the volume of nitrogen removed, i.e. $\delta v_K(1) = \delta v^l\ (1)$.

If the pores are cylindrical, we have a simple relation between the core volume $v_K(1)$ and the pore volume, $v_p(1)$, of the first, and largest, group of mesopores. Thus,

$$v_p(1) = \frac{\bar{r}_p^2(1)}{\bar{r}_K^2(1)}\, v_K(1) \tag{7.18}$$

where $\bar{r}_p(1)$ and $\bar{r}_K(1)$ are the mean pore and core radii of the first step.

As the stepwise removal proceeds ($j \neq 1$), we must allow for the contribution from the thinning of the multilayer thickness, $\delta t\ (j)$. For the step j:

$$\delta v(j) = \delta v_K(j) + \delta v_t(j) \tag{7.19}$$

where $\delta v_K(j)$ is the core volume emptied in step j and $\delta v_t(j)$ is the equivalent liquid volume removed from the multilayer.

The volume, $\delta v_p(j)$, of the group of pores emptied of condensate in step j is given by

$$\delta v(j) = \frac{\bar{r}_p^2(j)}{[\bar{r}_K(j) + \delta t(j)]^2} \times \delta v_K(j) \tag{7.20}$$

where $\bar{r}_p(j)$ and $\bar{r}_K\ (j)$ are now the mean pore and core radii for the step j.

We can make use of Equations (7.18), (7.19) and (7.20) to obtain all the successive contributions to the total pore volume, i.e. $\delta v_p(1)$, $v_p(2)$, ..., $\delta v_p(j)$; but to do this we need to know the individual values of $\delta v_t(j)$ (the changes in multilayer volumes) for each stage of the stepwise procedure.

Various methods have been devised for calculating the values of $\delta v_t(j)$ the simplest approach being to adapt Equation (7.16) for the individual groups of cylindrical pores and cores. For example, the core area is

$$\delta a_K(j) = 2\, \delta v_K(j)/\bar{r}_K(j) \tag{7.21}$$

and similarly the pore area is

$$\delta a_p(j) = 2\, \delta v_p(j)/\bar{r}_p(j)$$

The corresponding core and pore areas are related by the equation

$$\delta a_K(j) = \delta a_p(j) \frac{\bar{r}_p(j) - \bar{t}(j)}{\bar{r}_p(j)}$$

$$= \delta a_p(j) \times \rho(j) \tag{7.22}$$

In the original BJH method, $\rho(j)$ was given a single value, which corresponded to the most frequent pore size: whereas in the procedure adopted by Pierce (1953), it was considered enough to take $\rho(j) = 1$, i.e. to omit the correction. Of course, with the aid of a modern computer, it is not difficult to apply a separate correction factor for each individual step (Montarnal 1953).

The cumulative pore volumes and pore areas are obtained by the summation of all the respective contributions, $\delta v_p(j)$ and $\delta a_t(j)$. As a check on the overall consistency of the pore volume–area analysis, it is useful to compare the cumulative values of $v_p(j_{max})$ and $a_p(j_{max})$ with the corresponding Gurvich volumes and BET areas. In view of all the uncertainties and approximations, one should not expect to obtain perfect agreement (Gregg and Sing 1982). Indeed, agreement to within say 5% may be fortuitous!

Although many adsorbents possess exceedingly complex pore structures, the mesopore size analysis carried out by several groups (Dollimore and Heal, 1973; Havard and Wilson, 1976) appears to indicate that the calculated pore size distribution is rather insensitive to the model. However, as was pointed out by Haynes (1975) such results may be due in part to the over-simplification of the computations.

7.4.3. The multilayer thickness

It is evident that the corrections for multilayer thickness and thinning effects are of great importance. For example, for nitrogen adsorption at 77 K, $t \approx 0.6$ nm at $p/p^\circ = 0.5$, just before the condensation occurs in a cylindrical pore of $r_p \approx 2$ nm. The corresponding approximate values at $p/p^\circ = 0.8$ are $t \approx 0.9$ and $r_p \approx 5$ nm.

Values of t are obtained from n/n_m by assuming an average molecular layer thickness. Following the recommendation of Lippens, Linsen and de Boer (1964), the *average* adsorbed nitrogen layer thickness is usually taken as 0.35 nm. This value was based on the assumption of a hexagonally close-packed multilayer and molecular diameter of 0.43 nm.

The assumption that multilayer coverage of the mesopore walls proceeds in exactly the same manner as on the open surface has been questioned by several investigators (see Everett 1988). Evans and Marconi (1985) suggested on theoretical grounds that in a narrow mesopore the thickness of a multilayer is likely to be somewhat greater than on the non-porous surface. On the other hand, there is a considerable amount of experimental evidence in support of the long-standing view that in the pre-capillary condensation region, the corresponding isotherms on mesoporous and non-porous adsorbents follow the same path. This is clearly shown by the linearity of the α_S-plots (e.g. Section 6.3.3). Much effort has been expended in the determination and verification of the standard isotherm date (Sing 1970; Kaneko 1994; Milburn and Davis, 1997).

7.4.4. Validity of the Kelvin equation

We turn now to the question of validity of the Kelvin equation. Although the thermodynamic basis of the Kelvin equation is well established (Defay and Prigogine 1966), its reliability for pore size analysis is questionable. In this context, there are three related questions: (1) What is the exact relation between the meniscus curvature and the pore size and shape? (2) Is the Kelvin equation applicable in the range of narrow mesopores (say $w_p < 5$ nm)? (3) Does the surface tension vary with pore width? The answers to these questions are still elusive, but recent theoretical work has improved our understanding of mesopore filling and the nature of the condensate.

It was recognized many years ago (Foster, 1932) that the Kelvin equation is likely to break down as the meniscus curvature approaches a limiting value. Molecular simulation studies (Jessop *et al.*, 1991) have indicated that the Kelvin equation fails to account for the effects of the fluid-wall interactions and the associated inhomogeneity of the pore fluid. These and other studies (Lastoskie *et al.*, 1993) reveal that the Kelvin equation probably underestimates the pore size and that its reliability may not extend below a pore size of ≈7.5 nm.

Evans and his co-workers (1986) have shown that a statistical mechanical treatment may be used to derive the Kelvin equation. This approach, which was designed to avoid the difficulties associated with the exact form of the meniscus, led to a new mathematical description of the effect of confining a fluid in pores of different size and shape on its liquid–gas coexistence curve. An equation of the same mathematical form as Equation (7.10) was obtained, provided that the 'undersaturation' was not too great, i.e. that p/p° was not too low. It was shown that this simple equation becomes less accurate as r_K is reduced and is no longer applicable beyond a 'capillary critical point'. At a lower r_K or higher T, the two-phase relation fails because of the existence of only one stable fluid configuration in the pore.

Many early attempts were made to correct the Kelvin equation (see Brunauer, 1945). As already indicated, when the Kelvin equation is applied to capillary condensation it is normally assumed that the reduction in chemical potential is entirely dependent on the curvature of the meniscus. This assumption implies a sharp discontinuity between the state of the adsorbed layer and the condensate. However, as Derjaguin first pointed out (1957), the transition is more likely to be a gradual one. This problem was also discussed by Everett and Haynes (1973).

Since the capillary condensate in a particular mesopore is in thermodynamic equilibrium with the vapour, its chemical potential, μ^σ, must be equal to that of the gas (under the given conditions of T and p). As we have seen, the difference between μ^σ and μ^l (the chemical potential of the free liquid) is normally assumed to be entirely due to the Laplace pressure drop, Δp, across the meniscus. However, in the vicinity of the pore wall a contribution from the adsorption potential, $\phi(z)$, should be taken into account. Thus, if the chemical potential is to be maintained constant throughout the adsorbed phase, the capillary condensation contribution must be reduced.

In addition, within a particular mesopore, the curvature of the meniscus is not constant. In the middle of a cylindrical pore, where the wall effect is negligible, the

radius of curvature is r_K; whereas as the wall is approached, the radius of curvature is progressively increased.

The question of the constancy of the surface tension in porous media has been under consideration for many years and has been taken up again recently by Brown *et al.* (1997). Formerly, it was thought that for a concave liquid–vapour interface the surface tension should increase with increased curvature. The experimental findings that the hysteresis critical temperature is generally appreciably lower that the bulk critical temperature (see Section 7.5) is considered to be a strong indication that the surface tension of a capillary-condensate is reduced below the bulk value. More work on model pore structures is evidently required to settle this question.

7.5. Hysteresis loops

Hysteresis loops, which appear in the multilayer range of physisorption isotherms, are generally associated with capillary condensation. It is well known that most mesoporous adsorbents give distinctive and reproducible hysteresis loops (de Boer 1958; Sing *et al.*, 1985).

According to the laws of classical thermodynamics, the amount adsorbed is controlled by the chemical potential of the adsorptive (see Section 2.3). It follows that the two branches of a loop cannot both satisfy the requirement of thermodynamic reversibility. The appearance of reproducible and stable hysteresis therefore implies the existence of certain well-defined metastable states.

Many different forms of loop have been reported in the literature, but the major types are represented in the IUPAC classification (1985) given in Figure 7.3. Types H1, H2 and H3 were included in the first classification proposed by de Boer (1958). Type H1 (originally known as Type A) is a fairly narrow loop with very steep and nearly parallel adsorption and desorption branches. In contrast, the Type H2 loop (formerly Type E) is broad with a long and almost flat plateau and a steep desorption branch. Types H3 (formerly Type B) and H4 do not terminate in a plateau at high p/p° and the limiting desorption boundary curve is therefore more difficult to establish.

The characteristic features of some types of loop are associated with certain well-defined pore structures. Thus, Type H1 loops are given by adsorbents with a narrow distribution of uniform pores (e.g. open-ended tubular pores as in MCM-41 – see Section 12.3.1). Many inorganic oxide gels give the more common Type H2 loops. The pore structures in these materials are complex and tend to be made up of interconnected networks of pores of different size and shape.

Type H3 loops are usually given by the aggregates of platy particles or adsorbents containing slit-shaped pores. Hysteresis loops of Type H4 are also given by slit-shaped pores, as in many activated carbons, but in this case the pore size distribution is mainly in the micropore range. It can be seen that H3 and H4 loops do not close until the equilibrium pressure is at, or very close to, the saturation pressure. With loops of this type the location of the desorption branch is likely to depend on the maximum pressure attained before the commencement of desorption. A new

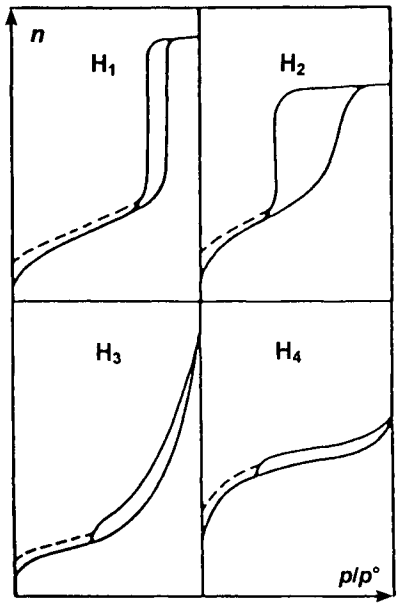

Figure 7.3. The IUPAC classification of hysteresis loops (Sing *et al.*, 1985).

experimental procedure introduced by Murray *et al.* (1998) is designed to overcome this difficulty. Thus, by starting the desorption run from a 'bulk condensation' state (i.e. the adsorbent immersed in liquid adsorptive) it is possible to determine the true boundary desorption isotherm, and hence the extent and stability of the hysteresis loop.

A feature common to many loops is that for a given adsorptive (at a particular temperature) the very steep region of the desorption branch joins the adsorption branch at a limiting relative pressure. This lower limit of hysteresis is thus dependent on the adsorptive and the operational temperature, but not on the adsorbent. In the case of nitrogen adsorption at 77 K, the lower closure point is often located at the lower limit of $p/p° = 0.42$.

In principle, the processes of capillary condensation and evaporation should occur reversibly in a closed tapering pore (Everett 1967). At low relative pressures there is an enhanced concentration of adsorbed molecules in the narrow end of the pore (i.e. a micropore filling effect) as in Figure 7.4. At a certain $p/p°$, a meniscus begins to form which, with the increase of $p/p°$, then moves steadily up towards the pore entrance. Evaporation proceeds in the reverse direction but involves the same elemental steps (i.e. the meniscus configurations) and therefore the entire isotherm is reversible.

The systematic studies of adsorption hysteresis made over a period of many years by Everett and his co-workers revealed that the phenomena are temperature-dependent (Amberg *et al.*, 1957; Everett, 1967; Burgess *et al.*, 1989). Thus, with increase in temperature most hysteresis loops undergo a reduction in size. More recently these findings have been extended by adsorption measurements on mesoporous controlled-pore glass

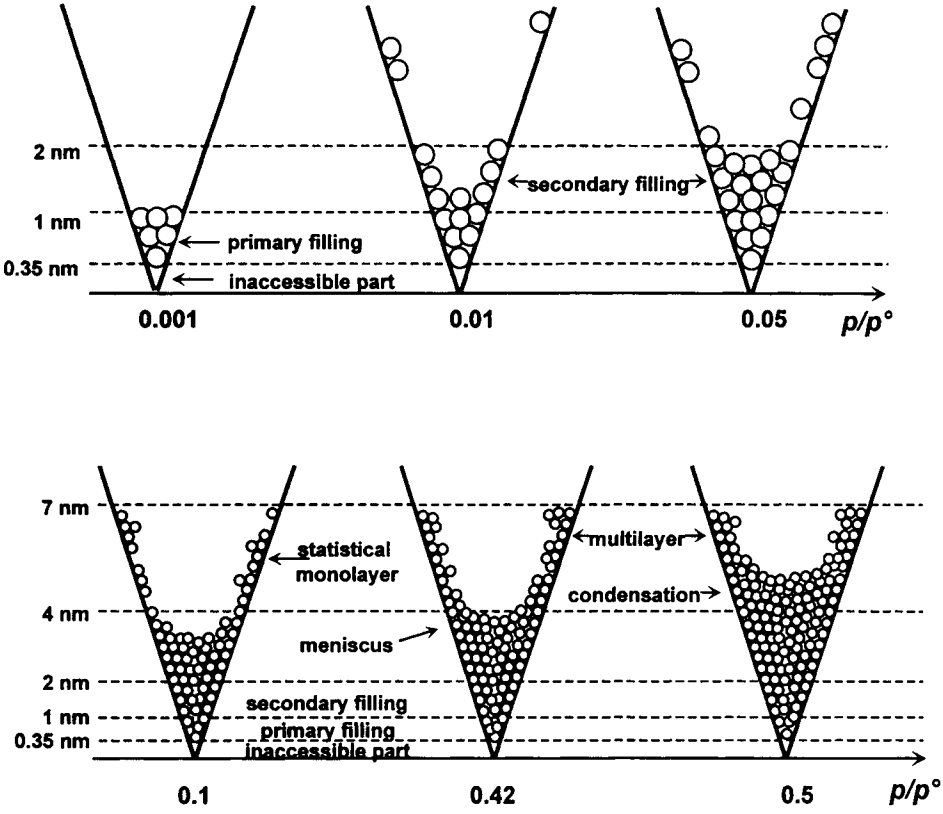

Figure 7.4. Main steps of the successive filling of micropores and mesopores during adsorption. The pressure scale gives orders of magnitudes for the case of N_2 at 77 K. The size scale is twice as large in the upper row.

(Machin, 1994; Findenegg *et al.* 1994; Brown *et al.*, 1997) MCM-41 (Branton *et al.*, 1997) and graphitic carbons (Lewandowski *et al.*, 1991).

As with bulk liquid–vapour equilibria, hysteresis (or capillary) phase diagrams can be presented in different ways. By taking the lower and upper hysteresis closure points to represent the limits of the region of coexistence of the vapour and capillary condensed liquid, one can obtain, for example, a smooth curve relating the two densities of the condensed phase to the temperature. The two curves come together at the hysteresis critical temperature, $T_c(h)$ for the given system. Such hysteresis phase diagrams are similar in shape to the phase diagrams for the corresponding bulk liquids (e.g. CO_2/Vycor), but with the important difference that $T_c(h)$ is consistently much lower than the corresponding bulk critical temperature T_c.

The fact that the isotherms become reversible at temperatures above $T_c(h)$ may seem to indicate that the distinction between the pore condensate and vapour must

disappear and that the surface tension becomes zero, i.e. that the adsorbate loses its liquid-like properties at T_c(h). However, this explanation is probably oversimplified in the light of recent work on highly uniform pore structures such as MCM-41 (see Section 12.3.1). As already indicated in Section 7.4.1 and will be discussed later, it is now evident that adsorption hysteresis can originate in different ways and also that *reversible*, stepwise condensation can occur under certain conditions.

Most of the older theories of adsorption hysteresis made explicit use of the Kelvin equation. Zsigmondy (1911) was the first to suggest that the phenomenon was due to a difference in the contact angles of the condensing and evaporating liquid. This explanation may account for some of the anomalous effects produced by the presence of surface impurities, but in its original form it cannot explain the permanence and reproducibility of the majority of recorded loops. However, as will become evident, the notion of delayed condensation is still of great importance.

Another early theory, which also attracted a great deal of attention, was the 'ink-bottle theory': this was originally put forward by Kraemer (1931) and subsequently developed by McBain (1935). Kraemer pointed out that the rate of evaporation of a liquid in a relatively large pore is likely to be retarded if the only exit is through a narrow channel. This argument led Brunauer (1945) to conclude that the liquid in the pore cannot be in true equilibrium with its vapour during the desorption process and therefore it is the *adsorption* branch of the loop which represents thermodynamic reversibility.

The mechanisms of meniscus formation, modification and removal have been discussed by many investigators including Foster (1932), Cohan (1944), de Boer (1958), Everett (1967, 1979), Broekhoff and Linsen (1970), Haynes (1975), Lewandowski *et al.*, (1991), Machin (1992) and Findenegg *et al.*, (1994). A substantial amount of evidence is now available in support of Foster's view that condensation does not always occur in accordance with the simple Kelvin equation. The most striking examples of delayed meniscus formation are afforded by many clays and oxides, which give Type H3 loops. In a slit-shaped pore the meniscus is formed only at high $p/p°$ and consequently over a wide range the *adsorption* isotherm is of Type II (but is not reversible) and in some cases appears to approach the $p°$ axis asymptotically. Such an isotherm could be regarded as a pseudo-Type II isotherm, but we prefer to adopt the designation Type IIb since there may be virtually no detectable capillary condensation on the adsorption branch.

Cohan (1938) suggested that in an open-ended pore a difference in meniscus shape is involved in the processes of condensation and evaporation. According to this view, condensation is governed by the initial formation of a cylindrical meniscus, whereas two hemispherical menisci are developed once the pore has been filled. By applying Equations (7.11) and (7.13) we find that a given value of r_K represents the corrected *width*, $2(r_p - t)$, for pore filling and the corrected *radius*, $(r_p - t)$, for pore emptying. This approach indicates that the hysteresis in the filling and emptying of a single open-ended tubular pore is due to the processes of condensation and evaporation occurring at different relative pressures.

Everett (1979) has pointed out that several irreversible steps are involved when

condensation occurs in an open-ended cylinder. Since a cylindrical meniscus is unstable, a spontaneous change leads to the development of an unduloid. In the next stage, the pore becomes blocked by the formation of a biconcave lens of liquid. The evaporation process proceeds in a thermodynamically reversible manner, however, and in accordance with the Kelvin equation, the relative pressure is now dependent on the radius of curvature of the hemispherical menisci. Thus, in the case of this simple system, it is the location of the desorption branch which should be used for the calculation of r_p.

A different approach was adopted by Saam and Cole (1975), who attempted to explain the hysteresis exhibited by a cylindrical pore in terms of the regimes of stability, metastability and instability of the multilayer film. The applicability of the Saam–Cole theory has been explored in some detail by Findenegg *et al.* (1994), Lewandowski *et al.* (1991) and Michalski *et al.* (1991).

According to the Saam–Cole theory, there are two opposing effects which govern the range of metastability of a multilayer film in a cylindrical mesopore. Thus, long-range adsorption forces help to stabilize the film, while capillary forces are responsible for the condensation of the liquid. At a critical film thickness, t_c, the curved film becomes unstable and condensation occurs. Evaporation of the liquid condensate requires a lower $p/p°$ and now the residual film thickness, is t_m. We may therefore regard the difference $(t_c - t_m)$ as the metastability thickness range of the multilayer film.

On the basis of the Saam–Cole–Findenegg approach, we are now able to revise the 'ideal isotherm' for capillary condensation. A more realistic isotherm for the physisorption of a vapour in an assemblage of uniform cylindrical mesopores is shown in Figure 7.5. Here, C represents the limit of metastability of the multilayer (of thickness t_c) and M the point at which the three phases (multilayer, condensate and gas) all coexist. Along MC the multilayer and gas are in metastable equilibrium.

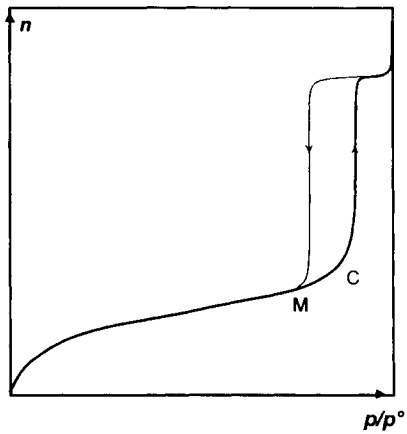

Figure 7.5. An adsorption–desorption isotherm for a mesoporous solid with cylindrical pores, all having the same radius.

The chemical potential of an adsorbed multilayer film in a cylindrical pore may be expressed as

$$\mu_m = \mu_0 + \phi(r_p) - \gamma/r_K \, \Delta\rho \tag{7.23}$$

where $\phi(r_p)$ is the interaction energy between the film and the adsorbent, r_K is the inner radius ($r_K = r_p - t$) and $\Delta\rho$ is the difference in density between the liquid and vapour. The term $\gamma/r_K \, \Delta\rho$ represents the energy associated with the curved film—vapour interface.

If the multilayer is sufficiently thick, the interaction energy, ϕ (r_p), is obtained by integration of the C/r^6 pair potentials. From the Saam–Cole theory it then becomes possible to arrive at the critical film thickness, t_c, and metastable limit, t_m, in terms of t/r_p. The following qualitative behaviour was predicted (Findenegg *et al.*, 1994): (1) as the pore radius is decreased, the stability limits are shifted to larger relative film thickness, t/r_p; (2) for a given pore radius, the stability limits are temperature dependent. The latter effect is dominated by the negative temperature coefficient of the surface tension and therefore the stability limits are shifted to larger reduced film thickness as $T \longrightarrow T_c$.

The applicability of the Saam–Cole theory has been tested by Findenegg and his co-workers (1993, 1994). Their adsorption measurements of certain organic vapours on carefully selected grades of controlled-pore glass provide semi-quantitative confirmation of the theoretical treatment adopted so far. However, it is evident that some refinement is required in the assessment of $\phi(r_p)$ for materials of small pore size and that the experimental choice of the mesoporous adsorbent is important. To make further progress it will be necessary to study adsorbents having narrow size and shape distributions of easily accessible mesopores.

In recent years, a number of investigators have studied the phase equilibria of simple fluids in pores by the application of *density functional theory*. Seminal studies were carried out by Evans and his co-workers (1985, 1986). Their approach was considered to be 'the simplest realistic model for an inhomogeneous three-dimensional fluid'. The starting point was a model intrinsic Helmholtz free energy functional $F(\rho)$, with a mean-field approximation for the attractive forces and hard-sphere repulsion. As explained in Section 7.6, the equilibrium density profile of the fluid in a pore was obtained by minimizing the grand potential functional.

In the case of wide mesopores, the density profiles $\rho(w_p)$ found for a given μ and T corresponded to both liquid and gas solutions. In this case, the solution with the lower grand potential was the stable one, while the other was the metastable solution. The coexistence of the two phases was indicated when the grand potentials were equal (for specified μ and T). The capillary critical point was reached when the two distinctive fluid configurations became indistinguishable. When pre-wetting occurred in the pore, three solutions were found, the 'gas' film now being thin or thick. Only one solution was found when the pore width was small, and the phase transition to the 'liquid' phase was then unable to take place.

It was concluded by Evans and his co-workers (1986) that if the pore width is sufficiently large, a first-order phase transition should occur at an appropriate chemical potential from gas to metastable bulk liquid, with an accompanying jump in the

adsorption. It was suggested that adsorption hysteresis was likely to be associated with this discontinuous jump. The expectation that the magnitude of the first-order transition should be reduced with increase in temperature would explain the experimental observation of the effect of temperature in decreasing the size of the hysteresis loop (Burgess *et al.*, 1989; Machin 1994).

Early attempts were made by Everett (1955, 1967) to formulate the behaviour of groups of pores in terms of domain theory. The independent domain theory assumed that each pore behaves as though it were interacting in isolation with the vapour, and therefore the overall behaviour was considered to depend on the statistical distribution of the individual pore properties. The pathways of crossing the loop (i.e. scanning behaviour) were predicted. For example, according to the independent domain model, if scanning loops are traced within given limits, the areas of these subsidiary loops should be constant and independent of their location within the main loop. Generally, this prediction is not fulfilled and it must be concluded that the domains do not behave independently (Everett, 1979).

In fact, most mesoporous adsorbents possess complex networks of pores of different size. It is therefore unlikely that the condensation–evaporation processes can occur independently in each pore. The complexity of capillary condensation in porous materials is illustrated by the recent Monte Carlo computer simulation studies of Page and Monson (1996) and Gelb and Gubbins (1998). The well-defined hysteresis loops observed in the simulation results of both studies were attributed to the presence of thermodynamically metastable states and not to kinetic effects. However, it appears that the extent of the hysteresis was associated with the overall heterogeneity of the adsorbent structure and not simply due to capillary condensation within individual pores.

Let us postulate that the condensate cannot leave a pore (or segment of a pore) at the 'Kelvin relative pressure' unless there is a continuous channel of *vapour* leading to the adsorbent surface. It follows that the probability that a portion of the condensate will be trapped will depend on the nature of the pore network and the numerical and spatial distribution of pore size. Thus, a large amount of entrapment – and hence pronounced hysteresis – will be observed if a high proportion of the pore volume is only accessible through narrow channels with a relatively low level of pore connectivity.

Computer modelling of physisorption hysteresis is simplified if it is assumed that pore filling occurs 'reversibly' (i.e. in accordance with the Kelvin equation) along the adsorption branch of the loop. Percolation theory has been applied by Mason (1988), Seaton (1991), Liu *et al.*, (1993, 1994), Lopez-Ramon *et al.*, (1997) and others (Zhdanov *et al.*,1987; Neimark 1991). One approach is to picture the pore space as a three-dimensional network (or lattice) of cavities and necks. If the total neck volume is relatively small, the location of the adsorption branch should be mainly determined by the cavity size distribution. On the other hand, if the evaporation process is controlled by percolation, the location of the desorption branch is determined by the network coordination number and neck size distribution.

An alternative structural model, favoured by Seaton (1991), is one made up of an

aggregate of small particles which contain a network of mesopores (and possibly also micropores). The interstices between the particles form a continuous network of macropores. In Seaton's model, the mesopore network is represented by a simple cubic lattice. In percolation terminology, each pore is regarded as a bond in the lattice and each pore junction is a node. The average size of the small particles is expressed as the number of pore lengths L.

During the desorption process, the liquid condensate leaves the pore when two conditions are satisfied: (1) the relative pressure must be low enough for vaporization to be thermodynamically favourable; (2) the pore must have direct access to the vapour phase, either because it is at the surface or because it is adjacent to another pore from which the condensate has already been vaporized.

At the beginning of the desorption process, some condensate is removed from the wider pores (i.e. unoccupied bonds) near the surface. As the pressure is reduced, the vapour-filled pores (occupied bonds) form clusters, which eventually extend across the particle. The stage at which a spanning cluster is formed across the particle corresponds to the percolation threshold, when the pore emptying becomes rapid. This stage corresponds to the knee of an H2 hysteresis loop.

Seaton and his co-workers (Liu *et al.*, 1992) have simulated the desorption percolation for nitrogen from a simple cubic lattice. Their hypothetical results in Figure 7.6 are plotted in the form of the fraction of the pores retaining liquid nitrogen, $(1 - x^{A})$, against the fraction of pores containing nitrogen in its *stable* condensed form. Here, x is defined as the fraction of pores large enough to allow vaporization at p/p° and x^{A} is the fraction of pores from which nitrogen is able to vaporize at p/p°. As the adsorption run is not influenced by the connectivity, x is the fraction of pores in which condensation has not yet occurred at p/p° (i.e. over the adsorption branch of the loop). Thus, the linear relation, $(1 - x^{A}) = (1 - x)$, represents the adsorption branch.

In percolation terminology, the fraction of vapour-occupied bonds is x, which increases from zero to unity during the course of the simulation. This is achieved by choosing bonds at random and changing their state from unoccupied to occupied assuming a random distribution of pore sizes in the porous material.

In Figure 7.6, each curve has been plotted for a given value of lattice size, L. With these coordinates, the simulation data give a series of transformed desorption isotherms, which provide an indication of vapour accessibility as a function of bond occupation probability. As expected, above a certain fraction of occupation, the location of the accessibility curve is highly dependent on the value of L. When this treatment was extended to other lattices with different values of the coordination number, Z, it was found that the effect of increasing Z was to move the percolation threshold to the right. Of course, this is because there is a greater chance that the liquid in a given pore can find a pathway of vapour-filled pores to the surface. It follows that the size of the hysteresis loop is increased as the mean coordination number is reduced.

Seaton and his co-workers have been mainly concerned with derivation of the connectivity, Z, from experimental hysteresis loops. In practice, Z and L are both unknown and Seaton's method for the analysis of nitrogen adsorption–desorption

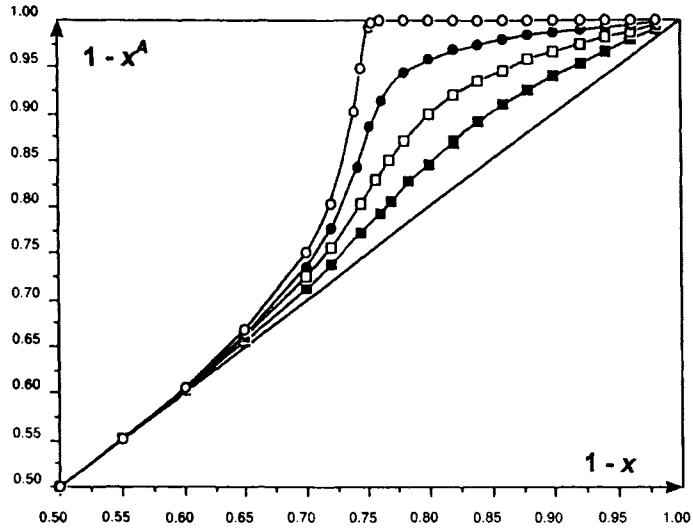

Figure 7.6. Fraction of pores containing liquid nitrogen, $(1-x^A)$, plotted against fraction of pores containing the thermodynamically stable liquid $(1-x)$ for various values of lattice size L: 10 (solid squares), 20 (open squares), 60 (solid circles), ∞ (open circles) reproduced courtesy of Liu *et al.*, 1994).

data involves the following steps:

1. The pore size distribution is obtained from the *adsorption* isotherm. An appropriate pore shape must be assumed.
2. The accessibility, x^A, is assessed from the pore size distribution to give a percolation transform of the desorption isotherm.
3. Z and L are calculated by comparison of the experimental percolation plot with the simulation data. This is essentially a curve-fitting procedure.

It is too early to assess the full potential of this promising method of isotherm analysis. So far it has been applied to only a limited number of experimental isotherms and some of the findings have been puzzling. For example, a few unrealistically high values of Z have been derived (Seaton, 1991). Furthermore, the physical significance of L is difficult to understand. It seems likely that this method of isotherm analysis (and possibly other procedures based on percolation theory) will become especially useful when the range of applicability can be clearly specified in terms of isotherm type and the range of pore size, shape and disposition.

At present, it must be recognized that adsorption hysteresis may be generated in a number of different ways. In the context of the assessment of mesoporosity, we have seen that there are two major contributing factors: (a) on the adsorption branch, the development of a metastable multilayer and the associated delay in capillary condensation; (b) on the desorption branch, the entrapment of condensate through the effect of network-percolation.

7.6. Density Functional Formulation

The pioneering work in this area was carried out by Seaton *et al.* (1989), who adapted a statistical mechanical approach originally known as mean field theory (Ball and Evans, 1989). At the time of their early work (Jessop *et al.*, 1991) mean field theory was already known to become less accurate as the pore size was reduced, but even so it was claimed to offer a more realistic way of determining the pore size distribution than the classical methods based on the Kelvin equation.

Over the past few years a revised form of density functional theory DFT, has become a powerful tool for the interpretation of physisorption data (Balbuena and Gubbins, 1992, 1993; Lastoskie *et al.*, 1993; Olivier 1995; Cracknell *et al.*, 1995; Maddox and Gubbins, 1995). In particular, the approach must now be regarded as a valuable alternative procedure for evaluating the pore size distribution (Lastoskie *et al.*, 1994; Olivier *et al.*, 1994).

Let us consider a one-component fluid confined in a pore of given size and shape which is itself located within a well-defined solid structure. We suppose that the pore is open and that the confined fluid is in thermodynamic equilibrium with the same fluid (gas or liquid) in the bulk state and held at the same temperature. As indicated in Chapter 2, under conditions of equilibrium a uniform chemical potential is established throughout the system. As the bulk fluid is homogeneous, its chemical potential is simply determined by the pressure and temperature. The fluid in the pore is not of constant density, however, since it is subjected to adsorption forces in the vicinity of the pore walls. This *inhomogeneous* fluid, which is stable only under the influence of the external field, is in effect a layerwise distribution of the adsorbate. The density distribution can be characterized in terms of a *density profile*, $\rho(r)$, expressed as a function of distance, r, from the wall across the pore. More precisely, r is the generalized coordinate vector.

In the DFT treatment the statistical mechanical grand canonical ensemble is utilized. The appropriate free energy quantity is the grand Helmholtz free energy, or grand potential functional, $\Omega[\rho(r)]$. This free energy functional is expressed in terms of the density profile, $\rho(r)$: then by minimizing the free energy (at constant μ, V, T) it is possible in principle to obtain the equilibrium density profile.

For a one-component fluid, which is under the influence of a spatially varying external potential, the grand potential functional becomes

$$\Omega[\rho(r)] = \mathrm{F}[\rho(r)] + \int \mathrm{d}r\rho(r)[\phi(r) - \mu] \tag{7.24}$$

where $\mathrm{F}[\rho(r)]$ is the intrinsic Helmholtz free energy functional, $\phi(r)$ is the external potential, and the integration is performed over the pore volume, V.

The $\mathrm{F}[\rho(r)]$ functional can be separated into an ideal gas term and contributions from the repulsive and attractive forces between the adsorbed molecules (i.e. the fluid–fluid interactions). Hard-sphere repulsion and pairwise Lennard–Jones 12-6 potential are usually assumed and a mean field treatment is generally applied to the long-range attraction. However, the evaluation of the density profile of an inhomogeneous hard-sphere fluid presents a special problem since its free energy is

dependent on the density at positions near r as well as at r itself. The mean field approach therefore provides an unrealistic picture of the density profile in this region. For this reason, it is now customary to apply non-local density functional theory (NLDFT), which involves the incorporation of short-range smoothing functions. In this manner, it has been possible to obtain good agreement with the density profiles determined by Monte Carlo molecular simulation (Lastoskie *et al.*, 1993; Cracknell *et al.*, 1995).

In the special case of the interaction of nitrogen with two graphitic slabs (i.e. within a carbon slit), the Steele 10-4-3 potential has been used to obtain the effective external potential (Lastoskie *et al.*, 1993). It is this system which has so far received most attention and generally the surface is assumed homogeneous so that the potential is constant in the xy plane.

Once the density profile is defined for a given pressure, the amount adsorbed by a particular pore can be obtained from the area under the curve. The surface excess number of molecules adsorbed, which as we have seen corresponds to the experimentally determined adsorption, is then given by $[\rho(r) - \rho_B]\,dr$, where ρ_B is the density of the bulk phase at (μ, T).

Lastoskie *et al.* (1993) have applied NLDFT to generate series of hypothetical 'individual pore isotherms' for a range of pore sizes and wall potentials. The results appeared to provide a basis for a new classification based on three regimes: continuous pore filling, capillary condensation and layering transitions. It was therefore proposed that the filling behaviour rather than the pore width should be adopted for the classification of physisorption systems. Thus, according to the DFT model, the critical pore widths which correspond to the boundaries between these regimes are strongly dependent on temperature. Furthermore, it is the magnitude of the solid–fluid interactions which govern the pressure at which pore filling occurs, the type of filling being dependent on the ratio of pore width to adsorbate molecular diameter.

So far it has been assumed that the adsorbent surface is homogeneous and that all the pores are of the same size and shape. In practice these conditions are rarely fulfilled. To arrive at the pore size distribution, it has been assumed that a porous adsorbent has an array of non-interacting pores (i.e. there are no network percolation effects) and that the distribution of pore widths can be described by a continuous function f(w). The experimental isotherm can then be regarded as a composite of isotherms for each group of pores. The amount adsorbed is presumed to be given by the general equation

$$n(p) = \int_0^\infty \rho(p, w)\mathrm{f}(w)\,dw \tag{7.25}$$

Various procedures have been proposed for solving this equation. For example the pore size distribution may be assumed to be of log-normal form (Seaton *et al.*, 1989), or alternatively integration may be replaced by summation and a numerical deconvolution approach adopted (Olivier *et al.*, 1994).

It is still too early to give a definitive appraisal of the value of DFT for pore size analysis. Considerable progress has already been made in the theoretical treatment of

physisorption mechanisms and there appears to be considerable scope for further development.

References

Adkins B.D. and Davis B.H. (1986) *J. Phys.Chem.* **90**, 4866.

Adkins B.D. and Davis B.H. (1987) *Langmuir* **3**, 722.

Amberg C.H., Everett D.H., Ruiter L.H. and Smith E.W. (1957) In: *Solid/Gas Interface*, Proceedings of the 2nd International Congress of Surface Activity, Butterworths Scientific Publications, London, p. 3.

Avery R.G. and Ramsay J.D.F. (1973) *J. Colloid Interface Sci.* **42**(3) 597.

Balbuena P.B. and Gubbins K.E. (1992) *Fluid Phase Equilibria* **76**, 21.

Balbuena P.B. and Gubbins K.E. (1993) Langmuir **9**, 1801.

Ball P.C. and Evans R. (1989) *Langmuir* **5**, 714.

Barrett E.P., Joyner L.G. and Halenda P.H. (1951) *J. Am. Chem. Soc.* **73**, 373.

Branton P.J., Sing K.S.W. and White J.W. (1997) *J. Chem. Soc., Faraday Trans.* **93**, 2337.

British Standards Institution (1992) BS 7591, Part 2.

Broekhoff J.C.P. and Linsen B.G. (1970) In: *Physical and Chemical Aspects of Adsorbents and Catalysts* (B.G. Linsen, ed.), Academic Press, London, p. 1.

Brown A.J., Burgess C.G.V., Everett D.H. and Nuttall S. (1997) In: *Characterization of Porous Solids IV* (B. McEnaney, T.J. Mays, J. Rouquerol, F. Rodriguez-Reinoso, K.S.W. Sing and K.K. Unger, eds) The Royal Society of Chemistry, Cambridge, p. 1.

Brunauer S. (1945), *The Adsorption of Gases and Vapours*, Oxford University Press, London, p. 126.

Bukowiecki S.T., Straube B. and Unger K.K. (1985) In: *Principles and Applications of Pore Structural Characterization* (J.M. Haynes and P. Rossi-Doria, eds), Arrowsmith, Bristol, p. 43.

Burgess C.G.V., Everett D.H. and Nutall S. (1989) *Pure Appl. Chem.* **61**, 1845.

Carrott P.J.M. and Sing K.S.W. (1989) *Pure Appl. Chem.* **61**, 1835.

Cohan L.H. (1938) *J. Am. Chem. Soc.* **60**, 433.

Cohan L.H. (1944) *J. Am. Chem. Soc.* **66**, 98.

Cracknell R.F., Gubbins K.E., Maddox M. and Nicholson D. (1995) *Accounts Chem. Res.* **28**, 281.

Cranston R.W. and Inkley F.A. (1957) In: *Advances in Catalysis*, vol. 9, Academic Press, New York, p. 143.

de Boer J.H. (1958) In: *The Structure and Properties of Porous Materials* (D.H. Everett and F.S. Stone, eds), Butterworths, London, p. 68.

Defay R. and Prigogine I. (1951) *Tension Superficielle et Adsorption*, Dunod, Paris.

Defay R. and Prigogine I. (1966) *Surface Tension and Adsorption*, Longmans, Green and Co., Bristol.

Derjaguin B.V. (1957) In: *Proceedings of the Second International Congress on Surface Activity II*, Butterworths, London, p. 154.

Dollimore D. and Heal G.R. (1964) *J. Appl. Chem.* **14**, 109.

Dollimore D. and Heal G.R. (1973) *J. Colloid Interface Sci.* **42**, 233.

Evans R. and Marconi U.M.B. (1985) *Chem. Phys. Lett.* **114**, 415.

Evans R., Marconi U.M.B. and Tarazona P. (1986) *J. Chem. Phys.* **84**, 2376.

Everett D.H. (1955) *Trans. Faraday Soc.* **51**, 1551.

Everett D.H. (1958) In: *Structure and Properties of Porous Materials* (D.H. Everett and F.S. Stone, eds), Butterworths, London, p. 95.

Everett D.H. (1967) In: *The Solid–Gas Interface* (E.A. Flood, ed.), Edward Arnold, London, p. 1055.

Everett D.H. (1979) In: *Characterization of Porous Solids* (S.J. Gregg, K.S.W. Sing and H.F. Stoeckli, eds), Society of Chemical Industry, London, p. 229.

Everett D.H. (1988) In: *Characterization of Porous Solids I* (K.K. Unger, J. Rouquerol, K.S.W. Sing and H. Kral, eds) Elsevier, Amsterdam, p. 1.

Everett D.H. and Haynes J.M. (1973) In: *Colloid Science*, The Chemical Society, London p. 123.

Findenegg G.H., Groß S. and Michalski Th. (1993) In: *Fundamentals of Adsorption* (M. Suzuki, ed.), Kodanska, Tokyo, p. 161.
Findenegg G.H., Groß S. and Michalski Th. (1994) In: *Characterization of Porous Solids III* (J. Rouquerol, F. Rodriguez-Reinoso, K.S.W. Sing and K.K. Unger, eds) Elsevier Science BV, Amsterdam, p. 71.
Foster A.G. (1932) *Trans. Faraday Soc.* **28**, 645.
Gelb, L.D. and Gubbins, K.E. (1998) *Langmuir* **14**, 2097.
Gregg, S.J. and Sing K.S.W. (1982) *Adsorption, Surface Area and Porosity*, Academic Press, London, p. 169.
Gurvich L. (1915) *J. Phys. Chem. Russ.* **47**, 805.
Havard D.C. and Wilson R. (1976) *J. Colloid Interface Sci.* **57**, 276.
Haynes J.M. (1975) In: *Colloid Science*, vol. 2, The Chemical Society, London, p. 101.
Jessop C.A., Riddiford S.M., Seaton N.A., Walton J.P.R.B. and Quirke N. (1991) In: *Characterization of Porous Solids II* (F. Rodriguez-Reinoso, J. Rouquerol, K.S.W. Sing and K.K. Unger, eds) Elsevier, Amsterdam, p. 123.
Kaneko K. (1994) *J. Membrane Sci.* **96**, 59.
Kanellopoulos N.K., Petrou J.K. and Petropoulos J.H. (1983) *J. Colloid Interface Sci.* **96**, 90.
Karnaukhov A.P. (1971) *Kinetics and Catalysis* **12**, 908, 1096.
Karnaukhov A.P. (1979) In: *Characterization of Porous Solids* (S.J. Gregg, K.S.W. Sing and H.F. Stoeckli, eds) Society of Chemical Industry, London, p. 301.
Kraemer E.O. (1931) In: *A Treatise of Physical Chemistry* (H.S. Taylor, ed.) Macmillan, New York, p. 1661.
Lastoskie C., Gubbins K.E. and Quirke N. (1993) *J. Phys. Chem.* **97**, 4786.
Lastoskie C., Gubbins K.E. and Quirke N. (1994) In: *Characterization of Porous Solids III* (J. Rouquerol, F. Rodriguez-Reinoso, K.S.W. Sing and K.K. Unger, eds) Elsevier, Amsterdam, p. 51.
Lewandowski H., Michalski T. and Findenegg G.H. (1991) In: *Fundamentals of Adsorption III* (A.B. Mersmann and S.E. Scholl, eds) Technical University of Munich, p. 497.
Lippens B.C., Linsen B.G. and de Boer J.H. (1964) *J. Catalysis* **3**, 32.
Liu H., Zhang L. and Seaton N.A. (1992) *Chem. Eng. Sci.* **47**, 4393.
Liu H., Zhang L. and Seaton N.A. (1993) *Langmuir* **9**, 2576.
Liu H., Zhang L. and Seaton N.A. (1994) In: *Characterization of Porous Solids III* (J. Rouquerol, F. Rodriguez-Reinoso, K.S.W. Sing and K.K. Unger, eds) Elsevier Science BV, p. 129.
Llewellyn P.L., Sauerland C., Martin C., Grillet Y., Coulomb J.P., Rouquerol F. and Rouquerol J. (1997) In: *Characterization of Porous Solids IV* (B. McEnaney, T.J. Mays, J. Rouquerol, F. Rodriguez-Reinoso, K.S.W. Sing and K.K. Unger, eds) The Royal Society of Chemistry, Cambridge, p. 111.
Lopez-Ramon M.V., Jagiello J., Bandosz T.J. and Seaton N.A. (1997) In: *Characterization of Porous Solids IV* (B. McEnaney, T.J. Mays, J. Rouquerol, F. Rodriguez-Reinoso, K.S.W. Sing and K.K. Unger, eds) The Royal Society of Chemistry, Cambridge, p. 73.
McBain J.W. (1935) *J. Am. Chem. Soc.* **57**, 699.
McKee D.W. (1959) *J. Phys. Chem.* **63**, p. 1256.
Machin W.D. (1992) *J. Chem. Soc. Faraday Trans.* **88**, 729.
Machin W.D. (1994) *Langmuir* **10**, 1235.
Machin W.D. and Murdey R.J. (1997) In: *Characterization of Porous Solids IV* (B. McEnaney, T.J. Mays, J. Rouquerol, F. Rodriguez-Reinoso, K.S.W. Sing and K.K. Unger, eds) The Royal Society of Chemistry, Cambridge, p. 221.
Maddox M.W. and Gubbins K.E. (1995) *Langmuir* **11**, 3988.
Mason G. (1971) *J. Colloid Interface Sci.* **35**, 279.
Mason G. (1988) In: *Characterization of Porous Solids I* (K.K. Unger, J. Rouquerol, K.S.W. Sing and H. Kral, eds) Elsevier, Amsterdam, p. 323.
Michalski T., Benini A. and Findenegg G.H. (1991) *Langmuir* **7**, 185.
Milburn D.R. and Davis B.H. (1997) In: *Characterization of Porous Solids IV* (B. McEnaney, T.J. Mays, J. Rouquerol, F. Rodriguez-Reinoso, K.S.W. Sing and K.K. Unger, eds) The Royal Society of Chemistry, Cambridge, p. 274.
Montarnal R. (1953) *J. Phys. et Rad.* **12**, 732.

Murray K.L., Seaton N.A. and Day M.A. (1998) *Langmuir* in press.
Neimark A.V. (1991) In: *Characterization of Porous Solids II* (F. Rodriguez-Reinoso, J. Rouquerol, K.S.W. Sing and K.K. Unger, eds) Elsevier, Amsterdam, p. 67.
Olivier J.P. (1995) *J. Porous Materials* **2**, 9.
Olivier J.P., Conklin W.B. and Szombathely M.V. (1994) In: *Characterization of Porous Solids III* (J. Rouquerol, F. Rodriguez-Reinoso, K.S.W. Sing and K.K. Unger, eds) Elsevier, Amsterdam, p. 81.
Page, K.S. and Monson, P.A. (1996) *Phys. Rev. E*, **54**, 6557.
Pierce C. (1953) *J. Phys. Chem.* **57**, 149.
Roberts B.F. (1967) *J. Colloid Interface Sci.* **23**, 266.
Rouquerol J., Avnir D., Fairbridge C.W., Everett D.H., Haynes J.M., Pernicone N., Ramsay J.D.F., Sing K.S.W. and Unger K.K. (1994) *Pure Appl. Chem.* **66**, 1739.
Saam W.F. and Cole M.W. (1975) *Phys. Rev. B* **11**, 1086.
Seaton N.A. (1991) *Chem. Eng. Sci.* **46**, 1895.
Seaton N.A., Walton J.P.R.B. and Quirke N. (1989) *Carbon* **27**, 853.
Sing K.S.W. (1970) In: *Surface Area Determination* (D.H. Everett and R.H. Ottewill, eds) Butterworths, London, p. 25.
Sing K.S.W., Everett D.H., Haul R.A.W., Moscou L., Pierotti R.A., Rouquerol J. and Siemieniewska T. (1985) *Pure Appl. Chem.* **57**(4) 603.
Thomson W.T. (1871) *Phil. Mag.* **42**, 448.
Wade W.H. (1964) *J. Phys. Chem.* **68**, 1029.
Wade W.H. (1965) *J. Phys. Chem.* **69**, 322.
Zhdanov V.P., Fenelonov V.B. and Efremov D.K. (1987) *J. Colloid Interface Sci.* **120**, 218.
Zsigmondy A. (1911), *Z. Anorg. Chem.* **71**, 356.

This Page Intentionally Left Blank

CHAPTER 8

Assessment of Microporosity

8.1. Introduction

We recall that the filling of micropores (of width < 2 nm) takes place in the pre-capillary condensation range of a physisorption isotherm. If the pore width, w, is no greater than a few molecular diameters (i.e. in an ultramicropore), the pore filling occurs at a very low $p/p°$. This process, which we refer to as the 'primary micropore filling', is associated with enhanced adsorbent–adsorbate interactions and always involves some distortion of the sub-monolayer isotherm. Wider micropores (super-micropores) are filled by a co-operative process over a somewhat higher range of $p/p°$, which may extend into the multilayer region.

Recent theoretical, simulation and experimental studies of physisorption energetics and phase equilibria have helped to improve our understanding of the differences between these two mechanisms of micropore filling. It is now evident that there are six main variables which must be taken into account:

(a) the adsorbent solid structure;
(b) the surface composition;
(c) the pore width and shape;
(d) the polarizabilities and polarities of the interacting centres;

(e) the adsorptive molecular size and shape;
(f) the operational temperature.

In addition, we should keep in mind that the micropore filling capacity is dependent on both the available pore volume and the packing of the adsorbed molecules.

In this chapter, we introduce the currently most popular adsorption methods used for micropore size analysis: our aim is to outline in general terms the relative merits and limitations of these procedures. Their application is discussed more fully in later chapters in relation to the characterization of particular adsorbents.

As we have already seen, an ideal Type I isotherm has a long, almost horizontal plateau, which extends up to $p/p^\circ \longrightarrow 1$, as in Figure 8.1a. In this case, the micropore capacity, n_p(mic), is registered directly as the amount adsorbed at the plateau. Such well-defined Type I isotherms are given by large crystals of a molecular sieve zeolite.

Many porous adsorbents contain pores with a wide range of sizes which cross the micropore–mesopore boundary. Also, some microporous adsorbents are composed of very small agglomerated particles, which exhibit a significant external area. Such materials give composite isotherms with no distinctive plateau. The presence of mesopores can often be detected by the appearance of a hysteresis loop – as in Figure 8.1b.

A third possibility is a Type I isotherm with a short plateau, which terminates at $p/p^\circ < 1$. An upward deviation, as indicated in Figure 8.1c, occurs at high p/p° when the microporous adsorbent also contains some wide mesopores or narrow macropores. Since the wall area of such relatively wide pores is likely to be much smaller than the micropore area, the scale of multilayer development or mesopore filling may be quite small.

Many attempts have been made to obtain the micropore capacity by the analysis of composite isotherms. The calculation of the micropore volume, v_p(mic), from n_p(mic) is almost invariably based on the assumption that the adsorbate in the micropores has the same density as the adsorptive in the liquid state at the operational

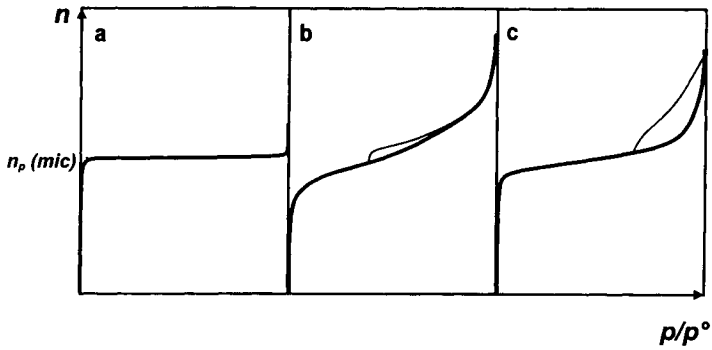

Figure 8.1. Nitrogen isotherms corresponding to adsorption: (a) in ultramicropores; (b) in wider micropores and on external surfaces; (c) in micropores and wide mesopores.

temperature. As we saw in Chapter 7, for the condensate in a mesoporous adsorbent this assumption (i.e. the Gurvich rule) appears to be justified. The situation is quite different, however, with a microporous material – particularly when the pore dimensions are in the ultramicropore range.

Studies of the packing of molecules in cylindrical and slit-shaped pores have revealed the importance of both the width and the shape of narrow pores (Carrott *et al.*, 1987; Balbuena and Gubbins, 1994). An indication of the effect of pore size on the packing density of spherical molecules is given in Figure 8.2. Here, the degree of packing in cylinders and slits is expressed as a percentage of the packing density in the corresponding close-packed state. Although this is an oversimplified picture since it does not allow for the adsorption forces, it does illustrate the difficulty of arriving at an unambiguous assessment of the accessible pore volume. Inspection of

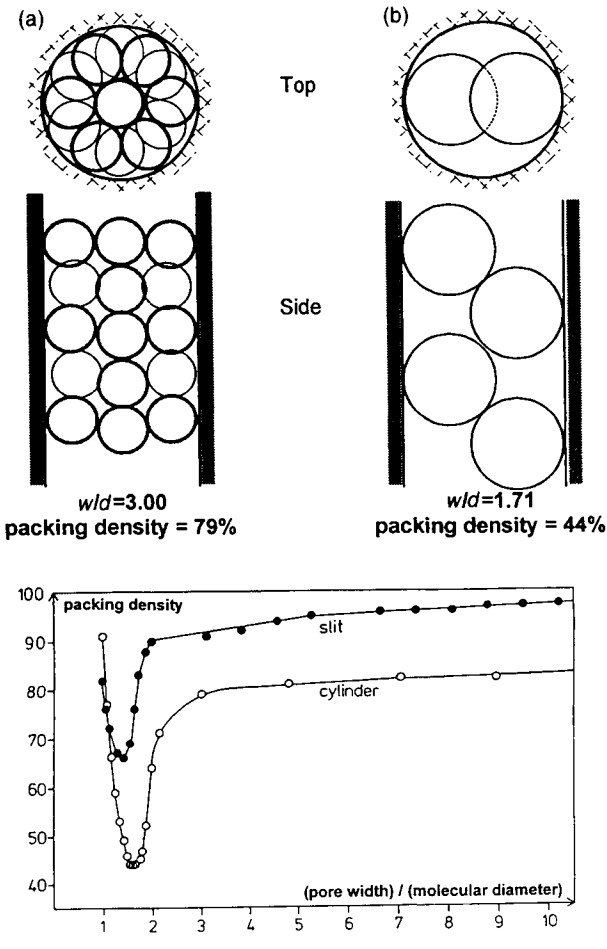

Figure 8.2. Packing of spherical molecules in narrow cylinders and slits.

Figure 8.2 reveals that the Gurvich rule is more likely be obeyed if $w/d > 4$. Of course, conformity to the Gurvich rule does not by itself guarantee that the packing densities are the same as in the bulk liquid.

The most striking feature of Figure 8.2 is the effect of the additional degree of freedom provided by a parallel-sided slit. Indeed, this difference in the packing density in slits and cylinders will be seen to be of great importance when we consider the adsorptive properties of molecular sieve carbons and certain zeolites.

In assessing the packing densities within narrow slits and cylinders, we have assumed that the same width is available for all molecules within a given slit or cylinder. This cannot be strictly true, however, since the effective pore width is to some extent dependent on the molecular interactions (Everett and Powl, 1976). Indeed, the adsorbate can be regarded as an inhomogeneous fluid with a density which varies from one point to another within a given pore.

Of course, one possible reason for an observed large departure from the Gurvich rule is as a direct result of molecular sieving: that is, the inability of larger adsorptive molecules to enter a certain range of narrow pores. Behaviour of this type is well documented for many zeolites and some activated carbons. Size exclusion measurements (gas adsorption or immersion calorimetry) provide an obvious way of determining the micropore size distribution (Gonzalez *et al.*, 1997; Lopez-Ramon *et al.*, 1997). Even when exclusion effects are small, or even absent, the use of molecules of different size is strongly recommended for the characterization of microporous adsorbents.

8.2. Isotherm Analysis

8.2.1. Empirical methods

Several early attempts were made to adapt the *t*-method for micropore analysis. In their original work, Lippens and de Boer (1965) had proposed that the total surface area of a porous solid was directly proportional to the slope of the initial linear section of a *t*-plot (see Section 6.3.2). In the MP (micropore)-method of Mikhail *et al.*, (1968), tangents to the *t*-plot were taken to represent the surface areas of different groups of micropores. The pore volume distribution was then determined for a given pore shape (e.g. parallel-sided slits). Although this apparently simple procedure attracted a good deal of interest, Dubinin (1970) and others (Gregg and Sing, 1976) pointed out that the MP method is fundamentally unsound. Since the isotherm is distorted as a result of primary micropore filling, it cannot be assumed that surface coverage or the effective molecular area are the same as on the open surface.

In principle, a *t*-plot can be used to assess the micropore capacity provided that the standard multilayer thickness curve has been determined on a non-porous reference material with a similar surface structure to that of the microporous sample. In our view, it is not safe to select a standard isotherm with the same BET C value (i.e. the procedure recommended by Brunauer (1970) and Lecloux and Pirard (1979)) since this does not allow for the fact that the sub-monolayer isotherm shape is dependent on both the surface chemistry and the micropore structure.

An important advantage of the α_s-method (see Section 6.3.3) is that it does not depend on any *a priori* assumptions concerning the mechanism of adsorption by the reference material and therefore its application is not restricted to nitrogen adsorption. For this reason it can be used to explore the various stages of micropore filling with a number of different adsorptives. As explained in Chapter 6, the standard isotherm is plotted in the reduced form, $(n/n_x)_s$ versus $p/p°$, the normalizing factor, n_X, being taken as the specific amount adsorbed at a pre-selected $p/p°$ (generally, it is convenient to take $p/p° = 0.4$).

To construct an α_S-plot for a given microporous adsorbent, the amount adsorbed, n, is plotted against the reduced standard adsorption, $\alpha_s = (n/n_X)_S$. Hypothetical α_S-plots for two different microporous adsorbents are shown in Figure 8.3. In the case of (a), there is no initial linear region since the isotherm is distorted at low $p/p°$ as a result of the enhanced adsorbent–adsorbate interactions in ultramicropores. However, the initial linear section of the α_S-plot in (b) corresponds to monolayer adsorption on the walls of supermicropores. Co-operative filling of the supermicropores occurs progressively over a range of higher $p/p°$ and in some cases is manifested by an upward deviation of the α_S-plot.

Once the micropores have been filled, both plots in Figure 8.3 become linear, provided that capillary condensation is absent (or only detectable at high $p/p°$). The low slope signifies that multilayer adsorption has occurred on a relatively small external surface. Back-extrapolation of the linear multilayer section gives the specific micropore capacity, n_p(mic), as the intercept on the n axis.

As already noted, the effective micropore volume, v_p(mic) is

$$v_p(\text{mic}) = n_p(\text{mic}) \times M/\rho \tag{8.1}$$

where M is the molar mass of the adsorptive and ρ is the average absolute density of the adsorbate, which is generally assumed to be the same as the absolute density of the liquid adsorptive.

The α_s-method has been used by a number of investigators to study the various stages of micropore filling (Fernandez-Colinas *et al.*, 1989; Carrott *et al.*, 1989; Kenny *et al.*, 1993; Kaneko, 1996). For example, high-resolution nitrogen measurements have

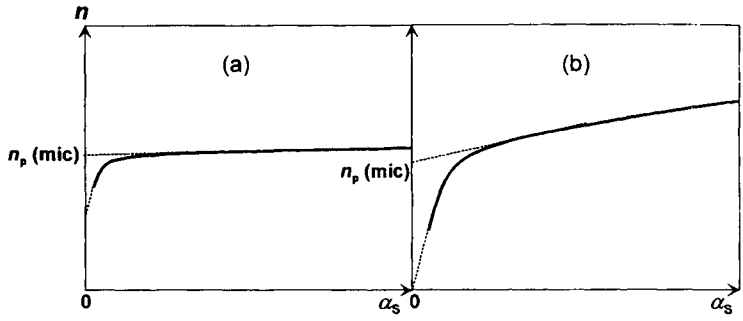

Figure 8.3. Hypothetical α_S plots for a sample with ultramicropores (a) and for a sample with only wider micropores or 'supermicropores' (b).

confirmed the differences in the adsorptive behaviour of ultramicroporous and supermicroporous carbons. Also, by constructing the α_S-plots for probe molecules of different size, one can study the effect of changing the ratio of pore width/molecular size, w/d, on the mechanism of pore filling (Carrott *et al.*, 1987, 1988). In this manner it is possible to gain a semi-quantitative estimate of the pore size distribution. This approach as applied to the characterization of activated carbons is illustrated in Chapter 9.

8.2.2. Dubinin–Stoeckli methods

The Dubinin–Radushkevich (DR) equation, which in Chapter 4 was given as Equation (4.43), can also be expressed in the form

$$\log_{10}(\boldsymbol{n}) = \log_{10}(\boldsymbol{n}_p(\text{mic})) - D \log^2_{10}(p°/p) \qquad (8.2)$$

where D is an empirical constant – as defined in Equation (4.44). Thus, according to the DR theory, a plot of $\log_{10}(\boldsymbol{n})$ against $\log^2_{10}(p°/p)$ should be linear with slope D and intercept $\log_{10}(\boldsymbol{n}_p(\text{mic}))$. As before, Equation (8.1) is used to obtain $v_p(\text{mic})$ from $\boldsymbol{n}_p(\text{mic})$.

Various DR plots for activated carbons are given in Chapter 9. For our present purpose, the two hypothetical examples in Figure 8.4 will suffice to illustrate some important features.

As a general rule, an ultramicroporous carbon gives a linear DR plot over a wide range of $p/p°$ (see Figure 8.4a) provided that the isotherm is reversible (i.e. there is no low-pressure hysteresis). Generally, any significant adsorption in wider pores or on an external surface leads to a departure from linearity (see Figure 8.4b). On the

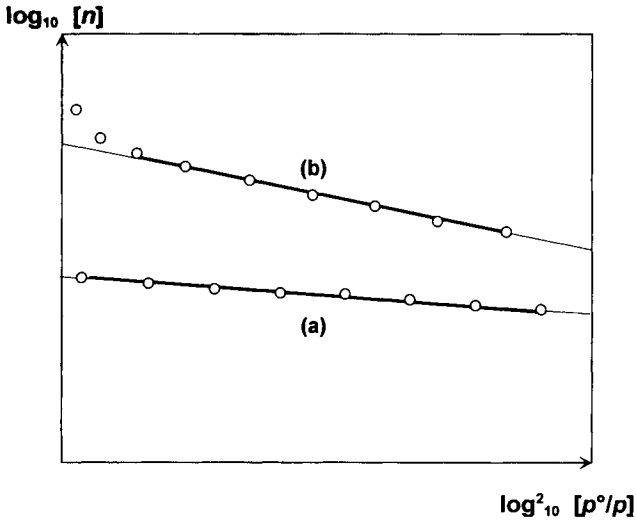

Figure 8.4. Hypothetical DR plots for a sample with only ultramicropores (a) and for a sample also including wider pores (b).

other hand, some DR plots on non-porous or mesoporous solids do exhibit limited ranges of linearity. In fact, it was this behaviour which led Kaganer (1959) to propose an analogous form of Equation (8.2) in which v_m(mic) is replaced by $\boldsymbol{n}_m$, the monolayer capacity.

It is apparent that any limited range of linearity of a simple DR plot cannot be used to give a reliable evaluation of the pore size distribution. In order to describe a bimodal micropore size distribution, Dubinin (1975) applied a two-term equation, which we may write in the form

$$\boldsymbol{n} = \boldsymbol{n}_{p,1} \exp[-(A/E_1)^2] + \boldsymbol{n}_{p,2} \exp[-(A/E_2)^2] \tag{8.3}$$

where $\boldsymbol{n}_{p,1}$ and $\boldsymbol{n}_{p,2}$ are the micropore capacities of the two groups of pores and E_1 and E_2 are the corresponding characteristic energies.

Of course, the application of Equation (8.3) is based on the assumption that there are two separate ranges of pore size. This led Dubinin (1975) to refer to the group of wider pores as the 'supermicropores', the width of which was considered to be *c.* 1.5 nm. In principle, Equation (8.3) could be extended to include a much larger number of different groups of pores, but in practice the resulting multi-term summations become intractable.

An important advance in the application of the DR equation to heterogeneous micropore structures was made by Stoeckli. By assuming a Gaussian distribution, Stoeckli and co-workers attempted to allow for a continuous distribution of pore size by replacing the summation of the individual DR contributions by integration (Stoeckli, 1977; Stoeckli *et al.*, 1979) (see Chapter 4). The integral transform was then solved by the use of a mathematical device equivalent to an 'error function' to give an exponential relation between the micropore size distribution and the Gaussian half-width, Δ. In other words, Δ was taken to be a measure of the dispersion of B around a mean value of B_0 in Equation (4.47).

To explain the significance of the various terms adopted by Dubinin and Stoeckli, it is convenient to write the Dubinin–Astakov equation – Equation (4.45) – in the form

$$\boldsymbol{n} = \boldsymbol{n}_p \exp[-(A/\beta E_0)^N] \tag{8.4}$$

where β and N are as defined in Chapter 4 and E in Equation (4.45) is replaced by βE_0. On the basis of a limited amount of experimental evidence, an inverse relation was proposed (Dubinin, 1979) between E_0 and the pore width, w:

$$w = K/E_0 \tag{8.5}$$

where K is an empirical constant, which was reported to be ≈ 17.5 nm kJ mol^{-1} for a series of activated carbons (see Bansal *et al.*, 1988). However, it was concluded that active carbons with characteristic E_0 values < 20–22 kJ mol^{-1} were likely to be heterogeneous. It appeared that the micropore size became smaller and the distribution also more homogeneous with increase in N over the range 1.5 to 3.0. The extreme value of $N = 3$ was found with a carbon molecular sieve, which had a particularly narrow distribution of pore size (Dubinin and Stoeckli, 1980).

The mathematical elegance of the Dubinin–Stoeckli approach is impressive, but it remains to be seen whether the basic DR equation is strictly applicable to a narrow

group of micropores of any size. It is noteworthy that the method appears to be most successful when applied to a relatively narrow range of ultramicropores in molecular sieve carbons, i.e. when only primary micropore filling is involved (Martin-Martinez *et al.*, 1986). Although the DA equation can be applied to physisorption isotherms on molecular sieve zeolites, the results are much more difficult to interpret. This is an indication that consideration must be given to both the pore structure and the surface chemistry.

8.2.3. Nonane pre-adsorption

A novel method for the evaluation of microporosity was introduced by Gregg and Langford (1969). The aim was to fill the micropores of an adsorbent with *n*-nonane, whilst leaving the wider pores and open surface still available for the adsorption of nitrogen at 77 K. Nonane was chosen as the pre-adsorptive because of its relatively large physisorption energy, which in turn results in a high energy barrier (i.e. activation energy) for desorption. As a consequence, elevated temperatures are required to remove the nonane molecules from the narrow pores at a measurable rate. Moreover, the long-chain molecules of *n*-nonane are able to enter narrow micropores of width as low as 0.4 nm, which is not the case with more bulky hydrocarbon molecules.

The following experimental procedure was used by Gregg and Langford. The outgassed adsorbent was first exposed to *n*-nonane vapour at 77 K, re-outgassed at room temperature and the first nitrogen isotherm determined at 77 K. The sample was then outgassed at a number of increasingly higher temperatures and nitrogen isotherms successively determined after each stage of outgassing until the nonane had been completely removed.

The first material to be studied in this way was an activated sample of carbon black. It was found that prolonged outgassing at a temperature of 350°C was required to achieve complete removal of the pre-adsorbed nonane. All the intermediate nitrogen isotherms were found to be parallel in the multilayer range and the vertical separation between the isotherms obtained after outgassing at 20° and 350°C provided a satisfactory measure of the micropore capacity. Convincing evidence was also obtained that the nonane was removed only from the external surface at 20°C.

Some more recent investigations of the pre-adsorption method have shown, however, that the results are not always so easy to interpret (Martin-Martinez *et al.*, 1986; Carrott *et al.*, 1989). As would be expected, the nonane molecules are more strongly trapped in ultramicropores than in supermicropores. However, since many microporous adsorbents have complex networks of pores of different size, the retention of the nonane molecules in narrow pores also leads to blocking of some wider pores.

8.2.4. Generalized adsorption isotherm (GAI)

A generalized expression for the adsorption isotherm given by a porous solid can be written in the integral form

$$n(\mathrm{p}) = \int n'(p, w)\mathrm{f}(w)\,\mathrm{d}w \tag{8.6}$$

where $n(p)$ is the total amount adsorbed at pressure p, $n'(p,w)$ represents a single-pore isotherm and $f(w)$ is a function of the pore size distribution. It is apparent that Equation (8.6) is equivalent to Equation (4.52), which is not explicitly related to the pore size distribution.

It follows that the derivation of a meaningful pore size distribution from an experimental isotherm is dependent on the availability of the appropriate single-pore isotherm data on a series of adsorbents of controlled pore size and shape (McEnaney and Mays, 1991). In practice, this requirement poses a serious problem with microporous adsorbents. As we have seen, it is unlikely that the same mathematical form of isotherm can hold for the complete range of filling of micropores of different size. The recent attempts to overcome this difficulty are discussed in the following sections.

8.3. Microcalorimetric Methods

Because of the appreciable enhancement of the adsorption potential in micropores of a few molecular diameters in width (see Section 1.7 and Figure 1.6), microcalorimetry can provide a useful means of assessing microporosity. The available experimental procedures are outlined in the following sections.

8.3.1. Immersion microcalorimetry

Immersion of various dry samples in the same liquid

For this approach, the liquid is usually selected to fill the micropores as completely as possible. The most popular liquids are water, methanol, benzene, cyclohexane and *n*-hexane; the choice depends on the expected polarity of the surface and shape of the micropores (cylindrical, slit-shaped, etc.).

The first stage is usually a simple comparison of the specific energies of immersion. In the absence of a relatively large external surface area, the energies are controlled by the nature of the microporous network (see for instance Stoeckli and Ballerini, 1991, or Rodriguez-Reinoso *et al.*, 1997).

For a more detailed evaluation of the microporosity, one must be able to interpret the energy of immersion data. At present, there are two procedures favoured by different investigators.

The first procedure is based on the Dubinin–Stoeckli principles of volume filling (see Section 4.4.4). The energy of immersion $\Delta_{\text{imm}}U$ is related to the *micropore volume* $W_0(d)$ and the 'characteristic energy' E_0 for a given micropore size and immersion liquid (Bansal *et al.*, 1988) by the expression:

$$\frac{\Delta_{\text{imm}}U}{m_s} = [-\beta E_0 W_0(d)(1+\alpha T)\sqrt{\Pi}/2V_{\text{m}}^{\text{l}}] + u^{\text{i}}a(\text{ext}) \qquad (8.7)$$

where m_s is the mass of adsorbent, d is the molecular diameter, V_{m}^{l} is the molar volume of the liquid, u^{i} is the energy of immersion of 1 m^2 of external surface area

a(ext), β is a scaling factor and α is the coefficient of thermal expansion of the liquid. Provided the external surface area is negligible, the energy of immersion appears to provide an approximate comparative assessment of the microporous volume $W_0(d)$ accessible to the immersion liquid. However, this only holds if the characteristic energy, E_0, remains the same for all samples or if allowance can be made for the likely variation in E_0. Generally, this poses a serious problem.

The second procedure directly relates the energy of immersion $\Delta_{imm}U$ to the *micropore surface area* a(mic), as described in Section 6.5.2. As we saw, very simply:

$$\Delta_{imm}U = u_i a(\text{mic}) + u_i a(\text{ext}) \tag{8.8}$$

In spite of their great difference in complexity, Equations (8.7) and (8.8) are at least mutually consistent: since E is an inverse function of the pore width w, EW_0 may be approximately proportional to a(mic).

Immersion of dry samples in liquids of different molecular size

This method is designed to take advantage of molecular sieving. The basic data are simply in the form of a curve of the specific energy of immersion versus the molecular size of the immersion liquid. This provides immediate information on the micropore size distribution. For room-temperature experiments one can use the liquids listed in Table 8.1, which are well suited for the study of carbons. Because of the various ways of expressing the 'critical dimension' of a molecular probe or its 'molecular size', one must be careful to use a consistent set of data (hence the two separate lists in Table 8.1). Again, one can process the microcalorimetric data to compare either the micropore volumes accessible to the various molecules (see Stoeckli *et al.*, 1996), or the micropore surface areas, as illustrated in Figure 8.5.

A particular advantage of using immersion microcalorimetry for the study of ultramicroporous materials is that the molecular entry into very fine pores takes place much more rapidly from the liquid phase than from a gas. There are two reasons for this difference: gaseous diffusion may be slow (thermally activated) – especially at 77 K – and the higher liquid density also favours a more rapid molecular penetration.

Table 8.1 Immersion liquids used to probe micropore size

Liquid	Critical dimension[a] (nm)	Liquid	Molecular size[b] (nm)
Dichloromethane	0.33	Benzene	0.37
Benzene	0.41	Methanol	0.43
Cyclohexane	0.54	Isopropanol	0.47
Carbon tetrachloride	0.63	Cyclohexane	0.48
1,5,9-Cyclododecatriene	0.76	ter-Butanol	0.6
Tri 2,4-xylylphosphate	1.5	α-Pinene	0.7

[a] After Stoeckli (1993)
[b] After Denoyel *et al.*, (1993)

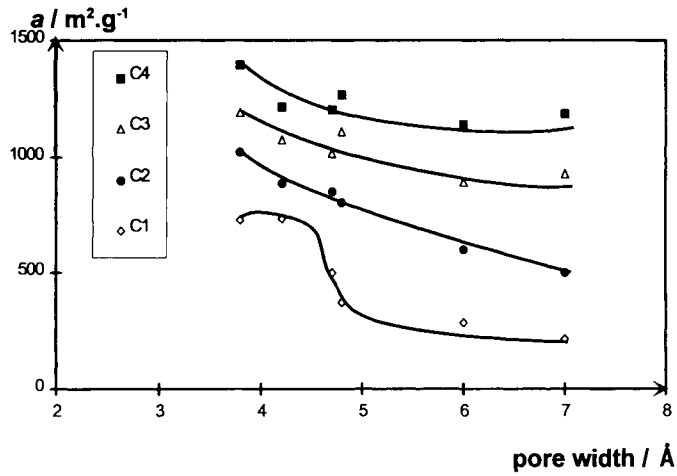

Figure 8.5. Accessible surface area versus pore width, from immersion microcalorimetry in the liquids listed in Table 8.1 (right-hand side) for a set of charcoals (activation increasing from C1 to C4) (Denoyel *et al.*, 1993).

Immersion of samples partially pre-covered by vapour adsorption

This is an indirect way of assessing the energetics of gas adsorption in micropores. The pre-adsorbed vapour can be that of the immersion liquid or it can be another adsorptive: for instance, to study the water filling mechanism in microporous carbons, Stoeckli and Huguenin (1992) devised an experiment with water pre-adsorption prior to immersion calorimetry (in water or in benzene).

8.3.2. Gas adsorption microcalorimetry

The enhancement of the potential energy in micropores can be directly assessed by microcalorimetric measurements of $\Delta_{ads} u$. Moreover, a comparison between N_2 and Ar adsorption allows one to distinguish between the enhancement due to the confinement in micropores and that due to specific adsorbent–adsorbate interactions. Both effects are manifested in the low-pressure range of the nitrogen isotherm, but the specific interactions are virtually absent with argon.

An important feature of gas adsorption microcalorimetry for the study of microporosity is that its highest sensitivity is in the low-pressure region (say, $p/p° < 0.05$), which is precisely the region of micropore filling and where the adsorption isotherm measurement often lacks accuracy. It follows that it is usually advisable to plot $\Delta_{ads} u$ versus n rather than versus $p/p°$. It is then possible to distinguish various types of micropores from the value of $\Delta_{ads} u$ and to obtain information on their effective volumes. This is illustrated by the microcalorimetric curves of Figure 9.14, obtained for nitrogen and argon adsorption on two activated carbons. In this manner, microcalorimetry is an independent way of checking the analysis of the isotherm. Values of $\Delta_{ads} u$ can be meaningful. For instance, with molecular sieve carbons, the

initial values of $\Delta_{ads}\dot{u}$ for nitrogen and argon are *c.* two-fold higher than those obtained on non-porous carbon black: this is the maximum enhancement predicted for the adsorption in slit-shaped micropores (Everett and Powl, 1976).

8.4. Modelling Micropore Filling: Theory and Simulation

8.4.1. Potential energy functions

Successful computer modelling of physisorption is dependent, *inter alia*, on the validity of the solid–fluid and fluid–fluid potential functions (Cracknell *et al.*, 1995). A rigorous description of the attractive and repulsive components is complex (see Nicholson, 1997); however, as was indicated in Chapter 1, the pairwise interaction between a single adsorbate atom and a solid atom is still usually expressed in the form of the 12-6 Lennard-Jones potential. For our present purpose, we may write

$$\varepsilon(r) = 4\,\varepsilon_{gs}[(\sigma/r)^{12} - (\sigma/r)^{6}] \tag{8.9}$$

where r is the distance between the centres of the two atoms, ε_{gs} is the depth of the potential energy well and here σ is the distance at which $\varepsilon(r) = 0$ (σ can also be regarded as the effective mean atomic diameter). According to the Lorentz combining rules, $\varepsilon_{gs} = (\varepsilon_g \times \varepsilon_s)^{1/2}$ and $\sigma = (\sigma_g + \sigma_s)/2$, where the subscripts g and s represent the gas and solid phases, respectively.

It was pointed out in Chapter 1 that it is usually assumed that the overall interaction energy between an adsorbate molecule and the adsorbent is given by the summation of the pairwise interactions. Furthermore, if the assemblage of discrete force centres in the solid can be treated as a continuum, the summation can be replaced by integration (Hill, 1952). In this case, the non-specific Lennard-Jones interaction energy between a single molecule and a semi-infinite slab of solid takes the 9-3 form (Steele, 1974):

$$\phi_{gs}(z) = 0.667\pi\rho\sigma^{3}\varepsilon_{gs}[0.133(\sigma/z)^{9} - (\sigma/z)^{3}] \tag{8.10}$$

where ρ is the density of force centres in the adsorbent.

However, if the adsorbate–adsorbent interactions are confined to a single solid lattice plane, integration over the two dimensions of the solid gives a 10-4 potential function in place of Equation (8.10).

Everett and Powl (1976) applied both the 9-3 and the 10-4 expressions in their theoretical treatment of potential energy profiles for the adsorption of small molecules in slit-like and cylindrical micropores. As one would expect, the two corresponding potential energy curves were of a similar shape, but the differences between them became greater as the pore size was reduced. Strictly, the replacement of the summation by integration is dependent on the distance between the molecule and the surface plane, becoming more accurate as the distance is increased (Steele, 1974).

For the important case of the adsorption of a small molecule on a slab of graphite, Steele (1973) proposed a 10-4-3 potential:

$$\phi_{gs}(z) = 2\pi\rho\varepsilon_{gs}\sigma^{2}\Delta\{0.4(\sigma/z)^{10} - (\sigma/z)^{4} - \sigma^{4}/[3\Delta(0.61\Delta + z)^{3}]\} \tag{8.11}$$

where z is the distance from the graphite surface, Δ is the distance between the graphite layers (0.335 nm) and ρ is the number of carbon atoms per unit volume (114 nm^{-3}). The derivation of this 10-4-3 potential function involved integration over the basal plane and summation over the successive layers. The 10- and 4- terms, therefore, represent the repulsive and attractive interactions with the basal plane, while the 3- term takes care of the summation over the remaining layers. This form of potential function has been favoured in recent computer simulation studies of the adsorption of molecules by porous carbons (Nicholson, 1996, 1997).

If the micropores can be pictured as uniform slits of width H within a graphitic structure, we have

$$\phi(z)_{pore} = \phi_{gs}(z) + \phi_{gs}(H - z) \tag{8.12}$$

where $\phi(z)_{pore}$ now represents the interaction of an adsorbate molecule with the two opposite walls of the slit. As we shall see later, H is the distance between the centres of the carbon atoms and must not be confused with the effective pore width, w.

The composition and size of the adsorbate molecule must be taken into account in the application of Equations (8.11) and (8.12). The nitrogen molecule is sufficiently small to be treated either as a single spherical interacting centre (Walton and Quirke, 1989) or alternatively as a diatomic species in which each atom is regarded as an interacting centre (Nicholson, 1996). For methane adsorbed on graphite, the continuum solid approximation appears to give satisfactory results at temperatures as low as 80 K (Cracknell *et al.*, 1995). In this case, the diameter of the molecule (0.381 nm) is large in comparison with the C—C spacing (0.142 nm) in the basal plane: the molecule therefore appears to move parallel to the surface at constant z.

8.4.2. Horvath–Kawazoe (HK) method

A novel method for determining the micropore size distribution was introduced by Horvath and Kawazoe in 1983. In its original form, the HK analysis was applied to nitrogen isotherms determined on molecular sieve carbons, the assumption being made that these adsorbents contained slit-shaped graphitic pores. More recently, the HK treatment has been extended to argon and nitrogen adsorption in cylindrical and spherical pores of zeolites and aluminophosphates (Venero and Chiou, 1988; Davis *et al.*, 1989; Saito and Foley, 1991; Cheng and Yang, 1995; Horvath and Suzuki, 1997).

The HK method is based on the general idea that the relative pressure required for the filling of micropores of a given size and shape is directly related to the adsorbent –adsorbate interaction energy. As in the FHH theory (see Section 4.2.5), the assumption is made that the entropy contribution to the free energy of adsorption is small in comparison with the large change of internal energy, which is itself largely dependent on the depth of the potential energy well. Expressed in another way, it is assumed that the molar entropy of the adsorbed phase is not very sensitive to a change in the pore dimensions.

By combining a simple 10-4 potential function and Equation (8.12), we have

$$\phi(z)_{\text{pore}} = k\int\left[\left(\frac{\sigma}{z}\right)^{10} - \left(\frac{\sigma}{z}\right)^{4} + \left(\frac{\sigma}{H-z}\right)^{10} - \left(\frac{\sigma}{H-z}\right)^{4}\right] \tag{8.13}$$

where z, σ and H are all as previously defined, and k is a constant for a given gas–solid system and temperature.

Equation (8.13) gives the potential at the distance z from each surface plane in the graphitic slit of width H. The average potential, ϕ_{pore}, in a given pore is obtained by integration across the effective pore width. In this manner, it is possible to evaluate the required relative pressure, $(p/p^\circ)_{\text{pore}}$, since it is assumed that

$$RT\ln(p/p^\circ)_{\text{pore}} = \text{f}[\phi(z)_{\text{pore}}] \tag{8.14}$$

By making use of the Kirkwood–Müller equation and substituting the available experimental data for the physical properties of nitrogen and carbon, Horvath and Kawazoe (1983) arrived at the following equation for the adsorption of nitrogen by molecular sieve carbons at 77 K:

$$\ln(p/p^\circ) = \frac{61.23}{(H-0.64)}\left[\frac{1.895\times10^{-3}}{(H-0.32)^3} - \frac{2.709\times10^{-7}}{(H-0.32)^9} - 0.05014\right] \tag{8.15}$$

Here, H is expressed in nm.

A few representative values of $(p/p^\circ)_{\text{pore}}$ obtained by the application of Equation (8.15) are given in Table 8.2. Although the HK method is based on questionable principles and is now overshadowed by the application of density functional theory, it merits recognition as the first stage in the development of a unified theoretical treatment of micropore filling.

Although the estimated values of $(p/p^\circ)_{\text{pore}}$ in Table 8.2 are unlikely to agree exactly with the equivalent experimental values, the predicted range is of interest. Thus, the filling of ultramicropores is expected to occur at very low relative pressures. In fact, the recent high-resolution adsorption studies of Conner (1997) and Maglara *et al.* (1997) have revealed that to investigate the first stages of micropore filling, it is necessary to work at $p/p^\circ < 10^{-5}$.

Table 8.2 HK predicted values of p/p° of N_2 required to fill carbon slit-shaped pores

Effective pore width w (nm)	$(p/p^\circ)_{\text{pore}}$
0.4	1.46×10^{-7}
0.5	1.05×10^{-5}
0.6	1.54×10^{-4}
0.8	2.95×10^{-3}
1.5	7.59×10^{-2}

8.4.3. Computer simulation and density functional theory

As indicated in Chapter 1, there is now considerable interest in the application of computer simulation (e.g. GCMC) and density functional theory (DFT) to physisorption in model pore structures. It is already possible to predict the behaviour of some simple fluids in model micropores of well-defined size and shape and further progress is to be expected within the next few years.

We have seen that the earlier methods of micropore analysis were either essentially empirical or based on questionable assumptions. In contrast, molecular simulation and DFT offer the prospect of a more rigorous treatment since they are based on the fundamental principles of statistical mechanics. However, it must be kept in mind that to solve the statistical mechanical Hamiltonian, it is necessary to know the exact position of the force centres in the solid structure and also the potential functions which govern the solid–fluid and fluid–fluid interactions. In view of the complexity of most porous adsorbents, it is not surprising that so far most attention has been given to the adsorption of small, spherical molecules in pores of uniform geometry –particularly cylindrical or slit-shaped pores (Steele and Bojan, 1997).

Because of its diatomic nature and permanent quadrupole moment, the physisorption of nitrogen at 77 K presents special problems. The application of DFT is facilitated if the molecules are assumed to be spherical, which was the approach originally adopted by Seaton *et al.* (1989) and also by Lastoskie *et al.* (1993). The analytical procedures already outlined in Chapter 7 (Section 7.6) do not depend on the meniscus curvature and are in principle applicable to both capillary condensation and micropore filling. The non-local version of the mean field theory (NLDFT), which was used by Lastoskie, gave excellent agreement with computer simulation when applied to the carbon slit pore model. However, as pointed out earlier, these computational procedures are not entirely independent since they involve the same model parameters.

With the aid of NLDFT, Lastoskie *et al.* (see Gubbins, 1997) have generated the 'individual pore isotherms' for nitrogen adsorption at 77 K for a wide range of slit-shaped pores. Wider pores (e.g. of $H/\sigma \approx 4$) were found to give Type IV isotherms: in this case the pore filling riser appeared to correspond to capillary condensation. At a smaller pore width a transition from the discontinous capillary condensation in mesopores to continuous filling in supermicropores was observed. Other continuous–discontinuous transitions were also detected at smaller pore widths, the double minima of the solid–fluid potential coming together to form a single deep well at $H \approx 0.8$ nm. At $H \approx 0.69$ nm, the enhancement of the potential well depth appeared to be maximized to approximately double its original depth on the open surface. At a smaller pore width, the repulsive forces became increasingly important and at 0.6 nm the pore space became inaccessible to nitrogen.

By computing a series of model single-pore isotherms for nitrogen adsorption at 77 K, Seaton, Gubbins, Olivier, Quirke and their co-workers (see Gubbins, 1997; Olivier, 1995) have been able to make use of Equation (8.6) in order to determine the micropore size distribution. It is assumed that all the pores are of the same shape (i.e. slits or cylinders of semi-infinite length) and that the distribution,

f(w), can be mathematically described by a function such as the gamma or log-normal distribution.

In applying DFT or MC simulation for the determination of pore size distribution, most investigators have not allowed for pore blocking or any other form of diffusion control. However, in a very recent study by Lopez-Ramon *et al.* (1997) an attempt has been made to make use of percolation theory along with GCMC simulation to interpret the isotherms of CH_4, CF_4 and SF_6 given by a microporous carbon. Although still at an early stage of development, it is already evident that there are a number of advantages in using various adsorptives at different temperatures. In principle, it becomes possible to assess the internal consistency of the derived pore size distribution and expose any aberrations due to networking or molecular sieving.

Most simulation studies of nitrogen adsorption have been made at 77 K. A higher operational temperature is likely to have the advantage that the effects due to quadrupolar interaction will become less important as the kinetic energy is increased. In the work of Kaneko *et al.* (1994), GCMC simulation was used to study the adsorption of nitrogen in slit-shaped graphitic micropores at 303 K.

The comparison of the GCMC isotherms with experimental data has brought to light the uncertainties involved in defining the effective pore width (i.e. the experimental property). Since the effective width of the pore depends on the temperature of measurement and the size of the probe molecule, it is virtually impossible to give a single value for the internal volume of a micropore (Rowlinson, 1985). However, Kaneko *et al.* (1994) suggest that it is practicable to take $\phi(z) = 0$ as a basis for defining the limits of pore width.

The question of the location of the interacting centres in the adsorbate molecule was also examined by Nicholson (1996). It was concluded that the differences between the one-centre and two-centre models, which are significant for the high fractional filling of nitrogen of a narrow micropore, can be attributed to differences in molecular packing. Thus, in the absence of quadrupolar interactions, the two-centre molecules are amenable to higher packing densities than the hypothetical one-centre molecules.

References

Balbuena P.B. and Gubbins K.E. (1994) In: *Characterization of Porous Solids III* (J. Rouquerol, F. Rodriguez-Reinoso, K.S.W. Sing and K.K. Unger, eds) Elsevier, Amsterdam, p. 41.

Bansal R.C., Donnet J.B. and Stoeckli H.F. (1988) In: *Active Carbon*, Marcel Dekker, New York, p. 139.

Brunauer S. (1970) In: *Surface Area Determination* (D.H. Everett and R.H. Ottewill, eds) Butterworths, London, p. 63.

Carrott P.J.M. and Sing K.S.W. (1988) In: *Characterization of Porous Solids I* (K.K. Unger, J. Rouquerol, K.S.W. Sing and H. Kral, eds) Elsevier, Amsterdam, p. 77.

Carrott P.J.M., Roberts R.A. and Sing K.S.W. (1987) *Chem. Ind.* 855.

Carrott P.J.M., Roberts R.A. and Sing K.S.W. (1988) In: *Characterization of Porous Solids I* (K.K. Unger, J. Rouquerol, K.S.W. Sing and H. Kral, eds) Elsevier, Amsterdam, p. 89.

Carrott P.J.M., Drummond F.C., Kenny M.B., Roberts R.A. and Sing K.S.W. (1989) *Colloids and Surfaces*, **37**, 1.

Cheng L.S. and Yang R.T. (1995) *Adsorption* **1**, 187.

Conner W.C. (1997) In: *Physical Adsorption: Experiment, Theory and Applications* (J. Fraissard and W.C. Conner, eds) Kluwer, Dordrecht, p. 33.
Cracknell R.F., Gubbins K.E., Maddox M.W. and Nicholson D. (1995) *Accounts Chem Res.* **28**, 281.
Davis M.E., Montes C., Hathaway P.E., Arhancet J.P., Hasha D.L. and Garces J. E. (1989) *J. Am. Chem. Soc.* **111**, 3919.
Denoyel R., Fernandez-Colinas F., Grillet Y. and Rouquerol J. (1993) *Langmuir* **9**, p. 515.
Dubinin M.M. (1970) In: *Surface Area Determination* (D.H. Everett and R.H. Ottewill, eds) Butterworths, London, p. 123.
Dubinin M.M. (1975) In: *Progress in Surface and Membrane Science* vol. 9 (D.A. Cadenhead, ed.) Academic Press, New York, p. 1.
Dubinin M.M. (1979) In: *Characterisation of Porous Solids* (S.J. Gregg, K.S.W. Sing and H.F. Stoeckli, eds) *Society of Chemical Industry*, London, p. 1.
Dubinin M.M. and Stoeckli H.F. (1980) *J. Colloid Interface Sci.* **75**, 34.
Everett D.H. and Powl, J.C. (1976) *J. Chem. Soc. Faraday Trans. I* **72**, 619.
Fernandez-Colinas J., Denoyel R., Grillet Y., Rouquerol F. and Rouquerol J. (1989) *Langmuir* **5**, 1205.
Gonzalez M.T., Rodriguez-Reinoso F., Garcia A.N., Marcilla A. (1997) *Carbon* **35**, 8.
Gregg S.J. and Langford J.F (1969) *Trans. Faraday Soc.* **65**, 1394.
Gregg S.J. and Sing K.S.W. (1976) In: *Surface and Colloid Science*, Vol 9 (E. Matijevic, ed.) Wiley, New York, p. 336.
Gubbins K.E. (1997) In: *Physical Adsorption: Experiment, Theory and Applications* (J. Fraissard and C.W. Conner, eds) Kluwer, Dordrecht, p. 65.
Hill T.L. (1952) *Adv. Catalysis IV* 236.
Horvath G. and Kawazoe K. (1983) *J. Chem. Eng. Japan* **16**, 470.
Horvath, G. and Suzuki, M. (1997), In: *Physical Adsorption: Experiment, Theory and Applications* (J. Fraissard and C.W. Conner, eds) Kluwer, Dordrecht, p. 133.
Kaganer M.G. (1959) *Zhur. Fiz. Khim.* **33**, 2202.
Kaneko, K. (1996), In: *Adsorption on New and Modified Inorganic Sorbents* (Dabrowski A. and V.A. Tertykh, eds) Elsevier, Amsterdam, p. 573.
Kaneko K., Cracknell R.F. and Nicholson D. (1994) *Langmuir*, **10**, 4606.
Kenny M.B., Sing K.S.W. and Theocharis C. (1993) In: *Proc. 4th Int. Conf. on Fundamentals of Adsorption* (M. Suzuki, ed.) Kodansha, Tokyo, p. 323.
Lastoskie C., Gubbins K.E. and Quirke N. (1993) *J. Phys. Chem.* **97**, 4786.
Lecloux A. and Pirard J.P. (1979), *J. Colloid Interface Sci.* **70**, 265.
Lippens, B.C. and de Boer, J.H. (1965) *J. Catalysis* **4**, 319.
Lopez-Ramon M.V., Jagiello J., Bandosz T.J. and Seaton N.A. (1997) *Langmuir* **13**, 4435.
Maglara E., Pullen A., Sullivan D., Conner W.C. (1997) *Langmuir* **10**, 11.
Martin-Martinez J.M., Rodriguez-Reinoso F., Molina-Sabio M. and McEnaney B. (1986) *Carbon* **24**, 255.
McEnaney B. and Mays T.J. (1991) In: *Characterization of Porous Solids II* (F. Rodriguez-Reinoso, J. Rouquerol, K.S.W. Sing and K.K. Unger, eds) Elsevier, Amsterdam, p. 477.
Mikhail R. Sh., Brunauer S. and Bodor E.E. (1968) *J. Colloid Interface Sci.* **26**, 45.
Nicholson D. (1996) *J. Chem. Soc., Faraday Trans* **92**, 1.
Nicholson D. (1997) In: *Physical Adsorption: Experiment, Theory and Applications* (J. Fraissard and C.W. Conner, eds) Kluwer, Dordrecht, p. 105.
Olivier J.P. (1995) *J. Porous Materials.* **2**, 9.
Rodriguez-Reinoso F., Molina Sabio M., Gonzalez M.T. (1997) *Langmuir* **13**, 8.
Rowlinson J.S. (1985) *Proc. Roy. Soc. A.* **402**, 67.
Saito A. and Foley H.C. (1991) *AIChEJ* **37**, 429.
Seaton N.A., Walton J.P.R.B. and Quirke N. (1989) *Carbon* **27**, 853.
Steele W.A. (1973) *Surface Sci.* **36**, 317.
Steele W.A. (1974) *The interaction of gases with solid surfaces*, Pergamon, Oxford, p. 14.
Steele W.A. and Bojan M. J. (1997) In: *Characterization of Porous Solids IV* (B. McEnaney, T.J. Mays, J. Rouquerol, F. Rodriguez-Reinoso, K.S.W. Sing and K.K. Unger, eds) The Royal Society of Chemistry, Cambridge, p. 49.

Stoeckli H.F. (1977) *J. Colloid Interface Sci.* **59**, 184.
Stoeckli F. (1993) *Adsorption Sci. Tech.* **10**, 3.
Stoeckli H.F. and Ballerini L. (1991) *Fuel* **70**, 557.
Stoeckli H.F. and Huguenin D. (1992) *J. Chem. Soc., Faraday Trans.* **88**(5), 737.
Stoeckli H.F., Houriet J.Ph., Perret A. and Huber U. (1979) In: *Characterisation of Porous Solids* (S.J. Gregg, K.S.W. Sing and H.F. Stoeckli, eds) *Society of Chemical Industry*, London, p. 31.
Stoeckli H.F., Centeno T.A., Fuertes A.B. and Muniz J. (1996) *Carbon* **34**, 10.
Venero A. F. and Chiou J. N. (1988) *M.R.S. Symp. Proc.* **111**, 235.
Walton J.P.R.B. and Quirke N. (1989) *Mol. Simul.* **2**, 361.

CHAPTER 9

Adsorption by Active Carbons

9.1. Introduction

There is no precise definition of an 'active carbon', but it is generally understood to be a carbonaceous material of appreciable specific surface area. If it is to be an effective adsorbent, an active carbon must have a surface area of at least 5 $m^2 g^{-1}$. Active carbons used as industrial adsorbents have much larger BET-areas, which may extend well above 2000 $m^2 g^{-1}$. In accordance with this broad definition, an active carbon may be porous or non-porous. The term 'activated carbon' has a more specific connotation, however, since it is reserved for a highly porous carbon produced from a carbon-rich material by some form of chemical or physical activation.

There are three main crystalline forms of carbon with well-defined lattice parameters (i.e. having long-range order): graphite, diamond and the fullerenes. Graphite is the stable form at ambient temperature and pressure. Its normal structure is shown in Figure 9.1.

The basal plane of graphite is made up of benzene-like hexagonal nets of carbon atoms. In the normal α (or hexagonal) graphite the layers are arranged in the sequence –ABAB–, whereas in β (or rhombohedral) graphite the stacking sequence is –ABCABC–. In both forms, the carbon–carbon distance within the basal plane is 0.142 nm and the interplanar spacing is 0.335 nm.

In graphite, three of the outer electrons of the C atom hybridize to form localized

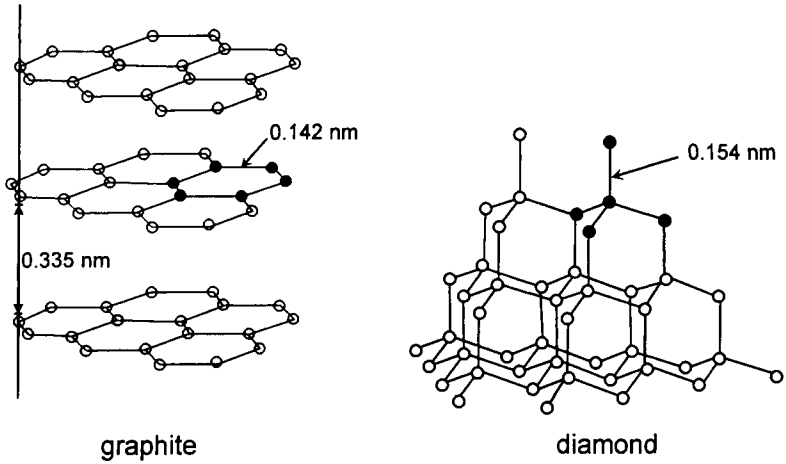

Figure 9.1. Structure of hexagonal graphite and of diamond. Centre of carbon atoms denoted by open or black circles. Black circles show basic hexagonal ring and tetrahedron.

sp^2 bonds (i.e. three trigonal σ–sp^2 planar orbitals), while the remaining electrons are delocalized in the form of π molecular orbitals. This arrangement accounts for the strong directional dependence of the electrical and thermal conductivity of graphite and also for its high thermal stability.

In diamond, each carbon atom is tetrahedrally surrounded by four equidistant neighbours (see Figure 9.1). In this case, the C–C distance is 0.154 nm and four interlinked tetrahedra make up the cubic unit cell of eight carbon atoms. The tetrahedral bond symmetry is the result of sp^3 hybridization. Diamond is an extremely poor conductor of electricity since the energy of the empty conduction band lies considerably above the filled valence band.

The fullerenes are composed of five- and six-membered rings and their structures and electronic properties are quite distinctive. Thus, the aromatic character of the graphitic basal plane is modified by a reduction in the degree of π bonding and an increase in the σ character. The consequential curvature of the carbon layers therefore allows the formation of C_{60} and other giant molecules including the carbon nanotubes (see Chapter 12).

Many different forms of active carbon exhibit short-range order. In the context of adsorption, the most important are carbon blacks, which are essentially non-porous, and a wide range of activated carbons, which are all porous.

Carbon blacks can be obtained by the controlled pyrolysis or combustion of a variety of organic precursors (solids, liquids and gases). They are composed of discrete or aggregated spheroidal particles, generally within the size range of 10–1000 nm. The carbon atoms are arranged in localized graphitic layers (graphene layers). These layers are disordered in the centre of the particles, but tend to lie parallel to the particle surface.

Carbon blacks are strong absorbers of light over the entire spectrum and are the

preferred black pigments and fillers in printing inks, paints, plastics and pneumatic tyres. These applications are dependent on the control of the surface chemistry, particle size and aggregate structure. Interaction of the particle surface with a dispersion medium involves adsorption at the solid–liquid interface, which in turn affects the dispersibility and stability of the dispersion. In this respect changes in the surface chemistry can have a major effect on the performance of a carbon black. For example, a high concentration of chemisorbed oxygen renders the surface more hydrophilic and leads to improved dispersibility in an aqueous medium.

Progressive graphitization of a carbon black occurs as a result of heat treatment in an inert atmosphere. This change is of great importance for the study of mechanisms of adsorption. Because of the uniformity of their surface, graphitized blacks have been adopted as model adsorbents in many fundamental investigations of adsorption from both the gas phase and the liquid phase. Some technological grades of ungraphitized carbon blacks have BET areas of over 200 $m^2 g^{-1}$, but the surface areas of the graphitized materials are smaller (<100 $m^2 g^{-1}$). Special techniques have been used to prepare exfoliated graphites with surface areas of *c.* 20 $m^2 g^{-1}$ (Dash, 1975; Thomy and Duval, 1969).

Over a period of almost a century activated carbons have remained the most widely used of all the general-purpose industrial adsorbents. In 1995, the world annual production of activated carbons was estimated to be in the region of 400 000 tonnes, with consumption increasing at about 7% per annum (Derbyshire *et al.*, 1995). They are manufactured from a variety of precursors, but cheap and readily available materials such as wood, peat, coal and nut shells are still generally used for large-scale production (Baker, 1992).

Activated charcoal was originally regarded as a relatively inexpensive adsorbent with an assortment of pores of ill-defined size and shape. However, in recent years considerable progress has been made in the development of tailor-made porous carbons such as molecular sieves, activated carbon fibres and carbon composites (Marsh *et al.*, 1997). Superactive carbons are now made on a commercial scale with BET areas of around 3000 $m^2 g^{-1}$. Activated carbons can be manufactured as fine particles or granules or in the form of a cloth, felt or consolidated membrane. The properties of some of these special types of activated carbon are discussed in Chapter 12.

Optimization of the pore size distribution is important for the control of both the equilibria and the dynamics of physisorption (see Ruthven, 1984; Do *et al.*, 1993). Most activated carbons are highly microporous, but for some purposes it is desirable to extend the range of pore size into the mesopore or macropore range – or even eliminate the microporosity. Progress in this direction has been made by the use of special pre-treatment procedures and the careful control of the conditions of carbonization and activation. In this connection, physisorption measurements have an important role to play in characterizing the material at various stages of manufacture.

In view of the commercial importance of active carbons, it is not surprising that a great deal of attention has been given to the presentation and interpretation of adsorption data. Much of the discussion in the literature has been concerned with the derivation of the internal and external surface area and the micropore and mesopore size

distribution. It would be impossible to review all of this work in a single chapter; indeed, it is doubtful whether such a task would be worthwhile. As in the other chapters of this book, our approach is essentially a pragmatic one in order to arrive at useful procedures for the analysis of adsorption isotherm and calorimetric data. However, since the behaviour of an adsorbent is dependent on its structure and surface chemistry, it is appropriate to include a brief account of the physical and chemical properties of the various forms of active carbon. It is also pertinent to comment on the changes which occur as a result of carbonization and activation.

9.2. Formation and Structure of Carbon Blacks

Various manufacturing processes are employed for the production of different grades of carbon black (Medalia and Rivin, 1976). The most important is the oil furnace process, in which petroleum residue is subjected to partial combustion and cracking in a refractory furnace. Colloidal carbon is produced in the form of a hot smoke of small globular particles, which on cooling undergo aggregation to give branched chain-like structures.

Globular particles of relatively large size (≈200 nm) and low specific surface area ($\approx 10\ m^2\ g^{-1}$) can be produced by the thermal process, which involves the thermal cracking of natural gas. The thermal blacks (e.g. Sterling FT) have lower ash content than the furnace blacks; for this reason, and because of the discrete nature of their primary particles, they are favoured for adsorption studies.

Although the mechanisms of carbon black formation and particle growth are still not entirely clear, it now seems likely that polyaromatic hydrocarbons are the most important precursors (Lahaye and Ehrburger-Dolle, 1993). However, it appears that only about 10% of the final mass is deposited during the initial stages of particle nucleation. Most of the carbon yield is due to particle growth and this is probably dependent on both particle–particle and particle–vapour interactions, with acetylene and other unsaturated hydrocarbons involved in the surface reactions.

By applying the newer techniques of scanning tunnelling microscopy (STM) and atomic force microscopy (AFM), along with X-ray diffraction, transmission electron microscopy (TEM), inverse gas chromatography (IGC) and Raman spectroscopy, it is possible to gain a more detailed picture of the particles and their surface structure than has been possible hitherto. For example, the work of Donnet and Custodero (1993) has indicated that the carbon black surface is not atomically smooth, but is instead made up of overlapping 'quasi-graphitic scales' (Donnet, 1994). The scale formation appears to be consistent with the surface growth mechanism as envisaged by Lahaye and Ehrburger-Dolle (1993).

Other recent work (Hess and Herd, 1993) on the microstructure of carbon blacks has confirmed earlier findings (Medalia and Rivin, 1976) that the particles of some partially graphitized blacks are composed of hollow graphitic shells. Thus, voids are formed in the interior of the particles and agglomerates as a result of localized densification.

It was shown by Schaeffer *et al.* in 1953 that the degree of graphitization was a function of the temperature of heat treatment and also depended on the nature of the

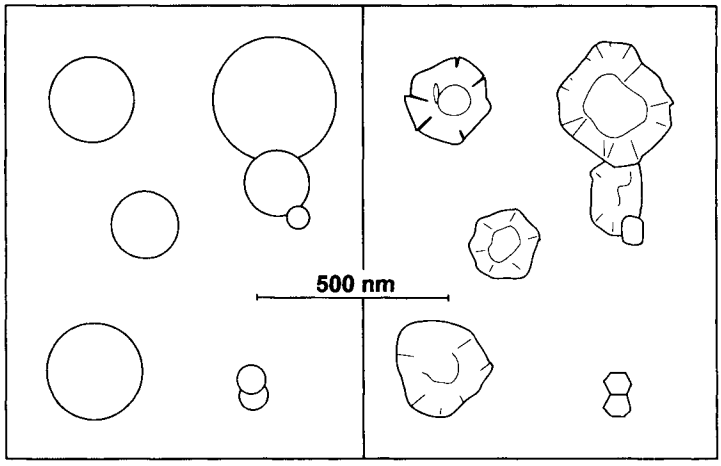

Figure 9.2. Particles of a medium thermal black (Sterling MT) before (left) and after (right) graphitization at 3000°C.

original black. The relatively large particles in the thermal blacks are converted into relatively well-defined polyhedra, as illustrated in Figure 9.2. In this case, a high proportion of the resultant surface is in the form of the graphitic basal planes.

It has been known for some time that Raman spectroscopy can be used to characterize the size of crystalline domains in graphite. Gruber *et al.* (1994) have found that the study of Raman intensities can also give a clearer understanding of the changes which accompany graphitization. It now seems that the microcrystallite growth is mainly due to the rearrangement of existing layer planes and that crystallization of amorphous carbon is of secondary importance.

Graphitization brings about a much greater reduction in the overall reactivity of a carbon black than would be expected from the decrease in surface area. Oxygen, hydrogen, chlorine and other reactive gases are strongly chemisorbed on edge or defect sites. It is of importance that this initial stage of chemisorption can lead indirectly to attack of the basal plane (Thomas,1965).

It is well known that the surface properties of carbon blacks are to a great extent influenced by the presence of surface oxides and oxygen-containing groups (Medalia and Rivin, 1976). The acidity of aqueous dispersions of carbon blacks is dependent on their oxygen content; this has been attributed to the presence of carboxyl and other functional groups such as lactols and phenols (Boehm, 1966, 1994). Carbon blacks with low oxygen contents generally exhibit basic properties. This behaviour is to some extent associated with the basic character of the aromatic ring structure.

Most carbon blacks have a low affinity for water, i.e. they are hydrophobic. However, the level of hydrophobicity is reduced by the presence of chemisorbed oxygen and certain functional groups (Walker and Janov, 1968; Bradley *et al.*, 1995). The relative extents of the polar and hydrophobic areas of carbon blacks have been studied by various methods (Boehm, 1994), including energy of immersion measurements (Barton and Harrison, 1975) and by liquid flow calorimetry (Groszek,

1970). These procedures make use of the differences between (a) the strong specific interactions given by certain polar molecules (e.g. *n*-butanol) with polar surface sites and (b) the non-specific interactions given by the adsorption of hydrocarbon molecules (e.g. n-$C_{32}H_{66}$) on the graphitic basal plane.

9.3. Physisorption of Gases by Carbon Black and Graphite

9.3.1. Adsorption of nitrogen

Because of their globular shape, carbon black particles were used in some of the earliest attempts to validate the BET method (Emmett and DeWitt, 1941). Comparison of the values of surface area obtained by nitrogen adsorption and electron microscopy appeared to provide sound evidence for the validity of the BET areas (Brunauer, 1945; Gregg and Sing, 1982, p. 64). However, in the light of more recent work (Sing, 1994), it seems likely that the excellent agreement obtained in the early measurements may have been to some extent fortuitous.

Many of the original adsorption studies were undertaken on Spheron 6, a channel black having a BET-nitrogen area of *c.* 120 $m^2 g^{-1}$. Graphon, the graphitized form of this material (prepared by heat treatment at 2700°C), has a BET-nitrogen area of *c.* 90 $m^2 g^{-1}$. In particular, Graphon was used in some of the first systematic calorimetric measurements of the energetics of physisorption on graphitized carbons (see Holmes, 1966).

Spheron 6 is now known to be made up of clusters (i.e. agglomerates) of strongly bonded particles (see Figure 9.2). Its surface is energetically heterogeneous and there is an indication that it may be slightly microporous (Carrott *et al.*, 1987). It is not surprising that Graphon has been found to exhibit some surface heterogeneity, with a small proportion of high-energy sites. On the other hand, graphitized Sterling FT appears to be almost entirely free of surface irregularities and strong adsorption sites (see Parkyns and Sing, 1975).

In the work of Isirikyan and Kiselev (1961), adsorption isotherms of nitrogen were determined at 77 K in considerable detail on four different graphitized thermal blacks (with BET areas in the range 6.5–29.1 $m^2 g^{-1}$). The isotherms are plotted in Figure 9.3 in a normalized form, as the amount adsorbed per unit area (in $\mu mol\ m^{-2}$) against the relative pressure, $p/p°$. Kiselev and his co-workers referred to such isotherm plots as 'absolute adsorption isotherms', but of course they are not strictly absolute since they are dependent on the validity of the BET-nitrogen areas – with the usual assumption that $\sigma(N_2) = 0.162\ nm^2$.

Inspection of the common normalized isotherm in Figure 9.3 reveals a number of distinctive features. At very low $p/p°$, the isotherm is slightly convex with respect to the $p/p°$ axis and it is evident that the linear, Henry's law region does not extend above $p/p° \approx 5 \times 10^{-4}$. Although the isotherm is not truly stepwise (i.e. not a true Type VI isotherm), it does exhibit a characteristic monolayer step. This is followed by a wavy second layer region and then a smooth multilayer curve. Thus, as the multilayer coverage is increased, the isotherm appears to conform to the normal Type II shape.

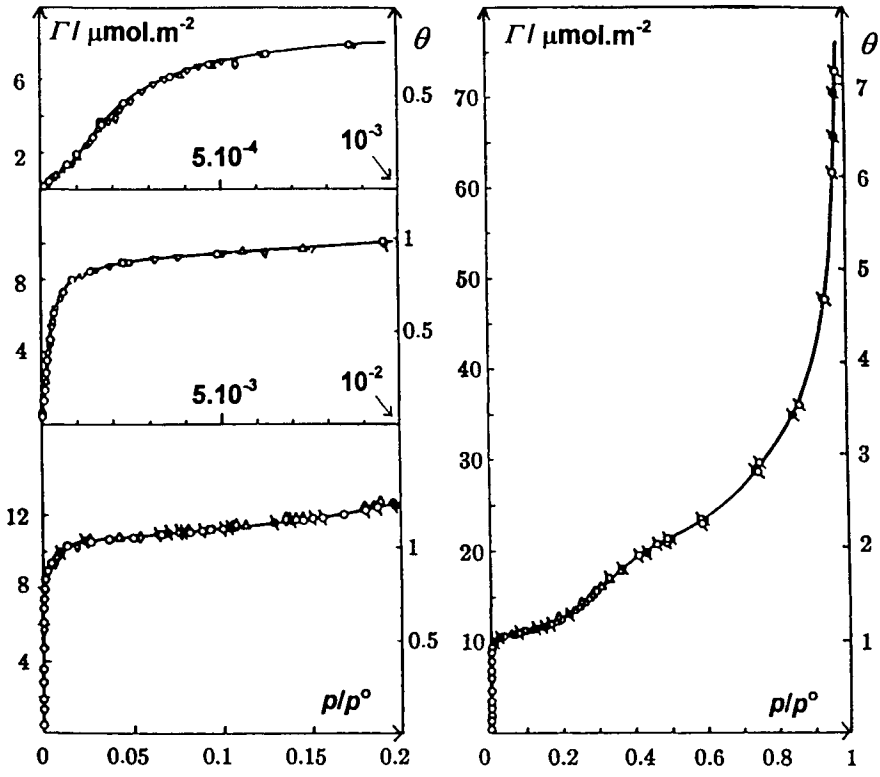

Figure 9.3. Adsorption isotherm of N_2 at 77 K on size different graphitized thermal blacks, at various scales of $p/p°$ (after Isirikyan and Kiselev, 1961).

The effect of graphitization on the shape of the nitrogen isotherm is revealed in Figure 9.4a. Here, isotherms on a number of graphitized and ungraphitized carbon blacks are plotted together in the reduced form of $n/n_{0.4}$ against $p/p°$, where $n_{0.4}$ is the amount adsorbed at $p/p° = 0.4$. It is apparent that all the isotherms follow a nearly common path over the multilayer range of $p/p° = 0.3 - 0.8$, but that only the ungraphitized blacks give completely smooth Type II isotherms.

A more rigorous test of the multilayer conformity is provided by linearizing the multilayer isotherms in the FHH coordinates. The Frenkel–Halsey–Hill (FHH) plots of the isotherms in Figure 9.4a are shown in Figure 9.4b. Here, several of the plots of $\log_{10}(n/n_{0.4})$ versus $\log_{10}[\log_{10}(p°/p)]$ are linear over a wide multilayer range, in accordance with the FHH equation,

$$\ln(p°/p) = k(n/n_{0.4})^s \tag{9.1}$$

where s is an empirical constant. From the slope of the linear section of the FHH plots we obtain $s = 2.70 \pm 0.05$.

Many attempts have been made to determine standard nitrogen isotherms on well-defined non-porous carbons, but it is evident that there is no single isotherm which

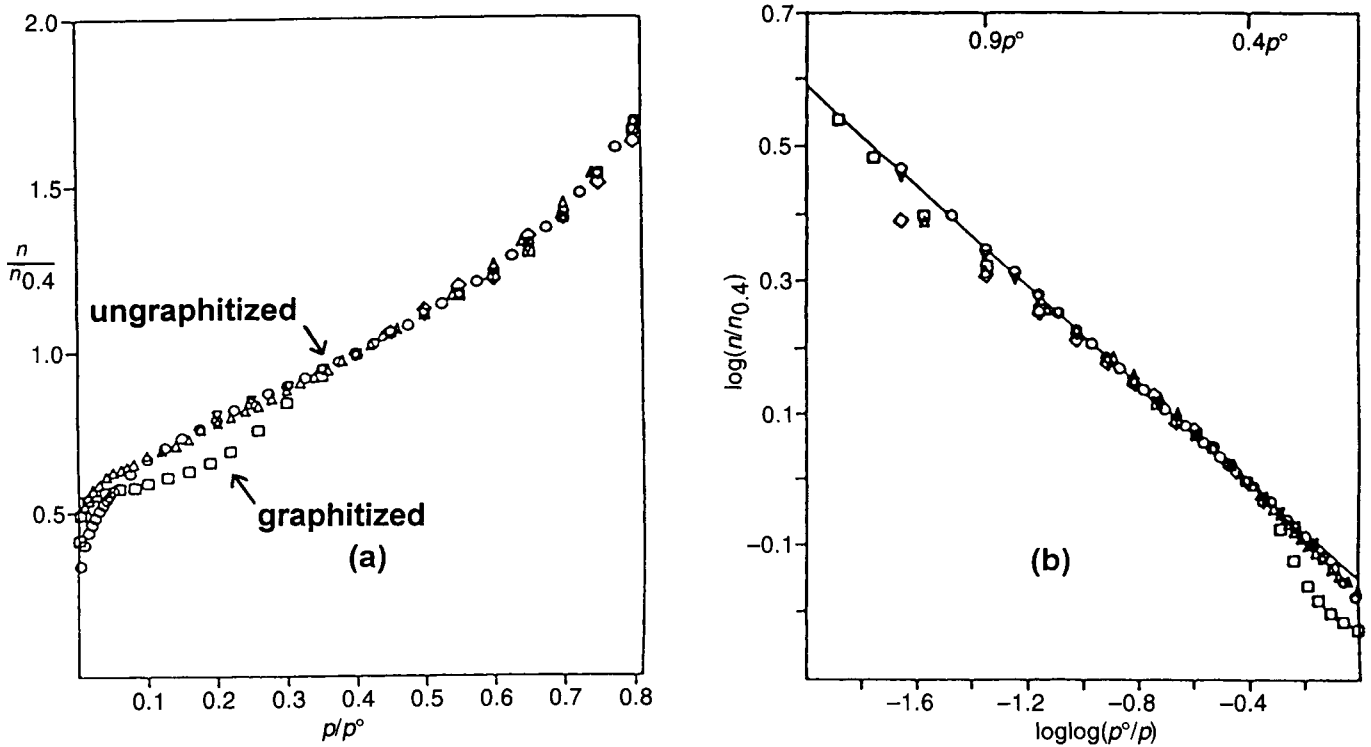

Figure 9.4. Standard nitrogen isotherms for carbons (a), and corresponding FHH plots (b) (circles, Carrott *et al.*, 1988a; diamonds, Voloshchuk *et al.*, 1988, squares, Isirikyan and Kiselev, 1961; triangles down, Pierce, 1968; triangles up, Rodriguez-Reinoso *et al.*, 1987). Reproduced from Carrott and Sing (1989).

could serve as standard for both graphitized and non-graphitized carbons. There are three main reasons why there are significant discrepancies between proposed standard data to be found in the literature. First, any significant differences in the graphitic surface structure will have some effect on the isotherm shape – especially at low surface coverage. Second, any interparticle capillary condensation will produce an upward deviation in the multilayer/capillary condensation region. Third, any microporosity will enhance the adsorption in the sub-monolayer region and will tend also to reduce the isotherm slope in the multilayer region.

As explained in Chapters 6 and 8, by applying the α_S-method we have a simple way of checking the validity of the BET area and detecting the presence of microporosity. Many carbon blacks have been found to be essentially non-microporous (Carrott *et al.*, 1987; Bradley *et al.*, 1995), in which case the corresponding values of BET area and α_S area are in good agreement. However, in a few cases the back-extrapolation of the α_S-plot has given a positive intercept on the adsorption axis which is an indication of some microporosity. The microporous nature of some carbon blacks has been confirmed in several recent investigations (Stoeckli *et al.*, 1994a; Kruk *et al.*, 1996). As one might expect, oxidation leads to a considerable increase in the level of the microporosity (Bradley *et al.*, 1995).

The strong energetic heterogeneity exhibited by Spheron 6 was first shown calorimetrically by Beebe and his co-workers (Beebe *et al.*, 1947; Kington *et al.*, 1950). This work also revealed that the surface of Graphon was much less heterogeneous than that of the original carbon black. The results of a more detailed investigation of the effect of thermal treatment of carbon black on the energetics of nitrogen adsorption (i.e. variation of $\Delta_{ads}h$ with coverage θ) are shown in Figure 9.5. Microcalorimetric measurements were undertaken on a sample of heat-treated Sterling FT-FF (i.e. a thermal black).

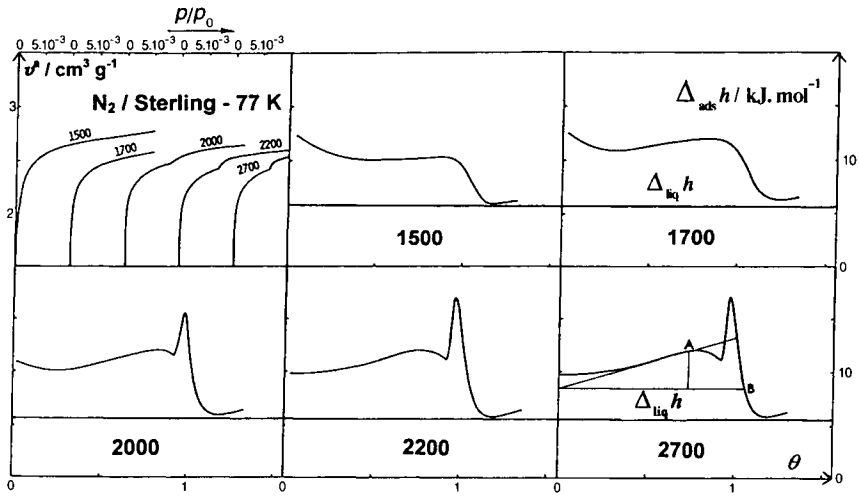

Figure 9.5. Differential enthalpies of N_2 adsorption at 77 K on heat-treated blacks (at temperatures from 1500 to 2700°C), as a function of coverage (Grillet *et al.*, 1979).

The interpretation of the microcalorimetric data in Figure 9.5 seems at first sight to be quite straightforward. Thus, heat treatment at temperatures >2000°C evidently removed much of the adsorbent–adsorbate heterogeneity since in the region of low θ the differential enthalpy underwent very little variation. This is, of course, consistent with the picture of the development of a uniform surface composed largely of the graphitic basal planes.

However, it is possible that this interpretation is somewhat oversimplified. The simulation study of the energetics of nitrogen adsorption on graphite by Steele and Bojan (1989) has indicated that there is a steady decrease in the adsorbent–adsorbate interaction with increase in surface coverage. This unexpected finding was attributed to a change in the orientation of the nitrogen molecules as a result of molecule–molecule interactions. Thus, as the surface population is increased, there is a greater probability that the adsorbed molecules will adopt a vertical orientation with respect to the basal plane. It follows that the almost constant adsorption energy observed experimentally is the result of compensation between an increase in adsorbate–adsorbate interactions and a decrease in the adsorbent–adsorbate interactions.

Turning now to the regions of high surface coverage in Figure 9.5, we note the appearance of two maxima in the differential enthalpy curves for the high-temperature graphitized Sterling. The first is a broad peak with a maximum attained at $\theta \approx 0.8$ and the second is a sharp peak in the vicinity of $\theta \approx 1$. The initial increase in $\Delta_{ads}\dot{h}$ can be attributed to the normal attractive interactions between neighbouring adsorbate molecules, whereas the second peak is the result of a two-dimensional phase transformation (Rouquerol *et al.*, 1977).

The use of the 'continuous quasi-equilibrium technique' (see Chapter 3) made it possible to determine the corresponding adsorption isotherm in sufficient detail to reveal the sub-step shown in Figure 9.5 and located at the same θ as the sharp calorimetric peak. The isotherm sub-step and associated calorimetric peak are evidently associated with an increase in packing density of the adsorbate. Rouquerol *et al.* (1977) and Grillet *et al.* (1979) concluded that these changes were due to a degenerated first-order transition from a hypercritical two-dimensional (2-D) fluid state to a 2-D localized state.

Many years ago, Isirikyan and Kiselev (1961) and Pierce and Ewing (1962, 1967) came to the conclusion that the nitrogen monolayer on graphite was localized at 77 K, the most favourable site being at the centre of the hexagon of carbons (see Figure 9.6). At that time, however, it was thought that because of its size and diatomic shape, each nitrogen molecule would demand the space provided by four hexagons. A simple calculation indicates that this is equivalent to a molecular area, σ (N_2), of 0.21 nm^2 for the completed monolayer. After making a detailed empirical analysis of the isotherms of nitrogen and other gases on Sterling MT (3100°C), Pierce and Ewing (1967) concluded that 0.194 nm^2 was a more realistic value for the effective area of nitrogen in the BET monolayer on graphitized carbons. This value was remarkably close to that (0.195 nm^2) proposed independently by Carrott *et al.*, (1987).

However, a number of other investigators have come to a different conclusion. They have proposed that a commensurate 'herringbone' structure could be adopted if

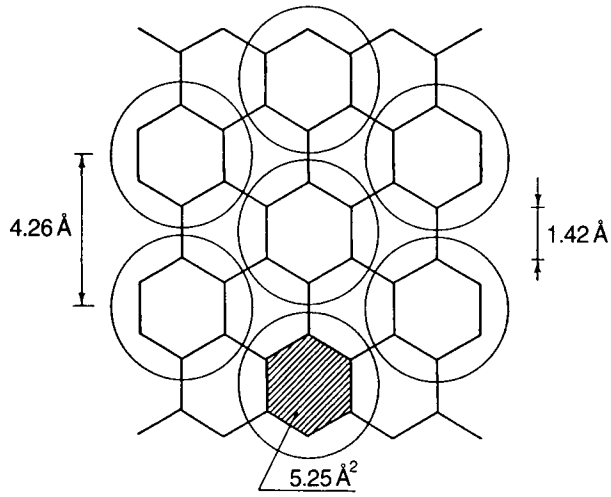

Figure 9.6. Localization of N_2 molecules on graphite (Rouquerol *et al.*, 1977).

the adsorbed nitrogen molecules occupied one in three of the neighbouring hexagonal sites (Rouquerol *et al.*, 1977; Bojan and Steele, 1987; Ismail, 1990). This arrangement, which is illustrated in Figure 9.6, would reduce the value of $\sigma_m(N_2)$ to 0.157 nm^2 and therefore the commensurate monolayer would have a packing density only slightly greater than that of the hypothetical close-packed 'liquid' monolayer. Since independent support for this state has been obtained by neutron diffraction and X-ray scattering (see Ismail,1992), this value would now seem to be the preferred one for the effective molecular area of nitrogen in the localized monolayer on the graphitic basal plane.

It is significant that the second calorimetric peak and the associated isotherm sub-step were detectable only if the graphitized thermal black had been heated at temperatures above 1700°C. These results suggest that the 2-D phase transformation is very sensitive to the perfection of the surface basal planes and this is a further indication that the phase change leads to the development of a commensurate structure.

9.3.2. Adsorption of noble gases

The stepwise character of the low-temperature isotherms of argon and krypton on graphitized carbon blacks was firmly established by the pioneering investigations of Beebe *et al.* (1953), Polley *et al.* (1953), Beebe and Young (1954), Beebe and Dell (1955) and Prenzlow and Halsey (1957). The early measurements revealed *inter alia* that argon isotherms at 77 K underwent a progressive change from Type II to Type VI as carbon blacks were heated at increasingly higher temperatures over the range 1000–2700°C.

The energetic heterogeneity of the original ungraphitized surface was revealed by the careful adsorption calorimetric measurements undertaken by Beebe *et al.*, (1953). By comparing the changes in the differential energies of adsorption for argon on Spheron and Graphon, these investigators found that the initial steep decline in 'differential heat of adsorption' was largely removed as a result of graphitization. Instead, an increase in the differential energy was observed at a higher surface coverage: it is now generally agreed that this was due to the adsorbate–adsorbate interaction becoming apparent as the degree of energetic heterogeneity was reduced.

A systematic study of krypton adsorption on exfoliated graphite was subsequently undertaken by Thomy and co-workers (Thomy and Duval, 1969; Thomy *et al.*, 1972). Their stepwise isotherm, determined at 77.3 K, is shown in Figure 4.1. The layer-by-layer nature of the physisorption process is clearly evident – at least up to four molecular layers. This isotherm shape is remarkably similar to that of the krypton isotherm on graphitized carbon black reported by Amberg *et al.*, (1955).

The work of Thomy and co-workers (Thomy and Duval, 1969; Thomy *et al.*, 1972) provided the first well-documented evidence for the presence of a sub-step in the krypton isotherm. The effect of temperature on the shape and the location of the sub-step is shown in Figure 9.7. The fact that the riser of the sub-step remained vertical over the temperature range of 77.3–96.3 K served to confirm that the sub-step was

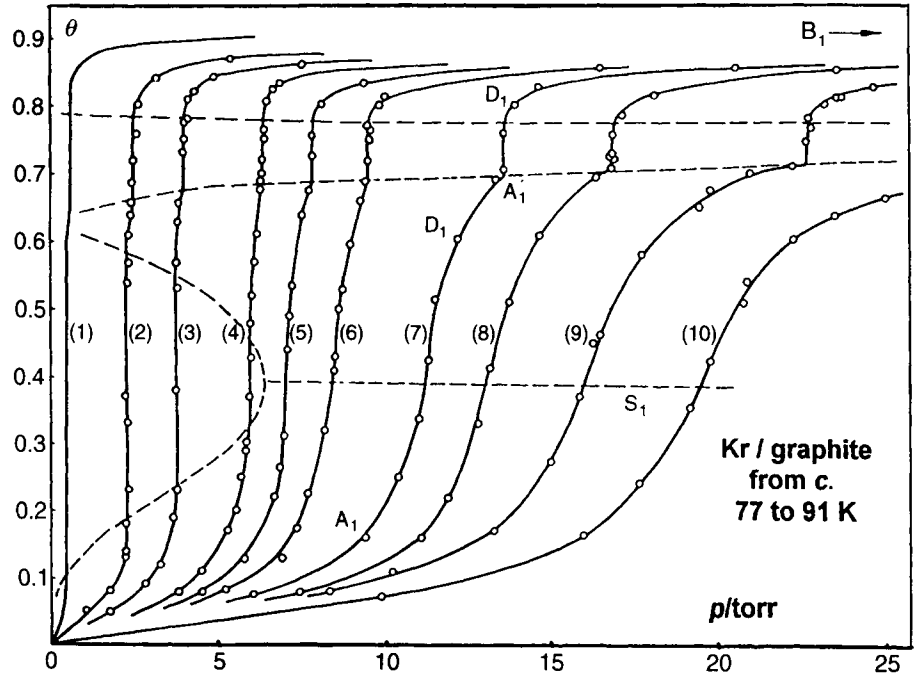

Figure 9.7. Adsorption isotherms of krypton on exfoliated graphite. Curves labelled from 1 to 10, obtained at 77.3, 82.4, 84.1, 85.7, 86.5, 87.1, 88.3, 89.0, 90.1 and 90.9 K, respectively (courtesy Thomy *et al.*, 1972).

due to a first-order two-dimensional phase change. It was thus evident that at a given temperature the two sub-monolayer phases were in thermodynamic equilibrium at a characteristic pressure, $p_{2\text{-D}}$. As discussed in Chapter 4, the 2-D phase diagram is then obtained as the plot of $p_{2\text{-D}}$ against T.

As already noted, adsorption microcalorimetry is one of the most useful techniques for studying 2-D phase changes. Tian–Calvet microcalorimetry was used to investigate the adsorption of argon on graphitized carbon black (Grillet *et al.*, 1979). As with nitrogen, the argon phase change was accompanied by a peak in $\Delta_{ads}\dot{h}$, but in this case on a smaller scale. The difference in the magnitude of the calorimetric peak was consistent with the lower height of the argon sub-step. Furthermore, the amounts adsorbed at 77 K were different, the monolayer of nitrogen being the more densely packed. It follows that, unlike nitrogen, the 2-D 'solid' argon was not in registry with the graphite structure.

According to Larher (1983), the behaviour of argon is also unlike that of krypton and xenon since its melting transition does not appear to be first-order at any recorded temperature. The differences in size and likely location of these three adsorbate molecules are illustrated in Figure 9.8 in relation to the graphitic basal plane. Here, a hypothetical commensurate hexagonal structure is shown in comparison with the dense 2-D (111) plane of the noble gases, Ar, Kr and Xe. It can be seen that the lattice mismatch is likely to be quite small for Kr and Xe, but significantly larger for

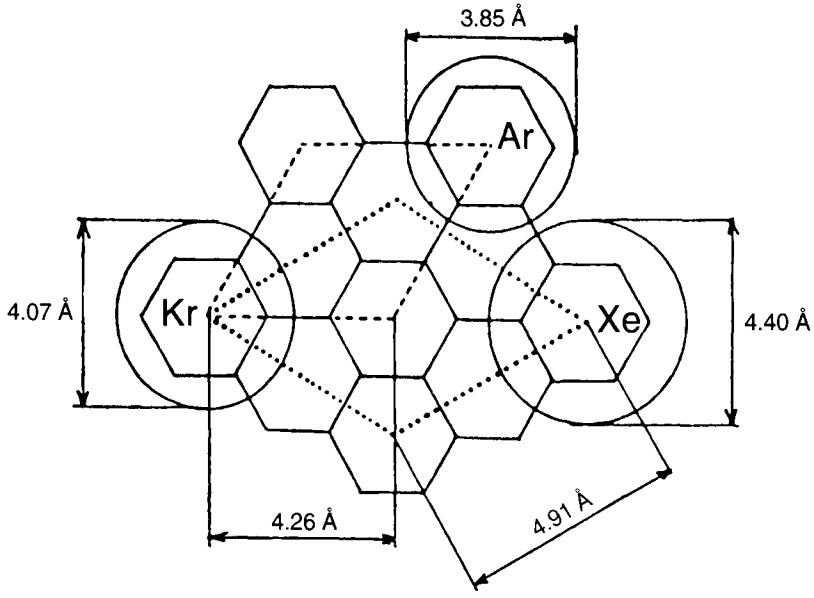

Figure 9.8. Possible structures for argon, krypton and xenon adsorbed in registry with graphite. Dotted unit cell: Xe linearly expanded by (4.91 – 4.40)/4.40 = 11.6%. Dashed unit cell: Xe linearly compressed by (4.40 – 4.26)/4.26 = 3.2%. Kr expanded by (4.26 – 4.07)/4.07 = 4.7% and Ar expanded by (4.26 – 3.85)/3.85 = 10.6% (reproduced courtesy of Larher, 1974).

Ar and evidently much larger for Ne. Therefore, we would expect Kr and Xe to undergo the commensurate–incommensurate phase changes more easily than Ar or Ne.

The 'best' value for the effective molecular cross-sectional area, σ(Kr), of krypton in the BET monolayer at 77 K has been under discussion for many years. In their original work on krypton adsorption, Beebe *et al.* (1945) recommended the value 0.195 nm^2 for σ(Kr) and this empirical value is still used by many investigators. For the adsorption of krypton on graphitized carbon, Ismail (1990, 1992) gives preference to the value σ(Kr) = 0.157 nm^2, which is fairly close to the values of molecular area calculated from the liquid density and determined by X-ray scattering. This, of course, implies that Kr and N_2 molecules undergo localized adsorption on the same sites. For ungraphitized carbons, Ismail (1992) recommends σ(Kr) = 0.214 nm^2.

It seems likely that the effective molecular area of krypton is dependent on the surface structure, but the extent of this variation is unknown. In practice, there is another problem which is encountered when the krypton-BET plot is not strictly linear (Malden and Marsh, 1959): the calculated value of n_m then varies according to where the tangent is drawn.

There is a similar difficulty in the selection of the effective molecular area with argon adsorption at 77 K on graphitized and ungraphitized carbon blacks. The results of a number of comparisons with nitrogen have led to recommended values of σ(Ar) in the range 0.130–0.165 nm^2 (Gregg and Sing, 1982, p. 75), but according to Ismail (1992) the most appropriate values are 0.138 and 0.157 nm^2 for graphitized and ungraphitized carbons, respectively.

As explained in Chapter 6, the evaluation of the BET monolayer capacity of either Kr or Ar at 77 K is dependent on the choice of $p°$ for the construction of the BET plot at 77 K, that is whether the saturation pressure of the stable 3-D solid, $p°$(sol), or the extrapolated liquid value, $p°$(liq), is used. Until recently, most workers have followed the early recommendation of Beebe *et al.* (1945) that the supercooled $p°$(liq) value should be adopted since many Type II isotherms of argon and krypton at 77 K appear to cut the $p°$(sol) axis at a sharp angle (Gregg and Sing, 1982, p. 74). However, Ismail (1990) has presented new evidence in favour of $p°$(sol). The case for $p°$(sol) is especially strong in relation to the adsorption of Kr on graphitized carbon since a liquid-type of multilayer seems unlikely to develop at 77 K after the formation of a 2-D 'solid' in registry with the basal plane. In our view the evidence for the more general use of $p°$(sol) is not entirely convincing and we consider that more work is required to settle this question.

9.3.3. Adsorption of organic vapours

At appropriately low temperatures, many organic molecules undergo localized adsorption on graphite. The mode of adsorption of small molecules (e.g. methane and ethane) is highly dependent on temperature, the monolayer becoming more mobile with increase in thermal energy.

The adsorption isotherm of methane at 77 K on exfoliated graphite is shown in Figure 9.9: the stepwise character is clearly very similar to that of krypton at 77 K

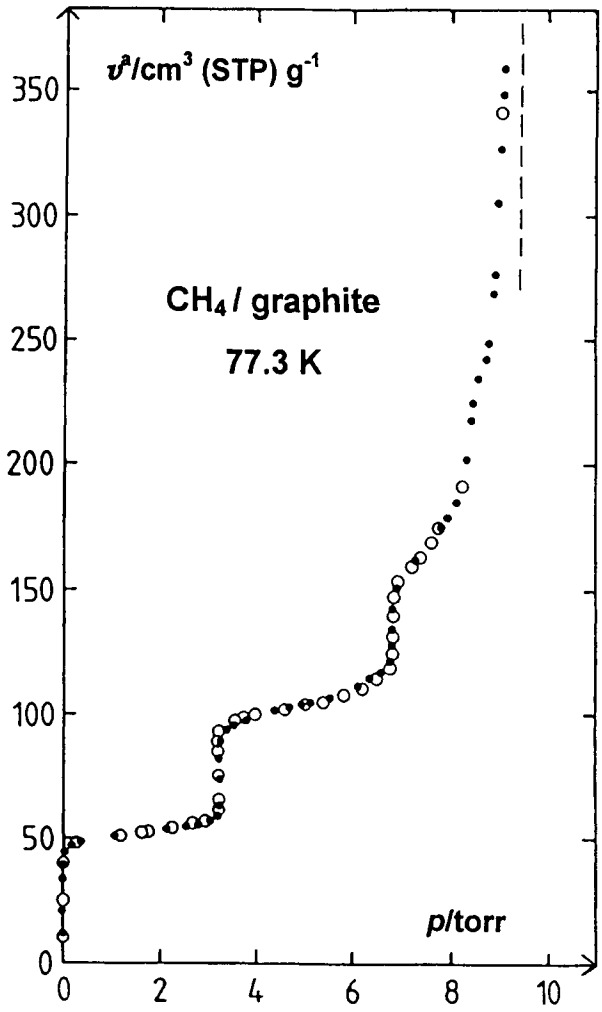

Figure 9.9. Stepwise isotherm of CH_4 on graphite foam (open circles) and exfoliated graphite (solid circles) at 77.3 K (reproduced courtesy of Bienfait *et al.*, 1990).

(see Figure 4.1). Stepwise isotherms are also given by ethane on graphite (Bienfait, 1985) and ethyl chloride on graphitized Sterling MT (Davis and Pierce, 1966). On the other hand, the isotherms of benzene and hexane at 293 K on graphitized Sterling MT are essentially Type II – although the hexane isotherm is similar to that of nitrogen in having a slight indication of a second-layer step. The isotherms of propane (at 196 K), isobutane (at 261 K) and neopentane (at 273 K) on graphitized carbon blacks are all typical Type II (Carrott and Sing, 1989).

We conclude that, provided the temperature is not too high, the simplest organic adsorptives can undergo stepwise adsorption on the graphitic basal plane to give well-defined Type VI isotherms. However, most organic adsorptives give Type II

isotherms with values of C (BET) tending to be high and therefore clearly marked monolayer capacities.

Sub-steps, similar to those in Figure 9.7, have been observed with both methane and ethane (Bienfait, 1980, 1985). It has been possible to construct 2-D phase diagrams for several of these systems (Gay *et al.*, 1986; Suzanne and Gay, 1996). LEED and neutron diffraction have provided information on the 2-D structures. For example, seven different 2-D phases have been reported for ethane on graphite over the temperature range 64–140 K. Thus, three 'solid' commensurate phases were identified at temperatures <85 K, the S_3 phase apparently having a close-packed hexagonal structure, with $\sigma(C_2H_6) = 0.157$ nm^2.

In the case of hexane on graphite, the adsorbate molecules appear to adopt an ordered herringbone structure at temperatures below 151 K, whereas a fluid-like phase is formed at higher temperatures (Krim *et al.*, 1985). Several investigators (e.g. Avgul and Kiselev, 1970; Clint, 1972; Gregg and Sing, 1982, p. 80) have concluded that long-chain alkane molecules tend to lie flat and parallel to the basal plane, which explains the constant incremental increase in adsorption energy and molecular area with chain length.

In their comparative study of the adsorption of *n*-hexane and benzene on graphitized thermal blacks, Isirikyan and Kiselev (1961) found a significant difference in the behaviour of the two adsorptives. This difference is illustrated in Figure 9.10, where the differential energies of adsorption are plotted against the surface coverage. In the case of benzene, the nearly constant adsorption energy over a wide range of coverage is a clear indication of a low level of lateral interaction between neighbouring adsorbate molecules. In contrast, the pronounced increase in hexane adsorption energy provides unambiguous evidence for the steady increase in adsorbate–adsorbate interaction as the monolayer becomes more densely populated.

As a result of their study of the adsorption of CH_2Cl_2 and C_6H_6 by various carbon blacks, Stoeckli *et al.* (1994a) have demonstrated the importance of using a number of adsorption and calorimetric techniques. This work has confirmed that the high surface area of some carbon blacks is not confined to the external surface. That particular blacks were to some extent microporous was revealed by immersion microcalorimetry, gas-phase microcalorimetry and by the form of their comparison and DR plots. These findings strengthen the view that the BET method cannot be relied upon to give an accurate evaluation of the surface area of carbon black.

9.4. Carbonization and Activation

Organic materials undergo pyrolytic decomposition when heated in an inert atmosphere. Polyaromatic ring structures are developed in the early stages of carbonization. As the heat-treatment temperature (HTT) is increased the solid char or coke begins to acquire short-range order with the formation of distorted graphitic lamellae. In addition, localized and anisotropic densification leads to the development of free space between the lamellae.

Wood and other naturally occurring precursors are composed of three-dimensional

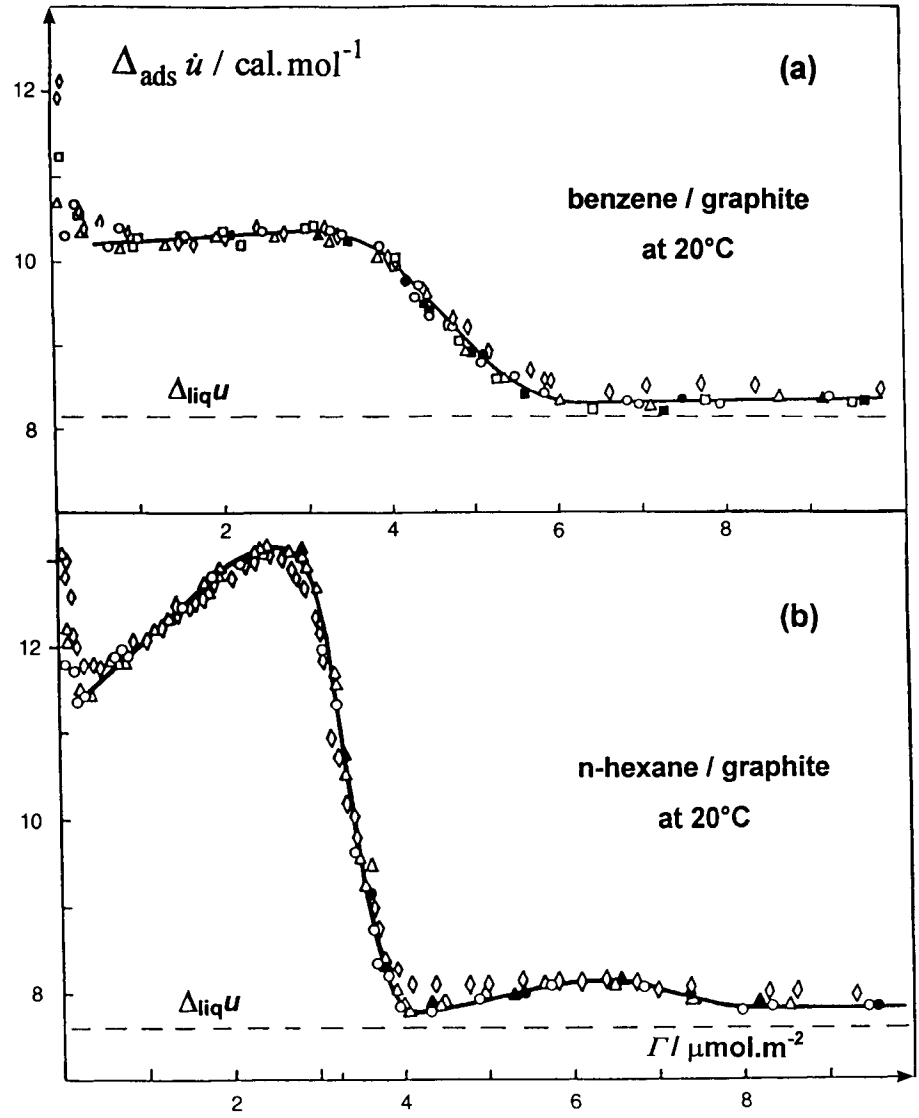

Figure 9.10. Differential energies of adsorption of benzene (top) and *n*-hexane (bottom) at 20°C on three different graphitized thermal blacks (after Isirikyan and Kiselev, 1961).

polymeric networks of cellulose and lignin. Pyrolysis at temperatures <700°C results in the loss of water, carbon dioxide and a wide range of organic molecules (e.g. alcohols, ketones, acids). There follows a progressive increase in the C/H and C/O ratios, but heteroatoms (O, H, Cl, N, S, etc.) remain chemically bonded at the edges of the aromatic macromolecules and these are finally transformed into surface complexes. Some of the purest chars are derived from sugars, regenerated cellulose and certain

synthetic polymers, but even these do not possess clean carbon surfaces unless they have been subjected to special treatment.

With the aid of high-resolution electron microscopy and other techniques, Oberlin and her co-workers have been able to follow the changes in microstructure which accompany carbonization (Bonijoly *et al.*, 1982; Rouzard and Oberlin, 1989). The basic structural units (BSU) were identified as small assemblages of the polyaromatic rings. Increase in HTT caused the BSU to form distorted stacks (or columns), but crystal growth of the long-range graphitic structure required the removal of various defects. The 'non-graphitizable' chars produced from sugar contained highly disordered stacks with defects in the form of functional groups firmly attached to the BSU. In contrast, the 'graphitizable coke' derived from anthracene appeared to undergo a progressive ordering of the BSU stacks with the formation of the long-range graphitic structure.

In a char which has been subjected to HTT of, say, 800–900°C the interstices between the BSU have the dimensions of narrow micropores, but generally they are not easily accessible to adsorptive molecules. 'Activation' of the char is undertaken to improve the accessibility of the pore structure and also, if required, to increase the pore width and pore volume.

Activation always involves some form of chemical attack. However, *chemical activation* is a term often used to indicate the prior impregnation of the precursor with a chemical agent such as phosphoric acid or zinc chloride before heat treatment. *Physical activation*, on the other hand, signifies the heat treatment of the char in a mildly reactive atmosphere such as steam or carbon dioxide. This type of process is preferably referred to as *thermal activation* (Baker, 1992). The apparent distinction between 'chemical' and 'physical' is somewhat unsatisfactory for two reasons: first, it implies a fundamental difference in the mechanism of activation; and second, it does not allow for the many procedures which involve both types of treatment.

The extent of the activation reaction is characterized by the *burn-off* as determined by the change in mass of the char, expressed as the percentage weight loss of the carbonized material as a result of HTT under controlled conditions. With some chars, the burn-off increases linearly with the time of HTT at a constant temperature. This form of linear dependence has been reported by Rodriguez-Reinoso (1986) for the activation of carbonized olive stones and almond shells in CO_2 at temperatures around 850°C. The extensive linear relationship was a clear indication that the reaction rate was almost constant over a very wide range of burn-off (i.e. 8–80%).

Activation in CO_2 is often used on a laboratory scale, but steam activation is generally favoured for the large-scale production of most activated carbons of industrial importance (Baker, 1992). The steam reaction is considerably faster than the carbon dioxide reaction (Wigmans, 1989). Steam activation is normally carried out at temperatures of 750–950°C. Direct contact between oxygen and carbon must be avoided since at these temperatures oxygen would aggressively attack the carbonized material.

Many investigations have been made of the surface chemistry of activated carbons (Bansal *et al.*, 1988, p. 29; Boehm, 1966, 1994; Mikhalovsky *et al.*, 1994). It is generally agreed that the presence of carbon–oxygen complexes have a great influence

on the chemical reactivity of an activated carbon. Surface functional groups such as carboxyls, phenols, aldehydes, ketones, lactones and quinones have been identified, but the overall surface composition is not easy to establish.

In spite of the experimental difficulty of using infrared spectroscopy to study the surface structure of carbon, IR spectroscopic measurements (especially in the form of Fourier transform IR, FTIR) have brought to light important information on the changes in surface chemistry produced by oxidation and substitution reactions. As a result of the systematic FTIR studies of Starsinic *et al.* (1983), van Driel (1983) and others (see Zawadzky, 1989; Boehm, 1994), considerable progress has been made in the assignment of IR bands.

It has been known for many years that activated carbons appear to exhibit both acidic and basic properties (Boehm, 1966; Puri, 1970; Bansal *et al.*, 1978a,b). The acidic properties have been attributed to the presence of phenolic and carboxylic acid groups (and possibly surface lactones), whereas the basic character has been more difficult to explain (see Bansal *et al.*, 1988, p. 102).

9.5. Physisorption of Gases by Activated Carbons

9.5.1. Adsorption of argon, nitrogen and carbon dioxide

Many investigators have used nitrogen adsorption at 77 K to study the porosity of activated carbons (e.g. see de Vooys, 1983; Fernandez-Colinas *et al.*, 1989a; Rodriguez-Reinoso *et al.*, 1989; Sing, 1989, 1995; Freeman and Sing, 1991; Bradley and Rand, 1995).

As explained in Chapter 7, since the *multilayer* isotherm path is rather insensitive to differences in surface chemistry, for routine mesopore analysis it is possible to make use of a 'universal' form of nitrogen isotherm. However, most activated carbons are highly microporous and the determination of the micropore size distribution remains a more difficult problem. Indeed, as discussed in Chapter 8, even the assessment of the total micropore volume presents conceptual difficulties. We should therefore regard the measurement of a nitrogen adsorption isotherm as only the first stage in the characterization of a microporous carbon.

Nitrogen isotherms on some activated carbons and the corresponding α_S-plots and Dubinin–Radushkevich (DR) plots are shown in Figure 9.11. The isotherms on Carbosieve and the carbon cloth JF005 are of well-defined Type I in the IUPAC classification, but the isotherms on the carbon cloth JF517 and the superactive carbon AX21 are evidently more complex.

The *multilayer* section of each α_S-plot in Figure 9.11b exhibits an appreciable range of linearity. By assuming that this linear section represents unrestricted multilayer adsorption on the external surface, we can arrive at an approximate estimate of the external area, a(ext). Thus, if the amounts adsorbed, v^σ, or v^a, are expressed in the units cm^3 (STP) g^{-1}, the values of a(ext) in Table 9.1 are obtained by application of the equation

$$a(\text{ext}) = 2.86v^\sigma/\alpha_S \tag{9.2}$$

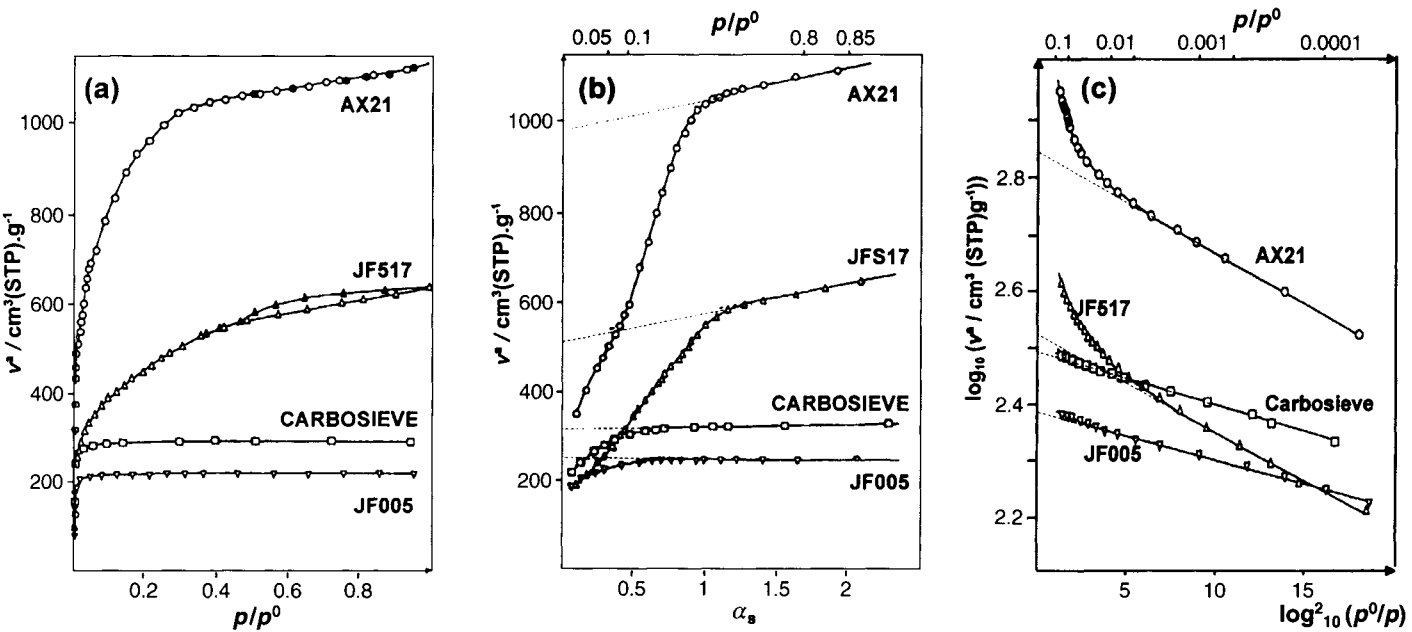

Figure 9.11. (a) Adsorption isotherms on microporous carbons (open symbols adsorption; solid symbols, desorption); (b) α_S-plots for microporous carbons; (c) DR plots for microporous carbons (after Carrott *et al.*, 1987).

Table 9.1. Surface areas and pore volumes of some microporous carbons (N_2)

Carbon	a(BET) ($m^2\,g^{-1}$)	a(ext) ($m^2\,g^{-1}$)	v_p(mic, S) ($cm^3\,g^{-1}$)	v_p(mic, D) ($cm^3\,g^{-1}$)
PX21	3700	178	1.75	0.99
AX21	3393	233	1.52	1.00
JF516	2053	246	0.98	
JF517	1657	218	0.76	0.47
JF142	1479	54	0.55	
Carbosieve	1179	41	0.43	0.45
JF005	882	19	0.33	0.35

where the factor 2.86 has been evaluated by calibration against the BET areas of several non-porous carbon blacks (Carrott *et al.*, 1987).

The values of a(BET) in Table 9.1 are the BET-nitrogen areas, which were derived from the linear regions of the BET plots, with the molecular area assumed to be 0.162 nm^2. The values of a(ext) in Table 9.1 are obviously much smaller than the corresponding values of a(BET). The question naturally arises: does the BET method provide a reliable assessment of the *total area* (i.e. internal plus the external area)? The non-linear character of the *low-pressure* region of each α_S-plot is a clear indication that the isotherm is distorted in the monolayer region and we may therefore conclude that a(BET) does *not* represent a real surface area. Additional support for this interpretation comes from the microcalorimetric data, which are discussed later in this section. More detailed discussion of some of the results in Table 9.1 is given in Chapter 12.

Backward extrapolation of the linear multilayer section of the α_S-plot allows us to assess the total micropore capacity (as indicated in Chapter 8) and hence to evaluate the *effective* micropore volume, v_p(mic, S). The values of v_p(mic, S) in Table 9.1 were obtained by making the usual assumption that the pores are filled with *liquid* nitrogen (density 0.808 g cm^{-3}).

The DR plots in Figure 9.9c are all linear at very low $p/p°$, but those for JF517 and AX21 show strong deviations at $p/p° > 0.01$. Nitrogen DR plots of similar appearance have been reported in other studies of activated carbons (e.g. Dubinin, 1966; Atkinson *et al.*, 1984; Rodriguez-Reinoso, 1989). According to the DR theory (see Section 4.4.4), the intercept of the linear plot should equal $\log_{10} v_p$(mic, D), where v_p^o(mic) is the volume of gas required to fill the micropores. The apparent micropore volumes, v_p(mic, D), in Table 9.1 are obtained from the values of v^o(mic, D) – again, by taking the liquid density.

Generally, long linear DR plots are given by carbons with narrow micropores; whereas the more restricted linearity is an indication of the presence of wider micropores and mesopores (Gregg and Sing, 1982, p. 223; Atkinson *et al.*, 1984). The wider micropores were designated 'supermicropores' by Dubinin (1975). It is evident that the corresponding values of v_p(mic, S) and v_p(mic, D) in Table 9.1 are in close agreement only if the supermicropores are absent. Similar results have been reported by Rodriguez-Reinoso (1989). Since the primary filling of the very narrow

micropores (i.e. the ultramicropores) occurs at very low $p/p°$, the change in amount adsorbed at $p/p° > 0.01$ is quite small (Atkinson *et al.*, 1987; Kenny *et al.*, 1993) and therefore it is not surprising to find that the DR plot is virtually linear over a fairly wide range of $p/p°$.

In some investigations (Fernandez-Colinas *et al.*, 1989a; Kakei *et al.*, 1991; Kenny *et al.*, 1993; Kaneko, 1996) it has been found that the shapes of high-resolution α_S-plots and DR plots provide strong evidence for a sequential filling of several groups of micropores. For example, the nitrogen isotherms in Figure 9.12a were determined on a series of activated pine wood charcoals (Fernandez-Colinas *et al.*, 1989a). The change in isotherm shape is the first indication that pore widening has occurred as a result of progressive activation in steam. The α_S-plots in Figure 9.12b confirm this interpretation and indicate that this was mainly due to the development of a supermicropore structure. It appears that the initial stage of primary micropore filling at very low $p/p°$ (i.e. $p/p° < 0.01$) was followed by the more gradual filling of supermicropores.

Surface coverage of the supermicropore walls is indicated by the appearance of a short linear section at $\alpha_S > 0.5$. Extrapolation of this section to $\alpha_S = 0$ provides an approximate evaluation of the *effective ultramicropore volume*, $v_p(u, mic)$.

The second linear section extends over the multilayer range of each α_S-plot in Figure 9.12b. Backward extrapolation of this branch gives the total effective micropore volume, $v_p(mic)$, from the intercept on the v^a axis. It follows that the effective supermicropore volume, $v_p(sup, mic)$, can be regarded as the difference $v_p(mic) - v_p(u, mic)$. It is of interest that after an initial small change in $v_p(u, mic)$, this has remained constant during further activation while the magnitude of $v_p(sup, mic)$ has increased steadily.

As discussed in Chapter 8, the pre-adsorption of *n*-nonane can be used as a means of blocking narrow micropore entrances (see Section 8.2.3). Thus, in the case of an ultramicroporous adsorbent such as Carbosieve, the pre-adsorption of nonane leads to complete blockage of the pore structure. The effect of progressively removing the pre-adsorbed nonane from a supermicroporous carbon is shown in Figure 9.13. The adsorbent used in this work was a well-characterized carbon cloth with the following properties: $a(BET)$, $1330\ m^2\ g^{-1}$; $a(ext)$, $25\ m^2\ g^{-1}$; $v_p(mic)$, $0.44\ cm^3\ g^{-1}$; w_p, 0.6–2.0 nm (Carrott *et al.*, 1989).

Inspection of the α_S-plots in Figure 9.13 is instructive. It can be seen that there are two linear sections, back-extrapolation of the first giving a zero intercept when part of the pre-adsorbed nonane was removed by prolonged outgassing at 50°C. We may conclude that the initial stage of nitrogen adsorption is by monolayer adsorption on the walls of the supermicropores. This is followed by the formation of a quasi-multilayer until pore filling is complete at $p/p° \approx 0.4$. Increase of outgassing temperature leads to the progressive removal of nonane from the ultramicropores and narrow entrances and the original nitrogen isotherm is restored after prolonged outgassing at 200°C. Thus, we may compare the change in the extent of total micropore capacity, $v_p(mic)$ (obtained as described earlier by back-extrapolation of the linear multilayer branch), with the magnitude of the restoration of the ultramicropore capacity, $v_p(u, mic)$ (as defined above). The fact that at each stage $v_p(mic) > v_p(u, mic)$ is a

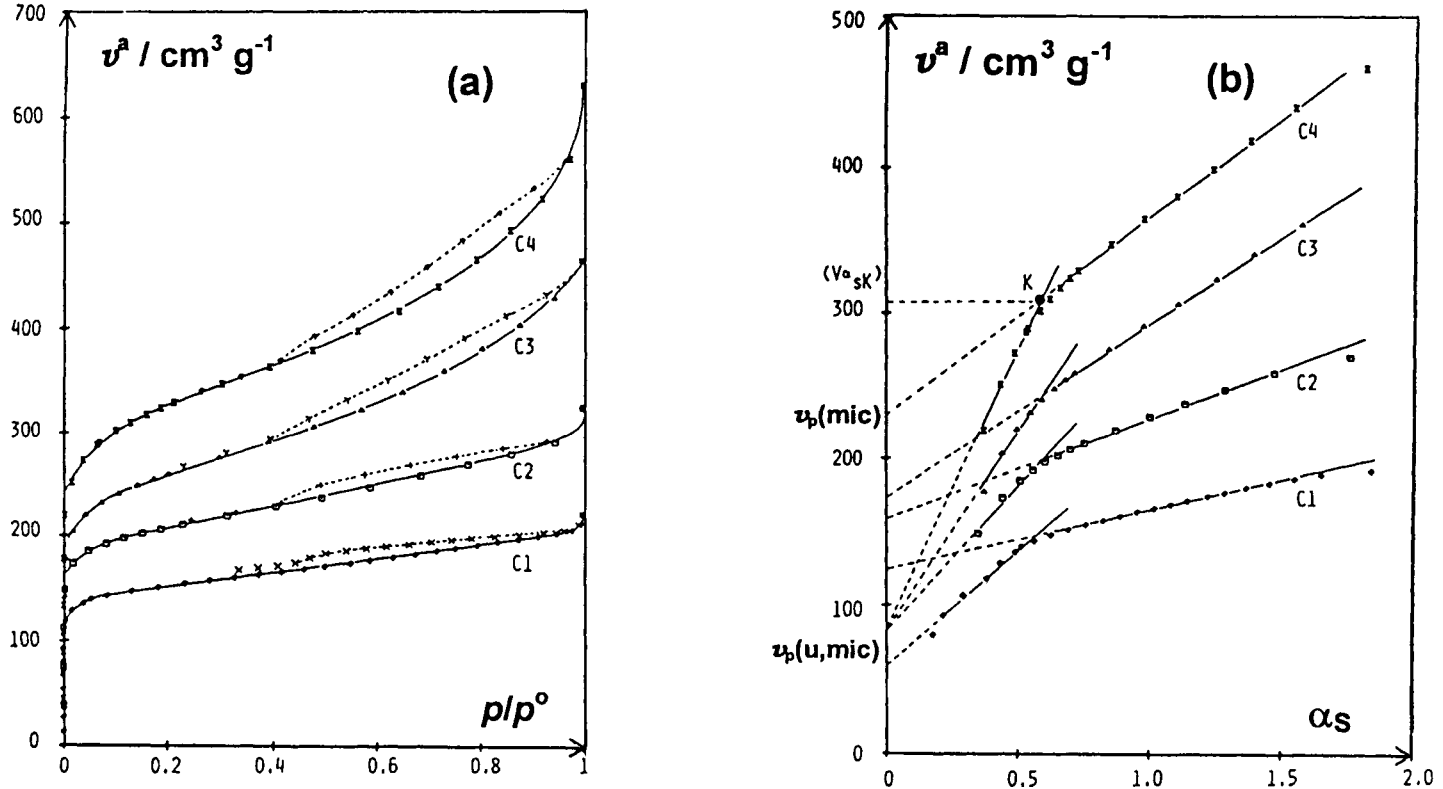

Figure 9.12. N_2 adsorption isotherms at 77 K (a) and corresponding α_S plots (b) on four activated carbons (Fernandez-Colinas *et al.*, 1989a).

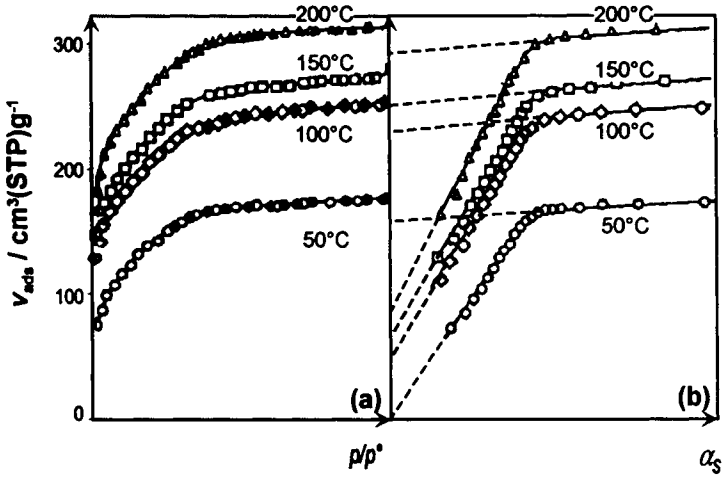

Figure 9.13. Nitrogen adsorption isotherms ar 77 K (a) and corresponding α_S plots (b) for charcoal cloth JF012 after pre-adsorption of nonane followed by outgassing at indicated temperature (after Carrott *et al.*, 1989).

clear indication that the pre-adsorption of nonane has resulted in the blockage of narrow entrances of some supermicropores.

A possible disadvantage of nitrogen is that, because of its diatomic molecular shape and quadrupolar nature, it is an unrepresentative adsorptive for the investigation of micropore filling. It is instructive therefore to compare the results of nitrogen and argon adsorption measurements on a series of activated carbons. For this purpose, adsorption microcalorimetry is an invaluable tool. Differential enthalpies of adsorption for argon and nitrogen are plotted in Figure 9.14 (i.e. $\Delta_{ads}\dot{h}$ versus θ) for two of the activated charcoals, C1 and C4, featured in Figure 9.12. As expected, over most of the micropore filling range, the nitrogen adsorption energies are appreciably above the corresponding argon energies. As discussed in Chapter 1, this difference is likely to be due to the specific field gradient–quadrupole interaction experienced by nitrogen. However, it is evident that with both C1 and C4 the corresponding adsorption energy curves have the same general appearance.

Inspection of the adsorption enthalpy curves for nitrogen in Figure 9.14 reveals that three characteristic stages of physisorption can be identified: Point A is at the end of the first plateau; Point B is at the beginning of a second, less well-defined, plateau; Point C is the point where the pore-filling curve crosses the corresponding curve for monolayer adsorption on ungraphitized carbon (Spheron 1500). We can attribute the high initial adsorption enthalpies ($\Delta_{ads}\dot{h} \approx 18$ kJ mol^{-1} for nitrogen and ≈ 16 kJ mol^{-1} for argon) to primary micropore filling within pores of molecular dimensions. This is followed by the transitional region AB and finally the mainly co-operative filling range of BC.

As pointed out in Chapter 1, high physisorption energies are produced by the overlap of the adsorbent–adsorbate interactions in pores of molecular dimensions (Everett and Powl, 1976). In the case of slit-shaped pores in carbons, a significant

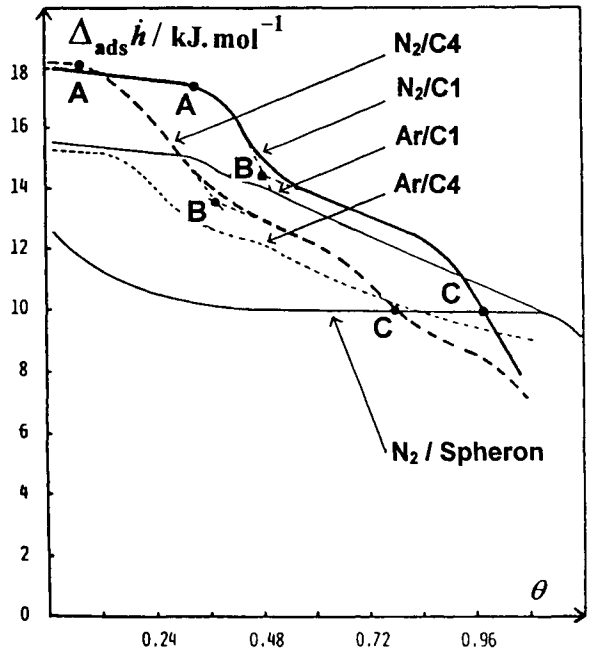

Figure 9.14. Differential enthalpies of adsorption of N_2 and Ar at 77 K on carbons C1 and C4 (same as in Figure 9.12) and on Spheron 1500 (Fernandez-Colinas *et al.*, 1989a).

enhancement of adsorption energy would be expected for an effective pore width, $w < 2d$ (d is the molecular diameter). A two-fold enhancement of adsorption energy would be the maximum expected for the entry of molecules in narrow slit-shaped pores. Such values are recorded in Table 1.3, but it is evident that the initial values in Figure 9.14 are at a somewhat lower level. These findings indicate that the narrowest pore width in the series of activated charcoals is probably in the region of 0.8 nm.

A detailed microcalorimetric study of the adsorption of argon and nitrogen by a selection of microporous carbons was reported by Atkinson *et al.* (1987). The differential enthalpies of adsorption are presented in two ways: in Figure 9.15a and 9.15b they are plotted in the usual manner, as a function of the fractional micropore filling, v/v_p(mic); and in Figures 9.16a and 9.16b they are plotted as a function of the equilibrium $p/p°$. The latter presentation is of particular interest since it reveals the considerable differences in the energetics of adsorption at low $p/p°$. As indicated in Chapter 3, Tian–Calvet microcalorimetry is the preferred technique for this type of investigation because the adsorption enthalpy measurements are made at a virtually constant temperature.

The nitrogen isotherms and corresponding α_S-plots for the microporous carbons JF005, JF142, JF516 and PX21 were very similar to those for carbons JF005, Carbosieve, JF517 and AX21 in Figure 9.11. Thus, JF005 and JF142 were both

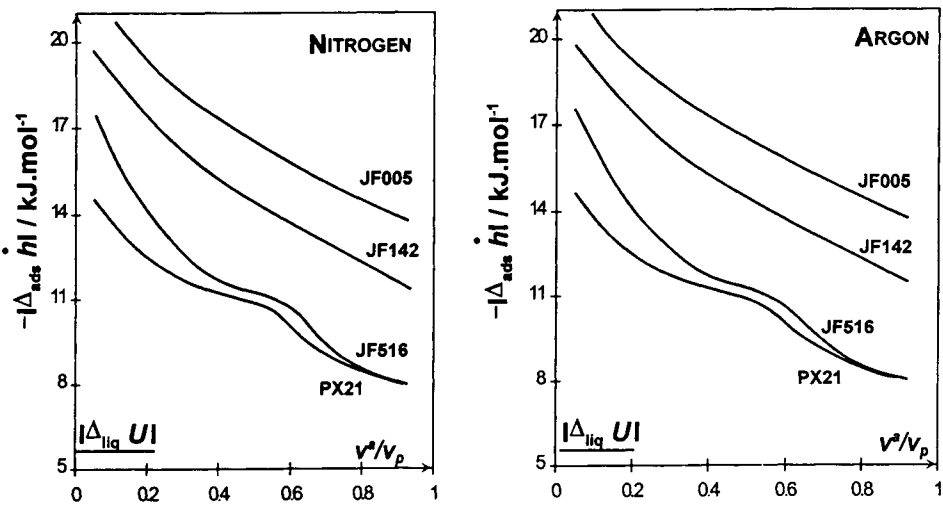

Figure 9.15. Differential enthalpies of adsorption of N_2 and Ar on microporous carbons, plotted versus fractional pore filling (after Atkinson *et al.*, 1987).

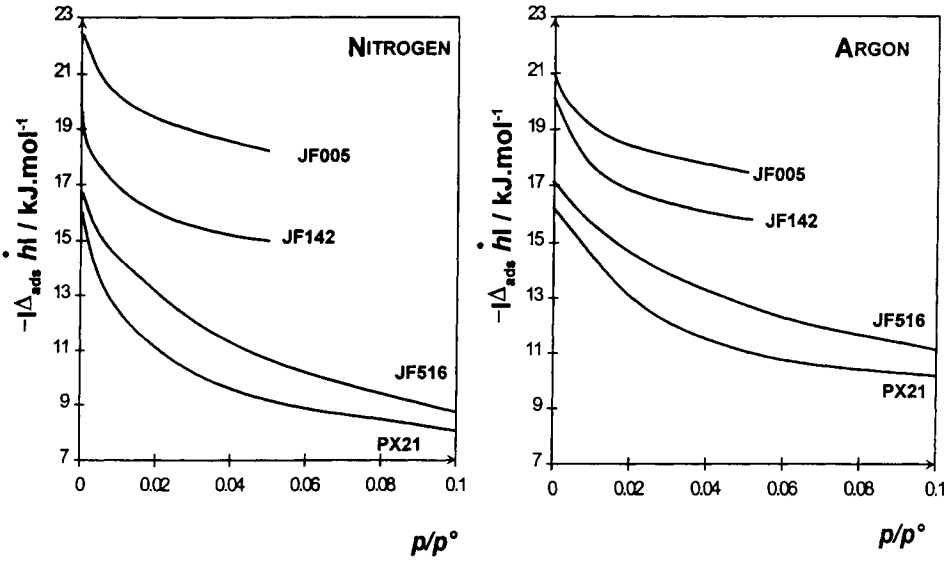

Figure 9.16. Differential enthalpies of adsorption of N_2 and Ar on microporous carbons, plotted versus relative pressure (after Atkinson *et al.*, 1987).

molecular sieve carbons, whereas JF516 and PX21 contained wide ranges of micropores. Values of a(BET), a(ext) and v_p, derived from the nitrogen isotherms, are included in Table 9.1.

The changes in the differential enthalpies of adsorption revealed in Figures 9.15 and 9.16 illustrate the strong energetic heterogeneity associated with micropore filling by all four carbons. However, it is evident that for both nitrogen and argon adsorption the differential enthalpy curves are of two types. Of special interest is the high level of adsorption enthalpy given by JF005 and JF142 over almost the complete range of micropore filling, which is in contrast to the more complex behaviour of JF516 and PX21. With the latter adsorbents, the two stages of micropore filling are clearly evident. It is also apparent that with the two molecular sieve carbons JF005 and JF142 over 80% of the pore filling (i.e. primary micropore filling) has taken place at $p/p^\circ < 0.01$.

In the light of these results, it is of interest to obtain accurate adsorption isotherm data at very low p/p°. As explained in Chapter 3, such high resolution adsorption (HRADS) measurements are not easy to make, but a preliminary investigation (Kenny *et al.*, 1993) indicated that the primary filling of the micropores in Carbosieve by nitrogen at 77 K begins at $p/p^\circ < 10^{-5}$ and is complete at $p/p^\circ \approx 10^{-2}$. These findings have been broadly confirmed by the recent work of Conner (1997) and Kaneko (1997).

By applying non-local density functional (DFT) theory, Gubbins and his co-workers (Balbuena *et al.*, 1993) have predicted that the stepwise filling of very narrow slit-shaped micropores takes place at $p/p^\circ < 10^{-5}$. The non-local DFT theory also predicts that there are layering transitions in the filling of supermicropores. A homogeneous graphitic-type surface was assumed in these calculations, but it was also shown (Balbuena and Gubbins, 1994) that the filling pressure is highly dependent on the relative strengths of the intermolecular interactions (i.e. solid–fluid/fluid–fluid).

Brauer *et al.* (1993) have carried out GCMC simulations for argon adsorption in carbon micropores. As expected, as the pore width was increased from 0.7 nm to *c.* 1 nm the potential energy curves underwent a change from a single deep potential energy well to two minima, which became progressively separated into the normal wall potentials with a further increase of pore width. The simulation experiments indicated that at 87 K stepwise filling of the 0.7 nm pore would occur at $p/p^\circ \approx 10^{-5}$. Pore widening causes this sharp filling to separate into two stages. The results of computer simulation are thus consistent with the DFT calculations.

In their extensive investigations of the porosity of activated carbons, Rodriguez-Reinoso and his co-workers (Garrido *et al.*, 1987; Rodriguez-Reinoso *et al.*, 1989; Rodriguez-Reinoso, 1989; Molina-Sabio *et al.*, 1995) have found it useful to employ carbon dioxide as an adsorptive (generally at 273 K) alongside nitrogen (at 77 K). Indeed, it has been shown that the two sets of adsorption measurements are essentially complementary. When studying the properties of some carbonized organic polymers, Marsh and Wynne-Jones (1964) had found that the levels of uptake of carbon dioxide at 195 K were much larger than could be accommodated on the BET-nitrogen areas. At first sight this seems surprising because the two molecules are not

very different in size: the kinetic diameter of N_2 is 0.36 nm and that of CO_2 is 0.33 nm; and the corresponding minimum dimensions are 0.30 and 0.28 nm. However, by far the most important factor in causing the greater uptake of CO_2 is the higher operational temperature (Gregg and Sing, 1982, p. 230).

This effect is exploited to an even greater extent when the carbon dioxide measurements are undertaken at 273 or 298 K. At these temperatures the carbon dioxide saturation pressures are extremely high (e.g. at 298 K $p^\circ = 63.4$ bar) so that the range of p/p° is limited to ≈ 0.02 at sub-atmospheric pressures. This has the advantage that the initial part of the isotherm can be determined with a much greater accuracy than is normally possible with nitrogen at 77 K, and in addition the DR plots are generally more linear (Rodriguez-Reinoso, 1989).

Rodriguez-Reinoso and his co-workers have identified three groups of porous carbons: (a) carbonized materials and activated carbons of low burn-off, giving much larger CO_2 uptake, because of restricted diffusion of nitrogen into very narrow pores; (b) activated carbons of low-to-medium burn-off, having fairly narrow micropores and giving approximately equivalent uptakes of CO_2 and N_2; and (c) activated carbons of medium-to-high burn-off, having a range of wider micropores and giving larger uptakes of N_2 than CO_2.

Recent experiments by Cazorla-Amoros *et al.* (1996) have involved the measurement of CO_2 isotherms up to pressures of 4 MPa at 273 and 298 K. These investigators have confirmed that CO_2 adsorption at subatmospheric pressures is a useful complementary technique for the characterization of very narrow micropores and that at higher pressures the adsorption of CO_2 is similar to nitrogen.

9.5.2. Adsorption of organic vapours

Benzene was the most popular adsorptive in many early studies of the pore structure of activated carbons (Dubinin, 1958, 1966; Cadenhead and Everett, 1958; Smisek and Cerny, 1970). Indeed, in order to construct the characteristic curve for a given microporous carbon, Dubinin and his co-workers (Dubinin, 1966) originally adopted benzene as the standard adsorptive: thus, in the context of the Dubinin theory of the volume filling of micropores (TVFM), the scaling factor β (C_6H_6) = 1 (see Chapter 8).

Polanyi's concept of the temperature invariance of the characteristic curve became an important feature of the TVFM proposed by Dubinin (1966). The approach provided a way of bringing together a family of isotherms determined at different temperatures. The resulting common curve may be regarded as the relation between the fractional filling of the pores of a microporous carbon by a particular adsorptive and the 'adsorption potential', defined as $RT \ln (p^\circ/p)$. An example of a typical characteristic curve is shown in Figure 9.17, where it is evident that for the active carbon CK the common characteristic curve is given by all the benzene isotherms determined over the temperature range of 20–140°C.

Not all characteristic curves are temperature invariant (Aranovich, 1991; Tolmachev, 1993). Invariance over a wide temperature range has thermodynamic implications, which are unlikely to be consistent with the behaviour of many systems – especially when strong adsorbent–adsorbate interactions or a combination of

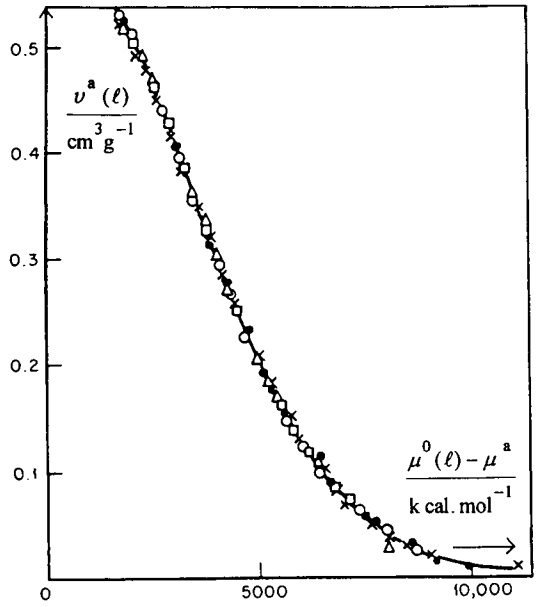

Figure 9.17. DR characteristic curve for benzene adsorption on active carbon CK, for temperatures ranging from 20°C (triangles) to 140°C (solid circles) (from Dubinin, 1975).

adsorption mechanisms are involved. As might be expected, different characteristic curves are often obtained when the isotherms of various adsorptives are determined on the same microporous carbon; in fact there are relatively few well-documented examples of an identical characteristic curve being derived from the isotherms of different vapours (Bansal *et al.*, 1988, p. 102). Recently, Bradley and Rand (1995) have compared the characteristic curves derived from the isotherms of a series of lower alcohols on a coal-based activated carbon. The characteristic curves for methanol and ethanol are in good agreement, but the corresponding curves for propan-2-ol and butan-1-ol deviate at low fractional loading (as does nitrogen). The authors conclude that the deviations are probably the result of molecular packing restrictions within ultramicropores.

Over the past 30 years many organic molecules of different size, shape and polarity have been used as molecular probes. A high proportion of the experimental isotherms on porous carbons have been analysed by application of the Dubinin–Radushkevich (DR) equation or, in a few cases, by the Dubinin–Astakhov (DA) equation. So far, the more sophisticated Dubinin–Stoeckli (DS) treatment (Stoeckli, 1993) has been applied by very few other investigators.

As indicated earlier, an extensive range of linearity of a DR plot is usually associated with primary micropore filling. However, it must be kept in mind that the micropore filling mechanism is dependent on the nature of adsorption system and the temperature as well as on the pore size. Since it contains an additional adjustable parameter, the DA equation is obviously more adaptable than the simple DR

equation. With most activated carbons values of the empirical exponent N in Equation (4.45) are in the range 1.5–3.

Stoeckli (1981), McEnaney and Mays (1991), Hutson and Yang (1997) and others (see Rudzinski and Everett, 1992) have attempted to provide a theoretical basis for the DR and DA equations in terms of an integral transform or a generalized adsorption isotherm, which may be expressed in the form of Equation (4.52). However, in practice the DR and DA equations are usually applied empirically and consequently the derived quantities (micropore volume, characteristic energy and structural constant) are not always easy to interpret.

An alternative, and perhaps more pragmatic, approach is to compare the pore filling behaviour of a number of non-polar vapours of different molecular size (Carrott and Sing, 1988). Although this approach is still at a preliminary stage of development, the following few examples will illustrate its applicability.

The adsorption isotherms and corresponding α_S-plots for nitrogen, propane, isobutane and neopentane on five different activated carbons are given in Figures 9.18–9.22. The isotherms in Figure 9.18 were determined on Carbosieve and those in Figures 9.19–9.21 on different grades of carbon cloth. To facilitate comparison of the levels of uptake, the amounts adsorbed are expressed as the equivalent volumes of *liquid* adsorptive, but it is recognized that the adsorbates are unlikely to have liquid-like properties.

Although some of the isotherms in Figures 9.18–9.22 are more complex than others, they are all essentially Type I in the IUPAC classification. The five carbons are evidently predominantly microporous, but with different ranges of pore size. Before any attempt is made to assess the pore size distribution of each carbon, it is worth examining the significance of the various characteristic features of the isotherms.

A striking feature of the isobutane and neopentane isotherms in Figures 9.18 and 9.19 is their pronounced low-pressure hysteresis. Since the rate of uptake of the bulky isobutane and neopentane molecules was very slow, thermodynamic equilibration was not established and therefore these isotherms are not amenable to detailed analysis. In contrast, the smaller nitrogen and propane molecules are more rapidly adsorbed and their isotherms on Carbosieve and JF005 are reversible (apart from the small capillary condensation hysteresis loop in Figure 9.19). The four isotherms on JF144 in Figure 9.20 are all reversible, the paths of the isobutane and neopentane being virtually identical. In Figure 9.21 all three hydrocarbon isotherms on JF518 are in remarkably close agreement and the first part of the nitrogen isotherm is only slightly removed. The hydrocarbon isotherms in Figure 9.22 are also fairly close (especially at low p/p°), but the nitrogen isotherm deviates markedly in the multilayer range.

The α_S-plots in Figures 9.18–9.22 have been constructed with the aid of standard adsorption data obtained with Elftex 120 and other non-porous carbon blacks (Carrott *et al.*, 1987, 1988a). As noted earlier, each α_S-plot has two linear sections (Section 8.2.1). The first linear section (at $\alpha_S < 1.0$: $p/p^\circ < 0.4$) can be attributed to adsorption on the walls of the supermicropores and therefore its back-extrapolation to $\alpha_S = 0$ gives the ultramicropore capacity. The second linear section is obtained at $\alpha_S > 1.0$ and is associated with multilayer adsorption on the external surface and the intercept gives the total micropore capacity.

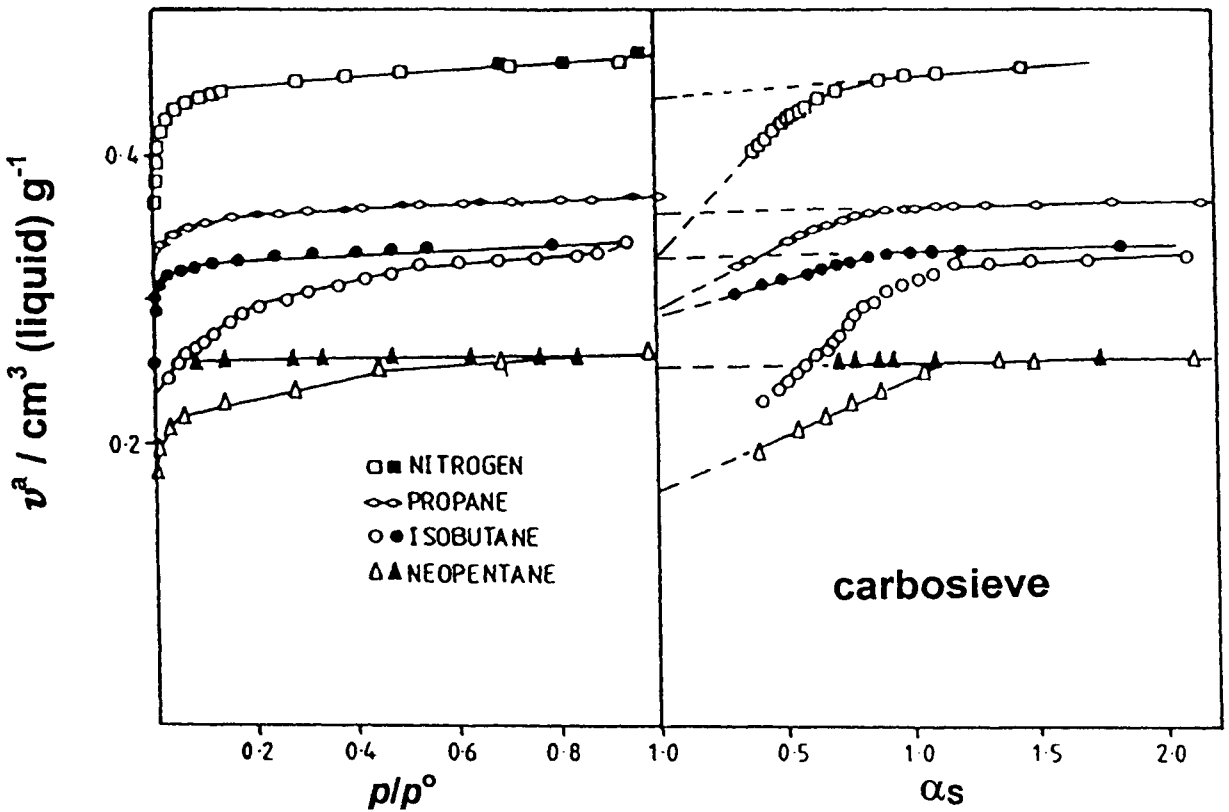

Figure 9.18. Adsorption isotherms and corresponding α_S plots for Carbosieve S (open symbols, adsorption; solid symbols, desorption) (Carrott *et al.*, 1988b).

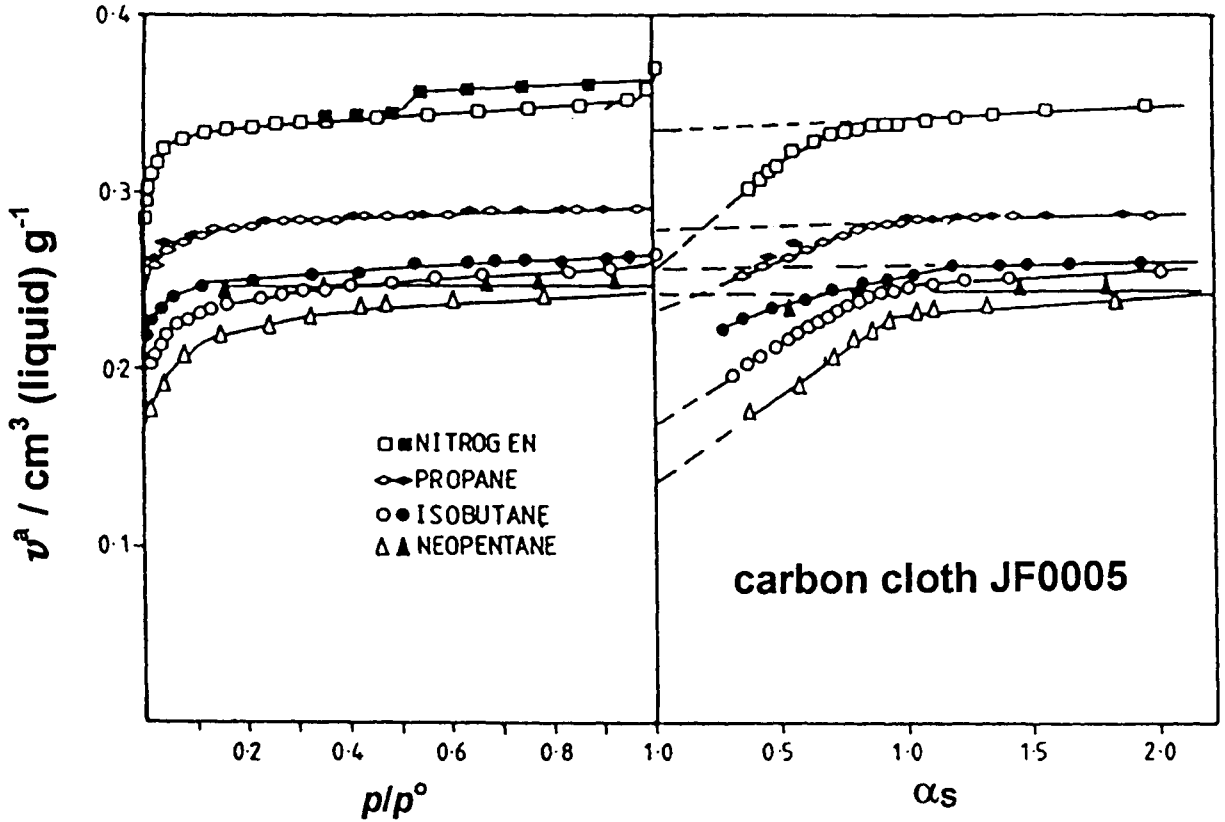

Figure 9.19. Adsorption isotherms and corresponding α_S plots for charcoal cloth JF005 (open symbols, adsorption; solid symbols, desorption) (Carrott *et al.*, 1988b).

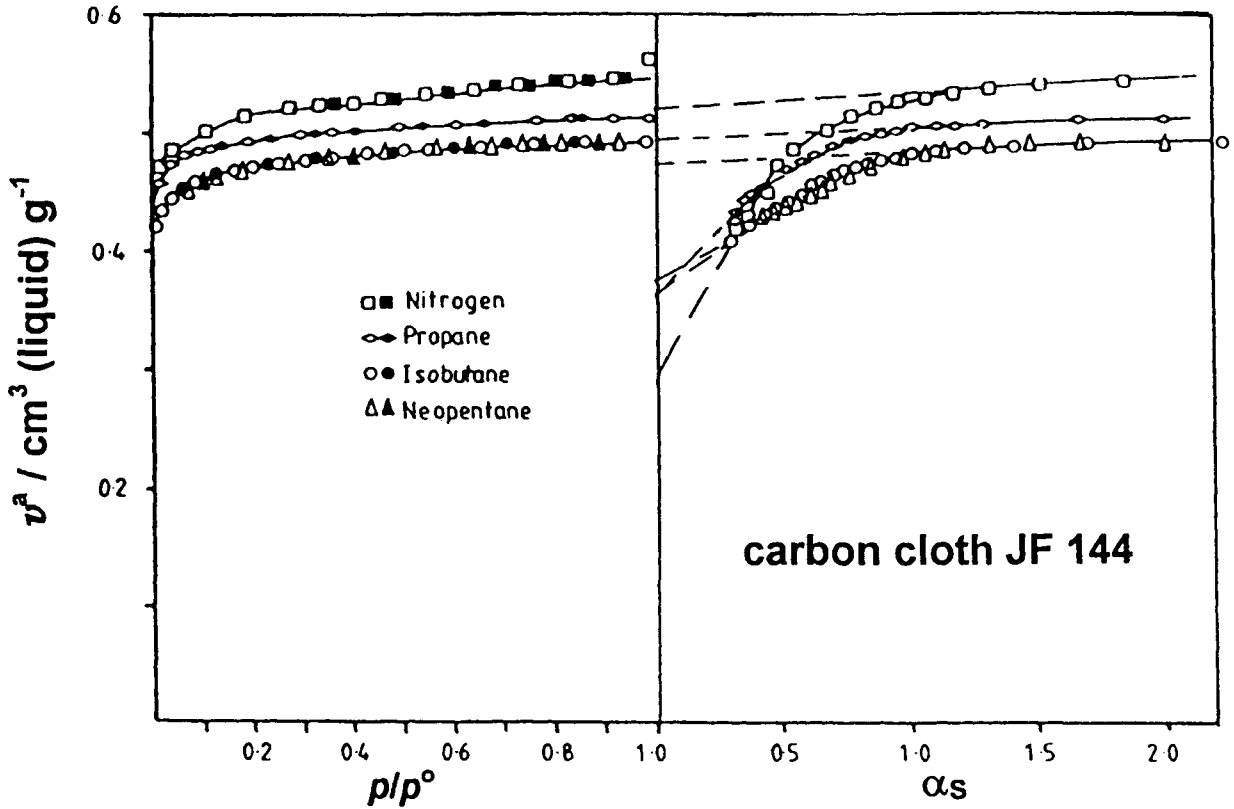

Figure 9.20. Adsorption isotherms and corresponding α_S plots for charcoal cloth JF144 (open symbols, adsorption; solid symbols, desorption) (Carrott *et al.*, 1988b)

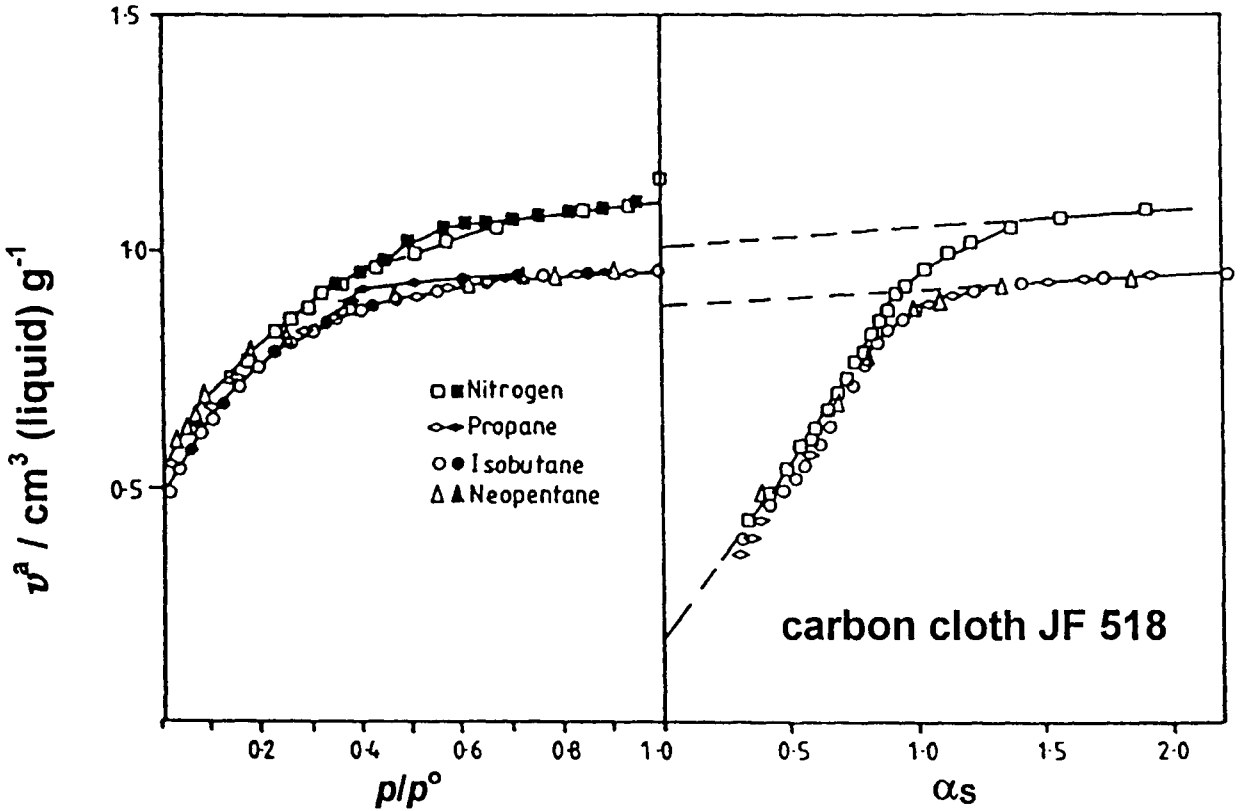

Figure 9.21. Adsorption isotherms and corresponding α_S plots for charcoal cloth JF518 (open symbols, adsorption; solid symbols, desorption) (Carrott *et al.*, 1988b)

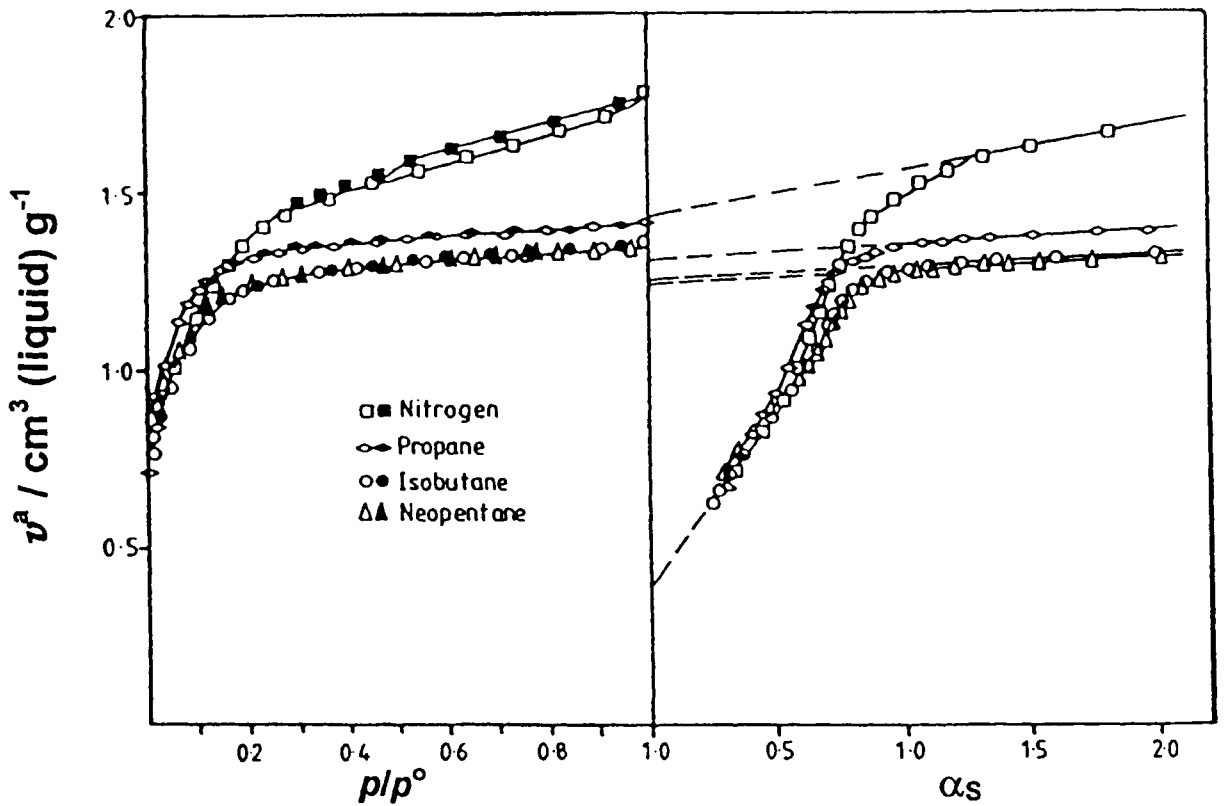

Figure 9.22. Adsorption isotherms and corresponding α_s plots for active carbon AX21 (open symbols, adsorption; solid symbols, desorption) (Carrott *et al.*, 1988b).

The isotherms in Figures 9.18 and 9.19 confirm the ultramicroporous character of Carbosieve and JF005. Both adsorbents exhibit a high affinity for the relatively small nitrogen and propane molecules and their α_S-plots reveal that about 70% of the total micropore capacity is associated with primary micropore filling. The situation is quite different in the case of the isotherms on the JF144 (Figure 9.20). The location of the low-coverage intercepts indicates a fairly high proportion of primary micropore filling (60–70%), but it is significant that at least 90% of the micropore-nitrogen capacity is available for neopentane adsorption. All the isotherms on JF518 (Figure 9.21) exhibit a more gradual approach to the plateau. The predominance of secondary micropore filling is confirmed by the small scale of the primary intercepts (*c.* 10% of the total micropore capacity).

In attempting to make a semi-quantitative estimation of the range of pore size in the four carbons, we assume: (a) that the pores are rigid and remain so during the physisorption measurements; (b) that the micropores are all slit-shaped; and (c) that primary micropore filling occurs in pores of width $< 2d$ and secondary micropore filling in pores of up to $\approx 5d$ (where d is the molecular diameter). Since N_2 molecules are not able to enter 0.4 nm zeolite channels at 77 K (Breck, 1974), it is assumed that this is also the lower limit for their entry into slit-shaped pores. On the basis of these assumptions, the permitted ranges of primary and secondary micropore filling are given in Table 9.2.

From the limits of the two stages of pore filling in Table 9.2 we are able to arrive at the tentative ranges of pore size summarized in Table 9.3. However, caution must be exercised in the acceptance of these limits in view of the the complexity and non-rigidity of the pores in activated carbons. Since there appears to be no sharp boundary between the completion of co-operative micropore filling and the beginning of reversible capillary condensation, we cannot at present define the upper limit of secondary micropore filling.

The series of isotherms in Figures 9.18–9.22 and the derived values of pore volume in Table 9.3 serve to illustrate the inescapable difficulties involved in the characterization of microporous adsorbents. It can be seen that the values of v_p(mic) derived from the nitrogen isotherms are consistently larger than those obtained from the hydrocarbon isotherms. As other authors have also pointed out (Aukett *et al.*, 1992; Bradley and Rand, 1995), adsorbate densities in micropores are unlikely to be the same as the corresponding liquid densities. Furthermore, the degree of molecular packing is to some extent dependent on both pore size and shape (Carrott and Sing, 1988). For these and other reasons, it is advisable to refer to the *effective* or *apparent*

Table 9.2. Primary and secondary filling of slit-shaped pores.

Adsorptive	d (nm)	Effective pore widths, w (nm)	
		Primary	Secondary
Nitrogen	0.36	0.4–0.7	0.7–1.8
Propane	0.43	0.45–0.9	0.9–2.2
Isobutane	0.50	0.5–1.0	1.0–2.5
Neopentane	0.62	0.6–1.2	1.2–3.1

Table 9.3. Effective pore sizes of activated carbons

Carbon	Effective pore volume, v_p(mic) ($cm^3\ g^{-1}$)	Pore range, w (nm)
Carbosieve	0.36[a]–0.43[b]	U: 0.4–0.7
JF005	0.28[a]–0.33	U: 0.4–0.8
JF144	0.51[a]–0.55	U + S: 0.4–2
JF518	0.90[a]–0.98	U + S: 0.4–3
AX21	1.29[a]–1.52	U + S: 0.4–3

[a] For propane.
[b] For nitrogen.
U, ultramicroporous; S, supermicroporous.

pore size or volume (Rouquerol *et al.*, 1994) and also specify the adsorptive and operational temperature.

9.5.3. Adsorption of helium

Helium is often used in adsorption manometry for the determination of the 'dead space' volume (see Chapter 3), but this procedure is based on the presupposition that the gas is not adsorbed at ambient temperature and that it does not penetrate into regions of the adsorbent structure which are inaccessible to the adsorptive molecules. In fact, with some microporous adsorbents, significant amounts of helium adsorption can be detected at temperatures well above the normal boiling point (4.2 K). For this reason, the apparent density (or so-called 'true density') determined by helium pycnometry (Rouquerol *et al.*, 1994) is sometimes dependent on the operational temperature and pressure (Fulconis, 1996).

Because of its small size (collision diameter $\approx$ 0.20 nm), helium would appear to be a useful probe molecule for the study of ultramicroporous carbons. The experimental difficulty of working at liquid helium temperature (4.2 K) is the main reason why helium has not been widely used for the characterization of porous adsorbents. In addition, since helium has some unusual physical properties, it is to be expected that its adsorptive behaviour will be abnormal and dependent on quantum effects.

In their recent investigations of helium adsorption by microporous carbons, Kaneko and his co-workers (Kuwabara *et al.*, 1991; Setoyama *et al.*, 1993; Setoyama and Kaneko, 1995; Setoyama *et al.*, 1996) have obtained strong evidence that the density of physisorbed helium is not the same as that of bulk liquid helium at 4.2 K (i.e. 0.102 g cm^{-3}). By adopting the value 0.202 g cm^{-3}, which had been proposed on theoretical grounds by Steele (1956), Kaneko and his co-workers were able to obtain fairly good agreement between the corresponding uptakes of He and N_2 by certain microporous carbons – as indicated in Figure 9.23. With some other porous carbons, the presence of narrow ultramicropores was demonstrated by the much larger apparent pore volumes available for helium adsorption.

The shapes of a series of helium and nitrogen isotherms are compared in Figures 9.24 and 9.25. To facilitate comparison, the amount adsorbed is expressed in the form

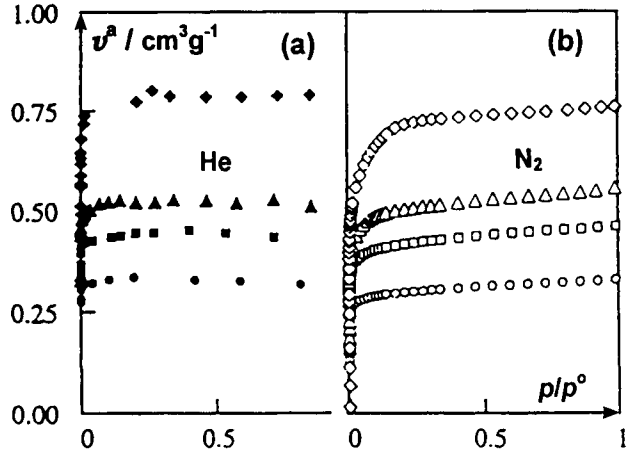

Figure 9.23. Adsorption isotherms of He at 4.2 K (a) and of N_2 at 77 K (b) on a carbon activated up to 19% (circles), 34% (squares), 52% (triangles) and 80% (diamonds) burn-off, respectively (reproduced courtesy of Setoyama *et al.*, 1996).

of a liquid-like volume. As already indicated, the adjusted density of the adsorbed helium is taken as 0.202 g cm^{-3}, whereas the adsorbed nitrogen is assumed to have the normal liquid density of 0.808 g cm^{-3}. It is evident that on this basis the corresponding saturation levels are again in quite close agreement, in accordance with the Gurvich rule. A notable feature of the helium isotherms is their relative steepness at very low p/p°. The striking difference between the helium and nitrogen isotherms is revealed in Figure 9.24, where on the abscissa p/p° is replaced by log (p/p°). It is now apparent that micropore filling by helium has begun at $p/p^\circ < 10^{-6}$ in comparison with the corresponding nitrogen micropore filling at $p/p^\circ \approx 10^{-4}$.

The observed difference in the low-pressure character of the helium and nitrogen isotherms is all the more remarkable in the light of the agreement already noted between the Gurvich volumes. The explanation given by Kaneko for this difference is based on the theory originally proposed by Steele (1956) that the abnormally high adsorption of helium on a graphitic surface at 4.2 K is due to 'an accelerated bilayer adsorption'. In view of this unusual behaviour, it might be expected that distinctive micropore filling mechanisms would be exhibited by helium at 4.2 K. It turns out, however, that there appears to be a close similarity between the helium and nitrogen primary and secondary stages of micropore filling.

The helium and nitrogen α_S-plots in Figure 9.25 were derived from the isotherms in Figure 9.23 with the aid of standard isotherm data determined on a non-porous carbon black (Setoyama *et al.*, 1996). In spite of the appreciable difference in the range of p/p°, it is apparent that the shapes of the corresponding He and N_2 α_S-plots are remarkably similar. We may conclude that with both adsorptives, the initial stage of physisorption is either predominantly surface coverage of supermicropore walls or primary micropore filling of ultramicropores. These findings are entirely consistent with the conditions of activation of these and the other porous carbons, which had

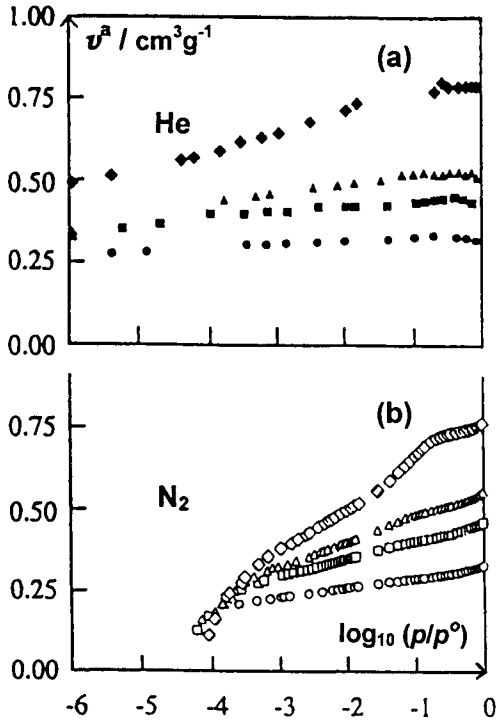

Figure 9.24. Logarithmic plot of isotherms in Figure 9.23 (reproduced courtesy of Setoyama *et al.*, 1996).

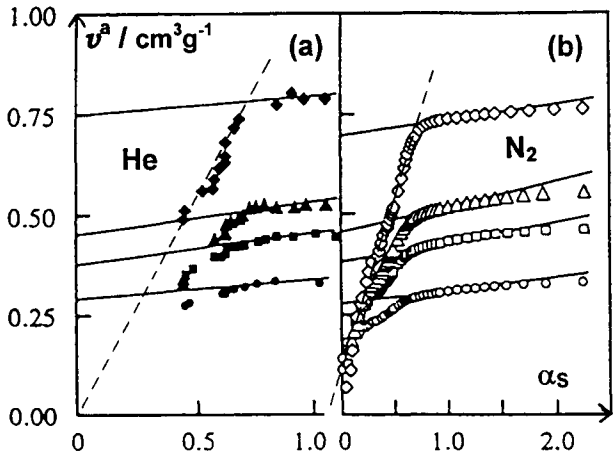

Figure 9.25. α_S plots of adsorption isotherms given in Figures 9.23 and 9.24 (reproduced courtesy of Setoyama *et al.*, 1996).

been prepared from olive stones, the levels of burn-off being indicated by the sample designation (i.e. 80 and 19%, respectively).

As we have seen, the apparent density of He at 4.2 K in the slit-shaped micropores of some activated carbons appears to be *c.* 0.20 g cm^{-3}. However, the true density must depend on both the nature of the adsorption system and the pore size and shape. Setoyama and Kaneko (1995) have given a possible range of 0.20–0.23 g cm^{-3} for the density of helium in the micropores of activated carbons.

9.5.4. Adsorption of water vapour

It is well known that the surface of graphite is 'hydrophobic': it has a very low affinity for water. Thus, the adsorption of water vapour on pure graphitized carbon quite difficult to *detect* at $p/p^\circ < 0.8$ (Avgul *et al.*, 1957) and also the energy of immersion of graphitized carbon in water is extremely low (Zettlemoyer *et al.*, 1953). Indeed, water isotherms of extreme Type III character can be obtained by the high-temperature treatment of carbon blacks in hydrogen to remove chemisorbed oxygen and other polar groups.

A pioneering investigation of the adsorption of water vapour by Saran charcoal (an ultramicroporous carbon) was carried out by Dacey *et al.*, (1958). The isotherm at 55°C had the well-defined Type V character with a steep riser at $p/p^\circ \approx 0.5$–0.6. There was a small amount of low-pressure hysteresis, but the isotherm appeared to be completely reversible at $p/p^\circ > 0.55$.

Typical examples of water isotherms on microporous carbons are shown in Figure 9.26. Although Carbosieve and AX21 are both highly microporous, their pore size distributions are quite different (see Chapter 12). It is apparent that the very narrow pores ($w \approx 0.4$–0.8 nm) in the ultramicroporous Carbosieve begin to fill with water at $p/p^\circ \approx 0.3$, while filling of the wider pores ($w \approx 1$–2 nm) of AX21 does not take place

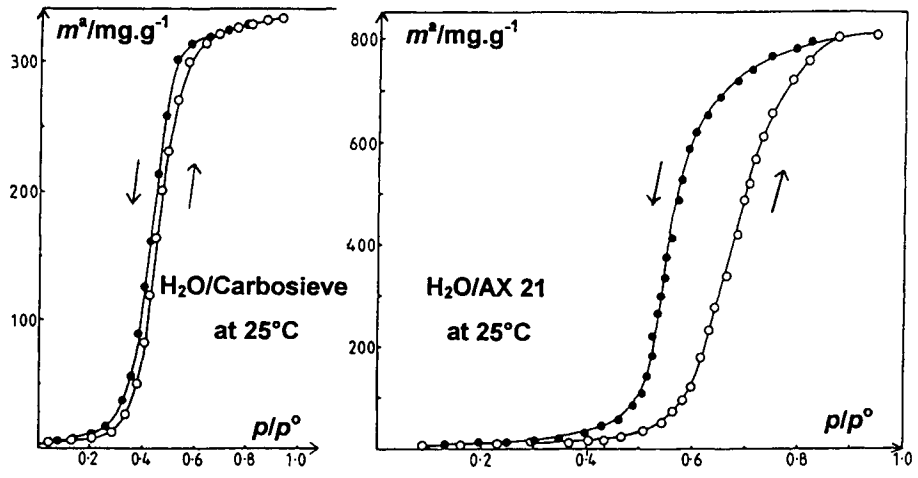

Figure 9.26. Water isotherms at 25°C on microporous carbons outgassed at 300°C (Sing, 1991).

until $p/p^\circ > 0.5$. Another interesting difference between the two water isotherms in Figure 9.26 is the size of their hysteresis loops: the loop given by Carbosieve is steep and narrow, while the loop obtained with AX21 is broader and more rounded.

A qualitative explanation for isotherms of the type shown in Figure 9.26 was first put forward by Pierce and Smith (1950), who postulated that initially a few water molecules are adsorbed on polar sites (e.g. oxygen complexes) and, with increase in p/p°, clusters of molecules are then hydrogen-bonded around these favourable sites. The clusters grow with increased pressure until they merge together and the pores are filled. According to Pierce and Smith, the hysteresis is due to a difference between the steps involved in pore filling and emptying, the latter representing a more stable state. The two-stage process was the basis of the model adopted by Dubinin and Serpinski (1981) and further developed by Barton and Koresh (1983).

The latter authors found that a *reversible* water isotherm was obtained after the low-temperature (i.e. 40°C) evacuation of a carbon cloth, which had been activated by oxidative HNO_3 treatment. The molecular sieve character of this material was reduced by evacuation at 400°C and this also led to the appearance of hysteresis in the water vapour isotherm. Barton and Koresh (1983) conclude that such hysteresis is mainly due to the concentration of surface oxides 'which dictate the adsorption value at which the change from cluster adsorption to a continuous adsorbed phase takes place'. The relationship between the adsorption of water and the surface concentration of chemisorbed oxygen was first established by Walker and Janov (1968). Bansal *et al.* (1978a,b) also investigated the influence of the surface oxygen on the adsorption of water: they concluded that at $p/p^\circ < 0.5$ the level of water uptake is determined by the concentration of surface oxygen-containing structures.

Truly reversible Type V isotherms are quite rare. It is significant that the example reported by Dubinin (1980) was obtained on a low burn-off (5.7%) carbon, which was certainly ultramicroporous. It was pointed out that with an activated carbon obtained by 20% burn-off, the hysteresis extended over virtually the whole range of pore filling – the water isotherm then having a very similar appearance to that of the Carbosieve isotherm in Figure 9.26.

A study of the hydrophilic sites on the surface of activated carbon fibres has been made recently by Kaneko *et al.* (1995) with the aid of X-ray photoelectron spectroscopy (XPS). In this work cellulose (CEL)- and polyacrylonitrile (PAN)-based activated carbon fibres were used and samples were either chemically treated with H_2O_2 or heated in H_2 at 1000°C. As expected, surface oxidation by the H_2O_2 treatment increased the initial uptake of water, while the H_2 reduction caused a marked decrease in the amount of water adsorbed at low p/p°. Measurement of the peak areas of the XPS spectra provided a means of determining the fractional surface coverage by the hydrophilic sites. In this way a linear relationship was found between the low-pressure adsorption of water vapour and the number of hydrophilic sites (mainly —COOH).

The low affinity of the surface of pure carbon for water is associated with the unusually weak non-specific interactions between the non-polar surface and the adsorbate. When certain functional groups are present on the carbon surface, specific interactions come into play and the adsorption affinity is thereby increased (see Chapter 1).

The effects produced by changing the surface chemistry of porous carbons have been studied by a number of investigators. In the systematic work of Hall and Holmes (1991, 1992, 1993) chemical modification of activated carbons was brought about by treatment with such agents as chlorine, phosgene, fluorine, dinitrogen tetroxide (NO_2) and 1,1-difluoroethene (DFE). Significant changes were observed in the p/p° required for pore filling by water vapour. In some cases the behaviour of the modified adsorbent was found to be dependent on the reaction conditions: for example, the degree of hydrophobicity produced by chlorination was affected by the reaction temperature. Although temperatures of around 180°C were required to produce relatively hydrophobic material, it seems that chlorination at low temperature may offer a new way of attaching different functional groups to the carbon surface (Hall and Holmes, 1993).

The recent contribution by Kaneko *et al.* (1995) has revealed that it is possible to produce highly hydrophobic fluorinated microporous carbon fibres. Two fluorinated carbons were reported to have apparent surface areas of 420 and 340 $m^2\,g^{-1}$ and micropore volumes of, respectively, 0.19 and 0.14 $cm^3\,g^{-1}$. These materials gave Type I nitrogen and methanol isotherms, but the adsorption of water vapour was too small to measure at $p/p^\circ < 0.8$ and the uptake was very low even at $p/p^\circ \approx 1$.

It is evident that there is ample evidence to support the view that the initial stage of water vapour adsorption is dependent on the presence of a number of polar sites on the carbon surface. In the theory of Dubinin and Serpinski (1981), these sites are pictured as primary adsorption centres of uniformly high energy. Water molecules are first adsorbed on the primary centres in a 1:1 ratio and these molecules then act as secondary adsorption centres for the adsorption (by H-bonding) of other molecules.

The Dubinin–Serpinski (DS) equation, which was based on this model, can be expressed in the form

$$p/p^\circ = \boldsymbol{n}/[k_1(n_0 + \boldsymbol{n})(1 - k_2\boldsymbol{n})] \tag{9.3}$$

where $\boldsymbol{n}$ is the specific amount of water adsorbed at p/p°, n_0 is the specific amount of primary centres, k_1 is the ratio of the rate constants for adsorption and desorption and k_2 is a constant related to the uptake at $p/p^\circ = 1$.

In some studies it has been found that Equation (9.3) is applicable to experimental water adsorption data in the region of $0.4 < p/p^\circ < 0.8$ (Stoeckli *et al.*, 1994). In practice, the range of fit has been found to depend on both the nature of the carbon surface and the pore structure (Carrott *et al.*, 1991; Carrott, 1993). The range of fit has been extended by Barton *et al.* (1991, 1992) by the addition of a fourth empirical parameter.

Stoeckli and his co-workers (1994b) have shown that the adsorption branch of a water isotherm can be described by a Dubinin–Astakov (DA) type of equation,

$$\boldsymbol{n} = \boldsymbol{n}_p \exp\,[-(A/E)^N] \tag{9.4}$$

where $\boldsymbol{n}_p$ is the micropore capacity, $A = RT \ln (p^\circ/p)$ and N and E are temperature-invariant parameters.

As we saw in Chapter 8, Equation (9.4) has been customarily applied to Type I isotherms. However, if the value of E is sufficiently low (i.e. $E < 2$–3 kJ mol^{-1} near room temperature), it can be applied to the major part of a Type V isotherm.

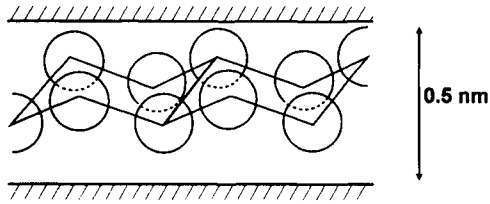

Figure 9.27. Hydrogen-bonded structure of water in a slit-shaped pore (Carrott *et al.*, 1991).

Furthermore, with at least some systems, it has been found that E and N do not vary appreciably with temperature and therefore the temperature-invariance condition is satisfied (Stoeckli *et al.*, 1994b). On the other hand, so far it has not been possible to define the exact meaning of these terms.

Recently, Iiyama *et al.* (1995) have obtained a series of distinctive X-ray diffraction patterns for water adsorbed in the 1.3 nm slit-shaped pores of a supermicroporous carbon. The diffraction patterns and derived electron distribution functions appear to confirm the existence of some long-range order in the structure of the adsorbed water. These interesting results are consistent with the fact that water can be easily accommodated in narrow slit-shaped pores of carbon in contrast to the pore-filling hydrophobicity of the tubular pores of Silicalite (Carrott *et al.*, 1991). As indicated in Figure 9.27, a thin slab of hydrogen-bonded water can be placed in a slit of width greater than ≈0.5 nm with very little distortion of its structure. Moreover, we can begin to see why the size of the hysteresis loop is dependent on pore size as well as surface chemistry. It seems likely that the adsorbate in the central layer will become more liquid-like as the pore width is increased. Therefore, the filling and emptying of a very narrow pore occurs reversibly in one step, whereas a wider pore is filled/emptied in two stages.

A novel method for determining the location of the primary water adsorbing sites has been developed by Bailey *et al.*, (1995). This approach involves the pre-adsorption of naphthalene, which was chosen because of its planar molecular shape and immiscibility with water. With some activated carbons it was found that the growth of the H-bonded water clusters was inhibited by the presence of naphthalene, while in other cases there was very little effect. It was thought that sites in larger micropores were prone to obstruction by the pre-adsorbed naphthalene. It is too early to judge the success of this interesting approach, which may turn out to be a useful alternative to pre-adsorption by *n*-nonane.

9.6. Immersion Microcalorimetry and Adsorption From Solution

9.6.1. Immersion microcalorimetry

Immersion calorimetry can be used to study either the surface chemistry or the texture of active carbons. A sensitive Tian–Calvet microcalorimeter is adaptable for either purpose, the main difference being in the choice of wetting liquids.

A selection of polar liquids is required for a systematic study of the surface chemistry. In the early work of Zettlemoyer and Chessick (1974), liquids of different dipole moment were used with the aim of obtaining a linear relation between the energy of immersion and the specific interaction of the dipole and the surface electrostatic field. Differences in the non-specific interaction energies were minimized by maintaining a constant hydrocarbon moiety (e.g. by comparing the energies of immersion of *n*-butylamine and *n*-butanol).

In a more recent investigation, Rodriguez-Reinoso *et al.* (1987) were able to characterize two different species of surface oxygen groups on the surface of activated carbons by making their immersion energy measurements with benzene, methanol and water. In this manner it was possible to distinguish between the properties of the functional groups which were thermally displaced in the form of either CO or CO_2.

As already described in Section 6.5.2, the surface area of active carbons can be directly assessed by immersion calorimetry with non-polar liquids (e.g. *n*-hexane). Satisfactory agreement with BET-nitrogen areas has been found with the supermicroporous carbons. As expected, because of the unreliability of the BET areas, the ultramicroporous carbons gave poor agreement. However, we consider that this does not invalidate the use of immersion calorimetry.

For the pore size analysis of microporous carbons, a series of liquids of different molecular size should be employed (see Section 8.3.1). The energy of immersion can be converted into an effective area, which is accessible to each liquid, and the micropore size distribution obtained from the plot of surface area versus molecular size (see Figure 8.5).

9.6.2. Adsorption from solution

Adsorption at the solution–carbon interface is already widely used on a large scale for water treatment, decolorizing, gold recovery, etc. (Derbyshire *et al.*, 1995). In addition to these well-established applications, considerable interest is now being shown in the potential use of activated carbons for the removal of a wide range of pollutants such as aromatic hydrocarbons, humic acids and heavy metal ions (Costa *et al.*, 1988; Youssef *et al.*, 1996) and for the treatment of radioactive waste (Qadeer and Saleem, 1997). The aims of the applied research are generally to optimize the performance of the available commercial grades of activated carbon, to develop new products and to elucidate the mechanisms of adsorption (Blasinski *et al.*, 1990).

In the past, much attention was given to the study of dye and iodine adsorption by active carbons (Brunauer, 1945; Orr and Dalla Valle, 1959). Many studies have been made with dye molecules of well-known size, shape and chemical properties, but the results have not been easy to interpret (Giles *et al.*, 1970; McKay, 1982, 1984). In a systematic study of iodine adsorption (from aqueous solution) on a carbon black and four activated carbons (Fernandez-Colinas *et al.*, 1989b), it was found that the iodine isotherms could be analysed by the α_S-method. In this way it was possible to assess values of the available volume in pores of effective width of 0.5–1.5 nm. The adsorption of iodine was also featured in a recent study by Ziolkowska and Garbacz (1997), who applied the Langmuir, Freundlich and other isotherm equations.

References

Amberg C.H., Spencer W.B. and Beebe R.A. (1955) *Canad. J. Chem.* **33**, 305.

Aranovich G.L. (1991) *J. Colloid Interface Sci.* **141**, 30.

Atkinson D., McLeod A.I. and Sing K.S.W. (1984) *J. Chim. Phys.* **81**, 791.

Atkinson D., Carrott P.J.M., Grillet Y., Rouquerol J. and Sing K.S.W. (1987) In: *Proc. 2nd Conf. on Fundamentals of Adsorption* (A.I. Liapis, ed.), Engineering Foundation, New York, p. 89.

Aukett P.N., Quirke N., Riddiford S.M. and Tennison S.R. (1992) *Carbon* **30**, 913.

Avgul N.N. and Kiselev A.V. (1970) *Chem. Phys. Carbon* **1**, 1.

Avgul N.N., Kiselev A.V., Kovalyova N.V. and Khrapova E.V. (1957) In: *Proc. 2nd Int. Congress on Surface Activity*, vol. II (J.H. Schulman, ed.), Butterworths, London, p. 218.

Baker F.S. (1992) In: *Kirk-Othmer Encyclopedia of Chemical Technology*, vol. 4, John Wiley, New York, p. 1015.

Bailey A., Lawrie G.A. and Williams M.R. (1995) *Adsorption Sci. Tech.* **12**, 193.

Balbuena P.B., Lastoskie C., Gubbins K.E. and Quirke N. (1993) In: *Proc. 4th Int. Conf. on Fundamentals of Adsorption* (M. Suzuki, ed.) Kodansha, Tokyo, p. 27.

Balbuena P.B. and Gubbins K.E. (1994) In: *Characterization of Porous Solids III* (J. Rouquerol, F. Rodriguez-Reinoso, K.S.W. Sing and K.K. Unger, eds), Elsevier, Amsterdam, p. 41.

Bansal R.C., Bhatia N. and Dhami T.L. (1978a) *Carbon* **16**, 65.

Bansal R.C., Dhami T.L. and Parkash S. (1978b) *Carbon* **16**, 389.

Bansal R.C., Donnet J.-B. and Stoeckli F. (1988) In: *Active Carbon*, Marcel Dekker, New York.

Barton S.S. and Harrison B.H. (1975) *Carbon* **13**, 47.

Barton S.S. and Koresh J.E. (1983) *J. Chem. Soc., Faraday Trans. I* **79**, 1147–1165.

Barton S.S., Evans M.J.B. and MacDonald J.A.F. (1991) *Carbon* **29**(8), 1099.

Barton S.S., Evans M.J.B. and MacDonald J.A.F. (1992) *Carbon* **30**(1), 123.

Beebe R.A. and Dell R.M. (1955) *J. Phys. Chem.* **59**, 746.

Beebe R.A. and Young D.M. (1954) *J. Phys. Chem.* **58**, 93.

Beebe R.A., Beckwith J.B. and Honig J.M. (1945) *J. Am. Chem. Soc.* **67**, 1554.

Beebe R.A., Biscoe J., Smith W.R. and Wendell C.B. (1947) *J. Am. Chem. Soc.* **69**, 95.

Beebe R.A., Millard B. and Cynarski J. (1953) *J. Am. Chem. Soc.* **75**, 839.

Beebe R.A., Gale R.L. and Kleinsteuber T.C.W. (1966) *J. Phys. Chem.* **70**, 4010.

Bienfait M. (1980) In: *Phase Transitions in Surface Films* NATO ASI B51 (J.G. Dash and J. Ruvalds, eds), Plenum, New York, p. 29.

Bienfait,M. (1985) *Surface Sci.* **162**, 411.

Bienfait M., Zeppenfeld P., Gay J.M. and Palmari J.P. (1990) *Surface Sci.* **226**(3), 327.

Blasinski H., Kamionowska U., Kazmierczak J. and Pustelnik A. (1990) *Adsorption Sci. and Techn.* **7**, 228.

Boehm H.P. (1966) In: *Advances in Catalysis*, vol. 16 (D.D. Eley, H. Pines and P.B. Weisz, eds), Academic Press, New York, p. 179.

Boehm H.P. (1994) *Carbon* **32**, 759.

Bojan M.J. and Steele W.A. (1987) *Langmuir* **3**(6), 1123.

Bonijoly M., Oberlin M. and Oberlin A. (1982) *Int. J. Coal Geol.* **1**, 283.

Bradley R.H. and Rand B. (1995) *J. Colloid Interface Sci.* **169**, 168.

Bradley R.H., Sutherland I. and Sheng E. (1995) *J. Chem. Soc., Faraday Trans.* **91**, 3201.

Breck D.W. (1974) In: *Zeolite Molecular Sieves*, John Wiley, New York, p. 636.

Brauer P., Poosch H.-R., Szombathely M.V., Heuchel M. and Jaroniec M. (1993) In: *Proc. 4th Int. Conf. on Fundamentals of Adsorption* (M. Suzuki, ed.), Kodansha, Tokyo, p. 67.

Brunauer S. (1945) In: *The Adsorption of Gases and Vapours*, Oxford University Press, London, p. 293.

Cadenhead D.A. and Everett D.H. (1958) In: *Industrial Carbon and Graphite*, S.C.I., London, p. 272.

Carrott P.J.M. (1993) *Adsorption Sci Tech* **10**, 63.

Carrott P.J.M. and Sing K.S.W. (1988) In: *Characterization of Porous Solids I* (K.K. Unger, J. Rouquerol, K.S.W. Sing and H. Kral, eds), Elsevier, Amsterdam, p. 77.

Carrott P.J.M. and Sing K.S.W. (1989) *Pure Appl. Chem.* **61**, 1835.

Carrott P.J.M., Roberts R.A. and Sing K.S.W. (1987) *Carbon* **25**, 59.
Carrott P.J.M., Roberts R.A. and Sing K.S.W. (1988a) *Langmuir* **4**, 740.
Carrott P.J.M., Roberts R.A. and Sing K.S.W. (1988b) In: *Characterization of Porous Solids I* (K.K. Unger, J. Rouquerol, K.S.W. Sing and H. Kral, eds), Elsevier, Amsterdam, p. 89.
Carrott P.J.M., Drummond F.C., Kenny M.B., Roberts A. and Sing K.S.W. (1989) *Colloids and Surfaces* **37**, 1.
Carrott P.J.M., Kenny M.B., Roberts R.A., Sing K.S.W. and Theocharis C.R. (1991) In: *Characterization of Porous Solids II* (F. Rodriguez-Reinoso, J. Rouquerol, K.S.W. Sing and K.K. Unger, eds), Elsevier, Amsterdam, p. 685.
Cazorla-Amoros D., Alcaniz-Monge J. and Linares-Solano A. (1996) *Langmuir* **12**, 2820.
Clint J.H. (1972) *J. Chem. Soc., Faraday Trans I* **68**, 2239.
Conner W.C. (1997) In: *Physical Adsorption: Experiment, Theory and Applications* (J. Fraissard and W.C. Conner, eds), Kluwer, Dordrecht, p. 33.
Costa E., Calleja G. and Marijuan L. (1988) *Adsorption Sci. Techn.* **5**, 213.
Dacey J.R., Clunie J.C. and Thomas D.G. (1958) *Trans. Faraday Soc.* **54**, 250.
Dash J.G. (1975) *Films on Solid Surfaces*, Academic Press, New York, p. 53.
Davis B.W. and Pierce C. (1966) *J. Phys. Chem.* **70**, 1051.
Derbyshire F., Jagtoyen M. and Thwaites M. (1995) In: *Porosity in Carbons* (J.W. Patrick, ed.), Edward Arnold, London, p. 227.
de Vooys F. (1983) In: *Activated Carbon: a Fascinating Material* (A. Capelle and F. de Vooys, eds), Norit N.V., Amersfoort, p. 13.
Do D.D., Hu, X., Gray P. and Mayfield P. (1993) In: *Fundamentals of Adsorption*, vol. IV (M. Suzuki, ed.), Kodansha, Tokyo, p. 145.
Donnet J.-B. (1994) *Carbon* **32**, 1305.
Donnet J.-B. and Custodero E. (1993) In: *The Second International Conference on Carbon Black*, Mulhouse, p. 177.
Dubinin M.M. (1958) In: *Industrial Carbon and Graphite*, Society of Chemical Industry, London, p. 219.
Dubinin M.M. (1966) In: *Chemistry and Physics of Carbon*, vol. 2 (P.L. Walker, ed.), Marcel Dekker, New York, p. 51.
Dubinin M.M. (1975) In: *Progress in Surface and Membrane Science*, vol. 9 (D.A. Cadenhead, ed.), Academic Press, New York, p. 1.
Dubinin M.M. (1980) *Carbon* **18**, 355.
Dubinin M.M. and Serpinski V.V. (1981) *Carbon* **19**, 402.
Emmett P.H. and DeWitt T. (1941) *Ind. Eng. Chem.* Anal Ed **13**, 28.
Everett D.H. and Powl J.C. (1976) *J. Chem. Soc., Faraday Trans. I* **72**, 619.
Everett D.H. and Ward R.J. (1986) *J. Chem. Soc., Faraday Trans. I* **82**, 2915.
Fernandez-Colinas J., Denoyel R., Grillet Y., Rouquerol F. and Rouquerol J. (1989a) *Langmuir* **5**, 1205.
Fernandez-Colinas J., Denoyel R. and Rouquerol J. (1989b) *Adsorption Sci. Techn.* **6**, 18.
Freeman J.J. and Sing K.S.W. (1991) In: *Adsorptive Separation* (M. Suzuki, ed.), Institute of Industrial Science, Tokyo, p. 261.
Fulconis J.M. (1996), Thèse, Université d'Aix-Marseille III, Marseille.
Garrido J., Linares-Solano A., Martin-Martinez J.M., Molina-Sabio M., Rodriguez-Reinoso, F. and Torregrosa R. (1987) *Langmuir* **3**, 76.
Gay J.-M., Suzanne J. and Wang R. (1986) *J. Chem. Soc., Faraday Trans II* **82**, 1669.
Gierak A. (1996) *Adsorption Sci. Techn.* **14**, 47.
Giles C.H., D'Silva A.P. and Trivedi A.S. (1970) In: *Surface Area Determination* (D.H. Everett and R.H. Ottewill, eds), Butterworths, London, p. 317.
Gregg S.J. and Sing K.S.W. (1982) In: *Adsorption, Surface Area and Porosity*, Academic Press, London.
Grillet Y., Rouquerol F. and Rouquerol J. (1979) *J. Colloid Interface Sci.* **70**, 239.
Groszek A.J. (1970a) *Proc. Roy. Soc. (London) A* **314**, 473.
Groszek A.J. (1970b) In: *Surface Area Determination*, Proc. Int. Symposium, Bristol (1969), *Pure Appl. Chem.*, 313.
Gruber T., Zerda T.W. and Gerspacher M. (1994) *Carbon* **32**, 1377.
Hall C.R. and Holmes R.J. (1991) *Colloids and Surfaces* **58**, 339.

Hall C.R. and Holmes R.J. (1992) *Carbon* **30**, 173.
Hall C.R. and Holmes R.J. (1993) *Carbon* **31**, 881.
Hess W.M. and Herd C.R. (1993) In: *The Second International Conference on Carbon Black*, Mulhouse, p. 251.
Holmes J.M. (1966) In: *The Solid–Gas Interface* (E.A. Flood, ed.), Marcel Dekker, New York, vol. 1, p. 127.
Hutson N.D. and Yang R.T. (1997) *Adsorption* **3**, 189.
Iiyama,T., Nishikawa K., Otowa T. and Kaneko K. (1995) *J. Phys. Chem.* **99**, 10075.
Isirikyan A.A. and Kiselev A.V. (1961) *J. Phys. Chem.* **65**, 601.
Ismail I.M.K. (1990) *Carbon* **28**, 423.
Ismail I.M.K. (1992) *Langmuir* **8**, 360.
Kakei K., Ozeki S., Suzuki T. and Kaneko K. (1991) In: *Characterization of Porous Solids II* (F. Rodriguez-Reinoso, J. Rouquerol, K.S.W. Sing and K.K. Unger, eds), Elsevier, Amsterdam, p. 429.
Kaneko K. (1996) In: *Adsorption on New and Modified Inorganic Sorbents* (A. Dabrowski and V.A. Tertykh, eds), Elsevier, Amsterdam p. 573.
Kaneko K. (1997) In: *Equilibria and Dynamics of Gas Adsorption on Heterogeneous Solid Surfaces* (W. Rudzinski, W.A. Steele and G. Zgrablich, eds), Elsevier, Amsterdam, p. 679.
Kaneko Y., Ohbu K., Uekawa N., Fujie K. and Kaneko K. (1995) *Langmuir* **11**, 708.
Kenny M.B., Sing K.S.W. and Theocharis C. (1993) In: *Proc. 4th Int. Conf. on Fundamentals of Adsorption* (M. Suzuki, ed.), Kodansha, Tokyo, p. 323.
Kington G.L., Beebe R.A., Polley M.H. and Smith N.R. (1950) *J. Am. Chem. Soc.* **72**, 1775.
Krim J., Suzanne J., Shechter H., Wang R. and Taub H. (1985) *Surface Sci.* **162**, 446.
Kruk M., Jaroniec M. and Bereznitski Y. (1996) *J. Colloid Interface Sci.* **182**, 282.
Kuwabara H., Suzuki T. and Kaneko K. (1991) *J. Chem. Soc., Faraday Trans* **87**, 1915.
Lahaye J. and Ehrburger-Dolle F. (1993) In *The Second International Conference on Carbon Black*, Mulhouse, p. 11.
Larher Y. (1974) *J. Chem. Soc., Faraday Trans I* **70**, 320.
Larher Y. (1983) *Surface Sci.* **134**, 469.
Malden P.J. and Marsh J.D.F. (1959) *J. Phys. Chem.*, **63**, 1309.
Marsh H. and Wynne-Jones W.F.K. (1964) *Carbon* **1**, 281.
Marsh H., Heintz E.A. and Rodriguez-Reinoso F. (1997) In: *Introduction to Carbon Technologies*, Publicaciones de la Universidad de Alicante, Spain.
McEnaney B. and Mays T.J. (1991) In: *Characterization of Porous Solids II* (F. Rodriguez-Reinoso, J. Rouquerol, K.S.W. Sing and K.K. Unger, eds), Elsevier, Amsterdam, p. 477.
McKay G. (1982) *J. Chem. Technol. Biotechnol.* **32**, 759.
McKay G. (1984) *J. Chem. Technol. Biotechnol.* **34A**, 294.
Medalia A.I. and Rivin D. (1976) In: *Characterization of Powder Surfaces* (G.D. Parfitt and K.S.W. Sing, eds), Academic Press, London, p. 279.
Mikhalovsky S.V., Glushakov V.G., Noscov A.M. and Rudakov D.B. (1994) In: *Characterization of Porous Solids III* (J. Rouquerol, F. Rodriguez-Reinoso, K.S.W. Sing and K.K. Unger, eds), Elsevier, Amsterdam, p. 705.
Molina-Sabio M., Munecas M.A., Rodriguez-Reinoso F. and McEnaney B. (1995) *Carbon* **33**, 1777.
Orr C. and Dalla Valle J.M. (1959) *Fine Particle Measurement*, Macmillan, New York.
Parkyns N.D. and Sing K.S.W. (1975) In: *Specialist Periodical Report: Colloid Science*, vol. 2 (D.H. Everett, ed.), The Chemical Society, London, p. 26.
Pierce C. (1968) *J. Phys. Chem.* **72**, 3673.
Pierce C. and Smith N. (1950) *J. Phys. Colloid. Chem.* **54**, 784.
Pierce C. and Ewing B. (1962) *J. Am. Chem. Soc.* **84**, 4072.
Pierce C. and Ewing B. (1967) *J. Phys. Chem.* **71**, 3408.
Polley M.H., Schaeffer W.D. and Smith W.R. (1953) *J. Phys. Chem.* **57**, 469.
Prenzlow C.F. and Halsey G.D. (1957) *J. Phys. Chem.* **61**, 1158.
Puri B.R. (1970) In: *Chemistry and Physics of Carbon*, vol. 6 (P.L. Walker, ed.), Marcel Dekker, New York, p. 191.

Qadeer R. and Saleem M. (1997) *Adsorption Sci. Techn.* **15**, 373.
Rodriguez-Reinoso F. (1986) In: *Carbon and Coal Gasification* (J.L. Figueredo and J.A. Moulijn, eds), Martinus Nijhoff, Dordrecht, p. 601.
Rodriguez-Reinoso F. (1989) *Pure Appl. Chem.* **61**, 1859.
Rodriguez-Reinoso F., Martin-Martinez J.M., Prado-Burguete C. and McEnaney B. (1987) *J. Phys. Chem.* **91**, 515.
Rodriguez-Reinoso F., Garrido J., Martin-Martinez J.M., Molina-Sabio M. and Torregrosa, R. (1989) *Carbon* **27**, 23.
Rouquerol J., Partyka S. and Rouquerol F. (1977) *J. Chem. Soc., Faraday Trans. 1* **73**, 306.
Rouquerol J., Avnir D., Fairbridge C.W., Everett D.H., Haynes J.M., Pernicone, N., Ramsay J.D.F., Sing K.S.W. and Unger K.K. (1994) *Pure Appl. Chem.* **66**, 1739.
Rouzard J.N. and Oberlin A. (1989) *Carbon* **27**, 517.
Rudzinski W. and Everett D.H. (1992) In: *Adsorption of Gases on Heterogeneous Surfaces*, Academic Press, London, p. 142.
Ruthven D.M. (1984) *Principles of Adsorption and Adsorption Processes*, John Wiley, New York, p. 124.
Schaeffer W.D., Smith W.R. and Polley M.H. (1953) *Ind. Eng. Chem.* **45**, 1721.
Setoyama N. and Kaneko K. (1995) *Adsorption* **1**, 1.
Setoyama N., Ruike M., Kasu T., Suzuki T. and Kaneko K. (1993) *Langmuir* **9**, 2612.
Setoyama N., Kaneko K. and Rodriguez-Reinoso F. (1996) *J. Phys. Chem.* **100**(24), 10331.
Sing K.S.W. (1989) *Carbon* **27**, 5.
Sing K.S.W. (1991) In: *Third Int. Conf. on Fundamentals of Adsorption* (A.B. Mersmann and S.E. Scholl, eds), Engineering Foundation, New York, p. 69.
Sing K.S.W. (1994) *Carbon* **32**, 1311.
Sing K.S.W. (1995) In: *Porosity in Carbons* (J.W. Patrick, ed.), Edward Arnold, p. 49.
Smisek M. and Cerny S. (1970) In: *Active Carbon*, Elsevier, Amsterdam, p. 10.
Starsinic M., Taylor R.L. and Walker P.L. (1983) *Carbon* **21**, 69.
Steele W.A. (1956) *J. Chem. Phys.* **25**, 819.
Steele W.A. and Bojan M.J. (1989) *Pure. Appl. Chem.* **61**, 1927.
Steele W.A., Vernov A.V. and Tildesley D.J. (1987) *Carbon* **25**, 7.
Stoeckli H.F. (1981) *Carbon* **19**, 325.
Stoeckli H.F. (1993) *Adsorption Sci. Tech.* **10**, 3.
Stoeckli H.F., Huguenin D. and Laederach A. (1994a) *Carbon* **32**, 1359.
Stoeckli F., Jakubov T. and Lavanchy A. (1994b) *J. Chem. Soc., Faraday Trans.* **90**, 783.
Strelko V.V. (1997) In: *Characterisation of Porous Solids*, vol. IV (B. McEnaney, T.J. Mays, J. Rouquerol, F. Rodriguez-Reinoso, K.S.W. Sing and K.K Unger, eds), The Royal Society of Chemistry, Cambridge, p. 245.
Suzanne J. and Gay J.M. (1996) In: *Handbook of Surface Science*, vol. 1, Physical Structure, W.N. Unertl, vol. ed., N.V. Richardson and S. Holloway, series ed., North-Holland Elsevier, Amsterdam, p. 503.
Thomas J.M. (1965) In: *Chemistry and Physics of Carbon*, vol. 1 (P.L. Walker, ed.), Marcel Dekker, New York, p. 121.
Thomy A. and Duval X. (1969) *J. Chim. Phys.* **66**, 1966.
Thomy A., Regnier J. and Duval X. (1972) In: *Thermochimie*, Colloques Internationaux du CNRS, no. 201, Editions du CNRS, Paris, p. 511.
Tolmachev A.M. (1993) *Adsorption Sci. Tech.* **10**, 155.
van Driel J. (1983) In: *Activated Carbon: A Fascinating Material* (A. Capelle and F. de Vooys, eds), Norit N. V., Netherlands, p. 40.
Voloshuck A.M., Dubinin M.M., Moskovskaya T.A., Ivakhnyuk G.R. and Federov N.F. (1988) *Izv. Akad. Nauk. SSSR, Ser. Khim.* 277.
Walker P.L. and Janov J. (1968) *J. Colloid Interface Sci.* **28**, 499.
Wigmans, T. (1989) *Carbon* **27**, 13.
Youssef A.M., El-Wakil A.M., El-Sharkawy E.A., Farag A.B. and Tollan K. (1996) *Adsorption Sci. Techn.* **13**, 115.

Zawadzky J. (1989) In: *Chemistry and Physics of Carbon*, vol. 21 (P.A. Thrower, ed.), Marcel Dekker, New York, p. 147.

Zettlemoyer A.C. and Chessick J.J. (1974) In: *Advances in Chemistry*, no. 43, American Chemical Society, Washington DC, p. 58.

Zettlemoyer A.C., Young G.J, Chessick J.J. and Healey F.H. (1953) *J. Phys. Chem.* **57**, 649.

Ziolkowska D. and Garbacz J.K. (1997) *Adsorption Sci. Techn.* **15**, 155.

This Page Intentionally Left Blank

CHAPTER 10

Adsorption by Metal Oxides

10.1. Introduction

Some metal oxides (notably alumina, magnesia and silica) can be readily prepared in a stable state of high specific surface area. Because of their technical importance as adsorbents, they have been featured in many fundamental and applied investigations of adsorption. Other oxides (e.g. those of chromium, iron, nickel, titanium and zinc) tend to give surfaces of lower area, but exhibit specific adsorbent and catalytic activity. These oxides have also attracted considerable interest.

In their bulk properties, oxide adsorbents range from amorphous solids (e.g. silica)

to various crystalline forms (e.g. anatase and rutile), but they all tend to undergo surface hydration and/or hydroxylation as a means of achieving coordinative stabilization. The presence of other surface ligands can also be detected by infrared spectroscopy. An important consequence of the presence of surface hydroxyls is that many polar adsorptive molecules can interact in a specific manner with the surface. In some cases, surface dehydration leads to the exposure of strong cationic sites, while other parts of the surface may become less reactive. The possible types of specific interaction include hydrogen bonding and Lewis electron acceptor–donor exchange.

The most active oxide adsorbents are generally highly porous. In the past, the porosity was easy to produce but difficult to control, and therefore industrial adsorbents such as many silica gels and activated aluminas had complex micropore or mesopore structures. However, considerable progress has been made in recent years in the elucidation of the mechanisms of pore formation and development.

The aims of this chapter are: (a) to indicate the progress made in the development and characterization of some of the more important oxide adsorbents and (b) to illustrate the procedures described in earlier chapters for the interpretation of adsorption data.

10.2. Physisorption of Gases by Silica Powders and Gels

10.2.1. Pyrogenic and crystalline silicas

The pyrogenic silicas are formed at high temperatures. The most common type of 'fume silica', which is produced by the flame hydrolysis of silicon tetrachloride, is widely known as Aerosil. This term has become generic for the fume silicas, although strictly Aerosil is the trade mark of Degussa (Ferch, 1994). Other pyrogenic silicas are made by the high-temperature fusion or vaporization of sand in an arc or plasma.

From the standpoint of adsorption, the pyrogenic silicas can be regarded as essentially non-porous. Electron microscopic examination has demonstrated that the arc silicas (e.g. Degussa TK800 or TK900) consist of discrete spheroidal particles. However, the application of high-resolution electron microscopy has also revealed that the globules (typically of diameter 10–100 nm) are in fact agglomerates of much smaller spheroidal units of diameter around 1 nm (Barby, 1976). The coordination number of these primary particles is generally so high that there is no detectable micropore structure within the secondary globules.

In their original unaged and uncompacted state, the pyrogenic silicas give reversible Type II nitrogen isotherms at 77 K (as in Figure 10.1). When plotted in a reduced, dimensionless form (e.g. α_s versus p/p°), the isotherms lie on a common curve over a wide range of p/p° (Carruthers *et al.*, 1968; Bhambhani *et al.*, 1972).

The corresponding argon isotherms at 77 K also give a common reduced isotherm (Payne *et al.*, 1973), but in this case monolayer completion cannot be identified as a single point on the isotherm (i.e. Point B is not well defined). Another difference is that at 77 K the argon multilayer development is restricted at high p/p° (see Figure 10.1).

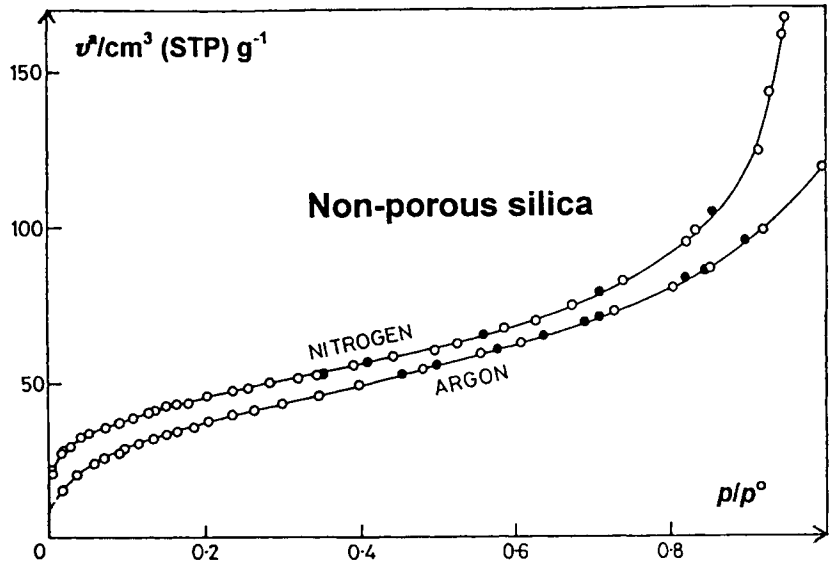

Figure 10.1. Argon and nitrogen isotherms at 77 K on non-porous silica TK800 (Payne *et al.*, 1973).

Standard isotherm data for nitrogen and argon adsorption at 77 K on non-porous hydroxylated silica are recorded in Tables 10.1 and 10.2, respectively. The original isotherms were determined on five different arc silicas having specific surface areas over the range 36–166 $m^2 g^{-1}$ (Carruthers *et al.*, 1968; Bhambhani *et al.*, 1972; Payne *et al.*, 1973). Close agreement is obtained in the monolayer and lower multilayer regions with reduced isotherms on Aerosil 200 and on mesoporous silica gels (Bhambhani *et al.*, 1972). However in view of the wide particle size distribution and the heterogeneous nature of these materials, it would now be of interest to determine the standard isotherms for a range of carefully prepared non-porous silicas.

The early work of Kiselev (1957) revealed that the adsorption isotherms of *n*-pentane and *n*-hexane on non-porous quartz were intermediate in character between Types II and III. Values of C(BET) < 10 were obtained and the differential enthalpies of adsorption decreased steeply at low surface coverage. More recently, the isotherms of isobutane (at 261 K) and neopentane (at 273 K) on TK800 have been found to be of a similar shape (Carrott *et al.*, 1988; Carrott and Sing, 1989). Unlike those of benzene, these alkane isotherms do not undergo a pronounced change of shape as a result of surface dehydroxylation. This is consistent with the non-specific nature of their molecular interactions (see Chapter 1).

The usefulness of the Frenkel–Halsey–Hill (FHH) equation for multilayer analysis was discussed in Chapters 4 and 9. FHH plots for nitrogen on various pyrogenic silicas are given in Figure 10.2. As expected, each FHH plot is linear over a wide range of $p/p°$, but this is rather more extensive (i.e. $p/p° \approx 0.3$–0.9) with the arc

Table 10.1. Standard data for the adsorption of nitrogen at 77 K on non-porous hydroxylated silica.

Relative pressure, $p/p°$	Adsorption per unit area (μmol m^{-2})	α_S ($= n/n_{0.4}$)
0.001	4.0	0.26
0.005	5.4	0.35
0.01	6.2	0.40
0.02	7.7	0.50
0.03	8.5	0.55
0.04	9.0	0.58
0.05	9.3	0.60
0.06	9.4	0.61
0.07	9.7	0.63
0.08	10.0	0.65
0.09	10.2	0.66
0.10	10.5	0.68
0.12	10.8	0.70
0.14	11.3	0.73
0.16	11.6	0.75
0.18	11.9	0.77
0.20	12.4	0.80
0.22	12.7	0.82
0.24	13.0	0.84
0.26	13.3	0.86
0.28	13.6	0.88
0.30	13.9	0.90
0.32	14.2	0.92
0.34	14.5	0.94
0.36	14.8	0.96
0.38	15.1	0.98
0.40	15.5	1.00
0.42	15.6	1.01
0.44	16.1	1.04
0.46	16.4	1.06
0.50	17.0	1.10
0.55	17.8	1.14
0.60	18.9	1.22
0.65	19.9	1.29
0.70	21.3	1.38
0.75	22.7	1.47
0.80	25.0	1.62
0.85	28.0	1.81
0.90	37.0	2.40

silicas, TK800 and TK900, when outgassed at 140°C. Dehydroxylation of the TK 800, by outgassing the adsorbent at 1000°C, has resulted in a deviation of the FHH plot from linearity at $p/p° < 0.5$. This deviation is likely to be associated with the reduction in the specific field gradient–quadrupole interactions as a result of the removal of surface hydroxyls. In the case of the FHH plot on the Aerosil 200, the small upward deviation from linearity, which is detectable at $p/p° > 0.8$, is due to interparticle capillary condensation.

Table 10.2. Standard data for the adsorption of argon at 77 K on non-porous hydroxylated silica

Relative pressure $p/p°$	α_S (= $n/n_{0.4}$)	Relative pressure $p/p°$	α_S (= $n/n_{0.4}$)
0.01	0.243	0.30	0.876
0.02	0.324	0.32	0.900
0.03	0.373	0.34	0.923
0.04	0.413	0.36	0.948
0.05	0.450	0.38	0.973
0.06	0.483	0.40	1.000
0.07	0.514	0.42	1.022
0.08	0.541	0.44	1.048
0.09	0.563	0.46	1.064
0.10	0.583	0.48	1.098
0.11	0.602	0.50	1.123
0.12	0.620	0.52	1.148
0.13	0.638	0.54	1.172
0.14	0.657	0.56	1.198
0.15	0.674	0.58	1.225
0.16	0.689	0.60	1.250
0.17	0.705	0.62	1.275
0.18	0.719	0.64	1.300
0.19	0.733	0.66	1.327
0.20	0.748	0.68	1.354
0.22	0.773	0.70	1.387
0.24	0.801	0.72	1.418
0.25	0.813	0.74	1.451
0.26	0.826	0.76	1.486
0.28	0.851	0.78	1.527

FHH plots have also been constructed from the isotherms of isobutane and neopentane on the pyrogenic silicas (Carrott *et al.*, 1988). Derived values of the FHH exponent, s, for neopentane s (np) and nitrogen s (N_2) are recorded in Table 10.3. Also included in this table are the BET-nitrogen surface areas a(BET-N_2), and the BET C values for nitrogen and neopentane C (N_2) and, C (np). As expected, the high-temperature treatment of TK800 and Aerosil 200 resulted in the removal of a high proportion of the surface OH groups: this in turn led to a significant reduction in the nitrogen–adsorbent interaction energy and consequently a decrease in the values of C (N_2).

The remarkable constancy of the values of s(N_2) and s(np) in Table 10.3 follows from the fact that the linear FHH plots are parallel in the multilayer range. These results confirm that the multilayer character of each adsorptive is rather insensitive to changes in surface chemistry.

The α_S-method has been used for the analysis of the isotherms of the following gases on porous and non-porous silicas: nitrogen (Bhambhani *et al.*, 1972; Carrott and Sing, 1984) argon (Carruthers *et al.*, 1971; Payne *et al.*, 1973) carbon tetrachloride (Cutting and Sing, 1969) and neopentane (Carrott *et al.*, 1988). A consistent pattern of behaviour has emerged from the study of different samples of the pyrogenic silicas. The derived α_S-plots are all linear over the monolayer and lower multilayer range. In

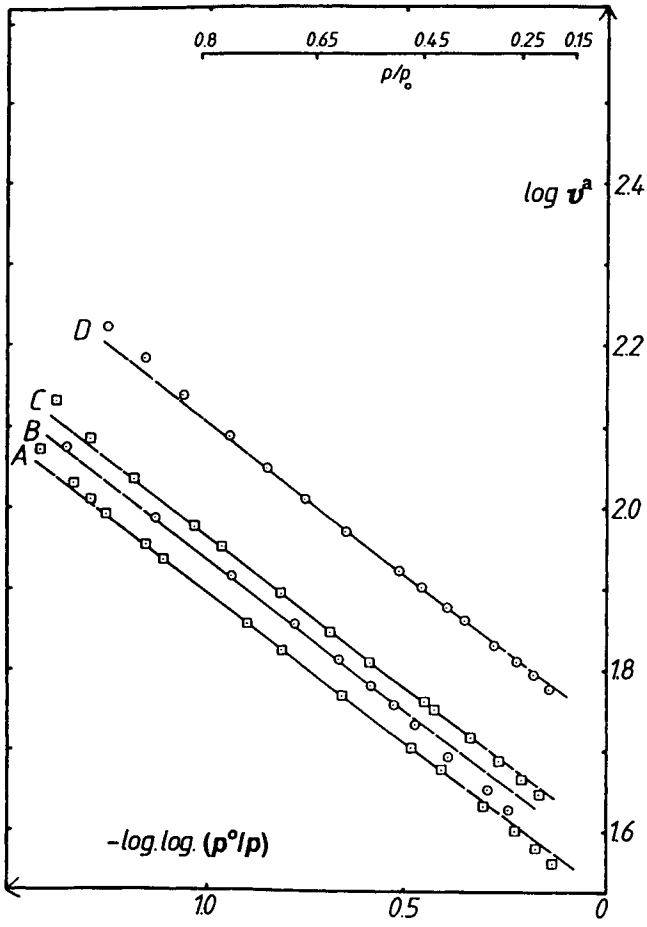

Figure 10.2. FHH plots for nitrogen adsorption on pyrogenic silicas. (A) TK900, 140°C; (B) TK800, 1000°C; (C) TK800, 140°C; (D) Aerosil 200, 140°C (Carrott *et al.*, 1982).

each case, back-extrapolation gives a zero intercept, which confirms the absence of microporosity. The α_S-plots on samples of Aerosil 200 exhibit an upward deviation in the higher multilayer region (see Figure 10.3) which is consistent with the FHH evidence that some interparticle capillary condensation has occurred.

As to be expected from the shape of the nitrogen isotherms and the linearity of the α_S-plots in Figure 10.3, satisfactory agreement is obtained between the corresponding values of the BET area, a(BET), and the area a(S), calculated from the slope of the α_s-plot – as indicated in Table 10.4. Here, the value of a(S) is given by

$$a(\mathrm{S}) = 0.0641 n/\alpha_S \qquad (10.1)$$

where the amount adsorbed, n, is expressed in μmol g^{-1} and the factor 0.0641 has been obtained by calibration against Fransil – a well-characterized arc silica having a BET area of 38.7 $m^2 g^{-1}$ (Bhambhani *et al.*, 1972).

Table 10.3. FHH s values for nitrogen (at 77 K) and neopentane (at 273 K) on pyrogenic silicas.

Silica	a(BET-N_2) ($m^2\ g^{-1}$)	$C(N_2)$	$s(N_2)$	C(np)	s(np)	σ(np) (nm^2)
TK800	158	94	2.72	6	1.97	0.62
TK900	136	101	2.71	7	1.97	0.60
TK900[a]	120	47	2.69	8	1.96	0.58
Aeros 200	205	95	2.67	7	2.01	0.60
Aeros 200*	192	43	2.68	8	2.00	0.59

[a]Heated in pure N_2 for 8 hours at 950°C.
Results taken from Carrott *et al.* (1988).

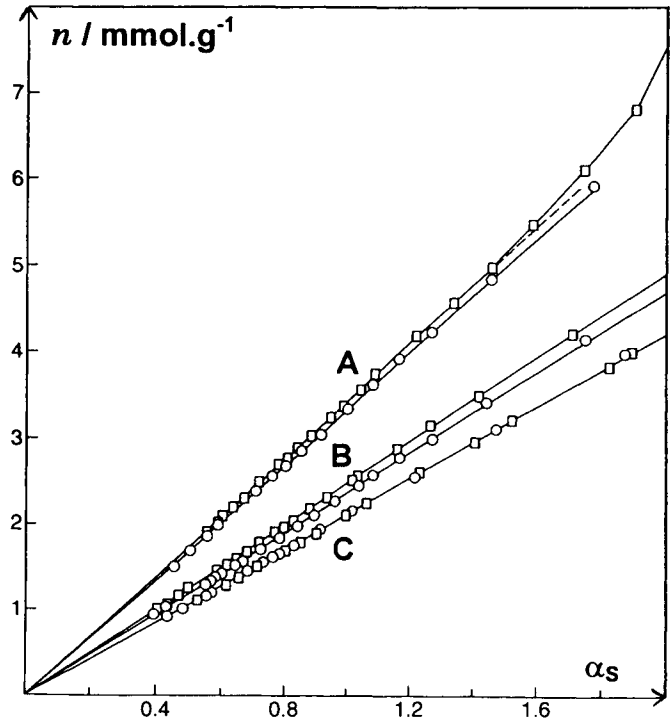

Figure 10.3. Representative α_S-plots for nitrogen adsorption on pyrogenic silicas. (A) Aerosil 200; (B) TK800; (C) TK900, outgassed at 298 K (circles) or at 413 K (squares) (Carrott and Sing, 1984).

The situation is more complicated when Point B is either non-existent (as with the alkanes) or ill-defined (as with argon and krypton) since the physical significance of the BET monolayer capacity, n_m, is now questionable. However, some progress can be made if we proceed in the following way: instead of using an assumed value of molecular area σ, to obtain a(BET), we now derive the apparent value of σ from a(S) and n_m. The values of apparent molecular area, σ(np), of adsorbed neopentane in Table 10.3 are calculated from its BET monolayer capacity, n_m(np), and the surface

Table 10.4. Comparison of surface areas of pyrogenic silicas evaluated by the BET and α_S-method.

Silica	Outgassing T(K)	a(BET) ($m^2\,g^{-1}$)	a(S) ($m^2\,g^{-1}$)
TK800	298	153	151
	413	158	158
TK900	298	136	136
	413	136	135
Aerosil 200	298	215	213
	413	221	218

area $a(N_2)$ determined by nitrogen adsorption. Thus,

$$\frac{\sigma(\text{np})}{\text{nm}^2} = \frac{1.66a(N_2)/\text{m}^2\,\text{g}^{-1}}{n_m(\text{np})/\mu\text{mol}\,\text{g}^{-1}} \tag{10.2}$$

The five σ(np) values in Table 10.3 are in close agreement (i.e. 0.595 ± 0.015 nm^2), but they are much larger than the value, 0.40 nm^2, calculated for a close-packed monolayer of freely rotating neopentane molecules. However, it must be kept in mind that the C(BET) values are very low (i.e. 6–8) and therefore it is unlikely that n_m(np) represents the true statistical monolayer capacity.

Prolonged storage of a pyrogenic silica can result in slow ageing, as indicated by a loss of BET area. For example, the original specific surface area of a master batch of TK800, as evaluated from the measurements of Payne *et al.* (1973) and Baker and Sing (1976), was 163–166 $m^2\,g^{-1}$. A loss of area of *c.* 6 $m^2\,g^{-1}$, which occurred over a period of eight years, was evidently due to the development of some interparticle mesoporosity since this led to the development of a narrow hysteresis loop in the nitrogen isotherm at high nitrogen $p/p°$ (Carrott and Sing, 1984). A partial restoration in area was achieved by raising the outgassing temperature from 25°C to 140°C (see Table 10.4). This restoration was probably due to the removal of water from the particle interstices: it is likely that the presence of residual water and compaction were together responsible for the loss of area.

A number of detailed studies have been made of the physisorption of gases on compacted silica powders (Avery and Ramsay, 1973; Gregg and Langford, 1977). The changes in the character of nitrogen adsorption as a result of increasing the compacting pressure are shown in Figure 10.4.

It is striking that the isotherms in Figure 10.4 change first from Type II to IV and finally to Type I. Thus, the results of Avery and Ramsay (1973) have clearly demonstrated that mesopores and micropores can be produced by the progressive compaction of a non-porous powder. However, a drastic loss of surface area accompanied this change (from 630 to 219 $m^2\,g^{-1}$) and Avery and Ramsay point out that this was associated with a marked increase in the particle packing density.

The importance of surface silanol (hydroxyl) groups in controlling the specific physisorption interactions was studied by Kiselev (1958, 1971). Kiselev and his coworkers found that fully hydroxylated silica has a surface OH concentration of 7–9 μmol m^{-2}, which corresponds to a surface population, N(OH), of *c.* 5 OH nm^{-2}

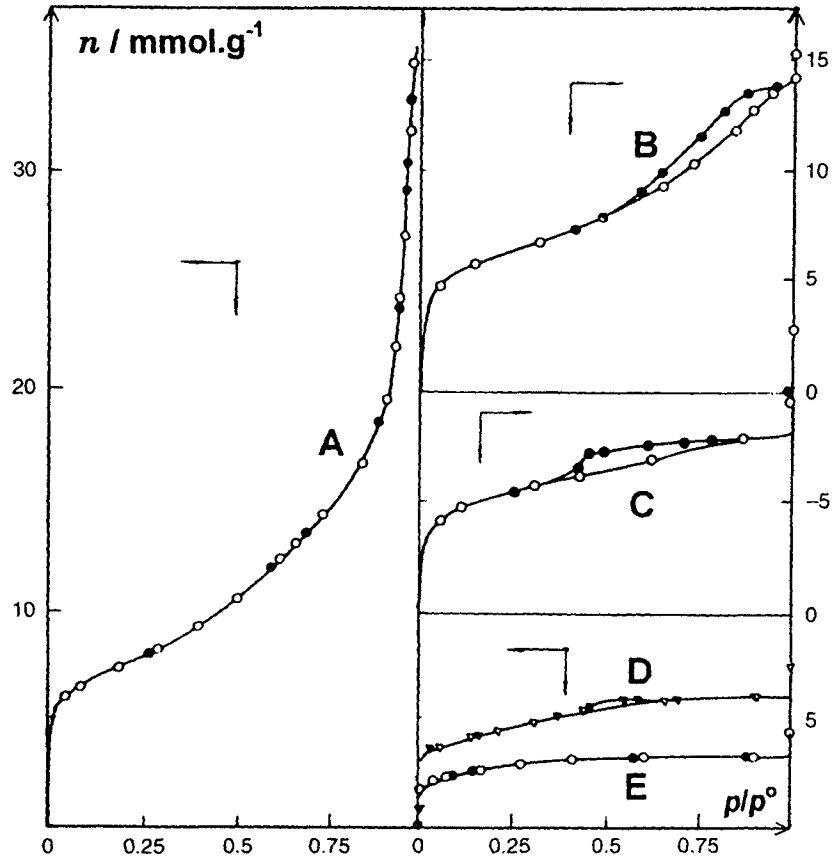

Figure 10.4. Effect of compaction of Aerosil on nitrogen adsorption isotherms at 77 K; (A) uncompressed or compressed under (B) 1.5, (C) 6, (D) 7.5 or (E) 15 kbar (reproduced courtesy of Avery and Ramsay, 1973).

(Zhuravlev and Kiselev, 1970). More recently, Zhuravlev (1987) reported a mean N(OH) value of 4.9 OH nm^{-2} (after outgassing at 180–200°C) for 100 fully hydroxylated amorphous silicas. This value is not far removed from N(OH) = 4.6 OH nm^{-2}, originally proposed by Vleeskens (see Okkerse, 1970).

A fully hydroxylated state in which all the OH groups are bound to Si atoms (with N(OH) = 4.6 OH nm^{-2}) would correspond to the octahedral, (111), face of β-cristobalite or the basal face of β-tridymite. However, as indicated in Table 10.5, the surface hydroxyl concentrations found on some arc and fume silicas are significantly lower, typical values being in the range 3.4–4 OH nm^{-2} (Baker and Sing, 1976; Unger, 1979, p. 62; Gallas *et al.*, 1991).

As was noted earlier, the level of surface OH concentration has very little effect on either the isotherms or the energetics of adsorption of non-polar molecules such as argon or the alkanes. Specific interactions become significant when the adsorptive

Table 10.5. Levels of hydroxylation and sorption of water vapour by pyrogenic and precipitated silicas and mesoporous silica gels.

Silica	Outgassing θ (°C)	N(OH) (nm^2)	Water adsorption at $p/p^\circ = 0.2$ ($\mu mol\ m^{-2}$)
Fransil	25	4	5.3
TK800	25	3.6	5.0
	1000	~0	1.3
VN3	25	14[a]	22
SiO_2 gels	25	3.4, 5[a]	6.4, 6.5[b]
	1000	~0	1.3

[a]Results of Gallas *et al.* (1991).
[b]Results of Kiselev (1958, 1971).

molecules are quadrupolar (e.g. nitrogen and carbon dioxide) and even more so when hydrogen bonding is involved (e.g. with water or the lower alcohols).

Many investigations have been made of the adsorption of water vapour on amorphous silicas (e.g. Zettlemoyer, 1968; Baker and Sing, 1976; Iler, 1979, p. 651; Unger, 1979, p. 196; Burneau *et al.*, 1990). There is general agreement that the removal of surface silanols by heat treatment causes a drastic reduction in the level of water adsorption (see Table 10.5). It might be expected that there would be a simple correlation between the surface OH concentration and the affinity for water vapour. However, systematic adsorption calorimetric and infrared spectroscopic investigations by Fubini *et al.*, (1992) and Gallas *et al.*, (1991) have revealed a more complex behaviour.

It is now apparent that isolated silanols have relatively low affinity for water. Thus, the hydrophobic nature of silica is manifested after dehydroxylation when only the siloxane bridges and some isolated silanols (giving an IR band at *c.* 3750 cm^{-1}) remain. On the dehydroxylated surface the net adsorption enthalpy for water is negative. In this case, the enthalpy of adsorption is lower than the normal enthalpy of condensation. Application of adsorption microcalorimetry has allowed an assessment to be made of the relative extents of the hydrophilic and hydrophobic areas of the surface (Bolis *et al.*, 1991). On the hydrophilic surface, it appears that water is adsorbed via two hydrogen bonds to two silanols – one acting as the hydrogen donor and the other as the acceptor. In the case of the weaker attachment to the isolated OH, the attachment involves one hydrogen bond.

Comparisons made between the properties of crystalline and amorphous silicas (Bolis *et al.*, 1991; Fubini *et al.*, 1992) have brought to light some interesting differences. For example, quartz is much less easily dehydroxylated than the pyrogenic silicas, which is consistent with its more persistent hydrophilic character (Pashley and Kitchener, 1979). In their study of the adsorption of water on α-cristobalite Fubini and her co-workers (1992) obtained a number of irreversible water isotherms, the nature of which depended on the thermal pre-treatment. The complete rehydroxylation of a hydrophobic silica by exposure to water vapour is usually slow, but with some dehydroxylated samples a fairly rapid stage of dissociative chemisorption leads to pronounced hysteresis, which extends across the complete range of p/p° as in Figure 10.13 (Baker and Sing, 1976).

Adsorption microcalorimetry has shown that the surfaces of both amorphous and crystalline silicas are energetically heterogeneous. Furthermore, the IR spectroscopic evidence reveals that their surface structures are dependent on the conditions of preparation and treatment (Unger, 1994).

10.2.2. Precipitated silicas

Although commercially important, the precipitated silicas have received much less attention in the scientific literature than either the Aerosils or silica gels. In certain respects they are similar to pyrogenic silicas: indeed, at one time they were treated as alternative non-porous silicas. Thus, the reversible Type II isotherms of nitrogen and argon obtained by Basset *et al.* (1968) were assumed to represent uncomplicated monolayer–multilayer adsorption. More recent work (Carrott and Sing, 1984) has shown that the Type II character is here the result of adsorption both on the external surface and within some micropores.

In contrast to the general behaviour of the pyrogenic silicas, the level of physisorption by precipitated silicas has been found to be sensitive to changes in the conditions of outgassing. Physisorption equilibration is more difficult to attain and consequently the isotherms often have a more complicated appearance. For example, the behaviour of a batch of VN3 (a Degussa product) is illustrated by the results in Figure 10.5 (Carrott and Sing, 1984). It can be seen that the increase in outgassing temperature from 25°C to 110°C has produced a significant upward movement in the nitrogen isotherm. In addition it has led to the appearance of a small step in the amount adsorbed at $p/p^\circ \approx 0.6$ and to the development of a small amount of low pressure hysteresis. Similar features are exhibited by the isotherms determined after outgassing at the temperatures of 200°C and 300°C, but in the latter case the step is located at a much lower relative pressure ($p/p^\circ \approx 0.2$) and the open hysteresis extends over the complete isotherm. It is evident that these steps cannot be explained in terms of any well-defined phase transitions. They are more likely to be due to the slow diffusion of the adsorptive molecules into inner regions of the particles, which are not easily accessible.

The α_S-plots for nitrogen on VN3 in Figure 10.5 have been constructed from the *desorption* isotherms. In each case, the back-extrapolated linear portion gives a positive intercept on the n axis and an upward deviation can be seen at $p/p^\circ \approx 0.7$. This behaviour is typical of adsorption at low p/p° occurring both on the external surface and within narrow micropores. At higher p/p°, the upward deviation indicates that the multilayer adsorption on the external surface is accompanied by interparticle capillary condensation, which is partly responsible for the narrow hysteresis loop.

The α_S-plots in Figure 10.5 have been analysed by the method described in Chapter 8. The values of the external surface area, a(ext, S), and micropore volume, v_p(mic, S), in Table 10.6 have been calculated from the slope and intercept, respectively, of each α_S-plot. It can be seen that the external area does not change to any significant extent over the range 110–300°C and that the changes in the BET area, a(BET), are due to the development of a small micropore volume.

Further confirmation of the development of microporosity has been obtained by the application of the nonane pre-adsorption method of Gregg and Langford (1969).

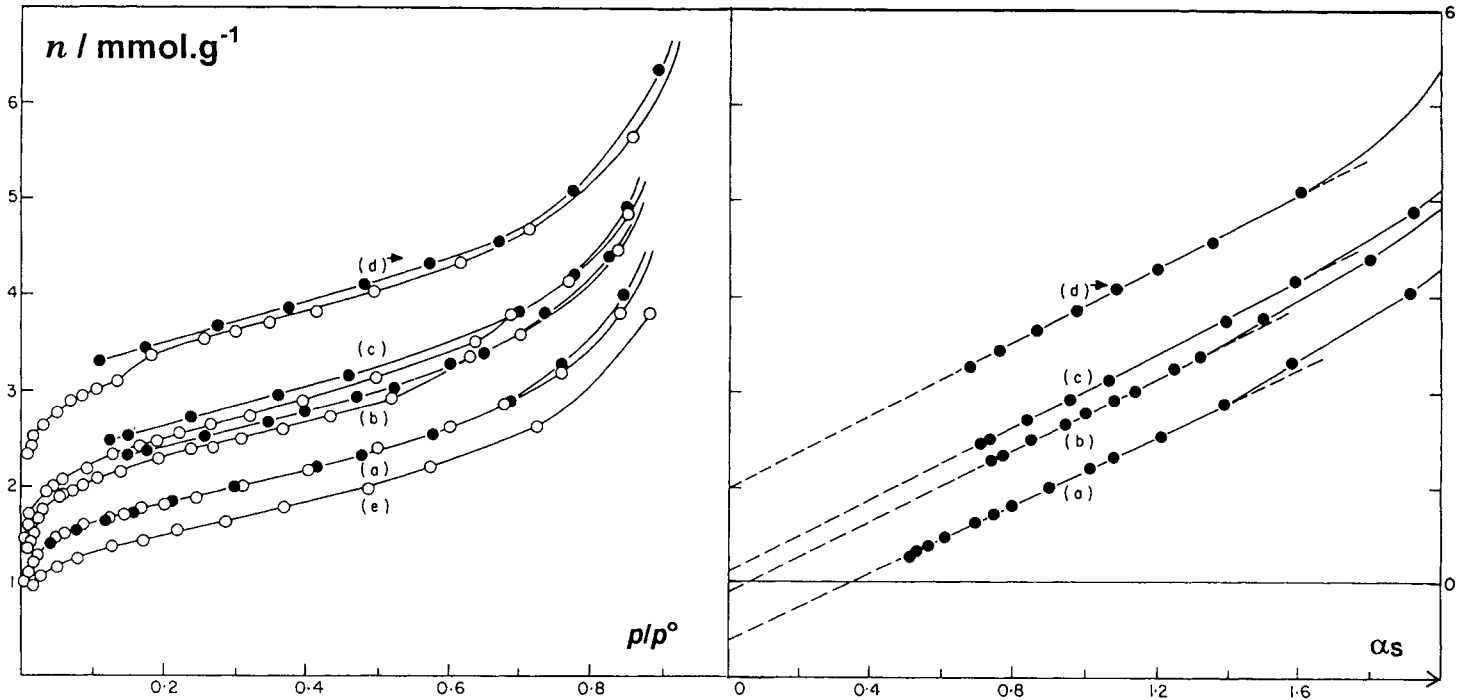

Figure 10.5. Nitrogen isotherms (left, with open circles for adsorption and closed circles for desorption) and α_S plots (right) for precipitated silica VN3 outgassed at (a) 25°C, (b) 110°C, (c) 200°C and (d) 300°C, with ordinate shifted upwards of 1 mmol g^{-1}, for clarity). Run (e) after outgassing at 200°C and *n*-nonane pre-adsorption (Carrott and Sing, 1984).

Table 10.6. Values of BET area, external area and micropore volume given by a precipitated silica, VN3, outgassed at various temperatures.

Outgassing temperature (K)	a(BET)($m^2\ g^{-1}$)	a(ext, S)($m^2\ g^{-1}$)	v_p(mic, S)($cm^3\ g^{-1}$)
298	146	114	0.014
383	178	122	0.027
473	195	124	0.034
573	174	125	0.030

After it had been outgassed at 200°C, the sample of VN3 was exposed to *n*-nonane vapour, then outgassed at 25°C and the nitrogen isotherm redetermined. The result is isotherm (e) in Figure 10.5 and the derived value of a(BET) is now 122 $m^2\ g^{-1}$, which is in good agreement with the external area a(ext S) = 124 $m^2\ g^{-1}$.

Gallas *et al.* (1991) noted the exceedingly high value of the silanol population (14 OH nm^{-2}) in their sample of precipitated silica, which they attribute to the presence of many inner hydroxyls. This is consistent with the abnormally large water uptake by VN3 – as indicated in Table 10.5. This is much greater than the amount (*c.* 15.7 $\mu mol\ m^{-2}$) required to give a close-packed water monolayer and is further evidence of the microporous nature of precipitated silicas.

We conclude that in the precipitation process, the trapping of water has resulted in the formation of a more open intraparticle microstructure than in the pyrogenic silicas. The internal surface remains hydroxylated, but is not easily accessible to most adsorptive molecules. Water molecules are able to undergo specific interactions with the internal OH groups which accounts for the abnormally high uptake of water vapour.

10.2.3. Silica gels

Over the past 70 years a large number of physisorption studies have been reported on silica gels (Deitz, 1944; Brunauer, 1945; Okkersee, 1970; Barby, 1976; Iler, 1979, p. 488). It is not difficult to prepare stable adsorbent silica xerogels in a highly porous and fairly dense granular form. Although other more refined routes are now available, commercial silica gels are still prepared in large quantity by the dehydration of the hydrogels produced by reacting sodium silicate with acid (Patterson, 1994). These materials are widely used as relatively inexpensive adsorbents, desiccants and catalyst supports.

Many of the early physisorption measurements were undertaken on ill-defined silica gels of unknown origin. However, as a result of systematic work on the formation of the hydrogel and its ageing and conversion to the xerogel, it is now possible to control the adsorptive properties within quite narrow limits (Barby, 1976; Iler 1979, p. 488; Unger, 1979, p. 196; Kenny and Sing, 1994).

Monosilicic acid is stable in aqueous solution only at low pH and very low concentration (Iler, 1979, p. 209). The rate of condensation-polymerization of silicic acid is dependent on pH, concentration and temperature. At a certain stage, the polysilicic acid sol is converted into either a precipitate (i.e. a flocculated system) or a hydrogel.

Further changes take place when the hydrogel is brought into contact with an ageing medium. The mechanisms of ageing include aggregation-cementation and Ostwald ripening and result in changes in the size and packing density of the colloidal particles. Particle growth and particle–particle siloxane (Si–O–Si) bonding are largely irreversible, but it is possible to achieve a certain degree of depolymerization, e.g. by acid treatment (Mitchell, 1966).

The hydrogel has an open structure (i.e. a low particle coordination number) and is mechanically weak. The removal of the aqueous liquid phase normally leads to a drastic shrinkage of the silica framework and the formation of additional siloxane bonds (Fenelonov *et al.*, 1983). The resulting xerogel is therefore much stronger and more compact, but inevitably has a lower pore volume.

Until the availability of high-resolution electron microscopy, the structure of silica xerogels remained a matter of conjecture. Now, there is no longer any doubt that the amorphous framework is made up of very small globular units (see Figure 10.6). These primary particles are isotropic and have fairly uniform size of 1–2 nm (with a molar mass $\approx 2000\ \text{g mol}^{-1}$). In some xerogels the primary particles are densely packed within secondary particles, whereas in other systems there is a more open arrangement (Barby, 1976).

The texture of the dry xerogel depends partly on the properties of its parent hydrogel and partly on the conditions of the conversion. The dependence of the final xerogel porosity on the conditions of gelation and after-treatment have been investigated in some detail (see Barby, 1976; Iler, 1979, p. 209; Kenny and Sing, 1994). In the early work of Madeley and Sing (1953, 1954, 1962) microporous products were obtained from hydrogels prepared by the addition of sodium silicate to sulfuric acid at relatively low pH (e.g. ≈pH 3.5). Mesoporous products were produced when the reaction was carried out at a higher pH (≈pH 6). On the other hand, changes in the silicic acid concentration over a wide range had little effect, provided that the gelation was conducted in a buffered aqueous medium (Madeley and Sing, 1962).

Neimark *et al.* (1964) carried out extensive investigations of the effects of ageing silica hydrogels in various media. It was found that the dispersed state was stabilized when the hydrogel was left in contact with acids (at pH 2–5) which appeared to be due to the protection afforded by hydrogen-bonded water (i.e. a 'hydrate shell') around the particles. The effect that acid washing has in enhancing the adsorption activity is illustrated by the results in Figure 10.7. In this case, the original hydrogel was prepared at pH 5.4 and portions were then subjected to different forms of after-treatment (Wong,1982). Soaking in HCl (at pH 2.0 for 24 h) resulted in a significant upward movement of the complete nitrogen isotherm: analysis of the adsorption data revealed an increase in BET-nitrogen area, a(BET), from 284 to 380 $\text{m}^2\,\text{g}^{-1}$ and an increase in pore volume, v_p, from 0.44 to 0.55 $\text{cm}^3\,\text{g}^{-1}$.

The fact that the shape of the isotherms in Figure 10.7 has remained almost unchanged after the acid treatment is an indication that the mesopore structure was not altered to any signifiant extent. However, as pointed out in Chapter 7, this form of H2 hysteresis loop is not easy to interpret since it is associated with pronounced percolation effects in an irregular pore network.

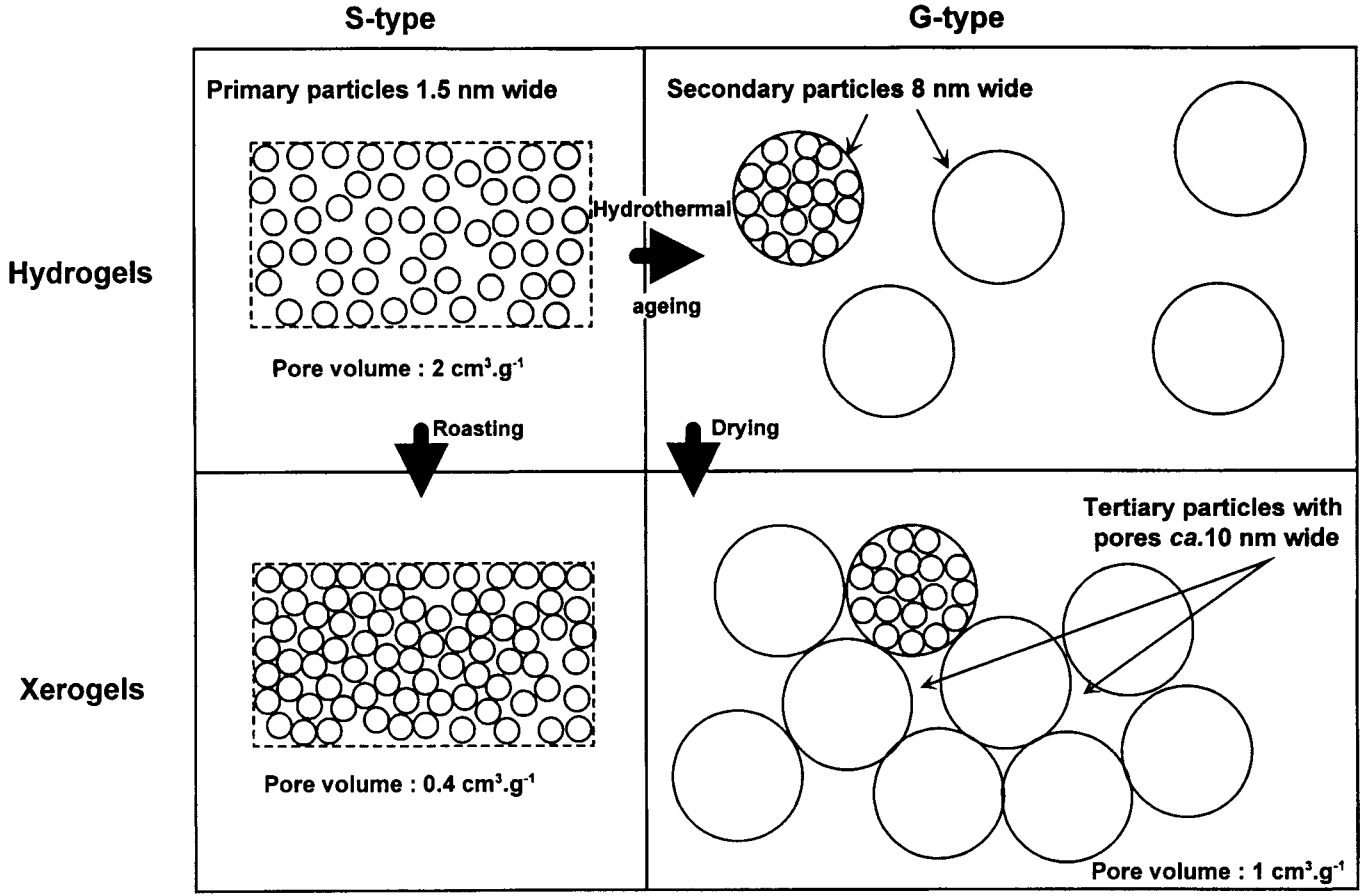

Figure 10.6. Morphology of silica gel (after Barby, 1976).

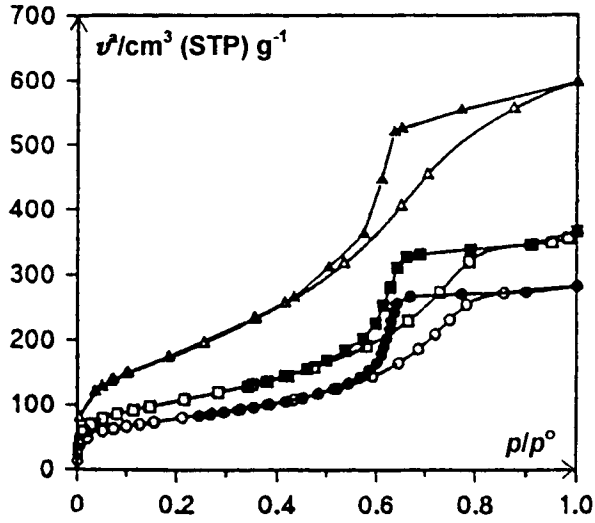

Figure 10.7. Nitrogen isotherms at 77 K for xerogel (circles), acid-washed xerogel (squares; HCl, pH2, 24 h) and alcogel (triangles) (Kenny and Sing, 1994).

The most striking result in Figure 10.7 was obtained when the hydrogel was washed with ethyl alcohol. The vacuum-dried material, which we shall refer to as an 'alcogel', gave a much larger uptake of nitrogen over the complete range of $p/p°$: $a(\text{BET}) = 641\ \text{m}^2\,\text{g}^{-1}$ and $v_p = 0.93\ \text{cm}^3\,\text{g}^{-1}$. It is evident that by replacing water as the continuous liquid phase, it was possible to reduce the large capillary forces which are responsible for the considerable shrinkage normally found when water is removed from the hydrogel.

An even larger pore volume can be obtained if the liquid phase is removed under supercritical conditions to give an 'aerogel'. This type of gel has an extremely high surface area and pore volume (see Table 10.7), but it tends to be mechanically weak and unstable when exposed to water vapour because the particle coordination number is low. The upper limiting area of a silica composed of discrete primary particles would be $\approx 2000\ \text{m}^2\,\text{g}^{-1}$, but specific surface areas of this magnitude are unlikely to be attained.

Barby (1976) has defined two types of conventional silica xerogels (Table 10.7). The S-type gels can be either microporous or mesoporous and are produced in the normal way, which allows considerable loss of suface area and pore volume to occur during the removal of water from the hydrogel. If the hydrogel is subjected to hydrothermal treatment, the primary particles undergo more drastic aggregation-cementation with the result that after drying the porosity is largely confined to the interstitial space between the secondary particles, as in Figure 10.6. The resulting G-type xerogel has a somewhat lower surface area, but a larger and more uniform pore volume (Barby, 1976).

In view of the complexity of the structure of most silica xerogels, it is to be expected that their adsorptive behaviour would be equally complex. The following

Table 10.7. The properties of typical silica gels.

Gel type	Porosity	a(BET) ($m^2\,g^{-1}$)	v_p ($cm^3\,g^{-1}$)
Aerogel	Macro	800	2.0
G-Xerogel	Meso	350	1.2
S-Xerogel	Meso	500	0.6
	Micro	700	0.4

questions are pertinent:

(a) How reliable are the derived values of a(BET) and pore size distribution?
(b) Can we identify the various stages of micropore and mesopore filling?

The following discussion of some typical data for the adsorption of nitrogen and argon will throw light on these questions and also illustrate the value of using the α_S-method of isotherm analysis.

The isotherms and corresponding α_S-plots in Figures 10.8 and 10.9 are for the adsorption of nitrogen on representative mesoporous and microporous silica gels (Bhambhani *et al.*, 1972). The derived values of the specific surface area are given in Table 10.8. The values of the BET nitrogen area, a(BET), in Table 10.8 are based on the usual assumption that the adsorbed molecules were close-packed in the completed monolayer (i.e. $\sigma(N_2) = 0.162$ nm^2). The corresponding values of $a(S, N_2)$ were calculated from the initial slope of the α_S-plots by the relation

$$a(S, N_2) = 2.89\, v^{\sigma}(STP) / \alpha_S \qquad (10.3)$$

which is another form of Equation (10.1). Here v^{σ}(STP), or v^{a}, is the volume of nitrogen adsorbed, expressed in cm^3 (STP) g^{-1}, and the factor 2.89 has been obtained by calibration against the BET area of Fransil.

The good agreement between the corresponding values of $a(BET, N_2)$ and $a(S, N_2)$ in Table 10.8 is an indication that gels A, G and J were mesoporous, which is confirmed by the characteristic shapes of the isotherms and α_S-plots in Figure 10.8. However, the range of linearity of each α_S-plot does not extend above $p/p^\circ = 0.4$, which in the case of gels G and J is just below the lower limit of hysteresis. This result is consistent with the likehood of some reversible capillary condensation occurring around the contact regions of the globular particles.

The nitrogen isotherms on the microporous gels D and E in Figure 10.9 are of Type I in the IUPAC classification (now designated Type Ib). The gradual approach to the plateau at $p/p^\circ \approx 0.4$ is an indication that both gels contained a wide distribution of micropores (see Chapter 8). The α_s-plot on gel D confirms that there were two stages of micropore filling: primary micropore filling at $p/p^\circ < 0.01$ has resulted in some initial distortion of the isotherm while secondary (co-operative) micropore filling of supermicropores has taken place over the range $p/p^\circ \approx 0.02$–0.2. Comparison of the derived areas for gels D and E in Table 10.8 confirms the expected differences in the corresponding values of a(BET) and a(S). It is evident that the BET method cannot be relied upon to provide an accurate evaluation of the internal surface areas of such microporous silica gels.

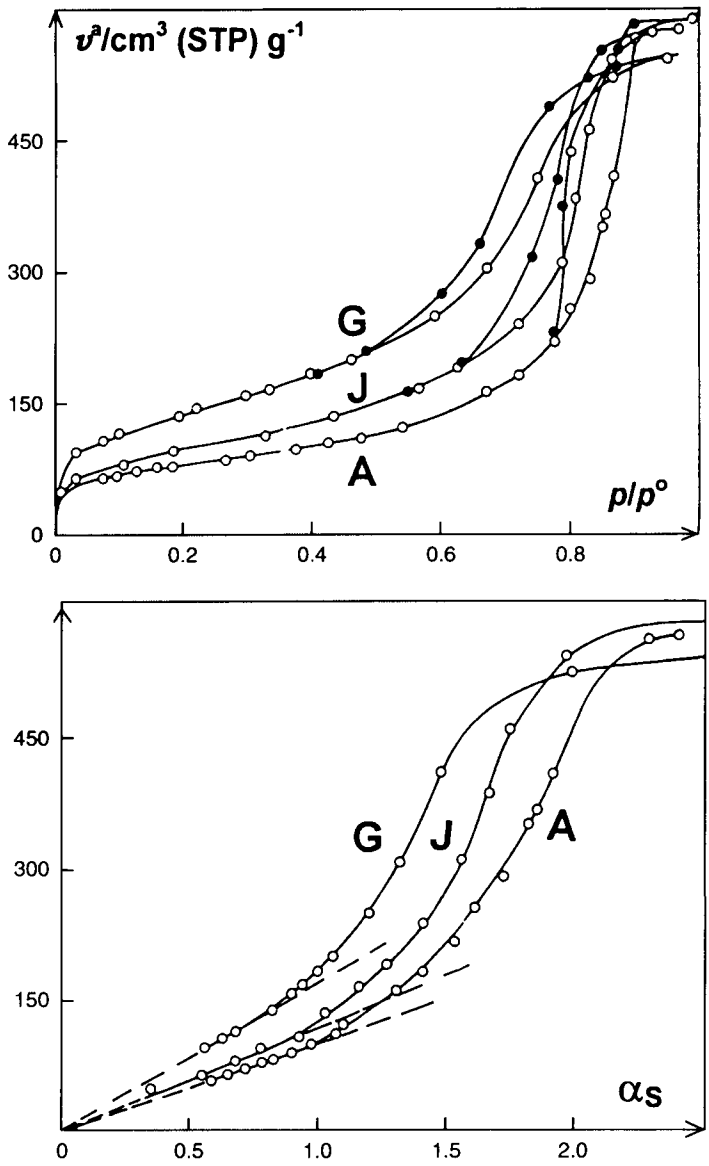

Figure 10.8. Nitrogen isotherms (top) and α_S-plots (bottom) for mesoporous silica gels A, J and G (from Bhambhani *et al.*, 1972).

As explained in Chapter 8, the external surface area, a(ext, S), available for multilayer adsorption can be calculated from the high $p/p°$ section of an α_S-plot, provided that there is an adequate range of linearity to confirm the absence of capillary condensation. This condition is clearly fulfilled with gels D and E, and their external areas are therefore recorded in Table 10.8.

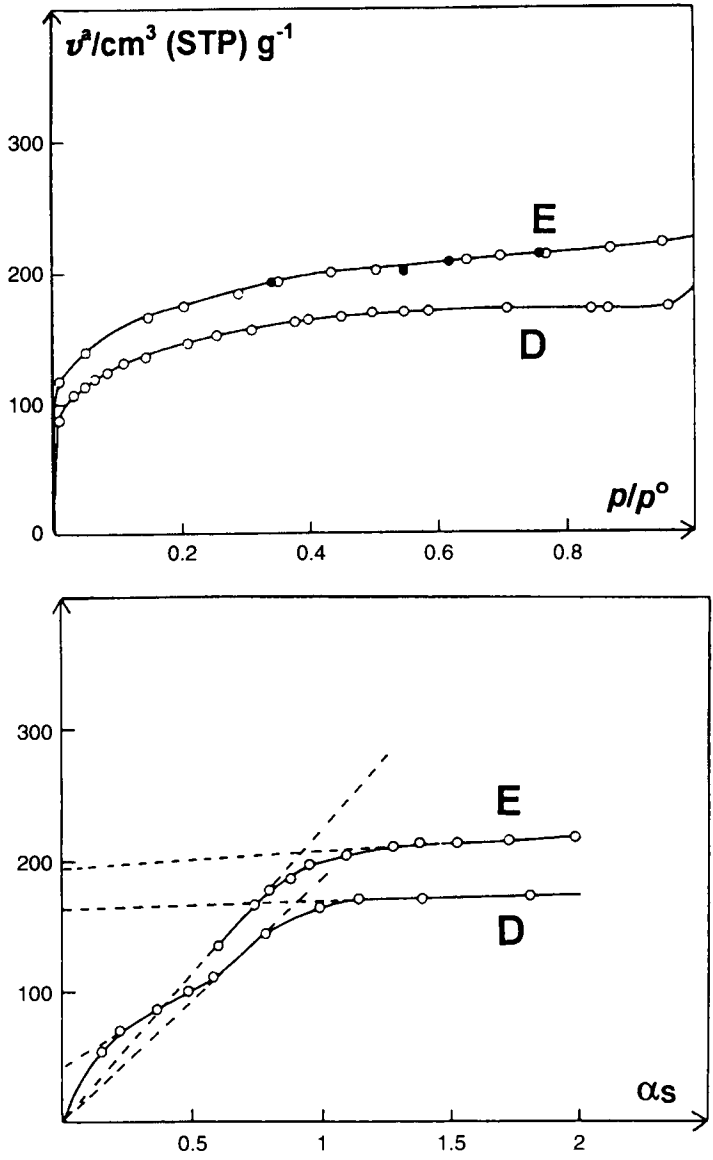

Figure 10.9. Nitrogen isotherms (top) and α_S-plots (bottom) for microporous silica gels D and E (from Bhambhani *et al.*, 1972).

We turn now to the argon isotherms and α_S-plots, respectively, in Figures 10.10 and 10.11 (from the data of Payne *et al.*, 1973). Here, the experimentally determined value of $p°$(i.e. $p°$(solid)) at 77 K has been used to calculate $p/p°$. It is of interest to compare the shapes of the argon isotherms with those of nitrogen on the same adsorbents (mesoporous gel B and microporous gel C). The nitrogen isotherm on gel B has

Table 10.8. Comparison of values of surface area derived from nitrogen BET plots and α_S-plots.

Silica	Porosity	a(BET) ($m^2\ g^{-1}$)	a(S, N_2) ($m^2\ g^{-1}$)
Gel A	Meso	300	303
Gel G	Meso	504	503
Gel J	Meso	349	350
Gel D	Micro	767	810–960, 35[a]
Gel E	Micro	631	730, 20[a]

[a] Values of external area, a(ext).

a well-defined Point B (C(BET) ≈ 100), while the argon isotherm has a more gradual curvature and no distinctive Point B (C(BET) < 50). In the middle range, these two isotherms run roughly parallel. It will be recalled that this behaviour is very similar to that on TK800 (see Figure 10.1). The Type I isotherms on gel C in Figure 10.10 have the typical features of Type Ib isotherms but the most striking aspect is the crossover of nitrogen by argon which occurs at $p/p° \approx 0.1$.

The deviations from linearity shown by the α_S-plots on gels B and C in Figure 10.11 confirm the respective mesoporous and microporous nature of these silica gels. Thus, the α_S-plot on gel B is linear up to $p/p° = 0.4$ (i.e. $\alpha_S = 1$). This indicates that the argon monolayer has formed on the mesopore surface in the same manner as on the non-porous surface. The upward deviation is clearly due to the onset of capillary condensation.

The behaviour of gel C is quite different. In this case, there is a strong distortion of the isotherm at $p/p° < 0.02$, which results in the positive intercept of the α_S-plot. This is followed by two linear regions, the first being associated with surface coverage and filling of supermicropores and the second with multilayer coverage of the external surface. Back-extrapolation of these two linear parts provides a means of assessing the volume of the ultramicropores, v_p(u) (of width ⩽ 1 nm), and the total micropore volume, v_p(t).

The values of specific surface area, a(S, Ar), in Table 10.9 are calculated from the linear sections of the argon α_S-plots by application of the equation

$$a(\text{S, Ar}) = 3.30\ v^{\sigma}(\text{STP})/\alpha_S \qquad (10.4)$$

where v^{σ}(STP), or v^{a}, is the volume (cm^3 (STP) g^{-1}) of argon adsorbed and the factor 3.30 has been obtained by calibration against the BET-nitrogen areas of Fransil and TK800. Comparison is made with the corresponding areas determined by nitrogen adsorption.

The results in Table 10.9 and other data (Rouquerol *et al.*, 1979b) reveal that for non-porous and mesoporous silicas good agreement is obtained between the corresponding values of a(S, Ar), a(BET, Ar) and a(BET, N_2), provided that the apparent molecular area of argon, σ(Ar), is taken as *c.* 0.182 nm^2. It must be kept in mind that the argon BET plots are based on $p°$(solid): if the extrapolated $p°$(liquid) for liquid argon is used, the adjusted σ(Ar) becomes ≈ 0.17 nm^2 (Gregg and Sing, 1982). The value σ(Ar) = 0.138 nm^2, originally adopted by Brunauer and Emmett (1937), is for

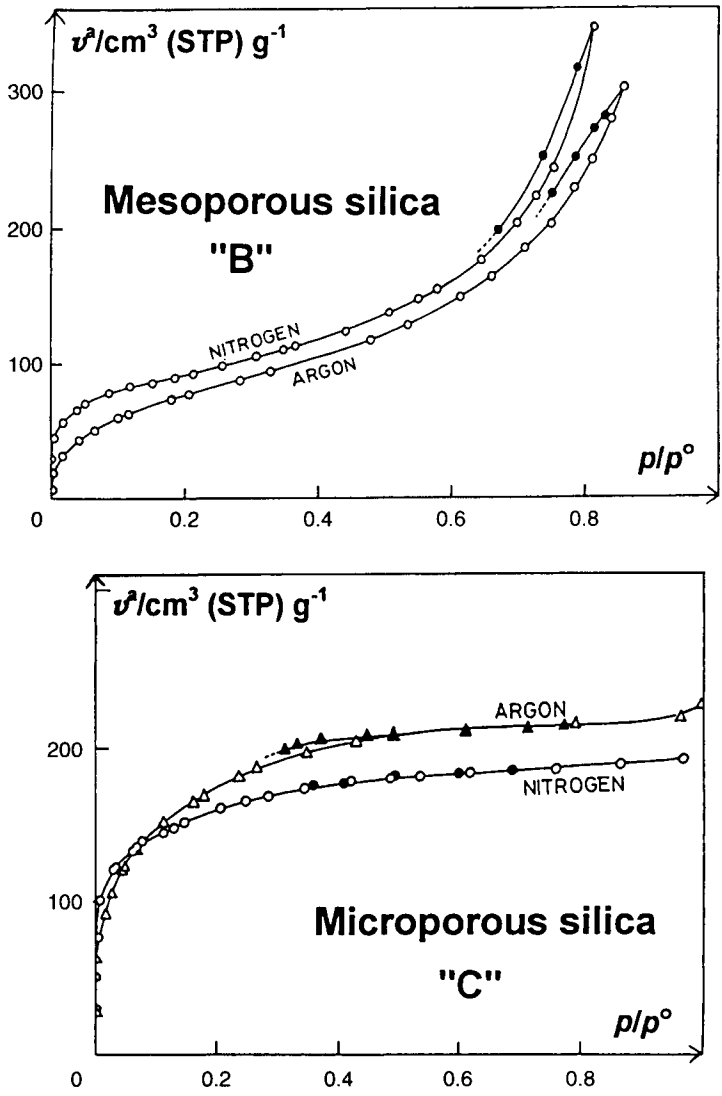

Figure 10.10. Argon and nitrogen isotherms at 77 K on mesoporous silica gel B (top) and microporous silica gel C (bottom) (Payne *et al.*, 1973).

close-packed liquid argon. In view of the limitations of the BET theory, the physical significance of both apparent values of σ(Ar) is questionable.

Dehydroxylated gels

When a silica gel is heated to progressively higher temperatures water is lost first from any mesopores and supermicropores then from any ultramicropores, and finally by the decomposition of surface hydroxyls. The dehydroxylation of the surface

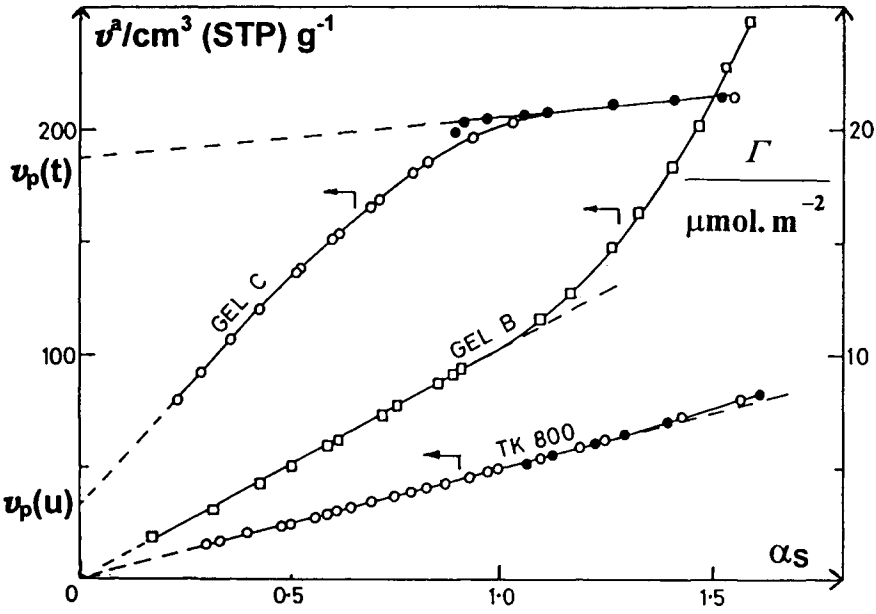

Figure 10.11. Argon α_S-plots for non-porous (TK800), mesoporous (gel B) and microporous (gel C) silicas (Payne *et al.*, 1973).

Table 10.9. Analysis of argon isotherms on silica gels.

Silica	a(BET, N_2) ($m^2\,g^{-1}$)	a(S, N_2) ($m^2\,g^{-1}$)	a(BET, Ar) ($m^2\,g^{-1}$)	a(S, Ar) ($m^2\,g^{-1}$)
Gel B	334	335	337	337
Gel K	216	217	214	222
Gel C	586	425–625, 29[a]	720	540–1150, 24[a]
Gasil	657	500–700	728	640–950

[a] Values of external area, a(ext).

generally takes place over the range 200–1000°C and is accompanied by some loss of surface area (see Iler,1979, p. 544). However, the precise changes in area and pore structure depend on a number of factors including the nature of the original hydroxylated gel and the conditions of heat treatment (e.g. in air, vacuo or water vapour).

The first systematic investigations of the adsorption of gases on dehydroxylated silicas were made by Kiselev and his co-workers (Kiselev, 1957, 1958). In a study of the adsorption of argon and nitrogen, Aristov and Kiselev (1965) found that, in contrast to nitrogen, the reduced argon isotherm did not appear to depend on the degree of surface hydroxylation.

The effect of surface dehydroxylation of a mesoporous silica on the Ar and N_2 energetics of adsorption is illustrated in Figure 10.12. In the work of Rouquerol *et al.* (1979b) Tian–Calvet microcalorimetry was used to determine the variation of the differential enthalpy of adsorption as a function of surface coverage. Although strong

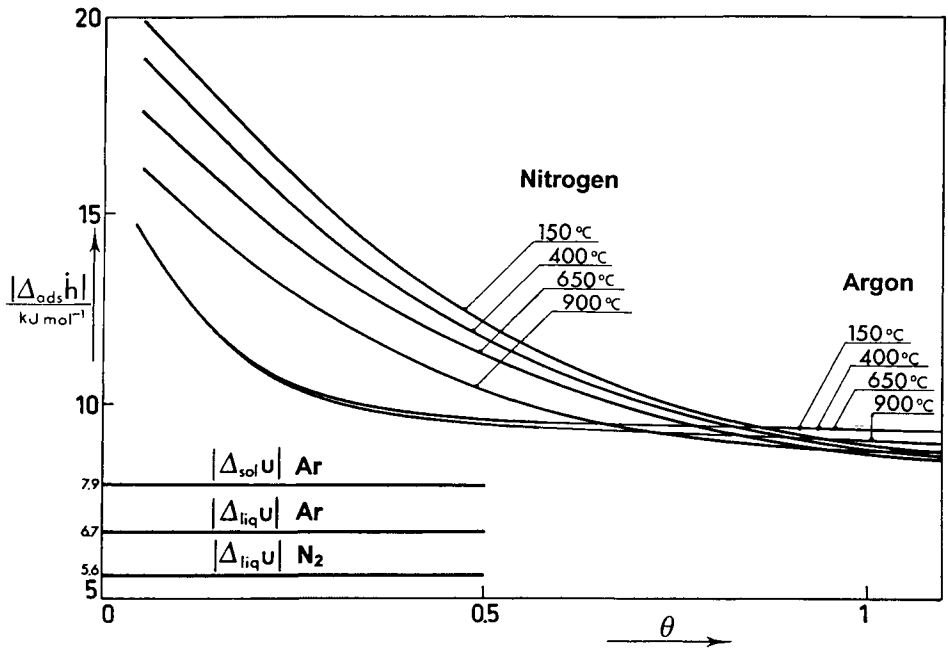

Figure 10.12. Differential enthalpies of adsorption of argon and nitrogen on a mesoporous silical gel: effect of outgassing at different temperatures (Rouquerol *et al.*, 1979b).

energetic heterogeneity is a feature of the adsorption of both gases, with Ar the variation of adsorption enthalpy is virtually unchanged over the outgassing temperature range 150–900°C. The striking difference in the behaviour of N_2 can only be due to the weakening of the specific field gradient–quadrupole interactions which is the result of the reduction in the number of surface hydroxyls. It is evident that the location of the N_2 curve on the 900°C sample is not far removed from the common Ar curve. This is to be expected because of the similarity of the non-specific interactions for both Ar and N_2 with the dehydroxylated surface. The remaining difference is probably due to the specific interaction of N_2 with the remaining isolated hydroxyls on the 900°C surface.

As noted in Chapter 1, the specific interactions between polar molecules and silica are virtually eliminated by the removal of all the surface hydroxyls and therefore the effect of partial dehydroxylation is to drastically reduce the adsorption energies of certain molecules. The polar adsorptives studied by Kiselev and his co-workers included alcohols, ketones, ethers and amines (Kiselev, 1965, 1971): with each adsorptive, the reduction in the adsorbent–adsorbate interaction energy was accompanied by a substantial change in the isotherm character.

It might be expected that a dehydroxylated silica surface would be more energetically homogeneous than the parent hydroxylated surface, and this is found in practice – as exemplified in Figure 10.12. However, the effect of outgassing a silica gel at high temperature may lead to the development of ultramicroporosity. To overcome this problem, much of the later work by Kiselev's group was undertaken on hydrother-

mally treated silicas (see Zhuravlev, 1994). In this manner, it was possible to convert the original skeletal globular structure of silica gel into a more homogeneous spongy structure (Kiselev, 1971) and thus avoid the development of ultramicroporosity.

As noted above, many investigations have been made of the adsorption of water on non-porous silicas. Less attention has been given to the dehydroxylation of porous silicas. An early study by Dzhigit *et al.* (1962) of the adsorption water vapour on a mesoporous silica gel involved both isotherm and calorimetric measurements. It was found that at very low surface coverage the adsorption enthalpy was not significantly affected by dehydroxylation, but a large difference became apparent as the surface coverage increased. A slow uptake of water vapour, which occurred after dehydroxylation, was attributed to chemisorption.

The dehydroxylation of microporous and mesoporous gels was investigated by Baker and Sing (1976). The reduced water isotherms in Figure 10.13 were determined on the non-porous TK800 and the mesoporous gel J and microporous gel E outgassed at 1000°C. All three isotherms exhibit pronounced hysteresis extending to very low $p/p°$, but the initial sections of the *adsorption* isotherms (at $p/p° < 0.3$) follow a similar path. This low affinity for water is clearly characteristic of the degree

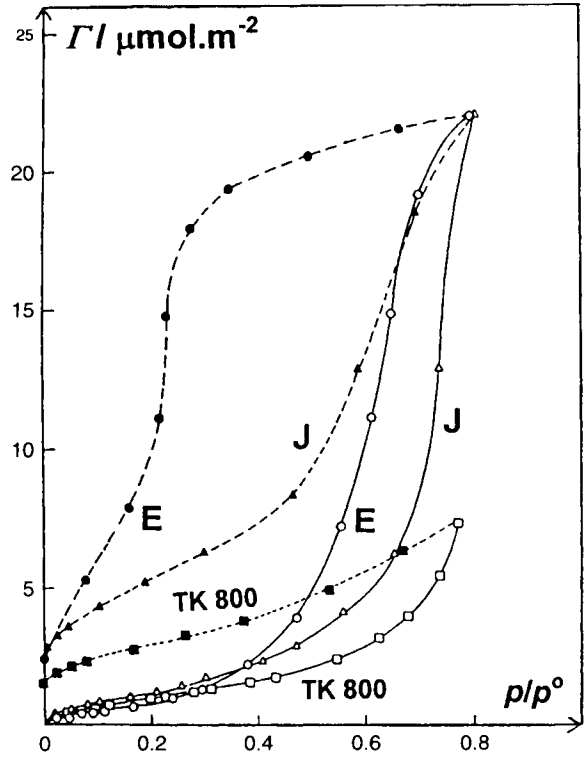

Figure 10.13. Adsorption isotherms of water vapour at 25°C on silicas TK800, gel E and gel J, evacuated at 1000°C (Baker and Sing, 1976).

of hydrophobicity shown by all dehydroxylated silicas. The surface rehydroxylation was very slow at $p/p° < 0.3$, but became rapid in the multilayer range; this phenomenon was evidently responsible for the low-pressure hysteresis. Indeed, it was found that the *desorption* branches of the isotherms on gels E and J were remarkably similar to the corresponding parts of the water isotherms on the two hydroxylated gels (Baker and Sing, 1976). We may conclude that the micropores in the rehydroxylated gel E regained their high affinity for water.

10.3. Aluminas: Structure, Texture and Physisorption

10.3.1. Activated alumina

The name 'activated alumina' is generally applied to an adsorbent alumina (usually an industrial product) prepared by the heat treatment of some form of hydrated alumina (i.e. a crystalline hydroxide, oxide-hydroxide or hydrous alumina gel). It has been known for many years that certain forms of activated alumina can be used as powerful desiccants or for the recovery of various vapours. It was apparent at an early stage that the adsorbent activity was dependent on the conditions of heat treatment. For example, in 1934 Bayley reported that the adsorption of H_2S by a commercial sample of activated alumina was affected by prior heating of the adsorbent at different temperatures, the maximum uptake being obtained after heat treatment at 550°C. During an investigation of the catalytic dehydration of alcohols, Alekseevskii (1930) found that a calcination temperature of *c.* 400°C was required to optimize the adsorption of the alcohol reactants, whereas calcination at 600°C was preferable for the adsorption of the olefine products.

Somewhat later it began to appear that there was a lack of agreement between the recorded dependence of surface area on the temperature of calcination (e.g. in the work of Krieger, 1941; Feachem and Swallow, 1948; Taylor, 1949; Gregg and Sing, 1951; de Boer, 1957). In fact, such differences are not really surprising. To obtain reproducible adsorbent properties it is necessary to control: (a) the chemical and physical nature of the starting material (i.e. its structure, crystal/particle size, amount of sample purity); (b) the conditions of heat treatment (type of furnace, atmosphere, time – temperature profile – preferably by a controlled rate thermal analysis (CRTA) heating procedure); and (c) the methods used to interpret the adsorption data (BET, BJH, etc.).

10.3.2. Aluminium trihydroxides

Although various modifications of aluminium trihydroxide, $Al(OH)_3$, have been described in the literature, there are only three common forms: gibbsite (originally also called hydrargillite) bayerite and nordstrandite. Gibbsite is the best known and most abundant. It is the main constituent of North and South American bauxite and is obtained as an intermediate product (i.e. 'Bayer Hydrate') in the Bayer process for the production of aluminium from bauxite.

The crystal structures of the three hydroxides are all based on a double layer of close-packed hydroxyl ions, two-thirds of the octahedral interstices being occupied by aluminium ions (see Figure 10.14). The layers are held together by hydrogen bonding between the nearest neighbour hydroxyls. Differences in structure thus reside in the inter-layer spacing, i.e. in the *c*-axis. In the case of gibbsite, the stacking of the double layers is in the sequence ABBAABBA. The distance

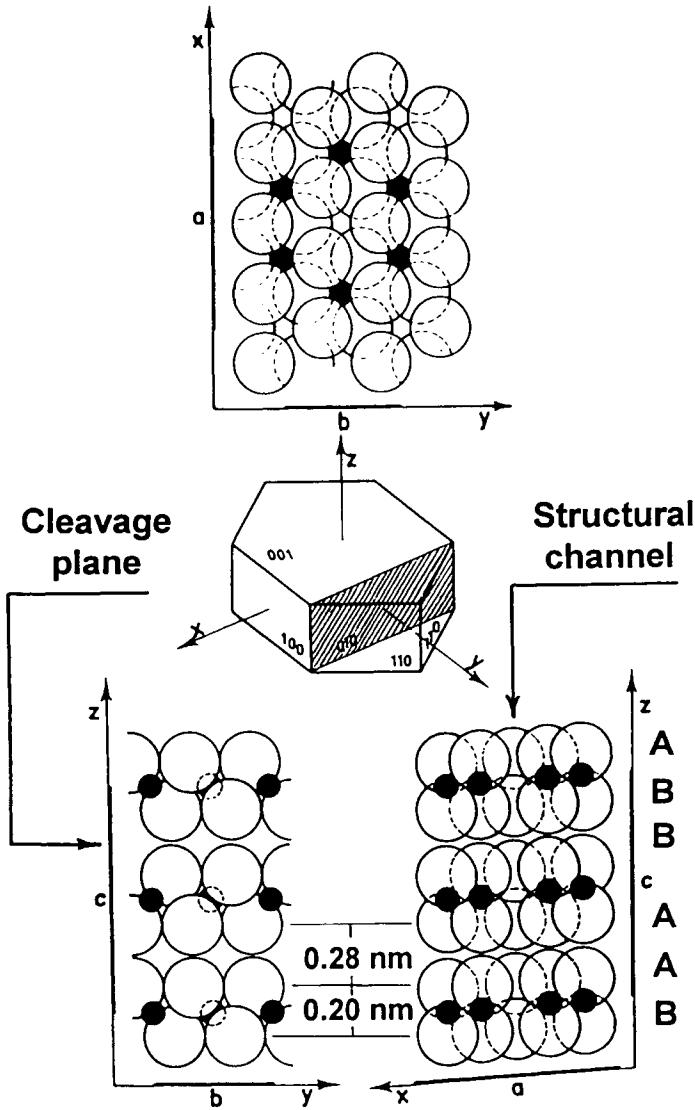

Figure 10.14. Crystalline structure of gibbsite. Small solid circles, aluminium ions; large open circles, hydroxyl ions (after Saafeld, 1960).

between two adjacent A (or B) layers is 0.28 nm whereas the A–B distance is 0.20 nm.

Bayerite does not occur in nature, but it can be made in a number of different ways (e.g. by the hydrolysis of an aluminium alkoxide). The OH layers in bayerite appear to be stacked in the order ABABAB.... Within the double layer the A–B distance is 0.21 nm and between the double layers the A–B distance is 0.26 nm. The density of bayerite is correspondingly a little higher than that of gibbsite.

Although deposits of nordstrandite have been found, this modification is not easy to prepare in a relatively pure form. For this reason, the exact structure is still under discussion. However, the layer stacking is likely to be made up of a combination of both bayerite and gibbsite.

In its most common industrial form, gibbsite is a sandy material, of *c.* 50–100 μm grain size. Each grain is itself a dense agglomerate of smaller hexagonal crystals, typically 5–15 μm in size, and the BET-nitrogen surface area is usually not more than 0.2 $m^2 g^{-1}$. Other forms of gibbsite have also been subjected to physisorption studies. These include loose, thin hexagonal crystals with BET-nitrogen areas of 5 and 15 $m^2 g^{-1}$ corresponding to mean crystal sizes of 1 and 0.2 μm, respectively (Rouquerol *et al.*, 1975), and also porous aggregates. For example, Ramsay and Avery (1979) found that a batch of very pure gibbsite powder gave a Type IV nitrogen isotherm with an H1 hysteresis loop at high $p/p°$. It appeared that the gibbsite was mesoporous and possibly also macroporous, the effective pore width being mainly > 20 nm. The BET-nitrogen area was 41 $m^2 g^{-1}$, which was consistent with the mean thickness of *c.* 25 nm of the thin hexagonal platelets, as determined by electron microscopy and X-ray line broadening. This rather ill-defined porosity was ascribed to the space between the gibbsite crystallites and was found to persist after heat treatment at 400°C. A batch of gibbsite of lower BET-nitrogen area (5.6 $m^2 g^{-1}$) was used by Stacey (1987). In this case, the polycrystalline grains of mean diameter 75 μm were composed of 0.3 μm platy crystallites.

A sample of microcrystalline nordstrandite was found to be somewhat mesoporous by Aldcroft and Bye (1967). The nitrogen hysteresis loop was Type H3, which indicated the existence of slit-shaped pores between the crystallites. The BET-nitrogen area of 34 $m^2 g^{-1}$ appeared to represent the external area of the crystallites.

A relatively low-area (8 $m^2 g^{-1}$) aged sample of bayerite (Bye and Robinson, 1964) which gave a reversible Type II nitrogen isotherm, was shown to be essentially non-porous (Payne and Sing, 1969). Electron microscopy revealed that this sample was composed of discrete conical crystals.

10.3.3. Aluminium oxide-hydroxides

There are two well-known oxide-hydroxides (AlOOH) with closely related structures: diaspore and boehmite. Diaspore occurs in some types of clay and bauxite. It has been produced by the hydrothermal treatment of corundum, α-Al_2O_3. Whereas boehmite is characterized by cubic close-packing of the anions, diaspore has a hexagonal close-packed structure. This difference probably accounts for the direct thermal transformation of diaspore to corundum at relatively low temperatures (450–600°C).

Boehmite is of considerable interest to the surface scientist. It was pointed out by Lippens and Steggerda (1970) that a clear distinction should be made between crystalline boehmite and the gelatinous forms of pseudoboehmite, which always contains some non-stochiometric, interlamellar water. Pseudoboehmite is the main constituent of European bauxites and can be easily prepared by the neutralization of aluminium salts, but hydrothermal conditions are required for the formation of crystalline boehmite.

In general, the BET area of the pseudoboehmites increases with decreasing crystallinity (Lippens and Steggerda, 1970). The gels prepared by the hydrolysis of aluminium alkoxides tend to be porous, but their complex nature means that the porosity is not always easy to characterize. However, by allowing the product to age in aqueous ethanol or ethanediol it is possible to obtain a well-defined mesopore structure (Bye *et al.*, 1967; Aldcroft *et al.*, 1971). This is believed to be the result of an aggregation-cementation type of ageing process, which involves a reduction in the solvent barrier and hence the promotion of particle–particle interaction with little particle growth (Bye and Sing, 1973).

A fibrillar type of boehmite (i.e. a du Pont product named Baymal colloidal alumina) was first described by Bugosh *et al.* (1962). The BET area was reported to be 275 $m^2 g^{-1}$. The discrete boehmite fibres of about 5 nm diameter and 100 nm length were protected by adsorbed acetate groups and were thus easily dispersible.

High-resolution adsorption measurements were undertaken recently by Fukasawa *et al.* (1994) on a porous boehmite glassy film prepared by slowly drying a boehmite sol. Small-angle X-ray measurements indicated that the 2.5 nm platelets of boehmite were densely stacked in the [0 1 0] direction with the inclusion of uniform slit-shaped pores of about 0.3 nm width. The nitrogen isotherm on the boehmite film was of Type Ib (see Chapter 13) and was somewhat unusual in that the gradual increase in the amount adsorbed (in the multilayer range) extended up to $p/p^\circ = 0.65$ (i.e. the beginning of the plateau). These results indicate that nitrogen adsorption had involved both primary and secondary micropore filling and also some multilayer adsorption on wider pores. With the aid of multiprobe adsorption measurements, it was concluded that there were indeed three groups of pores. However, the estimates of pore widths of 0.3, 0.7 and 1.3 nm must be in doubt because of the reliance placed on the Dubinin–Radushevich method of isotherm analysis.

10.3.4. Alumina structures

Alumina occurs in nature as corundum, α-Al_2O_3, which is noted for its great hardness, high electrical resistance and low chemical reactivity. It can be made by the high temperature treatment (at > 1200°C) of boehmite or gibbsite and normally has a low specific surface area (< 5$m^2 g^{-1}$).

The less compact 'transition' aluminas (γ-type) are highly porous, more reactive and do not occur in nature. They are prepared by the heat treatment of $Al(OH)_3$ or AlOOH at intermediate temperatures and undergo an irreversible change to α-Al_2O_3 at high temperature. Their BET areas are typically 300–400 $m^2 g^{-1}$ and they are widely used as catalysts and catalyst supports.

Various schemes have been proposed for the classification of the different alumina structures (Lippens and Steggerda, 1970). One approach was to focus attention on the temperatures at which they are formed, but it is perhaps more logical to look for differences in the oxide lattice. On this basis, one can distinguish broadly between the α-series with hexagonal close-packed lattices (i.e. ABAB...) and the γ-series with cubic close-packed lattices (i.e. ABCABC...). Furthermore, there is little doubt that both γ- and η-Al_2O_3 have a spinel ($MgAl_2O_4$) type of lattice. The unit cell of spinel is made up of 32 cubic close-packed O^{2-} ions and therefore 21.33 Al^{3+} ions have to be distributed between a total of 24 possible cationic sites. Differences between the individual members of the γ-series are likely to be due to disorder of the lattice and in the distribution of the cations between octahedral and tetrahedral interstices.

The detailed behaviour of a model γ-Al_2O_3 surface was first discussed by Peri (1965). It was supposed that a fully hydrated (100) plane of the spinel structure would have a monolayer of OH^- ions in a square lattice plane. On dehydration two adjacent OH^- ions would begin to combine at random. This simple pairwise condensation would be limited, however, since only two-thirds of the surface OH could be removed without changing the surface structure. According to this picture, the remaining OH^- ions would occupy different sites, which could be characterized by infrared spectroscopy and chemical activity. At high temperature, ionic migration would occur and various surface defects would be produced. Although this is an over-simplified model, it has been of great value for the discussion of the catalytic activity and chemical reactivity of the aluminas.

In fact, the surface structures of activated aluminas are exceedingly complex. After exposure to the air an alumina surface is always fully hydrated, but unlike silica it is not fully hydroxylated. Thus, 'bound' water is in the form of both hydroxyls and coordinated water molecules. Removal of the latter may take place at temperatures as low as 200°C and leave high-energy Al^{3+} sites exposed. As in the Peri model, with increase in temperature further cationic sites are formed with the combination of adjacent OH^- ions, ionic mobility and finally reorganization of the surface structure.

10.3.5. Physisorption by high-temperature aluminas

In view of the complexity of the γ-series, it is of interest to investigate the adsorption of gases by high-temperature aluminas, particularly α-Al_2O_3. Non-porous α-Al_2O_3 can be obtained by heating the spheroidal particles of a flame-hydrolysed alumina for a prolonged period at temperatures of at least 1200°C: this was the procedure adopted by Carruthers *et al.*, (1971). A master batch of Degussa 'Aluminiumoxid C' (designated alumina DC; $a(\text{BET}) = 111\ m^2\ g^{-1}$) was used as the starting material and also as the non-porous reference adsorbent. This was composed of discrete spheroidal particles and gave reversible Type II argon and nitrogen isotherms at 77 K. In the reduced α_S form, the nitrogen isotherm was virtually identical with the corresponding isotherms on samples of low-area bayerite and aged hydrous alumina (Bye *et al.*, 1967; Payne and Sing, 1969).

Samples of alumina DC were calcined in air at the recorded temperatures and for specified times. Thus, sample DC(1200)6 was prepared by calcination at 1200°C for

Table 10.10. Argon and nitrogen adsorption on high-temperature aluminas (Carruthers *et al.*, 1971)

Adsorbent	Crystal structure	a(BET, N_2) ($m^2\ g^{-1}$)	a(S, N_2) ($m^2\ g^{-1}$)	a(S, Ar) ($m^2\ g^{-1}$)
Alumina DC	δ-Al_2O_3	111	(111)	(111)
DC(1200)6	θ-Al_2O_3	74.8	74.6	77.0
DC(1200)114	α-Al_2O_3	5.9	5.9	6.6
DC(1300)6	α-Al_2O_3	4.5	4.3	4.9
DC(1400)6	α-Al_2O_3	2.5	2.3	2.7

6 hours and sample DC(1200)114 by calcination at 1200°C for 114 hours. The BET-nitrogen areas of these and other high-temperature samples are given in Table 10.10. It is noteworthy that after 6 hours at 1200°C, the specific surface area of sample DC(1200)6 was remarkably high and there had been no detectable conversion to α-Al_2O_3, whereas after 114 hours at 1200°C, sample DC(1200)114 had been completely converted to α-Al_2O_3.

The α_S-plots for sample DC(1200)6 were found to be linear over the recorded ranges of both isotherms. This correspondence of isotherm shape is to be expected since the adsorbent structure has not been appreciably changed as a result of the 6-hour calcination at 1200°C. The multilayer sections of the other α_S-plots were for the most part linear, but the monolayer sections all exhibited significant deviation. The fact that the linear multilayer plots can be back-extrapolated to the origin was an indication that the multilayer development had not been affected to any great extent by the change in structure of the adsorbent.

The values of surface area, a(S, N_2) and a(S, Ar), in columns 4 and 5 of Table 10.10 are derived from the linear *multilayer* α_S-plots. As was pointed out in Chapter 6, if unrestricted multilayer adsorption has occurred, the specific surface area can be evaluated from the slope of the α_S-plot. The following equations have been developed for the adsorption of argon and nitrogen on alumina:

$$a(\text{S, Ar}) = 3.22\ v^{\sigma}(\text{STP})/\alpha_S \tag{10.5}$$

$$a(\text{S, N}_2) = 2.87\ v^{\sigma}(\text{STP})/\alpha_S \tag{10.6}$$

where v^{σ}(STP), or v^{a}, is the volume of gas adsorbed expressed in cm^3(STP) g^{-1} and the proportionality factors have been obtained by calibration against the BET-nitrogen area of alumina DC.

The corresponding values of a(BET, N_2) and a(S, N_2) in Table 10.10 are evidently in good agreement, but the values of a(S, Ar) are somewhat higher. Of course this discrepancy could be partially rectified by a simple change in the proportionality factor for argon from 3.22 to 2.82, but this would be a departure from the appropriate value for other aluminas (Carruthers *et al.*, 1971).

A sample of non-porous α-Al_2O_3 (of a(BET) = 2.7 $m^2\ g^{-1}$) was used in an important investigation by Barto *et al.* (1966) of the adsorption of a series of *n*-aliphatic alcohols. The isotherms, which are displayed in Figure 10.15, show very clearly the effect of 'autophobicity'. Thus, the increase in hydrocarbon chain length from C1 to

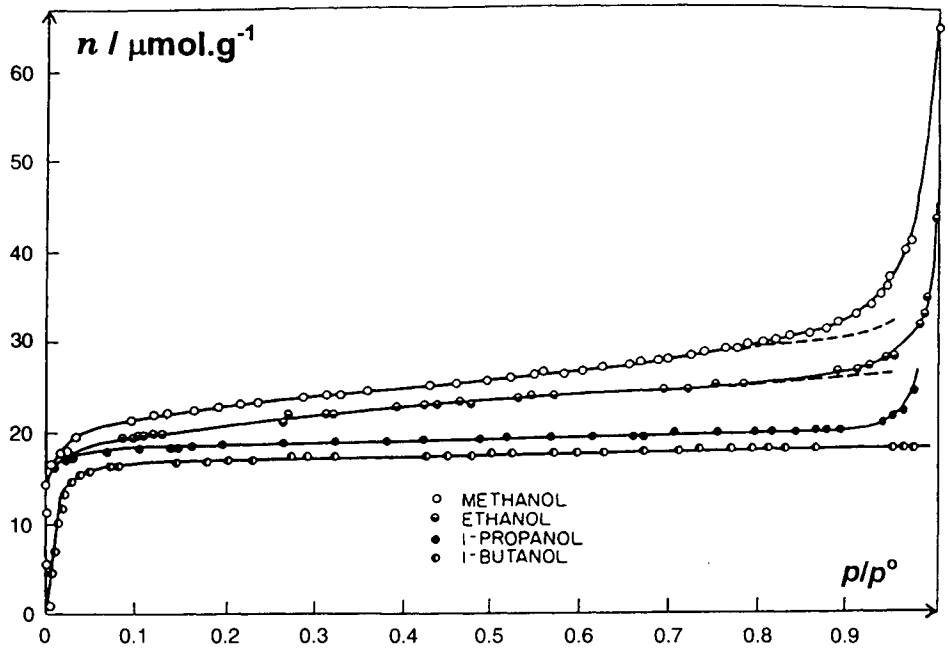

Figure 10.15. Adsorption isotherms of methanol, ethanol, propanol and butanol on α-Al_2O_3 (2.7 $m^2\,g^{-1}$) (from Barto *et al.*, 1966).

C4 has resulted in a drastic reduction in the extent of multilayer adsorption. The reason for this unusual physisorption behaviour is that the molecules in the localized monolayer are oriented to allow directional hydrogen bonding between their hydroxyls and the hydrated alumina surface. The alkyl groups are therefore directed away from the surface and thereby provide an effective low-energy screen against further adsorption.

Langmuir plots were constructed by Barto *et al.* (1966) from their alcohol isotherms: it is not surprising that the most extensive linearity was given by butanol. Values of the monolayer capacity were obtained from the linear regions of the Langmuir plots and by assuming the validity of the BET-nitrogen area it was possible to derive the apparent molecular areas for the four alcohols. For the C1–C4 series the following values were obtained: 0.205, 0.220, 0.234, 0.248 nm^2. It is noteworthy that 0.20 nm^2 is the area occupied by a long-chain alcohol in a close-packed insoluble monolayer. As expected it is methanol which gives the 'best' BET fit, but even in this case the range of linearity was limited to $p/p° < 0.15$.

In a further study of autophobicity by Blake and Wade (1971), adsorption isotherms were determined for water vapour and the first five *n*-aliphatic alcohols on the surface of oxidized aluminium foil. The results were very similar to those obtained for α-Al_2O_3. A Type II water isotherm was obtained, the initial steep slope being indicative of a high affinity of adsorption. The residual uptake of water was

significantly larger than expected (equivalent to 1.5 monolayers) and it was considered likely that the oxidized surface was microporous with respect to water.

The adsorption of water vapour by various forms of alumina was studied by Carruthers *et al.* (1971). To investigate the interaction of water with α-Al_2O_3, sample DC(1200)114 (see Table 10.10) was outgassed at 400°C. The subsequent water uptake was much larger than that given by the same sample outgassed at 25°C and the first adsorption–desorption cycle exhibited pronounced hysteresis over the complete range of $p/p°$. Indeed, the initial mass could not be regained by prolonged evacuation at 25°C. The amount irreversibly held (13.1 μmol m^{-2}) almost corresponded to a close-packed monolayer of water (i.e. 15.8 μmol m^{-2}). After 25°C evacuation, the water isotherm was reversible but the level of uptake was lower than expected for the adsorption of a close-packed monolayer.

The interaction of water with the transitional aluminas is more complex. With the original alumina DC and sample DC(1200)6, the water isotherms were irreversible – even after evacuation at 25°C – and it was not possible to establish thermodynamic equilibrium. It appears that there was a slow penetration of water molecules which involved the hydration of poorly ordered cations.

As we have seen, the formation of α-Al_2O_3 is normally associated with a considerable loss of surface area. It must not be assumed, however, that this is accompanied by the removal of all porosity. The pore structure is always changed by high-temperature treatment, but a distinction must be made between open and closed pores, and it is only the former that can be characterized by physisorption measurements.

The effect of high-temperature treatment of alumina fibres is an interesting example of the evolution of porosity. In the work of Stacey (1991), the alumina fibres made by sol-gel methods and calcined at 900°C consisted of η-Al_2O_3. Further calcination at 1300°C resulted in their conversion to α-Al_2O_3 and a considerable change in the mesopore structure. Although the BET-nitrogen area was reduced from 84 to 11 $m^2 g^{-1}$, the fibres continued to retain a well-defined mesopore structures. Pore widening appeared to involve a change from a bimodal to a more normal unimodal distribution. An improved picture of the changes in texture was obtained with the aid of optical and electron microscopy and small-angle neutron scattering. It was concluded that most of the residual mesoporosity in the α-Al_2O_3 fibres was oriented along the fibre axis and that the randomly distributed smaller mesopores had been preferentially eliminated during the transformation in crystal structure.

10.3.6. Thermal decomposition of trihydroxides

The structural and textural changes involved in the thermal decomposition of the three trihydroxides have been studied in considerable detail (Aldcroft *et al.*, 1968; Lippens and Steggerda, 1970; de Boer, 1972; Rouquerol *et al.*, 1975, 1979a; Ramsay and Avery, 1979; Stacey, 1987). It is now clear that the dehydration sequence is dependent not only on the crystalline structure of the trihydroxide, but also on its texture and the conditions of heat treatment.

It appears to have been first noted by Achenbach (1931) that the dehydration of a gibbsite crystal is pseudomorphic: the crystal shape and original lattice are retained and

therefore a highly porous product is formed. The fact that the loss of structural water precedes the formation of a new stable structure is obviously of great importance.

In Figure 10.16 the BET-nitrogen areas of the activated aluminas obtained by heating small crystals of bayerite and nordstrandite in air are plotted against the temperatures of calcination. In this work, each sample was put into the furnace at the recorded temperature and held there for 5 hours (Aldcroft *et al.*, 1968). It is evident that the trihydroxides underwent thermal decomposition at temperatures >200°C, with the maximum BET areas being generated at 250–300°C. Similar results had been previously reported for gibbsite, but the maximum BET areas were $\approx 300\ m^2\ g^{-1}$ at 300–400°C (Gregg and Sing, 1951; de Boer 1957). The changing isotherm type (II → I → IV) provides the first indication that microporous products were obtained by the heat treatment of the trihydroxides at 250–450°C and mesoporous products at higher temperatures (Aldcroft *et al.*, 1968; Lippens and Steggerda, 1970).

As already explained, the α_S-method of isotherm analysis can be used to derive the external area, a(ext, S), and the pore volume v_p(mic, S). Of course the first requirement is to obtain an appropriate standard isotherm on a non-porous alumina. Strictly, the surface chemistry of the reference material should be exactly the same as that of the porous adsorbent, but in practice this is not easy to achieve because of the complex surface structure of active aluminas. As before, standard isotherm data determined on the non-porous Degussa Aluminiumoxid C have been found suitable for the analysis of various isotherms on the porous aluminas (Sing,1970).

The α_S-method was used to analyse the nitrogen isotherms determined after the calcination of very small crystals of bayerite and nordstrandite (Aldcroft *et al.*, 1968). Thus, each value of the external area, a(ext), in Table 10.11 was obtained from the

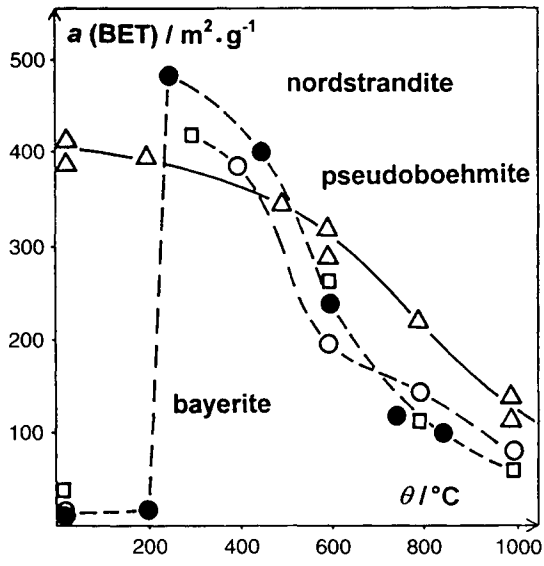

Figure 10.16. BET area of calcined hydrated aluminas versus the temperature of calcination for 5 hours (Lippens, 1961; Sing, 1972).

Table 10.11. Thermal decomposition of bayerite and nordstrandite.

Adsorbent[a]	a(BET) ($m^2\ g^{-1}$)	a(ext) ($m^2\ g^{-1}$)	v_p(mic) ($cm^3\ g^{-1}$)	Porosity
Bayerite	15	15	–	Non-porous
Bayerite (400)	382	30	0.20	Microporous
Bayerite (600)	199	23	0.21	Mesoporous
Nordstrandite	34	19	0.02	(Microporous)
Nordstrandite (300)	415	20	0.19	Microporous
Nordstrandite (600)	265	20	0.23	Meso + microporous
Nordstrandite (1000)	62	65	0.21	Mesoporous

[a] Temperature of calcination (°C) given in brackets. Each sample heated for 5 hours at recorded temperature (Sing, 1972).

slope of the linear *multilayer* section of the α_S-plot by the application of Equation (10.5). It is evident that the very large change in a(BET), which accompanied the thermal decomposition of the trihydroxide, was not associated with any significant change in a(ext). Indeed, the external surface area of the finely-divided nordstrandite remained remarkably constant up to at least 600°C. These results confirmed that the crystalline framework of the trihydroxide was preserved even after the thermal decomposition was virtually complete. Back-extrapolation of the multilayer plot to $\alpha_S = 0$ gave each v_p(mic) value recorded in Table 10.11. It can be seen that the pore volumes generated at 300 or 400°C remained remarkably constant after further heat treatment, although changes in the isotherm character indicated that pore widening had occurred at the higher temperatures.

By using fine crystals of bayerite and nordstrandite, Aldcroft *et al.* (1968) were able to ensure a fairly rapid release of the water produced during the removal of the structural hydroxyls. The importance of residual water in affecting the course of the thermal decomposition of gibbsite had been earlier demonstrated by Papée and Tertian (Tertian and Papée, 1953; Papée and Tertian, 1955). It was shown that at temperatures < 400°C, gibbsite was transformed partly into boehmite and partly into a porous form of ρ-alumina, a 'transition alumina'. The relative amounts of the products of these two parallel routes were found to depend on the controlled pressure of water vapour: over the 0–100 mbar range low water vapour pressure favoured a direct conversion to microporous, poorly ordered ρ-alumina; while at high water pressures, up to 42% of the gibbsite was converted into boehmite.

In the 1950s, de Boer and his co-workers (de Boer *et al.*, 1954, 1956; de Boer, 1957) used a variety of techniques in their studies of the thermal dehydration of gibbsite and bayerite and a more detailed picture was obtained of the conditions under which the two decomposition routes were manifested. For example, it was shown that relatively well-crystallized boehmite could be produced by the treatment of gibbsite or bayerite in saturated steam at temperatures of *c.* 165°C. These and other findings provided qualitative confirmation that the formation of boehmite involved an intragranular hydrothermal transformation.

Although reproducible results can be obtained by the simple calcination of samples taken from a particular batch of trihydroxide, the chemical composition and porosity

of the products are usually complex. As in other thermal decomposition studies, control of the dehydration reactions and sintering/ageing processes is considerably improved by the application of CRTA (controlled rate thermal analysis), together with the use of finely divided and well-characterized gibbsite. In this manner, Rouquerol and co-workers (Rouquerol *et al.*, 1975, 1979a; Rouquerol and Ganteaume, 1975) were able to obtain the results in Figures 10.17 and 10.18 and hence extend the work of Papée.

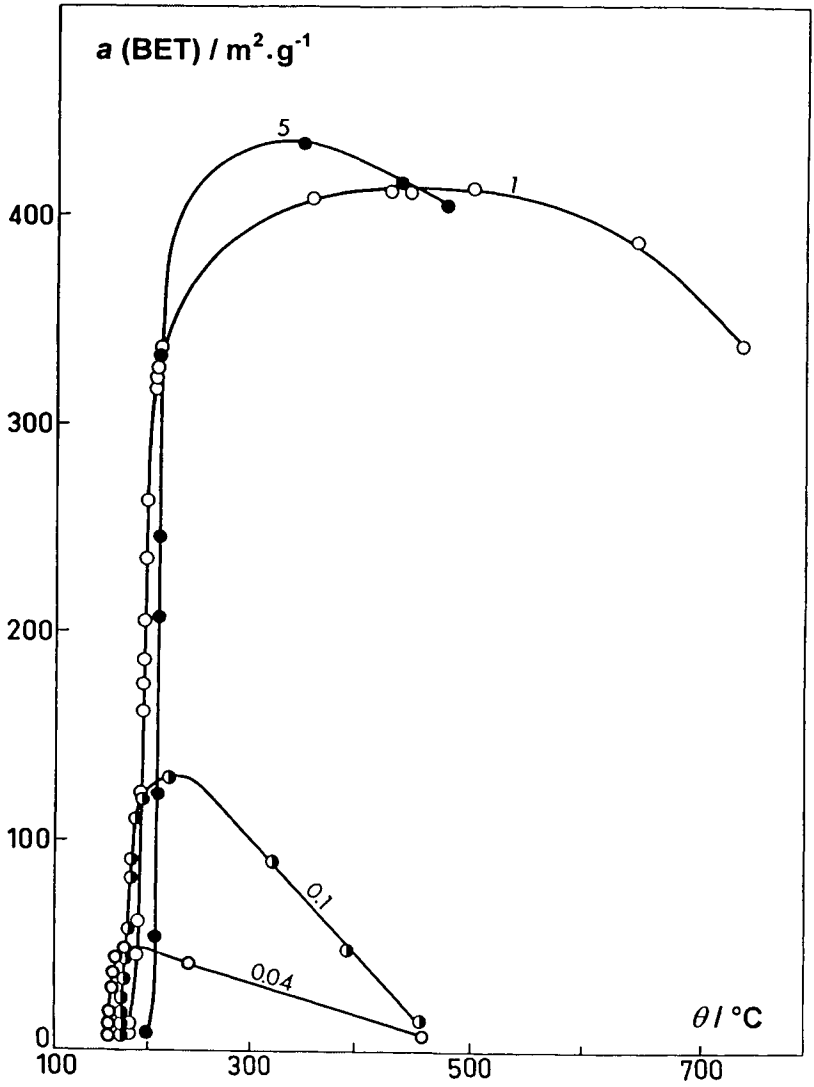

Figure 10.17. Development of the BET-nitrogen surface area during the dehydration, by CRTA, of a sample of fine gibbsite, 1 μm grain size. CRTA conditions: controlled pressure indicated in mbar on the curve; rate of dehydration, 11.4 mg h^{-1} g^{-1} (Rouquerol and Ganteaume, 1977).

The pronounced effect of changing the residual water vapour pressure from 0.1 to 1 mbar is shown in Figure 10.17. Values of a(BET) of over 400 $m^2 g^{-1}$ were recorded by conducting the CRTA in the presence of 1 or 5 mbar of water vapour. It is remarkable that under 1 mbar the BET area was still in the region of 350 $m^2 g^{-1}$ after the temperature had been taken to 700°C.

The same results are presented in Figure 10.18a, but here a(BET) is plotted against the percentage mass loss. It is apparent that there was no detectable development of BET-area until about 5% mass loss had occurred and thereafter the rate of increase in a(BET) was highly dependent on the water vapour pressure. Other evidence indicated that the latter stage was associated with dehydroxylation of the structural channels (see Figure 10.14) and therefore resulted in the formation of narrow, parallel micropores, which were 'drilled' in the z direction, i.e. normal to the basal (0 0 1) plane.

It is believed that the number of micropores so produced was not affected by the water vapour pressure, but that the pores were widened as the pressure was increased. This would explain the results in Figure 10.18b, where the steep increase in a a(BET) under 1 mbar pressure was due to appreciable micropore widening in contrast to the smaller rate of increase of a(BET) when the water vapour pressure was suddenly reduced to 0.04 mbar: in this way 'funnel-shaped' micropores were obtained.

In the work of Ramsay and Avery (1979) small quantities of microcrystalline gibbsite were heated at temperatures up to 425°C. The product obtained by decomposition *in vacuo* adsorbed very little nitrogen, although it did adsorb water. In the presence of water vapour the alumina was found to become more crystalline and to

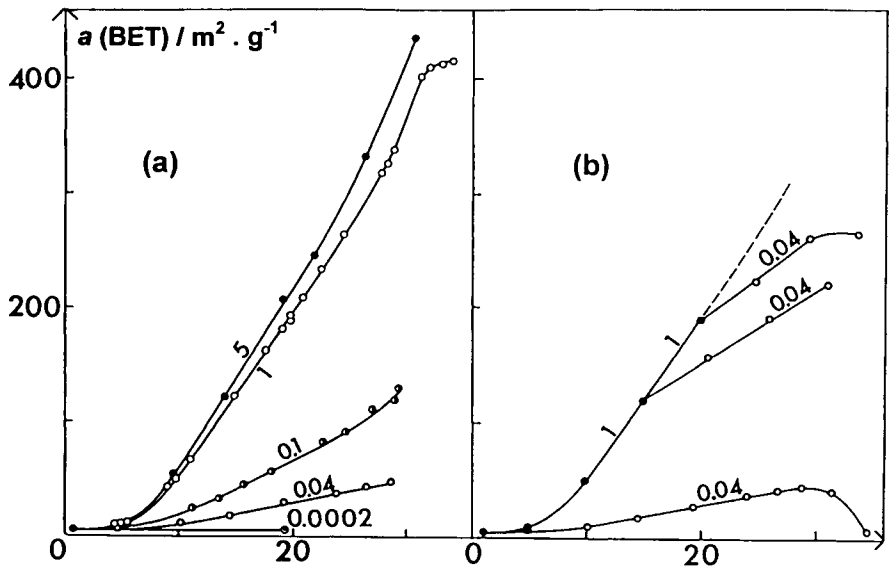

Figure 10.18. Development of the BET-nitrogen surface area during the dehydration of a fine gibbsite, versus % of mass loss. Same conditions as for Figure 1.17 (Rouquerol *et al.*, 1979a).

undergo pore widening: these results are consistent with the conclusions of the French investigators.

It is now clear that if the hydrothermal formation of boehmite is avoided (e.g. by using low-pressure CRTA and small crystals), then the three hydroxides lose their structural water at quite low temperature (≈ 200°C) to give the almost amorphous form, ρ-Al_2O_3. Complex changes occur as the temperature is increased to ≈250–800°C with the formation of certain members of the γ-series aluminas γ or η and θ. At temperatures ≈1200°C the conversion to the dense, low-area α-Al_2O_3 normally takes place.

10.3.7. Decomposition of boehmite and hydrous alumina

Boehmite is itself decomposed at *c.* 400–450°C. As expected, the calcined products have much lower specific surface areas than the activated aluminas produced from the trihydroxides. However, the results of de Boer and his co-workers (de Boer, 1972) indicate that a sample prepared at 580°C was highly microporous and that up to this temperature there was only a small change in the external area.

Some work has been undertaken on the decomposition of the poorly ordered forms of hydrous alumina. These materials can be prepared in the form of gels or flocs, but their surface properties are reproducible only if the conditions of gelation/flocculation, ageing, drying and storage are very carefully controlled (Bye and Sing, 1973). Exposure of microporous hydrous alumina gels to water vapour leads to the rapid and irreversible loss of BET area, but mesoporous pseudoboehmite gels tend to be more stable (Sing 1972). However, soaking either type of gel in liquid water generally results in its conversion to non-porous bayerite and consequently to a great reduction of specific surface area.

In contrast to the thermal activation of the well-defined hydroxides, the calcination of an amorphous or pseudoboehmite gel does not lead to any significant increase in specific surface area (see Figure 10.16). In this respect, a poorly ordered hydrous alumina is similar to silica gel. The results in Figure 10.16 also indicate that the surface areas of the calcined pseudoboehmite gels are rather more stable in the high temperature range (700–1000°C). For example, after being heated for 5 hours at 1000°C, a calcined hydrous alumina still possessed a specific surface area of 132 $m^2 g^{-1}$. Some alumina gels tend to remain poorly ordered at high temperature so that the final change to α-Al_2O_3 is delayed. Teichner and his co-workers have reported that amorphous alumina aerogels were slow to develop crystallinity when they were heated in vacuo (Teichner *et al.*, 1976; Teichner, 1986).

10.4. Titanium Dioxide Powders and Gels

10.4.1. Titanium dioxide pigments

Titanium dioxide (titania, TiO_2) is the major constituent of most commercial white pigments (Day, 1973; Wiseman, 1976; Solomon and Hawthorne, 1983). The

physical properties of typical grades of the common white pigments are given in Table 10.12. It can be seen that the main advantages of titania pigments over the older white pigments are their high refractive index in the visible region of the spectrum and their relatively low densities. Two other advantages of TiO_2 are its chemical stability and the fact that it can be manufactured in an optimum crystal size of *c.* 0.2 μm. As a consequence of their high degree of light scattering and low absorption of visible light, titanium dioxide pigments are the whitest and brightest of all the commercial white pigments.

There are three naturally occurring crystallographic forms of titanium dioxide: anatase, brookite and rutile. Rutile is the most common and stable form. Its structure, shown in Figure 10.19, is based on a slightly distorted hexagonal close-packing of oxygen atoms with the titanium atoms occupying half of the octahedral interstices. Anatase and brookite are both based on cubic packing of the oxygen atoms, but the coordination of the titanium is again octahedral.

Only anatase and rutile are manufactured on a large scale. Anatase was the first to become commercially available, but rutile is now the more important. The small pigmentary crystals of both forms are strong absorbers of UV light: this leads to photocatalysed degradation of organic molecules unless the TiO_2 surface is protected. The particularly high photoactivity of anatase renders it unsuitable for exterior finishes because of the rapid degradation of the protective film. The pigmentary rutile crystals are generally coated with alumina and/or silica and treated with organic compounds.

The early technological interest in anatase pigments was probably why anatase powder was for a time favoured as a non-porous adsorbent. Thus, anatase was one of the few finely divided crystalline solids used by Harkins and Jura (1944) in the development of new procedures for surface area determination. Anatase was also featured

Table 10.12. Physical properties of typical white pigments.

Pigments	Density ($g\ cm^{-3}$)	Refractive index	a(BET) ($m^2\ g^{-1}$)	Crystal size (μm)
Anatase	3.8	2.55	11	0.15
Rutile	4.2	2.76	6	0.25
ZnO	5.6	2.01	10	0.2
ZnS	4.0	2.37	6	0.25
White lead	6.9	2.0	2	1

From Wiseman (1976).

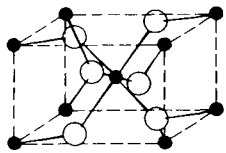

Figure 10.19. Unit cell of rutile. Black circles, titanium atoms; open circles, oxygen atoms (reproduced courtesy of Adamson 1986).

in some early adsorption calorimetric studies, e.g. by Kington *et al.*, (1950). However, it was soon evident that rutile was becoming increasingly important. Finely divided rutile was adopted by Drain and Morrison (1952) as the non-porous adsorbent for an important series of calorimetric adsorption energy measurements. In spite of the energetic heterogeneity shown by the low-temperature adsorption of argon, nitrogen and oxygen on rutile (Drain, 1954), the derived values of differential and molar entropies of adsorption provided valuable supporting evidence for the validity of the BET monolayer capacities.

Somewhat later, the surface and colloidal properties of rutile were studied in considerable detail (Day, 1973; Wiseman, 1976; Parfitt, 1981; Rochester, 1986). In the early 1970s, extensive use was made of infrared spectroscopy for characterizing the rutile surface and its interaction with water and other molecules. An improved understanding of the mechanisms involved in coating the rutile surface was also provided by studies of the energetics of immersion and electrokinetic behaviour together with the application of electron microscopy.

10.4.2. Rutile: surface chemistry and gas adsorption

The availability of pure rutile in a finely divided state has allowed progress to be made in the interpretation of adsorption isotherm and energy data. In particular, it has been possible to explain certain unusual features of the adsorptive properties of rutile in terms of its surface chemistry as characterized by infrared spectroscopy.

A puzzling dependence of the BET-nitrogen area on the outgassing temperature was first noted by Day and Parfitt (1967). It was found that the surface area appeared to undergo an increase of about 20% when the outgassing temperature was increased from ambient to 200°C and thereafter remained constant over a wide temperature range. A little later, Day *et al.* (1971) undertook a systematic investigation of the effect of pre-treating rutile with water and various alcohols. A sample was outgassed at 400°C, equilibrated with water vapour, and then outgassed at 25°C: as a result, the BET-nitrogen area underwent a decrease from 10.2 to 7.7 $m^2 g^{-1}$, the nitrogen C value being correspondingly reduced from 450 to 180. Pre-treatment with ethanol resulted in $a(\text{BET}, N_2) = 7.5\ m^2 g^{-1}$ and $C = 39$.

It was first thought that the changes in BET area were due to the presence of micropores in which water and other molecules could be trapped and removed only by an increase in the outgassing temperature. In the light of further adsorption and spectroscopic measurements, it now seems much more likely that these and other effects are associated with the surface chemistry of rutile rather than its porosity.

The external surface of a rutile crystal is almost entirely composed of the three crystal planes (1 1 0), (1 0 0) and (1 0 1). The relative area of each crystal face in a sample of finely divided rutile probably varies from one polycrystalline sample to another but it is generally assumed that 60–80% of the overall surface area of the powder is provided by the (1 1 0) plane, with the remainder divided equally between the two other planes (Jaycock and Waldsax, 1974; Boddenberg and Eltzner 1991).

The arrangement of the Ti^{4+} and O^{2-} ions in parallel rows on an exposed (1 1 0) surface is pictured in Figure 10.20. The surface structure is clearly consistent with the

composition of the unit cell (Bakaev and Steele, 1992). In this ideal model, the surface Ti^{4+} ions are coordinatively unsaturated ('cus') and on exposure to the atmosphere at ambient temperature they will be covered – either by ligand attachment or by some form of chemical bonding.

The most obvious way of removing the surface unsaturation is by reaction with water: this could involve dissociative chemisorption and/or molecular adsorption. Detailed infrared spectroscopic studies have shown that both processes occur (Griffiths and Rochester, 1977; Morishige *et al.*, 1985; Rochester, 1986). Although the interpretation of the infrared spectra is not entirely straightforward (see Parkyns and Sing, 1975) it appears to be generally agreed that the dominant infrared bands at 3655 cm^{-1} and 3410 cm^{-1} represent the stretching vibrations of terminal and bridged hydroxyl groups, respectively. It is likely that these hydroxyls are in the main located on the (1 1 0) face (Jaycock and Waldsax, 1974). However, other broad bands around 3400 cm^{-1} are probably due to hydrogen-bonded species. Dissociative chemisorption of water is believed to occur on the (1 1 0) face and coordinate bonding of water molecules on the Ti^{4+} sites exposed on the (1 0 0) and (1 0 1) faces.

Dehydration of rutile crystals involves the removal of hydrogen-bonded water, coordinately bonded water and surface hydroxyls (dehydroxylation). The temperature ranges corresponding to these three stages overlap and depend on the rutile sample and the conditions of heat treatment. Generally the removal of molecular water occurs at temperatures of up to about 300°C and progressive dehydroxylation

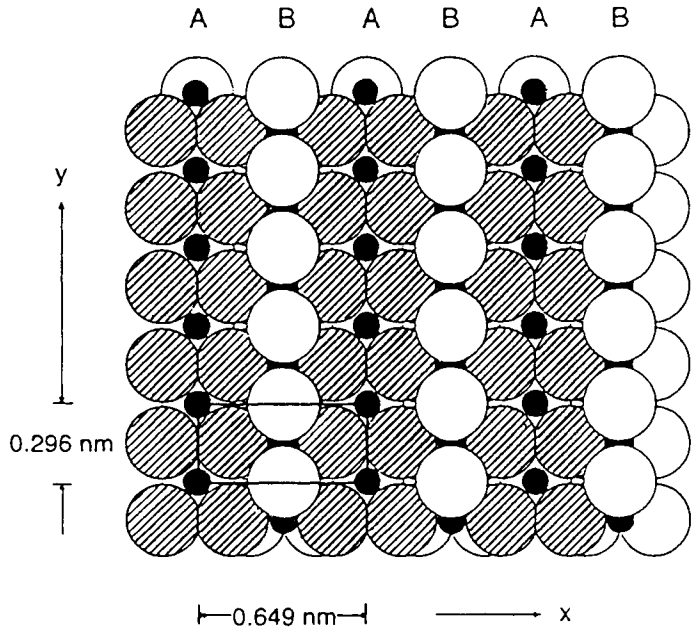

Figure 10.20. Top view of the (1 1 0) surface of rutile. Black circles, Ti atoms; open circles, O atoms above plane of Ti; hatched circles, O atoms under plane of Ti. (Reproduced courtesy of Rittner *et al.*, 1995).

over the range 200–500°C. In a study of the interaction of water vapour with the surface of rutile, Munuera and Stone (1971) concluded that molecular water could be completely removed by evacuation at 325°C, leaving the surface partially hydroxylated. They attributed a thermal analysis (TPD) peak at 250°C to the removal of coordinated water and a peak at 370°C to dehydroxylation from about 50% of the surface.

A striking difference has been found between the energetics of adsorption of argon and nitrogen on rutile (Furlong *et al.*, 1980a). A Tian–Calvet microcalorimeter was used to determine differential energies of adsorption of argon and nitrogen on nonporous rutile outgassed in stages at temperatures of 150, 250 and 400°C. The differential energies of adsorption, $\Delta_{ads}u$, obtained after each outgassing stage are plotted in Figure 10.21 against the surface coverage, θ.

The most striking feature of the results in Figure 10.21 is the very high initial energy of adsorption of nitrogen on rutile outgassed at 250 or 400°C, $\Delta_{ads}u$ being in excess of 20 kJ mol^{-1} at $\theta < 0.4$. With argon, the initial energies are closer together and the differences become more pronounced at higher coverage.

Values of $\Delta_{ads}u$ for nitrogen adsorption at $\theta = 0.1$ are recorded in Table 10.13, which also contains the corresponding adsorption energy data for silica-coated rutile. It was independently confirmed that the surface properties of the latter sample, which had a coating of 2.6% dense silica, were very similar to those of pure silica (Furlong *et al.*, 1980).

It is noteworthy that the corresponding values of $\Delta_{ads}u$ for nitrogen on rutile and silica-coated rutile in Table 10.13 are not very different, provided that the rutile is outgassed at 150°C. There is little doubt that the specificity of adsorption of nitrogen on hydroxylated silica is due to interaction between the nitrogen quadrupoles and the surface OH groups, and it appears that this is also true for rutile outgassed at 150°C. Clearly, the situation is changed when rutile is outgassed at higher temperatures. From the location of the adsorption energy curves in Figure 10.21 and the data in Table 10.13, we conclude that: (a) outgassing at 250°C has removed most, if not all,

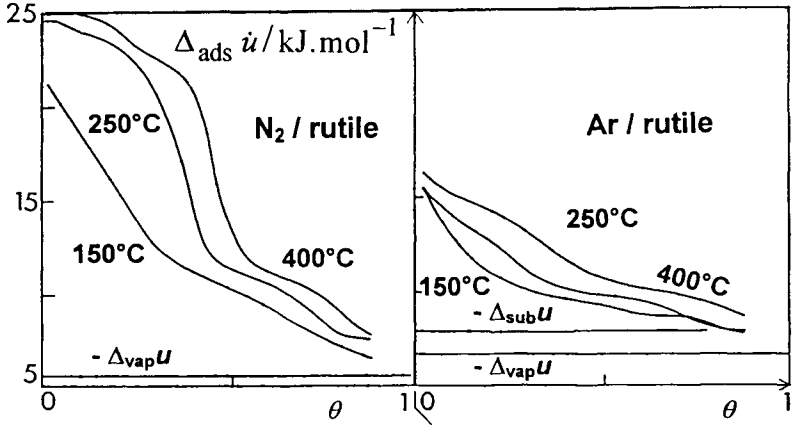

Figure 10.21. Differential energy of adsorption of nitrogen and argon, at 77 K, on rutile outgassed at 150°C, 250°C and 400°C (Furlong *et al.*, 1980a).

Table 10.13. Differential energies of adsorption of nitrogen at 77 K on rutile and silica-coated rutile.

Outgassing temperature (°C)	$\Delta_{ads}u$ (N_2 at $\theta = 0.1$) (kJ mol^{-1})	
	Rutile	Silica-coated rutile
150	18.5	19.3
250	24.0	20.0
400	24.9	20.6

the coordinated H_2O ligands from the cationic sites; (b) dehydroxylation at 400°C has resulted in the exposure of more high-energy sites; and (c) two types of cationic sites appear to occupy about 40% of the overall surface.

We are now in a position to explain in more detail why the BET area is found to increase as the outgassing temperature is raised. The picture of the exposed (1 1 0) surface in Figure 10.20 reveals that even an ideal plane of the dehydrated rutile surface cannot be regarded as smooth. Although the real surface is more complex and energetically heterogeneous, infrared spectroscopy and adsorption microcalorimetry give a remarkably consistent picture of the role of the cationic sites. We conclude that the interaction of adsorbate molecules with exposed 'cus' cations results in the incorporation of over 20% of the 'monolayer' within the surface structure. These adsorbate molecules take the place of water ligands (and also some hydroxyls) and are thus located in the gaps between the oxygen ions.

The adsorption of water vapour on rutile has been studied by a number of investigators (e.g. Dawson, 1967; Day *et al.*, 1971; Munuera and Stone 1971). In the work of Furlong *et al.* (1986), water isotherms were determined after successively outgassing the rutile adsorbent at: (1) 25°C, (2) 100°C, (3) 150°C, (4) 300°C and (5) 25°C. The resulting isotherms are shown in Figure 10.22. It can be seen that isotherms (4) and (5) exhibit a second knee (Points X and X') and are nearly parallel at $p/p^\circ > 0.1$. Isotherms (2) and (3) are almost parallel, but have no identifiable second knee.

Following the above reasoning, we arrive at the following interpretation of the isotherms in Figure 10.22. The first outgassing at 25°C has removed the free hydrogen-bonded water so that curve (1) is the physisorption isotherm on the remaining fully hydrated surface. Ligand water has started to leave the surface at 150°C and by 300°C all the ligand water has been removed, together with a high proportion of the hydroxyl groups. Isotherm (4) is therefore a composite isotherm of the specific adsorption on cationic sites and the additional physisorption. The latter has been removed by the final outgassing at 25°C, but is taken up again in the form of isotherm (5). Thus, the vertical separation of isotherms (5) and (4) – that is between X and X' – provides a measure of the ligand water retained after outgassing at 25°C (i.e. ~150 $\mu mol\ g^{-1}$). The fact that isotherms (1) and (5) follow different paths is a consequence of the change in the nature of the surface, which has involved the irreversible removal of hydroxyl groups. Physisorption accounts for *c.* 177 $\mu mol\ g^{-1}$, which corresponds to 0.21 nm^2 per water molecule a value close to that for water on hydroxylated silica.

We have seen that cations are exposed by the surface dehydration of rutile. These 'cus' ions act as Lewis acid (acceptor) sites for the adsorption of pyridine, ammonia

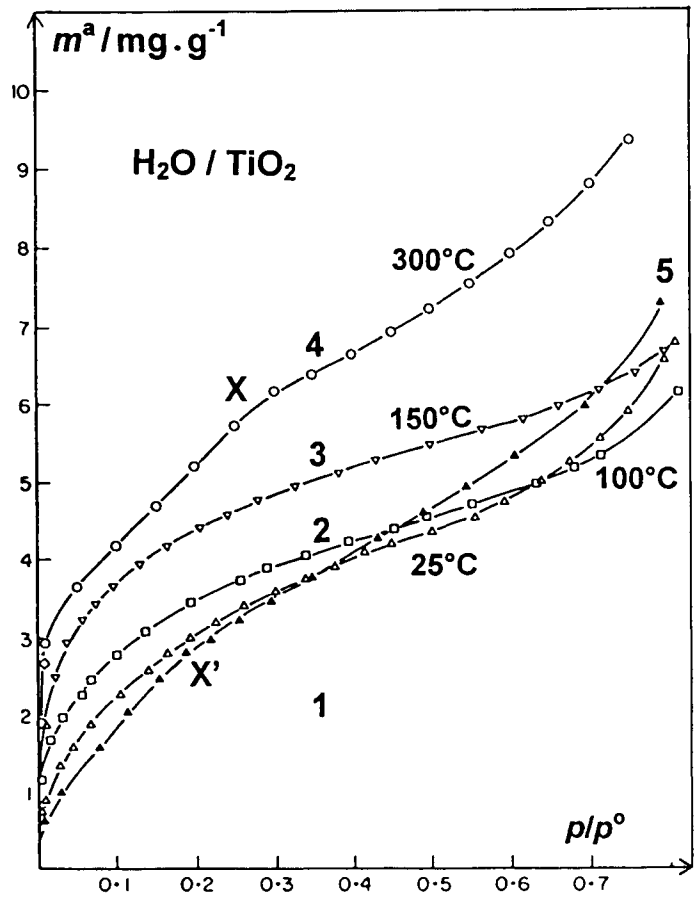

Figure 10.22. Isotherms of water vapour on rutile, outgassed between 25°C and 300°C. Run 5 follows run 4 with simple intermediate outgassing at 25°C (Furlong *et al.*, 1986).

and other bases. On the other hand, there appears to be no indication of Bronsted acidity, although this can be produced by surface treatment (e.g. with HCl). It is not surprising that the dehydrated surface of rutile can interact specifically with a wide range of polar molecules (Parkyns and Sing, 1975).

Parfitt and his co-workers pointed out (Day, Parfitt and Peacock, 1971) that there is an important difference between ethanol and isopropanol in their interactions with rutile. Whereas ethanol can displace water and undergo dissociative chemisorption to form the surface ethoxide, isopropanol is more readily adsorbed in the molecular form. This is consistent with the hydrophobic nature of ethanol-treated TiO_2 and the 'autophobic' nature of the ethanol monolayer. The latter effect is manifested in the form of a Type I isotherm, which is remarkably similar to that given by ethanol on alumina (see Figure 10.15).

A fairly low-area sample of polycrystalline TiO_2 (98.5% rutile) was used by Grillet

et al. (1985) in a combined manometric-calorimetric study of krypton adsorption at 77 K. Unlike nitrogen, the path of the krypton isotherm was not changed to any significant extent by the increase of outgassing temperature from 140 to 400°C. As can be seen in Figure 10.23, although the isotherm is essentially Type II in the IUPAC classification, it does exhibit some stepwise features. Thus, there are sub-steps at p/p° of 0.016 and 0.72 (i.e. at BET coverages of 0.66 and 1.45), which indicate changes in the mode of adsorption. The first sub-step is located in the sub-monolayer range of the isotherm. The microcalorimetric measurements revealed that it was accompanied by an energy change of 610 J mol^{-1} (hatched area), which is close to the thermal energy, RT, at 77 K (i.e. 644 J mol^{-1}). It therefore seems likely that this represents a change of state from a 2-D fluid to a 2-D solid.

There was no indication of any similar phase changes in the adsorbed monolayers of either nitrogen or argon on the same rutile surface. In the case of nitrogen, this is not surprising in view of its quadrupolar nature and specificity of adsorption. The difference between argon and krypton has been explained (Grillet *et al.*, 1985) in terms of the 'dimensional incompatibility factor'. According to this view, of the two adsorbate structures, krypton is more likely to be in registry with the rutile surface.

This work has again drawn attention to the difficulties involved in deriving the surface area from the BET-monolayer capacity. Grillet *et al.* (1985) have pointed out that the use of nitrogen may lead to an uncertainty of up to 30% in the area of rutile:

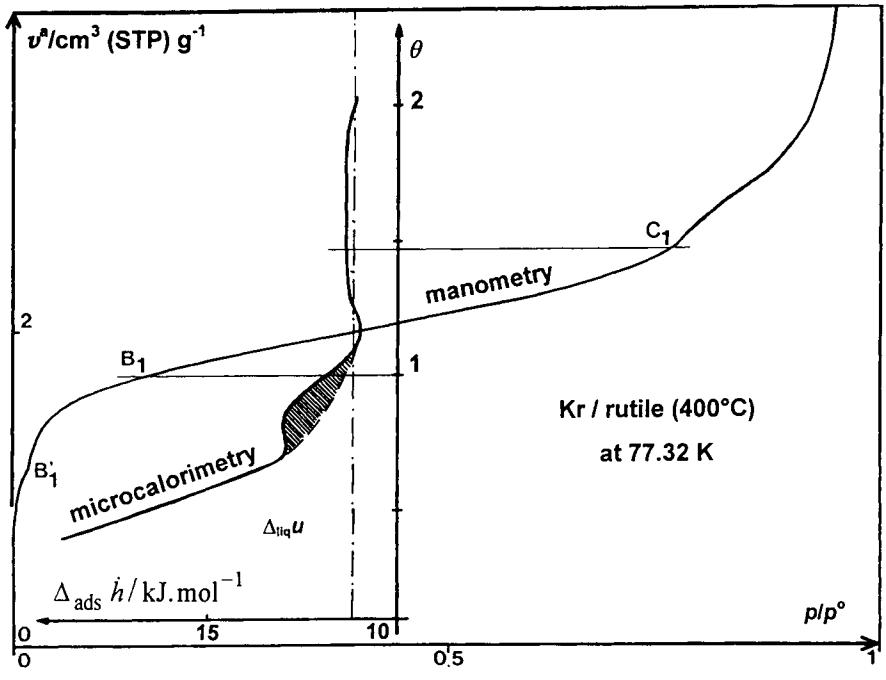

Figure 10.23. Isotherm and differential enthalpy of Kr adsorption on polycrystalline TiO_2 (Grillet *et al.*, 1985).

they suggest that consistency between krypton and argon is obtained if $\sigma(\mathrm{Kr}) = 0.15\ \mathrm{nm}^2$.

A recent computer simulation study has been made by Rittner *et al.* (1995) of the adsorption of xenon on the (1 1 0) face of rutile (as depicted in Figure 10.20). The simulated isotherms, obtained by the canonical ensemble Monte Carlo technique, were in fairly good agreement with experimental data determined over the temperature range 196–273 K. The Monte Carlo calculations indicate that the surface geometry of the (1 1 0) face has a predominant influence on the adsorption of xenon. At low surface coverage the adsorption is almost entirely confined to cationic rows, although the adsorbate structure is determined by the adsorbate–adsorbate interaction and therefore is not in registry with the 'cus' titanium sites. Increased translational mobility of the adsorbate is associated with the occupation of the surface oxygen sites at higher coverage. It is evident that the xenon atoms are not all in the same plane when the surface is fully covered. Although refinements are still required in this type of simulation approach, the results again illustrate the dependence of physisorption on surface structure.

10.4.3. The porosity of titania gels

Titanium dioxide gels of high surface area can be prepared in a number of different ways. In the early work of Harris and Whitaker (1962, 1963), porous gels were prepared by the steam-hydrolysis of titanium alkoxides in benzene solution. Bonsack (1973) obtained a range of microporous gels from Ti^{IV} sulfate in aqueous solution, the maximum BET-nitrogen area being $\approx 420\ \mathrm{m}^2\ \mathrm{g}^{-1}$. Carefully controlled stoichiometric amounts of water were used by Teichner and his co-workers (see Teichner *et al.*, 1976) to hydrolyse in an autoclave solution of alkoxide in the corresponding alcohol. A variety of macroporous aerogels of anatase structure could be produced in this manner.

In a systematic investigation of the porosity of titania gels, Ragai *et al.* (1980) and Ragai and Sing (1982, 1984) employed aqueous solutions of titanous ions, $[Ti(H_2O)_6]^{3+}$. The addition of aqueous ammonia gave black precipitates of the hydrous Ti^{III} oxide, which were then oxidized to produce the white hydrogels of Ti^{IV} oxide. The pH of the ammonia addition was recorded and the hydrogels were thoroughly washed and the compact xerogels obtained by oven-drying at 110°C.

A representative selection of the nitrogen isotherms and corresponding α_S-plots on the TiO_2 xerogels prepared by Ragai and Sing (1984) are displayed in Figure 10.24. Each α_S-plot is presented as the volume of nitrogen adsorbed plotted against the reduced adsorption, α_S, which had been determined on a nonporous reference TiO_2 (Ragai *et al.*, 1980). It is evident that in each case back-extrapolation of the initial linear section gives a zero intercept. This is a useful indication that pore filling was preceded by monolayer adsorption on the supermicropore walls and that there was no detectable primary micropore filling of ultramicropores.

The isotherms and α_S-plots in Figure 10.24 exemplify the adsorptive behaviour of three types of pore structure: (a) a wide range of open mesopores in gel E; (b) a well-defined mesoporous network in gel Al; and (c) a distribution of supermicropores and some mesopores in gels A3 and C.

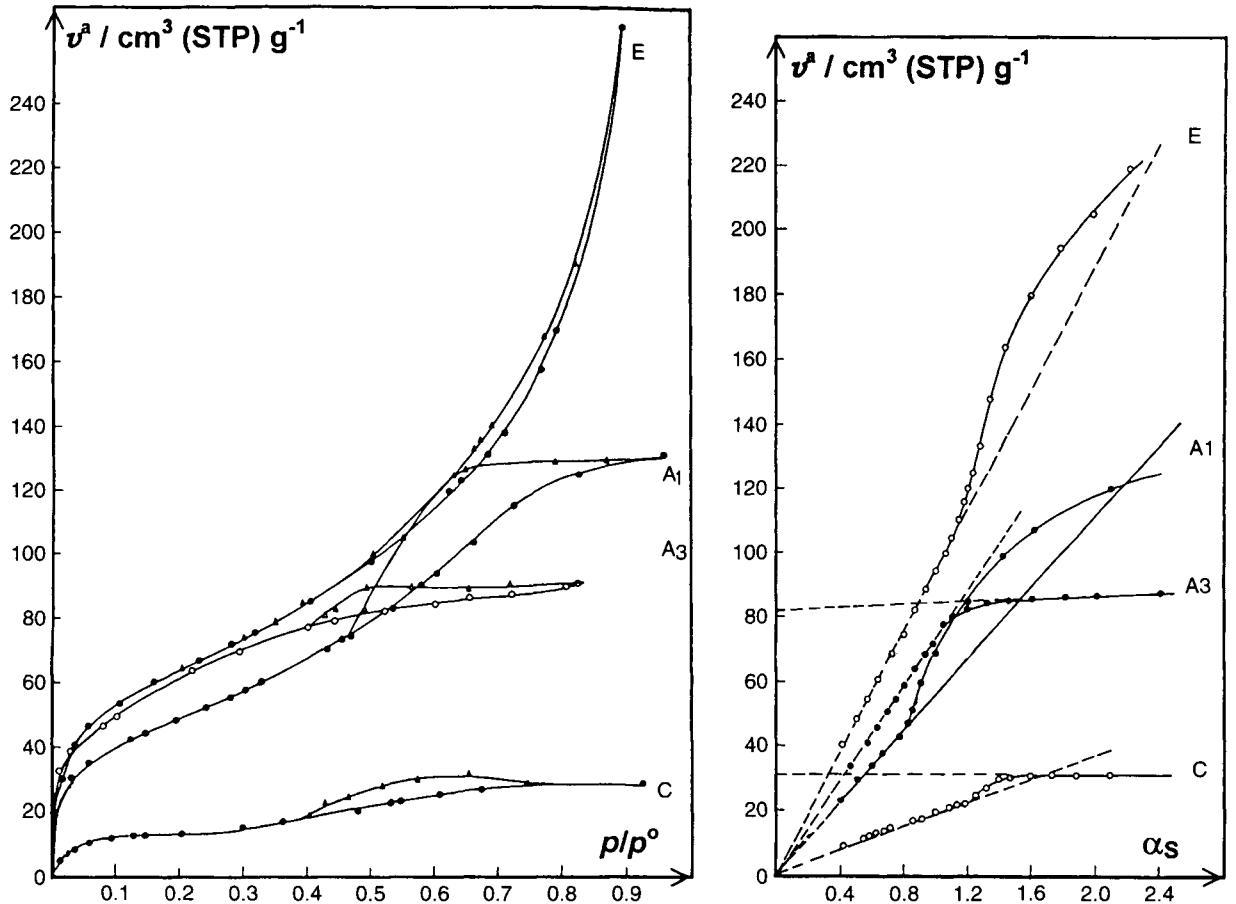

Figure 10.24. Adsorption isotherms of N_2 at 77 K on a selection of hydrous TiO_2 gels (left) and corresponding α_S-plots (right) (Ragai and Sing, 1984).

The development of porosity in many freshly prepared hydrous oxide gels (e.g. Al_2O_3, TiO_2, Cr_2O_3 and ZrO_2) is associated with the removal of the ligand water. Increase in pH generally leads to enhanced ligand displacement and consequently to the development of hydroxo and oxo bridges between neighbouring cations, and ultimately to the cementation of particles. The retention of the ligand water tends to retard the development of the gel network and to leave the system in a poorly ordered state (Bye and Sing, 1973).

The observed differences between the pore structures of the TiO_2 gels featured in Figure 10.24 have been explained in this manner (Ragai and Sing, 1984). The low uptake of nitrogen by gel C was probably due to the inaccessibility of many of the cavities which remained in the vicinity of the cations when the residual water ligands were removed at low temperature. Appreciable mesoporosity appeared only after the precipitation occurred above pH $\approx$ 5. For example gel E, prepared at pH 7.1, had a very open mesopore structure. It was found also that the transformation to rutile was facilitated if the gel was prepared at relatively low pH. Thus, gels C and Al were converted directly to rutile at 500°C, whereas anatase was formed by the same heat treatment of gel E. It seems likely that the removal of the residual water ligands has led to the formation of a defect structure and enhanced reactivity.

10.5. Magnesium Oxide

10.5.1. Physisorption of non-polar gases on non-porous MgO

It is well known that magnesium oxide smoke (an aerosol) is produced when magnesium ribbon is burnt in air. The dispersed material is in the form of small particles: when produced under controlled conditions these are single-crystal cubes in the size range 20–200 nm. Non-porous MgO powders prepared in this manner appear to have unique properties as adsorbents for physisorption measurements. In particular, it is possible to prepare a highly uniform MgO surface since the (1 0 0) crystal plane of the f.c.c. lattice is the most stable surface state (Henrich, 1976). Furthermore, although the MgO(1 0 0) surface is ionic, a relatively weak non-specific interaction is to be expected with non-polar molecules – in contrast to the strong non-specific interaction shown by the basal plane of graphite.

Remarkably uniform MgO smoke was prepared by Coulomb and Vilches (1984) by burning magnesium ribbons in dry O_2/Ar mixtures. The MgO particles were collected in the form of a coating on a clean aluminium surface and were subjected to heat treatment (at *c.* 950°C and pressures < 10^{-6} mbar). The specific surface area of the final MgO(1 0 0) powder was *c.* 8 $m^2 g^{-1}$ so that it was not difficult to undertake accurate physisorption measurements and also neutron scattering experiments.

The uniformity of the MgO(1 0 0) surface was demonstrated by the stepwise (Type VI) character of the isotherms of Kr, Xe and Ar (Coulomb *et al.*, 1984), CH_4 (Madih *et al.*, 1989) and C_2H_6 (Trabelsi and Coulomb, 1992). To obtain the required high degree of surface uniformity, it was necessary to exclude water vapour and control both the oxygen concentration and the conditions of thermal treatment (Coulomb and

Vilches, 1984). The deleterious effect of water vapour was attributed to the formation of surface layers of $Mg(OH)_2$. This conclusion was consistent with the inferior quality (i.e. non-stepwise character) of isotherms determined on MgO prepared by the thermal decomposition of $Mg(OH)_2$.

A family of isotherms for the Xe/MgO(1 0 0) system is shown in Figure 10.25. Similar results were obtained for the Kr/MgO(1 0 0) system (Coulomb *et al.*, 1984). The vertical risers corresponding to first and second layer formation are clearly evident, as are the first layer sub-steps. As with other systems, the sub-steps were attributed to 2-D 'fluid–solid' transitions. By following the approach adopted by Larher, Coulomb *et al.* (1984) were able to estimate the 2-D triple and critical points for Xe/MgO and Kr/MgO.

The Ar/MgO(1 0 0) isotherms determined by Coulomb *et al.* (1984) over the temperature range 48–69 K also exhibited well-defined first and second layer risers, but at these temperatures there appeared to be no first-layer sub-steps. This absence of monolayer phase transitions in the p–T range studied seemed to be associated with a large 2-D liquid–vapour coexistence region. However, subsequent work (Coulomb, 1991) revealed the existence of a 2-D solid-type structure at lower temperatures, with all the Ar atoms appearing to lie along the channels formed by the small Mg^{2+} ions. At a temperature of *c.* 38 K, the long-range order along the channels is lost.

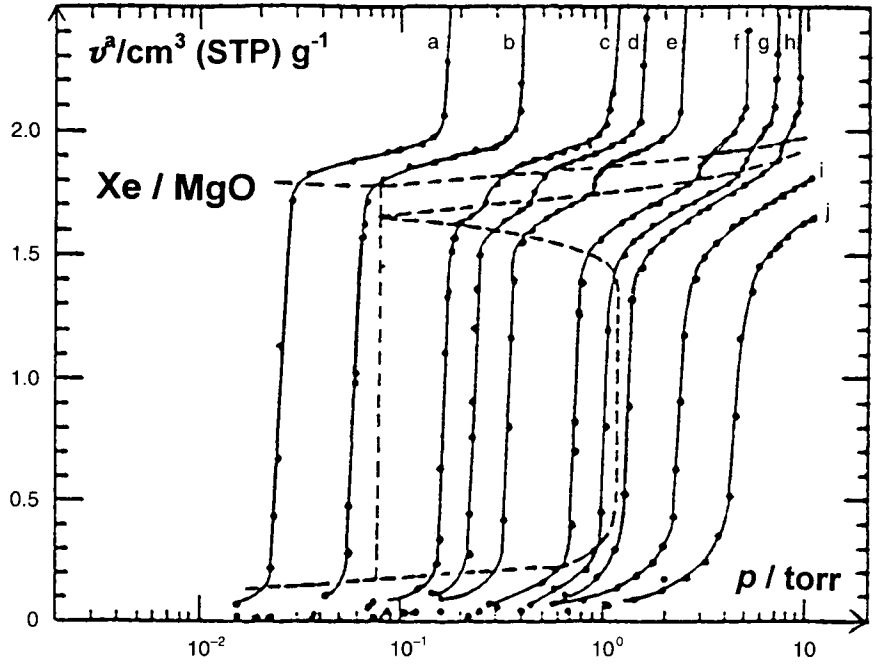

Figure 10.25. Isotherms of Xe on MgO at (a) 96.86, (b) 100.47, (c) 106.20, (d) 108.44, (e) 111.02, (f) 116.14, (g) 118.72, (h) 121.15, (i) 126.17 and (j) 131.19 K. Phase boundaries indicated by dashed lines (Coulomb *et al.*, 1984).

According to Coulomb, there occurs a kind of 'one-dimensional melting' with the formation of a 2-D 'liquid crystal' state.

A neutron diffraction study was undertaken by Madih *et al.* (1989) alongside methane adsorption measurements on the MgO(1 0 0) powder. The well-defined stepwise character of the CH_4 isotherm at 87.4 K in Figure 10.26 is again indicative of the layer-by-layer mode of adsorption. A somewhat similar isotherm was given by C_2H_6 on the MgO(1 0 0) surface at 119.68 K, although the higher steps were not as distinctive as those for CH_4.

Coulomb and his co-workers conclude that at 87.4 K up to four adsorbed layers of methane are ordered while the higher layers are disordered and liquid-like. In a normal 2-D 'solid' monolayer the CH_4 molecular area would be 0.178 nm^2. The neutron diffraction patterns for CD_4 methane indicate that the commensurate 2-D

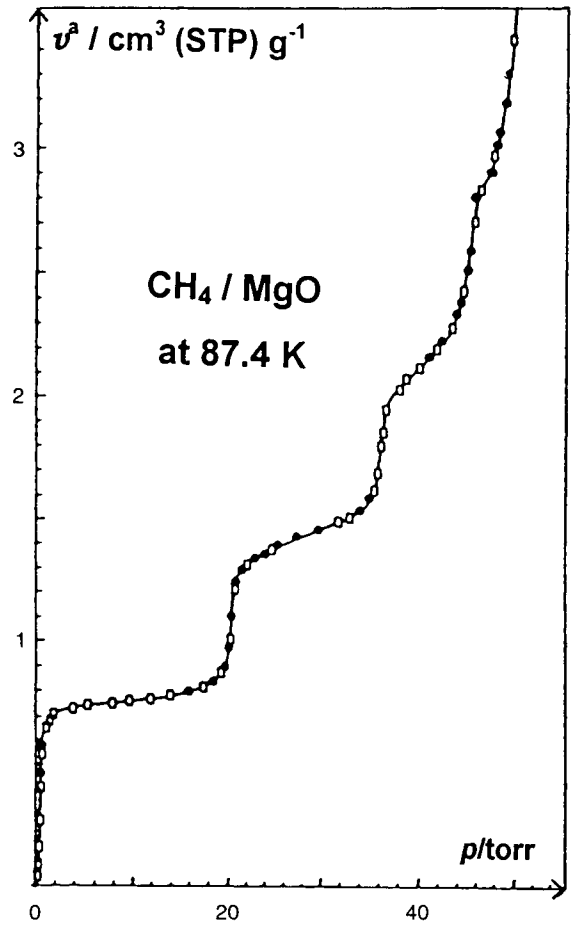

Figure 10.26. Adsorption isotherm of CH_4 on MgO (1 0 0) at 87.4 K. Open symbols, adsorption; solid symbols, desorption (reproduced courtesy of Gay *et al.*, 1990).

solid-like film is not completely melted above the triple point ($T_t = 89.7$ K) with over two statistical layers remaining ordered at 95 K. However, bulk crystallites, which are also formed at temperatures below the 2-D triple point, disappear as the melting point is approached.

As might be expected, ethane adsorption on MgO(100) is more complicated and is apparently characterized by short-range order. It seems that the size and shape of the C_2H_6 molecule play an important role in determining the structure of the 2-D film.

10.5.2. Physisorption by porous forms of MgO

Magnesium oxide of high surface area can be produced by the thermal decomposition of various magnesium compounds. In the early work of Gregg and Packer (1955), a maximum specific area of about 200 $m^2 g^{-1}$ was obtained by the calcination of $Mg(OH)_2$ at 380°C. This temperature was a little below the temperature required for the complete decomposition of the $Mg(OH)_2$ under these experimental conditions.

Vleesschauwer (1970) prepared two series of mesoporous batches of MgO by the heat treatment of crystalline $MgCO_3$ (magnesite) and crystalline $MgCO_3.3H_2O$ (nesquehonite). A maximum surface area of about 350 $m^2 g^{-1}$ was obtained by calcination of the latter precursor at 400°C. Although the thermal decomposition of magnesite resulted in the development of lower surface areas (< 140 $m^2 g^{-1}$) the products appeared to have a more uniform mesopore structure. Thus, the nitrogen isotherm determined on a sample calcined for 24 hours at 800°C exhibited a narrow, almost vertical, hysteresis loop at $p/p^\circ \approx 0.9$.

Mikhail *et al.* (1971) obtained a series of porous products by the thermal decomposition of magnesium oxalate dihydrate *in vacuo* at temperatures in the range 400–600°C. The BET areas derived from the adsorption isotherms of nitrogen and cyclohexane are given in Table 10.14. The values of $\sigma(N_2)$ and $\sigma(C_6H_6)$ have been taken as 0.162 nm^2 and 0.39 nm^2, respectively.

It is evident that the corresponding BET areas in Table 10.14 are in fairly good agreement only after the decomposition temperature was taken above 500°C. These results provide strong evidence for the initial formation of narrow micropores, which

Table 10.14. Comparison of BET areas derived from isotherms of nitrogen and cyclohexane on samples of MgO prepared by thermal decomposition of oxalate (Mikhail *et al*,. 1971).

θ_{decomp} (°C)	a(BET, N_2) ($m^2 g^{-1}$)	a(BET, C_6H_{12}) ($m^2 g^{-1}$)
400	482	204
430	471	259
460	481	370
510	263	246
560	145	141
600	42	44

would be inaccessible to cyclohexane molecules. However, as pointed out in Chapter 6, the validity of *both* values of BET area is questionable.

In other more recent studies of the formation of microporous MgO (Ribeiro Carrott *et al.*,1991a,b, 1993) microcrystalline $Mg(OH)_2$ was used as the precursor. The $Mg(OH)_2$ was thoroughly evacuated at room temperature before being heated *in vacuo* at progressively higher temperatures. The pressure was always maintained below 10^{-3} mbar. TEM revealed that the small hydroxide particles (150–7000 μm) consisted of hexagonal platelets and that this morphology was retained throughout the decomposition. The outgassed mass at 150°C corresponded to the exact stoichiometry $Mg(OH)_2$. About 85% decomposition occurred below 300°C, but temperatures of 700–800°C were required to achieve 100% decomposition. X-ray diffraction showed that the thermal decomposition was accompanied by a progressive development of the cubic MgO structure and a gradual decrease in the intensity of the $Mg(OH)_2$ lines.

Representative nitrogen isotherms and the corresponding comparison plots are shown in Figure 10.27. The latter have been constructed by taking the undecomposed $Mg(OH)_2$ as the reference material. Any change in isotherm shape is therefore manifested as a non-zero intercept and/or a deviation from linearity.

Each comparison plot in Figure 10.27 has two linear sections. Back-extrapolation of the first linear section gives a zero intercept whereas back-extrapolation of the second (multilayer) section gives a positive intercept. The interpretation of the features is based on the principles introduced in Chapter 8. An analysis of the isotherm data is given in Table 10.15.

The fact that the comparison plots in Figure 10.27 are parallel in the multilayer range indicates that the external area (a(ext) = 99 $m^2 g^{-1}$) has remained constant: this is in accordance with the absence of any detectable change in the particle morphology. The values of micropore volume, v_p(mic), in Table 10.15 have been calculated from the intercepts on the v^a axis, assuming liquid-like molecular packing.

Two sets of derived surface areas are recorded in Table 10.15: the values of a(BET) have been obtained by the usual BET method and a(com) from the slope of the initial linear part of the comparison plot. The close agreement between the corresponding values of surface area is consistent with the linearity and zero intercept of

Table 10.15. Analysis of nitrogen isotherms on thermally decomposed $Mg(OH)_2$.

θ (°C)	%	a(BET) ($m^2 g^{-1}$)	a(com) ($m^2 g^{-1}$)	v_p(mic) ($cm^3 g^{-1}$)	w_p (nm)
150	0	99	99	0	0
240	12.6	110	110	0.007	1.27
250	28.0	128	128	0.017	1.13
270	73.4	230	231	0.063	0.93
400	92.8	237	230	0.078	1.15
500	95.5	191	188	0.072	1.64
600	98.7	164	163	0.053	1.77
750	100	141	142	0.033	1.57

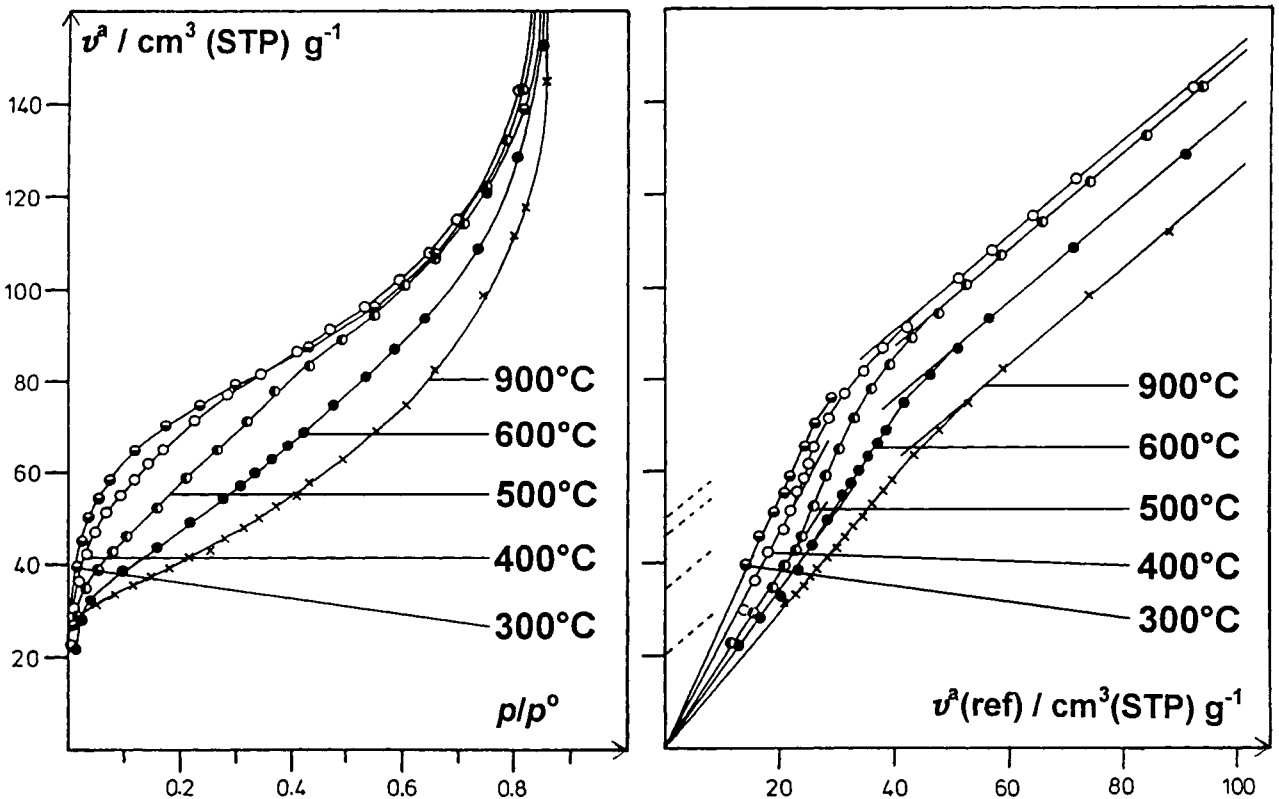

Figure 10.27. Nitrogen isotherms at 77 K on partially decomposed $Mg(OH)_2$ (left) and corresponding comparison plots with undecomposed ($Mg(OH)_2$) as reference (right) (Ribeiro Carrott *et al.*, 1991a).

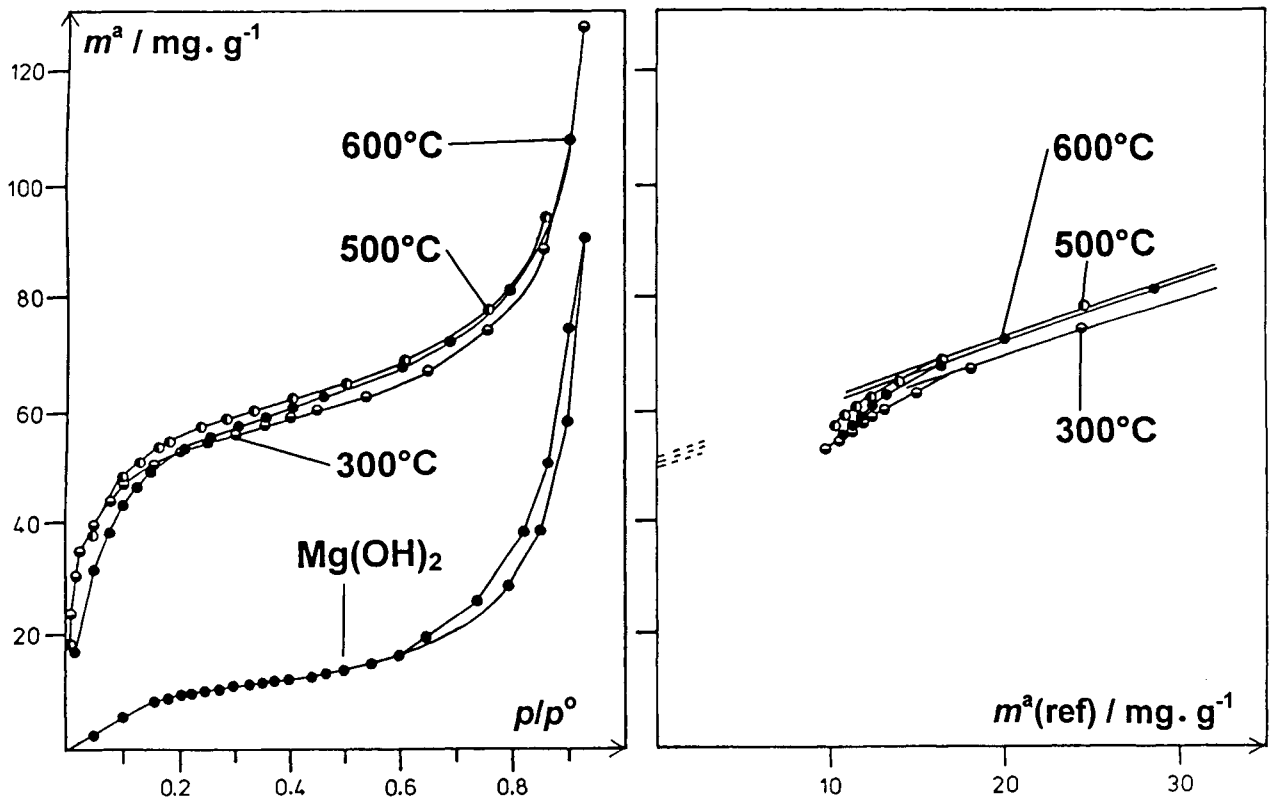

Figure 10.28. Neopentane iostherms at 273 K on partially decomposed and on starting $Mg(OH)_2$ (left) and corresponding comparison plots with undecomposed $Mg(OH)_2$ as reference (right) (Ribeiro Carrott *et al.*, 1991a).

the comparison plot. We conclude that the BET method appears to provide a reliable estimate of the total surface area of each adsorbent.

To obtain the values of mean pore width, w_p, in Table 10.15, we have assumed the validity of the BET area and all pores to be slit-shaped. Then by adopting the hydraulic pore width principle we have

$$w_p = \frac{2v_p(\text{mic})}{a(\text{BET}) - a(\text{ext})} \tag{10.7}$$

These and other results (Ribeiro Carrott *et al.*, 1991a) indicate that there is little variation in w_p between 30% and 90% decomposition. Supermicropores of width of *c.* 1 nm would be wide enough to allow monolayer adsorption of nitrogen to precede co-operative micropore filling, which is the mechanism best able to explain the features of the comparison plots in Figure 10.27.

However, more bulky adsorptive molecules would be expected to behave differently, provided their diameters are large enough to give primary micropore filling. This is exactly the position with neopentane: in terms of its molecular size (0.62 nm) the MgO pore sizes extend from *c.* 1.5 to 3 molecular diameters. This explains why the low-pressure regions of the neopentane comparison plots in Figure 10.28 are not linear and do not back-extraplolate to the origin. In this case, the physisorption forces are enhanced because of the proximity of the pore walls and the shape of the neopentane isotherm is consequently distorted at low $p/p°$.

It has been proposed that the slit-shaped micropores may be regarded as spaces between (1 1 1) planes in the freshly formed MgO structure. Thus, if the width of each micropore was equivalent to four (1 1 1) planes, its width would be 0.96 nm, which is quite close to the hydraulic values. It is not surprising to find pore widening to have occurred as the decomposition neared completion.

10.6. Miscellaneous Oxides

10.6.1. Chromium oxide gels

It has been known for many years that the adsorptive and catalytic properties of chromium oxide gels are very sensitive to the conditions of preparation, storage and heat treatment (Burwell *et al.*, 1960; Deren *et al.*, 1963; Carruthers and Sing, 1967; Baker *et al.*, 1970, 1971).

The amorphous hydrogels produced by the neutralization of chromium (III) salts generally retain large amounts of water. These products tend to undergo ageing (i.e. loss of surface area) but by careful drying they can be converted into highly porous xerogels. When such chromia gels are subjected to heat treatment in air or oxygen at temperatures above *c.* 200°C, there occurs an oxidation–reduction cycle, $Cr^{3+} \rightarrow Cr^{6+} \rightarrow Cr^{3+}$, which finally results in the formation of low-area crystalline α-Cr_2O_3 (Baker *et al.*, 1971).

The crystallization process is a highly exothermic transformation (or 'glow phenomenon') that normally occurs at remarkably low temperatures (350–400°C); this

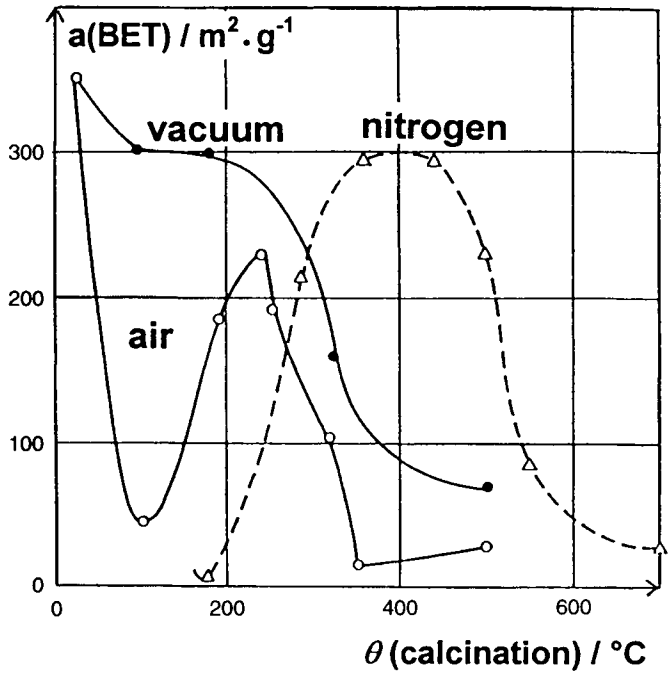

Figure 10.29. BET nitrogen area of chromia gel versus temperature of calcination (in air, *in vacuo* or in stream of dry nitrogen) (Carruthers and Sing, 1967).

can be delayed and minimized if the gel is heated in an inert atmosphere (Carruthers and Sing, 1967). The changes in BET-nitrogen area brought about by the heat treatment of a chromia gel *in vacuo* and in dry nitrogen are shown in Figure 10.29.

The results in Figure 10.29 illustrate the important influence of the surrounding atmosphere during heating. Particularly striking is the protection afforded by nitrogen until the temperature approached 500°C, which is consistent with the upward displacent of the glow temperature. It is also of interest that the drastic ageing at 100°C in air and nitrogen was eliminated by heating *in vacuo*.

The nitrogen isotherms in Figure 10.30 were determined on samples of another chromia preparation, gel B, which had been heated for different periods in air (A) or *in vacuo* (V). Temperature and duration of heat treatment are indicated for each sample.

For sample B (250°C, 2 h V), the nitrogen isotherm is irreversible, a long part of the desorption branch lying parallel to the p/p° axis. Prolonged outgassing (280°C, 27 h, V) has resulted in a reversible Type I isotherm. Heat treatment in air (280°C, 12 h, A and 280°C, 27 h, A) has led to further pore widening and a decrease in surface area (see Table 10.16). The curves 1, 2, 3 and 4 reveal a progressive change in the isotherm character from Type I to Type IV, which is indicative of the change from a microporous to a mesoporous structure.

The α_S -plots in Figure 10.30 provide a basis for the analysis of the corresponding

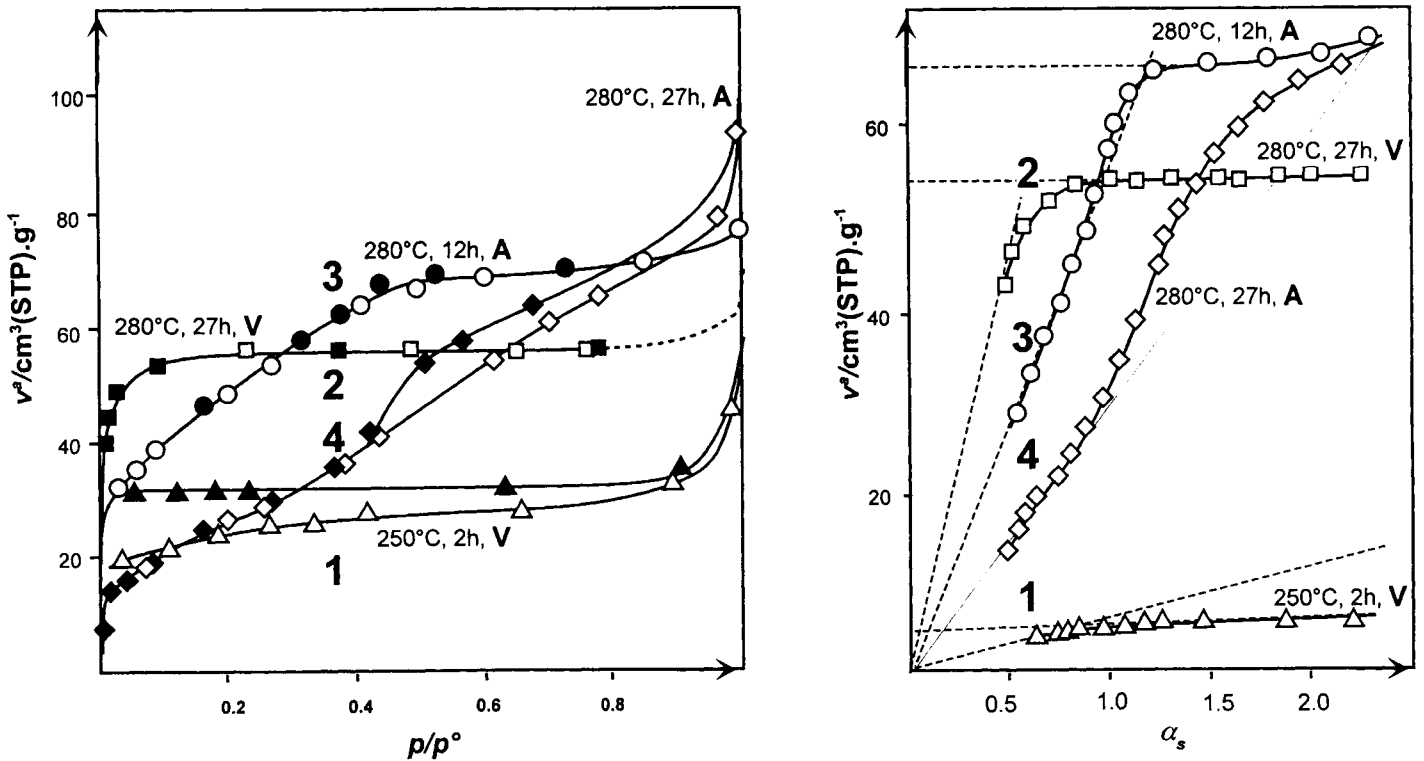

Figure 10.30. Nitrogen isotherms at 77 K (left) and α_S-plots (right) for chromia gel B heated in air (A) or *in vacuo* (V) (temperature and duration indicated on each curve) (Baker *et al.*, 1971).

nitrogen isotherms. The standard isotherm was determined on a non-porous sample of α-Cr_2O_3 (Baker *et al.*, 1971). As previously explained, curves 1 and 2 are characteristic of micropore filling followed by multilayer adsorption on a small external surface ($< 5\ m^2\ g^{-1}$). The values of micropore volume, v_p(mic), in Table 10.16 have been obtained by back-extrapolation of the linear multilayer branch to the adsorption axis and by assuming liquid-like molecular packing.

The long range of near-linearity of the α_S-curve 3 (for sample B: 280°C, 12 h, A) can be attributed to the reversible filling of supermicropores. In the case of curve 4, the upward deviation from linearity is due to capillary condensation in mesopores. In both cases the initial linear region can be back-extrapolated to the origin and we may conclude that pore filling was preceded by surface coverage of the pore walls. The values of total surface area, a(S), in Table 10.16 are calculated from the slope of this linear region by using Equation (10.3). It can be seen that fairly good agreement is obtained between the corresponding values of a(BET) and a(S) only for the supermicroporous and mesoporous samples.

It was established that the oxidation process $Cr^{3+} \longrightarrow Cr^{6+}$ is generally accompanied by pore widening, but that the reduction stage $Cr^{6+} \longrightarrow Cr^{3+}$, which involves the crystallization of α-Cr_2O_3, is associated with the removal of pores and a loss of surface area. It was also evident that the formation of the higher oxidation state is facilitated by the removal of the ligand water, thus reducing the stability of the Cr^{3+} ions (Baker *et al.*, 1971).

It was noted that the orthorhombic CrOOH and ferromagnetic CrO_2 structures were present in some chromia gels, which had been calcined under hydrothermal and oxidizing conditions (Carruthers *et al.*, 1967, 1969). This discovery prompted an investigation of the topotactic interconversion of the oxyhydroxide and the dioxide (Alario Franco and Sing, 1972, 1974), which involved the thermal decomposition *in vacuo* of small crystals of CrOOH. Gas adsorption and electron microscopy revealed that slit-shaped pores are first formed with little change in the external dimensions of the crystals (Alario Franco *et al.*, 1973). The CrO_2, which is formed as an intermediate product, is finally decomposed with the formation of larger pores and the growth of α-Cr_2O_3 crystals. As might be expected, the reduction of CrO_2 in H_2 similarly results in the formation of CrOOH with very little change in external area and with the generation of a relatively small micropore volume.

Table 10.16. Surface areas and porosities of chromia gel B heated *in vacuo* and in air.

Sample	Porosity	a(BET) ($m^2\ g^{-1}$)	a(S) ($m^2\ g^{-1}$)	v_p(mic) ($cm^3\ g^{-1}$)
B (250°C, 2 h, V)	Ultramicro	18		0.008
B (280°C, 12 h, V)	Ultramicro	235	(280)[a]	0.081
B (280°C, 27 h, V)	Ultramicro	240	(280)[a]	0.084
B (280°C, 12 h, A)	Supermicro	167	173	0.112
B (280°C, 27 h, A)	Meso	91	94	0.113 (meso)

[a] Afferent values.

10.6.2. Ferric oxide: thermal decomposition of FeOOH

In the early work of Goodman and Gregg (1959) it was found that a highly active hydrous ferric oxide (a(BET) ≈ 300 $m^2 g^{-1}$] underwent a progressive loss of surface area when calcined in air. Thus, after heat treatment at 400°C for 5 hours the BET area was reduced to *c.* 50 $m^2 g^{-1}$. One of the first systematic investigations of the thermal decomposition of a well-defined iron oxide precursor was undertaken by Bye and Howard (1971), who reported the formation of microporosity from goethite. More recently, the thermal transformation of goethite, α-FeOOH, into haematite, α-Fe_2O_3, has been investigated in a number of laboratories.

In the work of Naono *et al.* (1987), samples of the mineral form of goethite were heated *in vacuo* at different temperatures between 200 and 700°C (i.e. corresponding to the stoichiometric range of decomposition). Nitrogen adsorption measurements revealed that the BET area attained a maximum value of 151 $m^2 g^{-1}$ after the goethite had been outgassed for 10 h at 300°C. The nitrogen isotherms can be broadly separated into two groups as arranged in Figure 10.31. Most of those in (a) clearly have fairly pronounced Type I character, whereas those in group (b) are either Type IV or non-reversible Type II isotherms (now classified as Type IIb). All the isotherms exhibit hysteresis loops, the shape changing from H4 to H3.

The t-plots in Figure 10.32 were constructed from the isotherms in Figure 10.31. For this purpose, the standard t-curve was derived from nitrogen isotherms on two

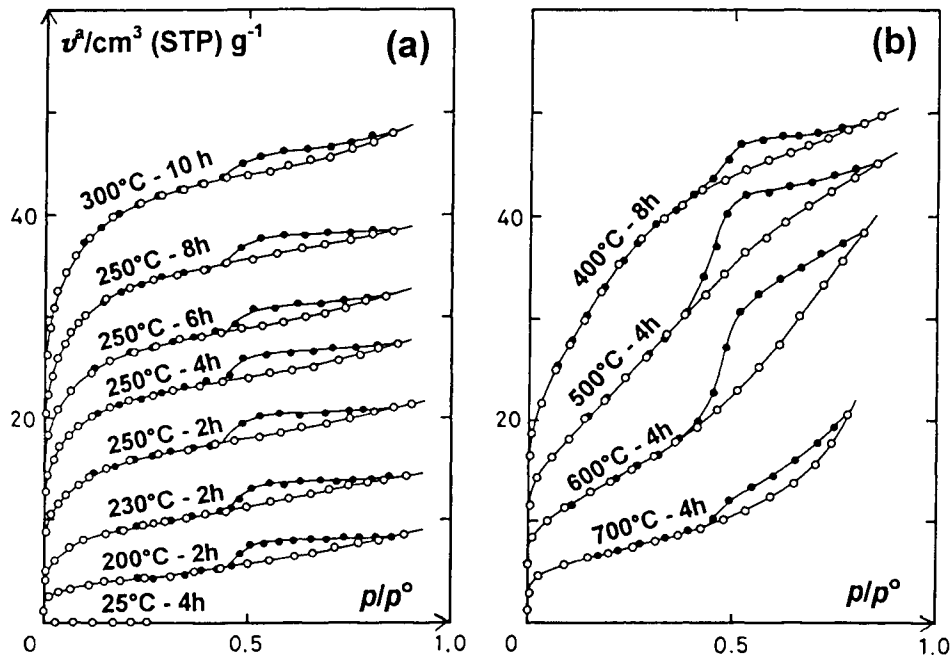

Figure 10.31. Nitrogen adsorption isotherms at 77 K on samples of goethite heated between 200°C and 700°C (reproduced courtesy of Naono *et al.*, 1987).

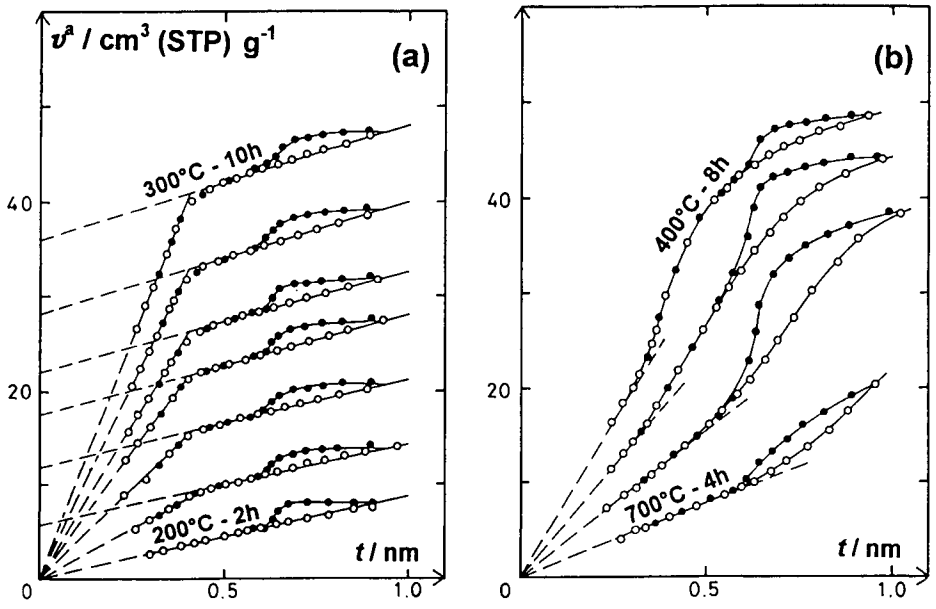

Figure 10.32. Nitrogen *t*-plots constructed from the isotherms in Figure 10.32, for samples of goethite heated between 200°C and 700°C (reproduced courtesy of Naono *et al.*, 1987).

samples of non-porous goethite. As with the isotherms, the *t*-plots are broadly divided into two groups: with the exception of the plot for the sample heated 2 h at only 200°C, those in group (a) are associated with supermicropore filling, while the group (b) plots indicate mainly capillary condensation in mesopores.

The *t*-plots in group (a) are of particular interest because of the linearity of the reversible region at low $p/p°$ and also of the *adsorption* branch of the hysteresis loop. Moreover, the first linear sections can be back-extrapolated to the origin. We may therefore conclude that monolayer adsorption has occurred on both an external surface and the walls of supermicropores, but multilayer adsorption has occurred only on an external surface. This evidence, together with the H4 hysteresis, points to a range of slit-shaped pores, which was confirmed by high-resolution electron microscopy (Naono *et al.*, 1987). Indeed, the electron micrographs of the porous samples have a remarkably similar appearance to the micrographs obtained with partially decomposed CrOOH (Alario Franco and Sing, 1972).

The change in the character of the isotherms and *t*-plots reveals that the loss of surface area which occurred when the outgassing temperature of the goethite was taken above 400°C, was associated with pore widening. The sample obtained at 400°C appears to have a broad range of pores extending from the supermicropore into the mesopore range. The oxide has become predominantly mesoporous at higher temperature, but it is evident that the limits of pore size are not discernible.

Naono and his co-workers have also studied the changes in texture produced by the thermal decomposition of γ-FeOOH (Naono and Nakai, 1989) and β-FeOOH

(Naono *et al.*, 1993). In the latter investigation, a partially decomposed sample gave reversible Type II nitrogen isotherms. However, the *t*-plots provided unambiguous evidence that a micropore structure was developed and that the external area remained virtually unchanged. Since the initial linear region could be back-extrapolated to the origin, it appears that there was no detectable distortion of isotherm shape and therefore no significant filling by ultramicropores.

10.6.3. Microcrystalline zinc oxide

The surface chemistry of zinc oxide is of particular interest in relation to its catalytic and photocatalytic properties. For example the (0 0 0 1) hexagonal crystal plane appears to have a special role in the catalytic methanol-synthesis reaction (Bowker *et al.*, 1983). The chemisorption of CO and dissociative chemisorption of H_2 occur on the exposed Zn^{2+} cations: Bolis *et al.* (1986) have found that the relative magnitude of this 'active' area of ZnO was highly dependent on the nature of the precursor (oxalate, carbonate of Zn). Similar conclusions can be drawn from the infrared spectroscopic measurements of Chauvin *et al.* (1986).

The adsorption isotherm of krypton determined at 77 K on a sample of zinc oxide powder (Grillet *et al.*, 1989) is shown in Figure 10.33. The adsorbent had been outgassed at temperatures up to 450°C by the CRTA technique. As first pointed out by Bonnetain and his co-workers (Audier *et al.*, 1981), it is possible to estimate the extent of surface homogeneity by taking the ratio of the step heights, Y_2/Y_1. In the case of an ideally homogeneous surface, one would expect to obtain $Y_2/Y_1 = 1$: the ZnO in Figure 10.33 gives 0.59 (cf. 0.9 for exfoliated graphite).

An unusual feature of the Kr isotherm in Figure 10.33 is the presence of the three small sub-steps (a b and c), which could be detected by the use of the continuous quasi-equilibrium procedure for the determination of the adsorption isotherm. At present, the significance of these sub-steps is not clear, but it seems more likely to be related to the adsorption on the different crystal faces rather than to any phase changes of the adsorbate. BET analysis of the adsorption isotherms of Kr, Ar and N_2

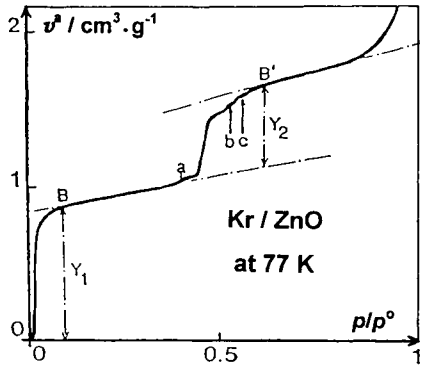

Figure 10.33. Adsorption isotherm of krypton on ZnO at 77 K (Grillet *et al.*, 1989).

on the sample of ZnO gave the following values of surface area: 3.53, 3.56 and 3.76 $m^2 g^{-1}$ (with σ taken as 0.143, 0.138 and 0.162 nm^2, respectively).

The differential enthalpies for the adsorption of N_2 and Ar are plotted against the surface coverage, θ, in Figure 10.34. It is significant that both N_2 and Ar give an almost constant differential enthalpy of adsorption up to *c.* half-coverage. This degree of energetic homogeneity is consistent with the stepwise character of the Kr and Ar isotherms. As with TiO_2, the initial N_2 adsorption energy is much greater than the corresponding Ar energy. The very high N_2 value is mainly due to its strong specific interaction with cationic sites. Thus, the outgassing at 450°C has removed protecting ligands such as H_2O or CO_2, leaving the unscreened Zn^{2+} ions freely exposed.

It can be seen that the N_2 plateau in Figure 10.34 is somewhat longer than the corresponding Ar plateau. It seems likely that the strong N_2 specific interaction is not confined to the (0 0 0 1) Zn^{2+} sites; it may also involve surface defects and edge sites. If we assume that the length of the Ar plateau provides a more reliable indication of the extent of the cationic surface, we arrive at estimated fractions of about 40 and 10%, respectively, for the effective areas of Zn^{2+} and other high-energy sites. There is a peak in the Ar differential energy curve at high surface coverage. The associated adsorbate–adsorbate interaction is probably the result of a two-dimensional phase change (possibly a 2-D fluid–solid transformation), but the smooth Ar isotherm shows no indication of a sub-step. These results illustrate the value of adsorption microcalorimetry for investigating the surface properties of microcrystalline powders.

10.6.4. Hydrous zirconia gels

Zirconium dioxide is notable for its chemical inertness and refractory nature. The first physisorption measurements on ZrO_2 appear to have been made around 1970 (Rijnten, 1970; Holmes *et al.*, 1972). The fact that relatively few adsorption studies

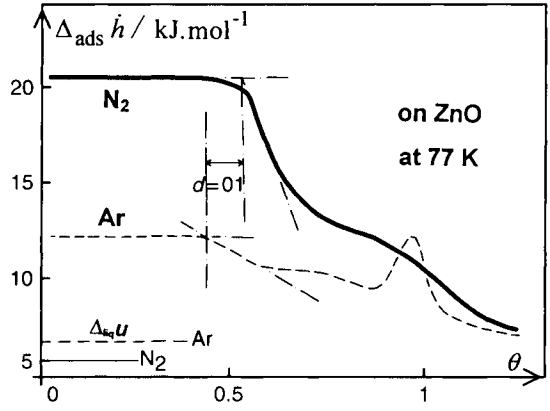

Figure 10.34. Differential enthalpy of N_2 and Ar on ZnO at 77 K (Grillet *et al.*, 1989).

have been undertaken since then may be due to the complexity of zirconium chemistry. Thus, in the preparation of a well-defined oxide-hydroxide structure it is necessary to take account of the exceptionally high coordination number generally exhibited by Zr^{IV} and its tendency to form polymeric ionic networks.

Non-porous ZrO_2 powders can be produced by high-temperature vapour phase condensation methods: in this manner discrete spherical particles of *c.* 4 nm diameter have been obtained (Avery and Ramsay, 1973). It is also possible to prepare colloidal dispersions of sub-micron sized, spheroidal particles of basic salts such as $Zr_2(OH)_6CO_3$ and $Zr_2(OH)_6SO_4$ with the aid of the carefully controlled sol-gel techniques developed by Matijevic (1988).

In the work of Rijnten (1970), a number of procedures were used for the preparation of hydrous zirconia gels. For example, a dilute solution of NH_4OH was added dropwise to a vigorously stirred solution of $ZrCl_4$ until a particular pH was attained. The nitrogen isotherms determined on the aged, washed and dried gels prepared at pH 4, 6 and 8 were of Types Ib, I + IV and IVb, respectively – indicating a change in the pore structure from supermicroporous to mesoporous. The corresponding BET areas were 244, 308 and 320 $m^2 g^{-1}$.

In the more recent adsorption studies by Gimblett *et al.* (1981, 1984) and Ragai and co-workers (Ragai, 1989; Ragai *et al.*, 1994), zirconyl chloride, $ZrOCl_2.8H_2O$, was adopted as the starting material. In one series of preparations, NH_3 gas was bubbled at a controlled rate through the $ZrOCl_2$ solution, the pH being continuously monitored. Nitrogen isotherms determined on gel ARZr3, prepared at pH 5, are shown in Figure 10.35a. The isotherm obtained after outgassing at 25°C is of Type Ib, which as we have seen is indicative of supermicroporosity. However, outgassing at 200°C resulted in the removal of a substantial fraction of the micropore capacity.

The corresponding water isotherms in Figure 10.35b were determined after a sample of ARZr3 had been outgassed at 25°C. Three successive sorption/desorption runs are depicted. The general Type I character again indicates microporosity, but now low-pressure hysteresis is observed. Outgassing after the first desorption run resulted in a substantial loss of weight (i.e. change from A to B). This behaviour extended into the second and third adsorption/desorption cycles, but smaller losses were involved.

Increasing the pH at which the gel was prepared led to the development of low-pressure hysteresis with both nitrogen and water. The gels prepared over the pH range 5–11 were all essentially microporous, although the proportion of larger supermicropores increased at higher pH. The BET-nitrogen areas and apparent pore volumes are summarized in Table 10.17. It can be seen that outgassing at 200°C has resulted in a drastic reduction in the BET area of each gel.

These and other results (Gimblett *et al.*, 1981; Ragai *et al.*, 1994) indicate that the microporosity of the hydrous ZrO_2 gels was largely dependent on the microstructure generated through the displacement of coordinated water. Thus, a proportion of the water removed by outgassing at 25°C was present in the form of weakly bound ligands in the coordination spheres of the Zr. Their removal at low temperature has led to the creation of vacancies and hence to the generation of microporosity. This

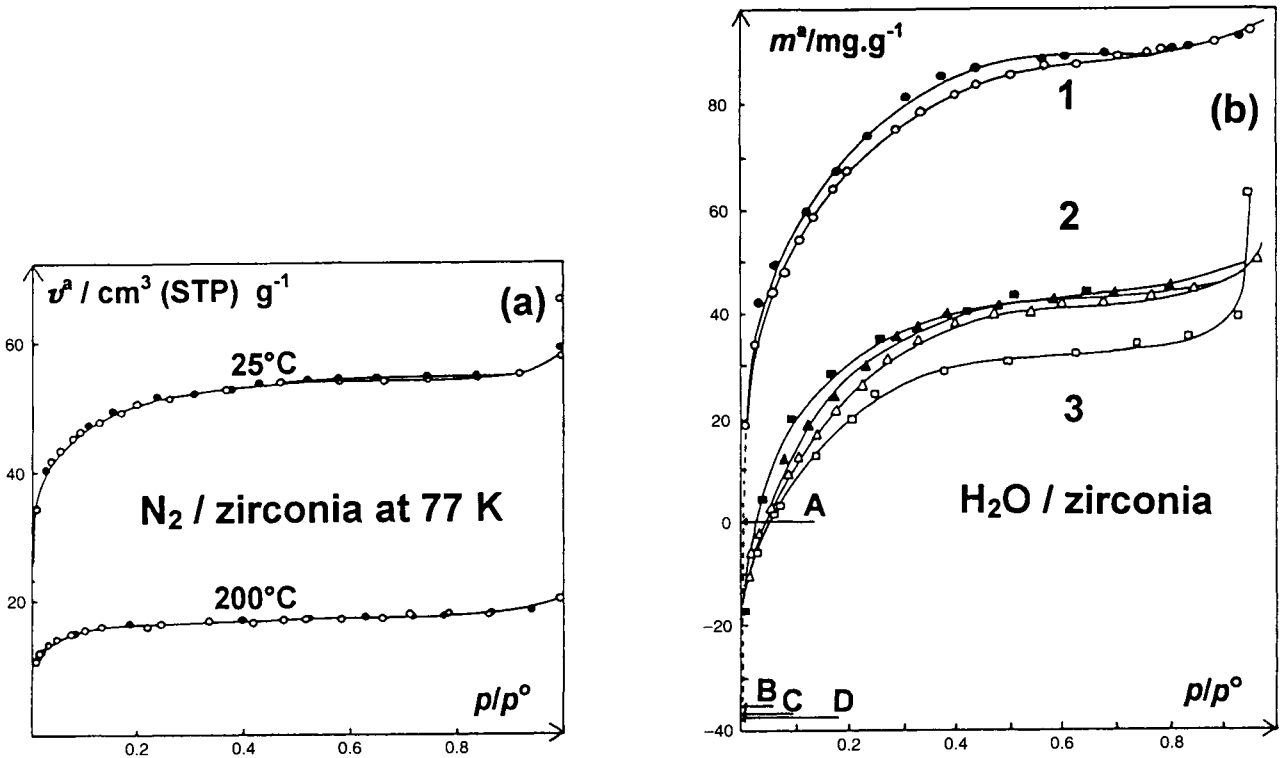

Figure 10.35. (a) Nitrogen adsorption isotherms at 77 K on zirconia gel ARZr3 outgassed at 25°C and 200°C (closed circles for desorption). (b) Water sorption isotherms on same gel outgassed at 25°C. Three successive runs. Runs 1, 2 and 3 start at points A, B and C, respectively. D is the final desorption point of run 3 (solid symbols for desorption) (Gimblett *et al.*, 1981).

Table 10.17. BET-nitrogen areas and apparent pore volumes of hydrous zirconia gels.

Sample	pH (prep)	Outgassing temperature, θ(°C)	a(BET) ($m^2\,g^{-1}$)	v_p (mic, N_2) ($cm^3\,g^{-1}$)	v_p (mic, H_2O) ($cm^3\,g^{-1}$)
ARZr3	5	25	162	0.093	0.091
		200	63	0.030	–
ARZr4	7	25	210	0.119	0.110
		200	88	0.042	0.050
		400	18	0.013	0.003
ARZr5	9	25	220	0.124	0.075
		200	100	0.056	0.056
ARZr6	11	25	226	0.136	–

mechanism is very similar to that proposed for the low-temperature formation of microporosity in chromia gels.

The similarity with chromia and other hydrous oxides is also evident in the loss of surface area which can occur through the removal (i.e. slow outgassing) and addition of water at quite low temperature. It is evident that the presence of the water ligands helps to stabilize the poorly ordered structure, whereas their removal renders the system more liable to undergo further change to a more thermodynamically favourable state. The sorption of water vapour makes this possible.

The use of bicarbonates as the precipitating agents has been found (Gimblett *et al.*, 1984) to lead to mixed microporous–mesoporous zirconia gels. The nitrogen adsorption and water vapour sorption measurements revealed that the microporosity obtained after outgassing the hydrous gel at low temperature (< 200°C) was due to removal of H_2O and NH_3 ligands, but that the removal of the bidentate carbonate groups required higher outgassing temperatures and resulted in the development of mesoporosity.

The hydrous ZrO_2 gel particle may be pictured as a three-dimensional agglomerate of indefinite size, shape and structure. It contains a large number of water molecules, many of which are coordinatively bound to the Zr^{4+} ions. The latter are linked in tetrameric units through hydroxo and oxo bridging. As the pH is increased the extent of these linkages also increases so that the gel becomes more rigid and compact. Spectroscopic and thermogravimetric measurements show the absence of any well-defined hydrates and instead indicate the presence of hydrogen-bonded and coordinated water (Gimblett *et al.*, 1980).

An interesting approach has been used by Hudson and Knowles (1996) to obtain mesoporous high-area ZrO_2. This involves the incorporation of cationic quaternary ammonium cations in the hydrous oxide and the subsequent calcination of the inorganic/organic intermediate. The incorporation is achieved by cation exchange at a pH above the isoelectric point of the hydrous oxide. After calcination at 723 K, ordering of the structure is detectable and appears to be a linear function of the chain length. Well-defined Type IVb nitrogen isotherms have been obtained on the calcined products, many of which have BET areas above 300 $m^2\,g^{-1}$.

References

Achenbach H. (1931) *Chem Erde* **6**, 307.

Adamson A.W. (1986) *Textbook of Physical Chemistry*, Academic Press, Orlando, p. 875.

Alario Franco M.A. and Sing K.S.W. (1972) *J. Thermal Anal.* **4**, 47.

Alario Franco M.A. and Sing K.S.W. (1974) *An. Quim.* **70**, 41.

Alario Franco M.A., Baker F.S. and Sing K.S.W. (1973) In: *Progress in Vacuum Microbalance Techniques*, vol. 2 (S.C. Bevan S.J. Gregg and N.D. Parkyns, eds) Heyden, London p. 51.

Aldcroft D. and Bye G.C. (1967) In: *Science of Ceramics*, vol. 3, Academic Press, London, p. 75.

Aldcroft D., Bye G.C., Robinson J.G. and Sing K.S.W. (1968) *J. Appl. Chem.* **18**, 301.

Aldcroft D., Bye G.C. and Chigbo G.O. (1971) *Trans. Br. Ceram. Soc.* **70**, 19.

Alekseevskii E.V. (1930) *J. Russ. Phys. Chem. Soc.* **62**, 221.

Aristov B.G. and Kiselev A.V. (1965) *Kolloid. Zh.* **27**, 299.

Audier M., Guinot J., Coulon M. and Bonnetain L. (1981) *Carbon* **19**, 99.

Avery R.G. and Ramsay J.D.F. (1973) *J. Colloid Interface Sci.* **42**(3) 597.

Bakaev V.A. and Steele W.A. (1992) *Langmuir* **8**, 1372.

Baker F.S. and Sing K.S.W. (1976) *J. Colloid Interface Sci.* **55**(3), 605.

Baker F.S., Sing K.S.W. and Stryker L.J. (1970) *Chem. & Ind.* 718.

Baker F.S., Carruthers J.D., Day R.E., Sing K.S.W. and Stryker L.J. (1971) *Disc. Faraday Soc.* **52**, 173.

Barby D. (1976) In: *Characterization of Powder Surfaces* (G.D. Parfitt and K.S.W. Sing, eds) Academic Press, London, p. 353.

Barto J., Durham J.L., Baston V.F. and Wade W.H. (1966) *J. Colloid Interface Sci.* **22**, 491.

Bassett D.R., Boucher E.A. and Zettlemoyer A.C. (1968) *J. Colloid Interface Sci.* **27**, 649.

Bayley C.H. (1934) *Can. J. Res.* **10**, 19.

Bhambhani M.R., Cutting P.A., Sing K.S.W. and Turk D.H. (1972) *J. Colloid Interface Sci.* **38**, 109.

Blake T.D. and Wade W.H. (1971) *J. Phys. Chem.* **75**, 1887.

Boddenberg B. and Eltzner K. (1991) *Langmuir* **7**, 1498.

Bolis V., Fubini B., Marchese L., Martra G. and Costa D. (1991) *J. Chem. Soc., Faraday Trans.* **87**, 497.

Bonsack J.P. (1973) *J. Colloid Interface Sci.* **44**, 430.

Bowker M., Houghton H., Waugh K.C., Giddings T. and Green M. (1983) *J. Catalysis* **84**, 252.

Brunauer S. (1945) *The Adsorption of Gases and Vapours*, Princeton University Press, Princeton.

Brunauer, S. and Emmett, P.H. (1937) *J. Am. Chem. Soc.* **59**, 2682.

Bugosh J., Brown R.L., McWhorter J.R., Sears G.W. and Sippel R.J. (1962) *Ind. Eng. Chem., Prod. Res. Dev.* **1**, 157.

Burneau A., Barres O., Gallas J.P. and Lavalley J.C. (1990) *Langmuir* **6**, 1364.

Burwell R.L., Littlewood A.B., Cardew M., Pass G. and Stoddart C.T.H. (1960) *J. Am. Chem. Soc.* **82**, 6272.

Bye G.C. and Howard C.R. (1971) *J. Appl. Chem. Biotechnol.* **21**, 324.

Bye G.C. and Robinson J.G. (1964) *Kolloid. Z.* **198**, 53.

Bye G.C. and Sing K.S.W. (1973) In: *Particle Growth in Suspensions* (A.L. Smith, ed.) Academic Press, London, p. 29.

Bye G.C., Robinson J.G. and Sing K.S.W. (1967) *J. Appl. Chem.* **17**, 138.

Carrott P.J.M. and Sing K.S.W. (1984) *Adsorption Sci. Tech.* **1**, 31.

Carrott P.J.M. and Sing K.S.W. (1989) *Pure Appl. Chem.* **61**, 1835.

Carrott P.J.M., McLeod A.I. and Sing K.S.W. (1982) In: *Adsorption at the Gas–Solid and Liquid–Solid Interface* (J. Rouquerol and K.S.W. Sing, eds) Elsevier, Amsterdam, p. 403.

Carrott P.J.M., Sing K.S.W. and Raistrick J.H. (1986) *Colloids and Surfaces* **21**, 9.

Carrott P.J.M., Roberts R.A. and Sing K.S.W. (1988) *Langmuir* **4**, 740.

Carruthers J.D. and Sing K.S.W. (1967) *Chem. & Ind.* 1919.

Carruthers J.D., Fenerty J. and Sing K.S.W. (1967) *Nature* **213**, 66.

Carruthers J.D., Cutting P.A., Day R.E., Harris M.R., Mitchell S.A. and Sing K.S.W. (1968) *Chem. & Ind.* 1772.

Carruthers J.D., Fenerty J. and Sing K.S.W. (1969) In: *6th International Symposium on Reactivity of Solids* (J.W. Mitchell, ed.) John Wiley, New York, p. 127.
Carruthers J.D., Payne D.A. Sing K.S.W. and Stryker L.J. (1971) *J. Colloid Interface Sci.* **36**(2) 205.
Chauvin C., Saussey J. and Rais T. (1986) *Appl. Catalysis* **25**, 59.
Coulomb J.P. (1991) In: *Phase Transitions in Surface Films II*, NATO-ASI Series B 267, Plenum, New York, p. 113.
Coulomb J.P. and Vilches O.E. (1984) *J. Physique* **45**, 1381.
Coulomb J.P., Sullivan T.S. and Vilches O.E. (1984) *Phys. Rev. B*, **30**, 4753.
Cutting P.A. and Sing K.S.W. (1969) *Chem. and Ind.*, 268.
Dawson P.T. (1967) *J. Phys. Chem.* **71**, 838.
Day R.E. (1973) In: *Progress in Organic Coatings 2*, Elsevier Sequoia, Lausanne, p. 269.
Day R.E. and Parfitt G.D. (1967) *Trans. Faraday Soc.* **63**, 708.
Day R.E., Parfitt G.D. and Peacock J. (1971) *Disc. Faraday Soc.* **52**, 215.
de Boer J.H. (1957) In: *2nd Int Congress on Surface Activity II* (J.H. Schulman, ed.) Butterworths, London, p. 93.
de Boer J.H. (1972) In: *Thermochimie*, Colloques Internationaux du CNRS no. 201, Editions du CNRS, Paris, p. 407.
de Boer J.H., Fortuin J.M.H. and Steggerda J.J. (1954) *Proc. Kon. Ned. Akad. Wetensch* **57B**, p. 170.
de Boer J.H., Steggerda J.J. and Zwietering P. (1956) *Proc. Kon. Ned. Akad. Wetensch* **59B**, p. 435.
Deitz V.R. (1944) *Bibliography of Solid Adsorbents*, National Bureau of Standards, Washington, p. 156.
Deren J., Haber J., Podgorecka A. and Burzyk J. (1963), *J. Catalysis* **2**, 161.
Drain L.E. (1954) *Sci. Progr.* **42**, 608.
Drain L.E. and Morrison J.A. (1952) *Trans. Faraday Soc.* **48**, 840.
Dzhigit O.M., Kiselev A.V. and Muttik G.G. (1962) *Kolloid Zh.* **24**, 15.
Feachem G. and Swallow H.T.S. (1948) *J. Chem. Soc.* 267.
Fenelonov V.A., Gavrilov V.Y. and Simonova L.G. (1983) In: *Preparation of Catalysts III* (G. Poncelet, P. Grange and P.A. Jacobs, eds) Elsevier, Amsterdam, p. 665.
Ferch H.K. (1994) In: *The Colloid Chemistry of Silica* (H.E. Bergna, ed.) American Chemical Society, Washington DC, p. 481.
Fubini B., Bolis V., Cavenago A. and Ugliengo P. (1992) *J. Chem. Soc., Faraday Trans.* **88**, 277.
Fukasawa J., Tsutsumi H., Sato M. and Kaneko K. (1994) *Langmuir* **10**, 2718.
Furlong D.N., Rouquerol F., Rouquerol J. and Sing K.S.W. (1980a) *J. Chem. Soc., Faraday Trans. I* **76**, 774.
Furlong D.N., Rouquerol F., Rouquerol J. and Sing K.S.W. (1980b) *J. Colloid Interface Sci.* **75**, 68.
Furlong D.N., Sing K.S.W. and Parfitt G.D. (1986) *Adsorption Sci. Tech.* **3**, 25.
Gallas J.P., Lavalley J.C., Burneau A. and Barres O. (1991) *Langmuir* **7**, 1235.
Gay J.M., Suzanne J. and Coulomb J.P. (1990) *Phys. Rev. B* **41**, 11346.
Gimblett F.G.R., Rahman A.A. and Sing K.S.W. (1980) *J. Chem. Tech. Biotechnol.* **30**, 51.
Gimblett F.G.R., Rahman A.A. and Sing K.S.W. (1981) *J. Colloid Interface Sci.* **84**, 337.
Gimblett F.G.R., Rahman A.A. and Sing K.S.W. (1984) *J. Colloid Interface Sci.* **102**, 483.
Goodman J.F. and Gregg S.J. (1959) *J. Chem. Soc.* 3612.
Gregg S.J. and Langford J.F. (1969) *Trans. Faraday Soc.* **65**, 1394.
Gregg S.J. and Langford J.F. (1977) *J. Chem. Soc., Faraday Trans. I* **73**, 747.
Gregg S.J. and Sing K.S.W. (1951) *J. Phys. Colloid Chem.* **55**, 592.
Gregg S.J. and Sing K.S.W. (1982) *Adsorption, Surface Area and Porosity*, Academic Press, London, p. 74.
Gregg S.J. and Packer R.K. (1955) *J. Chem. Soc.* 51.
Griffiths D.M. and Rochester C.H. (1977) *J. Chem. Soc., Faraday Trans. I* **73**, 1510.
Grillet Y., Rouquerol F. and Rouquerol J. (1985) *Surface Sci.* **162**, 478.
Grillet Y., Rouquerol F. and Rouquerol J. (1989) *Thermochim. Acta* **148**, 191.
Harkins W.D. and Jura G. (1944) *J. Am. Chem. Soc.* **66**, 1362.
Harris M.R. and Whitaker G. (1962) *J. Appl. Chem.* **12**, 490.
Harris M.R. and Whitaker G. (1963) *J. Appl. Chem.* **13**, 198.
Henrich V.E. (1976) *Surface Sci.* **57**, 355.

Holmes H.F., Fuller E.L. and Gammage R.B. (1972) *J. Phys. Chem.* **76**, 1497.
Hudson M.J. and Knowles J.A. (1996) *J. Mater. Chem.* **6**, 89.
Iler R.K. (1979) *The Chemistry of Silica*, John Wiley, New York.
Jaycock M.J. and Waldsax J.C.R. (1974) *J. Chem. Soc., Faraday Trans. I* **70**, 1501.
Kenny M.B. and Sing K.S.W. (1994) In: *The Colloid Chemistry of Silica* (H.E. Bergna, ed.) American Chemical Society, Washington DC, p. 505.
Kington G.L., Beebe R.A., Polley M.H. and Smith W.R. (1950) *J. Am. Chem. Soc.* **72**, 1775.
Kiselev A.V. (1957) In: *Second Int. Congress on Surface Activity* (J. Schulman, ed.) Butterworths, London, p. 229.
Kiselev A.V. (1958) In: *Structure and Properties of Porous Materials* (D.H. Everett and F.S. Stone, eds) Butterworths, London, p. 195.
Kiselev A.V. (1965) *Disc. Faraday Soc.* **40**, 205.
Kiselev A.V. (1971) *Disc. Faraday Soc.* **52**, 14.
Krieger (1941) *J. Am. Chem. Soc.* **63**, 2712.
Lippens B.C. (1961) PhD thesis, University of Delft.
Lippens B.C. and Steggerda J.J. (1970) In: *Physical and Chemical Aspects of Adsorbents and Catalysts*, (B.G. Linsen, ed.) Academic Press, London, p. 171.
Madeley J.D. and Sing K.S.W. (1953) *J. Appl. Chem.* **3**, 549.
Madeley J.D. and Sing K.S.W. (1954) *J. Appl. Chem.* **4**, 365.
Madeley J.D. and Sing K.S.W. (1962) *J. Appl. Chem.* **12**, 494.
Madih K., Croset B., Coulomb J.P. and Lauter H.J. (1989) *Europhys. Lett.* **8**, 459.
Matijevic E. (1988) *Pure Appl. Chem.* **60**, 1479.
Mikhail R.S., Nashed S. and Kahlil A.M. (1971) *Disc. Faraday Soc.* **52**, 187.
Mitchell S.A. (1966) *Chem. & Ind.* 924.
Morishige K., Kanno F., Ogawara S. and Sasaki S. (1985) *J. Phys. Chem.* **89**, 4404.
Munuera G. and Stone F.S. (1971) *Disc. Faraday Soc.* **52**, 205.
Naono H. and Nakai K. (1989) *J. Colloid Interface Sci.* **128**, 146.
Naono H., Nakai K., Sueyoshi T. and Yagi H. (1987) *J. Colloid Interface Sci.* **120**(2) 439.
Naono H., Sonoda J., Oka K. and Hakuman M. (1993) In: *Fundamentals of Adsorption IV* (M. Suzuki, ed.) Kodansha, Tokyo, p. 467.
Neimark I.E., Sheinfain R.Y., Lipkind B.A. and Stas O.P. (1964) *Kolloid Zh.* **26**, 734.
Okkerse C. (1970) In: *Physical and Chemical Aspects of Adsorbents and Catalysts* (B.G. Linsen, ed.) Academic Press, London, p. 213.
Papée D., Charrier J., Tertian R. and Houssemaine R. (1954) In: *Proceedings of the Congrès de l'Aluminium*, p. 31.
Parfitt G.D. (1981) *Dispersion of Powders in Liquids*, Applied Science, London, p. 1.
Parkyns N.D. and Sing K.S.W. (1975) In: *Specialist Periodical Report Colloid Science 2*, The Chemical Society, London, p. 1.
Pashley R.M. and Kitchener J.A. (1979) *J. Colloid Interface Sci.* **71**, 491.
Patterson R.E. (1994) In: *The Colloidal Chemistry of Silica* (H.E. Bergna, ed.), American Chemical Society, Washington DC, p. 617.
Payne D.A. and Sing K.S.W. (1969) *Chem. & Ind.* 918.
Payne D.A., Sing K.S.W. and Turk D.H. (1973) *J. Colloid Interface Sci.* **43**(2) 287.
Peri J.B. (1965) *J. Phys. Chem.* **69**, 211.
Ragai J. (1989) *Adsorption Sci. Tech.* **6**, 9.
Ragai J. and Sing K.S.W. (1982) *J. Chem. Tech. Biotechnol.* **32**, 988.
Ragai J. and Sing K.S.W. (1984) *J. Colloid Interface Sci.* **101**(2), 369.
Ragai J., Sing K.S.W. and Mikhail R.S. (1980) *J. Chem. Tech. Biotechnol.* **30**, 1.
Ragai J., Selim S., Sing K.S.W. and Theocharis C. (1994) In: *Characterization of Porous Solids III* (J. Rouquerol, F. Rodriguez-Reinoso, K.S.W. Sing and K.K. Unger, eds) Elsevier, Amsterdam, p. 487.
Ramsay J.D.F. and Avery R.G. (1979) In: *Characterization of Porous Solids* (S.J. Gregg, K.S.W. Sing and H.F. Stoeckli, eds) Society of Chemical Industry, London, p. 117.
Ribeiro Carrott M., Carrott P., Brotas de Carvalho M.M. and Sing K.S.W. (1991a) *J. Chem. Soc., Faraday Trans.* **87**(1) 185.

Ribeiro Carrott M., Carrott P.J.M., Brotas de Carvalho M.M. and Sing K.S.W. (1991b) In: *Characterization of Porous Solids II* (1961) (F. Rodriguez-Reinoso, J. Rouquerol, K.S.W. Sing and K.K. Unger, eds) Elsevier, Amsterdam, p. 635.

Ribeiro Carrott M., Carrott P., Brotas de Carvalho M.M. and Sing K.S.W. (1993) *J. Chem. Soc., Faraday Trans.* **89**, 579.

Rijnten H.T. (1970) In: *Physical and Chemical Aspects of Adsorbents and Catalysts* (B.G. Linsen, ed.) Academic Press, London, p. 315.

Rittner F., Paschek D. and Boddenberg B. (1995) *Langmuir* **11**, 3097.

Rochester C.H. (1986) *Colloids and Surfaces* **21**, 205.

Rouquerol J. and Ganteaume M. (1977) *J. Therm. Anal.* **11**, 201.

Rouquerol J., Rouquerol F. and Ganteaume M. (1975) *J. Catalysis* **36**, 99.

Rouquerol J., Rouquerol F. and Ganteaume M. (1979a) *J. Catalysis* **57**, 222.

Rouquerol J., Rouquerol F., Peres C., Grillet Y. and Boudellal M. (1979b) In: *Characterization of Porous Solids* (S.J. Gregg, K.S.W. Sing and H.F. Stoeckli, eds) Society of Chemical Industry, London, p. 107.

Saafeld (1960) *Neues Jahrb. Mineral. Abh.* **95**, 1.

Sing K.S.W. (1970) In: *Surface Area Determination* (D.H. Everett and R.H. Ottewill, eds) Butterworths, London, p. 25.

Sing K.S.W. (1972) In: *Thermochimie*, Colloques Internationaux du CNRS no. 201, Editions du CNRS, Paris, p. 601.

Solomon D.H. and Hawthorne D.G. (1983) *Chemistry of Pigments and Fillers*, John Wiley, New York, p. 51.

Stacey M.H. (1987) *Langmuir* **3**, 681.

Stacey M.H. (1991) In: *Characterization of Porous Solids II* (F. Rodriguez-Reinoso, J. Rouquerol, K.S.W. Sing and K.K. Unger, eds) Elsevier, Amsterdam, p. 615.

Taylor R.J. (1949) *J. Soc. Chem. Ind.* **68**, 23.

Teichner S.J. (1986) In: *Aerogels* (J. Fricke, ed.) Springer-Verlag, Berlin, p. 22.

Teichner S.J., Nicolaon G.A., Vicarini M.A. and Gardes G.E.E. (1976) *Adv. Colloid Interface Sci.* **5**, 245.

Tertian R. and Papée D. (1953) *C. R. Acad. Sci.* **236**, 1565.

Trabelsi M. and Coulomb J.P. (1992) *Surface Sci.* **272**, 352.

Unger K.K. (1979) *Porous Silica*, Elsevier, Amsterdam.

Unger K.K. (1994) In: *The Colloid Chemistry of Silica* (H.E. Bergna, ed.), American Chemical Society, Washington DC, p. 165.

Vleesschauwer W.F.M. (1970) In: *Physical and Chemical Aspects of Adsorbents and Catalysts* (B.G. Linsen, ed.) Academic Press, London, p. 265.

Wiseman T.J. (1976) In: *Characterization of Powder Surfaces* (G.D. Parfitt and K.S.W. Sing, eds) Academic Press, London, p. 159.

Wong W.K. (1982) PhD Thesis, Brunel University, UK.

Zettlemoyer A.C. (1968) *J. Colloid Interface Sci.* **28**, 343.

Zhuravlev L.T. (1987) *Langmuir* **3**, 316.

Zhuravlev L.T. (1994) In: *The Colloid Chemistry of Silica* (H.E. Bergna, ed.) American Chemical Society, Washington, p. 629.

Zhuravlev L.T. and Kiselev A.V. (1970) In: *Surface Area Determination* (D.H. Everett and R.H. Ottewill, eds) Butterworths, London, p. 155.

CHAPTER 11

Adsorption by Clays, Pillared Layer Structures and Zeolites

11.1. Introduction

It is well known that natural clays are the products of the weathering of rocks and are widely distributed. Their overall chemical compositions and textures vary from one

location to another, being dependent on their geological origin and the presence of organic and inorganic impurities. For our purpose, however, the term 'clay' is used to denote a structurally homogeneous 'clay mineral'.

Clay minerals are hydrous layer silicates of colloidal dimensions, with most if not all of the individual platy particles in the colloidal range of *c.* 1 nm–1 μm (van Olphen, 1976; Van Damme *et al.*, 1985). The term 'phyllosilicate' (*phyllo* = leaf like) is applied to the broad group of hydrous silicates with layer structures. The essential components of the phyllosilicate structure are two-dimensional tetrahedra and octahedra of oxygen atoms (or ions). The coordinating atoms (or cations) in the centre of the tetrahedra are for the most part Si, but Al^{3+} or Fe^{3+} may also be present. The coordinating cations in the octahedra are usually Al^{3+}, Mg^{2+}, Fe^{3+} or Fe^{2+}. Some clay structures (e.g. hectorite) can be synthesized in a reproducible and relatively homogeneous form.

Certain properties of clays were known and exploited in ancient times: in particular, clays were used for the fabrication of pottery, bricks and tiles. The chief constituent of china clay (or kaolin) is kaolinite, which is still used on a very large scale in the manufacture of paper and refractories. Ball clay, a fine-grained form of kaolinite, contains some mica and quartz and is now favoured for crockery, porcelain and floor tiles.

The swelling and thixotropic properties of the smectic clays have long been known and are of great importance in agriculture and civil engineering. Fuller's earth (mainly calcium montmorillonite) has high adsorbent and cation exchange properties, while bentonite (sodium montmorillonite) is extensively used as a constituent of drilling mud, mortar and putty – to provide the required degree of plasticity. The acidic nature of activated bentonite was exploited in an early catalytic cracking process (the Houdry process) for the production of gasoline from high molar mass oils.

More recently, various attempts have been made to develop cracking catalysts from pillared smectite clays, in which the layers are separated and held apart by the intercalation of large cations. Pillared clays (PILCs) have large surface areas within fairly well-ordered micropore structures (pore widths in the approximate range 0.6–1.2 nm). It is not surprising that these materials have attracted considerable interest with the prospect of an alternative type of catalytic shape selectivity (Thomas, 1994; Thomas *et al.*, 1997; Fripiat, 1997).

The aluminosilicate zeolites may be regarded as the most important and well-established members of a special class of microporous adsorbents in which the porosity is intra-crystalline. Although zeolites have been known for over 200 years, their potential value as highly selective adsorbents was first realized about 50 years ago (Barrer, 1945, 1978). Interest was further stimulated by the announcement by Breck *et al.* (1956) of the synthesis of the hitherto unknown zeolite A (i.e. Linde sieve A). Since then several hundred new porous zeolites have been synthesized.

The molecular sieve zeolites have attained great technological importance for catalysis, gas separation and drying and many other applications. They are now used as industrial catalysts for such reactions as the cracking of paraffins and the isomerization and disproportionation of aromatic compounds (Thomas and Theocharis, 1989; Thomas, 1995, Martens *et al.*, 1997).

One of the most significant stages in the development of zeolite catalysts was the synthesis by Mobil scientists (U.S. Patent 3, 702, 866) of the zeolite now universally known as ZSM-5 (i.e. Zeolite Socony Mobil-5). This was the first – and most important – member of a new class of shape selective catalysts, which have made viable the production of 'synthetic gasoline'. In this process, high-octane gasoline is produced by the catalytic conversion of methanol to a mixture of aromatic and aliphatic hydrocarbons (Derouane, 1980). Because of its unique combination of chemical nature and pore structure, ZSM-5 is a highly effective dehydration, isomerization and polymerization catalyst.

In 1978, the same year that the structure of ZSM-5 was first described, Flanigen and her co-workers reported the synthesis, structure and properties of 'a new hydrophobic crystalline silica molecular sieve' (Flanigen *et al.*, 1978). The new material, named Silicalite (now generally called Silicalite-I), has a remarkably similar channel structure to that of ZSM-5 but contains no aluminium. It was pointed out by the Union Carbide scientists that, unlike the aluminium-containing zeolites, Silicalite has no cation exchange properties and consequently exhibits a low affinity for water. In addition, it was reported to be unreactive to most acids (but not HF) and stable in air to over 1100°C.

The catalytic properties associated with the molecular shape-selectivity exhibited by ZSM-5 are now well known. Recent work by Martens *et al.* (1995) has revealed that the external surfaces of zeolite crystals have also to be considered as potential shape-selective environments. Thus, strong evidence has been obtained for a lock-and-key model, which involves a form of pore mouth catalysis with bulky long-chain molecules that cannot penetrate into the intracrystalline micropores. The proposed lock-and-key model for *n*-alkane isomerization over ZSM-22 zeolite (with tubular pore openings of 0.55×0.45 nm) seems likely to be valid for other catalytic reactions.

Over the past 20 years, pressure swing adsorption (PSA) has become one of the most important procedures for the separation and enrichment of industrial gases (Sircar, 1993). PSA technology is dependent on the selective adsorption of one, or more than one, of the components of a gas mixture. A change in composition occurs when the gas mixture is brought into contact with an adsorbent. Desorption of a selectively adsorbed component occurs when its partial pressure is sufficiently reduced and the adsorbent is thereby cleaned and ready for the next stage of adsorption. The PSA process thus consists of a cycle of stages of adsorption at high partial pressures and desorption at low partial pressures.

PSA technology is now extensively used for the fractionation of air. There are a number of different processes in industrial operation, the decision to use a certain design of plant and a particular adsorbent being governed by whether oxygen or nitrogen is required and by the level of purity. Formerly CaA and NaX zeolites were the preferred adsorbents for the separation of oxygen from nitrogen (Yang, 1987), but in recent years CaX and LiX have been featured in oxygen production patents.

It is not within the scope of this book to discuss the chemical engineering principles of PSA, but it is important to note that the application of a zeolite as the working adsorbent does *not* depend on molecular sieving. In this case, the achievable level of

separation is closely related to the separation factor (or selectivity ratio) – defined in terms of the equilibrium distribution of each component between the gas and the adsorbed phase (Yang, 1987).

In addition to its use as a selective adsorbent and powerful desiccant, zeolite A has turned out to be a highly efficient remover of calcium ions and in powder form is the preferred phosphate substitute in certain detergent formulations.

In a single chapter it would be impossible to consider all aspects of the physisorption properties of clays and zeolites. As in Chapters 9 and 10, our aim here is to apply and discuss the significance of the general principles propounded in Chapters 4–8. For this purpose, it is expedient to focus attention on particular systems (e.g. industrially important synthetic zeolites). However, since the adsorbent behaviour of clays and zeolites is to a large extent dependent on their solid structures, some attention is given in this chapter to structural chemistry.

11.2. Structure and morphology of layer silicates

As already indicated, a feature common to all clay minerals is the two-dimensional polymeric sheet which is composed of interlinked SiO_4 tetrahedra. These siloxane, O—Si—O, hexagonal (or 'tetrahedral') sheets are constructed from three of the four available oxygen atoms at the corners of the tetrahedra. The spare apical oxygens are directed away (upwards or downwards) from each sheet.

The other main component is an 'octahedral sheet': this is made up of oxygen and metal atoms, which are typically aluminium or magnesium (since Al is present in the majority of clay minerals, they are sometimes referred to as aluminosilicates). The junction plane between the hexagonal and octahedral sheets consists of the shared apical oxygens of the tetrahedra and also some hydroxyl groups. In one group of clay minerals, one octahedral sheet is directly attached to one silica sheet, thus giving a 1 : 1 type of two-sheet elemental structure. In another main group of clays, one octahedral sheet is sandwiched between two silica sheets, giving a 2:1 type of three-sheet layer structure.

Individual particles of clay minerals consist of stacks of layers, which in some systems are separated by interlayer materials. The individual layers are held together by secondary forces (i.e. van der Waals attractive forces, hydrogen bonding or weak electrostatic attraction).

11.2.1. Kaolinite

The best-known example of a 1 : 1 (two-sheet) type clay is kaolinite. A pictorial impression of the ideal kaolinite structure is given in Figure 11.1. The upper and lower basal surfaces of the two-sheet layer are clearly quite different. The layer repeat distance, or c-spacing, is c. 0.72 nm, which is the distance between atom centres in two contiguous layers. This is approximately the same as the sum of the atomic radii and therefore in an ideal structure there is insufficient space to accommodate any interlayer material such as intercalated water.

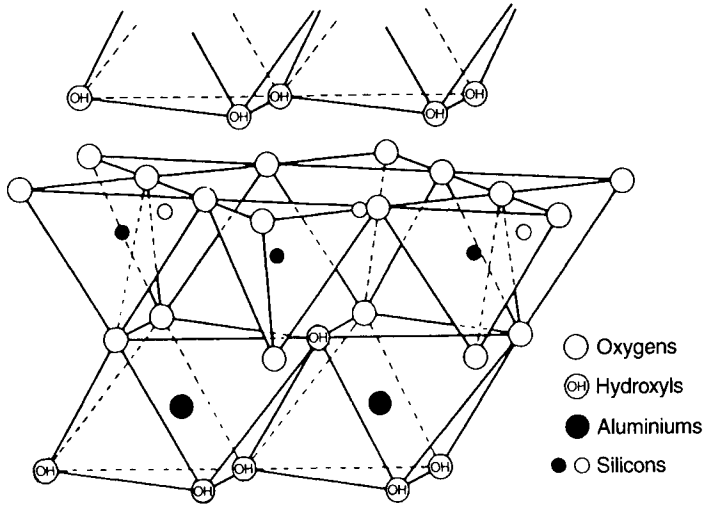

Figure 11.1. The ideal kaolinite structure.

In the perfect two-layer crystal of kaolinite the composition of the unit cell is $[Al_2(OH)_4(Si_2O_5)]_2$, but in most kaolitic clays there are defects due in part to isomorphous substitution of Si by Al and other small atoms. The excess negative charge is compensated by cations located on the outer surface of the crystallites.

11.2.2. Smectites and vermiculites

The 2:1 layer clays (i.e. with three-sheet layers) include a group of expanding or swelling clays, which comprise the smectites (e.g. montmorillonite, saponite and hectorite) and the vermiculites. The basic structure of a smectite is shown in Figure 11.2.

Pyrophyllite is the simplest layer aluminosilicate in which two tetrahedral SiO_4 layers are condensed on to the octahedral AlO_6 layer to produce a three-sheet layer, the composition of the unit cell being $[Al_2(OH)_2(Si_2O_5)_2]_2$. Another 'ideal' structure in which Al is replaced by Mg is that of talc. In both cases the three-sheet layer is electrically neutral and the layers are stacked in the ABAB... sequence. Because of the cohesive strength of this ideal structure, neither pyrophyllite nor talc occurs in the form of the very fine particles which generally characterize clay minerals.

An important feature of the smectites, vermiculites and other 2:1 layer silicates is that isomorphous substitutions can occur in both the tetrahedral and octahedral sheets. Thus, substitution of Si by Al occurs in the tetrahedral sheet, together with replacement of Al by Mg, Fe, Li or other small atoms in the octahedral sheet. The substitutions lead to a deficit of positive charge, which is compensated by the presence of exchangeable, interlayer cations.

Because of the presence of the cations, the *c*-spacing in the smectites and vermiculites is somewhat larger than in the uncharged pyrophyllite (*c.* 0.92 nm). Water

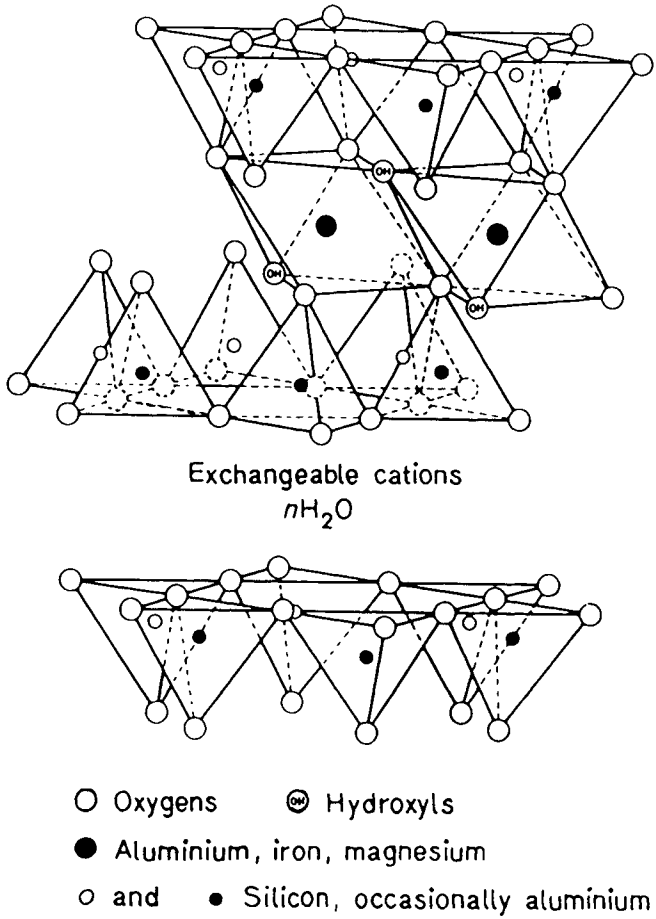

Figure 11.2. The ideal smectite structure.

molecules are able to penetrate between the layers, causing an expansion of the layer lattice – as indicated by an increase in the c-spacing. With some smectites, the expansion appears to occur in discrete steps corresponding to the formation of one to four layers of water between the lattice layers (van Olphen, 1976).

11.2.3. Palygorskites

Attapulgite and sepiolite are members of the palygorskite group of fibrous clay minerals. As before, the SiO_4 tetrahedra are linked together to form the polymeric silica layer, but now the vertices do not all point in the same direction. Instead, they are arranged in strips: in one strip all the vertices point up, while in the next strip they all point down. In attapulgite the strip width is of four tetrahedra and in sepiolite it is of six tetrahedra. The MgO_6 octahedra are arranged to give three-fold strips leaving channels parallel to the fibre axis containing water molecules (Barrer, 1978).

The idealized attapulgite composition for a half unit cell is $Mg_5Si_8O_{20}(OH)_2(H_2O)_4 \cdot 4H_2O$. Thus, four H_2O molecules are present in the channels (i.e. the 'zeolitic water') and four others are bound to the octahedral cations. On heating, water is lost in three stages: (a) zeolitic water and water adsorbed on the external surface are removed at temperatures < 75°C; (b) coordinated water is removed over the range 75–370°C; and (c) finally structural water is removed. An irreversible collapse of the structure begins to occur at temperatures of *c.* 130°C, corresponding to the loss of about half of the coordinated water (Grillet *et al.*, 1988; Cases *et al.*, 1991). The detailed study of these changes was made possible by the application of controlled rate thermal analysis (CTRA: see Chapter 3).

11.2.4. Morphology of clay particles and aggregates

Kaolinite particles (platelets) are relatively thick and rigid, usually containing 100 or more stacked layers. The platy particles tend to be of hexagonal shape with diameters of up to 1 μm The crystal shape is dependent on the basal (0 0 1) face and the prismatic edges: (1 1 0) etc. The interlayer attraction (mainly hydrogen bonding) is sufficiently strong to prevent cleavage under ordinary conditions. However, the crystallites do exhibit stacking faults. There appears to be an inverse relation between the number of structural defects and the particle size (Cases *et al.*, 1982).

The BET areas of refined natural kaolinites are generally in the range 10–20 $m^2 g^{-1}$ (Gregg *et al.*, 1954; Cases *et al.*, 1986). Comminution occurs under continuous grinding, although the extent of breakdown has been found to reach a maximum after a certain period of time (Gregg, 1968). For example, by the prolonged or repeated grinding of certain china clays, it is possible to reach maximum areas of *c.* 50 $m^2 g^{-1}$.

The smectite platelets (tactoids) are thin and flexible: the diameter is relatively large (up to 2 nm), but the individual platelet width is much smaller (e.g. 1 nm). It is evidently quite difficult to specify an unambiguous value of particle size. The BET-nitrogen areas of the montmorillonites are often in the region of 30 $m^2 g^{-1}$, while their particle sizes may appear to be 1 μm. In the case of laponite, the BET-nitrogen area may be as high as 300 $m^2 g^{-1}$ (Bergaya, 1995). Sepiolites have a fibrous morphology. Typical fibres have a length of 2–3 μm and a diameter of 0.1 μm. The more crystalline forms of sepiolite have a more rigid needle-like appearance.

In dilute suspensions clays tend to form gels. The classical model is the 'house of cards' structure of kaolinite in which the face-to-edge association leads to an open 3-D structure (van Olphen, 1965). In the case of smectite–water systems it now seems more likely that the microstructure is mainly controlled by the face-to-face interactions (Van Damme *et al.*, 1985).

11.3. Physisorption of Gases by Kaolinite

11.3.1. Nitrogen isotherms

In the uncompacted state, a sample of natural kaolinite was found to give the reversible Type II nitrogen isotherm shown in Figure 11.3 (Gregg, 1968). It is

apparent that the initial part of the isotherm (up to $p/p^\circ = 0.4$) was not changed to any detectable extent by the compaction of the kaolinite at a pressure of 96 ton in^{-2} (i.e. *c.* 1500 MN m^{-2}), but a narrow hysteresis loop appeared at higher relative pressure.

The adsorption isotherms in Figure 11.3 are of interest for several reasons. First, it may seem surprising that an assemblage of kaolinite platelets should give a *reversible* isotherm. The adsorbent had a specific surface area of 17 $m^2 g^{-1}$, which would appear to correspond to a platelet thickness of *c.* 50 nm. The particle rigidity and the house-of-cards packing have probably resulted in the formation of a macroporous aggregate, which accounts for the appearance of the reversible Type II isotherm.

It is striking that the high compaction pressure, which was sufficient to convert assemblages of spheroidal particles into well-defined mesopore structures (Gregg, 1968), had relatively little effect on the course of the *adsorption* isotherm. Although the *desorption* curve was displaced in the multilayer range, the isotherm remained pseudo-Type II (now termed Type IIb). We conclude that the resulting hysteresis loop is associated with both the development of a pore network and the delayed capillary condensation on the surface of the platelets.

In an early study of the effect of calcination on the surface area of kaolinite, Gregg and Stephens (1953) found a small but progressive decline in the BET area over the temperature range 100–800°C. These results were in contrast to a 12% loss of structural water at 450°C. It was concluded that there was no detectable activation and that the crystallite structure was not broken up as a result of thermal dehydroxylation.

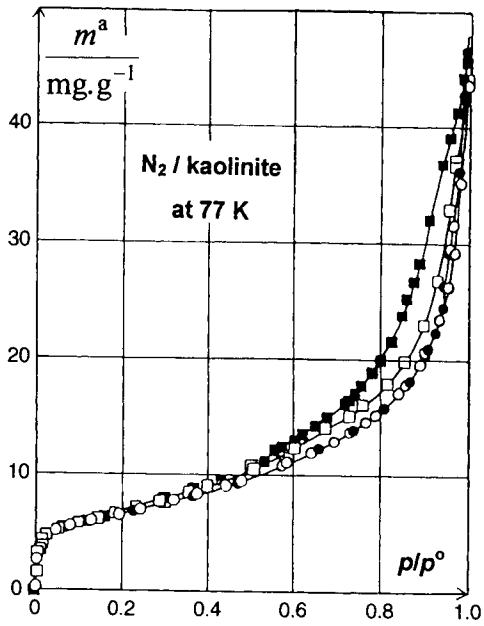

Figure 11.3. Adsorption–desorption isotherms (open and closed symbols, respectively) at 77 K on kaolinite, before (circles) and after (squares) compaction at 96 ton in^{-2} (after Gregg, 1968).

11.3.2. Energetics of argon and nitrogen adsorption

Cases *et al.* (1986) have used adsorption microcalorimetry along with other techniques in a study of the crystallographic and morphological properties of kaolinite. The differential adsorption energy curves in Figure 11.4 were determined on two different forms of kaolinite: sample GB3 was a well-ordered English china clay, whereas sample FU7 was a French kaolinite, which had been subjected to repeated dry grinding and fractionation. The BET areas, as determined by argon and nitrogen adsorption at 77 K, are given in Table 11.1.

For our present purpose, the results in Figure 11.4 and Table 11.1 can be summarized as follows:

1. The corresponding BET areas derived from the argon and nitrogen isotherms are in fairly good agreement (as also found with other samples of kaolinite).
2. Each adsorption energy curve can be divided into three distinctive parts: (a) an

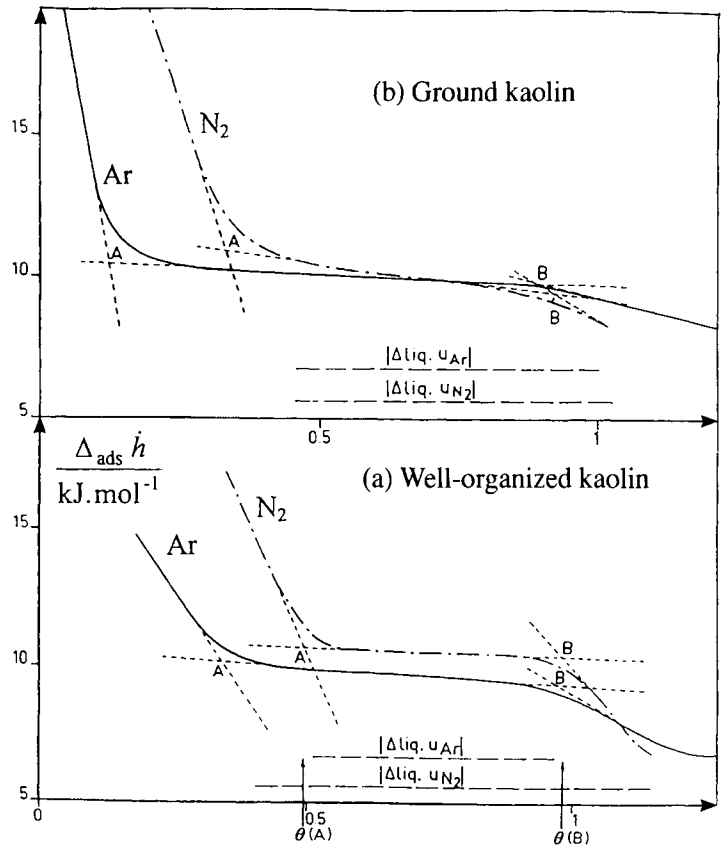

Figure 11.4. Differential molar energy of adsorption of Ar and N_2 on samples of kaolinite as a function of surface coverage. (a) On sample GB3; (b) On sample FU7 (reproduced courtesy of Cases *et al.*, 1986).

Table 11.1. Adsorption of Ar and N_2 on samples of kaolinite

Adsorbent	Adsorptive	a(BET) ($m^2\ g^{-1}$)	θ_A	θ_B	$100\ (\theta_B - \theta_A)$
GB3	Ar	11.6	0.34	0.97	63
	N_2	11.4	0.49	0.98	
FU7	Ar	47.3	0.12	0.91	79
	N_2	46.8	0.33	0.92	

initial steep decrease; (b) a long middle decline, AB; and (c) a multilayer declination.

3. Values of BET coverage, θ_A and θ_B, corresponding to the locations A and B are given respectively in columns 4 and 5 of the table.

We are now in a position to discuss the significance of these findings. The strong energetic heterogeneity at low coverage is probably due to adsorption on the edge sites (lateral faces) and defect sites (e.g. crevices) in the basal plane. In view of its specificity of interaction, it is not surprising to find that the nitrogen energies are appreciably greater than the corresponding argon values. The much smaller variation of adsorption energy in the middle region (along AB) is consistent with the energetic homogeneity of the (001) basal faces. It is of interest that the constant adsorption energy for argon on ground kaolin (FU7) extends over 79% of the surface coverage, whereas the comparable surface coverage is about 63% in the case of well-organized kaolin (GB3). These results appear to confirm that grinding has led to an appreciable increase in the fractional contribution of the basal faces to the total surface area.

Cases *et al.* (1986) found that the percentage areas corresponding to the lateral domains (i.e. the high-energy edge sites) evaluated from the differential energies of argon adsorption agreed quite well with the corresponding values obtained from the adsorption isotherms of alkyldodecylammonium ions. These results illustrate the value of adsorption microcalorimetry for the characterization of clay minerals.

11.4. Physisorption of Gases by Smectites and Vermiculites

Fuller's earth was traditionally used for the removal of grease from cloth and as a 'bleaching' or decolorizing agent. It has long been known that these sorption properties, although essentially physical in nature, are mainly dependent on the smectite structure. A number of attempts were made in the 1930s to explore the surface properties of natural and acid-activated bleaching clays, but the first important advances were made by Barrer and his co-workers in the 1950s.

11.4.1. Adsorption of non-polar molecules

The physisorption measurements by Barrer and MacLeod (1954) were undertaken on natural montmorillonite. The isotherms for the relatively non-polar molecules oxygen, nitrogen and benzene in Figure 11.5 are very similar in form to those reported subsequently (e.g. by Cases *et al.*, 1992). It is evident that the hysteresis

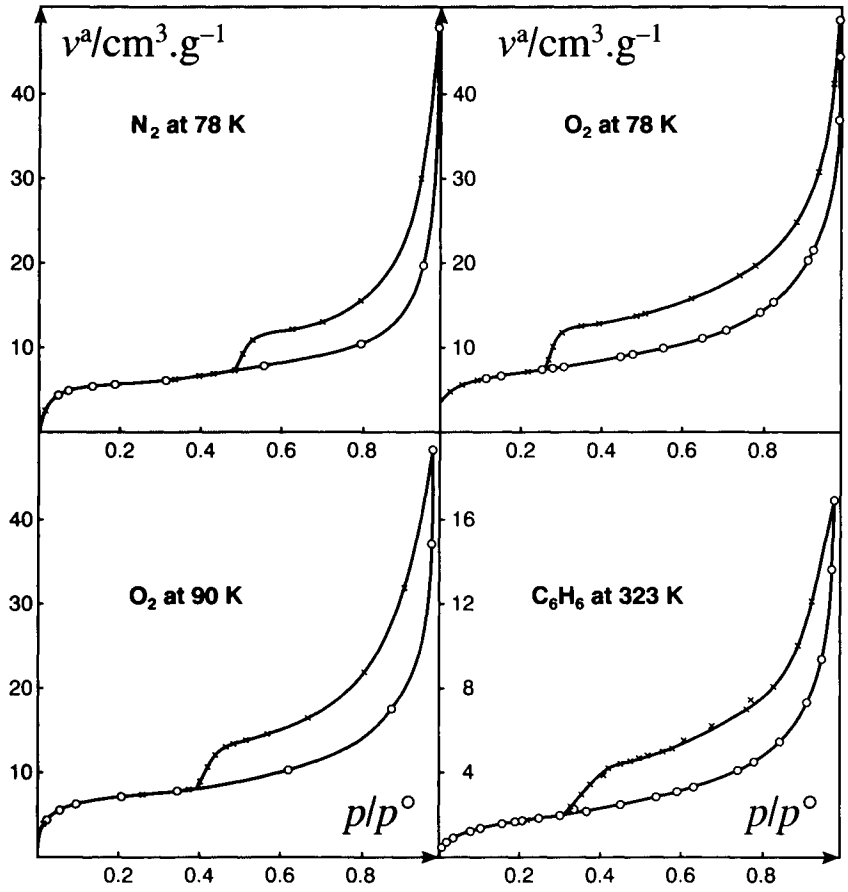

Figure 11.5. Isotherms for molecules of low polarity on natural montmorillonite (from Barrer, 1989).

loops are of Type H3 in the IUPAC classification, with no indication of a plateau at high p/p°, and therefore they should not be regarded as Type IV isotherms. Moreover, each *adsorption* branch appears to have the same typical Type II character as the nitrogen isotherms on kaolinite in Figure 11.3. The *desorption* branch follows a different path until a critical p/p° is reached.

As indicated earlier, the isotherms in Figure 11.5 could be termed pseudo Type II isotherms, but we prefer the designation Type IIb (see Figure 13.1). Such isotherms are given by either slit-shaped pores or, as in the present case, assemblages of platy particles. The fact that the montmorillonite particles are thin and flexible may be responsible for the closer proximity of the basal faces than in uncompacted kaolinite.

The properties of a well-characterized sample of sodium montmorillonite were investigated in some detail by Cases *et al.* (1992). As expected, the nitrogen isotherm at 77 K had a well-defined H3 hysteresis loop and was therefore a good example of a Type IIb isotherm in the new classification. The measurements were taken to a high

$p/p°$, which confirmed that there was no plateau and therefore no indication of the completion of mesopore filling. Thus, in our view the isotherm was mistakenly referred to by the investigators as a Type IV isotherm.

The nitrogen isotherm was replotted by Cases *et al.* (1992) in the usual BET coordinates and as a *t* plot. The derived BET area of 43.3 $m^2 g^{-1}$ appeared to be not far removed from the value of 45.9 $m^2 g^{-1}$ obtained from the amount adsorbed at Point B. The *t*-plot was constructed in the manner originally proposed by de Boer *et al.* (1966), which involved adopting a standard isotherm with the same value of *C*, which in this case was 485. It was not easy to interpret the *t*-plot, although three short linear sections were identified. From the initial slope, the total surface area appeared to be *c.* 50 $m^2 g^{-1}$. Back-extrapolation of a linear region at higher $p/p°$ gave an apparent micropore volume of *c.* 0.01 $cm^3 g^{-1}$.

The *t*-method of isotherm analysis adopted by Cases *et al.* (1992) is not entirely satisfactory and therefore the interpretation of the results is not altogether straightforward. However, the high BET *C* value is consistent with the conclusion that there was a small micropore filling contribution. To arrive at a more realistic quantitative assessment of the microporosity it would be desirable to obtain nitrogen isotherm data on a truly non-porous form of Na-montmorillonite. In practice, however, this may be difficult to accomplish and a more pragmatic approach would be to construct a series of comparison plots for the adsorption of N_2 (and preferably also Ar) on pairs of samples of differing particle sizes and defect structures. In this way it should be possible to establish quantitative differences in the micropore capacities.

In another investigation, nitrogen isotherms were determined on samples of acid-activated bentonite (Srasra *et al.*, 1989). The acid activation produced an increase in the BET area from 80 to 250 $m^2 g^{-1}$. From the change in shape of the nitrogen isotherm, it would appear that pore widening was associated with the removal of some microporosity in the original bentonite. The adsorption of β-carotene was also investigated, but there appeared to be no correlation with the adsorption of nitrogen at 77 K. This is hardly surprising in view of the differences in modes of adsorption and the complexity of the clay.

11.4.2. Sorption of polar molecules

The character of the isotherms for the polar molecules on natural montmorillonite in Figure 11.6 is quite different from that of the isotherms in Figure 11.5. The hysteresis now extends across the entire $p/p°$ range and is associated with the expansion and contraction of the layer structure (Barrer, 1978). The interlayer sorption, which is a form of intercalation, can be treated from the standpoint of a delayed phase change (Barrer, 1989).

An interesting approach was adopted by Annabi-Bergaya *et al.* (1979), who determined methanol and isopropanol *desorption* isotherms on a series of charge-deficient Ca-montmorillonites (prepared from Na- and Li-saturated montmorillonite). Each desorption isotherm was determined after a 'surface cleaning' process with the particular alcohol in order to prevent the irreversible collapse of the interlamellar space. The adsorbent was exposed to the alcohol vapour at $p/p° = 0.9$ and the stepwise mass

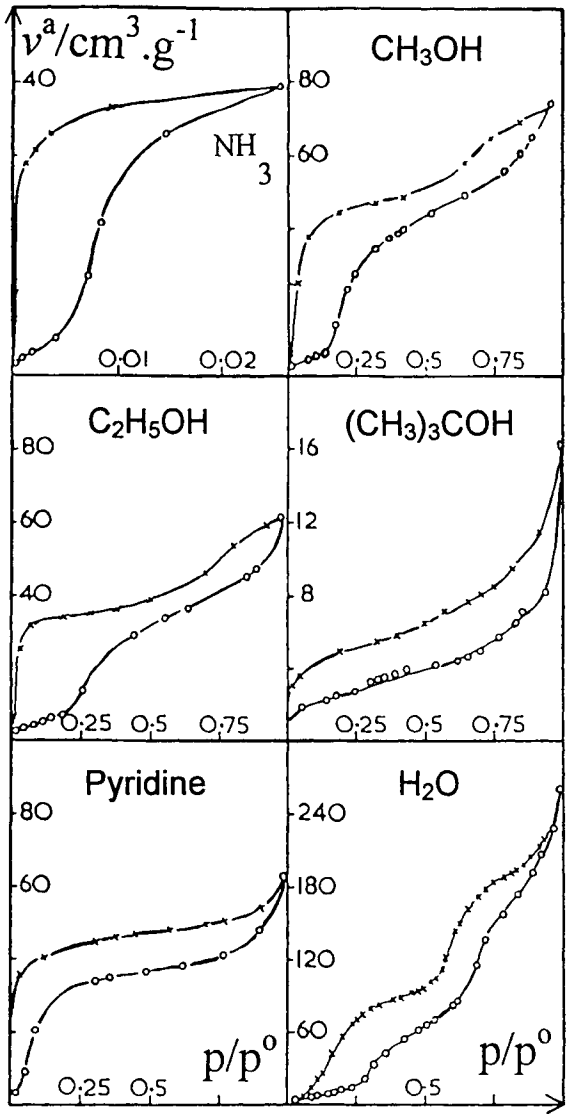

Figure 11.6. Isotherms for polar molecules on natural montmorillonite (from Barrer and Reay, 1957).

loss recorded as the $p/p°$ was reduced. At each stage, X-ray diffraction provided an independent measure of the change in the d_{001} spacings.

It was reasonably assumed that the experimental isotherm was composed of two parts: the 'internal' and 'external' isotherms. The external isotherm was defined as the isotherm on the external surface of the collapsed material, which remained independent of the extent of charge deficiency. The computed external isotherms for methanol and isopropanol turned out to have different shapes: the former was of

Type II character, whereas the latter was predominantly Type I. This difference is not surprising, but it is more difficult to explain the magnitude of the derived external area. Thus, a value of *c.* 300 $m^2 g^{-1}$ was obtained from the methanol isotherms, whereas the BET-nitrogen value was only 140 $m^2 g^{-1}$. It seems therefore that there may be an overestimate of the extent of the methanol adsorption on the external surface.

The mechanisms of methanol adsorption were discussed in a further paper by Annabi-Bergaya *et al.*, (1981). The authors drew particular attention to the importance of the hydrogen bonding between the adsorbed molecules, which is in competition with the dipole–cation interaction. In some cases, the latter is relatively strong and the cation may then adopt the structure-forming role, but with other smectites (e.g. Li-montmorillonite) the specific adsorbate–adsorbate interactions allow the formation of a continuous network of adsorbed species (analogous to the structure of crystalline CH_3OH).

Many investigations have been made of the sorption of water vapour by various forms of montmorillonite and vermiculite. In a study of the effect of increasing the outgassing temperature of natural vermiculite on the sorption of water vapour, Gregg and Packer (1954) obtained a set of unusual *stepwise* Type I isotherms, all of which displayed low-pressure hysteresis. It is of interest that the location of the step riser, at about $p/p^\circ = 0.02$, appeared to be almost independent of the outgassing temperature. The water sorption capacities were reported to be far greater than would be expected for adsorption on the external areas, as determined by the BET-nitrogen method (i.e. 1–2 $m^2 g^{-1}$).

The water isotherm on natural montmorillonite in Figure 11.6 (Barrer and Reay, 1957), has an ill-defined double step. Similar results were reported by van Olphen (1965) for the water/vermiculite system. After further work, van Olphen (1976) came to the conclusion that the sorption of water molecules produces a stepwise expansion of the layer lattice of smectites and vermiculites, with the interlayer formation of one to four monolayers of water.

A clearer picture of the sorption of water vapour by montmorillonite was obtained by Cases *et al.* (1992). Their adsorption–desorption isotherms of water on sodium montmorillonite are shown in Figure 11.7. The wavy nature of the adsorption and desorption branches (A_1 and D_1, respectively) of the full hysteresis loop in Figure 11.7 is evidently similar to that of the water isotherm in Figure 11.6 and is indicative of a complex mechanism. However, it was established that the scale of the hysteresis loop depended on the maximum relative pressure reached before the pressure was reduced. This dependency is illustrated by the appearance of the partial sorption isotherms also plotted in Figure 11.7. Here, a small hysteresis loop (desorption branch D3) was the result of $(p/p^\circ)_{max} < 0.25$, in contrast to much larger loop (desorption branch D2) when the adsorption was taken to $(p/p^\circ)_{max} = 0.35$.

The results in Figure 11.7 were consistent with the movement of the *c*-axis spacing, d_{001}: at $p/p^\circ < 0.25$, this remained close to the dry-state value of 0.96 nm, but as the water vapour pressure was increased, d_{001} underwent a stepwise change to *c.* 1.8 nm. The initial sharp increase in the region of $p/p^\circ = 0.25$ confirmed that at 25°C this represented the threshold relative pressure (and corresponding chemical potential) for the sorption of water within the interlamellar space.

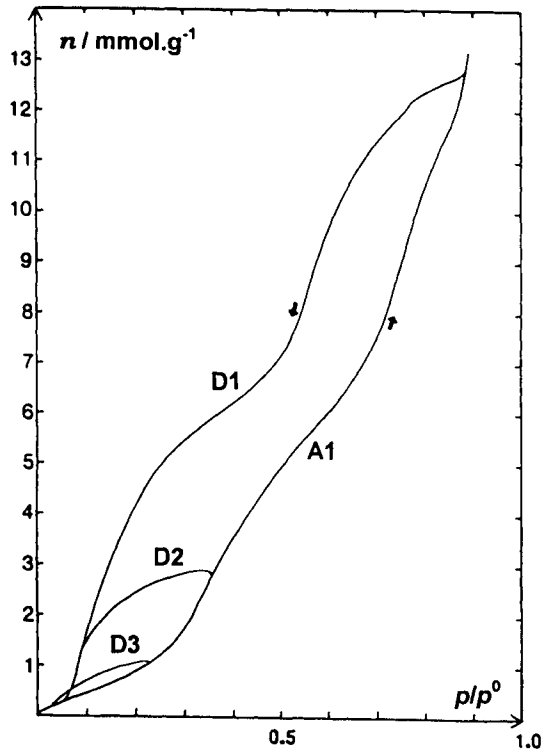

Figure 11.7. Adsorption–desorption isotherm for water vapour on sodium montmorillonite at 25°C. Desorption branches D1, D2 and D3 produced after adsorption up to relative pressures of 0.88, 0.35 and 0.25, respectively (after Cases *et al.*, 1992).

Immersion microcalorimetry was one of the techniques used by Cases *et al.* (1992) to provide additional information on the nature of the microstructural changes produced by the sorption of water vapour. The approach was based on the Harkins–Jura procedure (see Chapter 5), which involves the determination of the energy of immersion after the progressive preadsorption of water vapour.

The change in the energy of immersion as a function of the precoverage $p/p°$ is shown in Figure 11.8. In contrast to the behaviour of kaolinite, a relative pressure of *c.* 0.75 was required in order to reduce the immersion energy to its final constant level of 12.6 J g^{-1}. By assuming that this corresponds to the immersion of particles coated with liquid water, we obtain a value of 105 $m^2 g^{-1}$ for the *external* area (since the surface internal energy of pure liquid water is 0.119 J m^{-2}).

As already indicated, the surface area of the dry clay appeared to be about 50 $m^2 g^{-1}$. The platy particles (the tactoids) were therefore about 20 layers thick: during the first stage of water sorption, the particles were split into smaller tactoids of around six clay platelets (surface area of 105 $m^2 g^{-1}$). The external dimensions at $p/p° > 0.25$ remained fairly constant, but the interlamellar sorption was accompanied by swelling and the development of an accessible internal area (possibly as high as

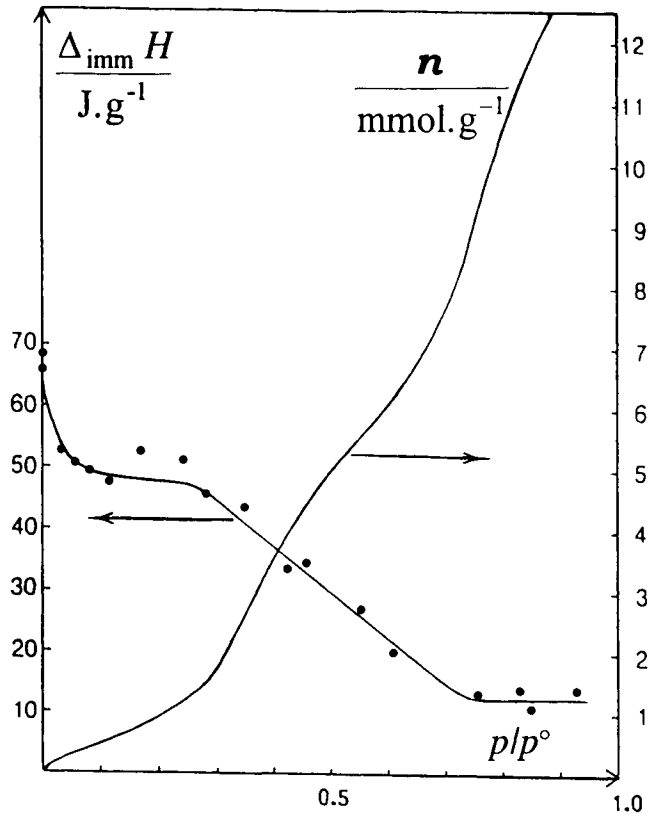

Figure 11.8. Energy of immersion in water versus pre-coverage relative pressure of water vapour (reproduced courtesy of Cases *et al.*, 1992).

800 m^2 g^{-1}). Cases *et al.* (1992) concluded that on the adsorption branch two-layer and three-layer hydrates were formed over the range $p/p° = 0.5–0.9$. On the desorption branch, the initial stage of the loss of some water from the external surface and mesopores was followed by a reduction in the amount of interlayer water.

A Monte Carlo simulation study of the adsorption of water was undertaken by Delville and Sokolowski (1993). The results appear to confirm that water molecules confined in 2 nm slits between montmorillonite sheets do not have the same properties as liquid water. The calculated water isotherms on open and confined clay surfaces appeared to be quite different and the results indicated a strong correlation between the wetting properties of a clay surface and its porosity and ionic nature.

11.4.3. Physisorption by expanded smectites

It was already known in 1955 that the exchangeable cations in montmorillonite lie between the negatively charged layers, the degree of separation being dependent on the size of the cation and its state of hydration. Barrer and MacLeod (1955)

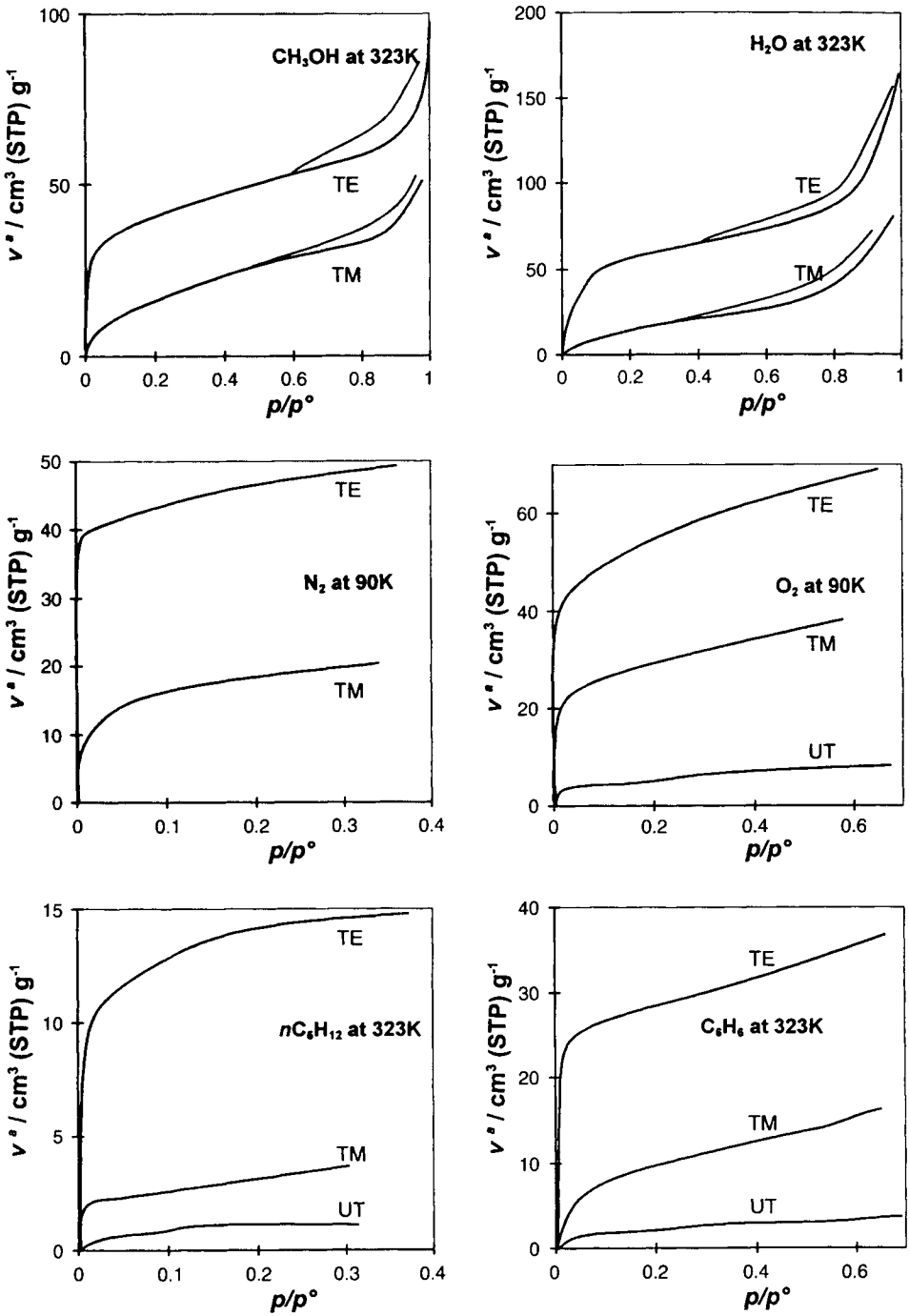

Figure 11.9. Isotherms for polar and non-polar molecules on alkylammonium-exchanged montmorillonite (from Barrer and Reay, 1957). UT, untreated; TM, tetramethylammonium ion treatment; TE, tetraethylammonium ion treatment.

conceived the idea that by replacing small cations by larger ones, it should be possible to hold the layers permanently apart so that the physisorption capacity would be considerably enhanced and possibly become selective. It was therefore decided to exchange the Na^+ ions for various alkyl ammonium ions (e.g. $(CH_3)_4N^+$ and $(C_2H_5)_4N^+$). The capacity of the clay for the non-polar molecules was greatly increased, as can be seen from the results in Figure 11.9. It is of particular interest that polar molecules were freely adsorbed, the low-pressure hysteresis in Figure 11.6 now being removed.

In an investigation of the adsorbent activities of other alkyl-ammonium montmorillonites, Barrer and Reay (1957) found that the $CH_3NH_3^+$ form exhibited molecular

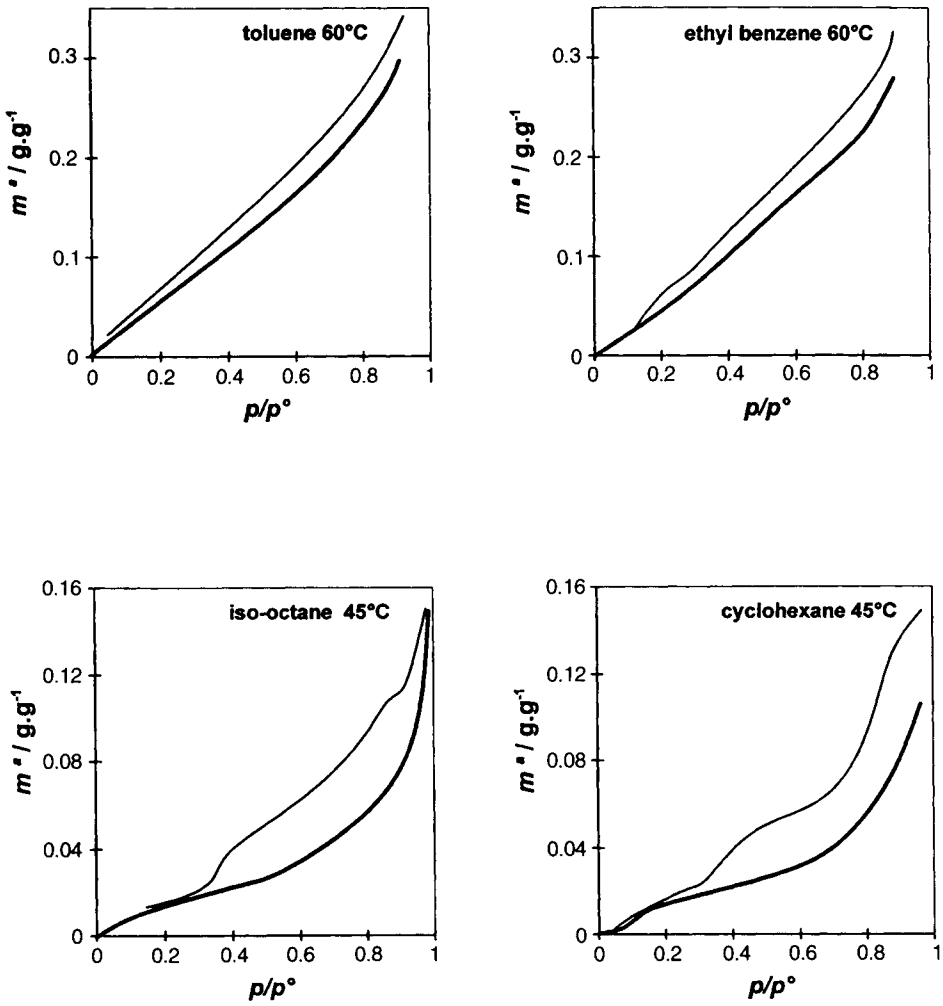

Figure 11.10. Hydrocarbon isotherms obtained with dimethyldioctadecylammonium bentonite (from Barrer, 1978).

sieve properties. However, the uptake of benzene was higher than expected, which confirmed that the expanded clays did not behave as completely rigid molecular sieves.

It was shown by Barrer and his co-workers that a great variety of organic cations can be introduced into the interlayer regions of smectites and vermiculites. The products have been referred to as organo-clays (Barrer, 1978) and some have been found to be useful thickeners in paints, inks, etc.

A selection of hydrocarbon vapour isotherms obtained with dimethyldioctadecylammonium bentonite is displayed in Figure 11.10. The toluene and ethyl benzene isotherms are almost linear over a wide range of $p/p°$ and are more like the sorption isotherms given by organic polymers than by inorganic porous adsorbents. On the other hand, the Type IIb character of the iso-octane and cyclohexane isotherms is apparent (Barrer, 1978, p. 455).

With the two aromatic hydrocarbons, Barrer and Kelsey (1961) found that the d_{001} spacing increased steadily with the increase in $p/p°$, but with the alkanes there was very little change. In the former case, it appeared that most of the uptake was in the interlamellar region. As indicated by the shape of the Type IIb isotherms, the sorption of the other organic vapours probably included an appreciable amount of multilayer adsorption on, and between, the clay platelets (cf. Figure 11.5).

11.5. Formation and Properties of Pillared Clays

As we have already seen, swelling is the direct result of the interlayer sorption of polar molecules by smectites. The generation of an internal area of about 800 $m^2 g^{-1}$ by the sorption of water vapour is associated with the development of an interlayer width of at least 0.6 nm, but the expanded structure lacks thermal stability. It is perhaps surprising that the work of Barrer on the sorption properties of expanded smectites, described in the previous section, did not immediately attract more attention. Twenty years were to elapse before the first successful attempts to produce stable permanently expanded smectites by the introduction of inorganic pillars were made by Vaughan *et al.* (1974) and Brindley and Sempels (1977).

The work by Vaughan's group in the laboratories of W.R. Grace and Co. was prompted by the need to develop new catalysts for the processing of heavy crude oils (Vaughan, 1988). The initial aim was to produce stable, wide-pore cracking catalysts, but so far progress in this direction has been disappointing. The present revival of interest in pillared clays (PILCs) is largely in the hope that they may find application in other areas such as separation technology (De Stefanis *et al.*, 1994; Fripiat, 1997).

11.5.1. Pillaring

A simplified picture of the stages involved in pillaring is shown in Figure 11.11. It is apparent that the replacement of the exchangeable cations by large inorganic ions is responsible for creation of the pore structure, which is then stabilized by thermal

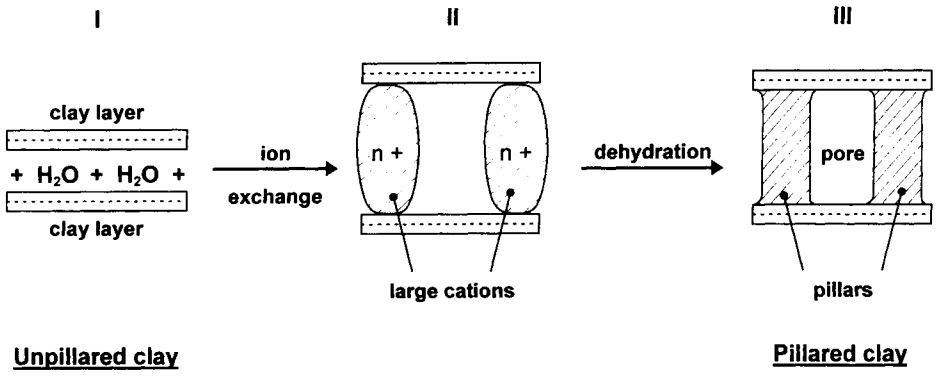

Figure 11.11. Simplified picture of pillaring.

treatment with the removal of H_2O and OH groups. In this manner, dense nanoscale oxide pillars are inserted into the interlayer 'galleries'.

It was established by Vaughan and his co-workers that certain inorganic polymeric cations could intercalate and thereby expand mineral and synthetic forms of smectic clays (Vaughan, 1988). Much of the early work involved the application of a large hydroxyaluminium cation, which can be readily prepared from aqueous aluminium chloride. The structure of the Al_{13} cation, $[Al_{13}O_4(OH)_{24}(H_2O)_{12}]^{7+}$, was already known and it was originally thought that this polymeric ion would retain its identity in the intercalated state. However, it became evident that complex changes accompany the exchange and ageing of the intercalated material (Vaughan, 1988; Fripiat, 1997).

In the initial stages, Vaughan and his co-workers were encouraged to find that their samples of PILC were catalytically active and also appeared to be thermally stable. However, an irreversible collapse of the pore volume was found to occur when the products were exposed to mild hydrothermal conditions at 600°C. The first successful way of stabilizing the pillar structure involved increasing the molar mass of the Al_{13} cation by further polymerization to give, for example, $[Al_{26}O_8(OH)_{52}(H_2O)_{20}]^{10+}$. Other procedures included the formation of larger co-polymers by reacting the Al_{13} ions with compounds of Mg, Si, Ti or Zr.

Experiments in the Grace laboratories were also carried out with solutions of $ZrOCl_2.xH_2O$, which tended to give more stable PILCs than those obtained by the Al_{13} route. On the other hand, it was more difficult to obtain reproducible products because of the complexity of the zirconia hydroxypolmers (Vaughan, 1988). Progress in this direction has been made by Burch (1987), Farfan-Torres *et al.* (1991) and Ohtsuka *et al.* (1993).

The possibility of pillaring smectites with various other large polyhydroxides (e.g. of titanium and various transition metals) is under active investigation. For example, the preparation of thermally stable TiPILCs (e.g. with BET areas $> 300\ m^2\ g^{-1}$ at 600°C) has been described by Sterte (1991) and characterized by Bernier *et al.* (1991). The use of different pillaring agents offers the prospect of the development of

a broad spectrum of different PILCs with pore sizes extending into the mesopore range (Barrer, 1989; Fripiat, 1997).

11.5.2. Chemical and physical nature of pillared clays

It is well known that the smectic clays exhibit both Bronsted and Lewis acidity: the former is associated with the clay surface and the latter with the exchangeable cations. It has been pointed out by Fripiat (1997) that pillaring the clay will modify the clay acidity in at least two ways: (a) the polycationic pillars replace a high proportion of the original cations, and (b) the pillars convey additional acidity. However, because of the pillar–smectite interaction, the net result is unlikely to be a simple substitution of one form of acidity by another. Further changes, which involve dehydroxylation and cationic dehydration, are brought about by thermal activation and lead to various forms of cross-linking between pillars and smectite framework. These changes have been followed by the application of infrared spectroscopy, magic angle spinning (MAS) NMR and thermal analysis.

Detailed investigations of clay morphology have revealed that Figure 11.11 gives an oversimplified impression of the microstructure (Van Damme *et al.*, 1985). Thus, there is normally an appreciable amount of disorder in the arrangement of aggregated clay platelets, resulting in a broad distribution of ill-defined interparticle pores. The BET areas of the calcined pillared clays are generally in the range 200–400 $m^2 g^{-1}$, although values of over 600 $m^2 g^{-1}$ have been recorded (Dailey and Pinnavaia, 1992).

11.6. Physisorption of Gases by Pillared Clays

Nitrogen isotherm measurements (at 77 K) have been used by many investigators for the evaluation of the surface area and porosity of pillared clays. Although the exact dimensions of the pillared pore structures are still under discussion (Fripiat, 1997), there is general agreement that the gallery (interlayer) pores are for the most part within the micropore range. Therefore, one might expect pillared clays to give Type I nitrogen isotherms. In fact, a few Type I isotherms have been reported (e.g. by Diano *et al.*, 1994; Cool and Vansant, 1996), but these are rarely fully reversible. The most common types of hysteresis loops are H3 and H4 in the IUPAC classification. With the majority of PILCs, the nitrogen isotherm turns out to be a combination of Types I and IIb, the exact shape depending on the relative extents of the interlamellar and external areas.

The values of BET area and apparent pore volume given by a particular PILC are of little use unless the external surface coverage and micropore filling contributions can be resolved. However, a useful initial step is to look for similarities and changes in the isotherm shape. For example, the nitrogen isotherms in Figure 11.12 were given by (a) the montmorillonite precursor, (b) the PILC, and (c) after autoclaving (Sterte, 1991).

It is evident that the multilayer sections of the isotherms in Figure 11.12 have a remarkably similar shape and indeed appear to lie parallel. This suggests that the

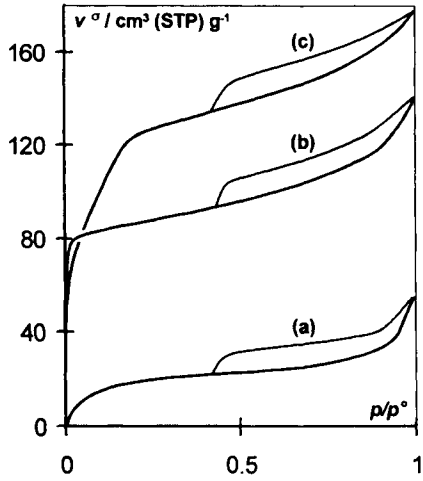

Figure 11.12. Nitrogen isotherms determined on (a) a montmorillonite, (b) the untreated La-Al-pillared montmorillonite, (c) after autoclaving treatment (after Sterte, 1991).

secondary pore structure of the smectic clay (i.e. its interparticle porosity) and its external area underwent little change. The steep low-pressure region of isotherm (b) indicates that the PILC contained narrow micropores, which were widened by the hydrothermal treatment – as can be seen by the appearance of isotherm (c).

Various procedures have been adopted for the analysis of the nitrogen isotherms. Some investigators have used the *t*-method of Lippens and de Boer in its original form. Other authors have preferred to follow the IUPAC recommendations of comparing the shape of a given isotherm with that of a standard on an appropriate non-porous adsorbent.

The latter approach was adopted by Trillo *et al.* (1993) in their study of the effect of thermal and hydrothermal treatment on the accessible microporosity of alumina-pillared montmorillonite. This work revealed that X-ray measurements of the d_{001} spacing taken alone may give a misleading impression of the thermal stability of the PILC micropore structure. For example, after heat treatment of the Al-PILC at 300°C, it was found that the apparent micropore volume available for nitrogen adsorption amounted to only *c.* 30% of that indicated by the d_{001} spacing.

The α_S-method was also used by Grange and his co-workers (Gil *et al.*, 1995; Gil and Grange, 1996) for analysing nitrogen isotherms on a series of pillared clays prepared from Na-montmorillonite. Hysteresis loops of Type H4 were associated with the secondary porosity and high values of the Langmuir constant b (see Equation (4.38)) indicated microporosity. In the case of a sample of Al-PILC, the micropore capacity was estimated to contribute about 60% to the total uptake at $p/p° = 0.99$.

Gil and Grange (1996) also attempted to apply the DR and DA equations (i.e. Equations (4.39) and (4.45)) – the latter is given later in this chapter as Equation (11.1). The pillared clays appeared to give bimodal adsorption potential distributions, but the significance of these findings is not entirely clear.

Some aspects of the interpretation of adsorption data were discussed by Bergaya *et al.* (1993), with the useful reminder that the packing of adsorbed molecules in narrow pores is strongly dependent on the pore width. It was suggested that the molecular confinement in interlamellar pores is a major source of underestimation of the gallery pore volume. These comments reinforce the IUPAC recommendation that no experimental method should be expected to provide an absolute assessment of the surface area or porosity of highly porous materials (Rouquerol *et al.*, 1994). The following summary of other recent work will also illustrate the importance of this recommendation.

In a study of the porosity of alumina-pillared montmorillonites (Al-PILCs), Zhu *et al.* (1995) have obtained values of the mean slit-width of 0.8–0.9 nm from the volume/surface ratio. In this case, the nitrogen adsorption values were in agreement with the corresponding d_{001} values of *c.* 0.8 nm. However, effective micropore volumes obtained from the nitrogen isotherms and from water sorption data were significantly different and it was suggested that the density of the sorbed water was lower than that of liquid water.

A different opinion has been expressed by Bergaoui *et al.* (1995), who consider that the characterization of Al-PILCs by nitrogen adsorption can lead to misleading results. These investigators have found that the Dubinin–Radushkevich (DR) analysis of carbon dioxide isotherms gave values of micropore volume in good agreement with the 'theoretical' values derived from the amounts of intercalated Al_{13} polymer in synthetic saponites. It is of interest that a quasi-equilibrium technique was used to determine the CO_2 isotherms at 273 and 293 K. The application of CO_2 adsorption for micropore characterization was originally devised by Rodriguez–Reinoso. The method is undoubtedly useful when applied to activated carbons, but the likelihood of a relatively strong field gradient–quadrupole interaction of CO_2 with clays and PILCs may complicate the interpretation of the adsorption data. This may explain the curvature of the DR plots obtained with intercalated saponites (Bergaoui *et al.*, 1995).

The importance of using a number of adsorptive molecules for the characterization of the porosity of PILCs is demonstrated by the recent work of Cool and Vansant (1996). The Zr-pillaring of natural hectorite and synthetic laponite was investigated with the aid of various techniques including measurements of the adsorption of nitrogen, oxygen and cyclohexane. The low-temperature N_2 isotherm on an uncalcined sample of Zr-laponite was of Type Ib in the new classification (Figure 13.1), but also had a small hysteresis loop. These features are indicative of a wide range of pores, which extended from narrow micropores (<0.7 nm) to supermicropores and narrow mesopores (*c.* 1.4–2.1 nm).

According to Cool and Vansant (1996), pores between 0.7 and 1.1 nm are probably present in all pillared clays, whereas the narrow and wider pores are particular features of the Zr-laponite and Zr-hectorite. A relatively high adsorption affinity (i.e. the low pressure capacity) of Zr-laponite for cyclohexane was attributed to the presence of a large number of narrow pores, giving rise to enhanced adsorbate–adsorbent interactions.

Reversible Type Ib isotherms have been reported by Galarneau *et al.* (1995) for the adsorption of nitrogen on some novel 'porous clay heterostructures' (PCHs). A

so-called 'intra-gallery templating process' was used to produce thermally stable pores of effective width of 1.4–2.2 nm (as evaluated by the Horvath–Kawazoe method). This interesting approach involved the use of intercalated quaternary ammonium cations and neutral amines as co-surfactants to direct the interlamellar hydrolysis and condensation of an organo-Si compound such as tetraethylorthosilicate. Removal of the surfactant by calcination then left a stable and highly developed supermicroporous/mesoporous structure.

11.7. Structure, Morphology and Synthesis of Zeolites

11.7.1. Zeolite structures

The basic unit of a zeolitic structure is the TO_4 tetrahedron, where T is normally a silicon or aluminium atom/ion (or phosphorus in an aluminophosphate). In this section we deal with the aluminosilicate zeolites, which have the general formula $M_{x/n}[(AlO_2)_x(SiO_2)_y].mH_2O$. The zeolite framework is composed of $[(AlO_2)_x(SiO_2)_y]$ and M is a non-framework, exchangeable cation.

Although some pure silica zeolites (notably the Silicalites) are known, it is not possible to obtain a zeolitic alumina. Indeed, according to Loewenstein's rule, to avoid any direct Al—O—Al linkage, the permitted Si/Al ratio is at least 1.0 (i.e. $y > x$).

The great variety of zeolites is made possible by the different arrangements of linked TO_4 tetrahedra within secondary building units (SBUs), which are themselves linked together in numerous three-dimensional networks. The two simplest SBUs are rings of four and six tetrahedra and others comprise larger single and double rings – up to 16 T atoms. The unit cell always contains an integral number of SBUs.

A zeolitic structure can be described in various crystallographic terms. For many systems it is now possible to specify the following structural features: the SBUs, the framework density, the coordination sequences, the unit cell dimensions and composition, the direction of the channels and the aperture (window) dimensions (*Atlas of Zeolite Structure Types*, 1992; Thomas *et al.*, 1997). The framework density, FD, is defined as the number of T atoms per 1000 $Å^3$ (i.e. per 1 nm^3) of the structure.

The sodalite unit (or β cage), which is a characteristic feature of the A, X and Y zeolites (see Figure 11.13), is made up of both four and six rings arranged in the form of a cubo-octahedron (i.e. a truncated octahedron). The cage has an internal effective diameter of about 0.6 nm.

Some of the most common structures are generated by linking the sodalite units in different ways. Thus, by bridging the sodalite units via the four rings we obtain zeolite A (Linde Type A). If the six rings are linked, on the other hand, the faujasite structure (essentially that of zeolites X and Y) is produced. It is evident that this mode of bridging is responsible for the generation of the 'supercages', i.e. the large cavities. Access to these regions is through the apertures (i.e. the 'windows').

The intracrystalline porosity is often taken as the fraction of volume occupied by liquid water evolved on heating and evacuating the zeolite. Typical values are:

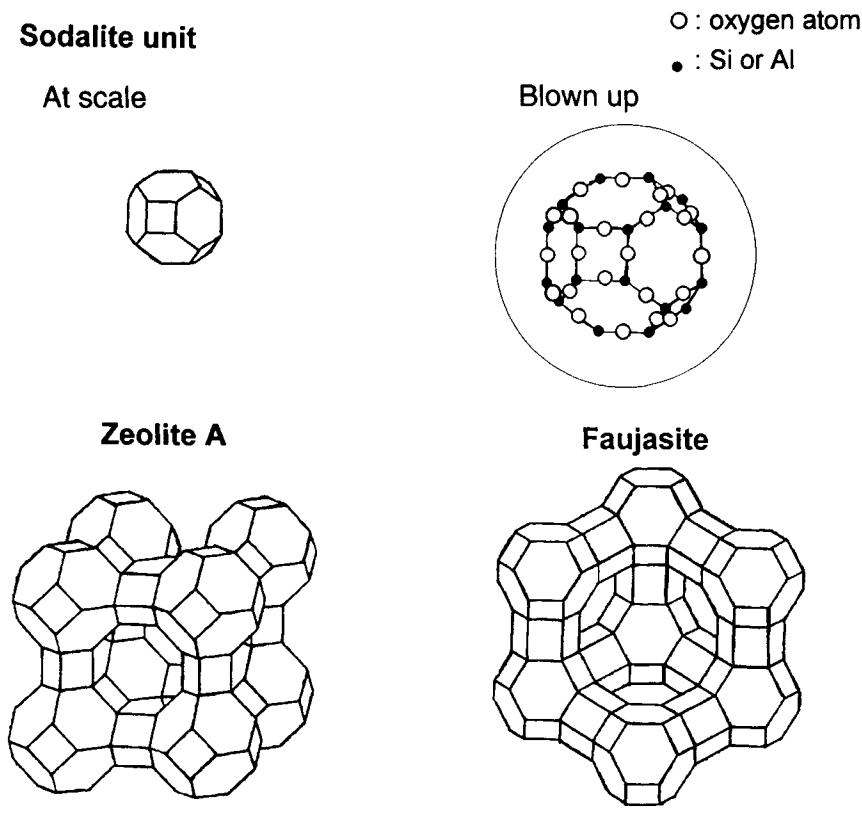

Figure 11.13. The composition of the sodalite cage and the structures of sodalite, zeolite A and faujasite (zeolites X and Y).

mordenite, 0.26; zeolite L, 0.28; zeolite A, 0.47; faujasite, 0.53 (Barrer, 1981). Because of the rigidity of the framework, there is little swelling or shrinking of the framework during adsorption or desorption. This behaviour is in contrast to that of clays and other aluminosilicates.

Zeolite A

The Linde Type A zeolite (Breck *et al.*, 1956; Reed and Breck, 1956) has a typical unit cell composition of $[Na_{12}\{Al_{12}Si_{12}O_{48}\}.27H_2O]_8$, the Si/Al ratio being always close to 1.0. The pseudo-cell pictured in Figure 11.13 consists of eight sodalite units (β cages). The SBUs are double four-rings and eight-rings. The FD is 12.9 nm^{-3}. Zeolite A crystallizes with cubic symmetry. The supercage (α cage) has a free diameter of about 1.14 nm and the 8-membered windows have free apertures of *c.* 0.42 nm, providing access to a three-dimensional isotropic channel structure. However, as discussed later, this window size is reduced by the presence of certain cations.

Zeolites X and Y

The faujasite-type zeolites all have the same framework structure, as indicated in Figure 11.13, and they crystallize with cubic symmetry. The general composition of the unit cell of faujasite is $(Na_2,Ca,Mg)_{29}[Al_{58}Si_{134}O_{384}].240H_2O$. The SBUs are double six-rings and the FD is 12.7 nm^{-3}. The unit cell contains eight cavities, each of diameter $\approx$1.3 nm. The three-dimensional channels, which run parallel to [1 1 0], have 12-ring windows with free apertures of about 0.74 nm. The difference between zeolites X and Y is in their Si/Al ratios which are 1–1.5 and 1.5–3, respectively.

Pentasil zeolites

The pentasil structure is based on double five-ring SBUs. The most important member is the MFI zeolite ZSM-5 (Silicalite-I in the pure silica form). This has the general formula $Na_n[Al_nSi_{96-n}O_{192}].16H_2O$, where $n < 27$ and crystallizes with orthorhombic symmetry. The FD of ZSM-5 is 17.9 nm^{-3}. A closely related structure is the MEL zeolite ZSM-11 with the same overall formula (but now $n < 16$). As is illustrated in Figure 11.14, ZSM-5 has intersecting straight and sinusoidal channels. Instead, ZSM-11 has intersecting straight channels. Intergrowths of the MFI and MEL forms are common and affect the catalytic properties (Thomas *et al.*, 1997).

In the orthorombic ZSM-5 and Silicalite-I crystal the sinusoidal (zigzag) channel runs along [1 0 0] and the other intersecting straight channel system along [0 1 0] (Kokotailo *et al.*, 1978). The pore openings are defined by ten-membered elliptical rings, the free diameters being 0.51 × 0.55 nm for the sinusoidal channels and 0.53 × 0.56 nm for the straight channels.

There are four interconnected cavities in the unit cell, each of *c.* 0.8 nm width. Each of the four interconnecting straight channels is 0.46 nm long and each of the four sinusoidal channels is 0.66 nm long.

Role of exchangeable cations

So far, we have not considered the role of the non-framework cations, M. Since the

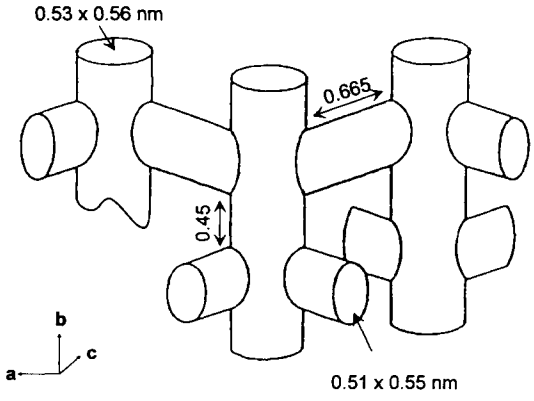

Figure 11.14. Channel structure of ZSM-5 (after Thamm, 1987).

aluminosilicate framework is composed of $(AlO_2)_x$ and $(SiO_2)_y$, it is anionic, the net negative charge being governed by the number of Al atoms in the T-positions. It is evident that a corresponding number of M cations are required to provide an overall balance of electric charge. A zeolite with a given Si/Al ratio normally has a certain number of exchangeable cations, which may be of different types, located at various sites within the cavities and channel structure.

In the case of zeolite A, three different cation sites have been identified: most of the cations occupy corner sites in the central cavity (Type I sites), but some of the total of twelve univalent ions (e.g. Na^+ or K^+) ions per cage must occupy sites within the eight-ring windows and therefore partially obstruct the channels. The effective window size of NaA (i.e. the 4A sieve) is thereby reduced from 0.42 nm to *c.* 0.38 nm. Since the K^+ ion is somewhat larger, the window size becomes even smaller (i.e the 3A sieve). When the Na^+ cations are exchanged for Ca^{2+} or Mg^{2+}, the number of requisite cations is reduced and the effective aperture size and pore volume are both increased (the 5A sieve).

The cation distribution in the faujasite zeolites is much more complex than in zeolite A. Five different sites have been identified and it is apparent that the distribution is dependent on the nature of the cations and the presence of water.

If the framework structure of a zeolite remains constant, the cation exchange capacity is inversely related to the Si/Al ratio. Furthermore, 'fine tuning' of the adsorptive and catalytic properties can be achieved by adjustment of the size and valency of the exchangeable cations. Dealumination of certain silica-rich zeolites can be achieved by acid treatment and the resulting 'hydrophobic' zeolites then become suitable for the removal of organic molecules from aqueous solutions or from moist gases.

11.7.2. Zeolite synthesis

Clearly, the time scales involved in the formation of natural zeolites cannot be reproduced in the laboratory, but in the 1940s it was shown by Barrer and his co-workers (see Barrer, 1982) that a number of the natural zeolites could be synthesized under hydrothermal conditions. The essential synthetic ingredients are suitably reactive forms of alumina, silica and base.

The initial formation of a poorly ordered aluminosilicate hydrogel is followed by the growth of oligomer precursors and the development of crystallinity. The crystalline zeolite may not be the most stable product and its formation will depend on the nature of the reactants, the reaction conditions and 'kinetic control'. The generally recognized stages of crystallization are supersaturation, nucleation and crystal growth. The key parameters governing zeolite formation are specified by Feijen *et al.* (1997) as hydrogel composition, pH, reaction conditions (temperature and time) and template.

Often organic ions (e.g. tetraalkylammonium cations such as tetramethylammonium, TMA^+, ions) or neutral molecules are used as templates (i.e. structure-directing agents). In the past certain templates were introduced empirically; although they are now widely used, their action is still not fully understood.

Crystals of synthetic zeolites often have a non-uniform distribution of their

trivalent T ions (i.e. they exhibit some degree of T-III zoning). The extent of this form of zoning appears to be the result of the synthesis procedure (Jacobs and Martens, 1987). Isothermal gas adsorption microcalorimetry was used in a novel manner to investigate the T-III zoning in MFI-type zeolites (Llewellyn *et al.*, 1994a).

11.7.3. Zeolite morphology

Crystals of the synthetic zeolites are usually quite small and often exhibit various forms of twinning and intergrowth. With some zeolites, individual crystallites (e.g. cube-shaped NaA) of size < 50 nm have been identified by electron microscopy, but the agglomerate sizes are generally in the approximate range 1–10 μm. For example, the particle size distribution over this range of a typical NaA powder was reported to be of a broad log-normal character (Breck, 1974, p. 388).

The particle size of many synthetic zeolites is too small for most applications and therefore they must be formed into polycrystalline aggregates (e.g. by pelletization). Binders are often added to improve the aggregate strength and durability. It must be kept in mind that these or other changes in the particle or aggregate morphology may significantly affect the equilibria or dynamics of adsorption.

11.8. Adsorbent properties of molecular sieve zeolites

It is evident that the channels and cavities within many zeolitic structures are of molecular dimensions and that their size and configuration are intrinsic properties of the particular crystalline framework. In addition, the local electrostatic fields, which emanate from the exchangeable cations, are to a large extent responsible for the strong affinity for water and other polar molecules. It follows that for a given zeolitic composition and structure, the adsorptive behaviour of a well-defined zeolite crystal is remarkably uniform and stable. Furthermore, within certain limits the adsorbent and ion exchange properties can be varied in a controlled manner by changing the framework structure, the Si/Al ratio and the nature of the exchangeable cations.

In the sub-monolayer range, the amount adsorbed on the external area of a 1 μm cubic zeolite crystal is very small in comparison with the adsorption within the micropore structure (the intracrystalline sorption). Also, apart from a small multilayer adsorption on the external surface, there should be no additional uptake at higher $p/p°$. However, there are three ways in which the non-zeolitic contribution may be increased: (a) the binder may have a relatively large specific surface; (b) the zeolite crystallite size may be much smaller than 1 μm; and (c) the zeolite may contain some amorphous aluminosilicate or silica. In practice, one or more of these effects can result in a significant distortion from the classical form of the Type I isotherm (see Sayari *et al.*, 1991).

11.8.1. Physisorption of gases by zeolite A

Certain forms of zeolite A (e.g. the 3A and 4A sieves) exhibit pronounced molecular sieving and consequently their physisorption capacities do not conform to the

Gurvich rule. At 77 K the uptake of argon or nitrogen by NaA is very small and too difficult to measure. The amounts adsorbed are appreciably increased as the temperature is raised, reaching maxima at *c.* 120 K for Ar and at *c.* 200 K for N_2. At 273 K the Ar adsorption is very small, whereas the N_2 adsorption is still significant.

These results reveal that at low temperature the rate of diffusion of Ar and N_2 into the intracrystalline pore structure is extremely slow. The increase in the adsorption with temperature is *not* thermodynamically controlled but is instead dependent on the molecules gaining enough kinetic energy to allow their passage through some of the 4A apertures. This process is probably assisted by enhanced vibrational amplitude of the oxygen ring structure.

Slightly smaller molecules such as O_2 are able to move more freely through the eight-ring apertures and in consequence the amount adsorbed decreases as temperature increases, in the normal manner. However, as indicated in Table 11.2, the derived values of v_p are not in close agreement (Breck, 1974, p. 428).

The exchange of sodium by calcium has a significant effect on the adsorbent properties of zeolite A. An abrupt change in the adsorptive properties occurs when between three and five Na^+ ions are replaced. Thus, Ar and N_2 are now both able to enter the channels at low temperature, although the lack of agreement between the different values of v_p in Table 11.2 is still evident.

The isotherms for the adsorption of oxygen and nitrogen by a 5A zeolite at the much higher temperatures of 273 and 293 K are shown in Figure 11.15. Of course, at these temperatures the isotherm curvature is much reduced: indeed, the oxygen isotherms are almost linear up to 10 bar (i.e. obeying Henry's law). The fact that the levels of nitrogen adsorption are significantly greater than those of oxygen is due

Table 11.2. Derived values of pore volume for zeolites A and X

Zeolite	Adsorptive	θ (°C)	V_p ($cm^3\,g^{-1}$)
$Na_{12}A$	H_2O	25	0.29
	CO_2	−75	0.25
	O_2	−183	0.21
Ca_6A	H_2O	25	0.31
	O_2	−183	0.24
	Ar	−183	0.26
	N_2	−196	0.30
	n-Butane	25	0.23
NaX(Si/Al = 1.25)	H_2O	25	0.36
	CO_2	−78	0.33
	Ar	−183	0.30
	O_2	−183	0.31
	N_2	−196	0.35
	n-Pentane	25	0.30
	Neopentane	25	0.26
	Benzene	25	0.30

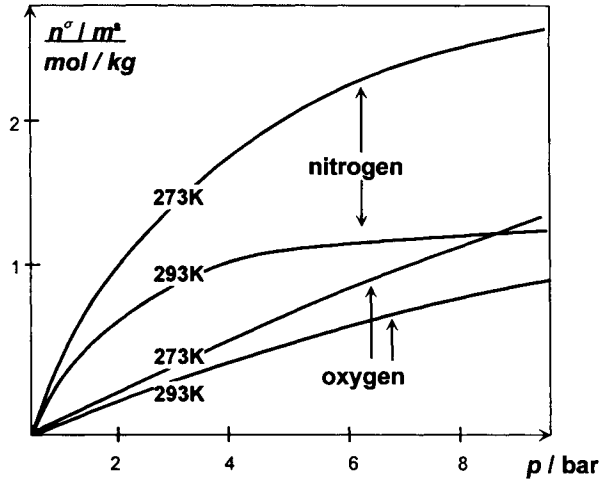

Figure 11.15. Adsorption isotherms for oxygen and nitrogen on a 5A zeolite at 273 and 293 K (after Kirkby, 1986).

mainly to its specific field gradient–quadrupole interaction. This enhancement of the nitrogen adsorbent–adsorbate interaction is responsible for the higher affinity of adsorption, which is indicated by the difference in the slopes of the isotherms at very low loading.

The 5A zeolite gives an N_2/O_2 selectivity ratio of 2–3 in the normal pressure swing adsorption (PSA) working range, although this is evidently reduced as the partial pressures are increased. At ambient temperature, adsorption equilibration is very rapid. At lower temperatures, the rates of adsorption are decreased and the separation becomes less efficient. At 293 K, argon gives an isotherm which is very close to that of oxygen and this component therefore tends to remain in the oxygen fraction. Since a selective adsorption of oxygen cannot be achieved with a zeolite, for nitrogen generation it is necessary to use a special type of molecular sieve carbon.

If the operational temperatures are not too high, many zeolites give reversible Type I isotherms. It might be expected that the Langmuir equation could be applied to these systems – at least over a certain range of pressure. The long ranges of linearity of the Langmuir plots in Figure 11.16 may appear to support the applicability of the Langmuir equation. However, as Ruthven (1984) has pointed out, the apparent conformity is deceptive. The three linear plots are given over different ranges of apparent surface coverage, θ, and the derived values of Henry's law constant and monolayer capacity, n_m, turn out to be incompatible with each other and with values obtained by a more detailed analysis of the adsorption data (e.g. virial treatment).

A more searching test of conformity to the Langmuir equation is obtained by plotting the adsorption data as a function of θ rather than p (Barrer, 1978, p. 407). Some pronounced deviations then appear, which are consistent with the inadequacy of the simple Langmuir model.

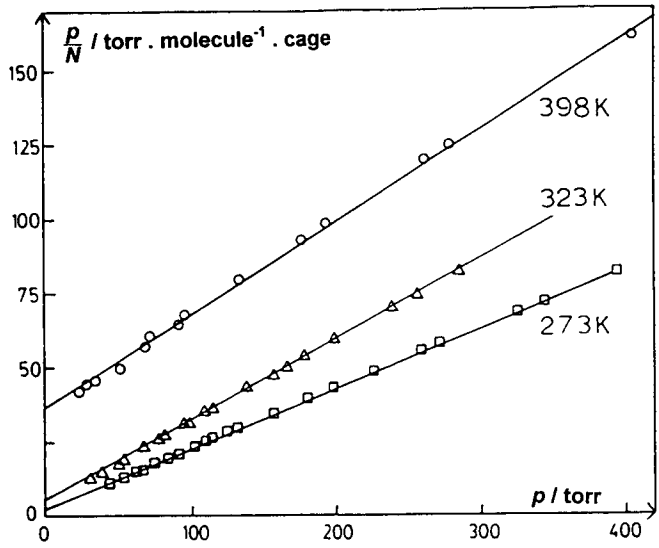

Figure 11.16. Langmuir plots for the adsorption of propane by 5A zeolite (reproduced courtesy of Ruthven and Loughlin, 1972).

11.8.2. Physisorption of gases by zeolites X and Y

Values of the effective pore volume of zeolite NaX, as determined by the adsorption of a selection of molecules, are included in Table 11.2. By omitting the water, nitrogen and neopentane values, we arrive at the value $V_p = (0.31 \pm 0.02)\ cm^3\ g^{-1}$, which is in agreement with a calculated supercage volume of $0.30\ cm^3\ g^{-1}$. This supports Breck's (1974, p. 428) conclusion that, with the possible exception of water, only the large supercages are available for physisorption, and is consistent with a supercage volume of about $6.7\ nm^3$ per unit cell.

The anomalous behaviour of water in both zeolite A and X is not surprising in view of its abnormal specificity, strong interactions with exchangeable cations and also the possibility of some penetration into the small β cages. The high nitrogen value is of interest since it provides further evidence that in ultramicropores adsorbed nitrogen does not adopt the normal liquid structure.

Various attempts were made by Dubinin and his co-workers to apply the fractional volume filling principle and thereby obtain a characteristic curve for the correlation of a series of physisorption isotherms on a zeolite (Dubinin, 1975). As was noted in Chapter 4, the original Dubinin–Radushkevich (DR) equation (i.e. Equation (4.39)) was found to be inadequate and in its place the more general Dubinin–Astakhov (DA) equation was applied (i.e. Equation (4.45)).

A convenient form of the DA equation is

$$n/n_p = \exp[-(A/E)^N] \tag{11.1}$$

where n_p is now the amount adsorbed when all the channels and cavities are full (i.e. the micropore capacity). The terms A and E are as defined in Chapter 4: A is a measure of the adsorption affinity (so-called 'adsorption potential') and E is a characteristic energy for the given system.

Dubinin (1975) found it necessary to distinguish between the adsorption of relatively large and small molecules by NaX and other faujasite zeolites. With large molecules, such as benzene and cyclohexane, it was apparently possible to apply Equation (11.1) in a fairly straightforward way: by using successive approximations the best values of n_p and E were obtained. For each system, this procedure gave a temperature-invariant characteristic curve, by which the fractional filling, n/n_p, was expressed as a function of *the potential*, A. For example, Equation (11.1) was applicable with $N = 4$ to the adsorption isotherms of cyclohexane on NaX over the remarkably wide fractional filling range $n/n_p = 0.10$–0.98 and within the temperature range 80–140°C (maximum deviation < 10%).

The adsorption of smaller polar molecules, such as water and carbon dioxide, was more complex, and Dubinin (1975) concluded that the overall pore filling process could be expressed as a two-term equation, each term having the mathematical form of Equation (11.1). In the low-filling region, the interaction with the cationic sites was considered to be the most important contribution, with the normal dispersion interactions becoming more important at higher loadings.

Although many experimental isotherms appear to obey the DA equation over appreciable ranges of pressure, the theoretical basis of this conformity is highly questionable. However, as Ruthven (1984) points out, even with NaX and other zeolites the temperature invariant characteristic curve can provide a useful empirical means of correlating engineering data.

It is generally agreed that a virial form of isotherm equation is of greater theoretical validity than the DA equation. As explained in Chapter 4, a virial equation has the advantage that since it is not based on any model it can be applied to isotherms on both non-porous and microporous adsorbents. Furthermore, unlike the DA equation, a virial expansion has the particular merit that as $p \rightarrow 0$ it reduces to Henry's law.

The exponential form of the virial isotherm favoured by Kiselev and his coworkers (e.g. Avgul *et al.*, 1973) was Equation (4.4), that is

$$p = n \exp (C_1 + C_2 n + C_3 n^2 + C_4 n^3 + \cdots) \tag{11.2}$$

By using the first three or four coefficients, Avgul *et al.*(1973) were able to satisfactorily apply Equation (11.2) up to 70–80% of the total filling of zeolites NaX and LiNaX by Ar and Xe.

The two-constant versions of Equation (11.2) and other virial expansions can be applied to the low fractional filling section of isotherms on the faujasite zeolites, provided that the temperature is not too low. In this manner it is then possible to obtain the Henry's law constant, k_H.

An alternative way of determining k_H is by a gas chromatographic method. This is the generally preferred approach at higher temperatures, where the isotherm curvature is reduced. A novel perturbation chromatographic technique was adopted by Denayer and Baron (1997) in their recent study of the adsorption of a range of normal

Table 11.3. Henry's law constants and low coverage energies of adsorption for various alkanes on NaY and HY

Adsorptive	NaY		HY	
	$k_H \times 10^5$ (mol g^{-1})	E_0 (kJ mol^{-1})	$k_H \times 10^5$ (mol g^{-1})	E_0 (kJ mol^{-1})
n-Hexane	1.9	45.5	1.7	44.2
2-Methylpentane	2.0	45.3	1.7	44.2
3-Methylpentane	2.0	44.5	1.7	43.5
2,3-Dimethylbutane	2.0	44.1	1.8	43.5
2.2-Dimethylbutane	2.1	43.2	1.8	43.5
n-Heptane	4.4	51.9	3.6	50.1
2,3-Dimethylpentane	5.1	50.6	3.6	50.1
n-Octane	10	57.5	7.9	56.0
2-Methylheptane	10	57.2	7.9	55.7
2,5-Dimethylexane	11	57.1	8.3	56.0
n-Nonane	23	63.4	17	62.0

From Denayer and Baron, (1997).

and branched paraffins by various forms of zeolite Y. By measuring the retention times corresponding to the perturbation of the adsorption system at different loadings, it was possible to derive the adsorption isotherm for each component. The measurements were made over the range 275–400°C. This study of the effect of chain length and branching of alkanes (from C_6 to C_{12}) followed earlier investigations of the adsorption of lower hydrocarbons by the faujasite zeolites (e.g. the work of Atkinson and Curthoys, 1981; Thamm *et al.*, 1983). Our present interest is in the behaviour of NaY and HY. Selected values of Henry's law constant, k_H, and low-coverage energy of adsorption, E_0, are given in Table 11.3.

Inspection of Table 11.3 reveals that there are relatively small differences between the corresponding values of k_H and E_0 for NaY and HY. This is to be expected since the adsorbent–adsorbate interactions are essentially non-specific (see Chapter 1). Decationization of zeolite Y thus has a minimal effect on the energetics of adsorption of the paraffins. The molecular shape of the adsorptive is also unimportant. In accordance with the results in Figures 1.5 and 1.6, the molar mass (number of carbon atoms) is much more important than the molecular shape. As before, there is a linear relation between E_0 and N_c. An exponential increase of k_H with N_c is of course consistent with the form of Equation (4.3).

The interaction of polar molecules with ionic and polar surfaces was briefly discussed in Chapter 1. A simplified form of Equation (1.6) was given as

$$E_0 = E_{ns} + E_{sp} \tag{11.3}$$

where E_{ns} represents the non-specific adsorbent-adsorbate interactions and E_{sp} the various specific contributions. When zeolites are used as adsorbents the E_{sp} term becomes extremely important (Kiselev, 1967; Barrer, 1978). The magnitude of the specific contributions is illustrated by the low-coverage adsorption calorimetric data in Table 11.4.

Comparison of the values of E_0 is made in Table 11.4 for pairs of molecules of very

Table 11.4. Adsorption energies at zero coverage for different adsorptives on NaX zeolite

Adsorptive	E_0 (kJ mol^{-1})	E_{sp} (kJ mol^{-1})
Argon	13.0	
Nitrogen	21.7	9
Ethane	25.9	
Ethylene	38.5	13
n-Hexane	61.4	
Benzene	75.2	14
n-Pentane	51.8	
Diethyl ether	87.8	36

Results of Kiselev (1967).

similar polarizabilities. By assuming that for each pair the corresponding E_{ns} values are approximately equal, we are able to obtain a rough estimate of the E_{sp} contribution given in column 3. On this basis, the most striking result is the very large E_{sp} contribution for diethyl ether.

Large E_{sp} contributions were also reported by Barrer (1978, p. 188) for the adsorption of carbon dioxide, ammonia and water vapour on NaX. Indeed, in the case of water, over 90% of the low-coverage adsorption energy was attributed to E_{sp}. With these highly polar molecules it is likely that the cation–adsorbate interaction provides a major contribution to E_{sp}.

In the work of Schirmer *et al.* (1980), a Tian–Calvet type microcalorimeter was used to determine the energetics of adsorption for *n*-hexane, cylohexane and benzene on NaY zeolite. The differential adsorption energies for *n*-hexane and benzene are plotted in Figure 11.17 as a function of the amounts adsorbed.

The results in Figure 11.17 are representative of the adsorption energy plots for various alkanes and aromatic hydrocarbons on faujasite zeolites. Thus, at low fractional filling by NaY, the benzene adsorption energy is greater than the *n*-hexane energy, although the difference ($\approx$6 kJ mol^{-1}) is much smaller than the corresponding difference ($\approx$14 kJ mol^{-1}) for NaX in Table 11.4. As already indicated, this is in accordance with the larger number of exhangeable cations in NaX. The pronounced maximum in the *n*-hexane curve in Figure 11.17 is indicative of strong adsorbate–adsorbate interactions at high loading, in contrast to benzene on graphitized carbon (see Figure 9.10a).

In view of the difference in the benzene adsorption energies on NaY and NaX, we would expect to find a difference in the benzene isotherms – especially at low loadings. The results of Kacirek *et al.* (1980) confirm that the benzene adsorption affinity of NaX is indeed significantly higher than that of NaY.

Generally, those polar adsorptives which have been found to exhibit the strongest specificity at very low coverage (e.g. H_2O and CO_2 on NaX) also give pronounced energetic heterogeneity: their differential adsorption energies decrease sharply with increased fractional pore filling (Kiselev, 1965; Barrer, 1978, p. 171). On the other hand, the adsorption energies of non-polar and weakly polar molecules tend not to undergo much initial change. As we have seen, the cation density is controlled by the

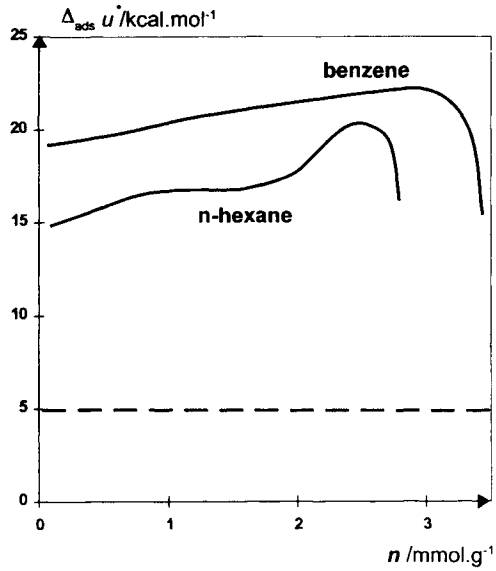

Figure 11.17. Differential energy of adsorption of *n*-hexane or benzene versus amount adsorbed by NaY zeolite (after Schirmer *et al.*, 1980).

Si/Al ratio and therefore a change from X to Y or dealumination generally leads to a higher degree of energetic uniformity (Barrer, 1978, p. 215; Schirmer *et al.*, 1980).

11.8.3. Physisorption of gases by ZSM-5 and Silicalite-I

In the early work on both ZSM-5 and Silicalite (e.g. by Flanigen *et al.* 1978; Ma, 1984) the adsorption isotherms of aliphatic and aromatic hydrocarbons and other vapours appeared to have an overall Type I appearance. However, the individual adsorption uptakes were widely spaced and generally desorption measurements appeared not to have been undertaken. More recent measurements by Rouquerol and Unger and their co-workers (e.g. Reichert *et al.*, 1991) have revealed that nitrogen and argon isotherms on well-defined crystals of Silicalite-I exhibit sub-steps within the micropore filling range of p/p°. Even more remarkable is the existence of a hysteresis loop in the pre-capillary condensation region of the nitrogen isotherm (Muller and Unger, 1986; Carrott and Sing, 1986).

As part of a systematic investigation of the adsorption of single and mixed gases by zeolites, Rees and his co-workers used an isosteric approach (i.e. by measuring a series of *p-T* isosteres) to compare the adsorptive properties of Silicalite I and zeolite NaY (Hampson and Rees, 1993). They concluded that, in contrast to NaY, Silicalite I was energetically homogeneous with respect to the adsorption of both propane and ethene. The results also indicate that the ethene–Silicalite interaction was largely non-specific.

The values of pore volume, v_p, of Silicalite-I in Table 11.5 were obtained from the saturation adsorption capacities in the usual manner: in each case, the uptake at

Table 11.5. Derived values of pore volume for Silicalite-I

Adsorptive	T (K)	v_p ($cm^3\ g^{-1}$)	Reference
Nitrogen	77	0.190	Kenny and Sing (1990)
Oxygen	90	0.185	Flanigen *et al.* (1978)
n-Butane	293	0.190	Flanigen *et al.* (1978)
n-Hexane	293	0.199	Flanigen *et al.* (1978)
n-Hexane	293	0.185	Ma (1984)
Benzene	293	0.134	Flanigen *et al.* (1978)
Benzene	293	0.126	Ma (1984)
p-Xylene	293	0.13	Ma (1984)
m-Xylene	293	0.085	Ma (1984)
o-Xylene	293	0.062	Ma (1984)
Neopentane	293	0.029	Ma (1984)
Water	293	0.019	Kenny and Sing (1990)

$p/p^\circ \longrightarrow 1$ was converted into the adsorbed volume by assuming the adsorbate to have the normal *liquid* density at the operational temperature.

There are a number of possible explanations to account for the lack of agreement between various values v_p in Table 11.5. First, it must be kept in mind that the total uptake at high p/p° is controlled by three mechanisms: (1) the intracrystalline filling at low p/p°, (2) the multilayer adsorption on the external surface, and (3) capillary condensation within a secondary pore structure. Process (2) and process (3) are manifested in the form of a finite multilayer slope and by a hysteresis loop in the capillary condensation range (Kenny and Sing, 1990).

Various procedures have been proposed for the evaluation of the true intracrystalline capacity and the external surface area (see Sayari *et al.*, 1991). The α_S-method is one way of analysing composite isotherms, which has been applied to nitrogen isotherms on different samples of ZSM-5 (Sing, 1989). This approach was used by Gil *et al.* (1995) in their recent study of the microporosity of pillared clays and zeolites. By this means, mesopores were estimated to have contributed about 25% to the total pore volume of a commercial sample of HZSM-5.

By using relatively large crystals of HZSM-5 (of length *c.* 350 μm), Müller and Unger (1988) were able to obtain the isotherms of Ar and N_2 shown in Figure 11.18. These results demonstrate the advantage of studying larger crystals than had been possible in previous work. With each adsorptive, the very low slope in the multilayer range provided unambiguous confirmation that the external surface area was very small and therefore that the amount adsorbed at the plateau corresponded to the micropore capacity.

In Figure 11.18 the argon isotherm is apparently a classical Type I isotherm, whereas the nitrogen isotherm has a well-defined hysteresis loop in the region of $p/p^\circ = 0.12$–0.15. The nitrogen loop has upper and lower closure points and is quite stable and reproducible. This phenomenon must not be confused with the more common form of low-pressure hysteresis, which is much less well defined and persists to the lowest attainable pressures. However, a loop in this region of a nitrogen

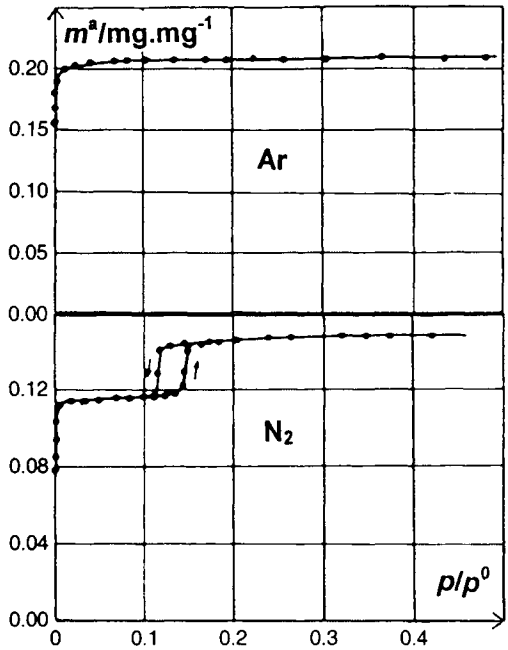

Figure 11.18. Adsorption isotherms of Ar and N_2 on HZSM-5 (reproduced courtesy of Müller and Unger, 1988).

isotherm is not associated with capillary condensation, since at 77 K this can occur only at $p/p^\circ > 0.4$ (see Chapter 7).

For reasons to be given later, Müller and Unger (1988) decided to evaluate the micropore volume from the uptakes of nitrogen and argon at $p/p^\circ = 0.1$. The nitrogen capacity was therefore taken near the end of the first plateau (i.e. before the hysteresis loop). As before, the adsorbate densities were assumed to be equal to the liquid density. But now, the values of intracrystalline pore volume are much lower than the previously estimated nitrogen value of v_p: 0.144 $cm^3\,g^{-1}$ (by nitrogen) and 0.147 $cm^3\,g^{-1}$ (by argon). The fact that the two values are in such close agreement is consistent with the apparent liquid-like character of *both* adsorbates. Also, by supposing that nitrogen has a solid-like packing at the second plateau, we can explain why the ratio of the uptakes (*c.* 0.78) is extremely close to the ratio of the nitrogen solid and liquid densities.

Detailed investigations (Müller and Unger, 1988) of the novel hysteresis loop revealed that it became more pronounced as the crystal size of the HZSM-5 was increased and its aluminium content was reduced. In fact, the most prominent loop was given by uniform crystals (of *c.* 150 μm) of pure Silicalite-I. In this case, the almost vertical riser of the associated substep corresponded to loadings of *c.* 25–30 molec uc^{-1} (molecules per unit cell).

Microcalorimetric and high-resolution adsorption measurements (Müller *et al.*, 1989)

have revealed the presence of smaller sub-steps in the isotherms of both argon and nitrogen at *c.* 22 molec uc^{-1}. These sub-steps can be seen in Figures 11.19 and 11.20.

Related studies of the energetics of adsorption have been made by means of Tian–Calvet isothermal microcalorimetry (Llewellyn *et al.*, 1993a,b). The results for argon and nitrogen adsorption on Silicalite I are given along with the corresponding isotherms in Figures 11.19 and 11.20. With each adsorptive on pure Silicalite, the differential adsorption enthalpy, $\Delta_{ads}\dot{h}$, remains almost constant over a wide range of loading, until $N^{\sigma} \approx 20$ molec uc^{-1}. In the case of argon, this is followed by a single broad peak in $\Delta_{ads}\dot{h}$ over the range $N^{\sigma} = 22$–30 molec uc^{-1}, which corresponds to the riser of the sub-step.

As might be expected, the behaviour of nitrogen on Silicalite-I is more complex. There are now two peaks, the first being located between two regions of minima of $\Delta_{ads}\dot{h}$. The first peak, labelled 1, is at $N^{\sigma} = 22$–25 molec uc^{-1}, and the second broad peak, labelled 2, is over the range $N^{\sigma} = 25$–30 molec uc^{-1}, again corresponding to the locations of the isotherm sub-steps.

Neutron diffraction experiments (Reichert *et al.*, 1991; Llewellyn *et al.*, 1993a,b) have confirmed that the sub-steps and associated energy changes are due to phase transitions in the adsorbate. In the case of argon, the sharp sub-step and exothermic change appeared to be due to a transition from a disordered phase to a solid-like structure with diffraction peaks which remained stable over the temperature range 10–100 K. Nitrogen underwent a similar overall change, but this took place in two stages. The first, transition 1, involved a change from a disordered mobile phase to a localized state (or lattice fluid-like phase). The second and larger, transition 2, led to the formation of a solid-like commensurate structure. It appears that the zeolite itself can undergo a change in structure, which may be initiated by the adsorption

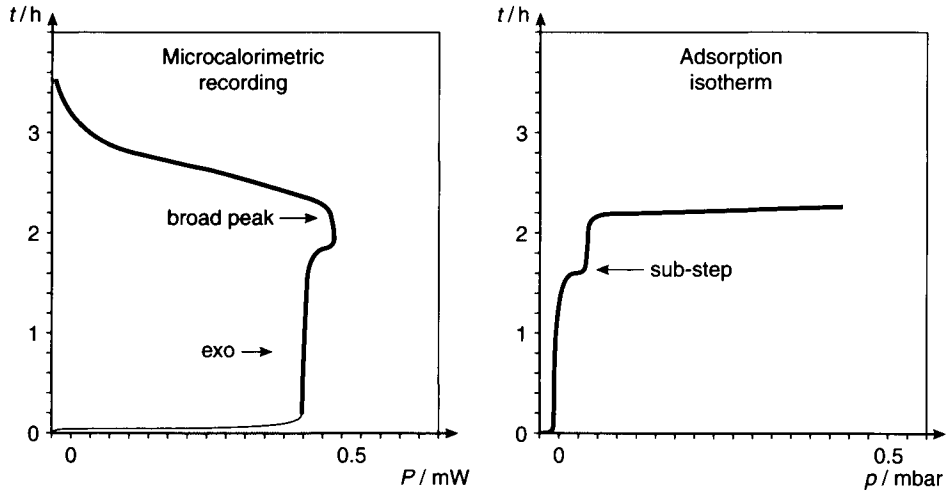

Figure 11.19. Adsorption isotherm and corresponding microcalorimetric recording for argon at 77 K on Silicalite-I (reproduced courtesy of Y. Grillet and P.L. Llewellyn, personal communication).

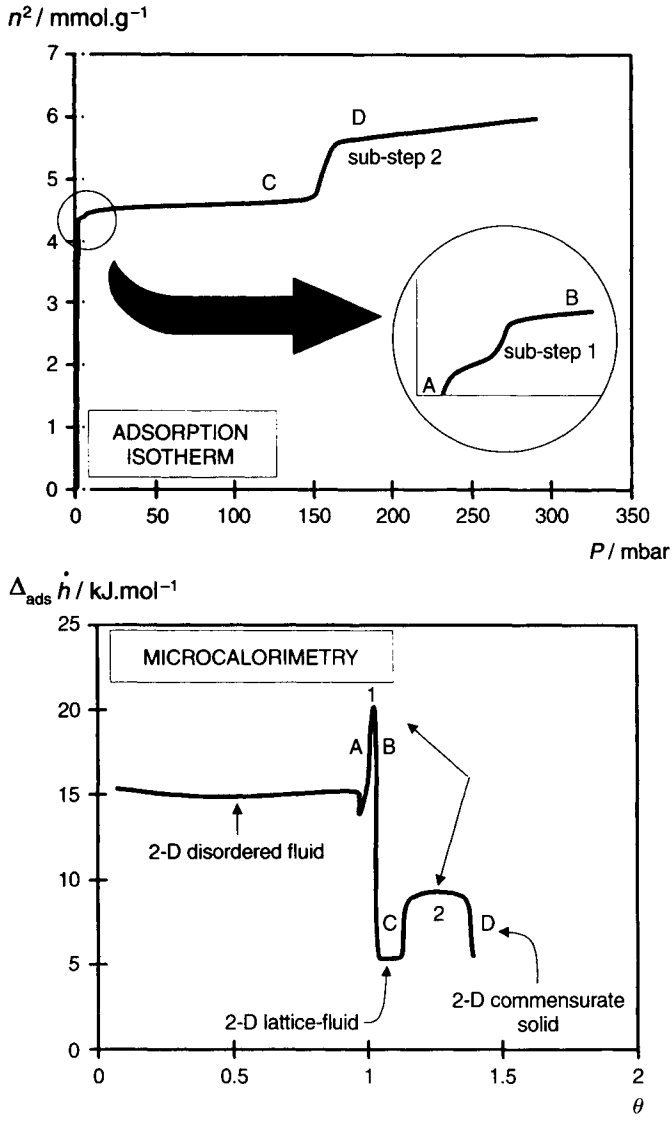

Figure 11.20. Isotherm and enthalpy of adsorption for nitrogen at 77 K on Silicalite-I (after Llewellyn *et al.*, 1993b).

process, but this alone would seem unlikely to account for the change in state of the adsorbate.

Because the 77 K isotherms are very steep (i.e. high adsorption affinity), it is very difficult to undertake any form of virial analysis. The few detailed nitrogen isotherms so far determined (Reichert *et al.*, 1991) at higher temperatures (i.e. 293–373 K) on Silicalite and HZSM-5 have indicated that Henry's law is obeyed at low fractional

loading. The derived values of isosteric enthalpies of adsorption are 15.0 ± 1.3 kJ mol^{-1} and within experimental error appear to be very similar for Silicalite-I and HZSM-5. These values are consistent with the microcalorimetric measurements of the energies of adsorption at 77 K.

The work of Llewellyn *et al.* (1993a,b) also showed the effect of changing the Si/Al ratio in the MFI structure. As noted in the earlier work of Müller and Unger (1988), the sub-steps become less distinctive and finally almost disappear completely as the Al content is increased. Furthermore, the nitrogen adsorption calorimetric measurements reveal a significant increase in energetic heterogeneity, which is due to the development of field gradient–quadrupole interactions between N_2 molecules and the Al and cationic sites.

Adsorbent–adsorbate potential energy calculations have been made for the adsorption of argon in the channels and intersections of Silicalite-I (Müller *et al.*, 1989). The most favourable sites for localized adsorption are within the straight and sinusoidal channels, which together should be able to accommodate 20 molec uc^{-1}. At a loading of 24 molec uc^{-1} all the available sites in the channels and intersections are probably occupied by localized molecules.

As predicted, at low loadings, argon and nitrogen are adsorbed in a very similar manner on pure Silicalite. Thus, in each case the adsorption energy remains almost constant until $N^{\sigma} = 20$ molec uc^{-1}. This suggests that localized adsorption is taking place with very little adsorbate–adsorbate interaction. The adsorbed molecules are mainly located in the channels and at a lower concentration in the intersections.

A small increase in adsorption energy may be due to co-operative interactions within the intersections, but this is quickly followed by the first phase transition, which involves a more drastic change in the packing density of argon than of nitrogen. The fact that the Ar transition 1 can take place at a much lower p/p° than the corresponding N_2 transition 2 is associated with the difference in the electronic properties of the two adsorbates. The non-polar nature of Ar must allow the adsorbed molecules to more readily undergo adsorbate–adsorbate interactions and hence give the opportunity for close-packing and hence densification of the adsorbate structure.

It seems likely that repulsion between the ends of the quadrupolar nitrogen molecules is responsible for the sharp fall in adsorption energy which precedes its transition 2. The sub-step 2 is probably accompanied by the reorientation of the molecules to permit a more favourable quadrupole–quadrupole interaction: i.e. to allow the end of one molecule to approach the centre of its neighbour. This transformation could lead to the development of the quasi-crystalline order by the formation of a chain-like structure (Sing and Unger, 1993). It is not surprising to find that hysteresis is involved in the more drastic molecular rearrangement of adsorbed nitrogen. An energy barrier must be overcome and since each molecular domain is so uniform, the macroscopic result is the appearance of a well-defined hysteresis loop with reproducible boundaries and scanning behaviour (Reichert *et al.*, 1991).

It is of interest to compare the behaviour of argon and nitrogen with that of other adsorptives on Silicalite-I. Recent work (Llewellyn *et al.*, 1993a,b) has shown that in certain respects krypton and argon behave in a similar way. Thus, up to the loading $N^{\sigma} \approx 20$ molec uc^{-1} the adsorption energies at 77 K are both constant and almost

identical. The type 2 sub-steps are also similar in character; but, in contrast to Ar, the Kr sub-step is associated with an endothermic change. At present, the explanation for this difference is not clear, but it must be kept in mind that the Kr molecule is rather more bulky than Ar and therefore the endothermic phenomenon may be the result of confinement effects within the micropore network (Derycke *et al.*, 1991). No indication of a phase transformation has so far been found with methane at 77 K. In this case, the adsorption energy also remains constant up to $N^{\sigma} \approx 20$ molec uc^{-1}, but thereafter it decreases sharply (Llewellyn *et al.*, 1993a).

It is perhaps not surprising to find that the adsorption of carbon monoxide at 77 K on the series of MFI-type zeolites is very similar to nitrogen adsorption (Llewellyn *et al.*, 1993). On Silicalite-I, CO also gives the transitions 1 and 2 and increase of Al in the MFI structure has the same effect of smoothing the isotherm and producing energetic heterogeneity. Indeed, because of the more polar character of CO, there is a somewhat larger change in the energetics of adsorption.

The Al content has an even greater influence on the level of the adsorption of water vapour by the MFI-type zeolites. In their original work, Flanigen *et al.* (1978) drew attention to the similarity of Silicalite to adsorbent carbons in having a low affinity for water. It has been found (Kenny and Sing, 1990; Carrott *et al.*, 1991) that the low uptake of water vapour by Silicalite-I (at say, 293 K) extends over virtually the complete range of p/p°. To illustrate this behaviour, the apparent fractional pore filling by water and nitrogen is compared in Figure 11.21.

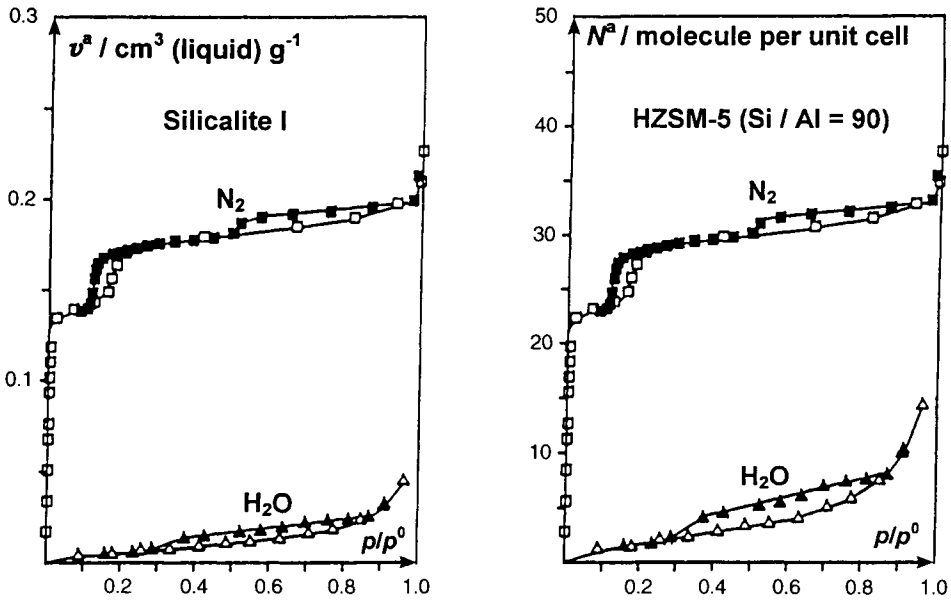

Figure 11.21. Adsorption of nitrogen and water vapour on Silicalite-I and water vapour on HZSM-5 (Si/Al = 90) (Sing, 1991).

A number of interesting features can be seen in Figure 11.21. First, the level of water adsorption at $p/p° = 0.90$ by Silicalite-I is only about 10% of the capacity available for nitrogen and other small adsorptive molecules (see Table 11.5). This is increased to about 18% for HZSM-5, when the Si/Al ratio is reduced to 90. The presence of the hysteresis loops in the capillary condensation range indicates that a high proportion of the water adsorption has occurred within the secondary pore structure or defect structure rather than in the zeolitic channel structure. Similar findings have been reported by Llewellyn *et al.* (1996).

Another interesting feature is the reversibility of the water isotherms at low $p/p°$. This is in marked contrast to the low-pressure hysteresis exhibited by water isotherms determined on most other forms of dehydroxylated silicas.The fact that there is no apparent tendency for rehydroxylation suggests that water does not easily penetrate into the intracrystalline pores of Silicalite or HZSM-5 to any great extent. However, in the work of Llewellyn *et al.* (1996), water was condensed on the Silicalite-I sample at $p/p° = 1.0$ and this did produce an irreversible change in the low pressure region of the water isotherm.

In seeking an explanation for these findings, we must take into account the geometry of the pores in addition to their size. As we have seen, the intracrystalline pores of the Silicalite/ZSM-5 system are for the most part tubular and of ≈0.55 nm diameter. In such a confined space, a three-dimensional array of the hydrogen-bonded water structure cannot be accommodated without some considerable distortion of the directional hydrogen bonds. The situation is quite different in the case of carbon molecular sieves, which have slit-shaped pores.

The molecular sieving behaviour of Silicalite-I, as illustrated in Table 11.5 by the low saturation uptakes of neopentane and *o*-xylene, is primarily dependent on size exclusion. It is of interest that *n*-nonane has been found to give an isotherm of essentially Type I character at 296 K (Grillet *et al.*, 1993). The initial part of this isotherm was completely reversible, but a small sub-step at $p/p° \approx 0.2$ was followed by a long plateau and associated narrow, Type H4, hysteresis loop. The plateau was located at $N^{\sigma} \approx 4$ molec uc^{-1}. This level of pre-adsorption was sufficient to block the whole of the intracrystalline pore structure. The accessibility to nitrogen was gradually restored by the progressive removal of the nonane. These results confirm the complexity of the nonane pre-adsorption and entrapment in relation to the pore network and indicate that there is no simple relation between the thermal desorption of *n*-nonane and the adsorbent pore structure.

References

Annabi-Bergaya F., Cruz M.I., Gatineau L. and Fripiat J.J. (1979) *Clay Minerals* **14**, 249.

Annabi-Bergaya F., Cruz M.I., Gatineau L. and Fripiat J.J. (1981) *Clay Minerals* **16**, 115.

Atkinson D. and Curthoys G. (1981) *J. Chem. Soc., Faraday Trans. I* **77**, 897.

Atlas of Zeolite Structure Types (1992) *Atlas of Zeolite Structure Types* (W.M. Meier and D.H. Olson, eds), International Zeolite Association, Butterworth-Heinemann, London.

Avgul N.N., Bezus A.G., Dobrova E.S. and Kiselev A.V. (1973) *J. Colloid Interface Sci.* **42**, 486.

Barrer R.M. (1945) *J. Soc. Chem. Ind.* **64**, 130.

Barrer R.M. (1966) *J. Colloid Interface Sc.* **21**, 415.
Barrer R.M. (1978) *Zeolites and Clay Minerals*, Academic Press, London.
Barrer R.M. (1981) *J. Chem. Tech. Biotechnol.* **31**, 71.
Barrer R.M. (1982) *Hydrothermal Chemistry of Zeolites*, Academic Press, London.
Barrer R.M. (1989) *Pure Appl. Chem.* **61**, 1903.
Barrer R.M. and Kelsey, K.E. (1961) *Trans. Faraday Soc.* **57**, 625.
Barrer R.M. and McLeod D.M. (1954) *Trans. Faraday Soc.* **50**, 980.
Barrer R.M. and MacLeod D.M. (1955) *Trans. Faraday Soc.* **51**, 1290.
Barrer R.M. and Reay J.S.S. (1957) In: *Proc. Second Int. Congress on Surface Activity II* (J.H. Schulman, ed.), Butterworths, London, p. 79.
Bergaoui L., Lambert J.F., Vicente-Rodriguez M.A., Michot L.J. and Villieras F. (1995) *Langmuir* **11**, 2849.
Bergaya F. (1995) *J. Porous Mater.* **2**, 91.
Bergaya F., Gatineau L. and Van Damme H. (1993) In: *Multifunctional Mesoporous Inorganic Solids* (C.A.C. Sequeira and M.J. Hudson, eds), Kluwer, Dordrecht, p. 19.
Bernier, A., Admaiai, L.F. and Grange, P. (1991) *Appl. Catalysis*, **77**, 269
Breck D.W. (1974) *Zeolite Molecular Sieves*, Wiley, New York.
Breck D.W., Eversole W.G., Milton R.M., Reed T.B. and Thomas T.L. (1956) *J. Am. Chem. Soc.* **78**, 5963.
Brindley G.W. and Sempels R.E. (1977) *Clay Mineral* **12**, 229.
Burch R. (1987) *Catalysis Today* **2**, 185.
Carrott P.J.M. and Sing K.S.W. (1986) *Chem. & Ind.* 786.
Carrott P.J.M., Kenny M.B., Roberts R.A., Sing K.S.W. and Theocharis C.R. (1991) In: *Characterization of Porous Solids II* (F. Rodriguez-Reinoso, J. Rouquerol, K.S.W. Sing and K.K. Unger, eds), Elsevier, Amsterdam, p. 685.
Cases J.M., Lietard O., Yvon J. and Delon J.F. (1982) *Bull. Mineral.* **105**, 439.
Cases J.M., Cunin P., Grillet Y., Poinsignon C. and Yvon J. (1986) *Clay Minerals* **21**, 55.
Cases J.M., Grillet Y., François M., Michot L., Villieras F. and Yvon J. (1991) In: *Characterization of Porous Solids II* (F. Rodriguez-Reinoso, J. Rouquerol, K.S.W. Sing and K.K. Unger, eds), Elsevier, Amsterdam, p. 591.
Cases J.M., Berend I., Besson G., François M., Uriot J.P., Thomas F. and Poirier J.E. (1992) *Langmuir* **8**, 2730.
Cool P. and Vansant E.F. (1996) *Microporous Mater.* **6**, 27.
Dailey J.S. and Pinnavaia T.J. (1992) *Chem. Mater.* **4**, 855.
de Boer J.H., Lippens B.C., Linsen B.G., Broekhoff J.C.P., van den Heuvel A. and Osinga Th.J. (1966) *J. Colloid Interface Sci.* **21**, 405.
De Stefanis A., Perez G. and Tomlinson A.A.G. (1994) *J. Mater. Chem.* **4**, 959.
Delville A. and Sokolowski S. (1993) *J. Phys. Chem.* **97**, 6261.
Denayer J.F.M. and Baron G.V. (1997) *Adsorption* **3**, 251.
Derouane E.G. (1980) In: *Catalysis by Zeolites* (B. Imelik, C. Naccache, Y. Ben Taarit, J.C. Vedrine, G. Coudurier and H. Praliaud, eds), Elsevier, Amsterdam, p. 5.
Derycke L., Vigneron J.P., Lambin P., Lucas A.A. and Derouane E.G. (1991) *J. Chem. Phys.* **94**, 4620.
Diano W., Rubino R. and Sergio M. (1994) *Microporous Mater.* **2**, 179.
Dubinin M.M. (1975) In: *Progress in Surface and Membrane Science*, vol. 9, Academic Press, New York, p. 1.
Farfan-Torres E.M., Dedeycker O. and Grange P. (1991) In: *Preparation of Catalysts V* (G. Poncelet, P. Grange and B. Delmon, eds), Elsevier, Amsterdam, p. 337.
Feijen E.J.P., Martens J.A. and Jacobs P.A. (1997) In: *Handbook of Heterogeneous Catalysis*, vol. 1 (G. Ertl, H. Knozinger and J. Weitkamp, eds), Wiley-VCH, Weinheim, p. 311.
Flanigen E.M., Bennett J.M., Grose R.W., Cohen J.P., Patton R.L., Kirchner R.M. and Smith J.V. (1978) *Nature* **271**, 512.
Fripiat J.J. (1997) In: *Handbook of Heterogeneous Catalysis*, vol. 1 (G. Ertl, H. Knozinger and J. Weitkamp, eds), Wiley-VCH, Weinheim, p. 387.
Galarneau A., Barodawalla A. and Pinnavaia T.J. (1995) *Nature*, **374**, 529.
Gil A. and Grange P. (1996) *Colloids and Surfaces*, **113**, 39.

Gil A., Massinon A. and Grange P. (1995) *Microporous Mater.* **4**, 369.
Gregg S.J. (1968) *Chem. & Ind.* 611.
Gregg S.J. and Packer R.K. (1954) *J. Chem. Soc.* 3887.
Gregg S.J. and Stephens M.J. (1953) *J. Chem. Soc.* 3951.
Gregg S.J., Parker T.W. and Stephens M.J. (1954) *J. Appl. Chem.* **4**, 666.
Grillet Y., Cases J.M., François M., Rouquerol, J. and Poirier J.E. (1988) *Clays and Clay Minerals* **36**, 233.
Grillet Y., Llewellyn P.L., Kenny M.B., Rouquerol F. and Rouquerol J. (1993) *Pure Appl. Chem.* **65**, 2157.
Hampson J.A. and Rees L.V.C. (1993) In: *Fundamentals of Adsorption*, vol. IV (M. Suzuki, ed.), Kodansha, Tokyo, p. 259.
Jacobs P.A. and Martens J.A. (1987) *Synthesis of High-silica Aluminosilicate Zeolites*, Elsevier, Amsterdam.
Kacirek H., Lechert H., Schweitzer W. and Wittern K.-P. (1980) In: *Properties and Applications of Zeolites* (R.P. Townsend, ed.), The Chemical Society, London, p. 164.
Kenny M.B. and Sing K.S.W. (1990) *Chem. & Ind.* 39.
Kirkby N.F. (1986) In: *Membranes in Gas Separation and Enrichment*, Special Publication 62, Royal Society of Chemistry, London, p. 221.
Kiselev A.V. (1965) *Disc. Faraday Soc.* **40,** 205.
Kiselev A.V. (1967) *Adv. Chromatogr.* **4**, 113.
Kokotailo G.T., Lawton S.L., Olson D.H. and Meier W.M. (1978) *Nature* **272**, 438.
Llewellyn P.L., Coulomb J.-P., Grillet Y., Patarin J., Lauter H., Reichert H. and Rouquerol J. (1993a) *Langmuir* **9**, 1846.
Llewellyn P.L., Coulomb J.-P., Grillet Y., Patarin J., Andre G. and Rouquerol J. (1993b) *Langmuir* **9**, 1852.
Llewellyn P.L., Grillet Y. and Rouquerol J. (1994a) *Langmuir* **10**, 570.
Llewellyn P.L., Pellenq N., Grillet Y., Rouquerol F. and Rouquerol J. (1994b) *J. Therm. Anal.* **42**, 855.
Llewellyn P.L., Grillet Y., Schüth F., Reichert H. and Unger K.K. (1994c) *Microporous Mater.* **3**, 345.
Llewellyn P.L., Grillet Y., Rouquerol J., Martin C. and Coulomb J.-P. (1996) *Surface Sci.* **352**, 468.
Ma Y.H. (1984) In: *Fundamentals of Adsorption* (A.L. Myers and G. Belfort, eds), Engineering Foundation, New York, p. 315.
Martens J.A., Souverijns W., van Rhijn W. and Jacobs P.A. (1997) In: *Handbook of Heterogeneous Catalysis, I* (G. Ertl, H. Knözinger and J. Weitkamp, eds), Wiley-VCH, Weinheim, p. 324.
Martens J.A., Souverijns W., Verrelst W., Parton R., Froment G.F. and Jacobs P.A. (1995) *Angew. Chem. Int. Ed.* **34**, 2528.
Müller U. and Unger K.K. (1986) *Fortschritte der Mineralogie* **64**, 128
Müller U. and Unger K.K. (1988) In: *Characterization of Porous Solids I* (K.K. Unger, J. Rouquerol, K.S.W. Sing and H. Kral, eds), Elsevier, Amsterdam, p. 101.
Müller U., Reichert H., Robens E., Unger K.K., Grillet Y., Rouquerol F., Rouquerol J., Pan D. and Mersmann A. (1989) *Fresenius Z. Anal. Chem.* 1.
Ohtsuka K., Hayashi Y. and Suda M. (1993) *Chem. Mater.* **5**, 1823.
Reed T.B. and Breck D.W. (1956) *J. Am. Chem. Soc.* **78**, 5972.
Reichert H., Muller U., Unger K.K., Grillet Y., Rouquerol F., Rouquerol J. and Coulomb J.-P. (1991) In: *Characterization of Porous Solids II* (F. Rodriguez-Reinoso, J. Rouquerol, K.S.W. Sing, and K.K. Unger, eds), Elsevier, Amsterdam, p. 535.
Rouquerol J., Avnir D., Fairbridge C.W., Everett D.H., Haynes J.M., Pernicone N., Ramsay J.D.F., Sing K.S.W. and Unger K.K. (1994) *Pure Appl. Chem.* **66**, 1739.
Ruthven D.M. (1984) *Principles of Adsorption and Adsorption Processes*, Wiley, New York, p. 51.
Ruthven D.M. and Loughlin K.F. (1972) *J. Chem. Soc., Faraday Trans. I* **68**, 696.
Sayari A., Crusson E., Kaliaguine S. and Brown J.R. (1991) *Langmuir* **7**, 314.
Schirmer W., Thamm H., Stach H. and Lohse U. (1980) In: *Properties and Applications of Zeolites* (R.P. Townsend, ed.), The Chemical Society, London, p. 204.
Sing K.S.W. (1989) *Colloids and Surfaces* **38**, 113.

Sing K.S.W. (1991) In: *3rd Fundamentals of Adsorption* (A.B. Mersmann and S.E. Scholl, eds), Engineering Foundation, New York, p. 78.
Sing K.S.W. and Unger K.K. (1993) *Chem. & Ind.* 165.
Sircar S. (1993) In: *Fundamentals of Adsorption IV* (M. Suzuki, ed.), Kodansha, Tokyo, p. 3.
Srasra E., Bergaya F., Van Damme H. and Ariguib N.K. (1989) *Appl. Clay Sci.* **4**, 411.
Sterte J. (1991) *Clays and Clay Minerals*, **39**, 167.
Thamm H. (1987) *Zeolites* **7**, 341.
Thamm H., Stach H. and Fiebig W. (1983) *Zeolites* **3**, 94.
Thomas J.M. (1994) *Nature* **368**, 289.
Thomas J.M. (1995) *Faraday Discuss.* **100**, C9
Thomas J.M. and Theocharis C.R. (1989) In: *Modern Synthetic Methods*, vol.5 (R. Scheffold, ed.), Springer-Verlag, Berlin, p. 249.
Thomas J.M., Bell R.G. and Catlow C.R.A. (1997) In: *Handbook of Heterogeneous Catalysis*, vol. 1 (G. Ertl, H. Knozinger and J. Weitkamp, eds), Wiley-VCH, Weinheim, p. 286.
Trillo J.M., Alba M.D., Castro M.A., Poyato J. and Tobias M.M. (1993) *J. Mater. Sci.* **28**, 373.
Van Damme H., Levitz P., Fripiat J.J., Alcover J.F., Gatineau L. and Bergaya F. (1985) In: *Physics of Finely Divided Matter* (N. Boccara and M. Daoud, eds), Springer-Verlag, Berlin, p. 24.
van Olphen H. (1965) *J. Colloid Sci.* **20**, 822.
van Olphen H. (1976) In: *Characterization of Powder Surfaces* (G.D. Parfitt and K.S.W. Sing, eds), Academic Press, London, p. 428.
Vaughan D.E.W. (1988) In: *Catalysis Today*, Elsevier, Amsterdam, p. 187.
Vaughan D.E.W., Maher P.K. and Albers E.W. (1974) U.S. Patent 3 838 037 (to WR Grace and Co).
Yang R.T. (1987) *Gas Separation by Adsorption Processes*, Butterworths, Boston, p. 263.
Zhu H.Y., Gao W.H. and Vansant E.F. (1995) *J. Colloid Interface Sci.* **171**, 377.

This Page Intentionally Left Blank

CHAPTER 12

Properties of Some Novel Adsorbents

12.1. Introduction

Before the mid-1940s few systematic attempts appear to have been made to optimize the properties of such common adsorbents as activated charcoal, silica gel and activated alumina. The increase in research and development activity after the Second World War was largely due to the demand for improved catalysts and adsorbents. It was already known that the extent of the accessible surface was of fundamental importance (Rideal, 1932). In the 1940s the interest in gas adsorption was undoubtedly stimulated by the perceived success of the BET method for the determination of the surface area.

The aim of much of the early post-war research was to maximize the specific surface of the traditional adsorbents. This work led to an improved understanding of the mechanisms of activation, ageing and sintering (Gregg, 1960, 1961; de Boer, 1972; Renou *et al.*, 1960; Rouquerol *et al.*, 1975, 1979, 1985; Rouquerol and Ganteaume, 1977; Sing, 1972, 1973). It became evident that reproducible adsorbent activity could be achieved only if a particular adsorbent was prepared under carefully controlled conditions. The three most important general procedures for the preparation of high-area (i.e. 'active') solids were: (a) precipitation-gelation, (b) grinding, and (c) heat treatment.

12.1.1. Precipitation-gelation

Dispersed solid particles are generally considered to exhibit colloidal behaviour when at least one dimension is in the range 1–1000 nm (Everett, 1988). If we take the simplest case of a colloidal system of equal-sized spheroidal particles, we may easily calculate the area of the liquid–solid interface with the aid of Equation (1.1), i.e. $a = 6/\rho d$. Thus, if the particle diameter, d, is 1 nm and its absolute density, ρ, is 3 g cm^{-3}, then $a = 2000$ m^2 g^{-1}, which of course represents the area of unit mass of the dispersed solid. It might be expected that by careful removal of the continuous liquid phase, it would be possible to convert such a colloidal dispersion of 1 nm particles into a powder of very high surface area. Although powders with specific areas of over 1000 m^2 g^{-1} can be produced in this way (e.g. from alumina flocs), they tend to undergo rapid ageing and consequently cannot be regarded as useful adsorbents.

The adsorbent properties are more stable and reproducible if the particles are cross-linked in the form of a gel. However, even in this case an appreciable change always occurs when an oxide hydrogel is dried in the normal manner and thereby converted into a stable xerogel. Thus, a drastic collapse of the weak solid framework is the result of the strong capillary forces associated with the formation of a curved liquid–vapour meniscus during the removal of capillary water from the hydrogel (see Section 10.2.3). As explained in Chapter 10, the collapse can be minimized if the wet gel is dried in an autoclave at a temperature above the critical temperature of the liquid; in this way an aerogel is produced. An alternative method is to hydrolyse an alkoxide with the minimum amount of water and then apply hypercritical conditions to remove the alcohol from the oxide 'alcogel'. This approach has been used to obtain aerogels with surface areas of over 1000 m^2 g^{-1} (Teichner, 1986).

12.1.2. Grinding

Comminution by grinding (or milling) is perhaps the most obvious way of attempting to increase the surface area of a given mass of solid. With some layer structures such as clays and graphite, an appreciable increase in specific area can be achieved by prolonged grinding (Gregg, 1961), but this is not on the scale required to give a highly active adsorbent. Also, the reduction of particle size by grinding is of limited applicability and is energy-demanding. The disintegration is opposed by the tendency of the fine particles to stick together – to minimize the free surface energy. A state of 'grinding equilibrium' is attained when the rate of surface formation is equal to the loss of surface by aggregation. Under these conditions, the surface area is not increased by further milling. Although particle size reduction is of great importance in powder technology, it is not a generally viable approach for the production of industrial adsorbents.

12.1.3. Heat treatment (calcination)

In reviewing the preparation of highly disperse solids, Gregg (1960) pointed out that an active solid can often be prepared by a thermal decomposition reaction of the type:

$$\text{Solid A} = \text{Solid B} + \text{Gas}$$

The specific surface of the freshly formed solid B is likely to be much larger than that of solid A. The reason for the generation of a large internal surface is that thermal decomposition of A generally occurs at a lower temperature than that required to bring about the crystal growth (and sintering) of B. Thus, the freshly formed crystallites of B adopt a form of pseudo-lattice of A, the pores and internal surface being created by the removal of the volatile component (Gregg, 1961).

Some of the best-known examples of this type of reaction are the thermal decomposition of hydroxides to give 'active' oxide-hydroxides and oxides (see Section 10.3.6). Another example is the calcination of a carbonate (e.g. $CaCO_3$). In fact, BET areas of up to 500 $m^2\ g^{-1}$ can be produced by the calcination of an aluminium trihydroxide. But, unless the heat treatment is carefully regulated, as in controlled rate thermal analysis (CRTA), the pore structure of the active product tends to be highly heterogeneous (Rouquerol and Ganteaume, 1977).

All active solids are metastable and the loss of area may occur at temperatures well below the Tamman temperature, at which the 'classical' form of sintering normally begins to become important. As we have seen in Chapter 10, water plays a key role in the ageing of the metastable oxides and oxide-hydroxides (Sing, 1972). This can be a serious problem when oxide adsorbents and catalysts are exposed to water vapour.

As the shortcomings of the traditional preparative methods outlined above became apparent, it was realized that alternative procedures were required to produce uniform or tailor-made adsorbents and shape-selective catalysts. As we saw in Chapter 11, one major route was opened up by the Linde synthesis in 1956 of the crystalline molecular sieve zeolite A. The search for new microporous crystalline materials has continued unremittingly and has resulted in the synthesis of novel zeolitic structures including the aluminophosphates, which are featured in this chapter.

With the growing interest in nanochemistry (Ozin, 1992), many attempts have been made in recent years to prepare porous crystals having larger channel widths than those in the aluminosilicate zeolites (i.e. ≈ 0.8 nm). In particular, great excitement was generated by the preparation of the wide-pore aluminophosphate , VPI-5, by Davis and his co-workers in 1988 and again when the first member of a new group of 'mesoporous molecular sieves', MCM-41, was prepared by Mobil scientists in 1992.

It was once taken for granted that adsorbents were required in the form of fine powders, porous granules or extrudates. However, other physical forms such as porous fibres are now available for special applications such as membranes for gas separation or water treatment. Carbon cloth provides an interesting example of a highly active form of fibrous carbon.

Another novel form of adsorbent is controlled pore glass (CPG), which is widely used as a stationary phase in chromatography (Schnabel and Langer, 1991). CPG is manufactured by leaching out the borate phase from phase-separated borosilicate glass. Although the CPG has a relatively narrow distribution of interconnected mesopores, the solid glass structure lacks any well-defined crystallinity. To overcome this problem, Gelb and Gubbins (1998) have adapted a new molecular dynamics

procedure to mimic the formation of CPG. In this manner, it is possible to generate a series of model CPG pore structures, which can be used as notional, but 'realistic', adsorbents for the calculation by GCMC simulation of adsorption isotherms. Since the chemical and physical properties of the simulated structures are known with great accuracy, this approach appears to offer a new basis for the comparison of the BET, BJH and other procedures for the determination of surface area and pore size distribution.

Our selection of 'novel adsorbents' for discussion in this chapter is somewhat arbitrary: the term 'novel' is used here to indicate some unusual aspect of particular interest. In discussing the distinctive properties of the few selected novel adsorbents, we aim to show the direction of current research and, as before, illustrate the principles developed in earlier chapters.

12.2. Carbons

12.2.1. Superactive carbons

It is not at all difficult to produce activated carbons with BET areas of at least 1000 $m^2 g^{-1}$. Indeed, the adsorbent activity can be increased well beyond this level by chemical activation with phosphoric acid (Baker, 1992) followed by the controlled heat treatment of certain impregnated precursors such as hardwoods (Jagtoyen and Derbyshire, 1993) or olive stones (Molina-Sabio *et al.*, 1995; Rodriguez Reinoso *et al.*, 1995). Typical commercial products have BET areas in the range 500–2000 $m^2 g^{-1}$ (Baker, 1992), but it is evidently more technologically demanding to manufacture 'superactive carbons' with significantly larger BET areas.

A novel method of chemical activation for producing some of the most active adsorbents so far developed was disclosed by AMOCO (Standard Oil Company) scientists in 1978 (Wennerberg and O'Grady, 1978). These superactive carbons were prepared by the high-temperature heat treatment of petroleum coke or coal mixed with excess amounts of potassium hydroxide. After removal of the remaining KOH and other soluble material, the products were reported to have BET areas of over 2300 $m^2 g^{-1}$.

Adsorption isotherms of nitrogen (at 77 K), toluene (at 293 K) and water vapour (at 294 K) on a sample of AMOCO superactive carbon, PX21, are shown in Figure 12.1. The magnitude of the adsorption capacities and the hydrophobic nature of the PX21 are clearly evident. Different samples of PX21 have been found to have BET-nitrogen areas of *c.* 3700 $m^2 g^{-1}$ and total pore volumes of *c.* 1.8 $cm^3 g^{-1}$ (Harrison *et al.*, 1979; Atkinson *et al.*, 1982).

The first commercial plant for the production of the AMOCO superactive carbons was constructed by the Anderson Development Company, Michigan. Their products were claimed to have BET areas in the range 2800–3500 $m^2 g^{-1}$ and total pore volumes of 1.4–2.0 $cm^3 g^{-1}$. The properties of one batch of the Anderson superactive carbon, designated AX-21 (BET area, 2960 $m^2 g^{-1}$; micropore volume, 1.4 $cm^3 g^{-1}$), have been investigated in some detail (Carrott *et al.*, 1987, 1988, 1989b). More

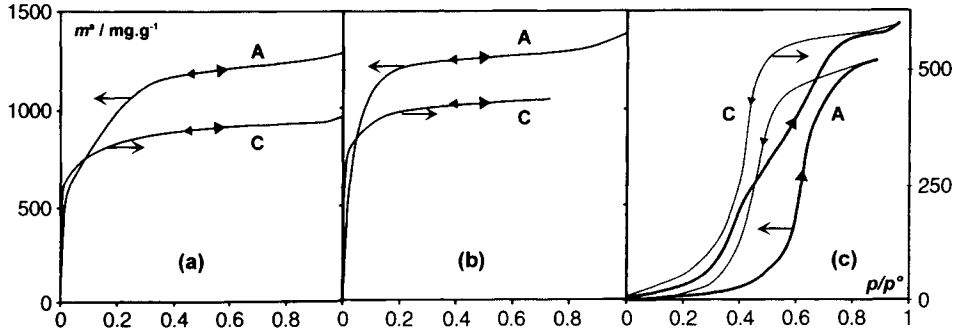

Figure 12.1. Adsorption–desorption isotherms of (a) nitrogen at 77 K, (b) toluene at 20°C and (c) water at 21°C, on AMOCO carbon PX21 (A) and charcoal cloth AM4 (C) (Atkinson *et al.*, 1982).

recently, the AMOCO process has been further developed and extended by the Kansai Coke and Chemicals Company of Japan. Their extremely active carbons, which are now marketed as powdered and granular forms of MAXSORB, are produced by the KOH activation of petroleum coke, coal or coconut shell char.

In the preparative procedure described by Otowa *et al.* (1993), mixtures of petroleum coke and excess amounts of KOH were dehydrated at 400°C and then heated under nitrogen flow at 600–900°C. The activated materials were washed thoroughly with water to remove KOH and K_2CO_3. Certain batches of MAXSORB prepared in this manner were reported to have BET areas $> 3100\ m^2\ g^{-1}$ and total pore volumes $> 2.5\ cm^3\ g^{-1}$ (Otowa, 1991; Otowa *et al.*, 1993, 1996). In a systematic investigation of the activation process, Otowa and his co-workers (1993, 1996) found that the K_2O, formed by the dehydration of KOH, reacted with CO_2 (produced by the water gas-shift reaction) to give K_2CO_3. Intercalation of metallic potassium, which was also formed at temperatures > 700°C, appeared to be responsible for the drastic expansion of the carbonized material and hence the creation of a large specific surface and enormous pore volume.

In view of the complexity of the system, it is not surprising that the untreated MAXSORB had a high concentration of surface functional groups (–COOH, –OCO and –OH, in similar proportions). However, it appears that these could be largely removed by further heat treatment in an inert atmosphere at 700°C (Otowa *et al.*, 1996). This form of after-treatment did not affect the excellent correlation obtained between methylene blue adsorption and the BET area, but it did lead to a considerable improvement in the breakthrough performance for the removal of $CHCl_3$ from water. On the other hand, the presence of the surface functional groups was found to be beneficial for some applications (e.g. for the double layer capacitance storage of electricity).

Argon and nitrogen adsorption measurements on PX21 and AX21 were displayed in Chapter 9 (see Figures 9.11, 9.15 and 9.16). The α_S-plots and differential energies of adsorption for Ar and N_2 have together revealed that physisorption at 77 K occurs in four stages: (1) primary micropore filling in ultramicropores at $p/p° < 0.01$; (2)

Table 12.1. Values of ultramicropore and supermicropore volumes and surface areas derived from nitrogen isotherms.

Adsorbent	PX21	AX21
Total micropore volume ($cm^3\ g^{-1}$)	1.75	1.52
Ultramicropore volume ($cm^3\ g^{-1}$)	0.39	0.36
Supermicropore volume ($cm^3\ g^{-1}$)	1.36	1.16
BET area ($m^2\ g^{-1}$)	3700	3390
Supermicropore area ($m^2\ g^{-1}$)	2140	2170
External area ($m^2\ g^{-1}$)	165	210

monolayer adsorption on the supermicropore surface at $p/p^\circ < 0.05$; (3) co-operative micropore filling of supermicropores and reversible capillary condensation in narrow mesopores; (4) multilayer adsorption on the external surface at $p/p^\circ > 0.4$. On this basis, we are now able to obtain a more detailed analysis of the nitrogen α_s-plots in Figure 9.11 than was given in Chapter 9. The effective values of the ultramicropore and supermicropore volumes and the supermicropore and external surface areas given in Table 12.1 are derived from nitrogen isotherms by the procedures described in Chapter 8.

The analysis in Table 12.1 indicates that about 20% of the total effective micropore volume of PX21 can be attributed to the volume of ultramicropores (i.e. those pores giving primary micropore filling by nitrogen at 77 K). Similarly, in the case of AX21, the primary micropore filling by nitrogen occurs in only about 25% of the total micropore volume. It is therefore apparent that a high proportion of the pore space is located within a supermicropore structure (i.e. with an effective pore size of *c.* 0.8–2 nm). This is consistent with the electron microscopic investigation of the AMOCO carbon by Marsh *et al.* (1982), which has revealed the presence of cage-like supermicropores of width > 1 nm.

As was pointed out in Chapter 6, the BET area cannot always be assumed to represent the true surface area of a microporous adsorbent. However, we consider that the derived values of supermicropore area and external area in Table 12.1 do give a useful indication of the extent of these regions of the overall surface.

The preponderance of supermicropores is responsible for the relative positions of the differential adsorption energy curves for nitrogen and argon in Figure 9.16 and also for the order of magnitude of the integral energies of adsorption plotted in Figure 12.3. As a result of the broad micropore size distribution in the AMOCO carbon PX21, the energies of adsorption are consistently lower than those obtained with many other microporous carbons. This aspect is discussed later in this chapter (see Section 12.2.2).

A gas chromatographic study (Carrott and Sing, 1990) of the adsorption of a series of hydrocarbons (C_2–C_6) by the AMOCO AX21 carbon has revealed some unusual features. Thus, values of the height equivalent to a theoretical plate (HETP) over the range 90–120°C were found to be independent of both the adsorptive and the temperature. Furthermore, over the range of gas flow rate studied, only the initial section of the Van Deemter plot could be observed (in contrast to the behaviour of other microporous carbons). At present, the explanation for this behaviour is not entirely

clear, but it seems likely that the chromatographic results are in part due to a very high degree of interconnectivity within the pore structure of AX21.

In this book we have generally adopted the convention of expressing the adsorption as the amount adsorbed by *unit mass* of the outgassed adsorbent. From a technological standpoint, however, it is sometimes more important to consider the amount adsorbed per *unit volume* of the adsorbent. It is evident that when this change is made for a powder of low bulk density such as AX21 (bulk density ≈ 0.3 g cm^{-3}) the available adsorbing capacity is much less impressive (Sing, 1989). For this reason, for a particular purpose it may be necessary to employ an adsorbent of moderate activity rather than one of very high specific activity.

12.2.2. Activated carbon fibres and carbon cloth

The first high-strength carbon fibres were produced in the 1950s (see Donnet and Bansal, 1984). The early carbonized products were rayon-based, but it was soon found that the mechanical properties and the carbon yield could be improved by the use of polyacrylonitrile (PAN) as the precursor. Also, less expensive fibres of somewhat lower strength and modulus could be made from various other precursors including petroleum pitch and lignin. However, cotton and other forms of natural cellulose fibres possess discontinuous filaments and the resulting mechanical properties were consequently found to be inferior to those of the rayon-based fibres.

It was not long before the first *activated* carbon fibres (ACFs) were developed. In the work of Economy and Lin (1971, 1976) highly porous carbon fibres were prepared from Kynol, a fibrous phenolic precursor. Carbonization was carried out in nitrogen at 800°C and activation occurred in steam at 750–1000°C. The products appeared to be predominantly microporous and were found to be effective for the removal of low levels of certain pollutants (e.g. phenol and pesticides) from air or aqueous solutions.

Another important development was the disclosure by Bailey and Maggs (1972; Bailey *et al.*, (1973) of a novel procedure for the manufacture of 'charcoal cloth'. The continuous process developed in the laboratories of the Chemical Defence Establishment, Porton Down, England, involved three main stages: (1) immersion of the roll of viscose rayon cloth in an aqueous solution of inorganic chlorides (e.g. $ZnCl_2$, $AlCl_3$ and NH_4Cl); (2) oven drying in nitrogen; (3) carbonization and activation in carbon dioxide.

The Type I character of the nitrogen and toluene isotherms displayed in Figure 12.1 indicates that a typical sample of activated charcoal cloth produced by the original Porton process had novel adsorbent properties. The activated material was strong and flexible and had a BET area of over 1200 m^2 g^{-1}, a wide distribution of micropores (no detectable mesoporosity) and a small external surface area (Atkinson *et al.*, 1982; Hall and Williams, 1986). In view of its early promise, it was logical to attempt to control the pore structure of charcoal cloth. A systematic study of the development of porosity was therefore undertaken by Atkinson *et al.* (1982, 1984) and Freeman *et al.* (1987–1991).

It was soon established that the micropore capacity of the chloride-impregnated rayon char was progressively increased by CO_2 activation and that the main effect of the pre-treatment with $ZnCl_2$, NH_4Cl or $AlCl_3$ was at the carbonization stage (Atkinson *et al.*, 1982). Indeed, micropore structures can be produced simply by the carbonization of untreated rayon in nitrogen at temperatures of *c.* 600°C (Bohra and Sing, 1985), but the pores are easily blocked and the adsorption data are difficult to interpret.

Nitrogen isotherms, which were determined after the CO_2 activation of untreated rayon chars, are analysed in Table 12.2, the derived areas and pore volumes being obtained by the procedures described in Chapter 8. It can be seen that the supermicropore volume and area increased progressively with percentage burn-off, whereas the ultramicropore volume remained virtually constant. The external area also underwent little change until the burn-off exceeded 70%. The extent of the mesoporosity remained very small throughout the series (Freeman *et al.*, 1990; Carrott and Freeman, 1991).

As already indicated, microporous materials are produced by the CO_2 activation of unimpregnated or chloride-impregnated viscose rayon. Other procedures are required to obtain mesoporous carbon cloth. One method is to use steam as the activating gas (Freeman *et al.*, 1990; Tomlinson and Theocharis, 1992). For example, activation in steam of a particular chloride-impregnated rayon to a 75% burn-off resulted in extensive mesopore formation, giving a three-fold increase in the total pore volume (to $\approx 1.5\ cm^3\ g^{-1}$). This enlargement of the pore volume appeared to be the result of overall widening of the original micropores since the impregnant residues had little effect on the gas/carbon reaction.

An alternative method of generating mesoporosity is to pre-treat the viscose rayon with aqueous solutions of either borates or phosphates. Pre-treatment with borate tends to lead to a CO_2-activated material having rather broad, ill-defined distribution of pore size (Freeman *et al.*, 1987), whereas phosphate impregnation results in a well-defined mesopore structure (Freeman *et al.*, 1988). The effect of the addition of 5% sodium dihydrogen phosphate is illustrated in Figure 12.2, where the micropore and mesopore volumes are plotted against percentage burn-off. Over the range of 10–70% burn-off, the mesopore volume has increased from *c.* 0.1 to $1.0\ cm^3\ g^{-1}$, while the micropore volume has remained almost constant.

With both the borate- and phosphate-impregnated rayon, the mesoporosity appears to be developed independently of the inherent microporosity and not as the result of

Table 12.2. Evolution of the micropore structure of untreated carbon cloth (analysis of nitrogen isotherms of Carrott and Freeman, 1991).

Micropore structure	Percentage burn-off				
	20	31.2	49.7	70.1	92.0
Total micropore volume ($cm^3\ g^{-1}$)	0.35	0.47	0.67	0.85	1.11
Ultramicropore volume ($cm^3\ g^{-1}$)	(0.34)	(0.34)	0.34	0.34	0.34
Supermicropore volume ($cm^3\ g^{-1}$)	(0.01)	(0.13)	0.33	0.51	0.77
Supermicropore area ($m^2\ g^{-1}$)	—	(500)	1030	1520	1690
External area ($m^2\ g^{-1}$)	20	30	30	50	200

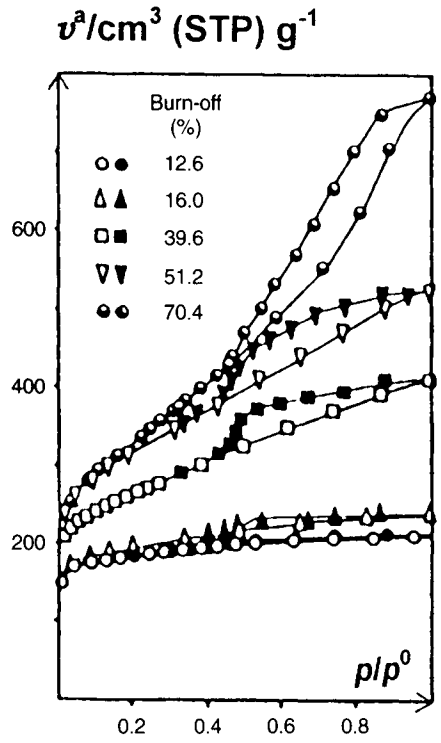

Figure 12.2. Nitrogen isotherms at 77 K, showing the development of mesopore volume in activated carbon cloth prepared by the impregnation of viscose rayon with 5% sodium dihydrogen phosphate and a mixture of chlorides (Freeman *et al.*, 1988).

overall pore widening (Freeman and Sing, 1991). The application of transmission electron microscopy has confirmed the difference in these mesopore structures and those produced by steam activation (Freeman *et al.*, 1989).

Other investigations of the porosity of activated carbon cloth explored the effects of impregnation with certain transition metal salts and oxo-complexes (Freeman *et al.*, 1989) and of activation in ammonia (Tomlinson *et al.*, 1993). In the latter case it was found that ammonia reacts with the viscose rayon chars to form various nitrogen-containing microporous products. An early study by Barton and Koresh (1983) had also demonstrated that the pore structure of carbon cloth and its affinity for water vapour can be modified by HNO_3 activation.

Exploratory investigations (Freeman *et al.*, 1991, 1993) of the use of more highly ordered polymeric precursors have shown that there remains considerable scope for the development of novel activated chars from synthetic textile fibres. For example, carbon dioxide breakthrough measurements revealed that activated carbons prepared from Kevlar interacted much more strongly with CO_2 than rayon-based chars. Thus, the latter showed very little ability to separate air and CO_2, in marked contrast to the Kevlar-derived materials.

One of the first industrial companies to appreciate the potential importance of charcoal cloth was Siebe Gorman & Co Ltd, UK, who developed a batchwise manufacturing process in the early 1970s. Their commercial 'C-Tex' grades are now produced in various forms including knitted and woven materials. Charcoal cloth is coming to be widely used for respiratory protection against noxious gases (Hall and Sing, 1988), the removal of unpleasant odours (e.g. in colostomy odour filters), water filtration and in medical dressings (Wright *et al.*, 1988). Specific adsorptive properties and catalytic activity can be generated by the impregnation of activated carbon cloth with silver, copper, platinum and some other metals (Hall *et al.*, 1985; Brown *et al.*, 1987; Gimblett *et al.*, 1989).

In separational and catalytic technology, there are several advantages of using fibres in place of powders, pellets or granules. An important operational advantage is the low resistance to fluid flow which, together with the relatively short molecular diffusion path within the fibre, can result in remarkably fast adsorption kinetics (Gimblett *et al.*, 1989; Suzuki, 1994). The unique combination of texture and adsorbent properties provided by carbon cloth has been found to be of potential significance for gas chromatography. Thus, it is possible to construct an efficient chromatographic 'column' by clamping together 15–20 discs of carbon cloth (Carrott and Sing, 1987). This arrangement can be used for studying the low-coverage energetics of alkanes, alkenes and other organic molecules (Carrott *et al.*, 1989a).

In characterizing the adsorptive properties of their original charcoal cloth, Bailey and Maggs (1972) adopted the traditional 'heat of wetting' (i.e. energy of immersion) method (see Smisek and Cerny, 1970). Although in this form, immersion calorimetry is now known to be of limited value, it can yield useful information provided that it is applied under carefully controlled conditions (see Chapter 5). In this manner, the Tian–Calvet microcalorimetric technique was used (Atkinson *et al.*, 1982) to determine the energies of immersion of the standard Porton charcoal cloth (AM4), a superactive carbon (PX21) and a graphitized carbon black (Vulcan 3G) in a series of organic liquids. The results are recorded in Table 12.3.

The results in Table 12.3 confirm that the areal energies of immersion (column 7) of graphitized carbon black increase progressively with increase in carbon number. This behaviour is of course consistent with the results presented in Figure

Table 12.3. Energies of immersion for charcoal cloth AM4, AMOCO carbon PX21 and graphitized carbon black Vulcan 3G in organic liquids at 300 K (Atkinson *et al.*, 1982).

Immersion liquid	AMOCO PX21		C cloth AM4		Vulcan 3G	
	($J\ g^{-1}$)	($mJ\ m^{-2}$)	($J\ g^{-1}$)	($mJ\ m^{-2}$)	($J\ g^{-1}$)	($mJ\ m^{-2}$)
n-Hexane	245	66	94	74	6.1	86
Cyclohexane	190	51	97	77	5.8	82
Neohexane	190	52	72	58	5.3	75
Toluene	271	73	155	123	8.2	115
Mesitylene	300	81	161	128	9.8	138
Isodurene	305	82	154	122	10.7	150

Areal values in $mJ\ m^{-2}$ are based on BET-nitrogen areas.

1.5. However, because of the unreliability of the BET areas, it is not possible to arrive at an unambiguous interpretation of the energy data on the two microporous carbons.

A thermodynamically rigorous treatment is to transform the energies of immersion into integral energies of adsorption. The derived values of $\Delta_{ads}U$ for the liquids listed in Table 12.3 are plotted against the carbon number of the adsorptive in Figure 12.3. As already indicated, the difference in the overall energies of adsorption by activated carbon cloth and superactive carbon is clearly evident in Figure 12.3. However, the information provided by the comparison of *integral* energies of adsorption is still of limited value.

To make further progress, it is appropriate to revisit the differential adsorption energies for argon and nitrogen in Figures 9.15 and 9.16. As previously pointed out, the difference in behaviour of carbon cloth JF005 and the AMOCO carbon PX21 is especially striking. Since this particular sample of carbon cloth contained a high proportion of ultramicropores, the large adsorption energy manifested at low $p/p°$ can be attributed to primary micropore filling within slit-shaped ultramicropores. This behaviour is consistent with the molecular sieve character of JF005 revealed in Figure 9.19 and is in marked contrast to the behaviour of carbon cloth JF518 in Figure 9.21.

In their adsorption properties, carbon cloth samples JF516 and JF518 appear to be somewhat similar to the AMOCO carbon PX21. Also, we note the intermediate nature of the two samples JF142 and JF144. These and many other adsorption measurements confirm that it is now possible to produce a wide range of activated carbons in stable cloth-form with remarkably well-controlled pore structures.

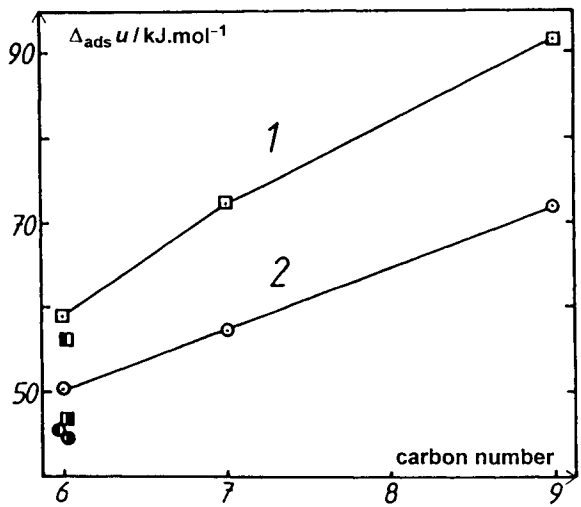

Figure 12.3. Integral molar energies of adsorption given by the immersion of carbon cloth AM4 (1) and superactive PX21 (2) in organic liquids plotted against carbon number (Atkinson *et al.*, 1984).

In recent years, extensive studies have been undertaken by Kaneko and his co-workers of the properties of activated carbon fibres (ACFs) produced from cellulose, polyacrylonitrile (PAN) and pitch. X-ray diffraction and electron microscopy revealed that the PAN-based and pitch-based fibres had a more homogeneous pore structure than that of the cellulose-based material, although the latter had the largest surface area and pore volume (Kakei *et al.*, 1990).

The distinctive shapes of the nitrogen isotherms and derived α_S-plots on the Japanese ACFs appeared to be consistent with a two-stage mechanism of micropore filling. However, the corresponding DR plots were composed of three or four linear regions, which were assumed to represent different steps in a multistage process (Kakei *et al.*, 1990). Analysis of the argon isotherms on the same adsorbents (Kakei *et al.*, 1991) appeared to provide further evidence for the three stages of physisorption within micropores (see Chapter 8): (1) the filling of ultramicropores; (2) monolayer adsorption on the walls of wider pores; and (3) co-operative filling of the wider micropores.

In discussing the significance of their results, Kaneko and his co-workers have pointed out that since their activated carbon fibres had a high level of micrographitic structure there was likely to be a close relationship between the pore width distribution and the graphitic interlayer spacing. Thus, the primary micropore filling process was thought to occur within bilayer-sized slit-shaped pores (≈ 0.7 nm), which were regarded as the ultramicropores. Monolayer adsorption (stage 2) was believed to occur on the walls of the tri- and four-layer-sized pores (i.e. the supermicropores of 1.1 and 1.5 nm width), to be followed by the filling (stage 3) of the inner supermicropore volume.

In our view this picture is probably oversimplified: electron microscopy has revealed that although the pores in activated carbons tend to be slit-shaped, they are not all strictly parallel-sided (Byrne and Marsh, 1995). Moreover, it is known that the physisorption of certain polar molecules is accompanied by some micropore swelling (Kaneko *et al.*, 1989). However, it seems reasonable to conclude that a hypothetical graphitic type of pore structure is a useful ideal model, to which some ACFs may conform more closely than others.

Recently, Setoyama *et al.* (1996) have extended their earlier investigations of the properties of fluorinated activated carbons. Nitrogen isotherms were determined both before and after the fluorination of cellulose-based ACF. Analysis of the α_S-plots and the corresponding DR plots has indicated that although the micropore capacity and width were reduced, the micropore structure appeared to become more homogeneous as a result of fluorination.

In another recent investigation, Wang and Kaneko (1995) determined SO_2 isotherms and energies of adsorption on a pitch-based ACF. The relatively strong adsorption at low p/p° was ascribed to a combination of enhanced non-specific dispersion interactions and specific permanent dipole-induced dipole interactions. The differential energies of SO_2 adsorption underwent little further change until the fractional micropore filling exceeded ≈ 0.6. The sharp increase observed at high fractional filling was attributed to dipole–dipole interactions between the adsorbed molecules.

12.2.3. Buckyballs and buckytubes

The discovery in 1985 of the buckminster fullerene C_{60} by Kroto, Curl, Smalley and their co-workers immediately created enormous interest in this new form of carbon. As is now well known, the spherical molecule (diameter ≈ 1 nm) has a soccerball-like structure, being composed of a stable cage of carbon atoms arranged in the form of six- and five-membered rings. The name 'buckminster fullerene' (now popularly reduced to 'buckyball') was inspired by the geodesic dome designed by the architect R. Buckminster Fuller. Although at first regarded as a rarity, it was soon discovered that C_{60} could be readily synthesized (along with C_{70}). The availability of gram quantities has allowed the chemical and physical properties of the C_{60} fullerene to be studied in some detail.

Several investigations have been undertaken of the physisorption of gases by C_{60} crystals. In the work of Ismail and Rodgers (1992) a very large difference was obtained between the apparent surface area available for nitrogen and krypton adsorption at 77 K ($\approx 5\ m^2\ g^{-1}$) and carbon dioxide adsorption at 298 K ($132\ m^2\ g^{-1}$). This apparent discrepancy cannot be explained in terms of molecular packing within the adsorbed monolayer. Instead, it was much more likely to be due to the greater translational energy of CO_2 (i.e. at the higher temperature), which allowed it to penetrate into regions that were inaccessible to N_2 and Kr. At first, it was not clear whether these regions were well-defined micropores or simply vacancies (defects) between the individual C_{60} molecules. The microporous character of a batch of C_{60} powder appeared to be confirmed by Kaneko *et al.* (1993): their Type I nitrogen isotherms were analysed by the α_S-method and the total surface area was estimated to be $24\ m^2\ g^{-1}$ and the external area to be about $1\ m^2\ g^{-1}$. The latter value was found to be in agreement with the crystal size determined by electron microscopy.

The porous nature of the C_{60} crystals has now been examined in more detail by Kaneko and his co-workers (Setoyama *et al.*, 1996; Thess *et al.*, 1996). The C_{60} powder was recrystallized from carbon disulfide and then studied before and after annealing by heat treatment. The nitrogen adsorption measurements revealed that the recrystallized material was both microporous and mesoporous; the mesoporosity was completely removed by heat treatment, but the sample remained microporous. Since the micropores and the C_{60} molecules appeared to be of similar size, it was concluded that the micropores were largely in the form of molecular defects and lattice vacancies.

Carbon nanotubes (or 'buckytubes') were first described by Iijima in 1991 as 'helical tubules of graphitic carbon'. They are multilayered hollow microtubes, each layer being a cylindrical graphitic (graphene) sheet. The diameter of the inner cavity is generally in the range 2–10 nm and the length is typically 200–500 nm (Cook *et al.*, 1996). The number of carbon layers (1–50) varies from one tube to another. Multi-walled buckytubes were first synthesized by the arc vaporization of carbon electrodes, but other preparative methods are now available including the laser vaporization of doped graphite rods (Thess *et al.*, 1996).

Although no experimental measurements of the adsorption of gases by buckytubes appear to have been reported, a useful molecular simulation study has been made by Maddox and Gubbins (1995). The value of this approach is two-fold: first, it predicts

the adsorption behaviour of buckytubes of various types and dimensions; and second, it improves our understanding of the mechanisms of pore filling.

In their study of three different buckytube models, Maddox and Gubbins used grand canonical Monte Carlo (GCMC) molecular simulation to calculate the isotherms and isosteric enthalpies for the adsorption of argon and nitrogen. The computational methodology was similar to that outlined in Chapter 8. The buckytube models were: (a) a semi-infinite, single-layer tube of diameter 1.02 nm; (b) a semi-infinite tube of diameter 4.78 nm of two rolled-up graphite sheets; and (c) an open-ended tube of diameter 4.78 nm of two rolled-up graphite sheets.

The above values of pore diameter are the distances between the centres of the carbon atoms in the pore walls. From a practical standpoint (as pointed out in previous chapters) it has been customary to refer to the *effective* pore diameter (or width). In the case of a cylindrical buckytube, an approximate evaluation of the effective diameter is arrived at by allowing for the radius of the carbon atom (*c.* 0.17 nm). Thus, for the two model diameters considered by Maddox and Gubbins (i.e. 1.02 and 4.78 nm), the corresponding effective pore diameters are *c.* 0.7 and 4.4 nm. These are the values used in the following discussion.

It is not surprising to find that the narrow single-layer buckytube exhibits reversible primary micropore filling by both argon and nitrogen at 77 K. The isotherms are Type Ia: since there is an appreciable wall-to-wall overlap of the adsorbent–adsorbate interactions, the isosteric enthalpies are high (*c.* 16 and 17 kJ mol^{-1}, respectively) and the isotherms rise steeply from the origin (i.e. high affinities of adsorption). The narrow buckytube is filled at reduced pressures of *c.* 0.04 (i.e. equivalent to the experimental p/p°) and thereafter the isotherms are flat.

The wider buckytube (4.4 nm effective diameter) is in the mesopore range and, as expected, the 77 K isotherms are essentially Type IV, although the argon isotherm also displays some stepwise, Type VI character – as can be seen in Figure 12.4. The initial isosteric enthalpies are now *c.* 12 kJ mol^{-1} and both adsorptives give well-defined monolayer adsorption, but the second layering stage is much more distinctive in the case of argon. This difference is similar to that observed with graphitized carbon black.

The first-order capillary condensation step for nitrogen in Figure 12.4 occurs at the reduced pressure of 0.5. It is of interest to compare the effective diameter of 4.4 nm in the simulation model with the corrected pore width obtained by application of the Kelvin equation (with allowance for the multilayer thickness). Thus, according to the classical evaluation of the pore size, cylindrical pores of *c.* 3.9 nm diameter should undergo capillary condensation by nitrogen at $p/p^\circ = 0.5$. It is too early to say whether GCMC simulation gives a fairly accurate estimate of the pore size, but in this region of the isotherm it is likely to be more reliable than the Kelvin evaluation.

A number of other interesting features are brought to light by the GCMC simulation. For example, with the open-ended mesoporous buckytubes of less than about 30 nm long, end effects become increasingly important. This is because the adsorbent–adsorbate interactions at the ends of the tube are not the same as in the semi-infinite environment. The difference is especially striking in the hysteresis region, the area of the loop becoming smaller and the desorption branch losing its first-order character. It is concluded by Maddox and Gubbins that for a given system the critical

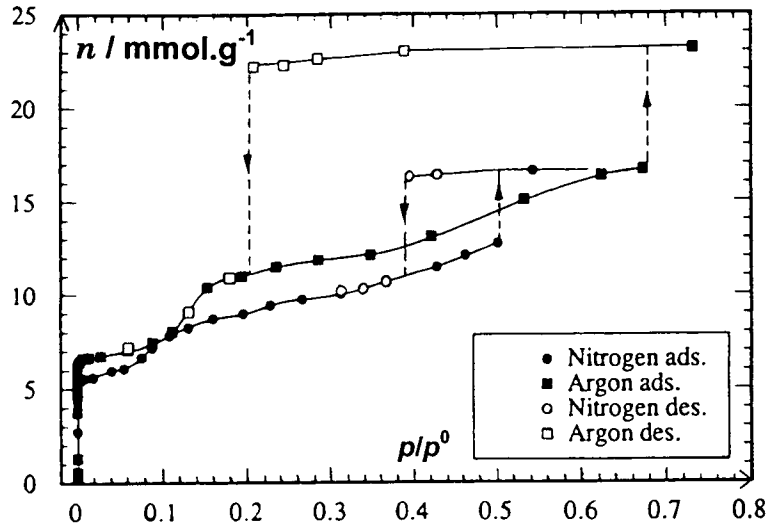

Figure 12.4. Simulated isotherms for the adsorption of argon and nitrogen at 77 K by a 4.4 nm bucky-tube (Maddox and Gubbins, 1995).

temperature for capillary condensation may be quite strongly dependent on the average pore length.

12.3. Nanoporous Inorganic Materials

12.3.1. MCM-41 and related structures

The synthesis of a new family of silicate/aluminosilicate mesoporous adsorbents was disclosed by Mobil scientists in 1992 (Kresge *et al.*, 1992; Beck *et al.*, 1992). These materials were first described as 'ordered mesoporous molecular sieves' and collectively designated M41S. So far, the most thoroughly investigated member of this new family is MCM-41 (Mobil Catalytic Material, number 41), which consists of an assemblage of non-intersecting tubular pores. As can be seen in Figure 12.5, the pore structure is composed of a hexagonal array of uniform channels of controlled size, typically of *c.* 4 nm diameter.

Formation

In their original synthesis of MCM-41, Beck *et al.* (1992) achieved the hydrothermal conversion of aluminosilicate gels in the presence of quaternary ammonium surfactants (e.g. hexadecyltrimethylammonium ions). The washed and air-dried products were calcined at 450°C to remove residual organic material.

It was considered by the Mobil scientists that the mesoporous structure was formed as a result of a 'liquid crystal templating' mechanism (see Figure 12.5) since the

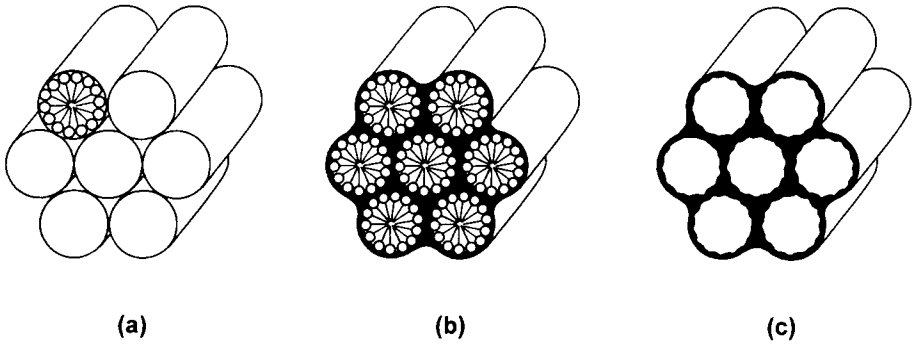

Figure 12.5. Schematic representation of the formation of MCM-41 by the liquid crystal templating mechanism first proposed by Kresge *et al.* (1992). (a) Hexagonal array of cylindrical micelles; (b) the same, with silicate species between the cylinders; and (c) hollow cylinders of MCM-41 after thermal elimination of organic material.

electron micrographs and diffraction patterns were remarkably similar to those given by the micellar phases of certain surfactant/water liquid crystals. The observed dependence of the pore width (within the range *c.* 1.5–10 nm) on the alkyl chain length and solubilization of organic oleophilic species was also consistent with the idea of a liquid crystal templating mechanism.

However, the exact nature of the intermediate products was unknown in 1992. Since then, Schüth, Stucky and their co-workers have studied in more detail the formation and morphology of various intermediate mesostructures (Monnier *et al.*, 1993; Huo *et al.*, 1994; Stucky *et al.*, 1994; Firouzi *et al.*, 1995). It now appears that a simple liquid crystal templating mechanism cannot explain the fact that the hexagonal surfactant/silicate phase can be produced at very low level surfactant concentrations, this being inconsistent with the pure surfactant phase diagram. It is therefore evident that the mesophase morphology is dependent *inter alia* on the nature of the lyotropic transformations and the interactions between the surfactant and the silicate phase. A generalized model, which makes use of the co-operative organization of inorganic and organic species into three-dimensional structured arrays, has been proposed for the synthesis of mesostructured oxides and nanocomposite materials (Ciesla *et al.*, 1994; Firouzi *et al.*, 1995).

Following the investigations of Schüth, Stucky and Unger and their co-workers, various procedures have been proposed for the preparation of M41S and other related materials. For example, Edler and White (1995) have described a method for the low-temperature synthesis of a pure silica form of MCM-41. An essential stage in their preparative route was the controlled ageing of the mixed solution of sodium silicate and cetyltrimethylammonium bromide (CTAB) before the intermediate product was filtered, washed, dried and finally calcined in air at 350°C. Comparison with standard hydrothermally produced material revealed no significant difference in the adsorption properties.

Inagaki *et al.* (1993) have reported the formation of highly ordered mesoporous materials from kanemite, a layered polysilicate, which was itself prepared from

hydrated sodium silicate. The kanemite was dispersed in an aqueous solution of hexadecyltrimethylammonium chloride and the mixture then heated at 70°C for several hours. HCl was added to bring the pH to 8.5. Finally, after it had been filtered and washed, the product was calcined in air at 700°C. Electron microscopy revealed the same type of hexagonal channel structure as that of MCM-41.

MCM-48 is another ordered mesoporous structure developed in the Mobil laboratories (Vartuli *et al.*, 1994); however, unlike MCM-41, it is composed of an interconnecting network of tubular pores. As in the case of MCM-41, it can be prepared in the form of a purely siliceous material or as an aluminosilicate. Schmidt *et al.* (1996) have described the synthesis of an MCM-48 of Si : Al ratio 22, in which the Al appeared to be only in the tetrahedral form.

Physisorption studies

Since 1992, physisorption isotherms have been reported on many different samples of MCM-41. Although all these isotherms have the general Type IV appearance, they are not all of exactly the same shape: a few are completely reversible, while others exhibit hysteresis. A series of systematic investigations (Branton *et al.*, 1993, 1995a, b, 1997) has shown that at certain temperatures the same adsorbent sample can give well-defined hysteresis with some adsorptives and reversible, or nearly reversible, isotherms with others. Furthermore, with certain systems (Ravikovitch *et al.*, 1995; Branton *et al.*, 1997), the hysteresis loop can be removed by increasing the operational temperature.

The nitrogen isotherm in Figure 12.6 was determined on a sample taken from a master batch prepared by Keung (1993) – in accordance with the original Mobil recipe. The most striking features are the sharp step over a narrow range of relative pressure, $p/p^\circ = 0.41–0.46$, and the overall reversibility of the isotherm. This is a rare example of a truly reversible Type IV isotherm, now designated a Type IVc isotherm (see Chapter 13). If the amount adsorbed is measured discontinuously (i.e. the usual procedure), it is necessary to allow at least 1 hour for the equilibration of each desorption point in the region of the step (Branton *et al.*, 1993). The absence of hysteresis with this particular grade of MCM-41 has been confirmed in several laboratories (Branton *et al.*, 1994; Llewellyn *et al.*, 1994a; Ravikovitch *et al.*, 1995). In the following discussion this grade is referred to as '4 nm MCM-41', or simply as the 4 nm sample of MCM-41.

The nitrogen isotherm data on non-porous hydroxylated silica in Table 10.1 (Bhambhani *et al.*, 1972) have been used to construct the α_S-plot in Figure 12.6. Since the initial linear section can be back-extrapolated to the origin, we are reasonably sure that monolayer–multilayer adsorption has occurred on the mesopore walls before the onset of pore filling at $p/p^\circ = 0.41$ and therefore that there was no detectable primary micropore filling at low p/p°. Similar results have been obtained by Kruk *et al.* (1997b) and Sayari *et al.* (1997).

The argon isotherm (at 77 K) on the 4 nm MCM-41, together with the corresponding α_S-plot, are given in Figure 12.7. The shape of the argon α_S-plot is again indicative of an abrupt change from monolayer–multilayer adsorption to pore filling. The adsorption isotherm of oxygen (at 77 K) on the same sample of 4 nm MCM-41 is also

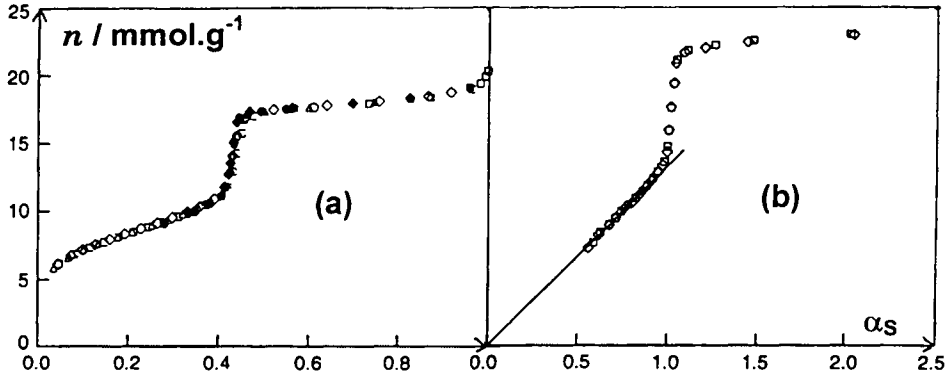

Figure 12.6. Adsorption isotherm of nitrogen (at 77 K) on 4 nm MCM-41. (b) The corresponding α_S-plot (Branton *et al.*, 1994).

shown in Figure 12.7. It is evident that the argon and oxgen isotherms have very similar hysteresis loops (of Type H1), in contrast to nitrogen.

The BET area, $a(\text{BET}, N_2) = 655\ \text{m}^2\ \text{g}^{-1}$, was derived from the slope and intercept of the nitrogen BET plot, which was linear over the range $p/p^\circ = 0.05$–0.32. By assuming that this area is also available for the adsorption of argon and oxygen, we may arrive at the values of apparent molecular area, σ, of each adsorptive in the BET monolayer. These values are given in Table 12.4. In the case of oxygen, the empirical value of σ is remarkably close to that ($\sigma = 0.143\ \text{nm}^2$) calculated from the liquid density. Although the argon value is in agreement with earlier empirical data obtained with non-porous and mesoporous oxides (Gregg and Sing, 1982), it is evidently appreciably larger than the area which would correspond to liquid packing (i.e. $0.138\ \text{nm}^2$).

Values of the total specific mesopore volume v_p(mes) in Table 12.4 have been obtained from the amounts adsorbed at $p/p^\circ = 0.95$, by making the usual assumption that the pores were filled with the condensed liquid adsorptive (i.e. assuming the validity of the Gurvich law). The fairly good agreement between the three values of v_p(mes) is consistent with the assumption that the capillary condensed state of argon is the supercooled liquid rather than the solid.

The sharp steps in the isotherms and α_S-plots suggest that capillary condensation has occurred in a narrow range of mesopores. The values of p/p° corresponding to the

Table 12.4. Adsorption of nitrogen, argon and oxygen on 4 nm MCM-41 by capillary condensation.

Adsorptive	n_m(BET) (mmol g^{-1})	σ (nm^2)	p/p° (range)	w_p (nm)	v_p(mes) ($cm^3\ g^{-1}$)
Nitrogen	6.71	(0.162)	0.41–0.46	3.3–4.3	0.64
Argon	6.51	0.167	0.38–0.42	3.5–4.8	0.61
Oxygen	7.52	0.145	0.34–0.37	3.1–4.4	0.64

From Branton *et al.* (1994).

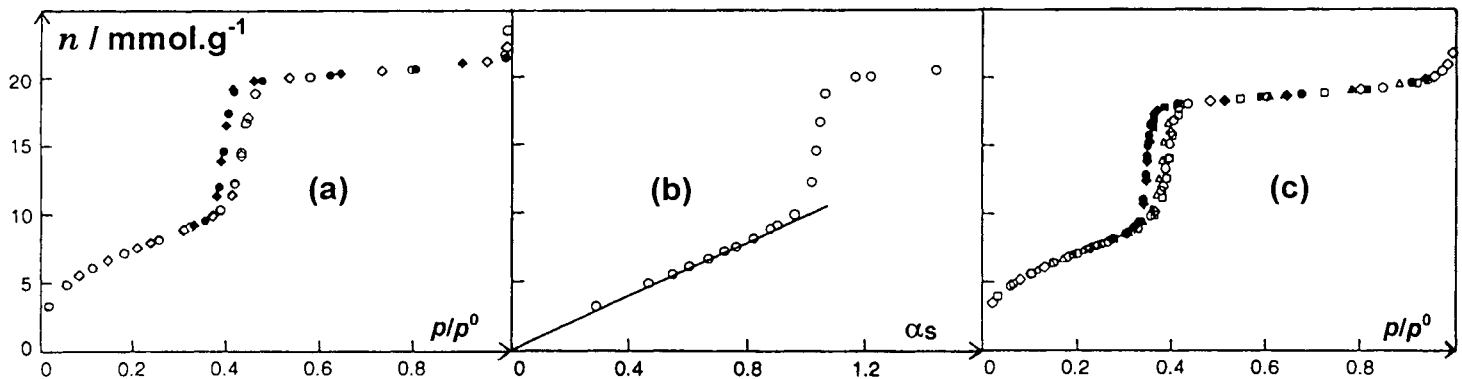

Figure 12.7. (a) Argon isotherm (at 77 K) on 4 nm MCM-41.
(b) Corresponding argon α_s-plot.
(c) Oxygen isotherm (at 77 K) on 4 nm MCM-41
(Branton *et al.*, 1994).

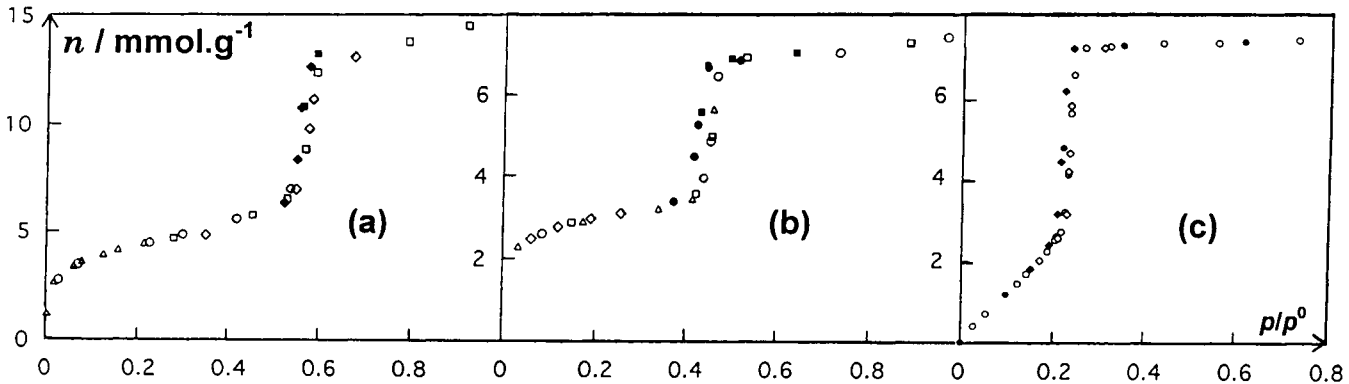

Figure 12.8. Adsorption isotherms of organic vapours.
(a) Methanol (at 290 K) on 4 nm MCM-41.
(b) Propan-1-ol (at 290 K) on 4 nm MCM-41.
(c) Carbon tetrachloride (at 303 K) on 3.4 nm siliceous MCM-41
(Branton *et al.*, 1995a, 1997).

beginning and end of each *desorption* step are indicated in Table 12.4 and the derived values of pore width, w_p, are obtained by application of Equations (7.10) and (7.11). Thus, the Kelvin equation is applied in its simplest form (assuming hemispherical meniscus and zero contact angle) with allowance made for multilayer adsorption on the pore walls. As pointed out in Chapter 7, there is little doubt that this is an over-simplification of the pore filling process. On the other hand, with MCM-41 it is to be expected that the tubular pore shape and absence of network percolation effects should at least minimize any deviation from the 'ideal' capillary condensation model. This appears to be confirmed by the fairly good agreement between the three ranges of w_p.

As already noted, although the nitrogen isotherm is reversible, the argon and oxygen isotherms exhibit well-defined hysteresis loops. Similar loops have been obtained with the following adsorptives on the same 4 nm sample of MCM-41: methanol, ethanol, propan-1-ol, butan-1-ol and water vapour (Branton *et al.*, 1995a), and carbon dioxide and sulfur dioxide (Branton *et al.*, 1995b). All of these loops are of Type H1 in the IUPAC classification, but there are significant differences in their widths. This is illustrated in Figure 12.8, where it can be seen that methanol at 290 K has given a narrower loop than propan-1-ol at 298 K.

Several recent investigations have been made of the dependence of isotherm shape on the pore size of MCM-41. The normalized nitrogen isotherms in Figure 12.9 exemplify the three types of isotherms given by MCM-41 adsorbents of different pore size. In accordance with previous work, a very steep and reversible pore filling riser is given by the 4 nm sample (over the range $p/p^\circ \approx 0.40$–0.44). The isotherm obtained on the 2.5 nm sample is also reversible, but in this case the pore filling has evidently occurred over a much wider range of p/p° (*c* 0.22–0.34). In contrast, the

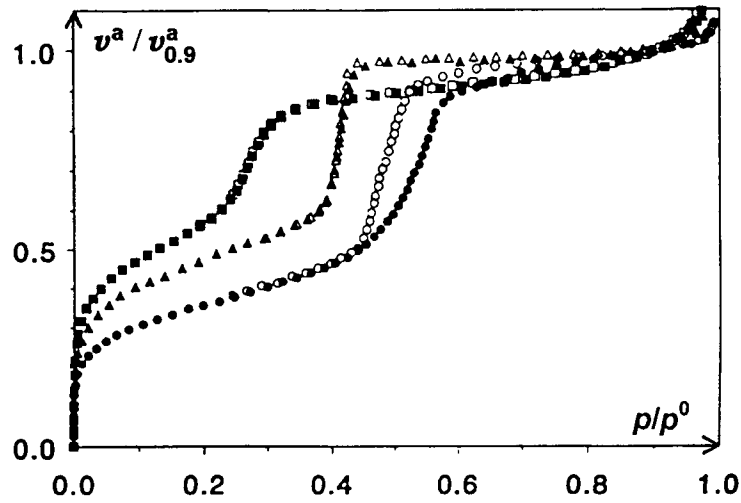

Figure 12.9. Normalized nitrogen isotherms on three samples of MCM-41 with apparent pore diameters of 2.5 (left), 4.0 (middle) and 4.5 nm (right) (Llewellyn *et al.*, 1994).

isotherm on the 4.5 nm sample is of a more usual Type IV shape with a well-defined hysteresis loop.

Somewhat similar differences in isotherm shape have been reported by other investigators (Franke *et al.*, 1993; Rathousky *et al.*, 1994; Ravikovitch *et al.*, 1995; Schmidt *et al.*, 1995; Llewellyn *et al.*, 1996). Very recently (Branton *et al.*, 1997), a 3.4 nm siliceous form of MCM-41 has been found to give a reversible Type IV nitrogen isotherm with a sharp pore-filling step in the range $p/p = 0.33–0.37$. The values of the BET area and pore volume derived from the nitrogen isotherm are recorded in Table 12.5. Carbon tetrachloride isotherms were determined on the 3.4 nm siliceous MCM-41 at the temperatures of 273, 288, 303 and 323 K. These isotherms were essentially of Type V: that at 325 K was completely reversible, while the others had narrow, almost vertical hysteresis loops of Type H1 (see Figure 12.8).

Samples of modified kanemite referred to earlier gave reversible pore filling by nitrogen over an appreciable range of $p/p°$ (Branton *et al.*, 1996), and the isotherm shape was similar to that given by the 2.5 nm MCM-41 in Figure 12.9. The BET areas and pore volumes of the modified kanemite adsorbents are shown along with other derived quantities in Table 12.5. This form of reversible nitrogen isotherm was also obtained by Schmidt *et al.* (1996) in their work on MCM-48, which had a BET area of 1157 $m^2 g^{-1}$ and a total specific pore volume of 0.96 $cm^3 g^{-1}$.

As already indicated, by applying the Kelvin equation (assuming hemispherical meniscus formation) and correcting for the adsorbed layer thickness, we are able to calculate the ranges of apparent pore width recorded in Table 12.5. The values of mean pore diameter, w_p^*, are obtained from the volume/surface ratio, i.e. by applying the principle of hydraulic radius (see Chapter 7) and assuming the pores to be non-intersecting cylindrical capillaries and that the BET area is confined to the pore walls.

The close agreement between the corresponding values of w_p and w_p^* in Table 12.5 is probably deceptive. It must be re-emphasized that it is unlikely that the Kelvin equation provides a reliable basis for the calculation of pore widths of around six molecular diameters. Also, as pointed out in Chapter 7, the application of the standard statistical multilayer thickness correction may be an oversimplification. For these reasons, the values of pore widths in Tables 12.4 and 12.5 should be regarded as *apparent* rather than real pore sizes.

We are now in a position to discuss the significance of the isotherm shape in relation to the appearance, or absence, of hysteresis. First, we note that all those hysteresis loops that have been given by various samples of MCM-41 are essentially of Type

Table 12.5. Surface areas, pore volumes and pore diameters of samples of MCM-41 and modified kanemite.

Adsorbent	a(BET) ($m^2 g^{-1}$)	v_p ($cm^3 g^{-1}$)	w_p range (nm)	w_p^* (nm)
4 nm MCM-41	655	0.64	3.3–4.3	3.9
3.4 nm MCM-41 (SiO_2)	980	0.84	2.8–3.5	3.4
Kanemite FSM-12	882	0.56	1.9–2.6	2.5
Kanemite FSM-16	977	0.91	2.8–3.9	3.7

H1. We believe this to be a useful indication that network-percolation effects are not playing a major role in the emptying of the mesopores (i.e. on the desorption branch). Thus, the narrow and almost vertical loops in Figure 12.8 are more likely to be associated with delayed condensation rather than the more complex percolation pore-blocking phenomena (see Chapter 7). Of course, this is to be expected in view of the non-intersecting tubular pore structure of the model MCM-41.

Next, we must consider the question of the lower limit of capillary condensation hysteresis. As pointed out in Chapter 7, a considerable amount of previous work has indicated that the lower closure point of this form of hysteresis loop is never located below a critical relative pressure, which is dependent on the adsorptive and temperature (but not on the adsorbent). In the case of nitrogen at 77 K, the lower limit of hysteresis appears to be at $p/p^\circ = 0.42$. So far, it would seem that the behaviour of MCM-41 is at least consistent with these findings.

The nitrogen isotherm on the 4 nm sample is of special interest because at first sight it appears to represent an almost 'ideal' case of reversible capillary condensation/evaporation in a narrow distribution of uniform cylindrical pores (cf. Figure 7.5). However, it must be kept in mind that the steep pore-filling riser is located at $p/p^\circ \approx 0.42$. Because of the pore geometry, there is no detectable interparticle condensation, which often results in a reversible deviation from the standard isotherm at $p/p^\circ < 0.42$. We may therefore conclude that the *condensate* has become unstable at the critical chemical potential corresponding to $p/p^\circ = 0.42$, while leaving the adsorbed multilayer (under the influence of surface forces) on the pore walls.

This system has been discussed in some detail by Ravikovitch *et al.* (1995, 1997). Model nitrogen isotherms at different temperatures (70–82 K) were computed for a wide range of pore sizes (1.8–8 nm) by using non-local density functional theory, NLDFT. Although it was necessary to assume energetic homogeneity of the adsorbent surface and to adopt a simplified treatment of the solid–fluid intermolecular potential, the computed isotherms were found to exhibit the same stepwise Type IV character as the experimental isotherms. However, wide hysteresis loops were generated and it was concluded that the magnitude of grand potential difference can be regarded as a measure of the degree of metastability. As observed experimentally, for a given pore size, the size of the loop becomes smaller with increase in temperature. Furthermore, at a given temperature, there is a critical pore size, below which irreversible pore filling – giving rise to hysteresis – is transformed into reversible pore filling.

In a very recent molecular simulation study of the adsorption of nitrogen by MCM-41, Maddox *et al.* (1997) have explored the effect of allowing for surface energetic heterogeneity. This approach was prompted by the fact that models in which the solid–fluid interaction potential was assumed homogeneous were incapable of reproducing an experimental isotherm, which had been accurately determined in the region of low surface coverage (at p/p° down to 2.7×10^{-6}). A heterogeneous surface model was developed which gave excellent agreement with the low-pressure adsorption isotherm data and which appears to be consistent with the variation of differential energies of adsorption with surface coverage (Coulomb *et al.*, 1997a,b). Maddox *et al.* (1997) point out that hysteresis loops obtained as a result of molecular

simulation arise from metastable states and may depend on the length of the simulation run; therefore, they are not directly comparable with experimental hysteresis loops.

It is of interest to compare the values of pore diameter obtained by molecular simulation and by the use of the corrected Kelvin equation. By comparing the nitrogen isotherm in Figure 12.6 with molecular simulation model isotherms, Maddox *et al.* (1997) have arrived at pore diameters of 4.1–4.3 nm. As indicated in Table 12.4, the corrected Kelvin diameters are 3.3–4.3 nm. The corresponding surface areas are ≈ 631 and 655 $m^2\ g^{-1}$. In view of the assumptions in the model and the shortcomings of the Kelvin and BET equations, this level of agreement must be considered to be encouraging.

Very recently, Kruk *et al.* (1997a) have analysed their detailed nitrogen isotherms determined on a series of siliceous MCM-41 samples of different pore size. The low-pressure data were used to calculate the adsorption energy distribution, which in general appeared to show little variation from one sample to another. However, it was found that the adsorption at the lowest accessible pressures ($5 \times 10^{-7} < p/p^\circ < 10^{-3}$) was significantly enhanced by the decrease in pore size. This may have been due to either corrugations in the pore walls or an overall increased curvature of the pore wall.

A striking feature of MCM-41 and other related ordered mesoporous materials is the magnitude of their specific surface areas. It is remarkable that it is possible to produce non-microporous structures with stable surface areas well in excess of 1000 $m^2\ g^{-1}$. Of course, the implication of the combination of high area *and* high pore volume is that the pore walls must be quite thin – in some cases the walls may be no more than two oxygen atoms thick!

In view of the surface heterogeneity of MCM-41, it might be expected that the adsorption of water vapour would involve some degree of specificity. It was found (Branton *et al.*, 1995b; Llewellyn *et al.*, 1995), however, that water isotherms on the 4 nm and 2.5 nm samples were of Type V in the IUPAC classification (cf. the carbon tetrachloride isotherm in Figure 12.8). The initial section of the isotherm on the 4 nm material was almost reversible – indicating that exposure to water vapour had led to very little rehydroxylation. Very recently, M.M.L. Ribeiro-Carrott, A.J. Estevao Candeias, P.J.M. Carrott and K.K. Unger (personal communication) have found that a high-area sample of MCM-41 underwent pronounced ageing when exposed to water vapour at high p/p°. S. Inagaki and Y. Fukushima (personal communication) also found that their sample of modified kanemite, FSM-16, which has similar properties to those of MCM-41, underwent a significant amount of rehydroxylation when exposed to water vapour. This behaviour is similar to that of most dehydroxylated silicas.

The considerable interest now being shown in MCM-41 by both experimentalists and theoreticians is an indication of its potential value as a model mesoporous adsorbent. As we have seen, remarkable progress has already been made in the synthesis and characterization of the non-intersecting assemblage of tubular pores. More work is now required to improve the uniformity of the pore structure and to investigate the stability of different forms of MCM-41 and related materials. Neutron diffraction has

already been shown to be a powerful tool for studying adsorbate structures in MCM-41 (Coulomb *et al.*, 1997) and should be capable of providing a better understanding of the effect of pore size on the confined fluid–solid phase transitions.

In general, there appears to be considerable scope for the application of ordered mesoporous structures in such fields as biochemical separations and nanocomposite materials. The potential value of MCM-41-based catalysts has been stressed by Thomas (1994, 1995). In principle, metal complexes, enzymes and other species can be attached to the channel walls to give high concentrations of structurally well-defined active sites. It should be possible therefore to take full advantage of the regularity of both the channel and the surface structure. Furthermore, the incorporation of heteroatoms such as Ti into the siliceous framework of MCM-41 should provide an elegant way of controlling catalytic selectivity (Thomas, 1995).

12.3.2. Aluminophosphate molecular sieves

Background

In reporting the results of a spectroscopic study of aluminium phosphate in 1971, Peri drew attention to the isostructural nature of $AlPO_4$ and SiO_2 and the likely value of $AlPO_4$ as an adsorbent and catalyst support. Stable high-area $AlPO_4$ gels could readily be prepared in 1971, but at that time there was no indication in the open or patent literature that zeolitic forms of aluminophosphate could be synthesized.

The synthesis of the first members of a new family of aluminophosphate molecular sieves (the ALPOs) was disclosed by Union Carbide scientists in the early 1980s (Wilson *et al.*, 1982a,b). The zeotype frameworks of the ALPO structures can be pictured as alternating $[AlO_2]^-$ and $[PO_2]^+$ units and so are electrically neutral with both Al and P occupying adjoining T-sites.

Great expectations were aroused by the discovery of a new large-pore ALPO, VPI-5 (VPI after Virginia Polytechnic Institute), by Davis *et al.* in 1988. It had been tacitly assumed by most investigators that the channel diameter of a zeolite structure could not exceed about 1 nm and therefore the discovery of a 1.2 nm channel structure has been regarded as a kind of 'psychological breakthrough' (Ozin, 1992).

The two relatively simple ALPOs that have been studied in most detail are $AlPO_4$-5 and VPI-5. The framework (0 0 1) plane projections of their structures are shown in Figure 12.10.

In $AlPO_4$-5 and VPI-5, the largest channels are essentially straight cylinders. However, as indicated in Table 12.6, there is an appreciable difference in the ring size, the number of T-atoms being 12 in $AlPO_4$-5 and 18 in VPI-5. The pore dimensions are derived from crystallographic data of Davis *et al.* (1989a,b).

Chemical modification of the ALPOs is required to create a new class of catalysts. In the metalloaluminophosphates (MeALPOs), the framework contains metal (Me), aluminium and phosphorus. Thus, it becomes possible to produce a wide range of active catalysts with Lewis and Bronsted acid sites and redox properties by the partial replacement of Al^{3+} by Me^{2+} ions (e.g. Co, Cu, Mg, Zn, etc.) in an ALPO framework (Thomas, 1995; Martens *et al.*, 1997).

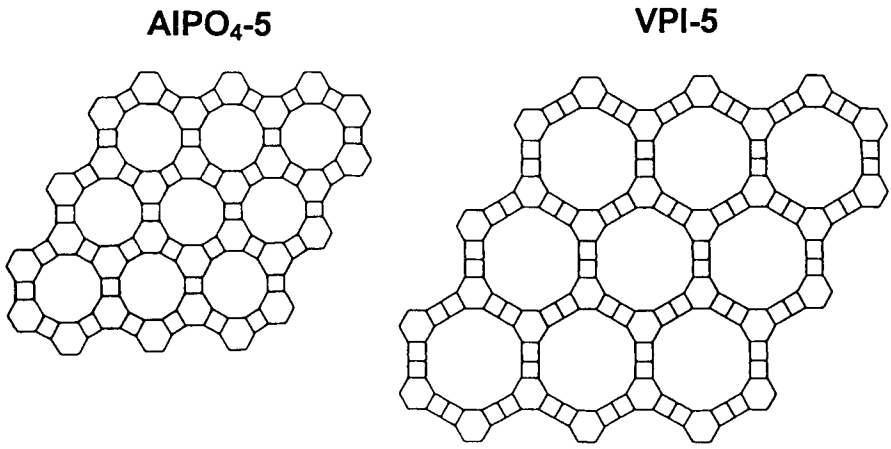

Figure 12.10. The framework (0 0 1) plane projections of $AlPO_4$-5 and VPI-5 (from Davis *et al.*, 1988).

Table 12.6. Properties of $AlPO_4$-5 and VPI-5.

	Ring sizes	Pore width (nm)	Pore volume ($cm^3\ g^{-1}$)	
$AlPO_4$-5	4, 6, 12	0.73	0.18	0.15[a]
VPI-5	4, 6, 18	1.21	0.31	0.26[a]

[a] Unidimensional pores.

The synthesis and properties of another group of acidic metallophosphates, having the general formula $Al_{100}P_xFe_y$, has been discussed by Petrakis *et al.* (1995). Products containing at least 15% phosphorus were found to be X-ray amorphous, mesoporous solids, but at a lower P content there was evidence of phase separation of the Fe and Al.

Physisorption of gases by $AlPO_4$-5

A series of high-resolution adsorption studies have been carried out at Marseille on different lots of 150 μm hexagonal crystals of $AlPO_4$-5, which had been synthesized by Unger and his co-workers (Müller and Unger, 1988). With the aid of CRTA it was first established that an outgassing temperature of 200°C was sufficiently high for the removal of physisorbed water without any significant structural change (Grillet *et al.*, 1993; Tosi-Pellenq *et al.*, 1992).

The initial measurements of nitrogen and argon adsorption at 77 K gave smooth Type I isotherms (Müller *et al.*, 1989). The corresponding differential energies of adsorption are shown versus molecules per unit cell in Figure 12.11. As expected, the nitrogen curve is above that of argon, but both systems apparently exhibit a high degree of energetic homogeneity. These results were therefore considered to confirm the theoretical prediction that $AlPO_4$-5 behaves as an essentially homogeneous adsorbent with a micropore capacity of about four molecules per unit cell.

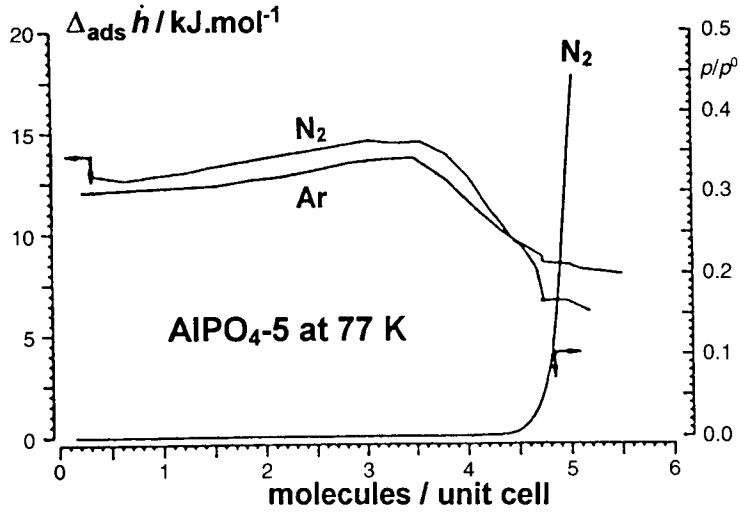

Figure 12.11. Nitrogen isotherm and differential enthalpy of adsorption of nitrogen and argon on $AlPO_4$-5 crystals (Müller *et al.*, 1989).

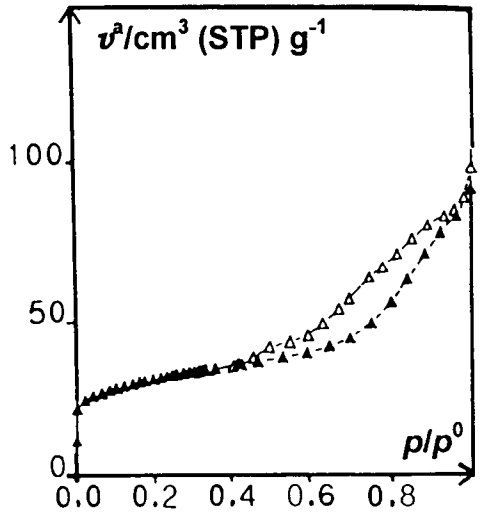

Figure 12.12. Adsorption isotherm of nitrogen at 77 K on $AlPO_4$-5 (Tosi-Pellenq *et al.*, 1992).

A nitrogen isotherm, determined at 77 K by static manometry on a second sample of $AlPO_4$-5, is shown in Figure 12.12 (Tosi-Pellenq *et al.*, 1992). In view of the crystalline nature of the $AlPO_4$-5, it was surprising to find that this adsorbent gave a fairly large hysteresis loop in the capillary condensation range. The shape of the loop indicates that the hysteresis was more closely associated with delayed condensation

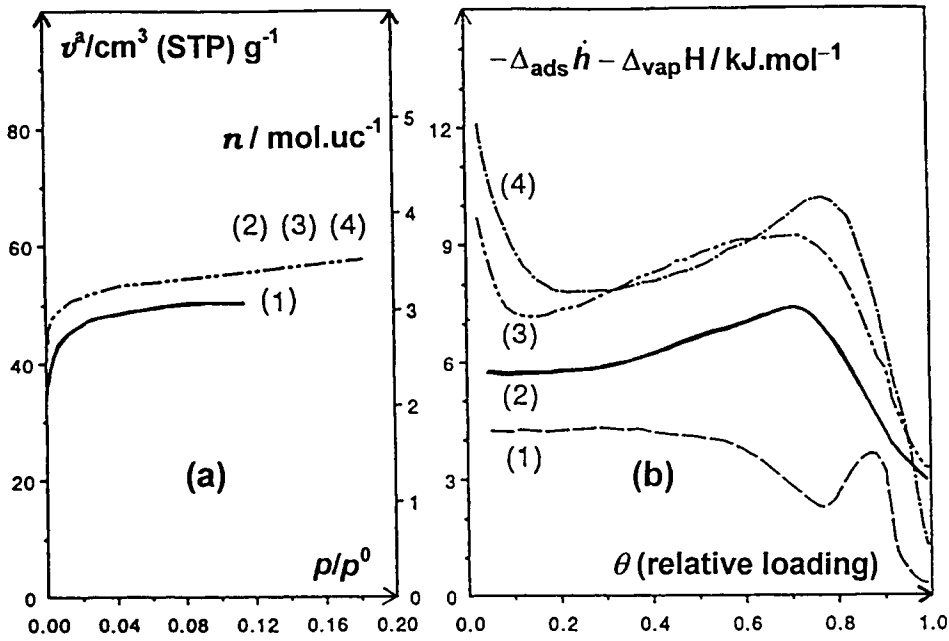

Figure 12.13. (a) Adsorption isotherms on $AlPO_4$-5 at 77 K of (1) methane, (2) argon, (3) nitrogen and (4) carbon monoxide.
(b) Net adsorption energies (Grillet *et al.*, 1993).

than with network percolation effects. Application of the BJH method of mesopore size analysis to the desorption branch gives a broad distribution of pore widths between 2 and 20 nm. However, this form of mesoporosity cannot be an intrinsic property of the ALPO structure: it was probably the result of structural defects and voids between the crystals.

The same sample of $AlPO_4$-5 was used to obtain the results shown in Figure 12.13. Here, the isotherms of methane, argon, nitrogen and carbon monoxide and the corresponding net adsorption energies were determined at 77 K after the adsorbent had been outgassed by CRTA to 353 K.

The adsorption isotherms of argon, nitrogen and carbon monoxide in Figure 12.13a all seem to follow an almost common path up to $p/p^\circ = 0.2$. In fact, there are significant differences in the isotherms at very low p/p° (Coulomb *et al.*, 1997a,b), as would be expected from the appearance of the net adsorption energy curves in Figure 12.13b. The uptake at the plateau corresponds to 3.5 molecules of argon, nitrogen or carbon monoxide adsorbed per unit cell and 3 molecules of methane. These values are slightly lower than the theoretical micropore capacity of 4 molecules per unit cell noted earlier.

The energetic heterogeneity shown by nitrogen and carbon monoxide at low loading is clearly evident and is probably due to specific interactions with hydroxyl groups and defect sites. With argon, nitrogen and carbon monoxide, the adsorbate–

adsorbate interactions are responsible for the energy maxima at loadings of 70–80%. The methane net energy curve is quite different and is indicative of an adsorbate phase change, which was originally thought to involve a change from a type of 'fluid' to a 'solid' phase.

Neutron diffraction studies (Coulomb *et al.*, 1994, 1997a,b) have provided more information on the methane phase transition. Adsorption isotherm and neutron diffraction measurements were made at different temperatures for D_2, ^{36}Ar, CD_4 and CF_4 on two samples: one of pure $AlPO_4$-5 and the other SAPO-5 (containing 5% Si). A characteristic sub-step was observed only with the $CD_4/AlPO_4$-5. The neutron diffraction patterns have indicated that two different solid-type phases are involved in the phase transition. It appears that the adsorbed phases are composed of ordered chains of CD_4 molecules and that a structural change occurs at the sub-step. It has been tentatively suggested that the chains are changed from a 'dimeric' form (at a loading of 4 molecules per unit cell) to 'trimers' (at 6 molecules per unit cell). However, since the kinetic diameter of methane is *c.* 0.38 nm, it would seem unlikely that the change in ordering is quite as simple as this would suggest! Another viewpoint has been provided by a related computer simulation study, which is discussed later.

Other neutron diffraction spectra obtained by Coulomb *et al.* (1997a,b) have revealed different phase 'signatures'. For example, the diffraction pattern for the Ar/SAPO-5 system underwent a change at high Ar loading, which was interpreted as an increase in short-range order. These results indicate that at low and medium loadings the adsorbed Ar has a relatively high mobility, while at high loading it 'solidifies' in a vitreous form. The preservation of a high degree of disorder would therefore appear to be responsible for the absence of a phase transformation. The presence of a weak sub-step in the $Kr/AlPO_4$-5 isotherm at 77.3 K is an indication of the intermediate behaviour of this system at the operational temperature.

Molecular simulation of the adsorption of gases by the ALPOs was pioneered by Cracknell and Gubbins (1993), who pointed out that the aluminophosphates should be easier to model than the aluminosilicates. There are two important advantages: first, the charge neutrality of the framework means that there are no exchangeable cations to be taken into account (this is, of course, also true for pure Silicalite); and second, the modelling is simpler because the pores are unidirectional with no interconnections.

Adsorption isotherms for argon in $AlPO_4$-5 and other ALPOs were simulated at 77 and 87 K by the grand canonical Monte Carlo (GCMC) method. Refined Lennard–Jones (12–6) potentials were used to model the argon–oxygen interactions, with some adjustment made for the less important contribution from the argon interactions with the T-atoms. The contribution from polarization, E_p, was considered to be very small and was ignored. The procedures for the GCMC simulations were based on the generally accepted approach for bulk fluids (Allen and Tildesley, 1987). The acceptance probabilities for the movement, creation and deletion of particles were chosen to allow the probability of a given state of the system, after a sufficiently high number of trials, to correspond to that of the grand canonical ensemble at constant μ, V and T. The simulations thus gave the ensemble average of the number of

argon atoms per unit cell, which could be plotted against the reduced pressure, thereby giving a model isotherm for each ALPO.

Cracknell and Gubbins (1993) found that the low-pressure region of their simulated isotherm for Ar/$AlPO_4$-5 agreed well with experimental data at 87 K, but that the curves began to diverge at $p/p^\circ \approx 10^{-4}$, with the simulated maximum loading lying about 25% above the experimental capacity determined by Hathaway and Davis (1990). The simulated variation of adsorption energy with uptake, although similar in general form to the argon curve in Figure 12.13, also deviated from the experimental microcalorimetric data. In seeking an explanation for these discrepancies, Cracknell and Gubbins drew attention to the assumptions made in the simulations including the use of the Lennard–Jones parameters and the supposed rigidity of the $AlPO_4$-5 structure. However, it was considered more likely that a more serious problem was an experimental one: that the unidimensional pores are particularly susceptible to pore blocking.

A detailed molecular simulation study of CH_4/$AlPO_4$-5 was undertaken by Lachet *et al.* (1996). The standard GCMC procedure was again used to equilibrate the system at a series of pressures and thereby allow an assessment to be made of the number of molecules per unit cell and the differential energies of adsorption. It was also assumed that the $AlPO_4$-5 structure remained rigid, but in this study various potentials were used to model the adsorbent–adsorbate and adsorbate–adsorbate interactions. Sub-steps could be generated with certain sets of parameters, but the position of the sub-step and the agreement with microcalorimetric data depended critically on the repulsive oxygen–methane parameter, and therefore indirectly on the pore size.

Lachet *et al.* (1996) have concluded that the experimental sub-step can be interpreted as a structural rearrangement of the adsorbed methane. On the other hand, they are undecided whether the phenomenon should be regarded as a true 'phase transition' and they point out that the exact structure at maximum loading is still unknown.

It is interesting that, unlike the situation with Silicalite-I, argon and nitrogen do not appear to undergo well-defined phase transitions in the unidirectional channels of $AlPO_4$-5. However, we must bear in mind the possibility that the transitions are obscured by the energetic heterogeneity, structural disorder or pore blocking. It is apparent from the foregoing discussion that significant differences have been noted in the properties of the various samples of $AlPO_4$-5.

The adsorption–desorption isotherm of water vapour in Figure 12.14 exhibits hysteresis over the entire range of p/p°. This form of hysteresis, which extends down to very low p/p°, cannot be attributed solely to the filling and emptying of mesopores. Low-pressure hysteresis is a common feature of water isotherms: the most likely explanation for the strong retention of water by the $AlPO_4$-5 is dissociative chemisorption of water on the defect sites to give Al-OH and P-OH. Indeed, the amount of water retained at an outgassed pressure of 10^{-3} hPa is consistent with the high-energy uptakes of nitrogen and carbon monoxide.

By using the quasi-equilibrium procedure, Grillet *et al.* (1993) were able to detect the sub-step, AB, in the water isotherm at $p/p^\circ \approx 0.15$. The fact that the sub-step can be seen in both the adsorption and desorption isotherms (although at slightly

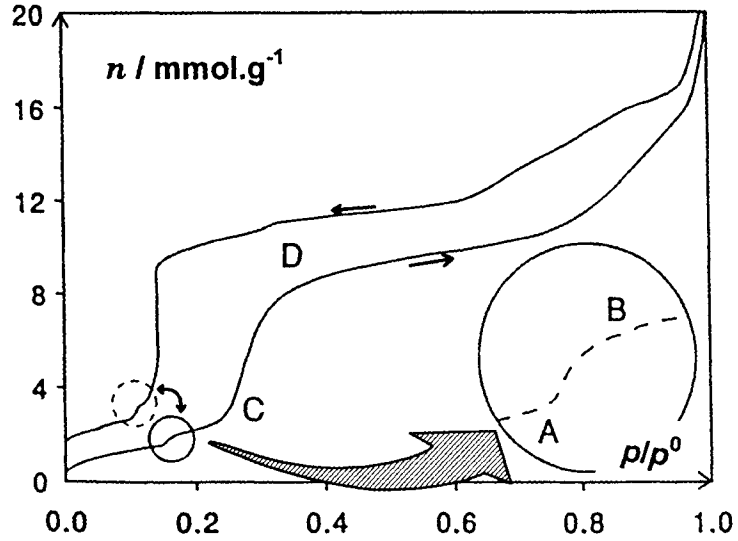

Figure 12.14. The adsorption–desorption isotherm of water vapour at 290 K on $AlPO_4$-5 (Grillet *et al.*, 1993).

different positions) suggests that it is associated with an adsorbate phase change. This explanation is consistent with a small change in the isosteric enthalpy of adsorption and by the changes in NMR spectra, but at this stage it is not possible to explain the nature of the transition.

The much larger step, CD, in the adsorption branch at $p/p^\circ \approx 0.3$ is unlikely to be due to a simple form of capillary condensation. It is significant that the corresponding – very sharp – desorption step is located at a much lower p/p°. Stach *et al.* (1986) have suggested that it corresponds to both capillary condensation and a slow coordinative hydration giving *inter alia* $Al(OP_4)\ (OH_2)_2$. This explanation is supported by the results of NMR spectrocopy.

Physisorption of gases by VPI-5

The physisorption isotherms obtained by Davis *et al.* (1988, 1989a,b) in their original investigations of VPI-5 were reported to show Type I behaviour. However, inspection of the isotherms of argon, oxygen and water vapour reveals that a significant amount of additional adsorption of each adsorptive occurred at $p/p^\circ > 0.4$. No desorption measurements were reported and therefore it is not possible to deduce whether the further uptake at high p/p° was due to multilayer adsorption, capillary condensation or an irreversible change in the adsorption system.

The more recent adsorption–desorption isotherms of some organic vapours of different molecular diameter are shown in Figure 12.15. These measurements were made on different samples of VPI-5, each having been outgassed for 16 hours at 673 K. Although essentially of Type I, the isotherms reveal some degree of thermodynamic irreversibility with hysteresis extending back to very low p/p°. Evidently,

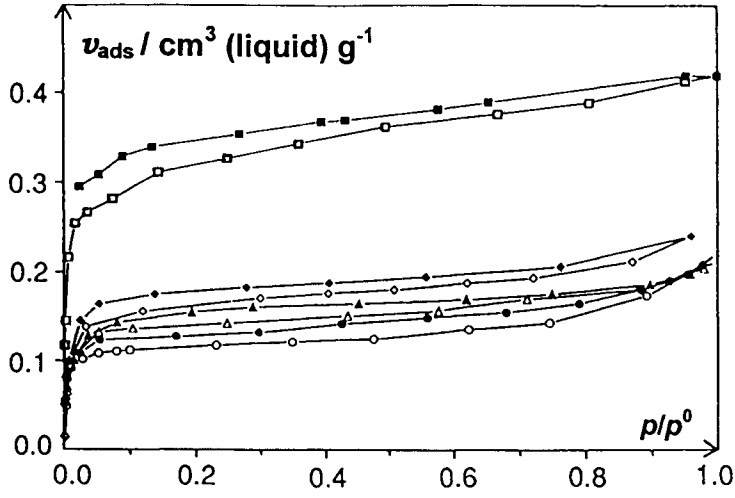

Figure 12.15. Adsorption–desorption isotherms on VPI-5 of methanol (squares), isobutane (diamonds), neopentane (circles) and propane (triangles) determined at 298, 261, 273 and 196 K, respectively (Kenny *et al.*, 1992).

this form of hysteresis cannot be attributed to capillary condensation, and is instead indicative of a more complex change in the adsorption system (e.g. activated entry of adsorptive molecules or swelling of the adsorbent).

Values of apparent specific micropore volume, v_p, of VPI-5 evaluated from the uptakes determined by Kenny *et al.* (1992) of various adsorptives at $p/p° = 0.4$ are recorded in Table 12.7. As before, the adsorbate densities are assumed equal to the respective liquid densities at the operational temperatures. Also included in Table 12.7 are values of v_p derived from the measurements of Davis *et al.* (1989b), Schmidt *et al.* (1992) and Reichert *et al.* (1994). The complexity of the behaviour of VPI-5 is

Table 12.7. Values of apparent micropore volume, v_p, of VPI-5 evaluated from the adsorption capacities of different vapours at $p/p° = 0.4$ (Kenny *et al.*, 1992).

Adsorptive	Kinetic diameter (nm)	Temperature (K)	Apparent v_p (cm^3 g^{-1})
Water	0.27	298	0.31–0.35[a]
Methanol	0.38	298	0.32
Oxygen	0.35	77	0.23[a]
Argon	0.34	77	0.17[b]
Nitrogen	0.36	77	0.187, 0.184[c], 0.146[b]
Methane	0.38	77	0.17[b]
Propane	0.43	196	0.17
Isobutane	0.50	261	0.18
Neopentane	0.62	273	0.12, 0.15[a]

[a] Davis *et al.* (1989b).
[b] Reichert *et al.* (1994).
[c] Schmidt *et al.* (1992).

illustrated by the poor agreement between some individual values of v_p and also the apparent molecular sieving effects.

In attempting to explain the anomalous results in Figure 12.15 and Table 12.7, Kenny *et al.* (1991a, 1992) undertook a systematic study of the stability of VPI-5. First, successive BET-nitrogen areas were determined (by the single-point method) on two samples taken from the same batch of VPI-5. Sample A was kept in a dry condition between successive nitrogen adsorption measurements, while sample B was exposed to water vapour. The same conditions of outgassing were adopted for both samples, namely 16 hours at 673 K. The BET area of sample A remained almost constant at $394 \pm 7\ m^2\ g^{-1}$, whereas that of sample B underwent the following progressive decrease: 404, 309, 179, 147 $m^2\ g^{-1}$.

In another set of experiments, the effect of changing the outgassing conditions was studied by outgassing one sample at increasingly higher temperatures over the range 273–1173 K and outgassing separate samples at the same temperatures. The separate samples had consistently higher BET areas, differences of *c.* 100 $m^2\ g^{-1}$ being recorded.

With the aid of thermal analysis, X-ray diffraction and diffuse reflectance FTIR, it was possible to deduce that the removal of the zeolitic water brought about a partial structural transformation of the VPI-5 to $AlPO_4$-8. Schmidt *et al.* (1992) have studied this phase transition in some detail and have shown that it can be avoided if the sample is heated slowly under reduced pressure (10^{-5} hPa). In this manner, VPI-5 can be heated to 450–500°C without any detectable change of structure.

Since the $AlPO_4$-8 structure has a ring opening of about 0.8 nm, one would expect it to accommodate all the molecules in Table 12.7. The low uptake of neopentane and the low-pressure hysteresis indicate that the aged material has an imperfect $AlPO_4$-8 structure. It seems likely that the phase transition has resulted in the development of constrictions and some blockage of the unidirectional channels.

The results in Table 12.7 appear to show that a considerably larger micropore volume is available for the adsorption of water and methanol than for the other adsorptives. A somewhat larger uptake of water is to be expected in view of its molecular size and apparent ability to enter the narrow six-membered rings (Davis *et al.*, 1989b), but the high uptake of methanol is unexpected and will require further investigation.

The unusual character of the water isotherm on VPI-5 can be seen in Figure 12.16. There are three distinct steps at low $p/p°$. Step 1 occurs at $p/p° < 0.001$, step 2 at $p/p° = 0.013$ and step 3 at $p/p° = 0.060$. Between steps 2 and 3 there is a narrow hysteresis loop, which in this region of the isotherm cannot be associated with capillary condensation.

Step 1 in Figure 12.16 must be the result of interactions between water molecules and highly active regions of the VPI-5 surface, which may be exposed P—OH groups and possibly other defect sites (Kenny *et al.*, 1991b). At present, the explanation for the two pore-filling steps, 2 and 3, must also be speculative. It is of interest that these risers are located at much lower relative pressures than the corresponding single pore-filling step for $AlPO_4$-5 (Carrott *et al.*, 1991). This suggests that the three-dimensional, hydrogen-bonded water structure can be more readily formed in the wider channels of VPI-5. It seems likely that a rearrangement of water molecules at the pore walls is responsible for the separation of steps 2 and 3 and the presence of the associated hysteresis loop.

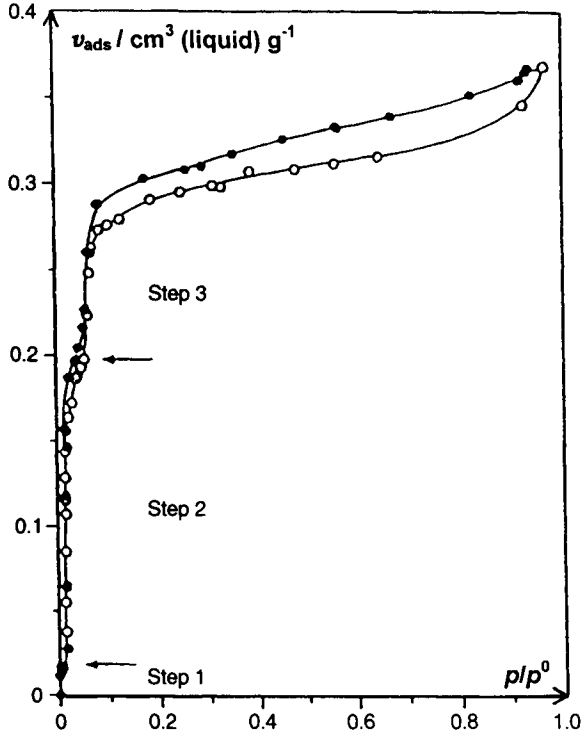

Figure 12.16. The adsorption–desorption isotherm of water vapour determined at 298 K on VPI-5 outgassed at 673 K for 16 hours (Kenny *et al.*, 1991b).

The difficulty of arriving at an unambiguous assessment of the micropore capacity is immediately apparent when we see the shape of the water isotherm in Figure 12.16. Since the micropore filling process is confined to the range $p/p^\circ < \approx 0.1$, there is an overestimate of $\approx 20\%$ in v_p if the molecular sieve capacity is taken as the uptake at $p/p^\circ = 0.4$.

Finally, we note that the maximum p/p° attained on the adsorption branch in Figure 12.16 is *c.* 0.95. As indicated earlier, exposure of the adsorbent to water vapour at $p/p^\circ \approx 1$ caused an irreversible partial conversion of the VPI-5 structure to $AlPO_4$-8. Furthermore, a significant decrease in the water adsorption capacity was found when the outgassing temperature was taken to 673 K in a stepwise manner (Kenny *et al.*, 1992). We conclude that CRTA would be admirably suitable for a more rigorous study of the properties and thermal stability of VPI-5.

References

Allen M.P. and Tildesley D.J. (1987) *Computer Simulation of Liquids*, Oxford University Press, Oxford.
Atkinson D., McLeod A.I., Sing K.S.W. and Capon A. (1982) *Carbon* **20**, 339.
Atkinson D., McLeod A.I. and Sing K.S.W. (1984) *J. Chim. Phys.* **81**, 791.

Bailey A. and Maggs F.A.P. (1972) British Patent 1 301 101.
Bailey A. and Maggs F.A.P. (1974) U.S. Patent 3 847 833.
Bailey A., Maggs F.A.P. and Williams J.H. (1973) British Patent 1 310 011.
Baker F.S. (1992) In: *Kirk-Othmer Encyclopædia of Chemical Technology*, 4th edn, vol. 4, John Wiley, New York, p. 1015.
Barton S.S. and Koresh J.E. (1983) *J. Chem. Soc., Faraday Trans. I* **79**, 1173.
Beck J.S., Vartuli J.C., Roth W.J., Leonowicz M.E., Kresge C.T., Schmitt K.D., Chu C.T.-W., Olson D.H., Sheppard E.W., McCullen S.B., Higgins J.B. and Schlenker J.L. (1992) *J. Am. Chem. Soc.* **114**, 10 834.
Bhambhani M.R., Cutting P.A., Sing K.S.W. and Turk D. (1972) *J. Colloid Interface Sci.* **38**, 109.
Bohra J.N. and Sing K.S.W. (1985) *Adsorption Sci. Tech.* **2**, 89.
Branton P.J., Hall P.G. and Sing K.S.W. (1993) *J. Chem. Soc., Chem. Commun.* 1257.
Branton P.J., Hall P.G., Sing K.S.W., Reichert H., Schüth F. and Unger K.K. (1994) *J. Chem. Soc., Faraday Trans.* **90**, 2965.
Branton P.J., Hall P.G. and Sing K.S.W. (1995a), *Adsorption* **1**, 77.
Branton P.J., Hall P.G., Treguer M. and Sing K.S.W. (1995b) *J. Chem. Soc., Faraday Trans.* **91**, 2041.
Branton P.J., Kaneko K., Setoyama N., Sing K.S.W., Inagaki S. and Fukusima Y. (1996) *Langmuir* **12**, 599.
Branton P.J., Sing K.S.W. and White J.W. (1997) *J. Chem. Soc., Faraday Trans.* **93**, 2337.
Brown P.N., Jayson G.G., Thompson G. and Wilkinson M.C. (1987) *J. Colloid Interface Sci.* **116**, 211.
Byrne J.F. and Marsh H. (1995) In: *Porosity in Carbons* (J.W. Patrick, ed.), Edward Arnold, London, p. 1.
Carrott P.J.M. and Freeman J.J. (1991) Carbon **29**, 499.
Carrott P.J.M. and Sing K.S.W. (1987) *J. Chromatogr.* **406**, 139.
Carrott P.J.M. and Sing K.S.W. (1990) *J. Chromatogr.* **518**, 53.
Carrott P.J.M., Roberts R.A. and Sing K.S.W. (1987) *Carbon* **25**, 59.
Carrott P.J.M., Roberts R.A. and Sing K.S.W. (1988) In: *Characterization of Porous Solids I* (K.K. Unger, J. Rouquerol, K.S.W. Sing and H. Kral, eds), Elsevier, Amsterdam, p. 89.
Carrott P.J.M., Brotas de Carvalho M. and Sing K.S.W. (1989a) *Adsorption Sci. Tech.* **6**, 93.
Carrott P.J.M., Drummond F.C., Kenny M.B., Roberts R.A. and Sing K.S.W. (1989b) *Colloids and Surfaces* **37**, 1.
Carrott P.J.M., Kenny M.B., Roberts R.A., Sing K.S.W. and Theocharis C.R. (1991) In: *Characterization of Porous Solids-II* (F. Rodriguez-Reinoso, J. Rouquerol, K.S.W. Sing and K.K. Unger, eds), Elsevier, Amsterdam, p. 685.
Ciesla U., Demuth D., Leon R., Petroff P., Stucky G., Unger K.K. and Schüth F. (1994) *J. Chem. Soc., Chem. Commun.* 1387.
Cook J., Sloan J. and Green M.L.H. (1996) *Chem. & Ind.* 600.
Coulomb J.P., Martin C., Grillet Y., Llewellyn P. and Andre G. (1997) In: *Studies in Surface Science and Catalysis*, vol. 105, Elsevier, Amsterdam, p. 1827.
Coulomb J.-P., Martin C., Grillet Y. and Tosi-Pellenq N. (1994) In: *Zeolites and Related Microporous Materials: State of the Art 1994* (J. Weitkamp, H.G. Karge, H. Pfeifer and W. Holderich, eds), Elsevier, Amsterdam, p. 445.
Coulomb J.-P., Martin C., Grillet Y., Llewellyn P.L. and André J. (1997a) In: *Progress in Zeolites and Microporous Materials*, Studies in Surface Science and Catalysis, Elsevier, Amsterdam, vol. 105, p. 1827.
Coulomb J.-P., Martin C., Llewellyn P.L. and Grillet Y. (1997b) In: *Progress in Zeolites and Microporous Materials*, Studies in Surface Science and Catalysis, Elsevier, Amsterdam, vol. 105, p. 2355.
Cracknell R.F. and Gubbins K.E. (1993) In: *Proc IVth Int. Conf. on Fundamentals of Adsorption* (M. Suzuki, ed.), Kodansha, Tokyo, p. 105.
Davis M.E., Saldarriaga C., Montes C., Garces J. and Crowder C. (1988) *Zeolites* **8**, 362.
Davis M.E., Hathaway P.E. and Montes C. (1989a) *Zeolites* **9**, 436.
Davis M.E., Montes C., Hathaway P.E., Arhancet J.P., Hasha D.L. and Garces J.M. (1989b) *J. Am. Chem. Soc.* **111**, 3919.

de Boer J.H. (1972) In: *Thermochimie*, Colloques Internationaux du CNRS no. 201, Editions du CNRS, Paris, p. 407.
Donnet J.-B. and Bansal R.C. (1984) *Carbon Fibers*, Marcel Dekker, New York.
Economy J. and Lin R.Y. (1971) *J. Mater. Sci.* **6**, 1151.
Economy J. and Lin R.Y. (1976) *Appl. Polymer Symp.* **29**, 199.
Edler K.J. and White J.W. (1995) *J. Chem. Soc., Chem. Commun.* 155.
Everett D.H. (1988) *Basic Principles of Colloid Science*, Royal Society of Chemistry, London, p. 5.
Firouzi A., Kumar D., Bull L.M., Besier T., Sieger P., Huo Q., Walker S.A., Zasadzinski J.A., Glinka C., Nicol J., Margolese D.I., Stucky G.D. and Chmelka B.F. (1995) *Science* **267**, 1138.
Franke O., Schulz-Ekloff G., Rathousky-Starek J. and Zukal A. (1993) *J. Chem. Soc., Chem. Commun.* 724.
Freeman J.J., Gimblett F.G.R., Roberts R.A. and Sing K.S.W. (1987) *Carbon* **25**, 559.
Freeman J.J., Gimblett F.G.R., Roberts R.A. and Sing K.S.W. (1988) *Carbon* **26**, 7.
Freeman J.J., Gimblett F.G.R. and Sing K.S.W. (1989) *Carbon* **27**, 85.
Freeman J.J., Sing K.S.W. and Tomlinson J.B. (1990) *Carbone-90*, Extended Abstracts, GFEC, Paris, p. 164.
Freeman J.J. Gimblett F.G.R., Hayes R.A., Mohd Amin Z. and Sing K.S.W. (1991) In: *Characterization of Porous Solids-II* (F. Rodriguez-Reinoso, J. Rouquerol, K.S.W. Sing and K.K. Unger, eds), Elsevier, Amsterdam, p. 319.
Freeman J.J. and Sing K.S.W. (1991) In: *Adsorptive Separation* (M. Suzuki, ed.), Institute of Industrial Science, Tokyo, p. 259.
Freeman J.J., Tomlinson J.B., Sing K.S.W. and Theocharis C.R. (1993) *Carbon* **31**, 865.
Gelb L.D. and Gubbins K.E. (1998) *Langmuir* **14**, 2097.
Gimblett F.G.R., Freeman J.J. and Sing K.S.W. (1989) *J. Mater. Sci.* **24**, 3799.
Gregg S.J. (1960) *Kolloid-Z.* **169**, 5.
Gregg S.J. (1961) *The Surface Chemistry of Solids*, Chapman & Hall, London, p. 300.
Gregg S.J. and Sing K.S.W. (1982) *Adsorption, Surface Area and Porosity*, Academic Press, London.
Grillet Y., Llewellyn P.L., Tosi-Pellenq N. and Rouquerol J. (1993) In: *Proc IVth Int. Conf. on Fundamentals of Adsorption* (M. Suzuki, ed.), Kodansha, Tokyo, p. 235.
Hall C.R. and Sing K.S.W. (1988) *Chemistry in Britain* **24**, 670.
Hall P.G. and Williams R.T. (1986) *J. Colloid Interface Sci.* **113**, 301.
Hall P.G., Gittins P.M., Winn J.M. and Robertson J. (1985) *Carbon* **23**, 353.
Harrison B.H., Barton S.S., Dacey J. and Sellors J.R. (1979) *J. Colloid Interface Sci.* **71**, 367.
Hathaway P.E. and Davis M.E. (1990) *Catalysis Lett.* **5**, 333.
Huo Q., Margolese D.I., Clesia U., Feng P., Gler T.E., Sieger P., Leon R., Petroff P.M., Schüth F. and Stucky G.D. (1994) *Nature* **368**, 317.
Iijima S. (1991) *Nature* **354**, 56.
Inagaki S., Fukushima Y. and Kuroda K. (1993) *J. Chem. Soc., Chem. Commun.* 680.
Ismail I.M.K. and Rodgers S.L. (1992) *Carbon* **30**, 229.
Jagtoyen M. and Derbyshire F. (1993) *Carbon* **31**, 1185.
Kakei K., Ozeki S., Suzuki T. and Kaneko K. (1990) *J. Chem. Soc., Faraday Trans.* **86**, 371.
Kakei K., Ozeki S., Suzuki T. and Kaneko K. (1991) In: *Characterization of Porous Solids-II* (F. Rodriguez-Reinoso, J. Rouquerol, K.S.W. Sing and K.K. Unger, eds), Elsevier, Amsterdam, p. 429.
Kaneko K., Fujiwara Y. and Nishikawa K. (1989) *J. Colloid Interface Sci.* **127**, 126.
Kaneko K., Setoyama N., Suzuki T. and Kuwabara H. (1993) In: *Proc. 4th Int. Conf. on Fundamentals of Adsorption* (M. Suzuki, ed.), Kodansha, Tokyo, p. 315.
Kenny M.B., Sing K.S.W. and Theocharis C.R. (1991a) *Chem. & Ind.* 216.
Kenny M.B., Sing K.S.W. and Theocharis C.R. (1991b) *J. Chem. Soc., Chem. Commun.* 974.
Kenny M.B., Sing K.S.W. and Theocharis C.R. (1992) *J. Chem. Soc., Faraday Trans.* **88**, 3349.
Keung M. (1993), PhD Thesis, Brunel University, UK.
Kresge K.D., Leonowicz M.E., Roth W.J., Vartuli J.C. and Beck J.S. (1992) *Nature* **359**, 710.
Kroto H.W., Heath J.R., O'Brien S.C., Curl R.F. and Smalley R.E. (1985) *Nature* **318**, 162.
Kruk M., Jaroniec M. and Sayari A. (1997a) *J. Phys. Chem. B* **101**, 583.
Kruk M., Jaroniec M. and Sayari A. (1997b) *Langmuir* **13**, 6267.

Lachet V., Boutin A., Pellenq R.J.M., Nicholson D. and Fuchs A.H. (1996) *J. Phys. Chem.* **100**, 9006.
Llewellyn P.L., Grillet Y., Schüth F., Reichert H. and Unger K.K. (1994a) *Microporous Mater.* **3**, 345.
Llewellyn P.L., Pellenq N., Grillet Y., Rouquerol F. and Rouquerol J. (1994b) *J. Therm. Anal.* **42**, 855.
Llewellyn P.L., Schüth F., Grillet Y., Rouquerol F., Rouquerol J. and Unger K.K. (1995) *Langmuir* **11**, 574.
Llewellyn P.L., Grillet Y., Rouquerol J., Martin C. and Coulomb J.-P. (1996) *Surface Sci.* **352**, 468.
Maddox M.W. and Gubbins K.E. (1995) *Langmuir* **11**, 3988.
Maddox M.W., Olivier J.P. and Gubbins K.E. (1997) *Langmuir* **13**, 1737.
Marsh H., Crawford D.C., O'Grady T.M. and Wennerberg A.N. (1982) *Carbon* **20**, 419.
Martens J.A., Souverijns W., Van Rhijn W. and Jacobs P.A. (1997) In: *Handbook of Heterogeneous Catalysis* (G. Ertl, H. Knozinger and J. Weitkamp, eds), Wiley-VCH, Weinheim, 1, p. 324.
Molina-Sabio M., Rodriguez-Reinoso F., Caturla F. and Selles M.J. (1995) *Carbon* **33**, 1105.
Monnier A., Schüth F., Huo Q., Kumar D., Margolese D., Maxwell R.S., Stucky G.D., Krishnamurty M., Petroff P.M., Firouzi A., Janicke M. and Chmelka B.F. (1993) *Science* **261**, 1299.
Müller U. and Unger K.K. (1988) *Z. Kristallogr.* **182**, 190.
Müller U., Unger K.K., Pan D., Mersmann A., Grillet Y., Rouquerol F. and Rouquerol J. (1989) In: *Zeolites as Catalysts, Sorbents and Detergent Builders* (H.G. Karge and J. Weitkamp, eds), Elsevier, Amsterdam, p. 625.
Müller U. *et al.* (1990) In: *Gas Separation Technology*, Elsevier, Amsterdam, p. 255.
Otowa T. (1991) In: *Adsorptive Separation* (M. Suzuki, ed.), Institute of Industrial Science, Tokyo, p. 273.
Otowa T., Tanibata R. and Itoh M. (1993) *Gas Separation and Purification* **7**, 241.
Otowa T., Nojima Y. and Itoh M. (1996) In: *Fundamentals of Adsorption* (M.D. LeVan, ed.), Kluwer, Boston, p. 709.
Ozin G.A. (1992) *Advanced Mater.* **4**, 612.
Peri J.B. (1971) *Disc. Faraday Soc.* **52**, 55.
Petrakis D.E., Hudson M.J., Pomonis P.J., Sdoukos A.T. and Bakas T.V. (1995) *J. Mater. Chem.* **5**, 1975.
Rathousky J., Zukal A., Franke O. and Schulz-Ekloff G. (1994) *J. Chem. Soc., Faraday Trans.* **90**, 2821.
Ravikovitch P.I., O Domhnaill S.C., Neimark A.V., Schüth F. and Unger K.K. (1995) *Langmuir* **11**, 4765.
Ravikovitch P.I., Wei D., Chueh W.T., Haller G.L. and Neimark A.V. (1997) *J. Phys. Chem.* **B101**, 3671.
Reichert H., Schmidt W., Grillet Y., Llewellyn P., Rouquerol J. and Unger K.K. (1994) In: *Characterization of Porous Solids III* (J. Rouquerol, F. Rodriguez-Reinoso, K.S.W. Sing and K.K. Unger, eds), Elsevier, Amsterdam, p. 517.
Renou J., François-Rossetti J. and Imelik B. (1960) *Bull. Soc. Chim. Fr.* 446.
Rideal E.K. (1932) In: *The Adsorption of Gases by Solids, Faraday Soc.*, p. 139.
Rodriguez-Reinoso F., Molina-Sabio M. and Gonzalez M.T. (1995) *Carbon* **33**, 15.
Rouquerol F., Rouquerol J. and Imelik B. (1985) In: *Principles and Applications of Pore Structural Characterization* (J.M. Haynes and P. Rossi-Doria, eds), J.W. Arrowsmith, Bristol, p. 213.
Rouquerol J. and Ganteaume M. (1977) *J. Therm. Anal.* **11**, 201.
Rouquerol J., Rouquerol F. and Ganteaume M. (1975) *J. Catalysis* **36**, 99.
Rouquerol J., Rouquerol F. and Ganteaume M. (1979) *J. Catalysis* **57**, 222.
Sayari A., Liu P., Kruk M. and Jaroniec M. (1997) *Chem. Mater.* **9**, 2499.
Schmidt W., Schüth F., Reichert H., Unger K. and Zibrowius B. (1992) *Zeolites* **12**, 2.
Schmidt R., Hansen E.W., Stocker M., Akporiaye D. and Ellestad O.H. (1995) *J. Am. Chem. Soc.* **117**, 4049.
Schmidt R., Junggreen H. and Stocker M. (1996) *J. Chem. Soc., Chem. Commun.* 875.
Schnabel R. and Langer P. (1991) *J. Chromatography* **544**, 137.
Setoyama N., Li G., Kaneko K., Okino F., Ishikawa R., Kanda M. and Touhara H. (1996) Adsorption **2**, 293.
Smisek M. and Cerny S. (1970) *Active Carbon*, Elsevier, Amsterdam, p. 317.
Sing K.S.W. (1972) In: *Thermochimie*, Colloques Internationaux du CNRS no. 201, Editions du CNRS, Paris, p. 601.

Sing K.S.W. (1973) In: *Pore Structure and Properties of Materials*, vol. III (S. Modry, ed.), Academia Prague, B-5.
Sing K.S.W. (1989) *Carbon* **27**, 5.
Stach H., Thamm H., Fiedler K., Grauert B., Wieker W., Jahn E. and Ohlmann G. (1986) *Stud. Surface Sci. Catalysis* **28**, 539.
Stucky G.D., Monnier A., Schüth F., Huo Q., Margolese D., Kumar D., Krishnamurty M., Petroff P., Firouzi A., Janicke M. and Chmelka B.F. (1994) *Mol. Cryst. Liq. Cryst.* **240**, 187.
Suzuki M. (1994) *Carbon* **32**, 577.
Teichner S. (1986) In: *Aerogels*, Springer-Verlag, Berlin, p. 22.
Thamm H. (1987) *Zeolites* **7**, 341.
Thess A., Lee R., Nikolaev P. and Dai H. (1996) *Science* **273**, 483.
Thomas J.M. (1994) *Nature* **368**, 289.
Thomas J.M. (1995) *Faraday Discuss.* **100**, C9.
Tomlinson J.B. and Theocharis C.R. (1992) *Carbon* **30**, 907.
Tomlinson J.B., Freeman J.J. and Theocharis C.R. (1993) *Carbon* **31**, 13.
Tosi-Pellenq N., Grillet Y., Rouquerol J. and Llewellyn P. (1992) *Thermochim. Acta* **204**, 79.
Vartuli J.C., Kresge C.T., Leonowicz M.E., Chu A.S., McCullen S.B., Johnson I.D. and Sheppard E.W. (1994) *Chem. Mater.* **6**, 2070.
Wang Z.-M. and Kaneko K. (1995) *J. Phys. Chem.* **99**, 16714.
Wennerberg A.N. and O'Grady T.M. (1978) U.S. Patent 4 082 684.
Wilson S.T., Lok B.M., Messina C.A., Cannan T.R. and Flanigen E.M. (1982a) *J. Am. Chem. Soc.* **104**, 1146.
Wilson S.T., Lok B.M. and Flanigen E.M. (1982b) U.S. Patent 4 310 440.
Wright J.E., Freeman J.J., Sing K.S.W., Jackson S.W. and Smith R.J.M. (1988) British Patent 8 723 447.

CHAPTER 13

General Conclusions and Recommendations

13.1. Physisorption at the Gas–Solid Interface

13.1.1 Interpretation and classification of adsorption isotherms

A useful indication of the mechanisms of surface coverage and/or pore filling can be obtained by visual inspection of an isotherm. However, it must be kept in mind that the overall shape of an isotherm is governed by the nature of the gas–solid system, the pore structure of the adsorbent and the operational temperature.

Linearity of the isotherm (i.e. Henry's law behaviour) is generally observed only at very low surface coverage and therefore cannot be easily detected at the temperatures and with the techniques normally used for studying the complete range of $p/p°$ (e.g. 77 K for nitrogen adsorption). The deviation from linearity may be either towards or away from the pressure axis, depending on the scale of surface heterogeneity and the magnitude of the adsorbate–adsorbate interactions. A virial form of equation is generally applicable to this low coverage region.

The six major types of isotherms in the IUPAC classification (see Figure 1.7) still provide a useful basis for the discussion of the various physisorption mechanisms,

but as a result of recent progress it is now possible to extend and refine the classification by the subdivision of Types I, II and IV.

Type I isotherms

The main feature of a reversible Type I isotherm is the long plateau, which is indicative of a relatively small amount of multilayer adsorption on the open surface. Micropore filling may take place either in pores of molecular dimensions (i.e. primary micropore filling) at very low $p/p°$ or in wider micropores (co-operative filling) over a range of higher $p/p°$. The corresponding isotherms are here designated Types Ia and Ib, respectively, as displayed in Figure 13.1. In their 'ideal' forms, both types are reversible and both have almost horizontal plateaux over a wide range of high $p/p°$.

Type II isotherms

A truly reversible Type II isotherm is normally associated with monolayer–multilayer adsorption on an open and stable external surface of a powder, which may be non-porous, macroporous or even, to a limited extent, microporous. This form of isotherm is now termed Type IIa (see Figure 13.1).

The smooth, non-stepwise character of a Type IIa isotherm is often associated with energetic heterogeneity in the adsorbent–adsorbate interactions. A sharp Point B and a correspondingly high value of C(BET) usually indicate a formation of a well-

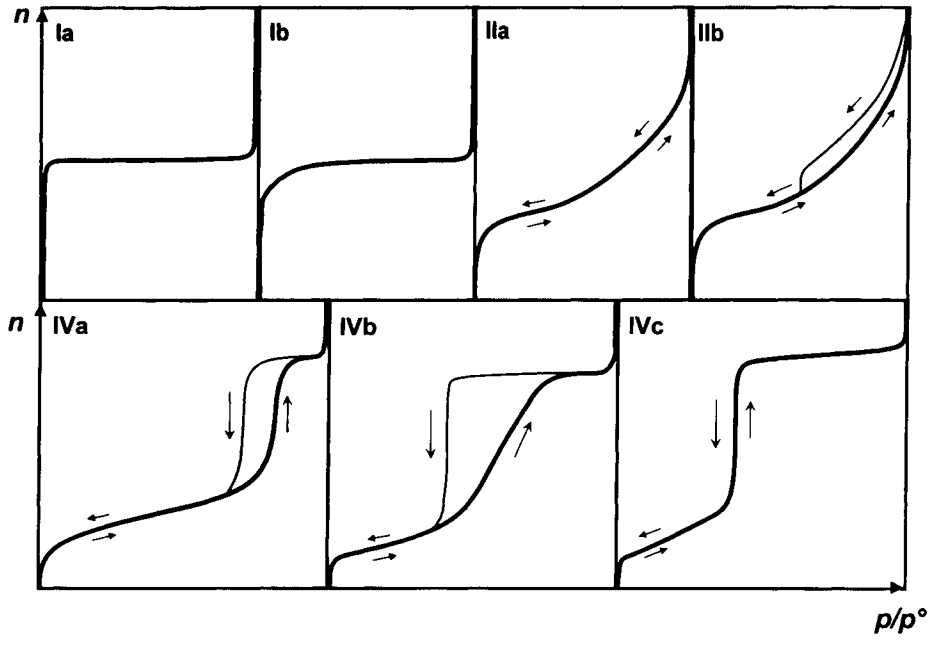

Figure 13.1. Subdivision of gas adsorption isotherms of type I, II and IV.

defined monolayer, while the absence of an identifiable Point B is a clear sign of a significant overlap of monolayer and multilayer adsorption. Increase of temperature leads to a smoothing of the isotherm, which may be generally ascribed to an increase in mobility of the adsorbed molecules, or alternatively to a decreased degree of localization.

There are many aggregated powders (clays, pigments, cements, etc.) that appear to give normal Type II adsorption isotherms, although their full adsorption–desorption isotherms exhibit Type H3 hysteresis. However, unlike Type IV isotherms, there is no plateau at high $p/p°$. These isotherms are now termed Type IIb, as indicated in Figure 13.1.

Generally, Type IIb isotherms are obtained with aggregates of plate-like particles, which therefore possess non-rigid slit-shaped pores. Because of delayed capillary condensation, multilayer adsorption is able to proceed on the particle surface until a high $p/p°$ is reached. Once the condensation has occurred, the state of the adsorbate is changed and the desorption curve therefore follows a different path until the condensate becomes unstable at a critical $p/p°$.

Type III isotherms

True Type III isotherms are confined to a few systems in which the overall adsorbent–adsorbate interactions are weak in comparison with relatively strong adsorbate–adsorbate interactions. The monolayer density tends to be unevenly distributed on the adsorbent surface with a relatively high concentration of molecules located on the most active areas. As the pressure is raised the average monolayer concentration is increased, but before it can become close-packed over the complete surface, the monolayer coverage is overtaken by a form of co-operative multilayer adsorption in which molecules are clustered around the most favourable sites. This results in the isotherm curvature remaining convex to the $p/p°$ axis with $C(\text{BET}) < 2$. In an extreme case (e.g. water/graphite) the adsorption may be quite difficult to detect, even at $p/p° \approx 0.8$.

Type IV isotherms

In the original IUPAC classification, the hysteresis loop was said to be a characteristic feature of a Type IV isotherm. It is now evident that this statement must be revised. Moreover, we can distinguish between two characteristic types of hysteresis loops. In the first case (a Type H1 loop), the loop is relatively narrow, the adsorption and desorption branches being almost vertical and nearly parallel; in the second case (a Type H2 loop), the loop is broad, the desorption branch being much steeper than the adsorption branch. These isotherms are illustrated in Figure 13.1 as Type IVa and Type IVb, respectively. Generally, the location of the adsorption branch of a Type IVa isotherm is governed by delayed condensation, whereas the steep desorption branch of a Type IVb isotherm is dependent on network-percolation effects.

The less common, completely reversible isotherm in Figure 13.1 is now designated a Type IVc isotherm. If the riser is almost vertical at a characteristic $p/p°$, reversible

pore filling and emptying appear to occur in a narrow range of uniform near-cylindrical pores of critical size – the reversibility being dependent on the adsorptive and the operational temperature.

Type V isotherms

The appearance of the initial section of a Type V isotherm is very similar to that of a Type III isotherm for a similar gas–solid system (e.g. water/carbon). In this case, however, the sharp increase in adsorption at higher p/p° is dependent on the pore size. For example, the ultramicropores in a molecular sieve carbon are filled with water at a much lower p/p° than are the wider pores in a supermicroporous carbon.

Type VI isotherms

The highly distinctive form of a Type VI isotherm is due to a stepwise layer-by-layer adsorption process. Such isotherms are given by the adsorption of simple non-polar molecules (e.g. argon, krypton and xenon) on uniform surfaces (e.g. the basal plane of graphite). The steps become less sharp as the temperature is increased. The vertical risers can be regarded as the adsorbed layer boundaries and the centres of the treads (inflection points) as the layer capacities. When present, sub-steps are associated with two-dimensional phase changes in the monolayer. Useful information concerning the surface uniformity and adsorbate structure can be obtained from the relative layer capacities and the presence of sub-steps.

Intermediate and composite isotherms

There are a few systems (e.g. butanol/alumina) which exhibit 'gas phase autophobicity'. Because of directional hydrogen bonding, the monolayer is much more strongly adsorbed than the second layer. The multilayer isotherm therefore has a very low slope and the isotherm has a Type I appearance. In this case, the monolayer completion is at the beginning of the plateau.

Since highly active adsorbents generally contain complex pore structures, it is not surprising that many physisorption isotherms are of a composite nature. Thus, most of the Type IV isotherms reported for oxide gels are exceedingly complex with features which are difficult to identify.

A few isotherms of an intermediate shape between Types Ib and IVc have been reported for the adsorption of argon and nitrogen on certain grades of MCM-41. In some instances, the isotherm is completely reversible, but the gradual slope of the Type IV riser presents a problem. Since the pore size distribution was believed to be very narrow, it would appear that pore filling has not taken place in accordance with the classical form of capillary condensation.

13.1.2. Energetics of physisorption

Adsorption energy studies serve a very useful purpose in three main areas: (1) to provide chemical engineering data; (2) to investigate adsorption mechanisms; and (3) to characterize the energetic heterogeneity of solid surfaces. To ensure that the evaluated adsorption energies have scientific validity, it is essential that the

thermodynamic states of the adsorption system are properly defined and that the reliability of the operational procedure is adequately checked.

The simplest way of obtaining the differential enthalpy of adsorption, $\Delta_{ads}\dot{h}$, is by the isosteric method, which involves the measurement of at least two isotherms for the given system at different temperatures and application of the Clausius–Clapeyron equation. The method is based on the assumption that the adsorbed phase remains unchanged and in thermodynamic equilibrium over the temperature range studied. In practice, the method is very sensitive to any errors in the measurement of the equilibrium pressures. For these reasons the derived isosteric enthalpies are often unreliable, particularly in the region of low surface coverage.

The requirement of thermodynamic reversibility also applies to the chromatographic method, but in this case it is necessary to work at very low surface coverage (at 'zero coverage') in the Henry's law region. Values of the specific retention volume, V_S, determined at different temperatures are inserted in the Clausius–Clapeyron equation in place of the equilibrium pressures to obtain $\Delta_{ads}\dot{h}$. Provided that a number of conditions are observed, the method is capable of providing a fairly easy and rapid assessment of the adsorbent–adsorbate interaction energy.

Many different calorimetric techniques are described in the literature for the direct determination of adsorption energies. Unfortunately, few of the older calorimeters can be used to determine well-defined thermodynamic quantities. However, by means of the modern design of microcalorimeter of the heat-flow type and a continuous manometric procedure, it becomes possible to determine highly accurate differential energies of adsorption at constant temperature (e.g. at 77 K) over a wide range of surface coverage. This approach also allows systematic investigations to be made of the energetics of two-dimensional phase changes and the various stages of pore filling.

13.1.3. Determination of surface area

To apply any gas adsorption technique for the determination of surface area, it must be assumed that the mode of monolayer and/or multilayer adsorption is not oversensitive to differences in surface structure. This requirement is more likely to be satisfied if the specific contribution to the adsorbent–adsorbate interaction is not too great. For this reason, water, alcohols and other highly polar molecules are not recommended for the determination of the *overall* area.

The BET model is strictly incompatible with the energetic heterogeneity exhibited by most solid surfaces. The range of linearity of the BET plot is always restricted to a limited part of a Type II isotherm, which rarely extends above $p/p^\circ \approx 0.35$ and in some cases no higher than $p/p^\circ \approx 0.1$. In fact, a more useful empirical relation for *multilayer* adsorption is the FHH equation, which is generally applicable over a wide range of p/p°.

In spite of the artificial nature of the BET theory, the BET method is still used as a standard procedure for surface area determination. In principle, the BET method can be applied to isotherms of Types Ib, IIa, IIb, IVa, IVb, IVc and VI, provided that there is no significant primary micropore filling contribution and that the structure of

the completed monolayer does not vary from one surface to another. Fractal analysis has shown that the latter requirement is fulfilled by only a few adsorption systems, and generally some arbitrary adjustment of the molecular areas is required to obtain agreement with the derived values of BET-nitrogen area.

For a number of reasons, nitrogen (at 77 K) is generally considered to be the most suitable adsorptive for standard surface area determination and for this purpose it is usually assumed that the BET monolayer is close-packed (with the molecular area taken as 0.162 nm^2). One advantage of nitrogen is that the path of its multilayer isotherm is not very sensitive to differences in adsorbent structure. A useful check on the validity of n_m is that the value of C(BET) should be neither too low nor too high: if C(BET) < 50, Point B is not sufficiently sharp; if C(BET) > 200, there is either a significant micropore filling contribution or localized adsorption on specific sites.

An empirical procedure (e.g. the α_s-method) can be used to verify the monolayer–multilayer mechanism and to provide an independent evaluation of the surface area. This approach has the merit that in favourable cases it can allow an assessment to be made of the total area and/or the external area of a microporous adsorbent.

13.1.4. Capillary condensation and mesopore analysis

The view is generally held that capillary condensation is responsible for mesopore and macropore filling (i.e. in pores of width $\omega > \approx 2$ nm). Since the filling of macropores ($\omega > 50$ nm) occurs at very high $p/p°$, we are essentially concerned with mesopore filling. Capillary condensation can be regarded as a secondary process, which is always preceded by adsorption on the pore walls.

According to the classical interpretation, the phenomenon is explained by application of the Kelvin equation: this gives the relationship between the relative pressure and the meniscus curvature of liquid condensed in a pore. When the Kelvin equation is used to evaluate the pore size, it is tacitly assumed that there is a direct relationship between the meniscus curvature and the dimensions of the mesopores. In principle, it is also necessary to define the pore shape.

The onset of capillary condensation is indicated by an upward departure of the isotherm from the standard curve determined on the same area of a non-porous surface of similar composition. The mesopore capacity is the amount adsorbed at the plateau of the Type IV isotherm: to obtain the mesopore volume, it is assumed that the condensate has the same density as the liquid adsorptive at the operational temperature.

Of the various classical procedures proposed for mesopore size analysis, the Barrett, Joyner and Halenda (BJH) method appears to remain the most popular. The application of the standard BJH method involves the following assumptions:

(a) Rigid pores of cylindrical shape.
(b) Hemispherical meniscus with zero contact angle.
(c) Applicability of simple Kelvin equation.
(d) Validity of the correction for multilayer adsorption.

If the pores are slit-shaped, the meniscus is assumed to be hemicylindrical. In principle, the pore width can be readily calculated from the Kelvin radius; in practice,

the metastable multilayer is likely to remain on the planar walls of a slit and thus considerably delay the onset of capillary condensation.

A long-standing problem is the interpretation of the hysteresis loop. For many years the desorption branch was favoured for pore size analysis, but this practice is now considered to be unreliable. There are three related problems: (a) network-percolation effects; (b) delayed condensation; and (c) instability of the condensate below a critical $p/p°$.

Validity of the derived pore size distribution should not be expected unless certain conditions are met and the following practice is recommended for mesopore size analysis: if the isotherm is of Type IVa, the desorption branch should be adopted; if the isotherm is of Type IVb, the adsorption branch is likely to provide a more reliable overall estimate of the pore size distribution. However, in the latter case the pore shape may be a critical factor. The procedure adopted for mesopore size analysis together with the branch of the hysteresis loop should always be clearly stated.

13.1.5. Micropore analysis

In the IUPAC classification of pore size the upper limit of micropore width was placed at about 2 nm. In fact, this limiting width is somewhat arbitrary since the mechanism of pore filling is controlled by the pore size, the adsorbate molecular size, the gas–solid interactions and the operational temperature. It is evident that capillary condensation cannot occur in ultramicropores of molecular dimensions and also that there can be no significant enhancement of initial adsorption energy in the supermicropores of larger pore width. In the latter case, our knowledge of the mechanisms of pore filling is still imprecise, although progress is being made with the aid of density functional theory and molecular simulation.

Various procedures have been used to evaluate the micropore capacity from the experimental isotherm data (e.g. the Dubinin–Radushkevich plot), but in practice these are all empirical methods. It should be kept in mind that no theoretical significance can be deduced from the fact that a particular equation gives a reasonably good fit over a certain range of an isotherm determined at only one temperature. In our view, a safer approach is to plot the amount adsorbed against standard data determined on a non-porous reference material (i.e. to construct a comparison plot or α_s-plot).

Another procedure proposed for micropore evaluation is by nonane pre-adsorption, which is dependent on the strong retention of *n*-nonane molecules in the ultramicropores. However, it is now apparent that the extent of the pore blocking is determined by the network connectivity as well as by the micropore size distribution.

To convert the micropore capacity into the micropore volume, it is usually assumed that the pores are filled with liquid adsorptive – as in the case of mesopore filling. This procedure does not allow for the dependency of molecular packing on both pore size and pore shape. For this reason, we recommend that the term 'apparent micropore volume' should be adopted and that the gas and temperature should always be specified.

The use of nitrogen adsorption alone cannot be expected to provide more than a

qualitative indication of the micropore size distribution. To obtain a quantitative evaluation it is advisable to employ a number of probe molecules of different size (e.g. methane, isobutane and neopentane). The number of adsorptive molecules can be minimized by taking account of the various stages of micropore filling. In this manner one can focus attention on the importance of the mechanism of pore filling.

13.2. Adsorption at the liquid–solid interface

13.2.1. Immersion energetics

Immersion calorimetry has much to offer for the characterization of powders and porous solids or for the study of adsorption phenomena. The technique can provide both fundamental and technologically useful information, but for both purposes it is essential to undertake carefully designed experiments. Thus, it is no longer acceptable to make ill-defined 'heat of immersion' measurements. To obtain thermodynamically valid energy, or enthalpy, or immersion data, it is necessary to employ a sensitive microcalorimeter (preferably of the heat-flow isothermal type) and adopt a technique which involves the use of sealed glass sample bulbs and allows ample time (usually one day) for outgassing and the subsequent temperature equilibration.

Once the essential experimental conditions are fulfilled, it is possible to use immersion microcalorimetry for the following purposes:

(a) Surface characterization. Information on the polarity, wettability, hydrophobicity and crystallinity of the surface can be obtained.
(b) Surface area determination. The external (non-microporous) area can be determined by the modified Harkins–Jura method, which has the advantage that it is completely independent of the BET method. The method can be applied to a wide range of powders, with surface areas in the range $1-100\ m^2\ g^{-1}$. The internal, micropore area of activated carbons and some other porous solids can also be determined, provided that the areal energies are already known.
(c) Micropore analysis. The indirect evaluation of the micropore size distribution can be achieved by using immersion liquids of different molecular size (i.e. by making use of molecular sieving). In this case, the area accessible to each liquid adsorptive is determined.

Our present understanding of the molecular interactions within micropores has resulted in a significant development in the interpretation of the immersion energy data. It was formerly thought that volume filling was solely responsible for the immersion energy enhancement, but the present view is that the energy of immersion is more directly related to the micropore area.

13.2.2. Adsorption from solution

Many of the technologically important adsorption from solution phenomena are exceedingly complex. Although most of the experimental data reported in the

scientific literature were determined for adsorption from relatively dilute binary solutions, even these are generally difficult to interpret.

Bearing in mind these problems, we can take advantage of the Gibbs presentation and also make use of the concept of reduced surface excess amount, which does not depend on the location of the Gibbs dividing surface. In this manner, we can avoid making any initial assumptions concerning the adsorption mechanism. The resulting isotherms are useful for surface characterization and in favourable cases for surface area determination or micropore analysis.

Values of apparent surface area can be derived only if the solute isotherm exhibits a long saturation plateau. Unfortunately, the derived values are often of questionable significance since the exact structure of the monolayer (containing both solute and solvent) is rarely known. The study of microporosity by adsorption from solution measurements is in its infancy, but the use of comparison plots appears to be a promising approach.

The energetics of adsorption at the solution–solid interface are conveniently expressed in terms of the enthalpy (or energy) of displacement of the solvent by the solute. Generally, the isosteric method and immersion calorimetry do not offer the same advantages as for gas–solid systems. Batch adsorption calorimetry appears to be a relatively simple technique which can be used with any grain size but its application is not straightforward. In contrast liquid-flow adsorption microcalorimetry is more versatile since it allows satisfactory control of pH, ionic strength, concentration, etc. and makes possible the study of desorption but it does demand a minimum grain size (say, 20 μm).

There are a number of different factors which may affect the level of uptake and the energetics of adsorption from solution: the chemistry and electrical properties of the solid surface and the molecular/micellar/polymeric structure of the solution must all be taken into account. Whenever possible, a study of both adsorption isotherms and enthalpies of displacement is worthwhile, but it is often necessary to complement these measurements with others including electrophoretic mobilities, FTIR spectra and various types of microscopy.

Author Index

Numbers in roman refer to citations in the text, numbers in italic indicate co-authors and numbers in bold refer to the pages on which references are listed at the end of each chapter.

Subject Index

This Page Intentionally Left Blank